DEVELOPMENT AND APPLICATION OF CLOSTRIDIA AS MICROBIAL CELL-FACTORIES FOR BIOFUELS AND BIOCHEMICALS PRODUCTION

EDITED BY: Hongxin Fu, Shang-Tian Yang, Chuang Xue, Weihong Jiang and Petra Patakova

PUBLISHED IN: Frontiers in Bioengineering and Biotechnology and Frontiers in Microbiology

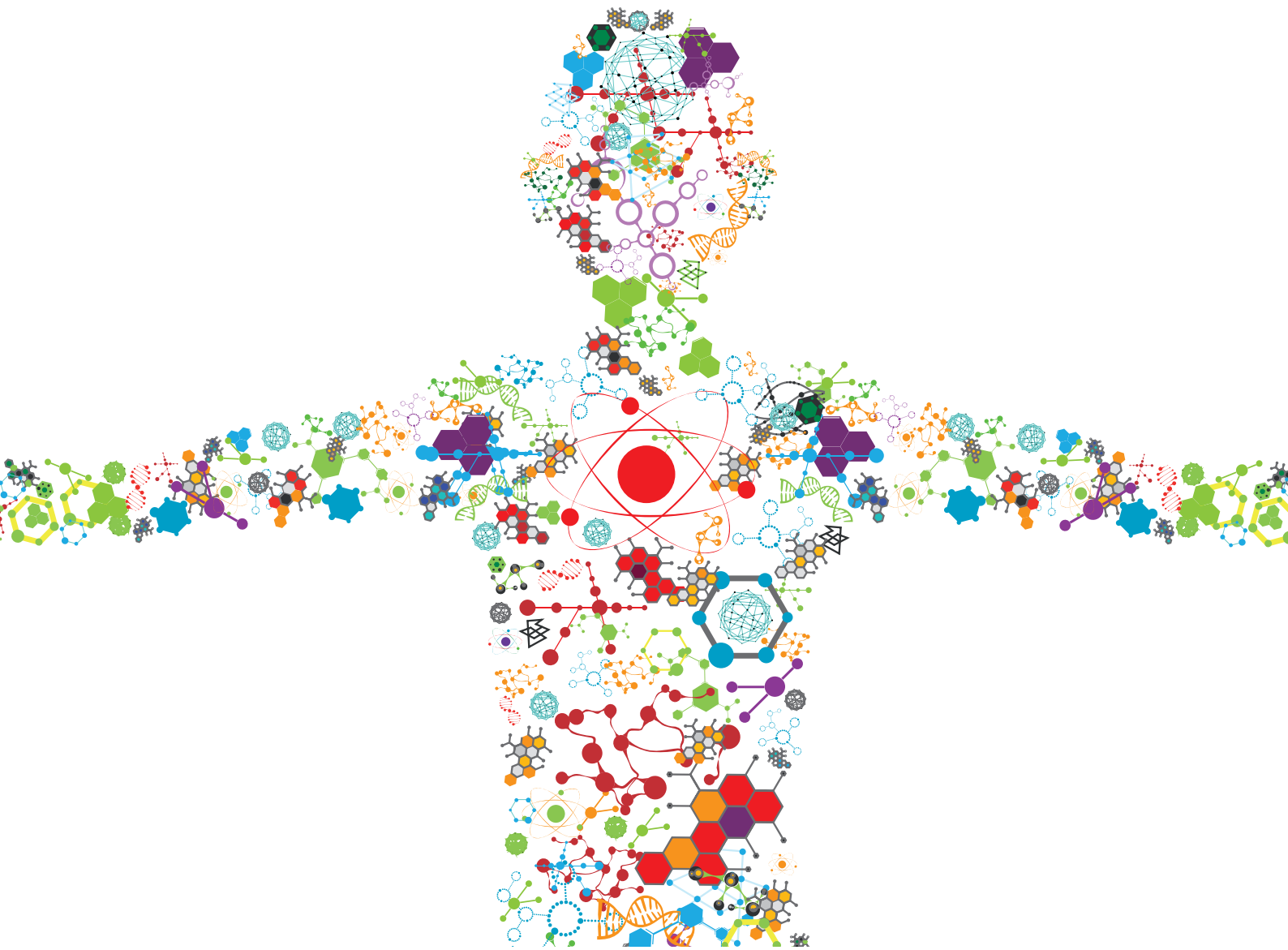

frontiers Research Topics

frontiers

ISSN 1664-8714
ISBN 978-2-88974-423-7
DOI 10.3389/978-2-88974-423-7

About Frontiers

Frontiers is more than just an open-access publisher of scholarly articles: it is a pioneering approach to the world of academia, radically improving the way scholarly research is managed. The grand vision of Frontiers is a world where all people have an equal opportunity to seek, share and generate knowledge. Frontiers provides immediate and permanent online open access to all its publications, but this alone is not enough to realize our grand goals.

Frontiers Journal Series

The Frontiers Journal Series is a multi-tier and interdisciplinary set of open-access, online journals, promising a paradigm shift from the current review, selection and dissemination processes in academic publishing. All Frontiers journals are driven by researchers for researchers; therefore, they constitute a service to the scholarly community. At the same time, the Frontiers Journal Series operates on a revolutionary invention, the tiered publishing system, initially addressing specific communities of scholars, and gradually climbing up to broader public understanding, thus serving the interests of the lay society, too.

Dedication to Quality

Each Frontiers article is a landmark of the highest quality, thanks to genuinely collaborative interactions between authors and review editors, who include some of the world's best academicians. Research must be certified by peers before entering a stream of knowledge that may eventually reach the public - and shape society; therefore, Frontiers only applies the most rigorous and unbiased reviews.
Frontiers revolutionizes research publishing by freely delivering the most outstanding research, evaluated with no bias from both the academic and social point of view. By applying the most advanced information technologies, Frontiers is catapulting scholarly publishing into a new generation.

What are Frontiers Research Topics?

Frontiers Research Topics are very popular trademarks of the Frontiers Journals Series: they are collections of at least ten articles, all centered on a particular subject. With their unique mix of varied contributions from Original Research to Review Articles, Frontiers Research Topics unify the most influential researchers, the latest key findings and historical advances in a hot research area! Find out more on how to host your own Frontiers Research Topic or contribute to one as an author by contacting the Frontiers Editorial Office: frontiersin.org/about/contact

DEVELOPMENT AND APPLICATION OF CLOSTRIDIA AS MICROBIAL CELL-FACTORIES FOR BIOFUELS AND BIOCHEMICALS PRODUCTION

Topic Editors:
Hongxin Fu, South China University of Technology, China
Shang-Tian Yang, The Ohio State University, United States
Chuang Xue, Dalian University of Technology, China
Weihong Jiang, Institute of Plant Physiology and Ecology, Shanghai Institutes for Biological Sciences (CAS), China
Petra Patakova, University of Chemistry and Technology in Prague, Czechia

Citation: Fu, H., Yang, S.-T., Xue, C., Jiang, W., Patakova, P., eds. (2022). Development and Application of Clostridia as Microbial Cell-factories for Biofuels and Biochemicals Production. Lausanne: Frontiers Media SA. doi: 10.3389/978-2-88974-423-7

Table of Contents

frontiers in Bioengineering and Biotechnology

EDITORIAL
published: 11 January 2022
doi: 10.3389/fbioe.2021.831135

Editorial: Development and Application of Clostridia as Microbial Cell-Factories for Biofuels and Biochemicals Production

Hongxin Fu[1]* *and Shang-Tian Yang*[2]*

[1]Guangdong Key Laboratory of Fermentation and Enzyme Engineering, School of Biology and Biological Engineering, South China University of Technology, Guangzhou, China, [2]William G. Lowrie Department of Chemical and Biomolecular Engineering, The Ohio State University, Columbus, OH, United States

Keywords: clostridia, butanol, butyric acid, isobutanol, 1,3-butanediol (1,3-BDO), biofilm, short- and medium-chain ester, metabolic engineering

Editorial on the Research Topic

Development and Application of Clostridia as Microbial Cell-factories for Biofuels and Biochemicals Production

Clostridia are Gram-positive, spore-forming, obligate anaerobic bacteria with versatile substrate utilization and metabolite production capabilities (Xue et al., 2017). The exploitation of clostridia for large-scale production of commodity chemicals can be dated back to 100 years ago with solventogenic clostridia in acetone-butanol-ethanol (ABE) fermentation, which had fallen out of favor since the establishment of more economical petrochemical processes (Cheng et al., 2019a). However, the necessity of sustainable development has renewed interest in the production of biofuels and biochemicals from abundant renewable biomass. In recent years, several *Clostridium* species, including conventional solventogenic clostridia such as *C. acetobutylicum* and *C. beijerinckii*, cellulolytic clostridia like *C. thermocellum*, *C. cellulolyticum* and *C. cellulovorans* (Yang et al., 2015), acetogens such as *C. formicoaceticum* (Bao et al., 2019) and *C. carboxidivorans* (Cheng et al., 2019b), and acidogens including *C. tyrobutyricum* (Li et al., 2019; Bao et al., 2020; Fu et al., 2021) *and C. kluyveri*, have garnered immense interests in the field of industrial biotechnology for their abilities to produce various chemicals and biofuels from low-cost agricultural residues and industrial wastes.

The high toxicity of fermentative products (such as butanol and butyrate) is a drawback limiting Clostridia for industrial applications. Random chemical mutagenesis aiming at increasing butanol efflux capacity was used to improve butanol tolerance of *C. beijerinckii* (Vasylkivska et al.). Mutant strains obtained by different approaches behaved differently in terms of efflux pump substrates (butanol, ethanol, ethidium bromide and antibiotics) tolerance and metabolites production. The best mutant obtained with ethidium bromide for mutagenesis and selection showed a 127% improvement in butanol tolerance. The genomes of various mutant strains were sequenced and analyzed, and the results indicated that the improved butanol tolerance was attributed to mutations in genes related to stress responses (chemotaxis, autolysis or changes in cell membrane structure) and efflux pump regulators. This study confirmed the importance of efflux in butanol stress and provided new gene targets for rational strain engineering. On another hand, Gao et al. screened 5 *C. acetobutylicum* mutants through carbon ion beam irradiation, which had advantages of excellent biological effectiveness and dose conformity over traditional mutation methods. The mutant Y217 showed enhanced butanol tolerance and production of 13.67 g/L (vs. 9.77 g/L for the control), which was attributed to its ability to maintain cell membrane integrity and permeability under butanol stress. As strain mutagenesis and screening is a time-consuming process, Cao et al. developed and verified non-

Edited and reviewed by:
Jean Marie François, Institut Biotechnologique de Toulouse (INSA), France

***Correspondence:**
Hongxin Fu
hongxinfu@scut.edu.cn
Shang-Tian Yang
yang.15@osu.edu

Specialty section:
This article was submitted to Synthetic Biology, a section of the journal Frontiers in Bioengineering and Biotechnology

Received: *08 December 2021*
Accepted: *13 December 2021*
Published: *11 January 2022*

Citation:
Fu H and Yang S-T (2022) Editorial: Development and Application of Clostridia as Microbial Cell-Factories for Biofuels and Biochemicals Production. Front. Bioeng. Biotechnol. 9:831135. doi: 10.3389/fbioe.2021.831135

structured mathematical models which could reflect strain growth, glucose consumption, and butyric acid production of $^{12}C^{6+}$ irradiation-mutation strain of *C. tyrobutyricum*.

Although clostridia possess the ability to ferment a broad range of substrates, carbon catabolite repression (CCR), which usually happens when mixed sugars (glucose and non-glucose substrates) are present in the fermentation medium, is limiting their uses of lignocellulosic biomass hydrolysates as substrates (Fu et al., 2017). Although catabolite control protein A (CcpA) knockout resulted in simultaneous utilization of glucose and xylose in *C. acetobutylicum*, some negative influences were observed due to the multiple roles of CcpA (Wu et al., 2015). To solve this problem, Ujor et al. explored a ribozyme-mediated approach to downregulate CcpA in *C. beijerinckii*. The expression of CcpA-/DisA (encoding DNA integrity scanning protein A)-specific M1 RNA-based ribozyme led to obvious decreases in CcpA/DisA mRNA levels and modest increase in mixed sugars utilization and ABE production compared to the control. This study demonstrated that DisA played an important role in regulating solvent production and the feasibility of using ribozyme-mediated approach for gene knockdown in *C. beijerinckii*.

Isobutanol is an important platform chemical widely used in food, chemical, biofuel and pharmaceutical industries. The market of bio-based isobutanol reached $1 billion in 2019 and is expected to rise significantly in the near future. Weitz et al. introduced two different isobutanol synthesis pathways, ketoisovalerate ferredoxin oxidoreductase (Kor) and ketoisovalerate decarboxylase (Kivd), into two acetogenic bacteria, *Clostridium ljungdahlii* and *Acetobacterium woodii*, and evaluated their effects on isobutanol production under both heterotrophic and autotrophic conditions. When syngas was used as the substrate, the engineered *C. ljungdahlii* produced 0.4 and 1 mM isobutanol without and with ketoisovalerate addition via the Kivd pathway, which was better than the results (0 and 0.2 mM isobutanol) obtained via the Kor pathway. To identify the bottlenecks of autotrophic isobutanol production, syngas-based batch cultivation together with metabolic profiling and flux balance analysis were performed for various *C. ljungdahlii* strains (Hermann et al.), and the results indicated that further work could be focused on improving the activities of key enzymes and changing their coenzyme specificity or supply. The chirally pure (R)-1,3-butanediol (BDO) is used for fragrances, insecticides and as precursor molecules for penem and carbapenem antibiotic synthesis. Grosse-Honebrink et al. expressed acetoacetyl-CoA reductase gene *phaB* from *Cupriavidus necator* in *C. saccharoperbutylacetonicum* and optimized the heterologous pathway at transcriptional (promoters and gene expression methods optimization), translational (codon optimization), enzyme (point mutations), and population (medium optimization) levels for (R)-1,3-BDO production from glucose. The optimized mutant produced 1.8 g/L (R)-1,3-BDO, a 217% increase compared to the control. A higher concentration could be achieved by further optimizing the fermentation process.

C. acetobutylicum has long been and extensively used in industrial production of acetone, butanol, and ethanol in ABE fermentation, but little attention has been paid to its biofilm. Zhang et al. summarized the cell physiological changes, extracellular matrix components, production advantages, influencing factors and regulatory genes of *C. acetobutylicum* biofilm, which provided valuable insights into its molecular basis useful for developing efficient biofilm processes. Clostridia can produce a variety of organic acids and alcohols, and thus are promising whole cell biocatalysts for short- and medium-chain esters. Wang et al. reviewed the advances in ester production by Clostridia including *in vitro* lipase catalysis and *in vivo* acyltransferase reaction. In addition, the potential of several Clostridia and clostridial consortia which can utilize cheap substrates such as industrial waste gas and lignocellulose for bio-ester production and the recent development of synthetic biology in clostridial chassis development were also discussed. Furthermore, cellulolytic Clostridia in a constructed cellulolytic microflora played an important role in anaerobic co-digestion of pig manure and rice straw for methane production (Zhong et al.).

In summary, the original research and review papers published in this Research Topic provide valuable information on the selection and construction of robust and novel *Clostridium* strains for biofuels and biochemicals production from renewable resources, which will contribute to the further development of Clostridia as microbial cell-factories for industrial applications.

AUTHOR CONTRIBUTIONS

HF initiated the Research Topic and wrote the draft. S-TY revised and approved the final version for publication.

ACKNOWLEDGMENTS

We thank all authors, reviewers, topic editors, and editorial staff at Frontiers who contributed to this Research Topic.

REFERENCES

Bao, T., Cheng, C., Xin, X., Wang, J., Wang, M., and Yang, S.-T. (2019). Deciphering Mixotrophic *Clostridium Formicoaceticum* Metabolism and Energy Conservation: Genomic Analysis and Experimental Studies. *Genomics* 111 (6), 1687–1694. doi:10.1016/j.ygeno.2018.11.020

Bao, T., Feng, J., Jiang, W., Fu, H., Wang, J., and Yang, S.-T. (2020). Recent Advances in *N*-Butanol and Butyrate Production Using Engineered *Clostridium Tyrobutyricum*. *World J. Microbiol. Biotechnol.* 36, 138. doi:10.1007/s11274-020-02914-2

Cheng, C., Bao, T., and Yang, S.-T. (2019a). Engineering Clostridium for Improved Solvent Production: Recent Progress and Perspective. *Appl. Microbiol. Biotechnol.* 103 (14), 5549–5566. doi:10.1007/s00253-019-09916-7

Cheng, C., Li, W., Lin, M., and Yang, S.-T. (2019b). Metabolic Engineering of *Clostridium Carboxidivorans* for Enhanced Ethanol and Butanol Production from Syngas and Glucose. *Bioresour. Technology* 284, 415–423. doi:10.1016/j.biortech.2019.03.145

Fu, H., Hu, J., Guo, X., Feng, J., Yang, S. T., and Wang, J. (2021). Butanol Production from *Saccharina japonica* Hydrolysate by Engineered *Clostridium tyrobutyricum*: The Effects of Pretreatment Method and Heat Shock Protein Overexpression. *Bioresour. Technol.* 335, 129290. doi:10.1016/j.biortech.2021.125290

Fu, H., Yu, L., Lin, M., Wang, J., Xiu, Z., and Yang, S.-T. (2017). Metabolic Engineering of *Clostridium Tyrobutyricum* for Enhanced Butyric Acid Production from Glucose and Xylose. *Metab. Eng.* 40, 50–58. doi:10.1016/j.ymben.2016.12.014

Li, J., Du, Y., Bao, T., Dong, J., Lin, M., Shim, H., et al. (2019). n-Butanol Production from Lignocellulosic Biomass Hydrolysates without Detoxification by *Clostridium tyrobutyricum* Δ*ack-adhE2* in a Fibrous-Bed Bioreactor. *Bioresour. Technology* 289, 121749. doi:10.1016/j.biortech.2019.121749

Wu, Y., Yang, Y., Ren, C., Yang, C., Yang, S., Gu, Y., et al. (2015). Molecular Modulation of Pleiotropic Regulator CcpA for Glucose and Xylose Coutilization by Solvent-Producing *Clostridium Acetobutylicum*. *Metab. Eng.* 28, 169–179. doi:10.1016/j.ymben.2015.01.006

Xue, C., Zhao, J., Chen, L., Yang, S.-T., and Bai, F. (2017). Recent Advances and State-Of-The-Art Strategies in Strain and Process Engineering for Biobutanol Production by *Clostridium Acetobutylicum*. *Biotechnol. Adv.* 35 (2), 310–322. doi:10.1016/j.biotechadv.2017.01.007

Yang, X., Xu, M., and Yang, S.-T. (2015). Metabolic and Process Engineering of *Clostridium Cellulovorans* for Biofuel Production from Cellulose. *Metab. Eng.* 32, 39–48. doi:10.1016/j.ymben.2015.09.001

Conflict of Interest: The authors declare that the research was conducted in the absence of any commercial or financial relationships that could be construed as a potential conflict of interest.

Publisher's Note: All claims expressed in this article are solely those of the authors and do not necessarily represent those of their affiliated organizations, or those of the publisher, the editors and the reviewers. Any product that may be evaluated in this article, or claim that may be made by its manufacturer, is not guaranteed or endorsed by the publisher.

frontiers in Bioengineering and Biotechnology

ORIGINAL RESEARCH
published: 05 November 2020
doi: 10.3389/fbioe.2020.598392

Phenotypic and Genomic Analysis of *Clostridium beijerinckii* NRRL B-598 Mutants With Increased Butanol Tolerance

Maryna Vasylkivska[1], Barbora Branska[1], Karel Sedlar[2], Katerina Jureckova[2], Ivo Provaznik[2] and Petra Patakova[1]*

[1] Department of Biotechnology, University of Chemistry and Technology, Prague, Prague, Czechia, [2] Department of Biomedical Engineering, Faculty of Electrical Engineering and Communication, Brno University of Technology, Brno, Czechia

OPEN ACCESS

Edited by:
Fu-Li Li,
Qingdao Institute of Bioenergy and Bioprocess Technology (CAS), China

Reviewed by:
Yi Wang,
Auburn University, United States
Noppol - Leksawasdi,
Chiang Mai University, Thailand
Thaddeus Chukwuemeka Ezeji,
The Ohio State University, United States

***Correspondence:**
Maryna Vasylkivska
vasylkim@vscht.cz

Specialty section:
This article was submitted to Bioprocess Engineering, a section of the journal Frontiers in Bioengineering and Biotechnology

Received: *24 August 2020*
Accepted: *20 October 2020*
Published: *05 November 2020*

Citation:
Vasylkivska M, Branska B, Sedlar K, Jureckova K, Provaznik I and Patakova P (2020) Phenotypic and Genomic Analysis of Clostridium beijerinckii NRRL B-598 Mutants With Increased Butanol Tolerance. Front. Bioeng. Biotechnol. 8:598392. doi: 10.3389/fbioe.2020.598392

N-Butanol, a valuable solvent and potential fuel extender, can be produced via acetone-butanol-ethanol (ABE) fermentation. One of the main drawbacks of ABE fermentation is the high toxicity of butanol to producing cells, leading to cell membrane disruption, low culture viability and, consequently, low produced concentrations of butanol. The goal of this study was to obtain mutant strains of *Clostridium beijerinckii* NRRL B-598 with improved butanol tolerance using random chemical mutagenesis, describe changes in their phenotypes compared to the wild-type strain and reveal changes in the genome that explain improved tolerance or other phenotypic changes. Nine mutant strains with stable improved features were obtained by three different approaches and, for two of them, ethidium bromide (EB), a known substrate of efflux pumps, was used for either selection or as a mutagenic agent. It is the first utilization of this approach for the development of butanol-tolerant mutants of solventogenic clostridia, for which generally there is a lack of knowledge about butanol efflux or efflux mechanisms and their regulation. Mutant strains exhibited increase in butanol tolerance from 36% up to 127% and the greatest improvement was achieved for the strains for which EB was used as a mutagenic agent. Additionally, increased tolerance to other substrates of efflux pumps, EB and ethanol, was observed in all mutants and higher antibiotic tolerance in some of the strains. The complete genomes of mutant strains were sequenced and revealed that improved butanol tolerance can be attributed to mutations in genes encoding typical stress responses (chemotaxis, autolysis or changes in cell membrane structure), but, also, to mutations in genes X276_07980 and X276_24400, encoding efflux pump regulators. The latter observation confirms the importance of efflux in butanol stress response of the strain and offers new targets for rational strain engineering.

Keywords: butanol tolerance, random chemical mutagenesis, solventogenic *Clostridium* species, genome sequence, butanol efflux

INTRODUCTION

Butanol can be produced from renewable feedstocks of different kinds, including agricultural waste materials, by acetone-butanol-ethanol (ABE) fermentation using solventogenic clostridia (Lee et al., 2008). The most famous species of the group of solventogenic clostridia are *Clostridium acetobutylicum* and *Clostridium beijerinckii*, both of which share a common process bottleneck – low tolerance to butanol.

Butanol is a toxic metabolite that tends to incorporate into the cell membrane, increases membrane fluidity and may disrupt membrane functions (Bowles and Ellefson, 1985; Lepage et al., 1987; Patakova et al., 2018; Vasylkivska and Patakova, 2020). In *C. acetobutylicum*, at inhibitory levels, effects of butanol on cell membrane results in lower ATP generation by the cell, a malfunction in nutrient uptake and an inability of the cell to maintain its internal pH (Bowles and Ellefson, 1985). In Gram-negative bacteria, butanol damages the inner and outer membranes and can also result in a change in cell shape (Fletcher et al., 2016). Such damage, at the cellular level, results in low culture viability and decreased growth rate and, as a consequence, low final butanol concentrations achieved after fermentation (Ingram, 1986).

Different methods have been used to obtain butanol-tolerant strains of solventogenic clostridia, including targeted modifications, e.g., overexpression of genes encoding heat-shock proteins or modification of fatty acids synthesis (Tomas et al., 2003; Zhao et al., 2003; Mann et al., 2012; Liao et al., 2017), serial transfer and adaptation (Lin and Blaschek, 1983; Baer et al., 1987; Soucaille et al., 1987; Xue et al., 2012; Liu et al., 2013; Yang and Zhao, 2013) or random mutagenesis (Hermann et al., 1985; Matta-el-Ammouri et al., 1986; Annous and Blaschek, 1991; Jain et al., 1994; Mao et al., 2010; Kong et al., 2016; Tanaka et al., 2017). Use of these methods resulted in improved survival in the presence of butanol at a concentration of 10–12 g/L for the wild-type strain (WTS) to 16–18 g/L for mutant strains (Vasylkivska and Patakova, 2020), sometimes up to 23 g/L, as in the case of mutant strain *C. beijerinckii* BA101 (Qureshi and Blaschek, 2001). Surprisingly, random and targeted mutagenesis have apparently produced very similar improvements in butanol tolerance, although this probably reflects our incomplete understanding of butanol tolerance mechanisms and their regulation (Patakova et al., 2018). In most cases, obtained mutant strains in addition to higher tolerance exhibited higher butanol production, usually an improvement from approximately 9–12 g/L for WTS to 13–16 g/L for mutant strains, sometimes up to 19–21 g/L for selected mutants (Vasylkivska and Patakova, 2020). However, some authors have reported increased tolerance, but not increased butanol production for obtained mutants, both for random (Baer et al., 1987; Gallardo et al., 2017; Máté de Gérando et al., 2018) and targeted (Zhao et al., 2003; Alsaker et al., 2004; Mann et al., 2012; Jones et al., 2016) mutagenesis. Thus, although it is commonly accepted that increased butanol tolerance leads to higher production, such data suggest strain-specific dependence between butanol tolerance and production or even the absence of any direct connection.

Efflux is one of the innate mechanisms of stress response in bacteria and it is based on active transport of the substances from the cell. This mechanism is mostly associated with antibiotic resistance, however, it has been shown that it also takes part in the butanol stress response of *Pseudomonas putida* and *Escherichia coli* (Fisher et al., 2014; Bui et al., 2015; Basler et al., 2018; Zhang et al., 2018). It was suggested that efflux can be very effective when cells are dealing with high solvent concentrations (Segura et al., 2012), and enhancement of efflux pump activity could possibly shift metabolic flux, resulting in higher production (Mukhopadhyay, 2015).

Efflux, particularly butanol efflux, is rarely studied in solventogenic clostridia (Vasylkivska and Patakova, 2020). Up-regulation of ATP-binding cassette transporters (Schwarz et al., 2012) and putative efflux pump regulators (Sedlar et al., 2019) observed under cultivation with butanol stress are the only evidence of innate butanol efflux in the group. Recently, a butanol efflux pump from *P. putida* S12 was expressed in *Clostridium saccharoperbutylacetonicum*, resulting in improved butanol tolerance (Jiménez-Bonilla et al., 2020) and demonstrating that butanol efflux studies in solventogenic *Clostridium* have potential for the development of butanol-tolerant production strains. As no native butanol efflux pumps have yet been reported for solventogenic clostridia, targeted engineering cannot be used for the study. Nevertheless, it was shown that efflux enhancement can be achieved even by a point mutation in the efflux pump gene sequence (Bohnert et al., 2007) or in the efflux pump promoter or regulator. To generate such mutations, ethyl methanesulfonate (EMS) or ethidium bromide (EB) can be used. EMS can alkylate guanine bases in DNA, resulting in unidirectional random transition mutations between GC and AT base pairs. Such a type of mutation can lead to an amino acid change and even loss of protein function. EMS was previously successfully used by Jain et al. (1994) to obtain a high butanol producing stable asporogenic mutant, *C. beijerinckii* ATCC 55025, formerly *C. acetobutylicum* ATCC 55025 (Jain et al., 1994). EB is a known substrate of different efflux pumps in both Gram-positive (Patel et al., 2010) and Gram-negative bacteria (Paixao et al., 2009) and also a chemical mutagen (Ohta et al., 2001). Use of EB may enhance efflux in the strain, resulting in improved butanol tolerance. Therefore, for this study, we have chosen three approaches to develop butanol-tolerant mutants of solventogenic *C. beijerinckii* NRRL B-598:

(1) Random chemical mutagenesis using EMS with selection on butanol (EMS + butanol mutants).
(2) Random chemical mutagenesis using EMS with selection on EB (EMS + EB mutants).
(3) Random chemical mutagenesis using EB as a mutagenic agent, where strains were selected directly on agar plates containing EB (EB mutants).

Phenotypic behavior of selected mutant strains was observed by testing tolerance to different substances such as butanol, EB, ethanol and antibiotics, and metabolite production. The complete genomes of mutant strains that exhibited improved butanol tolerance were sequenced to understand their changes in

phenotype and to contribute to knowledge about mutations that lead to increased butanol tolerance. To the best of our knowledge, the genomic sequence of only a few butanol-tolerant strains obtained by random mutagenesis are available.

MATERIALS AND METHODS

Bacterial Strain

Clostridium beijerinckii NRRL B-598 (WTS), former *Clostridium pasteurianum* NRRL B-598 (Sedlar et al., 2017), obtained from the Agricultural Research Service Culture Collection (1815 N. University Street, Peoria, IL 61604) was used in this study. The culture was maintained in the form of a spore suspension [containing about $2.2{\cdot}10^8$ spores/ml, determined by method described by Branska et al. (2018)] in sterile distilled water at 4°C. For each cultivation experiment, 450 μl of spore preserve was used for 100 ml of cultivation medium.

Mutagenesis and Strain Selection

Mutagenesis

Mutant strains described in this work were obtained using three different approaches of random chemical mutagenesis (**Figure 1**). Firstly, ethyl methanesulfonate (EMS) was used as a mutagenic agent in combination with selection in butanol (EMS + butanol mutants), secondly, EMS was used for mutagenesis but selection was carried out in ethidium bromide (EB) (EMS + EB mutants) and, finally, EB was used as a mutagenic agent and strains were directly selected on agar plates containing EB without exposition to EMS (EB mutants).

For the first two approaches, when EMS was used as a mutagenic agent, a spore suspension of *C. beijerinckii* NRRL B-598 was heated to 80°C for 2 min, vortexed and transferred to Erlenmeyer flasks with TYA medium (Vasylkivska et al., 2019) containing 20 g/L of glucose (analytical reagent grade, PENTA, Chrudim, Czechia). The strain was cultivated in a Concept 400 anaerobic chamber (Ruskinn Technology) under a stable N_2 atmosphere at 37°C (**Figure 1**, step 1). After 24 h of cultivation, 2 ml × 2 ml of cell suspension were transferred into sterile Eppendorf tubes, centrifuged and 0.5 ml of fresh sterile TYA medium were added to the cell pellet. Eppendorf tubes were vortexed and 20 μl/ml of EMS (pure, Sigma-Aldrich) were added (**Figure 1**, step 2). The exposition time was 40 min, during which Eppendorf tubes were placed in the anaerobic chamber. The cell suspension with mutagen was further centrifuged and washed twice with sterile physiological solution. The washed cell suspension was transferred to Petri dishes (250 μl of suspension on each plate) containing HPLC-grade butanol (Sigma-Aldrich) (**Figure 1**, step A3) or EB (for molecular biology, 10 mg/mL in H_2O, Sigma-Aldrich) (**Figure 1**, step B3) for selection. Tolerance of WTS to butanol and EB was tested prior to mutagenesis procedure (details are described in section "Tolerance Testing") and twice as high a concentration of butanol (for EMS + butanol mutants) or twice as high a concentration of EB (for EMS + EB mutants) than WTS was able to tolerate were used for mutants selection on Petri dishes (**Figure 1**, step 3). Inoculated petri dishes were cultivated for 48 h at 37°C in the anaerobic chamber. Colonies obtained were transferred to test tubes containing 10 ml of TYA medium with 20 g/L of glucose, and cultivated overnight in the anaerobic chamber (**Figure 1**, step 4). The cell suspension was cryopreserved in 30% (v/v) glycerol (analytical reagent grade, PENTA, Chrudim, Czechia) solution below −80°C.

EB mutant strains, prepared by direct cultivation on agar plates containing EB without exposition to EMS, were obtained as follows: the spore suspension of *C. beijerinckii* NRRL B-598 was heated to 80°C for 2 min (**Figure 1**, step C1), vortexed and 50 μl of the spore suspension were transferred onto Petri dishes containing either 0.5 mg/L or 2 mg/L of EB (**Figure 1**, step C2). Agar plates were cultivated in the anaerobic chamber for 24 h, chosen colonies (**Figure 1**, step C3) were cultivated in TYA medium and the cell culture was cryopreserved (**Figure 1**, step 4).

Mutant strains obtained by all methods were tested for butanol tolerance (details are described in section "Tolerance Testing) (**Figure 1**, step 5). Selected mutant strains with improved butanol tolerance compared to the wild-type strain (WTS) were cultivated in TYA medium (EB mutants) or on TYA agar plates (EMS + butanol and EMS + EB mutants) until sporulation was observed (Olympus BX51 microscope); spore preserves were prepared (**Figure 1**, step 6). Inocula were prepared from the spore preserves and mutant strains were tested one more time for butanol tolerance (**Figure 1**, step 7). After this step, the selected strains were further used in the experiments described in this article.

Tolerance Testing

Inocula of the wild-type strain and of the mutant strains (except for the first butanol tolerance testing shown as step 5 in **Figure 1**) were prepared from spore suspensions, and inocula of the mutant strains for the first butanol tolerance testing were prepared from the cryopreserves. Prior to inoculation, the spore suspensions of strains were heated to 80°C for 2 min and vortexed (heat-shock); cryopreserves were thawed at room temperature and vortexed. TYA medium containing 20 g/L of glucose was used for the preparation of inocula and inoculated test tubes were transferred to the anaerobic chamber and cultivated at 37°C overnight.

Tolerance to various substances was tested in microtiter plates containing 120 μl of TYA medium and 10 μl of cell culture. Medium for the experiment additionally contained 0.02 g/L of acid base indicator, bromocresol purple (suitable for indicator, dye content 90%, Sigma-Aldrich), and each substance in different concentrations. Eight substances were tested: two metabolites [butanol in the range of 0 to 30 g/L and ethanol (analytical reagent grade, PENTA, Chrudim, Czechia) in the range of 0 to 65 g/L], efflux pump inducer ethidium bromide EB in the range of 0–6 mg/L and five antibiotics [chloramphenicol (≥98% (HPLC), Sigma-Aldrich] in the range of 0 to 150 mg/L, tetracycline [98.0–102.0% (HPLC), Sigma-Aldrich] in the range of 0–30 mg/L, streptomycin in a form of streptomycin sulfate [>95.0% (TN), Tokyo Chemical Industry] in the range of 0 to 35 mg/L, ampicillin in a form of sodium salt (pure Ph. EUr., AppliChem) in the range of 0–100 mg/L and erythromycin [(for microbiological assay, Sigma-Aldrich) in the range of 0–100 mg/L]. Inoculated microtiter plates were cultivated in the anaerobic chamber at 37°C for 24 h. Results of the

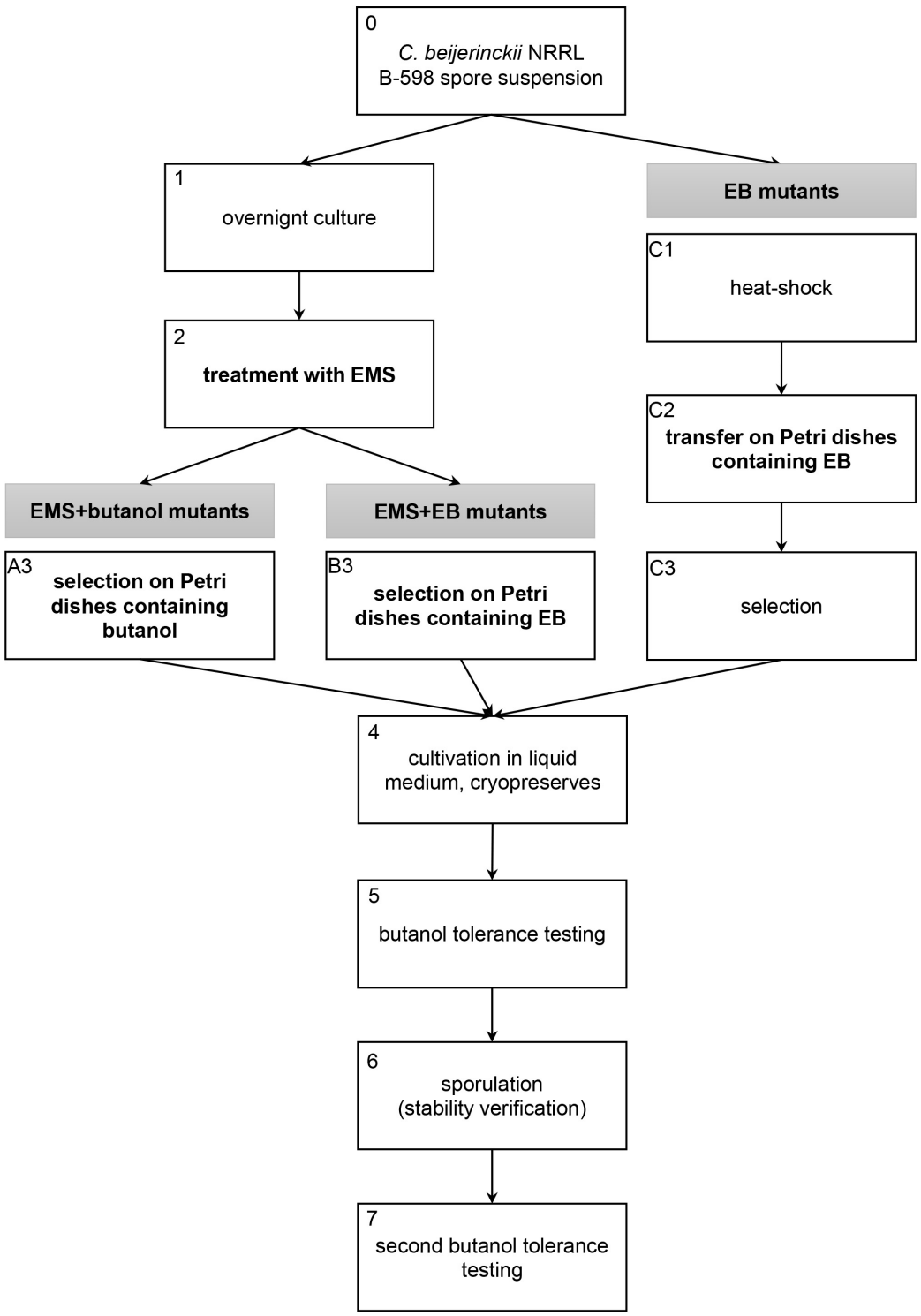

FIGURE 1 | Scheme of three random chemical mutagenesis approaches that were used to obtain mutant strains of *C. beijerinckii* NRRL B-598 with increased butanol tolerance. EMS, ethyl methanesulfonate; EB, ethidium bromide.

testing were evaluated visually as a change in color of the medium, from purple to yellow due to acid production and medium pH shift indicating growth of the strain. For each strain and each substrate, butanol tolerance was tested in at least three repetitions and TYA medium without additions was used as a control.

Cultivation Experiments

Cultivation in Erlenmeyer Flasks

For the determination of glucose consumption rate and metabolite production, WTS and mutant strains were cultivated in triplicates in non-shaken Erlenmeyer flasks. TYA medium containing 40 g/L of glucose was used for both inoculum preparation and cultivation experiment itself. The inoculum was prepared from the spore preserves after heat-shock (as described in section "Tolerance Testing") and cultivated in an anaerobic chamber under a stable N_2 atmosphere at 37°C overnight. For the cultivation experiment, flasks were inoculated with 10% (v/v) cell culture and cultivated in the anaerobic chamber for 72 h. At the end of cultivation, samples were taken for pH measurement and subsequent HPLC analysis (details of the analysis are described in section "Analytical Methods").

Cultivation in triplicates in non-shaken Erlenmeyer flasks with pH control was performed the same way as described above, but TYA medium after sterilization prior to inoculation was supplemented with $CaCO_3$ so that concentration 10 g/L of $CaCO_3$ was achieved.

Cultivation in Bioreactors

According to the result of experiment described in Section "Cultivation in Erlenmeyer Flasks," one selected mutant strain was chosen for batch cultivation alongside with WTS in triplicates in parallel Multiforce 1L bioreactors (Infors HT).

TYA medium for the inoculum was prepared with glucose concentrations of 20 g/L and for cultivation in bioreactors with concentrations of 40 g/L. The inoculum was prepared from the spore preserves as described in Section "Cultivation in Erlenmeyer Flasks.". Prior to inoculation of bioreactors, oxygen was exchanged with N_2 and the pH of the medium was adjusted to 6.4. Bioreactors were inoculated with 10% (v/v) cell culture. Cultivation temperature was 37°C and agitation speed was set to 3.3 s^{-1} throughout the cultivation, the pH was not controlled. During the cultivation, samples were taken for OD measurements and subsequent HPLC analysis (details of the analysis are described in section "Analytical Methods").

Analytical Methods

Culture growth was measured as the optical density OD of the culture broth at 600 nm (Varian Cary 50 UV-Vis spectrophotometer, Agilent) against TYA medium as a blank (Vasylkivska et al., 2019).

The concentrations of lactic acid (retention time t_R 6.9 min), acetic acid (t_R 8.1 min), ethanol (t_R 11.7 min), acetone (t_R 12.3 min), butyric acid (t_R 13.5 min), butanol (t_R 24.9 min), and glucose (t_R 4.8 min) were measured using HPLC with refractive index detection (Agilent Series 1200 HPLC). A column with stationary phase of Polymer IEX H from 8 μm (Watrex) was used for the separation. Samples of culture broth were centrifuged and the supernatants were microfiltered. The sample injection volume was 20 μl, the column temperature was 60°C, and 5 mM H_2SO_4 was used as the mobile phase with a flow-rate of 1 ml/min. The concentration of substances was determined from calibration curves (Sedlar et al., 2018).

DNA Isolation and Genome Sequencing

DNA was isolated from exponentially growing cultures prepared by inoculation of TYA medium with heat-shocked spores (as described above) using commercially available isolation kit DNeasy UltraClean Microbial Kit (Qiagen, Hilden, Germany), following recommended instructions. Library construction and sequencing of the sample was performed by CEITEC Genomics core facility (Brno, Czechia) on Illumina NextSeq 500, pair-end, 150 bp.

Bioinformatics Analysis

The quality assessment of particular steps of data processing were done using FastQC in combination with MultiQC to summarize the reports across all samples (Ewels et al., 2016). Adapter and quality trimming and filtering of singletons was performed with Trimmomatic v0.36 (Bolger et al., 2014). Remaining high quality paired reads were mapped to the genome sequence of the wild type strain with BWA-mem v0.7.15 (Li and Durbin, 2009). The latest genome assembly of the *C. beijerinckii* NRRL B-598 CP011966.3 (Sedlar et al., 2019) was used as a reference. Resulting SAM (Sequence Read Alignment/Map) files were indexed and transformed into more compact BAM (Binary Read Alignment/Map) format using SAMtools v1.9 (Li et al., 2009). Sequences in BAM files were cleaned, sorted, deduplicated and files were indexed with Picard Tools v2.21.6. Single nucleotide variants in genome sequences between wild type strain and particular mutant strains were called with GATK v4.1.4.1 (McKenna et al., 2010). Detected variants were further filtered in order to reduce the number of false positives. For this purpose, WTS resequencing data gathered within the same sequencing run, were used. All variants that were called simultaneously in the WTS and mutant were filtered out. Moreover, we used coverage of false detections in the WTS to set a threshold for filtering, and only variants covered by more than 25.9% of an average coverage of a strain were used. This threshold corresponded to the highest coverage of falsely detected mutations in the WTS. Moreover, not all variants were detected in the whole population. We again set a threshold using analysis of the WTS. Only variants that were called in at least 30.8% of the population were counted. Furthermore, we detected structural variations to the genome sequences, including copy number variations (CNV) with Pilon v 1.22 (Walker et al., 2014). All these analyses were performed with R/Bioconductor using functions from the genomeIntervals v1.42 (Gagneur et al., 2020), Biostrings v2.54 (Pagès et al., 2020), vcfR v1.11 (Knaus and Grünwald, 2017), and ggplot2 (Wickham, 2009) packages.

RESULTS

Mutant Strains, Tolerance Testing to Butanol, Ethanol and Tolerance to Known Efflux Pump Substrates

As a first step, WTS *C. beijerinckii* NRRL B-598 was tested for its tolerance to butanol, ethanol and EB. Testing revealed

that the strain was able to grow in medium containing no more than 11 ± 1 g/L of butanol, 38.5 ± 2.1 g/L of ethanol or 1.75 ± 0.40 mg/L of EB. EMS + butanol and EMS + EB mutants were, therefore, picked (**Figure 1**, step 3) from agar plates containing approximately twice as high a concentration of butanol or EB, which were 20 g/L and 4 g/L, respectively, prior to both butanol tolerance testing in microtiter plates (**Figure 1, steps 5** and **7**).

Number of strains being reduced through screening process is shown in **Table 1**. For mutagenesis using EMS as mutagenic agent, total of 45 colonies were selected during step A3 (**Figure 1**) and 45 during B3 (**Figure 1**). The first butanol tolerance testing (**Figure 1**, step 5) revealed that 32 strains exhibited increased butanol tolerance compared to WTS. To ensure that increased butanol tolerance was a result of mutation and not adaptation, these 32 strains were cultivated on TYA agar plates until sporulation was observed (**Figure 1**, step 6) and then spores were germinated and the strains were once again tested for butanol tolerance (**Figure 1**, step 7). After the second round of butanol tolerance testing, six strains exhibiting increased butanol tolerance were selected for further experiments: EMS + butanol mutants B33 and B44 and EMS + EB mutants E15, E28, E32, and E33 (**Table 1**).

Using another approach, mutagenesis of WTS was carried out on agar plates containing EB with no exposition to EMS (EB mutants, **Figure 1** steps C1–C3). 24 colonies (**Table 1**) were picked during C3 step (**Figure 1**). After the subsequent butanol tolerance test in microtiter plates (**Figure 1**, step 5), three EB mutants strains exhibited an increase in tolerance, strains A, B, and C. These strains were also cultivated until sporulation was observed (**Figure 1**, step 6) and then the spores were germinated and the strains were again tested for butanol tolerance (**Figure 1**, step 7). This confirmed that the acquired increase in tolerance was a stable phenotype.

All of mutant strains showed a significant increase in butanol and ethanol tolerance compared to WTS ($p < 0.05$, two-sample *t*-test) and were able to grow in a medium containing up to 25.0 g/L of butanol or up to 55.0 g/L of ethanol (**Figure 2**).

As the goal of the study was to increase the efflux capacity of mutant strains, the tolerance of mutant strains and the WTS to different substrates of efflux pumps, i.e., EB and antibiotics, was also tested. Mutants acquired increased EB (up to 5 mg/L) tolerance, see **Figure 3**.

Wild-type strain was tolerant to tetracycline, chloramphenicol and streptomycin at concentrations of 3.0 ± 0.0, 19.0 ± 1.4, and 20.0 ± 0.0 μg/ml, respectively, but was sensitive to ampicillin and erythromycin. The sensitivity toward ampicillin and erythromycin remained unchanged in all mutant strains, but tolerance to tetracycline and chloramphenicol was modified and, in some cases, increased. Surprisingly, tolerance to streptomycin decreased in all cases and strains B33 (EMS + butanol mutant), E15, E32, and E33 (EMS + EB mutants) exhibited complete growth inhibition in the presence of this antibiotic, see **Figure 4**.

Metabolites Production by WTS and Mutant Strains

Production of solvents and acids was tested in flasks containing TYA medium. Mutant strains A and C exhibited similar fermentation profiles as WTS and produced butanol in similar concentrations under standard cultivation conditions (**Supplementary Table 1**). Other mutant strains, B (EB mutant), B33, B44 (EMS + butanol mutants), E15, E28, E32, and E33 (EMS + EB mutants), probably developed the so-called "acid crash" phenotype and their respective fermentation outputs achieved higher concentrations of butyric, acetic or lactic acids compared to WTS.

Inspired by the study of the mutant strain *C. beijerinckii* BA105, which at first was seem to only exhibit the acid crash phenotype but it was later revealed that significantly higher butanol production can be achieved by the strain under pH regulation (Seo et al., 2017), we tested TYA medium with the addition of 10 g/L $CaCO_3$ for partial pH control (**Table 2**). WTS and mutant strains A and C (EB mutants) produced 11–16% higher concentrations of butanol and consumed the total amount of glucose present in the medium. Furthermore, mutant strain B (EB mutant) was able to produce butanol at a concentration of 4.7 ± 0.5 g/L, which is significantly ($p < 0.05$, two-sample *t*-test), almost 12 times, higher than that achieved in the medium without supplementation. However, EMS + butanol and EMS + EB stayed in the acidogenic phase of fermentation and the only difference compared to previous experiments was a significantly ($p < 0.05$, two-sample *t*-test) higher concentration of butyric acid at the end of fermentation.

The behavior of the mutant strain with the overall highest butanol production, EB mutant C, was compared with WTS

TABLE 1 | Number of mutant strains being reduced through screening process[1].

Mutagenesis method	Colonies picked after mutagenesis*	Strains exhibiting increased butanol tolerance (after 1st butanol testing)**	Strains exhibiting increased butanol tolerance (after 2d butanol testing)***	Strains selected for further experiments
EB	24	3	3	A, B and C
EMS + butanol	45	13	2	B33 and B44
EMS + EB	45	19	4	E15, E28, E32 and E33

[1] **Steps A3, B3, and C3 from **Figure 1**; **step 5 from **Figure 1**; ***step 7 from **Figure 1**.*
EB – strains obtained by random chemical mutagenesis using EB as a mutagenic agent, when strains were selected directly on agar plates containing EB; EMS + butanol – strains obtained by random chemical mutagenesis using EMS with selection on butanol; EMS + EB – strains obtained by random chemical mutagenesis using EMS with selection on EB.

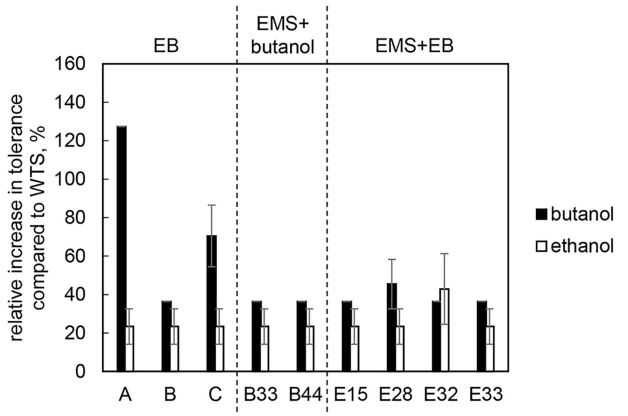

FIGURE 2 | Relative increase in butanol and ethanol tolerance of mutant strains compared to *C. beijerinckii* NRRL B-598 (WTS). Tolerance levels are expressed as the maximum concentration of butanol or ethanol in TYA medium at which growth of the strains was still detectable. The original tolerance of WTS to butanol and ethanol was 11 ± 1 g/L and 38.5 ± 2.1 g/L, respectively. EB – strains obtained by random chemical mutagenesis using EB as a mutagenic agent, when strains were selected directly on the agar plates containing EB; EMS + butanol – strains obtained by random chemical mutagenesis using EMS with selection on butanol; EMS + EB – strains obtained by random chemical mutagenesis using EMS with selection on EB.

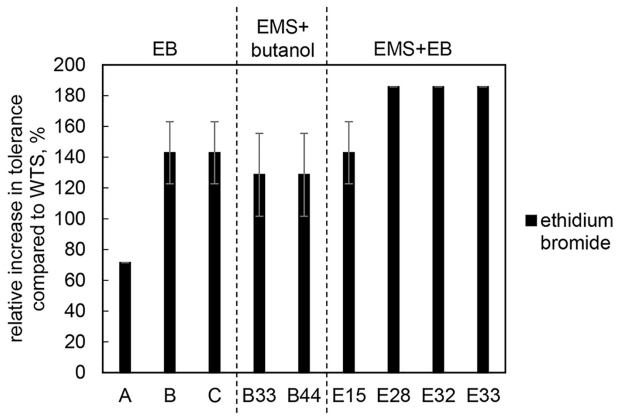

FIGURE 3 | Relative increase in tolerance to EB of mutant strains compared to *C. beijerinckii* NRRL B-598 (WTS). Tolerance levels are expressed as the maximum concentration of substances in TYA medium at which growth of the strains was still detectable. Original tolerance of WTS to EB was 1.75 ± 0.4 mg/L. EB – strains obtained by random chemical mutagenesis using EB as a mutagenic agent, when strains were selected directly on agar plates containing EB; EMS + butanol - strains obtained by random chemical mutagenesis using EMS with selection on butanol; EMS + EB – strains obtained by random chemical mutagenesis using EMS with selection on EB.

in parallel batch bioreactor fermentation (**Supplementary Figure 1**). At first sight, the fermentation profiles, growth curves and glucose consumption curves looked very similar, however, a thorough analysis of fermentation data revealed differences in the fermentation dynamics. The pH and growth curves show that the mutant strain C switched to solventogenesis earlier than the WTS and grew faster during the exponential phase. This was also confirmed by calculation of the specific growth rate (μ) for the exponential phase of growth (first 5 h of cultivation as no lag phase was observed), which was 0.32 ± 0.03 h^{-1} for the WTS and 0.48 ± 0.01 h^{-1} for the mutant strain C. Comparison of fermentation parameters for the first 24 h of cultivation and total fermentation time (48 h) is given in **Supplementary Table 2**. Although the strains reached the same butanol yield (**Supplementary Table 2**), productivity for mutant C was somewhat higher when calculated for the first 24 h of fermentation, which is in accordance with its higher glucose consumption rate during this period (**Supplementary Table 2**).

Genomic Analysis of Mutant Strains

To identify the causes of phenotypic changes in mutant strains, their genomes were sequenced and compared with the WTS genome. After quality trimming and deduplication, 2.4–4.5 million high quality (average Phred score $Q \approx 35$) paired sequences mapped to the reference genome suggesting coverage from 115 × to 221 × per mutant strain (see **Supplementary Table 3**). Sequencing of mutant strains revealed that most of the mutations were single-nucleotide polymorphisms (SNP). In unfiltered data, we detected from 21 to 51 SNPs or short indels per mutant strain and 18 false positive detections in the WTS (see **Supplementary Files 4**). Nevertheless, after filtering (see section "Materials and Methods"), the number of SNPs was reduced to the range from one to 17 per mutant strain (see **Table 3**). In total, 21 non-synonymous mutations were captured, including a mutation disrupting an open reading frame. SNPs in six genes were observed in at least two mutant strains (**Figure 4**). SNPs in X276_13415 encoding a putative S-layer family protein was detected in five mutant strains, SNPs in X276_14460 encoding cytochrome b5 was observed in four strains. EB mutants strain A, B and C included SNPs in the same genes, X276_22865 and X276_03000 encoding a carbohydrate ABC transporter permease and an AAA family ATPase, respectively (**Figure 4** and **Table 3**), and no mutations were observed in these gene when EMS was used as the mutagen.

In addition to SNPs, we detected several longer genome changes, including copy number variations (CNVs) (**Tables 4**, **5**). No copy number variations were detected for mutant strain E32. CNVs were detected for similar positions in strains A, B. C, B44, E28, and E33 (**Table 5**).

DISCUSSION

Using three different approaches of random chemical mutagenesis, we were able to obtain nine mutant strains of *C. beijerinckii* NRRL B-598 exhibiting from 36 to 127% increases in butanol tolerance (**Figure 2**). Similar increases in tolerance have been described for other solventogenic clostridia; in fact, the most well-studied and best-performing mutant strain, *C. beijerinckii* BA101, was likewise obtained by random chemical mutagenesis (Annous and Blaschek, 1991). *C. beijerinckii* BA101, an offspring of *C. beijerinckii* NCIMB 8052, exhibited around a 110% increase in butanol tolerance (Qureshi and Blaschek, 2001). Similarly, the asporogenic mutant *C. beijerinckii* ATCC

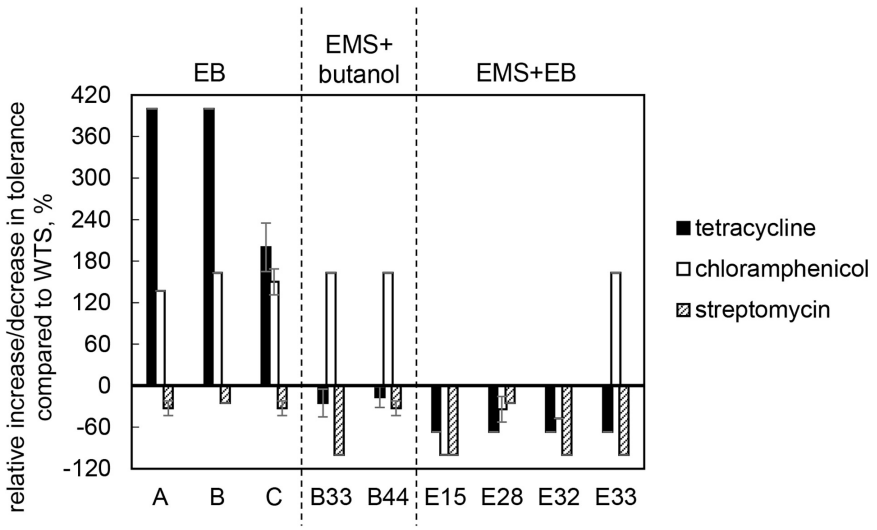

FIGURE 4 | Relative increase/decrease in tolerance to antibiotics tetracycline, chloramphenicol and streptomycin in mutant strains compared to *C. beijerinckii* NRRL B-598 (WTS). Tolerance levels are expressed as the maximum concentration of substances in TYA medium at which growth of the strains was still detectable. Tolerance of WTS was 3.0 ± 0.0, 19.0 ± 1.4, and 20.0 ± 0.0 μg/ml of tetracycline, chloramphenicol and streptomycin, respectively. EB – strains obtained by random chemical mutagenesis using EB as a mutagenic agent, when strains were selected directly on agar plates containing EB; EMS + butanol – strains obtained by random chemical mutagenesis using EMS with selection on butanol; EMS + EB – strains obtained by random chemical mutagenesis using EMS with the selection on EB.

TABLE 2 | Concentrations of glucose, acids and solvents and pH reached by *C. beijerinckii* NRRL B-598 (WTS) and its mutant strains in TYA medium containing 10 g/L of $CaCO_3$ after 72 h cultivation[1].

Mutagenesis method	Strain	Consumed glucose, g/L	Lactic acid, g/L	Acetic acid, g/L	Ethanol, g/L	Acetone, g/L	Butyric acid, g/L	Butanol, g/L	Final pH
–	WTS	38.4 ± 0.0	0.3 ± 0.0	3.0 ± 0.2	0.4 ± 0.0	1.3 ± 0.1	1.8 ± 0.1	**8.1 ± 0.2**	6.2 ± 0.0
EB	A	38.4 ± 0.0	0.2 ± 0.0	2.5 ± 0.1	0.3 ± 0.0	1.6 ± 0.1	1.7 ± 0.1	**8.1 ± 0.2**	6.4 ± 0.1
EB	B	34.4 ± 1.6	0.2 ± 0.0	3.3 ± 0.5	0.3 ± 0.1	0.1 ± 0.1	9.3 ± 0.7	**4.7 ± 0.5**	5.7 ± 0.0
EB	C	38.4 ± 0.0	0.2 ± 0.0	2.6 ± 0.1	0.4 ± 0.1	1.6 ± 0.1	1.7 ± 0.2	**8.1 ± 0.1**	6.4 ± 0.0
EMS + butanol	B33	26.1 ± 2.0	0.1 ± 0.1	1.5 ± 0.3	0.0 ± 0.0	0.0 ± 0.0	14.2 ± 0.8	**0.0 ± 0.0**	5.6 ± 0.0
EMS + butanol	B44	22.9 ± 0.5	0.1 ± 0.1	1.2 ± 0.0	0.0 ± 0.0	0.0 ± 0.0	12.7 ± 0.3	**0.0 ± 0.1**	5.7 ± 0.0
EMS + EB	E15	26.5 ± 1.1	0.2 ± 0.0	1.0 ± 0.2	0.0 ± 0.0	0.0 ± 0.0	15.2 ± 0.6	**0.0 ± 0.0**	5.7 ± 0.0
EMS + EB	E28	22.4 ± 0.6	0.1 ± 0.1	1.3 ± 0.1	0.0 ± 0.0	0.0 ± 0.0	12.8 ± 0.2	**0.1 ± 0.0**	5.7 ± 0.0
EMS + EB	E32	24.5 ± 1.0	0.2 ± 0.1	1.9 ± 0.2	0.0 ± 0.0	0.0 ± 0.0	13.4 ± 0.4	**0.0 ± 0.0**	5.7 ± 0.0
EMS + EB	E33	26.7 ± 0.8	0.2 ± 0.0	1.7 ± 0.1	0.0 ± 0.0	0.0 ± 0.0	15.0 ± 0.4	**0.0 ± 0.0**	5.7 ± 0.0

[1] *EB, strains obtained by random chemical mutagenesis using EB as a mutagenic agent, when strains were selected directly on agar plates containing EB; EMS + butanol, strains obtained by random chemical mutagenesis using EMS with selection on butanol; EMS + EB, strains obtained by random chemical mutagenesis using EMS with selection on EB. Bold values are the most important outcomes of the experiment.*

55025, an offspring of *C. acetobutylicum* ATCC 4259, was able to tolerate about 11.4 g/L of butanol while its WTS only 5 g/L (Jain et al., 1994). Interestingly, two of our nine mutant strains of *C. beijerinckii* NRRL B-598 with the highest increase in butanol tolerance were obtained by mutagenesis on agar plates containing EB (EB mutants) (**Figure 2**), a method that has not previously been used for this purpose in solventogenic *Clostridium*.

Despite increased butanol tolerance, no mutant strain exhibited an increase in butanol production compared with WTS (**Supplementary Table 1** and **Table 2**), which is a divergence from well-known mutant strains obtained in a similar way. For example, *C. beijerinckii* BA101 was able to produce around 20 g/L of butanol during batch cultivation (an increase of over 100%) (Annous and Blaschek, 1991; Chen and Blaschek, 1999) and *C. beijerinckii* ATCC 55025 displayed an increase in butanol concentration between 22 and 38% (Jain et al., 1994). However, it has previously been shown in multiple studies, both for random (Baer et al., 1987; Gallardo et al., 2017; Máté de Gérando et al., 2018) and targeted (Zhao et al., 2003; Alsaker et al., 2004; Mann et al., 2012; Jones et al., 2016) mutagenesis, that increased butanol tolerance does not always result in improved butanol production.

EMS + butanol and EMS + EB mutant strains exhibited the acid crash phenotype under standard cultivation conditions and under pH regulation via $CaCO_3$ supplementation (**Supplementary Table 1** and **Table 2**), producing high concentrations of butyric acid. It was shown for the WTS

TABLE 3 | List of single-nucleotide polymorphisms that occurred in mutant strains of *C. beijerinckii* NRRL B-598 exhibiting high butanol tolerance[1].

	Position	Ref	Alt	Locus	Product	Start	End	Strand	Feature	Aa_ref	Aa_alt
Mutant strain A*											
1	863781	T	G	X276_22865	Carbohydrate ABC transporter permease	863698	864525	+		I	M
2	1661343	C	T	X276_19395	Peptidase S8 and S53 subtilisin kexin sedolisin	1661151	1662989	+		L	F
3	2775912	T	C	X276_14460	Cytochrome b5	2775169	2775996	+		T	T
4	3007463	C	A	X276_13415	S-layer family protein	3005247	3009269	+		V	V
5	3008654	T	G	X276_13415	S-layer family protein	3005247	3009269	+		T	T
6	5443138	C	T	X276_03000	AAA family ATPase	5441786	5444533	–		E	K
Mutant strain B*											
1	863781	T	G	X276_22865	Carbohydrate ABC transporter permease	863698	864525	+		I	M
2	1190011	G	T						Non-coding		
3	2052101	G	T	X276_17580	Peptidase S8	2051180	2052916	+		G	C
4	3394324	C	T	X276_11885	16S ribosomal RNA	3393103	3394616	–		T	T
5	4087693	C	A						Non-coding		
6	5173544	A	AT	X276_04045	Chemotaxis protein CheC	5173215	5173817	–			
7	5443138	C	T	X276_03000	AAA family ATPase	5441786	5444533	–		E	K
Mutant strain C*											
1	863781	T	G	X276_22865	Carbohydrate ABC transporter permease	863698	864525	+		I	M
2	968295	C	T	X276_22430	Peptidase S8	967488	969206	+		H	Y
3	2775238	G	T	X276_14460	Cytochrome b5	2775169	2775996	+		E	*
4	2919727	T	A	X276_13825	Hypothetical protein	2919158	2919820	+		S	S
5	3004110	C	T	X276_13420	Collagen-like protein	3003304	3004570	+	Pseudogene	G	G
6	3025567	C	A	X276_13335	Collagen-like protein	3025298	3027013	+		G	G
7	4087693	C	A						Non-coding		
8	5443138	C	T	X276_03000	AAA family ATPase	5441786	5444533	–		E	K
9	5649791	C	A						Non-coding		
Mutant strain B33**											
1	81253	G	A	X276_26470	Prolipoprotein diacylglyceryl transferase	81069	81839	+		G	E
2	1115679	G	C						Non-coding		
3	1457462	G	A						Non-coding		
4	1913236	G	A	X276_18195	ABC transporter substrate-binding protein	1912234	1913397	+		D	N
5	3567763	C	T	X276_11100	Methyl-accepting chemotaxis protein	3566625	3568346	–		S	N
6	4087693	C	A						Non-coding		
7	4257246	C	T	X276_07910	DNA polymerase III subunit epsilon	4256489	4257421	–		S	N
8	4560040	C	T	X276_06635	Pyruvate, phosphate dikinase	4560023	4562566	–		V	I
9	5150062	T	A	X276_27350	Hypothetical protein	5146861	5150820	–		T	T
10	5150524	A	T	X276_27350	Hypothetical protein	5146861	5150820	–		S	S
11	5150526	A	T	X276_27350	Hypothetical protein	5146861	5150820	–		S	T
12	5150530	C	T	X276_27350	Hypothetical protein	5146861	5150820	–		V	V
13	5150532	C	T	X276_27350	Hypothetical protein	5146861	5150820	–		V	M
14	5150533	A	T	X276_27350	Hypothetical protein	5146861	5150820	–		I	I
15	5150538	C	T	X276_27350	Hypothetical protein	5146861	5150820	–		V	I
16	5150545	T	C	X276_27350	Hypothetical protein	5146861	5150820	–		G	G
17	5150568	T	C	X276_27350	Hypothetical protein	5146861	5150820	–		I	V

(Continued)

TABLE 3 | Continued

	Position	Ref	Alt	Locus	Product	Start	End	Strand	Feature	Aa_ref	Aa_alt
Mutant strain B44**											
1	3006134	C	A	X276_13415	S-layer family protein	3005247	3009269	+		T	T
2	3007658	C	A	X276_13415	S-layer family protein	3005247	3009269	+		G	G
3	4087693	C	A						Non-coding		
Mutant strain E15***											
1	654069	C	T	X276_23670	Nitrogenase iron protein	653549	654403	+		A	V
2	685966	C	T	X276_23545	tRNA 2-thiocytidine biosynthesis protein TtcA	685570	686436	+		P	S
3	724396	GT	G						Non-coding		
4	1809500	CA	C	X276_18715	YggS family pyridoxal phosphate-dependent enzyme	1809001	1809681	+			
5	2376845	G	A	X276_16220	MFS transporter	2376293	2377702	–		Y	Y
6	2453563	G	A	X276_15915	Sigma-54-dependent Fis family transcriptional regulator	2451932	2453896	+		E	E
7	2468045	G	A	X276_15855	HlyC/CorC family transporter	2467109	2468398	+		A	T
8	2482557	C	T	X276_15775	Bifunctional 4-hydroxy-2-oxoglutarate aldolase/2-dehydro-3-deoxy-phosphogluconate aldolase	2482286	2482915	+		A	V
9	3008051	C	A	X276_13415	S-layer family protein	3005247	3009269	+		T	T
10	3141441	C	CA	X276_12855	DUF4179 domain-containing protein	3141433	3142683	+			
11	4087693	C	A						Non-coding		
12	4243433	C	CT	X276_07980	MarR family transcriptional regulator	4243239	4243676	–			
Mutant strain E28***											
1	491837	G	A	X276_24400	MerR family transcriptional regulator	491399	492223	+		E	K
2	851273	T	G	X276_22910	16S ribosomal RNA	851024	852535	+		*	G
3	851321	T	G	X276_22910	16S ribosomal RNA	851024	852535	+		*	G
4	2775807	C	A	X276_14460	Cytochrome b5	2775169	2775996	+		G	G
5	2775912	T	C	X276_14460	Cytochrome b5	2775169	2775996	+		T	T
6	3004250	C	A	X276_13420	Collagen-like protein	3003304	3004570	+	Pseudogene	P	Q
7	3007799	C	A	X276_13415	S-layer family protein	3005247	3009269	+		T	T
8	3008654	T	G	X276_13415	S-layer family protein	3005247	3009269	+		T	T
Mutant strain E32***											
1	2207690	C	CT	X276_16910	IS110 family transposase	2206548	2207848	–	Pseudogene		
2	2775912	T	C	X276_14460	Cytochrome b5	2775169	2775996	+		T	T
3	3007397	C	A	X276_13415	S-layer family protein	3005247	3009269	+		G	G
4	3876973	C	A	X276_09805	Glycoside hydrolase	3876787	3877821	–		M	I
5	4087693	C	A						Non-coding		
6	4243379	C	CAT	X276_07980	MarR family transcriptional regulator	4243239	4243676	–			
7	4960470	G	A	X276_04930	Chemotaxis protein	4958594	4963015	–		T	I
8	4982628	C	T	X276_04840	Response regulator	4982393	4982745	–	Pseudogene	I	I
9	5011570	C	T	X276_04700	Non-ribosomal peptide synthase	5010682	5018304	–		W	*
10	5053669	C	T	X276_04620	Hypothetical protein	5053325	5055736	–		D	N
11	5083112	C	T	X276_04450	YigZ family protein	5082972	5083619	–		V	I

(Continued)

TABLE 3 | Continued

	Position	Ref	Alt	Locus	Product	Start	End	Strand	Feature	Aa_ref	Aa_alt
12	5084395	C	T	X276_04445	PLP-dependent aminotransferase family protein	5083996	5085438	–		M	I
13	5275399	G	A	X276_03630	Carboxynorspermidine decarboxylase	5274563	5275702	–		H	Y
Mutant strain E33* **											
1	2663675	G	A	X276_14895	PFL family protein	2663567	2664922	+		G	R

[1]*Ref, DNA base in the wild-type strain; Alt, DNA base in mutant strain; Start, position of the gene in the genome, start; End, position of the gene in the genome, end; Aa_ref, encoded amino acid in the wild-type strain; Aa_alt, encoded amino acid in mutant strain. *Strains obtained by random chemical mutagenesis using EB as a mutagenic agent, when strains were selected directly on agar plates containing EB; **strains obtained by random chemical mutagenesis using EMS with selection on butanol; ***strains obtained by random chemical mutagenesis using EMS with selection on EB.*

TABLE 4 | List of mutations that caused longer changes in the genomes of mutant strains of *C. beijerinckii* NRRL B-598 exhibiting high butanol tolerance[1].

Strain	Mutation position	Size (bp)	Note
B33*	5311613-5311767	155	Intergenic
E15**	2982416-2982635	220	Part of the gene X276_13505 encoding DNA mismatch repair protein MutS
	5311613-5311767	155	Intergenic
E33**	4243635-4244393	759	Part of the gene X276_07980 encoding MarR family transcriptional regulator

[1]*Strains obtained by random chemical mutagenesis using EMS with the selection on butanol; **strains obtained by the random chemical mutagenesis using EMS with selection on ethidium bromide.*

that it is possible to cultivate the strain at larger scale under constant pH regulation to produce butyric acid as the main fermentation product (Drahokoupil and Patáková, 2020). Therefore, these mutant strains can be further studied as alternative butyric acid producers.

Along with higher butanol tolerance, mutant strains of *C. beijerinckii* NRRL B-598 exhibited improved tolerance to ethanol and EB (**Figures 2**, **3**). Tolerance testing revealed that mutant strains obtained by different approaches behaved differently. While tolerance to ethanol increased similarly in all mutant strains (**Figure 2**), EMS + EB mutants exhibited higher tolerance to EB than other strains (**Figure 3**). In the case of antibiotics, EB mutants generally exhibited higher tolerance (**Figure 4**). On the other hand, antibiotic tolerance of EMS + EB strains was lower than the WTS, except for strain E33 when tested for chloramphenicol (**Figure 4**). These differences can be probably explained by different mutations that occurred in the strains, so to reveal the differences at the gene level, genomes of all mutant strains were sequenced and variant callings were analyzed.

Variant calling in bacteria is a neglected topic and mainly, attention is paid to eukaryotes. Nevertheless, one of the first benchmarking studies dealing with bacterial variant calling by Bush et al. (2020) showed that a combination of BWA for mapping and GATK HaplotypeCaller brought the best results for closely related strains. As this was the case in our study, we used these tools to capture SNPs (**Supplementary Files 4**). Moreover, we took advantage of our data containing resequencing of the WTS that was recently used to update its genome assembly (CP011966.3) (Sedlar et al., 2019). We used false positive detections of SNPs in the WTS sequencing data to infer our own filtering rules (see section "Materials and Methods") (**Table 3**). While this approach is good for SNP detection, it is unable to call structural variants. Thus, we utilized Pilon to detect longer changes in genomic sequences (**Tables 4**, **5**). The combination of various approaches for detection of short and longer changes is quite common for eukaryotes (Long et al., 2013). Utilization of Pilon is advantageous in our case as the reference sequence was constructed using this approach, and thus, we were again able to remove false positives by filtering variants that were falsely called in the WTS data. SNPs in individual genes of the mutants are discussed further in the text, however, it is difficult to discuss CNVs because the topic has been scarcely studied in bacteria. CNVs are usually studied in comparative analyses (Větrovský and Baldrian, 2013; Greenblum et al., 2015) and the approach cannot be applied in our case.

Only few genome sequences of butanol-tolerant mutant strains obtained by random mutagenesis are currently available [*C. beijerinckii* SA-1 (Sandoval-Espinola et al., 2013), *C. pasteurianum* M150B (Sandoval et al., 2015), *C. acetobutylicum* ATCC 55025 and *C. acetobutylicum* JB200 (Xu et al., 2017)]. Genomic sequences of *C. acetobutylicum* ATCC 55025 and *C. acetobutylicum* JB200, as well as *C. pasteurianum* M150B, included multiple mutations, for example, 143 SNPs and 67s SNP for *C. acetobutylicum* ATCC 55025 and *C. pasteurianum* M150B, respectively. On the other hand, similar to the case of *C. beijerinckii* SA-1, for which 10 genetic polymorphisms were confirmed, including eight SNPs, genomes of our mutant strains of *C. beijerinckii* NRRL B-598 included one to 17 SNPs (21–51 prior to filtering), one longer change in strains B33, E15, and E33 and one or more copy number variations

TABLE 5 | List of copy number variations in the genomes of mutant strains of *C. beijerinckii* NRRL B-598 exhibiting high butanol tolerance[1].

Strain	Position	Size	Locus	Putative product
A*	341278–349235	7.96 kb	X276_25195	DNA-3-methyladenine glycosylase 2 family protein
			X276_25190	Site-specific integrase
			X276_25185	XRE family transcriptional regulator
			X276_25180	Hypothetical protein
			X276_25175	Transcription factor
			X276_25170	Hypothetical protein
			X276_25165	Replication protein
			X276_25160	Hypothetical protein
			X276_25155	Hypothetical protein
			X276_25150	Hypothetical protein
			X276_25145	Hypothetical protein
B*	341243–349259	8.02 kb	X276_25195	DNA-3-methyladenine glycosylase 2 family protein
			X276_25190	Site-specific integrase
			X276_25185	XRE family transcriptional regulator
			X276_25180	Hypothetical protein
			X276_25175	Transcription factor
			X276_25170	Hypothetical protein
			X276_25165	Replication protein
			X276_25160	Hypothetical protein
			X276_25155	Hypothetical protein
			X276_25150	Hypothetical protein
			X276_25145	Hypothetical protein
C*	341297–349217	7.92 kb	X276_25195	DNA-3-methyladenine glycosylase 2 family protein
			X276_25190	Site-specific integrase
			X276_25185	XRE family transcriptional regulator
			X276_25180	Hypothetical protein
			X276_25175	Transcription factor
			X276_25170	Hypothetical protein
			X276_25165	Replication protein
			X276_25160	Hypothetical protein
			X276_25155	Hypothetical protein
			X276_25150	Hypothetical protein
			X276_25145	Hypothetical protein
B33**	167230–167409	180 bp	X276_26025	PIN/TRAM domain-containing protein
	499439–499573	135 bp	Only intergenic	–
	575045–575230	186 bp	Only intergenic	–
	728816–728957	142 bp	X276_23400	Hypothetical protein
	6042705–6042895	191 bp	X276_00695	Methyl-accepting chemotaxis protein
	6137871–6138337	467 bp	X276_00305	23S rRNA [pseudouridine(1915)-N(3)]-methyltransferase RlmH
B44**	341237–349270	8.03 kb	X276_25195	DNA-3-methyladenine glycosylase 2 family protein
			X276_25190	Site-specific integrase
			X276_25185	XRE family transcriptional regulator
			X276_25180	Hypothetical protein
			X276_25175	Transcription factor
			X276_25170	Hypothetical protein
			X276_25165	Replication protein
			X276_25160	Hypothetical protein
			X276_25155	Hypothetical protein
			X276_25150	Hypothetical protein
			X276_25145	Hypothetical protein
E15***	4901–5166	266 bp	X276_26795	DNA topoisomerase (ATP-hydrolyzing) subunit B

(Continued)

TABLE 5 | Continued

Strain	Position	Size	Locus	Putative product
E28***	341278–349256	7.98 kb	X276_25195	DNA-3-methyladenine glycosylase 2 family protein
			X276_25190	Site-specific integrase
			X276_25185	XRE family transcriptional regulator
			X276_25180	Hypothetical protein
			X276_25175	Transcription factor
			X276_25170	Hypothetical protein
			X276_25165	Replication protein
			X276_25160	Hypothetical protein
			X276_25155	Hypothetical protein
			X276_25150	Hypothetical protein
			X276_25145	Hypothetical protein
E33***	341393–349134	7.74 kb	X276_25190	Site-specific integrase
			X276_25185	XRE family transcriptional regulator
			X276_25180	Hypothetical protein
			X276_25175	Transcription factor
			X276_25170	Hypothetical protein
			X276_25165	Replication protein
			X276_25160	Hypothetical protein
			X276_25155	Hypothetical protein
			X276_25150	Hypothetical protein
			X276_25145	Hypothetical protein

[1] *Strains obtained by random chemical mutagenesis using EB as a mutagenic agent, when strains were selected directly on agar plates containing EB; **strains obtained by random chemical mutagenesis using EMS with selection on butanol; ***strains obtained by random chemical mutagenesis using EMS with selection on EB.

in all of the strains, except E32 (**Tables 3–5**). Some of the mutations revealed in *C. beijerinckii* NRRL B-598 mutant strains with increased butanol tolerance can be connected to tolerance mechanisms, while others may play roles in metabolic enhancement rather than tolerance improvement. Many of the mutations were membrane-related, which correlates with the fact that normal cellular responses of the strains to the solvent was mainly at the membrane level (Patakova et al., 2018). A similar result was observed in *E. coli* when a genomic library enrichment strategy was used under butanol challenge (Reyes et al., 2011). Examples of membrane-related mutations in *C. beijerinckii* NRRL B-598 mutant strains are mutations in genes encoding peptidases, transporters or cytochrome b5 (**Table 3**). Interestingly, mutations in genes encoding peptidase S8 were observed not only in our EB mutants A (X276_19395), B (X276_17580), and C (X276_22430) (**Table 3**), but also in a mutant strain of *C. beijerinckii* SA-1, the offspring of *C. beijerinckii* NCIMB 8052 (Sandoval-Espinola et al., 2013). Additionally, it seems that EB mutants A, B and C not only exhibited different phenotypes from other mutants for which EMS was used as a mutagenic agent, but were also different in terms of mutations and formed a distinguishable cluster, as shown in **Figure 5**.

We analyzed changes in the genomes of mutant strains to determine whether some of the mutations occurring in EMS + butanol and EMS + EB strains could lead to the acid-crash phenotype. In the case of strain E15, the mutation occurred in gene X276_15915 encoding the sigma-54-dependent Fis family transcriptional regulator (**Table 3**). This may be causing the acid crash phenotype. Sigma-54 regulates sugar consumption and carbon metabolism in *C. beijerinckii* (Hocq et al., 2019). Thus, a higher glucose uptake rate and acid production rate, the reasons for the acid crash phenotype (Maddox et al., 2000), may occur due to mutations in regulatory genes such as sigma-54. A similar hypothesis has already been proposed for the degenerate strain *C. beijerinckii* DG-8052 (Lv et al., 2016). Unfiltered data contained a mutation that might be responsible for the phenotype; it is situated in gene X276_15350 encoding NADP-dependent glyceraldehyde-3-phosphate dehydrogenase in mutant strain E28 (**Supplementary Files 4**). The gene product plays a role in the formation of NADPH, which is necessary for the biosynthetic processes and modulation of redox potential (Liu et al., 2015). The importance of the gene for metabolite production was shown when expression of NADP-dependent glyceraldehyde-3-phosphate dehydrogenase of *C. acetobutylicum* in *E. coli* resulted in improved productivity of lycopene and ε-caprolactone (Martínez et al., 2008). As in the case of solventogenic strain *C. saccharoperbutylacetonicum*, where defects in genes encoding enzymes responsible for NADH formation resulted in strain degeneration (Hayashida and Yoshino, 1990), mutations in genes encoding NADPH formation in mutant strain E28 could affect the cells in a similar way. Nevertheless, this mutation (in gene X276_15350) was later filtered (**Table 3**) and, therefore, acid crash in the E28 strain probably happened due to some other changes. The reason for the acid crash phenotype in other mutant strains was not clear and needs further investigation.

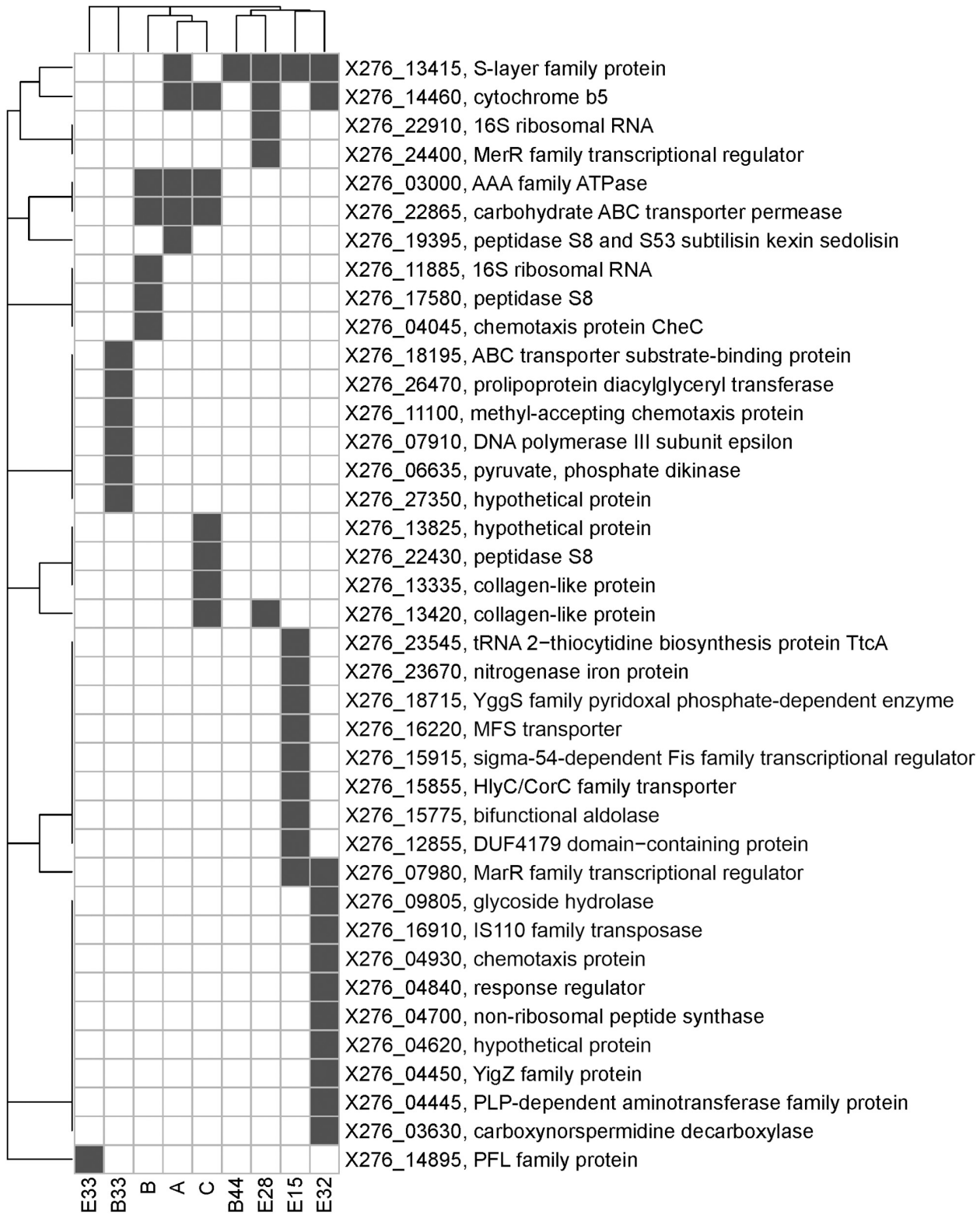

FIGURE 5 | A bi-clustered binary heatmap showing the distribution of genes with single-nucleotide polymorphisms among mutant strains of *C. beijerinckii* NRRL B-598 with improved butanol tolerance. Complete linkage clustering is based on binary distance between genes and mutants, respectively. Strains A, B, and C were obtained by random chemical mutagenesis using EB as a mutagenic agent, when strains were selected directly on agar plates containing EB; Strains B33 and B44 were obtained by random chemical mutagenesis using EMS with selection on butanol; strains E15, E28, E32, and E33 were obtained by random chemical mutagenesis using EMS with selection on EB.

The faster growth and somewhat higher butanol productivity of mutant C, observed during the first 24 h of cultivation (**Supplementary Table 2**), can probably be attributed to mutations in genes encoding a carbohydrate ABC transporter permease (X276_22865) and an AAA family ATPase (X276_03000), in which mutations were also detected for the other EB mutants, A and B (**Figure 5**). Use of non-PTS mechanisms of glucose uptake during the solventogenic phase, such as ABC transporters, resulted in more complete glucose utilization and increased butanol production in *C. beijerinckii* BA101 (Lee et al., 2005). A BLASTp (Gish and States, 1993) analysis of AAA family ATPase X276_03000 showed that it contained motifs similar to the PTS operon transcription anti-terminator in *Clostridioides difficile* 630, therefore it probably plays a part in PTS regulation. It was reported that the genome of the butanol-overproducing mutant *C. beijerinckii* SA-1 included mutations in PTS genes (Sandoval-Espinola et al., 2013) and that the mutant strain *C. beijerinckii* BA101 had a partially defective PTS (Lee and Blaschek, 2001; Lee et al., 2005). Therefore, a connection between PTS and regulation of solvent production, contributing to butanol overproduction, was hypothesized (Sandoval-Espinola et al., 2013).

Mutations in genes connected to butanol tolerance can also be identified in mutant strains of *C. beijerinckii* NRRL B-598. For example, in genes encoding chemotaxis proteins in strains B (X276_04045), B33 (X276_11100 and X276_00695), and E32 (X276_04930) (**Tables 3**, **5**). Chemotaxis is one the important mechanisms of adaptation to environmental stress (Zhao et al., 2007), in our case, the presence of produced butanol in the medium. It was shown that butanol acts as a repellent for *C. acetobutylicum*, meaning that it induces negative chemotaxis in the strain (Gutierrez and Maddox, 1987). For strain E32, mutations were observed in the gene X276_09805 encoding glycoside hydrolase, which belongs to family 25 (**Table 3**). This family includes enzymes with lysozyme activity and ones connected to autolysin production, for example, lyc gene (CA_C0554) of *C. acetobutylicum* ATCC 824. It was reported that enzymes that take part in autolysis and cell wall recycling in solventogenic clostridia are also connected to butanol tolerance (Patakova et al., 2018). In mutant strain B33, mutations were detected in X276_26470 encoding prolipoprotein diacylglyceryl transferase (**Table 3**), which catalyzes attachments of lipoproteins to cell membrane. Lipoproteins take part in multiple processes in the cell, including membrane transport, modifications of the cell wall, and antibiotic tolerance (Nielsen and Lampen, 1982; Chimalapati et al., 2012); therefore, mutations in prolipoprotein diacylglyceryl transferase can also be connected to butanol tolerance mechanisms.

One of most interesting mutations connected to improved butanol tolerance was revealed in EMS + EB mutants E15, E32, and E33 in the gene X276_07980 encoding the MarR family transcriptional regulator (**Tables 3**, **4**). Similarly to our result, mutations in genes encoding the MarR family transcriptional regulator occurred for the hyper butanol-tolerant and -producing strain, *C. acetobutylicum* JB200 and the authors hypothesized that this mutation contributed to enhanced butanol tolerance (Xu et al., 2017). Interestingly, MarR is a regulator that contributes to antibiotic resistance, as well as resistance to organic solvents and oxidative stress agents, by modulating the efflux pump and porin expression (Sharma et al., 2017). Thus, other regulators may also contribute to enhanced butanol tolerance. For example, mutations in gene X276_24400 encoding the MerR family transcriptional regulator in mutant strain E28 (**Table 3**). A BLASTp (Gish and States, 1993) analysis showed that the MerR gene shares similarity with the BmrR regulator from *Bacillus subtilis*, which controls the Bmr efflux pump for removal of antibiotics, dyes and disinfectants (Ahmed et al., 1994). Therefore, mutations in efflux pump regulators were found in all EMS + EB mutants.

These results suggest that the increased or decreased tolerance of mutant strains to antibiotics, EB or solvents (butanol and ethanol) (**Figures 2**–**4**) may also be due to altered activities of efflux pumps controlled by regulators. Transcriptional analysis of *C. beijerinckii* NRRL B-598 revealed upregulation of the TetR/AcrR family regulators putatively involved in efflux pump gene transcription after butanol addition to the medium (Sedlar et al., 2019), suggesting that efflux pumps might be involved in overcoming butanol stress in the strain. In the *C. beijerinckii* NRRL B-598 genome, 55 genes were identified as putatively encoding efflux pumps (Jureckova et al., 2018). Some of these pumps may be able to remove antibiotics, EB or solvents from a cell. For example, genes encoding Gram-positive efflux pumps capable of transporting tested antibiotics have been described for *Streptococcus pneumoniae*, *B. subtilis*, *Enterococcus faecalis*, *Lactococcus lactis*, and *Corynebacterium glutamicum* (Schindler and Kaatz, 2016). An efflux pump responsible for increased ethanol tolerance was reported for *Saccharomyces cerevisiae* BY4741 (Yang et al., 2013). Furthermore, native efflux pumps able to actively remove butanol were recently discovered in *Pseudomonas putida* and *E. coli* (Basler et al., 2018; Zhang et al., 2018), and heterologous expression of such a butanol efflux pump from *P. putida* in butanol-producing *C. saccharoperbutylacetonicum* led to increased butanol tolerance of the strain (Jiménez-Bonilla et al., 2020).

CONCLUSION

Our study shows that random chemical mutagenesis using EB can be successfully used for the generation of butanol-tolerant mutant strains in solventogenic *Clostridium*. While mutagenesis with EMS as a mutagenic agent, which is more commonly used for such a purpose, resulted in mutants exhibiting the acid-crash phenotype, use of EB alone did not disrupt solvent production. Moreover, use of EB for both mutagenesis and selection resulted in increased tolerance to several different substrates of efflux pumps.

We speculate that the acid crash phenotype in mutant strain E15 was acquired due to mutations in the gene encoding the sigma-54-dependent Fis family transcriptional regulator. Further investigations are needed to reveal the reasons for the phenotype in other EMS + butanol and EMS + EB strains.

Higher butanol tolerance of the strains may be connected to mutations in genes connected to the stress response, for example,

glycoside hydrolase or prolipoprotein diacylglyceryl transferase. However, the most prominent change in tolerance to substrates of efflux pumps, including butanol, can be explained by mutations in genes encoding efflux pump regulators, which were found in EMS + EB mutants. These regulators can be further studied in research connected to butanol tolerance mechanisms using targeted mutagenesis.

DATA AVAILABILITY STATEMENT

The genome sequencing data have been deposited in the NCBI Sequence Read Archive (SRA) under the project accession number PRJNA229510 (https://www.ncbi.nlm.nih.gov/sra/?term=PRJNA229510). WTS data are available under accession number SRX6419139 and mutant strains data under accession number within the range from SRX8614691 to SRX8614699.

AUTHOR CONTRIBUTIONS

MV, KS, IP, and PP designed the study. MV and BB performed the experiments and analyzed the data. KS and KJ performed the bioinformatics analyses. MV wrote the original draft, KS, BB, and PP contributed to manuscript writing. All authors read and approved the final manuscript.

FUNDING

This work was supported by GACR (Grantova Agentura Ceske Republiky), Czechia, project number 17-00551S.

ACKNOWLEDGMENTS

Computational resources were partially provided by the CESNET LM2015042 and the CERIT Scientific Cloud LM2015085, under the programme "Projects of Large Research, Development, and Innovations Infrastructures". We acknowledge the CF Genomics of CEITEC supported by the NCMG research infrastructure (LM2015091 funded by MEYS CR) for their support in obtaining the scientific data presented in this paper.

SUPPLEMENTARY MATERIAL

The Supplementary Material for this article can be found online at: https://www.frontiersin.org/articles/10.3389/fbioe.2020.598392/full#supplementary-material

REFERENCES

Ahmed, M., Borsch, C. M., Taylor, S. S., Vázquez-Laslop, N., and Neyfakh, A. A. (1994). A protein that activates expression of a multidrug efflux transporter upon binding the transporter substrates. *J. Biol. Chem.* 269, 28506–28513.

Alsaker, K. V., Spitzer, T. R., and Papoutsakis, E. T. (2004). Transcriptional analysis of *spo0A* overexpression in *Clostridium acetobutylicum* and its effect on the cell's response to butanol stress. *J. Bacteriol.* 186, 1959–1971. doi: 10.1128/JB.186.7.1959-1971.2004

Annous, B. A., and Blaschek, H. P. (1991). Isolation and characterization of *Clostridium acetobutylicum* mutants with enhanced amylolytic activity. *Appl. Environ. Microbiol.* 57, 2544–2548.

Baer, S. H., Blaschek, H. P., and Smith, T. L. (1987). Effect of butanol challenge and temperature on lipid composition and membrane fluidity of butanol-tolerant *Clostridium acetobutylicum*. *Appl. Environ. Microbiol.* 53, 2854–2861.

Basler, G., Thompson, M., Tullman-Ercek, D., and Keasling, J. (2018). A *Pseudomonas putida* efflux pump acts on short-chain alcohols. *Biotechnol. Biofuels* 11:136. doi: 10.1186/s13068-018-1133-9

Bohnert, J. A., Schuster, S., Fähnrich, E., Trittler, R., and Kern, W. V. (2007). Altered spectrum of multidrug resistance associated with a single point mutation in the *Escherichia coli* RND-type MDR efflux pump YhiV (MdtF). *J. Antimicrob. Chemother.* 59, 1216–1222. doi: 10.1093/jac/dkl426

Bolger, A. M., Lohse, M., and Usadel, B. (2014). Trimmomatic: a flexible trimmer for Illumina sequence data. *Bioinformatics* 30, 2114–2120. doi: 10.1093/bioinformatics/btu170

Bowles, L. K., and Ellefson, W. L. (1985). Effects of butanol on *Clostridium acetobutylicum*. *Appl. Environ. Microbiol.* 50, 1165–1170.

Branska, B., Pechacova, Z., Kolek, J., Vasylkivska, M., and Patakova, P. (2018). Flow cytometry analysis of *Clostridium beijerinckii* NRRL B-598 populations exhibiting different phenotypes induced by changes in cultivation conditions. *Biotechnol. Biofuels* 11:99. doi: 10.1186/s13068-018-1096-x

Bui, L. M., Lee, J. Y., Geraldi, A., Rahman, Z., Lee, J. H., and Kim, S. C. (2015). Improved n-butanol tolerance in *Escherichia coli* by controlling membrane related functions. *J. Biotechnol.* 204, 33–44. doi: 10.1016/j.jbiotec.2015.03.025

Bush, S. J., Foster, D., Eyre, D. W., Clark, E. L., De Maio, N., Shaw, L. P., et al. (2020). Genomic diversity affects the accuracy of bacterial single-nucleotide polymorphism-calling pipelines. *Gigascience* 9:giaa007. doi: 10.1093/gigascience/giaa007

Chen, C. K., and Blaschek, H. P. (1999). Acetate enhances solvent production and prevents degeneration in *Clostridium beijerinckii* BA101. *Appl. Microbiol. Biotechnol.* 52, 170–173. doi: 10.1007/s002530051504

Chimalapati, S., Cohen, J. M., Camberlein, E., MacDonald, N., Durmort, C., Vernet, T., et al. (2012). Effects of deletion of the *Streptococcus pneumoniae* lipoprotein diacylglyceryl transferase gene Lgt on ABC transporter function and on growth in vivo. *PLoS One* 7:e41393. doi: 10.1371/journal.pone.0041393

Drahokoupil, M., and Patáková, P. (2020). Production of butyric acid at constant pH by a solventogenic strain of *Clostridium beijerinckii*. *Czech J. Food Sci.* 38, 185–191. doi: 10.17221/95/2020-CJFS

Ewels, P., Magnusson, M., Lundin, S., and Kaller, M. (2016). MultiQC: summarize analysis results for multiple tools and samples in a single report. *Bioinformatics* 32, 3047–3048. doi: 10.1093/bioinformatics/btw354

Fisher, M. A., Boyarskiy, S., Yamada, M. R., Kong, N., Bauer, S., and Tullman-Ercek, D. (2014). Enhancing tolerance to short-chain alcohols by engineering the *Escherichia coli* AcrB efflux pump to secrete the non-native substrate n-butanol. *ACS Synth. Biol.* 3, 30–40. doi: 10.1021/sb400065q

Fletcher, E., Pilizota, T., Davies, P. R., McVey, A., and French, C. E. (2016). Characterization of the effects of n-butanol on the cell envelope of *E. coli*. *Appl. Microbiol. Biotechnol.* 100, 9653–9659. doi: 10.1007/s00253-016-7771-6

Gagneur, J., Toedling, J., Bourgon, R., and Delhomme, N. (2020). *genomeIntervals: Operations on Genomic Intervals. R package version* 1.44.2. Available online at: https://bioconductor.org/packages/release/bioc/html/genomeIntervals.html (accessed June 13, 2020).

Gallardo, R., Alves, M., and Rodrigues, L. R. (2017). Influence of nutritional and operational parameters on the production of butanol or 1,3-propanediol from glycerol by a mutant *Clostridium pasteurianum*. *N. Biotechnol.* 34, 59–67. doi: 10.1016/j.nbt.2016.03.002

Gish, W., and States, D. J. (1993). Identification of protein coding regions by database similarity search. *Nat. Genet.* 3, 266–272. doi: 10.1038/ng0393-266

Greenblum, S., Carr, R., and Borenstein, E. (2015). Extensive strain-level copy-number variation across human gut microbiome species. *Cell* 160, 583–594. doi: 10.1016/j.cell.2014.12.038

Gutierrez, N. A., and Maddox, I. S. (1987). Role of chemotaxis in solvent production by *Clostridium acetobutylicum*. *Appl. Environ. Microbiol.* 53, 1924–1927.

Hayashida, S., and Yoshino, S. (1990). Degeneration of solventogenic *Clostridium* caused by a defect in NADH generation. *Agric. Biol. Chem.* 54, 427–435. doi: 10.1271/bbb1961.54.427

Hermann, M., Fayolle, F., Marchal, R., Podvin, L., Sebald, M., and Vandecasteele, J. P. (1985). Isolation and characterization of butanol-resistant mutants of *Clostridium acetobutylicum*. *Appl. Environ. Microbiol.* 50, 1238–1243.

Hocq, R., Bouilloux-Lafont, M., Lopes Ferreira, N., and Wasels, F. (2019). σ 54 (σ L) plays a central role in carbon metabolism in the industrially relevant *Clostridium beijerinckii*. *Sci. Rep.* 9:7228. doi: 10.1038/s41598-019-43822-2

Ingram, L. O. (1986). Microbial tolerance to alcohols: role of the cell membrane. *Trends Biotechnol.* 4, 40–44. doi: 10.1016/0167-7799(86)90152-6

Jain, M. K., Beacom, D., and Datta, R. (1994). Mutant strain of *C. acetobutylicum and process for making butanol*. *Patent* 12:242. doi: 10.1016/0734-9750(94)90895-8

Jiménez-Bonilla, P., Zhang, J., Wang, Y., Blersch, D., De-Bashan, L.-E., Guo, L., et al. (2020). Enhancing the tolerance of *Clostridium saccharoperbutylacetonicum* to lignocellulosic-biomass-derived inhibitors for efficient biobutanol production by overexpressing efflux pumps genes from *Pseudomonas putida*. *Bioresour. Technol* 312:123532. doi: 10.1016/j.biortech.2020.123532

Jones, A. J., Venkataramanan, K. P., and Papoutsakis, T. (2016). Overexpression of two stress-responsive, small, non-coding RNAs, 6S and tmRNA, imparts butanol tolerance in *Clostridium acetobutylicum*. *FEMS Microbiol. Lett.* 363:fnw063. doi: 10.1093/femsle/fnw063

Jureckova, K., Koscova, P., Sedlar, K., Kolek, J., Patakova, P., and Provaznik, I. (2018). "*In silico* prediction of genes coding efflux pumps in *Clostridium beijerinckii* NRRL B-598," in *Proceedings of the 6th International Conference on Chemical Technology*, eds M. Vesely, Z. Hrdlicka, J. Hanika, and J. Lubojacky (Czech Republic: Czech Society of Industrial Chemistry), 86–90.

Knaus, B. J., and Grünwald, N. J. (2017). vcfr: a package to manipulate and visualize variant call format data in R. *Mol. Ecol. Resour.* 17, 44–53. doi: 10.1111/1755-0998.12549

Kong, X., He, A., Zhao, J., Wu, H., Ma, J., Wei, C., et al. (2016). Efficient acetone-butanol-ethanol (ABE) production by a butanol-tolerant mutant of *Clostridium beijerinckii* in a fermentation-pervaporation coupled process. *Biochem. Eng. J.* 105, 90–96. doi: 10.1016/j.bej.2015.09.013

Lee, J., and Blaschek, H. P. (2001). Glucose uptake in *Clostridium beijerinckii* NCIMB 8052 and the solvent-hyperproducing mutant BA101. *Appl. Environ. Microbiol.* 67, 5025–5031.

Lee, J., Mitchell, W. J., Tangney, M., and Blaschek, H. P. (2005). Evidence for the presence of an alternative glucose transport system in *Clostridium beijerinckii* NCIMB 8052 and the solvent-hyperproducing mutant BA101. *Appl. Environ. Microbiol.* 71, 3384–3387. doi: 10.1128/AEM.71.6.3384-3387.2005

Lee, S. Y., Park, J. H., Jang, S. H., Nielsen, L. K., Kim, J., and Jung, K. S. (2008). Fermentative butanol production by clostridia. *Biotechnol. Bioeng.* 101, 209–228. doi: 10.1002/bit.22003

Lepage, C., Fayolle, F., Hermann, M., and Vandecasteele, J. P. (1987). Changes in membrane lipid composition of *Clostridium acetobutylicum* during acetone-butanol fermentation: effects of solvents, growth temperature and pH. *Microbiology* 133, 103–110. doi: 10.1099/00221287-133-1-103

Li, H., and Durbin, R. (2009). Fast and accurate short read alignment with Burrows-Wheeler transform. *Bioinformatics* 25, 1754–1760. doi: 10.1093/bioinformatics/btp324

Li, H., Handsaker, B., Wysoker, A., Fennell, T., Ruan, J., Homer, N., et al. (2009). The sequence alignment/map format and SAMtools. *Bioinformatics* 25, 2078–2079. doi: 10.1093/bioinformatics/btp352

Liao, Z., Zhang, Y., Luo, S., Suo, Y., Zhang, S., and Wang, J. (2017). Improving cellular robustness and butanol titers of *Clostridium acetobutylicum* ATCC824 by introducing heat shock proteins from an extremophilic bacterium. *J. Biotechnol.* 252, 1–10. doi: 10.1016/j.jbiotec.2017.04.031

Lin, Y. L., and Blaschek, H. P. (1983). Butanol production by a butanol-tolerant strain of *Clostridium acetobutylicum* in extruded corn broth. *Appl. Environ. Microbiol.* 45, 966–973. doi: 10.1128/aem.45.3.966-973.1983

Liu, J., Qi, H., Wang, C., and Wen, J. (2015). Model-driven intracellular redox status modulation for increasing isobutanol production in *Escherichia coli*. *Biotechnol. Biofuels* 8:108.

Liu, X. B., Gu, Q. Y., and Yu, X. B. (2013). Repetitive domestication to enhance butanol tolerance and production in *Clostridium acetobutylicum* through artificial simulation of bio-evolution. *Bioresour. Technol.* 130, 638–643. doi: 10.1016/j.biortech.2012.12.121

Long, Q., Rabanal, F. A., Meng, D., Huber, C. D., Farlow, A., Platzer, A., et al. (2013). Massive genomic variation and strong selection in *Arabidopsis thaliana* lines from Sweden. *Nat. Genet.* 45, 884–890. doi: 10.1038/ng.2678

Lv, J., Jiao, S., Du, R., Zhang, R., Zhang, Y., and Han, B. (2016). Proteomic analysis to elucidate degeneration of *Clostridium beijerinckii* NCIMB 8052 and role of Ca2+ in strain recovery from degeneration. *J. Ind. Microbiol. Biotechnol.* 43, 741–750. doi: 10.1007/s10295-016-1754-6

Maddox, I. S., Steiner, E., Hirsch, S., Wessner, S., Gutierrez, N. A., Gapes, J. R., et al. (2000). The cause of "acid crash" and "acidogenic fermentations" during the batch acetone-butanol-ethanol (ABE-) fermentation process. *J. Mol. Microbiol. Biotechnol.* 2, 95–100.

Mann, M. S., Dragovic, Z., Schirrmacher, G., and Lutke-Eversloh, T. (2012). Over-expression of stress protein-encoding genes helps *Clostridium acetobutylicum* to rapidly adapt to butanol stress. *Biotechnol. Lett.* 34, 1643–1649. doi: 10.1007/s10529-012-0951-2

Mao, S., Luo, Y., Zhang, T., Li, J., Bao, G., Zhu, Y., et al. (2010). Proteome reference map and comparative proteomic analysis between a wild type *Clostridium acetobutylicum* DSM 1731 and its mutant with enhanced butanol tolerance and butanol yield. *J. Proteome Res.* 9, 3046–3061. doi: 10.1021/pr9012078

Martínez, I., Zhu, J., Lin, H., Bennett, G. N., and San, K. Y. (2008). Replacing *Escherichia coli* NAD-dependent glyceraldehyde 3-phosphate dehydrogenase (GAPDH) with a NADP-dependent enzyme from *Clostridium acetobutylicum* facilitates NADPH dependent pathways. *Metab. Eng.* 10, 352–359. doi: 10.1016/j.ymben.2008.09.001

Máté de Gérando, H., Wasels, F., Bisson, A., Clement, B., Bidard, F., Jourdier, E., et al. (2018). Genome and transcriptome of the natural isopropanol producer *Clostridium beijerinckii* DSM6423. *BMC Genom.* 19:242. doi: 10.1186/s12864-018-4636-7

Matta-el-Ammouri, G., Janati-Idrissi, R., Rambourg, J.-M., Petitdemange, H., and Gay, R. (1986). Acetone butanol fermentation by a *Clostridium acetobutylicum* mutant with high solvent productivity. *Biomass* 10, 109–119. doi: 10.1016/0144-4565(86)90059-4

McKenna, A., Hanna, M., Banks, E., Sivachenko, A., Cibulskis, K., Kernytsky, A., et al. (2010). The genome analysis toolkit: a MapReduce framework for analyzing next-generation DNA sequencing data. *Genome Res.* 20, 1297–1303. doi: 10.1101/gr.107524.110

Mukhopadhyay, A. (2015). Tolerance engineering in bacteria for the production of advanced biofuels and chemicals. *Trends Microbiol.* 23, 498–508. doi: 10.1016/j.tim.2015.04.008

Nielsen, J. B. K., and Lampen, J. O. (1982). Membrane-bound penicillinases in gram-positive bacteria. *J. Biol. Chem.* 257, 4490–4495.

Ohta, T., Tokishita, S. I., and Yamagata, H. (2001). Ethidium bromide and SYBR Green I enhance the genotoxicity of UV-irradiation and chemical mutagens in *E. coli*. *Mutat. Res. Genet. Toxicol. Environ. Mutagen.* 492, 91–97. doi: 10.1016/S1383-5718(01)00155-3

Pagès, H., Aboyoun, P., Gentleman, R., and DebRoy, S. (2020). *Biostrings: Efficient Manipulation of Biological Strings. R package version* 2.56.0. Available online at: https://bioconductor.org/packages/release/bioc/html/Biostrings.html (accessed June 13, 2020).

Paixao, L., Rodrigues, L., Couto, I., Martins, M., Fernandes, P., de Carvalho, C. C. C. R., et al. (2009). Fluorometric determination of ethidium bromide efflux kinetics in *Escherichia coli*. *J. Biol. Eng.* 3:18. doi: 10.1186/1754-1611-3-18

Patakova, P., Kolek, J., Sedlar, K., Koscova, P., Branska, B., Kupkova, K., et al. (2018). Comparative analysis of high butanol tolerance and production in clostridia. *Biotechnol. Adv.* 36, 721–738. doi: 10.1016/j.biotechadv.2017.12.004

Patel, D., Kosmidis, C., Seo, S. M., and Kaatz, G. W. (2010). Ethidium bromide MIC screening for enhanced efflux pump gene expression or efflux activity

in *Staphylococcus aureus*. *Antimicrob. Agents Chemother.* 54, 5070–5073. doi: 10.1128/AAC.01058-10

Qureshi, N., and Blaschek, H. P. (2001). Recent advances in ABE fermentation: Hyper-butanol producing *Clostridium beijerinckii* BA101. *J. Ind. Microbiol. Biotechnol.* 27, 287–291. doi: 10.1038/sj.jim.7000114

Reyes, L. H., Almario, M. P., and Kao, K. C. (2011). Genomic library screens for genes involved in n-butanol tolerance in *Escherichia coli*. *PLoS One* 6:e17678. doi: 10.1371/journal.pone.0017678

Sandoval, N. R., Venkataramanan, K. P., Groth, T. S., and Papoutsakis, E. T. (2015). Whole-genome sequence of an evolved *Clostridium pasteurianum* strain reveals Spo0A deficiency responsible for increased butanol production and superior growth. *Biotechnol. Biofuels* 8:227. doi: 10.1186/s13068-015-0408-7

Sandoval-Espinola, W. J., Makwana, S. T., Chinn, M. S., Thon, M. R., Andrea Azcárate-Peril, M., and Bruno-Bárcena, J. M. (2013). Comparative phenotypic analysis and genome sequence of *Clostridium beijerinckii* SA-1, an offspring of NCIMB 8052. *Microbiology* 159, 2558–2570. doi: 10.1099/mic.0.069534-0

Schindler, B. D., and Kaatz, G. W. (2016). Multidrug efflux pumps of Gram-positive bacteria. *Drug Resist. Updat.* 27, 1–13. doi: 10.1016/j.drup.2016.04.003

Schwarz, K. M., Kuit, W., Grimmler, C., Ehrenreich, A., and Kengen, S. W. M. (2012). A transcriptional study of acidogenic chemostat cells of *Clostridium acetobutylicum* - Cellular behavior in adaptation to n-butanol. *J. Biotechnol.* 161, 366–377. doi: 10.1016/j.jbiotec.2012.03.018

Sedlar, K., Kolek, J., Gruber, M., Jureckova, K., Branska, B., Csaba, G., et al. (2019). A transcriptional response of *Clostridium beijerinckii* NRRL B-598 to a butanol shock. *Biotechnol. Biofuels* 12:243. doi: 10.1186/s13068-019-1584-7

Sedlar, K., Kolek, J., Provaznik, I., and Patakova, P. (2017). Reclassification of non-type strain *Clostridium pasteurianum* NRRL B-598 as *Clostridium beijerinckii* NRRL B-598. *J. Biotechnol.* 244, 1–3. doi: 10.1016/j.jbiotec.2017.01.003

Sedlar, K., Koscova, P., Vasylkivska, M., Branska, B., Kolek, J., Kupkova, K., et al. (2018). Transcription profiling of butanol producer *Clostridium beijerinckii* NRRL B-598 using RNA-Seq. *BMC Genom.* 19:415. doi: 10.1186/s12864-018-4805-8

Segura, A., Molina, L., Fillet, S., Krell, T., Bernal, P., Muñoz-Rojas, J., et al. (2012). Solvent tolerance in Gram-negative bacteria. *Curr. Opin. Biotechnol.* 23, 415–421. doi: 10.1016/j.copbio.2011.11.015

Seo, S.-O., Janssen, H., Magis, A., Wang, Y., Lu, T., Price, N. D., et al. (2017). Genomic, transcriptional, and phenotypic analysis of the glucose derepressed *Clostridium beijerinckii* mutant exhibiting acid crash phenotype. *Biotechnol. J.* 12, 1700182. doi: 10.1002/biot.201700182

Sharma, P., Haycocks, J. R. J., Middlemiss, A. D., Kettles, R. A., Sellars, L. E., Ricci, V., et al. (2017). The multiple antibiotic resistance operon of enteric bacteria controls DNA repair and outer membrane integrity. *Nat. Commun.* 8:1444. doi: 10.1038/s41467-017-01405-7

Soucaille, P., Joliff, G., Izard, A., and Goma, G. (1987). Butanol tolerance and autobacteriocin production by *Clostridium acetobutylicum*. *Curr. Microbiol.* 14, 295–299. doi: 10.1007/BF01568139

Tanaka, Y., Kasahara, K., Hirose, Y., Morimoto, Y., Izawa, M., and Ochi, K. (2017). Enhancement of butanol production by sequential introduction of mutations conferring butanol tolerance and streptomycin resistance. *J. Biosci. Bioeng.* 124, 400–407. doi: 10.1016/j.jbiosc.2017.05.003

Tomas, C. A., Welker, N. E., and Papoutsakis, E. T. (2003). Overexpression of *groESL* in *Clostridium acetobutylicum* results in increased solvent production and tolerance, prolonged metabolism, and changes in the cell's transcriptional program. *Appl. Environ. Microbiol.* 69, 4951–4965. doi: 10.1128/AEM.69.8.4951-4965.2003

Vasylkivska, M., Jureckova, K., Branska, B., Sedlar, K., Kolek, J., Provaznik, I., et al. (2019). Transcriptional analysis of amino acid, metal ion, vitamin and carbohydrate uptake in butanol-producing *Clostridium beijerinckii* NRRL B-598. *PLoS One* 14:e0224560. doi: 10.1371/journal.pone.0224560

Vasylkivska, M., and Patakova, P. (2020). Role of efflux in enhancing butanol tolerance of bacteria. *J. Biotechnol.* 320, 17–27. doi: 10.1016/j.jbiotec.2020.06.008

Větrovský, T., and Baldrian, P. (2013). The variability of the 16S rRNA gene in bacterial genomes and its consequences for bacterial community analyses. *PLoS One* 8:e57923. doi: 10.1371/journal.pone.0057923

Walker, B. J., Abeel, T., Shea, T., Priest, M., Abouelliel, A., Sakthikumar, S., et al. (2014). Pilon: an integrated tool for comprehensive microbial variant detection and genome assembly improvement. *PLoS One* 9:e112963. doi: 10.1371/journal.pone.0112963

Wickham, H. (2009). *ggplot2*. New York, NY: Springer, doi: 10.1007/978-0-387-98141-3

Xu, M., Zhao, J., Yu, L., and Yang, S. T. (2017). Comparative genomic analysis of *Clostridium acetobutylicum* for understanding the mutations contributing to enhanced butanol tolerance and production. *J. Biotechnol.* 263, 36–44. doi: 10.1016/j.jbiotec.2017.10.010

Xue, C., Zhao, J., Lu, C., Yang, S. T., Bai, F., and Tang, I. C. (2012). High-titer n-butanol production by *Clostridium acetobutylicum* JB200 in fed-batch fermentation with intermittent gas stripping. *Biotechnol. Bioeng.* 109, 2746–2756. doi: 10.1002/bit.24563

Yang, K. M., Woo, J. M., Lee, S. M., and Park, J. B. (2013). Improving ethanol tolerance of *Saccharomyces cerevisiae* by overexpressing an ATP-binding cassette efflux pump. *Chem. Eng. Sci.* 103, 74–78. doi: 10.1016/j.ces.2012.09.015

Yang, S.-T., and Zhao, J. (2013). *Adaptive engineering of Clostridium for increased butanol production*. U.S. Patent No US8450093B1. Washington, DC: U.S. Patent and Trademark Office.

Zhang, Y., Dong, R., Zhang, M., and Gao, H. (2018). Native efflux pumps of *Escherichia coli* responsible for short and medium chain alcohol. *Biochem. Eng. J.* 133, 149–156. doi: 10.1016/j.bej.2018.02.009

Zhao, K., Liu, M., and Burgess, R. R. (2007). Adaptation in bacterial flagellar and motility systems: from regulon members to 'foraging'-like behavior in *E. coli*. *Nucleic Acids Res.* 35, 4441–4452. doi: 10.1093/nar/gkm456

Zhao, Y., Hindorff, L. A., Chuang, A., Monroe-Augustus, M., Lyristis, M., Harrison, M. L., et al. (2003). Expression of a cloned cyclopropane fatty acid synthase gene reduces solvent formation in *Clostridium acetobutylicum* ATCC 824. *Appl. Environ. Microbiol.* 69, 2831–2841. doi: 10.1128/AEM.69.5.2831-2841.2003

Conflict of Interest: The authors declare that the research was conducted in the absence of any commercial or financial relationships that could be construed as a potential conflict of interest.

frontiers in Microbiology

ORIGINAL RESEARCH
published: 18 December 2020
doi: 10.3389/fmicb.2020.602774

Effects of Carbon Ion Beam Irradiation on Butanol Tolerance and Production of *Clostridium acetobutylicum*

*Yue Gao[1,2], Miaomiao Zhang[1,2,3], Xiang Zhou[1,2], Xiaopeng Guo[1,2], Cairong Lei[1,2], Wenjian Li[1,2,3] and Dong Lu[1,2,3]**

[1] Institute of Modern Physics, Chinese Academy of Sciences, Lanzhou, China, [2] Chinese Academy of Sciences, University of Chinese Academy of Sciences, Beijing, China, [3] Gansu Key Laboratory of Microbial Resources Exploitation and Application, Lanzhou, China

OPEN ACCESS

Edited by:
Hongxin Fu,
South China University of Technology, China

Reviewed by:
Chi Cheng,
Dalian University of Technology, China
Hongzhen Luo,
Huaiyin Institute of Technology, China

***Correspondence:**
Dong Lu
ld@impcas.ac.cn

Specialty section:
This article was submitted to Microbiotechnology, a section of the journal Frontiers in Microbiology

Received: *04 September 2020*
Accepted: *30 November 2020*
Published: *18 December 2020*

Citation:
Gao Y, Zhang M, Zhou X, Guo X, Lei C, Li W and Lu D (2020) Effects of Carbon Ion Beam Irradiation on Butanol Tolerance and Production of Clostridium acetobutylicum. Front. Microbiol. 11:602774. doi: 10.3389/fmicb.2020.602774

Clostridium acetobutylicum (*C. acetobutylicum*) has considerable potential for use in bioenergy development. Owing to the repeated use of traditional mutagenesis methods, the strains have developed a certain tolerance. The rheology of the bioprocess and the downstream processing of the product heavily depend on the ability of *C. acetobutylicum* mutants to produce butanol. Carbon ion beam irradiation has advantages over traditional mutation methods for fermentative production because of its dose conformity and superb biological effectiveness. However, its effects on the specific productivity of the strains have not been clearly understood. In this study, we screened five mutants through carbon ion beam irradiation; mutant Y217 achieved a butanol-production level of 13.67 g/L, exceeding that of wild-type strain ATCC 824 (i.e., 9.77 g/L). In addition, we found that the mutant maintained normal cell membrane integrity under the stimulation of 15 g/L butanol, whereas the intracellular macromolecules of wild-type strain ATCC 824 leaked significantly. Subsequently, we used the response surface methodology (RSM) to determine if the mutant cell membrane integrity improved the butanol tolerance. We verified that with the addition of butanol, the mutant could be fermented to produce 8.35 g/L butanol, and the final butanol concentration in the fermentation broth could reach 16.15 g/L. In this study, we proved that under butanol stress, mutant Y217 features excellent butanol production and tolerance and cell membrane integrity and permeability; no prior studies have attempted to do so. This will serve as an interesting and important illustration of the complexity of genetic control of the irradiation mutation of *C. acetobutylicum* strains. It may also prove to be useful in the bioengineering of strains of the mutant for use in the predevelopment stage.

Keywords: *Clostridium acetobutylicum*, carbon ion beam irradiation, mutant, membrane permeability, response surface methodology

INTRODUCTION

The exhaustive exploitation of fossil fuels has led to a decline in the storage of fossil energy worldwide. Under the multiple pressures of energy depletion and environmental degradation, the development of alternative clean energy is urgently needed (Jiaquiang et al., 2018; Zhang et al., 2019). Presently, the main widely used alternative biofuels include biomethanol, biodiesel, bioethanol, and biobutanol. However, biobutanol significantly differs from other biofuels. As an essential product of microbial fermentation, biobutanol has the advantages of low volatility and high energy, and it can be mixed with gasoline in any ratio. Thus, it has significant potential for use in bioenergy development (Kikuchi et al., 2009). However, cost and efficiency are factors that limit the production of butanol by *Clostridium acetobutylicum*. Presently, acetone-butanol-ethanol (ABE) fermentation predominantly uses food crops (corn) and non-food crops (straw) as raw materials, which are expensive and have high pretreatment costs (Kumar et al., 2012). During the ABE fermentation process, when the concentration of butanol in the fermentation product exceeds 13 g/L, it has a toxic effect on *Clostridia*; the thallus begins to autolyzed, or spores are formed, and the fermentation process is gradually terminated, resulting in low butanol production and conversion rate, which limits the industrial production (Dadgar and Foutch, 1988). Therefore, rapid and efficient strain-modification techniques can improve the metabolic capacity and enhance the ABE production efficiency.

Mutagenesis is a reliable technology and widely used in strain improvement. Mutagenesis methods, including chemical and physical mutagenesis methods, are commonly used in mutagenic engineering to activate *Clostridia* strains. The strains are then screened by a selective medium to obtain mutants with excellent performance and applicability. Zhang et al. (1996) used N-methyl-N-nitro-N-nitrosoguanidine (NTG) and ethyl methane sulfonate (EMS) to obtain mutants with a high butanol ratio by performing chemical mutagenesis on *C. acetobutylicum*. The proportion of butanol in the total solvent is stable at approximately 70%, which is approximately 10% higher than that of the wild-type strain. Li et al. (2013) used *C. beijerinckii* as a starting strain and combined the low-energy ion beam implantation technology, NTG induction, and rational screening model to modify the strain; finally, they obtained a mutant with excellent cell performance and significantly increased the butanol production. The butanol yield of MUT3 reached 15.8 $\pm$ 0.7 g/L, which was 1.46 times higher than that of the starting strain in the P2 medium.

Owing to the repeated use of traditional mutagenesis methods, some industrial strains have developed a certain tolerance. Therefore, researchers have begun to develop new methods for microbial mutagenesis breeding; heavy ion beam irradiation, as a more efficient irradiation method, has been extended to a variety of scientific research and biological mutagenesis breeding, achieving a remarkable effect with high economic benefit. The metabolites of gentamicin-producing bacteria and respiration-deficient mutants were increased by heavy ion beam mutagenesis (Xie et al., 1995; Guo et al., 2019). In the food industry, new strains with a high conversion rate have also been obtained by heavy ion beam irradiation and industrialized; these include *Aspergillus Niger* and *Saccharomyces cerevisiae*, which have been screened for stable high-yield strains (Yan et al., 2009; Hu and Chen, 2012). In terms of microbial energy, the use of heavy ion beam irradiation produced poly-β-hydroxybutyrate (PHB) high-yield strain G15 (Xue et al., 2010) and oil-producing microalgae mutant strain D90G-19. Cell membranes provide an effective barrier to environment; therefore, adjusting the membrane permeability involves the regulation of passage of ions, nutrients, and toxic substances through the membrane (Qi et al., 2019). Related studies have been conducted to improve the solvent production by changing the cell membrane permeability of *C. acetobutylicum*. For example, Xin et al. (2018) reported that after supplementing 15% Tween 80 (v/v), the butanol production increased to 18.65 g/L, which is 38% higher than that for the control group, and the butanol tolerance increased to 18 g/L, which is 80% higher than that for the control group. Dhamole et al. (2012) conducted a series of tests with non-ionic surfactants (Triton X-114, L64, L62LF, L61, and L62) to increase the production of acetone and butanol. The results showed that L62 not only significantly improved the butanol yield but also produced a better butanol extractant. In addition, changes in cell membrane permeability are frequently identified as one of the main effects of butanol stress-induced toxicity (Qi et al., 2019).

The traditional exogenous butanol method, one-factor-at-a-time approach, is not feasible for establishing relationships between all the experimental input factors and the output response. Although the traditional approach can be useful to find the predominant factors, it consumes considerable time and energy. Furthermore, because the results are valid only under fixed experimental conditions, the predictions for other conditions may be inaccurate. To solve this problem, the design of experiment (DOE) offers a better alternative for studying the effects of butanol tolerance of *C. acetobutylicum* and their response with a minimum number of experiments. The response surface methodology (RSM) is a multifactor, multilevel test-design method that uses multiple quadratic regression equations to fit the functional relationship between factors and response values. It is typically used to obtain the best process parameters by analyzing the regression equations, which is a statistical method to solve multivariable problems (Ebrahimi et al., 2020; Figueroa-Torres et al., 2020). Liu et al. (2010) used the RSM to optimize the medium for xylose fermentation for producing butanol and established a regression equation. This optimized medium was obtained and the yield of butanol increased by 18.4%, reaching 6.69 g/L under optimized condition. Using the RSM-based DOE, the aggregate mix proportions can be obtained with a minimum number of experiments without the need for performing all the possible combination experiments. Further, the input levels of the different variables for a particular level of response can be determined. The RSM is a collection of statistical techniques for designing experiments, building models, evaluating the effects of factors, and searching for the optimum conditions of the factors. It also quantifies relationships between one or more measured responses and the vital input factors.

In this study, we used the heavy ion beam irradiation mutagenesis method for the selection of *C. acetobutylicum* to obtain a new strain with potential fermentation performance, attempt to use it in the studies of membrane permeability of the *C. acetobutylicum* mutant and responses of exogenous butanol with minimum numbers of experimental runs, determine the optimum tolerance using the RSM, and analyze the relationship between butanol tolerance and production of mutant. Improving butanol tolerance is critical for future applications of this process in the fermentation industry.

MATERIALS AND METHODS

Irradiation Treatment and Screening Process

Clostridium acetobutylicum strain ATCC 824 was preserved in 40% glycerol at −80°C. The growth medium of *C. acetobutylicum* strains was the liquid reinforced *Clostridial* medium (RCM) with 0.5% glucose or RCM agar plate at 37°C under anaerobic conditions. The following irradiation treatment was performed: wild-type strain *C. acetobutylicum* ATCC 824 was cultured on the RCM liquid medium at 37°C for 20 h (OD_{600} = 0.8–1.0); then, 1 ml of bacterial suspension was transferred onto a 35-mm irradiation dish. Six doses of cell suspension were irradiated at 30, 60, 90, 120, 150, and 200 Gy, and three samples were treated with every dose. Irradiation mutagenesis tests were conducted by the Heavy-Ion Research Facility in Lanzhou (HIRFL), Institute of Modern Physics, Chinese Academy of Sciences, with 80 MeV/u carbon ion beams. The survival fractions were measured by normalizing the colony counts of irradiated cells with those of untreated cells; survival fraction = (average number of colonies on treatment plates/average number of colonies on untreated plates) × 100%. The following screening process was performed: cell suspensions were diluted to 10^{-4}, and 200 μL of the dilution was spread on the RCM agar plate and cultured at 37°C for 36–38 h. Mutant strains were screened through the detection of starch utilization and butanol tolerance concentration. The screening agar plate, which contained 2.0% (v/v) butanol and 0.2% starch, was poured onto the RCM plate. The positive mutants were primarily selected by recording and comparing the diameter sizes of the transparent circles. The composition of RCM in distilled water was as follows: beef extract, 10.00 g/L; peptone, 10.00 g/L; yeast extract, 3.00 g/L; glucose, 5.00 g/L; starch, 1.00 g/L; NaCl, 5.00 g/L; sodium acetate, 3.00 g/L; cysteine hydrochloride, 0.50 g/L; (agar plate, 15 g/L).

Fermentation Conditions

The batch fermentation study was conducted in a 250 ml screw-capped bottle with 50 ml of corn- powder medium (CM). The spore suspension of *C. acetobutylicum* ATCC 824 or its mutant strains was anaerobically cultured to the stationary phase at 37°C in the RCM. The screw-capped bottles were inoculated with 5–10% seed culture of the total fermentation culture volume and the stationary culture at 37°C. The samples were drawn periodically to monitor the pH values and concentrations of the solvents and acids. The fermentation studies were performed in triplicate. The CM was used for the main batch fermentation. To prepare the CM, 70 g of corn powder was suspended in 1 L of distilled water and boiled for 1 h; the composition of CM in distilled water was as follows: 70 g/L corn powder, 3.0 g/L $(NH4)_2SO_4$, 3.0 g/L $CaCO_3$, 1.0 g/L $K_2HPO_4{\cdot}3H_2O$, 1.25 g/L KH_2PO_4, 0.1 g/L $MgSO_4{\cdot}7H_2O$, and 0.01 g/L $FeSO_4{\cdot}7H_2O$. All the purchased chemicals were >99% pure. To maintain complete anaerobic conditions, all the media were purged with N_2 to remove O_2, and agar plates were cultured in anaerobic jars.

Determination of the Genetic Stability of Mutants

The growth abilities and solvent yields were determined for 1–12 generations of the mutant and wild-type strain. A generation was defined as follows: a single colony was picked and inoculated into a 250 ml screw-capped bottle with 50 mL of the CM from the RCM plate and static culture at 37°C until OD_{600} approaches 1.0, after which the diluted suspension was plated on the RCM plate. The same procedure was followed for each generation. The growth rate was expressed by biomass concentration (dry cell weight, DCW). A 15 mL centrifuge tube was placed in an oven at 60°C for drying. The empty centrifuge tube was accurately weighted to X, 10 mL of fermentation broth was drawn into the centrifuge tube and centrifuged at 4000 × *g* for 15 min. After the supernatant was discarded, the bacterial pellet was washed five times with distilled water, dried in an oven at 60°C to a constant weight, and weighed to Y. DCW (g/L) = (Y–X)/10 × 1000. Fermentation experiments were performed as detailed previously. The butanol yield and total solvent content were detected.

Scanning Electron Microscopy (SEM) Sample Preparation

The suspension of the late logarithmic growth period liquid medium was collected by centrifugation at 8000 × *g* for 3–5 min and washed twice with a phosphate buffer (pH = 7.2) used for SEM observation. Thereafter, 2.5% glutaraldehyde was added to immobilize the cells at 4°C for 2–3 h. The cells were centrifuged (8000 × *g* for 3 min) and washed twice with a phosphate buffer (pH = 7.2), and a series of 10–100% ethanol was used for gradient dehydration. Each concentration was maintained for 15 min, and 100% dehydration was performed twice. Finally, the specimens were dried at room temperature (25°C) and sprayed with gold. The samples were used for SEM observation (FEI Nova NanoSem 450, working voltage: 15 kV, amplification factor: 80,000).

Detection of Intracellular Protein and Nucleotide Diffusion

After the sample was treated with 15 g/L butanol, the cells were collected by centrifugation (8000 × *g*, 4°C, 10 min) and washed and suspended in a phosphate buffer (pH = 7.2) to achieve a final concentration of 10^6–10^7 cells/mL. To ensure enzyme activity, all the samples were placed in an ice water bath for 2 h and then centrifuged (8000 × *g*, 4°C, 10 min) to collect the cells. The bicinchoninic acid (BCA) kit, Biyuntian, was used for protein determination. Following the BCA instruction,

the optical density (OD) of experimental group and Bovine Serum Albumin (BSA) standard group (0–200 μg/mL) were measured every 2 h at 560 nm after 37 h of incubation. The BSA standard group was used to draw the standard curve. In addition, the intracellular nucleotides were measured using the following formula: Nucleotide (μg/mL) = (11.87 × OD_{260} −10.40 × OD_{280}) × 100/9, where OD_{260} and OD_{280} are the optical density of the bacterial suspension at 260 and 280 nm, respectively.

Experimental Design and Validation by RSM

Based on the Box-Behnken design, the Design-Expert 8.0.6 software was used to analyze and select butanol concentration (X_1), temperature (X_2), and pH (X_3) as the investigation factors. The butanol production (Y) was the response value, and the RSM was used to evaluate the effects of three important factors on butanol fermentation and butanol tolerance of the carbon ion beam-irradiated mutant. The effect of each variable was studied at three different coded levels (−1, 0, +1) with low, medium, and high values (**Table 1**). The RSM analysis regression model is given by

$$Y = \beta_0 + \sum_{i=1}^{3} \beta_i X_i + \sum_{i=1}^{3} \beta_{ii} X_i^2 + \sum_{i<j=2}^{3} \beta_{ij} X_i X_j,$$

where Y is the predicted response, β_0 the offset term,β_i the linear coefficient,β_{ii} the squared coefficient,β_{ij} the interaction coefficient, and X_i and X_j are the independent variables.

Analytical Methods

The pH of the fermentation broth was measured using a Mettler Toledo pH meter (Giesen, Germany). Before the analysis of the product concentration, the fermentation broth was analyzed by centrifugation at 8000 *g* for 5 min, and the supernatant was filtered using a 0.22 μm syringe filter. Solvents (acetone, ethanol, and butanol) and acids (acetic acid and butyric acid) were determined by 456-GC gas chromatography (Bruker, Germany) on a HP-INNOWAX column (30 m × 0.320 mm × 0.50 μm; Agilent J&W, United States) equipped with a flame ionization detector.

Statistical Analysis

All experiments were performed at least three times and all the data were reported as mean ± SD. Statistical analysis software (Microsoft Excel 2016) was used to analyze the statistical significance of the experimental data, and $p < 0.05$ indicated a significant difference and $p < 0.01$ indicated a highly significant difference. RSM experiments were analyzed by ANOVA.

TABLE 1 | Actual values and level values of the variables employed in RSM.

Variables	Range and level		
	−1	0	+1
X_1: Butanol(g/L)	6	8	10
X_2: Temperature(°C)	34	36.5	39
X_3: pH	6.2	6.8	7.4

RESULTS

Survival and Mutagenesis of *C. acetobutylicum* Irradiated With the Carbon Ion Beam

This test successfully applied carbon ion beam irradiation to *C. acetobutylicum*. Due to a lack of reference conditions for the carbon ion beam irradiation of *C. acetobutylicum*, we investigated the survival fractions using six doses of carbon ion beam irradiation in this test, based on reference doses for other microbial strains irradiated with the carbon ion beam. Survival fraction reflects the damage degree to organisms caused by external stimuli. Studying the survival fraction of *C. acetobutylicum* cells after heavy ion beam irradiation can be used to evaluate the damage degree of *C. acetobutylicum* cells from heavy ion beams. It is also used to determine the optimal irradiation dose. The survival curve of *C. acetobutylicum* ATCC 824 cells after carbon ion beam irradiation was measured using a plate colony counting method. **Figure 1A** shows that at 30, 60, 90, 120, 150, and 200 Gy, the survival fractions were 0.85, 0.68, 0.51, 0.32, 0.25, and 0.14, respectively. With the increase in the irradiation dose, the survival fraction showed a significant downward trend. The 50% lethal dosage was 90 Gy and after 200 Gy irradiation, the cell survival fraction reduced to 14%. In this study, mutants were obtained using the higher carbon ion irradiation dose (120 Gy), causing a higher cell mortality (approaching 70%).

After two rounds of selective plate primary screening and secondary fermentation screening, five mutants with higher biobutanol accumulation were screened and selected. In comparison with the wild-type strain, butanol production by the screened strains Y007, Y009, Y207, Y217, and Y218 was greatly improved in terms of the final butanol concentration (**Figure 1B**). The wild-type strain and the five mutants, Y007, Y009, Y207, Y217, and Y218 could synthesize (9.78 ± 0.23), (13.61 ± 0.35), (13.39 ± 0.49), (11.58 ± 0.12), (13.60 ± 0.19), and (13.25 ± 0.39) g/L butanol, respectively. The increase in butanol production was considerable for the Y007, Y009, Y217, and Y218 strains, which showed the greatest production ability with an increase of 35–39% in butanol production. These results show that carbon ion beam irradiation can be applied as a useful candidate tool in *C. acetobutylicum* breeding.

Fermentation Kinetic Characteristics of the Wild-Type Strain and Mutants

The screw-capped bottle fermentation characteristic curves for the wild-type and five mutant strains are shown in **Figure 2**. There is a significant difference in final product concentrations; the five mutant strains produced higher butanol concentrations than the wild-type strain (9.81 g/L butanol). Y007, Y009, Y207, Y217, and Y218 produced 13.69, 13.30, 11.40, 13.50, and 13.10 g/L of butanol, respectively. Among them, mutant Y009 and Y207 reached the highest concentrations in 66 h, i.e., 6 h before the

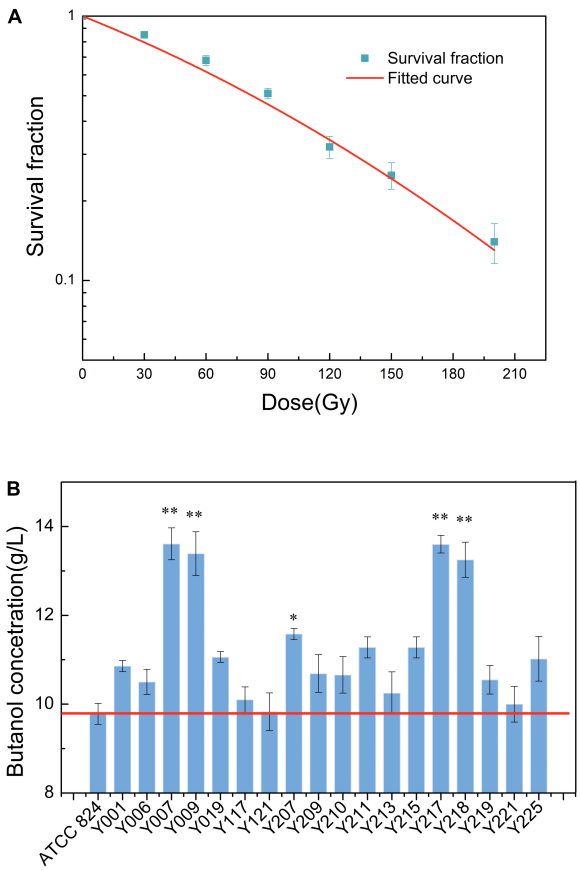

FIGURE 1 | (A) Survival fraction of *C. acetobutylicum* ATCC 824 treated with different doses (30, 60, 90, 120, 150, and 200 Gy) of carbon ion beam irradiation. **(B)** Carbon ion beam irradiation screening for high butanol-production mutants. Data of the total butanol concentrations of the mutants in 250 mL screw-capped bottles after carbon ion beam irradiation mutagenesis are presented. Y001–Y225 denote the mutants. $^{*}p < 0.05$, $^{**}p < 0.01$.

other strains (**Figures 2C,D**). The butanol productivity of Y009 reached 0.2 g/L/h, which indicates a 47.79% improvement over that of the wild-type strain. Correspondingly, the total solvents production of the five mutant strains was 18.38, 18.03, 16.59, 19.86, and 18.77 g/L, respectively, each of which was above the wild-type (15.46 g/L). Acid production by all strains showed a similar tendency, namely that it increased significantly before 20 h and then decreased gradually. The total acid (acetic acid and butyric acid) concentrations in cultures of the five mutant strains were 1.29, 1.35, 1.66, 1.41, and 1.63 g/L, respectively, each lower than that of the wild-type strain (3.20 g/L). Compared to the wild-type strain, butanol in Y007 and Y009 constituted over 70% of the total solvents. Strain Y217 (The raw sequence data of Y217 have been deposited in the Genome Sequence Archive in National Genomics Data Center, Beijing Institute of Genomics, Chinese Academy of Sciences, under accession number CRA003426, see **Supplementary Material** for details), with high butanol and solvent characteristics, selected from the 120 Gy irritated bacterial suspension, was chosen to be the experimental subject.

Discrepant Genetic Stability of Mutants

We determined the genetic stability of the mutant using consecutive generation experiments. We evaluated the genetic stability of the mutant by measuring the growth intensity and the butanol, ethanol, and acetone contents for 1–12 generations. For each strain, the change of measured value of each investigation index by generation was well linearly fitted, and the slope of the fitted straight line approached 0, which indicated that the measured indexes were very stable within the 12th generation of the mutant (**Figure 3**). In addition, the growth ability and fermentation performance of the mutant were significantly higher than the wild-type strain. These results indicate that the carbon ion beam mutagenesis technique can generate genetically stable microbial strains with strong product metabolite accumulation ability.

Intracellular Protein and Nucleotide Diffusion of *C. acetobutylicum* Under Butanol Stress

Figures 4A,B show the changes of the cell membrane surface produced by the two strains under the stimulation of 15 g/L butanol. It can be seen from the comparison that 15 g/L butanol caused a certain degree of damage to the surface of ATCC 824 cells, and the surface was wrinkled or even damaged, while Y217 maintained a complete and full surface morphology. Results of intracellular protein penetration and nucleotide diffusion detection of *C. acetobutylicum* ATCC 824 and Y217 under butanol stimulation are shown in **Figure 4**. It can be seen from **Figure 4C** that the protein penetration of ATCC 824 increases with extension of exposure time, and the osmolality gradually stabilizes after 10 h. Additionally, **Figure 4D** shows that the diffusion rate of ATCC 824 stagnated during 0–2 h and reached the logarithmic period of nucleotide diffusion from 4 to 8 h. It remained stable after 8 h, and the overall change trend was S-shaped. During the whole exposure time of Y217, no obvious protein penetration and nucleotide diffusion were observed.

Butanol Tolerance Was Verified by RSM

In this experiment three factors, including butanol (X_1), temperature (X_2), and initial pH (X_3), were used as independent variables, and the butanol production (Y) was used as the response value. The response surface analysis plan was designed to include 12 response surface analysis test points and five center points per block. The factors and levels of response surface analysis are shown in **Table 1**, and the test design and test results are shown in **Table 2**. Using Design Expert software, the response value and three factors are regression-fitted, and the ternary quadratic regression equation of Y to X_1, X_2, X_3 is:

$$Y = 8.46 - 0.14X_1 + 0.025X_2 + 0.21X_3 - 0.085X_1X_2 - 0.015X_1X_3 - 0.25X_2X_3 - 0.66X_1^2 - 0.57X_2^2 - 0.32X_3^2$$

The determination coefficient of the regression model $R^2 = 0.9752$ indicates that 97.52% change in response value comes from the selected variable, and only 2.48% total variation exists.

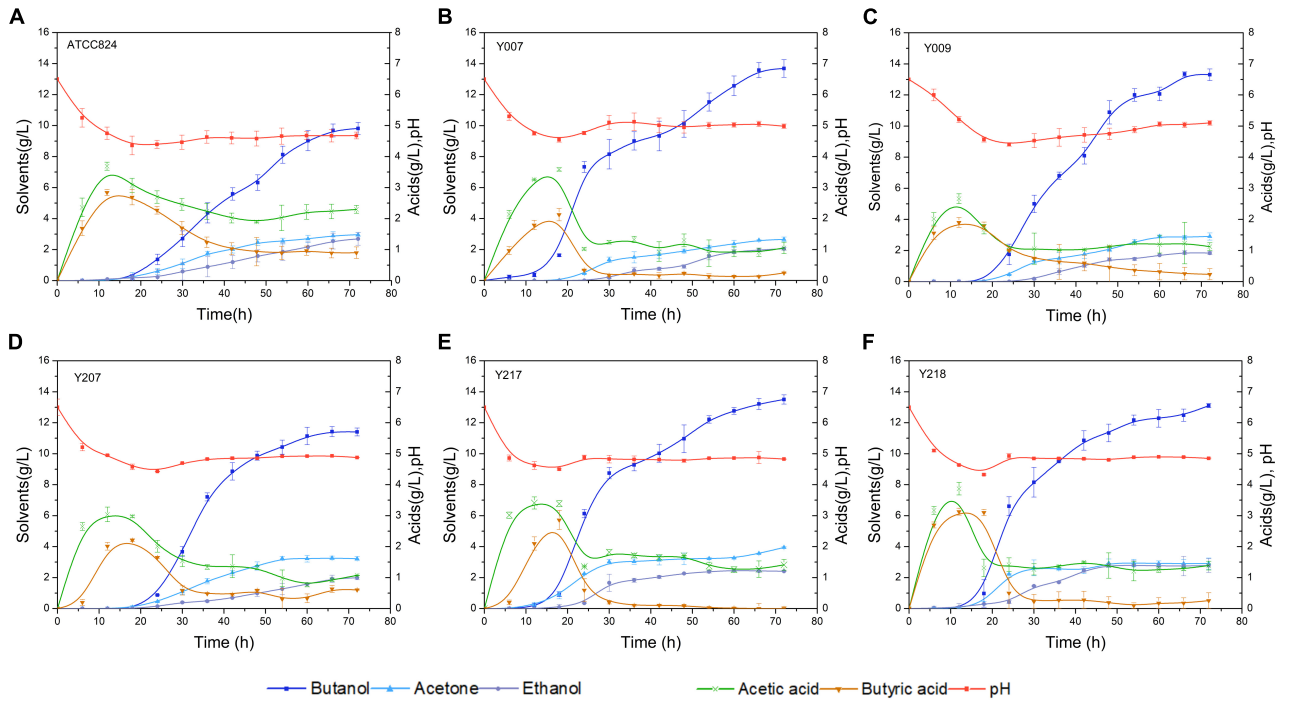

FIGURE 2 | Batch fermentation kinetics of wild-type strain and five mutants in 250 mL screw-capped bottles with an initial corn powder concentration of 70 g/L. **(A)** *C. acetobutylicum* ATCC 824. **(B)** Y007, **(C)** Y009, **(D)** Y207, **(E)** Y217, and **(F)** Y218. The data are the averages of three replicated experiments, and the error bar represents the standard deviation.

R^2 (adjusted) = 0.9433, which is close to the correlation coefficient (R^2) and is greater than 0.9, indicating that the test is highly reliable. Analysis of ANOVA (**Table 3**) of the regression model shows that *p*-value (Prob > F) is less than 0.0001, which indicates that model terms are significant. The lack of fit is not significant, indicating that the unknown error factors have little interference with the experimental results which indicate that the model fits well. Among the three factors, X_1, X_3, X_2 X_3, X_1^2, X_2^2, *and* X_3^2 all have significant effects. Comparing the *F* values, shows that the order of influence on butanol production is: (X_3) pH>(X_1) Butanol>(X_2) Temperature.

The response surfaces and contours of the interaction between the added butanol and temperature, the added butanol and pH, and the temperature and pH, were drawn by the Design-Expert 8.0.6 software, and the results were shown in **Figures 5A–F**. **Tables 2**, **3** and **Figure 5**, combined with the regression equation, indicate that the best conditions for the mutant to produce butanol when exogenous butanol is added are as follows: exogenous butanol, 7.79 g/L; temperature, 36.39°C; and initial pH, = 7.01. Under these fermentation conditions, the butanol production theoretical value is 8.49 g/L. To verify the practicability and accuracy of the model, the fermentation conditions were modified to add 7.8 g/L butanol exogenously, the fermentation temperature was 36.4°C, and initial pH = 7. Through the verification test, the final experimental result was 8.35 g/L. The output of butanol under optimal conditions is basically close to the theoretical value, indicating that the parameters of this model are reliable.

DISCUSSION

Carbon ion beam irradiation has a high mutation rate, and is an effective mutation-production method that has been widely used in industrial microbial breeding. Therefore, carbon ion beam irradiation can be an effective means to induce significant changes in the physiological characteristics of microorganisms. The mutant strain of baker's yeast, with a high yield of β-glucan and screened by carbon ion beam irradiation, was optimized under laboratory fermentation conditions, and its yield was 1.73 times higher than that of the original strain YS-00 (Li et al., 2017). Although carbon ion beam irradiation has been universally used in plant and microorganism breeding, it has not been widely reported in the breeding of *C. acetobutylicum*. In this study, we found that carbon ion beam irradiation can boost the butanol production characteristics of *C. acetobutylicum*. Due to the lack of reference mutagenesis conditions, a series of carbon ion irradiation doses was applied according to the previous reports on the use of carbon ion irradiation for the breeding of microorganisms (Ma et al., 2013). The results revealed that an increase in irradiation doses enhances the mortality rate from 15 to 86% (**Figure 1A**). According to our experience in mutagenesis breeding, high mutation rates often accompany high mortality (Ma et al., 2013). Thus, nearly 2000 clones, with a mortality rate of at least 50%, were selected for further mutation screening under irradiation doses of 90, 120, 150, and 200 Gy. The results revealed that carbon ion beam irradiation has obvious mutation effects on *C. acetobutylicum*. With an increase in irradiation

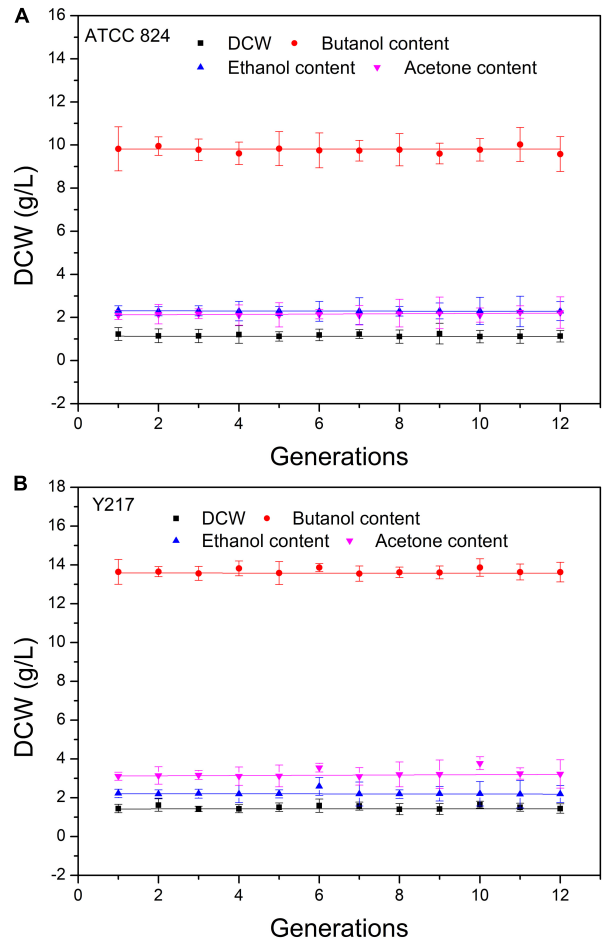

FIGURE 3 | Stability of mutant and the wild-type strain cell dry weight (DCW), butanol content, ethanol content, and acetone content were evaluated for 1–12 generations. **(A)** *C. acetobutylicum* ATCC 824. **(B)** Y217. The detected values of the indexes and generations were linearly fitted with slopes approaching 0.

dose, the lethality of *C. acetobutylicum* irradiation was enhanced, demonstrating that *C. acetobutylicum* is sensitive to high linear energy transfer (LET) carbon ion beam irradiation.

Based on the study of the fermentation kinetic curves of the five mutant strains, we aimed to select the one with the best performance as the research object for the follow-up experiment. Results showed that the butanol yield of Y007 and Y217 both exceeded 13.50 g/L, and that of Y007 reached 13.69 g/L. The two strains with the highest total solvent yield were Y217 and Y218, and Y217 was 19.86 g/L, indicating the fermentation performance of Y217 was excellent. Although the butanol yield of Y009 only reached 13.30 g/L, the total fermentation time of Y009 was 6 h shorter than other strains, and the productivity was 0.20 g/L/h, reaching the high production rate reported in the literature. The butanol yield of the Y207 strain was the lowest of those five mutants (11.40 g/L), but it reached the highest butanol concentration at 66 h, indicating that it shortened the fermentation time to some extent. The final concentration of acid in the fermentation medium of the five mutants was lower than that of the wild-type strain, indicating that the conversion rate of mutants increased during the acidogenesis-solventogenesis transformation period. Many studies have explored both external and internal factors that contribute to the transition from acid to solvent (Heipieper et al., 2007; Yang and Zhao, 2013). External factors include extracellular pH, extracellular undissociated acid concentration, nutritional factors, and temperature. Intracellular factors include intracellular pH, intracellular NAD(P), intracellular ATP/ADP, intracellular butyryl CoA, and butyryl phosphate concentration. Extracellular pH is considered the key factor determining the effect of fermentation to produce solvents. When the extracellular pH is high the bacteria mainly produce acid. When the extracellular pH is low the bacteria tend to produce solvents (Guo et al., 2013; Yang and Zhao, 2013). However, the pH scope for promoting bacterial-producing solvents is different for different strains and fermentation conditions (Yang et al., 1992; Kilonzo et al., 2009). The optimum pH range for solvent production of *C. acetobutylicum* ATCC 824 was 5.5–4.3. The experiment result shows that the acid production of Y007 and Y217 in acidogenesis was high, and the extracellular pH was 4.54 and 4.50, respectively, which may promote the occurrence of an acidogenesis-solventogenesis transformation period, during which acetic acid and butyric acid can be transformed to acetone and butanol in solventogenesis. The increase of pH in the fermentation broth reduced the toxicity of acid to cells, and thus increased the butanol yield. As shown in **Figure 2F**, strain Y218 had the highest acid yield compared with other strains in the acid production stage, but its butanol yield and total solvent yield were not suitable, and its final acid concentration was higher than that of Y007 and Y217. It is evident that the fermentation phenotypes of the five mutants were related to the complex changes during acidogenesis, solventogenesis, and acidogenesis-solventogenesis transformation stages. So far, there is no consensus on the regulation of the transition from the acid-producing stage to the solvent-producing stage (Heipieper et al., 2007). This complex physiological change may not be caused by a single factor, and there may be a mechanism of multifactor coordinated comprehensive regulation. These five mutants were mutated in different directions, and eventually increased the yield of butanol. They were independent strains that were different from each other. Based on the consideration of butanol, total solvent yield, and final acid quantity, we finally chose Y217 for the determination of genetic stability. Its growth (DCW), acetone, butanol, and ethanol yields were very stable within 12 generations. Results showed that carbon ion beam radiation mutagenesis, as an effective breeding method, could be successfully applied to the breeding of *C. acetobutylicum* strains with high yield. Jiang et al. (2018) used CGM medium with 60 g/L glucose to determine the solvent production capacity of the wild-type strain and mutant with heavy ions beam irradiation, and found that the butanol concentration of the irradiated strain was 8.096 g/L for 60 h, which was 1.959 g/L higher than the control. In this study, Y217 could stably produce butanol 13.67 g/L with 70 g/L corn powder, which was 3.9 g/L higher than the control (9.77 g/L).

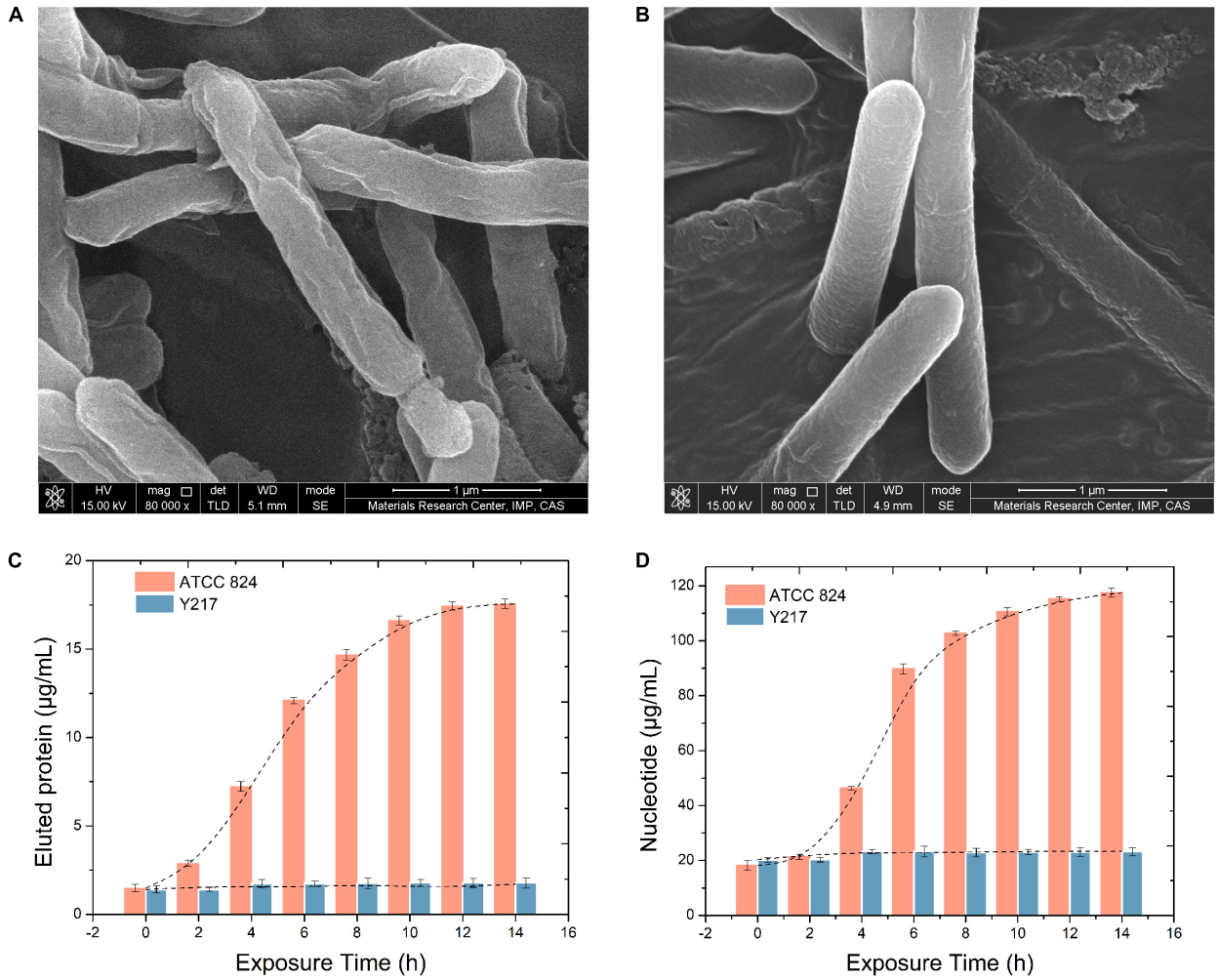

FIGURE 4 | SEM images of ATCC 824 **(A)** and Y217 **(B)** cultivated in a butanol medium (15 g/L). Intracellular protein penetration **(C)** and nucleotide diffusion **(D)** of *C. acetobutylicum* under 15 g/L butanol stress. The leakage trend of ATCC 824 is S-shaped.

In the process of microbial fermentation, whether the target product can be transferred to the extracellular optimally is very important. The growth and metabolism of microorganisms are directly related to the selective permeability of the membrane to compound in and out (Yang et al., 2015; Guan et al., 2018). The permeability of the cell membrane is changed, allowing intracellular metabolites to leak out of the cell quickly, thereby preventing the accumulation of metabolites in the cell and releasing the feedback regulation effect of the end product, and thus increasing the fermentation product (Wei et al., 2006; Hao, 2007). However, changes in cell membrane permeability are also beneficial for nutrients entering the cell, and can promote cell metabolism (Hao, 2007). Studies have also been conducted on the application of ultrasound technology to enhance cell membrane permeability in the butanol fermentation process, and promising results have been achieved. When the culture was sonicated at 0 h for 15 min, butanol and total solvent production were 30.2 and 22.8% higher than those of the control group, respectively (Qureshi and Maddox, 2005; Nitayavardhana et al., 2010). **Figure 4** shows that under butanol stimulation cell integrity of Y217 remains basically stable. After 4 h of butanol stimulation there was a very slight increase in permeability, and then a relatively balanced cell membrane permeability was maintained, indicating that within 4 h the cell membrane was in the delayed period of butanol stimulation. It is reasonable to assume that the cell membrane was responding to butanol stimulation during this period. Four hours later a moderate increase in membrane permeability increased the extent to which the Y217 strain transported the intracellular butanol product to the outside of the cell to reduce product inhibition, and thereby increased butanol production. Without lethal effect, 15 g/L butanol increased membrane permeability of Y217 and had a positive effect on butanol production. In contrast, 15 g/L butanol is fatal to ATCC 824, resulting in excessive intracellular extravasation and ultimately, loss of cell fermentability or death. Transmembrane transport and phosphorylation of glucose and other substances also depend on favorable membrane permeability. A key factor in determining

TABLE 2 | Design and results of response surface experiments.

Run No.	X_1:Butanol(g/L)		X_2:Temperature(°C)		X_3:pH		Y:Butanol(g/L)	
	Coded	Actual	Coded	Actual	Coded	Actual	Experimental	Predicted
1	−1	6.00	−1	34.00	0	6.80	7.22	7.25
2	−1	6.00	0	36.50	−1	6.20	7.28	7.38
3	0	8.00	−1	34.00	−1	6.20	7.22	7.09
4	0	8.00	−1	34.00	1	7.40	7.92	8.00
5	0	8.00	0	36.50	0	6.80	8.48	8.46
6	−1	6.00	0	36.50	+1	7.40	7.94	7.84
7	0	8.00	0	36.50	0	6.80	8.46	8.46
8	0	8.00	0	36.50	0	6.80	8.48	8.46
9	+1	10.00	+1	39.00	0	6.80	7.06	7.03
10	0	8.00	0	36.50	0	6.80	8.32	8.46
11	+1	10.00	0	36.50	−1	6.20	7.04	7.15
12	−1	6.00	+1	39.00	0	6.80	7.50	7.47
13	0	8.00	+1	39.00	+1	7.40	7.42	7.56
14	0	8.00	0	36.50	0	6.80	8.54	8.46
15	+1	10.00	−1	34.00	0	6.80	7.12	7.15
16	0	8.00	+1	39.00	−1	6.20	7.70	7.63
17	+1	10.00	0	36.50	+1	7.40	7.64	7.54

TABLE 3 | ANOVA for response surface quadratic model.

Source	Sum of Squares	Degree of freedom	Mean square	*F* value	*P* value Prob > *F*
Model	4.80	9	0.53	30.56	< 0.0001**
X_1-Butanol	0.15	1	0.15	8.36	0.0233*
X_2-Temperature	5.000E-003	1	5.000E-003	0.29	0.6090
X_3-pH	0.35	1	0.35	20.22	0.0028**
X_1X_2	0.029	1	0.029	1.66	0.2390
X_1X_3	9.000E-004	1	9.000E-004	0.052	0.8268
X_2X_3	0.24	1	0.24	13.76	0.0076**
X_1^2	1.84	1	1.84	105.29	< 0.0001**
X_2^2	1.37	1	1.37	78.55	< 0.0001**
X_3^2	0.43	1	0.43	24.79	0.0016**
Residual	0.12	7	0.017		
Lack of Fit	0.095	3	0.032	4.76	0.0829
Pure Error	0.027	4	6.680E-003		
Cor Total	4.92	16			
R-Squared	0.9752				
Adj R-Squared	0.9433				

*"**" means that the difference is extremely significant ($P < 0.01$); "*" means that the difference is significant ($P < 0.05$).*

whether nutrients can be used by microorganisms is if these nutrients can enter microbial cells. Only after the nutrients enter the cell can they be decomposed and utilized by the metabolic system, which in turn allows the normal growth and metabolism. Phosphoenolpyruvate-carbohydrate phosphotransferase system (PTS) is the main way for carbohydrates to enter the cells of *C. acetobutylicum*. Sugars such as glucose, fructose, and mannose are phosphorylated, mainly by the PTS system located on and in the membrane, and then enter the cell in the form of phosphorylated sugar (Lengeler, 1996). The diffusion of macromolecules under the action of butanol by Y217 and ATCC 824 shows that the same butanol concentration has a completely different effect on different strains. The toxic effects of solvents on bacteria mainly results in damage to the cell membrane (Weber and de Bont, 1996). Some prior studies indicate that engineering strategies regulating the membrane composition can be a potential target in the future for tuning membrane permeability to increase the stress tolerance of industrial strains. Thus, we believe that Y217 may be able to adapt to the solvent and improve the tolerance by changing the lipid composition of the membrane structure and membrane protein functions. Thus, Y217 may resist cell membrane permeability damage caused by butanol stress, maintain the proton gradient and cell electron potential, and avoid cell inactivation or death caused by the large leakage of intracellular proteins and nucleic acids due to the increased permeability (Ezeji et al., 2010;

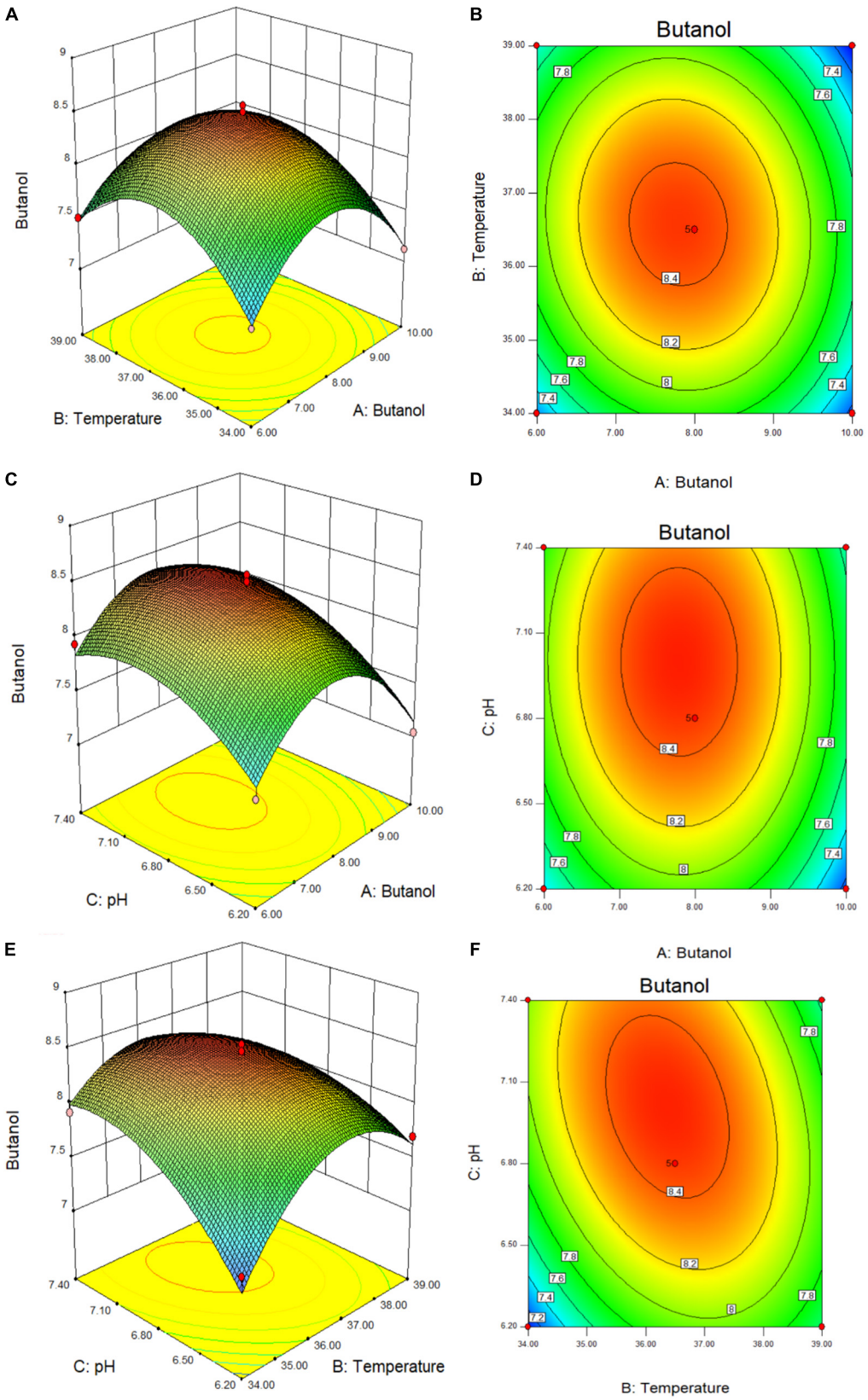

FIGURE 5 | 3D surfaces **(A–C)** and contour plots **(D–F)** of butanol produced by *C. acetobutylicum* mutant (Y217), showing interactions among three factors (exogenous butanol, temperature, and pH).

Isar and Rangaswamy, 2012). RSM analysis was used to verify the ability of Y217 to withstand high concentrations of butanol stress.

The 3D surface plots and contour plots of RSM are shown in the **Figure 5**. The 3D surface plot depicts the interaction between the other two variables in the experimental range when one of the variables remains constant at zero (Lin et al., 2011; Al-Shorgani et al., 2015). The slope of the surface reflects the strength of the interaction between the two experimental factors. Similarly, different shapes of contour plots indicate different interactions between variables. When there is perfect interaction between variables an elliptical profile is obtained. The response surface curve shows the influence of the interaction between various factors on the fermentation butanol (Sun et al., 2020). The steeper the response surface curve, the stronger is the interaction. If the contour line is elliptic, it indicates that the interaction of this factor has a great influence on the fermentation butanol. **Figures 5A,B** show that the contour line is oval, indicating that the added butanol concentration and temperature have a strong interaction. Furthermore, **Figures 5C,D** show that the gradient of added butanol concentration and pH is very steep, indicating that they have a great influence on the butanol production. Moreover, the contour line along the butanol addition axis is denser than the pH, indicating that when the two interact the external butanol addition has a greater influence on butanol fermentation than pH. From **Figures 5E,F**, it can be seen that the contour line is elliptic and that the response surface is extremely steep, indicating that temperature and pH interact, and the effect on the fermentation butanol differed significantly. RSM is commonly used to optimize fermentation process conditions to increase butanol and solvent production. Long et al. (2013) used fresh plantain as raw material to produce butanol with *C. acetobutylicum* CICC 8012. The central composite design was used to optimize the fermentation conditions and establish a mathematical model with butanol yield as the response value. Under optimized conditions butanol fermentation yield reached 12.73 g/L. Figueroa-Torres et al. (2020) evaluated the yield of ABE fermentation solvents under different initial medium concentrations of acetic acid and butyric acid by response surface analysis. In this study, RSM was used to verify the butanol tolerance of Y217, which can grow normally and ferment to produce butanol 7.04–8.54 g/L in 6–10 g/L added-butanol medium. The optimal conditions obtained by model optimization are: in 7.8 g/L butanol medium, 8.35 g/L butanol can be produced, and the final butanol concentration at the end of fermentation can reach 16.15 g/L, indicating that Y217 is also a high-tolerance butanol strain with good fermentation performance. To investigate the relevant mechanisms of butanol tolerance of strains, we will conduct extensive research on the cellular and genetic levels in the future.

CONCLUSION

In this study, we demonstrated the excellent butanol production and tolerance of mutant Y217 selected by carbon ion beam irradiation. The maintenance of its cell membrane surface structure and permeability under butanol stress, in particular, was demonstrated. The organic solvent environmental stress can cause changes in the structure of the protein or lipid molecules that make up the membrane structure such that while the fluidity of the cell membrane is affected, the permeability of the plasma membrane is often increased, and the selective permeability is reduced. External leakage causes changes in the structure and function of the cell membrane. Therefore, the cell membrane of the mutant Y217 not only forms a permeability barrier that regulates the entry channel between the cell and the external environment, but also has special significance for intracellular energy conduction, and different cell membrane structures directly affect the solvent resistance of the mutant. Therefore, further studies should explore the physiological and biochemical characteristics of cell membranes; further, the relevant metabolic mechanisms can be understood using omics to provide a theoretical basis for future breeding and construction of high-quality production bacteria.

DATA AVAILABILITY STATEMENT

The original contributions presented in the study are included in the article/**Supplementary Material**, further inquiries can be directed to the corresponding author.

AUTHOR CONTRIBUTIONS

DL and XZ coordinated and supervised the project. YG designed the experiments and wrote the manuscript. YG and CL analyzed the data. YG, MZ, and XG performed the experiments. MZ, DL, and WL corrected the manuscript. All authors read and approved the final manuscript.

FUNDING

This study was supported by the National Natural Science Foundation of China (11975284 and 11905265), Science and Technology Service Network Initiative of Chinese Academy of Sciences (KFJ-STS-QYZD-197), and Project of Lanzhou Science and Technology 2019-1-39. The funders had no role in study design, data collection and analysis, decision to publish, or preparation of the manuscript.

ACKNOWLEDGMENTS

We sincerely thank the National Laboratory of HIRFL and the National Natural Science Foundation of China for giving us opportunity to perform this project.

SUPPLEMENTARY MATERIAL

The Supplementary Material for this article can be found online at: https://www.frontiersin.org/articles/10.3389/fmicb.2020.602774/full#supplementary-material

REFERENCES

Al-Shorgani, N. K. N., Isa, M. H. M., Yusoff, W. M. W., Kalil, M. S., and Hamid, A. A. (2015). Response surface methodology for biobutanol optimization using locally isolated *Clostridium acetobutylicum* YM1. *Int. J. Green. Energy* 12, 1236–1243. doi: 10.1080/15435075.2014.895738

Dadgar, A. M., and Foutch, G. L. (1988). Improving the acetone-butanol fermentation process with liquid-liquid extraction. *Biotechnol. Progr.* 4, 36–39. doi: 10.1002/btpr.5420040107

Dhamole, P. B., Wang, Z., Liu, Y., Wang, B., and Feng, H. (2012). Extractive fermentation with non-ionic surfactants to enhance butanol production. *Biomass. Bioenerg.* 40, 112–119. doi: 10.1016/j.biombioe.2012.02.007

Ebrahimi, E., Amiri, H., Asadollahi, M. A., and Shojaosadati, S. A. (2020). Efficient butanol production under aerobic conditions by coculture of *Clostridium acetobutylicum* and *Nesterenkonia* sp. *strain F. Biotechnol. Bioeng.* 117, 392–405. doi: 10.1002/bit.27221

Ezeji, T., Milne, C., Price, N. D., and Blaschek, H. P. (2010). Achievements and perspectives to overcome the poor solvent resistance in acetone and butanol-producing microorganisms. *Appl. Microbiol. Biotechnol.* 85, 1697–1712. doi: 10.1007/s00253-009-2390-0

Figueroa-Torres, G. M., Wan, Mahmood, W. M. A. W., Pittman, J. K., and Theodoropoulos, C. (2020). Microalgal biomass as a biorefinery platform for biobutanol and biodiesel production. *Biochem. Eng. J.* 153:107396. doi: 10.1016/j.bej.2019.107396

Guan, W., Shi, S., and Blersch, D. (2018). Effects of Tween 80 on fermentative butanol production from alkali-pretreated switchgrass. *Biochem. Eng. J.* 135, 61–70. doi: 10.1016/j.bej.2018.03.015

Guo, T., He, A. Y., Du, T. F., Zhu, D.-W., Liang, D.-F., Jiang, M., et al. (2013). Butanol production from hemicellulosic hydrolysate of corn fiber by a *Clostridium beijerinckii* mutant with high inhibitor-tolerance. *Bioresource. Technol.* 135, 379–385. doi: 10.1016/j.biortech.2012.08.029

Guo, X., Zhang, M., Gao, Y., Cao, G., Yang, Y., Lu, D., et al. (2019). A genome-wide view of mutations in respiration-deficient mutants of *Saccharomyces cerevisiae* selected following carbon ion beam irradiation. *Appl. Microbiol. Biotechnol.* 103, 1851–1864. doi: 10.1007/s00253-019-09626-0

Hao, W. (2007). Principle and application of metabolic engineering for microbiology. *Biotechnol. Bull.* 5, 18–23. doi: 10.13560/j.cnki.biotech.bull.1985.2007.05.005

Heipieper, H. J., Neumann, G., Cornelissen, S., and Meinhardt, F. (2007). Solvent-tolerant bacteria for biotransformations in two-phase fermentation systems. *Appl. Microbiol. Biotechnol.* 74, 961–973. doi: 10.1007/s00253-006-0833-4

Hu, W., and Chen, J. H. (2012). Mutation breeding of *Aspergillus niger* for producing citric acid by heavy ion beam. *J. Radiat. Res. Radiat. Process.* 30, 53–57. doi: 10.11889/j.1000-3436.2012.rrj.30.120110

Isar, J., and Rangaswamy, V. (2012). Improved n-butanol production by solvent tolerant *Clostridium beijerinckii*. *Biomass. Bioenerg.* 37, 9–15. doi: 10.1016/j.biombioe.2011.12.046

Jiang, T. T., Zhou, X., and Liang, Y. (2018). A small-scale investigation process for the *Clostridium acetobutylicum* production of butanol using high-energy carbon heavy ion irradiation. *Eng. Life Sci.* 18, 721–731. doi: 10.1002/elsc.201800090

Jiaquiang, E., Pham, M. H., Deng, Y., Nguyen, T., Duy, V. N., Le, D. H., et al. (2018). Effects of injection timing and injection pressure on performance and exhaust emissions of a common rail diesel engine fueled by various concentrations of fish-oil biodiesel blends. *Energy* 149, 979–989. doi: 10.1016/j.energy.2018.02.053

Kikuchi, R., Gerardo, R., and Santos, S. M. (2009). Energy lifecycle assessment and environmental impacts of ethanol biofuel. *Int. J. Energ. Res.* 33, 186–193. doi: 10.1002/er.1435

Kilonzo, P., Margaritis, A., and Bergougnou, M. (2009). Airlift-driven fibrous-bed bioreactor for continuous production of glucoamylase using immobilized recombinant yeast cells. *J. Biotechnol.* 143, 60–68. doi: 10.1016/j.jbiotec.2009.06.007

Kumar, M., Goyal, Y., Sarkar, A., and Gayen, K. (2012). Comparative economic assessment of ABE fermentation based on cellulosic and non-cellulosic feedstocks. *Appl. Energ.* 93, 193–204. doi: 10.1016/j.apenergy.2011.12.079

Lengeler, J. W. (1996). *The Phosphoenolpyruvate-Dependent Carbohydrate: Phosphotransferase System (PTS) and Control of Carbon Source Utilization. In: Regulation of Gene Expression in Escherichia coli*. Boston, MA: Springer.

Li, H. G., Luo, W., Gu, Q. Y., Wang, Q., Hu, W.-J., and Yu, X. B. (2013). Acetone, butanol, and ethanol production from cane molasses using *Clostridium beijerinckii* mutant obtained by combined low-energy ion beam implantation and *N*-methyl-*N*-nitro-*N*-nitrosoguanidine induction. *Bioresource. Technol.* 137, 254–260. doi: 10.1016/j.biortech.2013.03.084

Li, L. Q., Ma, L., and Li, W. J. (2017). The selection for high-yield β-glucan production mutant strain by 12C 6+ ion irradiation. *Food Sci. Technol.* 42, 2–6. doi: 10.13684/j.cnki.spkj.2017.03.003

Lin, Y., Wang, J., Wang, X., and Sun, X. (2011). Optimization of butanol production from corn straw hydrolysate by *Clostridium acetobutylicum* using response surface method. *Chin. Sci. Bull.* 56, 1422–1428. doi: 10.1007/s11434-010-4186-0

Liu, Y., Liu, H. J., Zhang, J. N., and Chen, Z. D. (2010). Optimization of biobutanol production strain *Clostridiuml beijerinckii* with xylose medium by response surface methodology. *Sci. Technol. Food. Ind.* 31, 194–196. doi: 10.13386/j.issn1002-0306.2010.07.040

Long, F., Jin, Y., Zhao, Y., Gao, X., and Li, Y. (2013). Optimization of butanol production from *Canna edulis Ker* by *Clostridium acetobutylicum* using response surface methodology. *Chin. J. Appl. Environ. Biol.* 19, 54–60. doi: 10.3724/SP.J.1145.2013.00054

Ma, Y., Wang, Z., Zhu, M., Yu, C., Cao, Y., Zhang, D., et al. (2013). Increased lipid productivity and TAG content in *Nannochloropsis* by heavy-ion irradiation mutagenesis. *Bioresource. Technol.* 136, 360–367. doi: 10.1016/j.biortech.2013.03.020

Nitayavardhana, S., Shrestha, P., Rasmussen, M. L., Lamsal, B. P., van Leeuwen, J. H., and Khanal, S. K. (2010). Ultrasound improved ethanol fermentation from cassava chips in cassava-based ethanol plants. *Bioresource. Technol.* 101, 2741–2747. doi: 10.1016/j.biortech.2009.10.075

Qi, Y. L., Liu, H., Chen, X. L., and Liu, L. M. (2019). Engineering microbial membranes to increase stress tolerance of industrial strains. *Metab. Eng.* 53, 24–34. doi: 10.1016/j.ymben.2018.12.010

Qureshi, N., and Maddox, I. S. (2005). Reduction in butanol inhibition by perstraction: utilization of concentrated lactose/whey permeate by *Clostridium acetobutylicum* to enhance butanol fermentation economics. *Food Bioprod. Process.* 83, 43–52. doi: 10.1205/fbp.04163

Sun, X., He, S., Ye, Y., Cao, X., Liu, H., Wu, Z., et al. (2020). Combined effects of pH and thermal treatments on IgE-binding capacity and conformational structures of lectin from black kidney bean (*Phaseolus vulgaris* L.). *Food. Chem.* 329:127183. doi: 10.1016/j.foodchem.2020.127183

Weber, F. J., and de Bont, J. A. (1996). Adaptation mechanisms of microorganisms to the toxic effects of organic solvents on membranes. *Biochim. Biophys. Acta* 1286, 225–245. doi: 10.1016/S0304-4157(96)00010-X

Wei, N., Li, B. L., and Ou, J. (2006). Role of cell membrane permeability control on fermentation metabolic. *Food Sci. Technol.* 9, 14–17. doi: 10.13684/j.cnki.spkj.2006.09.012

Xie, H., Wei, Z., Li, W., Yang, W., Wang, L., Feng, J., et al. (1995). Preliminary study of QDMS reproductive actinomyces induced by 7 mev/u o6+ ions. *J. Radiat. Res. Radiat. Process.* 13, 99–101.

Xin, F. X., Liu, J., He, M. X., Wu, B., Ni, Y., Dong, W., et al. (2018). High biobutanol production integrated with in situ extraction in the presence of Tween 80 by *Clostridium acetobutylicum*. *Process. Biochem.* 67, 113–117. doi: 10.1016/j.procbio.2018.01.013

Xue, L., Zhao, X., Chang, S., Zhang, H., Wu, Z., and Jin, C. (2010). A strain of high PHB output by mutagenesis of 80 MeV/u C-12 ions. *Nucl. Tech.* 33, 284–288.

Yan, Y. P., Lu, D., Wang, J., Lu, D., Dong, X., Gao, F., et al. (2009). Study on yeast mutant with high alcohol yield fermented in sweet sorghum juice using carbon ion irradiation. *Nucl. Phy. Rev.* 26, 269–273.

Yang, M., Zhang, J., Kuittinen, S., Vepsäläinen, J., Soininen, P., Keinänen, M., et al. (2015). Enhanced sugar production from pretreated barley straw by additive xylanase and surfactants in enzymatic hydrolysis for acetone-butanol-ethanol fermentation. *Bioresource. Technol.* 189, 131–137. doi: 10.1016/j.biortech.2015.04.008

Yang, S. T., Tang, I. C., and Zhu, H. (1992). A novel fermentation process for calcium magnesium acetate (CMA) production from cheese whey. *Appl. Biochem. Biotechnol.* 34, 569–583. doi: 10.1007/BF02920579

Yang, S. T., and Zhao, J. (2013). *Adaptive Engineering of Clostridium for Increased Butanol Production*. U. S. Patent No 8450093 B1. Washington, DC: U.S. Patent and Trademark Office.

Zhang, Y., Chen, J., Yang, Y., and Jiao, R. (1996). Breeding of high-ratio butanol strains of *Clostridicum acetobutylicum* and application to industrial production. *Ind. Microbiol.* 26, 1–6.

Zhang, Z., Jiaqiang, J., Chen, J., and Zhu, H. (2019). Effects of low-level water addition on spray, combustion and emission characteristics of a medium speed diesel engine fueled with biodiesel fuel. *Fuel* 239, 245–262. doi: 10.1016/j.fuel.2018.11.019

Conflict of Interest: The authors declare that the research was conducted in the absence of any commercial or financial relationships that could be construed as a potential conflict of interest.

frontiers in Bioengineering and Biotechnology

ORIGINAL RESEARCH
published: 04 February 2021
doi: 10.3389/fbioe.2020.579405

Anaerobic Co-digestion of Rice Straw and Pig Manure Pretreated With a Cellulolytic Microflora: Methane Yield Evaluation and Kinetics Analysis

*Bin Zhong†, Xuejiao An, Fei Shen†, Weijuan An and Qinghua Zhang**

Jiangxi Engineering Laboratory for the Development and Utilization of Agricultural Microbial Resources, College of Bioscience and Biotechnology, Jiangxi Agricultural University, Nanchang, China

OPEN ACCESS

Edited by:
Petra Patakova, University of Chemistry and Technology in Prague, Czechia

Reviewed by:
Apilak Salakkam, Khon Kaen University, Thailand
Hongxin Fu, South China University of Technology, China

***Correspondence:**
Qinghua Zhang
zqh_net@163.com

†These authors have contributed equally to this work

Specialty section:
This article was submitted to Bioprocess Engineering, a section of the journal Frontiers in Bioengineering and Biotechnology

Received: *02 July 2020*
Accepted: *21 December 2020*
Published: *04 February 2021*

Citation:
Zhong B, An X, Shen F, An W and Zhang Q (2021) Anaerobic Co-digestion of Rice Straw and Pig Manure Pretreated With a Cellulolytic Microflora: Methane Yield Evaluation and Kinetics Analysis. Front. Bioeng. Biotechnol. 8:579405. doi: 10.3389/fbioe.2020.579405

Agricultural wastes, such as rice straw (RS) and pig manure (PM), cause serious environmental pollution due to the non-existence of effective disposal methods. Urgent investigations are needed to explore how such wastes can be transformed into resources. In this study, we comprehensively assessed methane yield and kinetics of RS and PM anaerobic co-digestion, with or without pretreatment of a previously developed cellulolytic microflora, under conditions of their maximum organic loading rate. The anaerobic co-digestion results revealed that the cumulative methane production of RS and PM after bio-pretreatment was 342.35 ml $(g\text{-}VS)^{-1}$, which is 45% higher than that of the control group [236.03 ml·$(g\text{-}VS)^{-1}$]. Moreover, the kinetic analysis showed the first-order kinetic, while the modified Gompertz models revealed higher fitting properties ($R^2 \geq 0.966$). After bio-pretreatment, the hydrolytic constant, maximum accumulative methane production, and maximum methane production rates of RS and PM reached 0.46 day^{-1}, 350.79 ml·$(g\text{-}VS)^{-1}$, and 45.36 ml·$(g\text{-}VS)^{-1}$·day^{-1}, respectively, which were 77, 45.1, and 84.3% higher than those without pretreatment. Also, we found that the lag phase and effective methane production time after bio-pretreatment decreased from 2.43 to 1.79 days and 10.7 to 8.92 days, respectively. Upon energy balance evaluation, we reported a net energy output of 5133.02 kWh·ton^{-1} after bio-pretreatment. Findings from this present study demonstrated that bio-pretreatment of RS and PM mixtures with cellulolytic microflora could greatly enhance methane production and anaerobic digestion efficiency.

Keywords: agricultural waste, biological pretreatment, anaerobic co-digestion, methane, kinetics, energy balance

INTRODUCTION

As a traditional agricultural country, nearly 29.69 million hectares of land in China is under rice production. In 2019, for instance, the rice output was 209.61 million tons (National Bureau of Statistics, 2019). Notably, due to the high grass-to-valley ratio (1–1.5) of rice (Kainthola et al., 2019), a large amount of rice straw (RS) is produced. On the other hand, with the large-scale development of pig farming in China, the environmental pressure brought by pig manure (PM) is gradually increasing (Wang et al., 2018). RS and PM are thus regarded as two types of typical agricultural wastes causing environmental pollution owing to the lack of efficient disposal measures

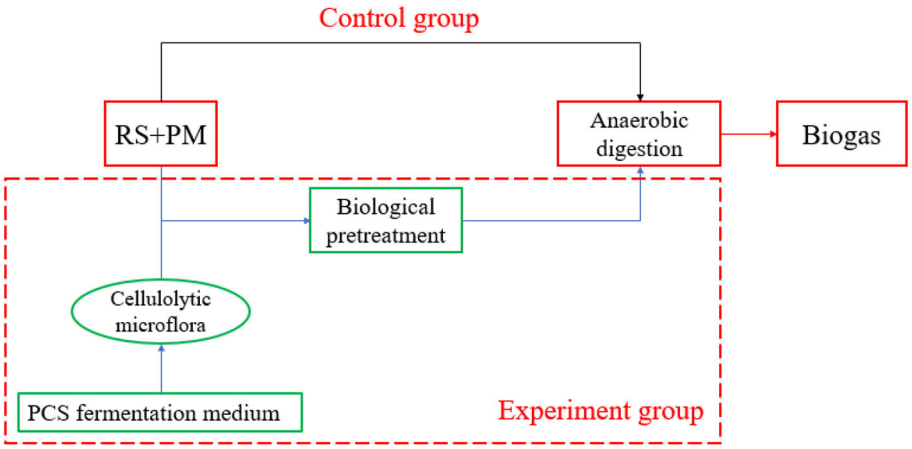

GRAPHICAL ABSTRACT | Flowchart with the followed procedure and methods.

(Chelme-Ayala et al., 2011; Yin et al., 2014). In previous studies, most of these wastes were processed either into feedstuffs or fertilizers (Qian et al., 2014); however, their utilization efficiencies remained relatively low. Therefore, there is an urgent need to explore new approaches to improve the utilization efficiency of these agricultural wastes.

Based on the current understanding, the bioconversion of these agricultural wastes into methane has attracted increasing attention across the globe (Deepanraj et al., 2015; Zhu et al., 2015; Andrew et al., 2018) for the advantages of low energy consumption, low equipment requirements, and milder operating conditions. It is generally believed that crop straw is rich in lignocellulosic content and a resultant high carbon/nitrogen (C/N) ratio, while this ratio in animal manure is relatively lower for its rich nitrogen content. Therefore, the direct digestion of these types of substrates will result in the lower conversion efficiency of organic carbon or ammonia accumulation (Yangin and Ozturk, 2013). To curb these drawbacks, mixing two or more types of substrates into an anaerobic digestion (AD) system (i.e., co-digestion) is regarded as one of the simple and acceptable strategies, which has received some positive impacts as highlighted by literature reports (Gopi et al., 2014; Logan and Visvanathan, 2019; Villa Gomez et al., 2019). However, the recalcitrant lignocellulosic structures of the substrates will still restrict the hydrolysis efficiency and further result in a lower methane yield (Karimi et al., 2013). Therefore, it is necessary to break up these recalcitrant structures using pretreatment strategies before AD. Compared with physicochemical methods, bio-pretreatment, especially through microbial co-culture methods (i.e., microflora), is more advantageous in terms of high enzymatic activity and lack of metabolite repression and feedback regulation problems (Haruta et al., 2002) and has attracted far much attention in recent AD research (Hu et al., 2016; Ali et al., 2017; Kong et al., 2018).

To further comprehend an AD system and predict its methane production, it is necessary to analyze the kinetics of methane production and evaluate the anaerobic performance. Generally, it is believed that AD has four phases, including hydrolysis, acidogenesis, acetogenesis, and methanogenesis. Currently, hydrolysis and methanogenesis have widely been investigated because most researchers believe that these phases greatly limit the dynamic process of AD (Taricska et al., 2011). In recent decades, numerous modeling studies using the modified Gompertz model, ADM1 model (Anaerobic Digestion Model No. 1), first-order kinetic model, cone model, Weibull model, and others have been carried out to characterize AD processes (Zhang et al., 2015; Lyu et al., 2019; Nguyen et al., 2019; Villamil et al., 2019). Among these models, the first-order kinetic model, regarded the most classical, has been widely used in systems involving complex wastes due to its simplicity and practicability (Mata-Alvarez et al., 1993). It could be used on the hypothesis that the hydrolysis phase limits the AD process, and meanwhile, the lag phase will not be considered. Also, it was reported that with the use of lignocellulose substrates such as stalks, the first-order kinetic model could efficiently describe the AD process (Lo et al., 2010). Furthermore, the cumulative methane production in the AD process is believed to conform to the sigmoidal curve, and such a process owns a significant lag phase stage. The modified Gompertz model, which has widely been considered to be the most suitable in describing the sigmoidal curve, can better fit the relationship between cumulative methane production and time in batch AD experiments (Zhai et al., 2015; Luz et al., 2018). Many researchers have received some positive results by applying these models to estimate methane production from AD using different substrates (Shen and Zhu, 2016; Li et al., 2018; Zahan et al., 2018). Although reports on anaerobic co-digestion with different substrates using different pretreatment strategies have been well-documented (Liu et al.,

Abbreviations: RS, rice straw; PM, pig manure; C/N, carbon/nitrogen ratio; AD, anaerobic digestion; ADM1 model, Anaerobic Digestion Model No.1; TS, total solids; VS, volatile solids; MS, mixed substrates; PCS, peptone–cellulose solution; CBPs, cellulose-binding proteins; OLR, organic loading rate; COD, chemical oxygen demand; CK, blank groups; TBMP, theoretical biochemical methane potential; λ, lag phase; k, hydrolysis constant; sCOD, soluble chemical oxygen demand; ALK, alkalinity; VFAs, volatile fatty acids; HPLC, high-performance liquid chromatography.

2014; Mustafa et al., 2016; Zhao et al., 2018), relevant literature reports that comparatively investigated the methane yields and kinetics of RS and PM anaerobic co-digestion with or without bio-pretreatment are scarce. Although previous studies have determined the feasibility of biological pretreatment (Shen et al., 2018), it is inaccurate to directly compare the AD data in different studies due to differences in substrates and processing methods. By establishing a mathematical model to predict the performance of AD with and without biological pretreatment, and comparing the kinetic parameters of AD in other studies, the feasibility of the pretreatment strategy can be better evaluated. Additionally, bio-pretreatment is an environmentally friendly pretreatment method, and a few reports exist on the energy balance and AD. Rodriguez's research shows that biological pretreatment can increase methane yield by 30–50% and can generate 834 kW of net energy (Rodriguez et al., 2017).

In the present study, RS and PM anaerobic co-digestion was conducted with or without bio-pretreatment using a previously constructed cellulolytic microflora. The main genera that synergistically degrade cellulose in the microflora are *Clostridium, Petrobacter, Defluviitalea,* and *Paenibacillus* (Zhang et al., 2011a), among them, *Clostridium* is the key genera that degrade cellulose, which could efficiently disintegrate filter paper via the secretion of cellulose-binding proteins (Zhang et al., 2011a). The aims of this study are (i) to investigate the effect of cellulolytic microflora on methane yield in RS and PM AD system, (ii) to establish the first-order kinetic and modified Gompertz models to accurately predict methane production and assess the relationship between AD process and kinetic parameters, and (iii) to determine the economic feasibility of applying composite microbial pretreatment substrates, whereby the energy production and consumption were balanced. Moreover, we used kinetic parameters to provide technical guidance for large-scale AD of RS and PM and to provide a basis for pretreating other fibrous agricultural wastes.

MATERIALS AND METHODS

Substrates and Anaerobic Sludge

RS and PM were collected from Jiangxi Agricultural University, Nanchang, China. The straw was dried and crushed using a solid crusher but was not sieved. PM was placed in the refrigerator at 4°C, during which no other treatment was done. The major components of RS and PM were as follows (**Table 1**).

TABLE 1 | The major components of raw materials.

	Rice straw	Pig manure	Sludge
Total carbon (%)	36.8 ± 1.21	7.95 ± 1.12	–
Total nitrogen (%)	0.623 ± 0.03	1.03 ± 0.04	–
Total hydrogen (%)	5.45 ± 0.18	5.52 ± 0.21	–
Total oxygen (%)	30 ± 1.42	31 ± 1.68	–
Total solids (TS, %)	–	–	10.20 ± 0.31
Volatile solids (VS, %)	–	–	5.22 ± 0.04

± the following value represents the standard deviation of the measurement, obtained as average values of three replicates.
Expressed as weight percent on a dry basis.
–, represents not determined.

Activation of the Cellulolytic Microflora

A peptone–cellulose solution (PCS) medium containing 5.0 g of filter paper (the round medium-speed qualitative filter paper) with a diameter of 12.5 cm was used. For convenience, it was cut into a rectangular shape measuring 1 × 10 cm. Then, 0.9 g of $CaCO_3$, 5.0 g of NaCl, 5.0 g of peptone, 1.0 g of yeast extract, 1.8 g of PM, and 1 L of water (pH 7.6) were added to activate the cellulolytic microflora, which was isolated from decaying straw and silt in nature and the filter paper could be completely decomposed at 55°C under 40 h of incubation by secreting cellulose-binding proteins (CBPs) (Zhang et al., 2011a, 2016). A total of 10% (v/v) of the microflora solution was inoculated into the PCS fermentation medium and incubated at 55°C under static conditions for 36 h.

Biological Pretreatment

A total of 99 g RS (51.15 g) and PM (47.85 g) mixture with a C/N ratio of 30:1 was combined at the biological pretreatment stage. Thereafter, the activated microflora solution was inoculated at the ratio of 10% (v/v) and supplemented with water to achieve a total volume of 1,000 ml, where pH was adjusted to 7.6 using 2 mol·L^{-1} NaOH solution. All these mixtures were incubated at 55°C under static conditions for 30 h. The above bio-pretreatment experiments were performed in triplicate for the subsequent AD.

AD Design

The whole study was conducted in nine parallel AD reactors with 9-L working volume, and a 2-L free space was left at the top of the reactor for gas generation. A similar amount (300 g) of anaerobic sludge collected by centrifugation (8,000 r·min^{-1}, 10 min) was inoculated into each reactor and mixed with 9 L of water. Thereafter, the bio-pretreated RS and PM mixtures with a cellulolytic microflora were transferred into three AD reactors at a maximum organic loading rate [OLR, 2.5 kg COD/(m^3·day)], in which the maximum accumulative methane production and maximum methane production rate were the highest. Meanwhile, the control groups (without biological pretreatment) were set up by adding RS and PM mixtures with equal volume of sterilized cellulolytic microflora solution into another three reactors using the same OLR condition. Furthermore, the blank groups (CK) were carried out in the remaining three AD reactors, where we only evaluated the methane produced from a mixture of 9 L of water and 300 g of anaerobic sludge. Each reactor was purged with N_2 gas for 5 min before sealing with rubber gaskets to maintain the anaerobic condition and mesophilic (35 ± 0.5°C) operating condition for 15–20 days. Moreover, the stirring speed of these reactors was maintained at 30 r·min^{-1}. To observe the changes in AD parameters, a small amount of supernatant from fermentation broth was collected via centrifugation (8,000 r·min^{-1}, 10 min) every day. Detailed information on the mounts of the substrates added with or without biological pretreatment is summarized in **Table 2**.

TABLE 2 | Details of the additional amounts of substrates.

OLR (g COD·L^{-1}·day^{-1})	Control group			Experimental group			
	RS (g)	PM (g)	Water (ml)	RS (g)	PM (g)	Water (ml)	Cellulolytic microflora solution (ml)
2.5	34.93	32.67	1,000	51.15	47.85	900	100

Calculating the Accumulative Methane Production and Methane Production Rate

Methane produced from RS and PM mixtures with or without biological pretreatment was determined through the water displacement method, where the carbon dioxide and H_2S were removed using 2 mol·L^{-1} of NaOH solution and the volume of the discharged NaOH solution was equivalent to the methane (Zhang et al., 2011b). Furthermore, the volume of methane produced by the sludge inoculums (i.e., blank group) was deducted from the entire volume produced by RS and PM with or without biological pretreatment. The rate of methane production and accumulated methane production were calculated as follows:

$$R(t) = \frac{V_t - V_{\mathrm{CK,\,t}}}{\text{VS of RS and PM mixtures added}} \quad (1)$$

$$M(t) = \sum_{t=1}^{t} \frac{V_t - V_{\mathrm{CK,\,t}}}{\text{VS of RS and PM mixtures added}} \quad (2)$$

where $R(t)$ denotes the methane production rate [(ml·(g-VS)$^{-1}$·day^{-1}] at AD time t (days), V_t denotes the methane volume (ml) of RS and PM with or without biological pretreatment at AD time t (days), $V_{CK,t}$ represents the methane volume (ml) of sludge inoculum at AD time t (days), and $M(t)$ denotes the cumulative methane production [ml·(g-VS)$^{-1}$] at AD time t (days).

Calculating the Theoretical Methane Yield and Biodegradability

The theoretical biochemical methane potential (TBMP) under standard conditions (0°C, 1 bar) was assessed based on the elemental composition of the substrates, according to Buswell's formula:

$$\mathrm{C_cH_hO_oN_n} + (\frac{4c-h-2o+3n}{4})\mathrm{H_2O} \quad (3)$$
$$= (\frac{4c+h-2o-3n}{8})\mathrm{CH_4} + (\frac{4c-h+2o+3n}{8})\mathrm{CO_2} + \mathrm{nNH_3}$$

$$CH_4^{TBMP}(\mathrm{ml\ CH_4/g\ VS}) \quad (4)$$
$$= 22.4\times[(\frac{4c+h-2o-3n}{8})/(12c+h+16o+14n)]\times 1000$$

The substrate biodegradability was calculated according to Equation (5) (James et al., 2014):

$$\text{Biodegradability} = \frac{\text{cumulative methane production (ml/g VS)}}{\text{theoretical methane production (ml/g VS)}} \times 100\% \quad (5)$$

Kinetic Assessment

The first-order kinetic model (Equation 6) was used to describe the hydrolysis constant (Liu et al., 2015).

$$M(t) = M_{\max} \cdot [1 - \exp(-kt)] \quad (6)$$

where $M(t)$ denotes the cumulative methane production [ml·(g-VS)$^{-1}$] at AD time t (days), $M_{\max}$ denotes the maximum cumulative methane production potential [ml·(g-VS)$^{-1}$], and k denotes the hydrolysis constant (day^{-1}); the data of lag phase was eliminated before fitting.

The modified Gompertz model, as shown in Equation (7), was proposed to fit the cumulative methane production results obtained from the AD experiments to predict the methane potential (Lay et al., 1998).

$$M(t) = M_{\max} \cdot \exp\{-\exp[\frac{R_{\max} \cdot e}{M_{\max}} \cdot (\lambda - t) + 1]\} \quad (7)$$

where $M(t)$ denotes the cumulative methane production [ml·(g-VS)$^{-1}$] at AD time t (days), $M_{\max}$ denotes the maximum cumulative methane production potential [ml·(g-VS)$^{-1}$], $R_{\max}$ denotes the maximum methane production rate [ml·(g-VS)$^{-1}$·day^{-1}], e is Euler's constant (2.7183), and λ is the lag phase (days).

Energy Balance

Energy balance is necessary before and after adding the biological pretreatment steps.

$$\Delta E = E_{\mathrm{out}} - E_{\mathrm{in}} - E_{\mathrm{escape}} \quad (8)$$

$$E_{\mathrm{out}} = E_{out}^{pretreament} + E_{out}^{digestion} \quad (9)$$

$$E_{\mathrm{in}} = E_{in}^{pretreament} + E_{in}^{digestion} \quad (10)$$

$$E_{in}^{pretreament} = \frac{c \times \left(T\,final - T\,initial\right) \times V \times \rho}{3600} \quad (11)$$

$$E_{\mathrm{escape}} = E_{escape}^{pretreatment} + E_{escape}^{digestion} \quad (12)$$

$$E_{escape}^{pretreatment} = \frac{c \times \left(T\,pretreatment - T\,anbient\right) \times V \times \rho}{3600} \quad (13)$$

$$E_{escape}^{digestion} = \frac{c \times \left(T\,digestion - T\,anbient\right) \times V \times \rho}{3600} \quad (14)$$

where ΔE = net energy, kWh; E_{out} = output energy, kWh; E_{in} = input energy, kWh; c = specific heat capacity of water, 4.18 kJ·kg^{-1}·°C $^{-1}$; T_{final} = pretreatment temperature, 55°C; T_{initial} = the initial temperature of the material, 25°C; V =

volume of pretreatment; ρ = density of pretreatment liquid, 1,050 kg·$(m^3)^{-1}$

$$E_{in}^{digestion} = E_{in}^{filling} + E_{in}^{mixing} + E_{in}^{recycling} + E_{in}^{CHP} \quad (15)$$

$$E_{out}^{pretreament} = \frac{c \times \left(T\ pretreatment - T\ digestion\right) \times V \times \rho}{3600} \quad (16)$$

where c = specific heat capacity of water, 4.18 kJ·kg^{-1}·°C $^{-1}$; $T_{\text{pretreatment}}$ = pretreatment temperature, 55°C; $T_{\text{digestion}}$ = digestion temperature, 35°C; V = the volume of digestive liquid; ρ = the density of the digestive liquid, 1,050 kg·$(m^3)^{-1}$; $E_{in}^{filling}$ is the energy required to fill the material into the reactor, 3.8 W·$(m^3)^{-1}$; E_{in}^{mixing} is the electricity required for the mixture in the AD process, 3.8 W·$(m^3)^{-1}$; $E_{in}^{recycling}$ is the electricity required by the heat pump for water circulation, 2.4 W·$(m^3)^{-1}$; and E_{in}^{CHP} is the energy consumed by combined heat and power unit (CHP), 74 W·$(m^3)^{-1}$ (Dahunsi et al., 2017; Sagarika et al., 2020).

$$E_{out}^{digestion} = E_{out}^{heat} + E_{out}^{electricity} \quad (17)$$

$$E_{out}^{heat} = E_{boiler}^{heat} + E_{CHP}^{heat} \quad (18)$$

$$E_{boiler}^{heat} = 0.05 Y_{\text{yield}} m_{\text{vs}} \zeta \eta_{boiler}^{heat} \quad (19)$$

$$E_{CHP}^{heat} = 0.9 Y_{\text{yield}} m_{\text{vs}} \zeta \eta_{CHP}^{heat} \quad (20)$$

$$E_{out}^{electricity} = 0.9 Y_{\text{yield}} m_{\text{vs}} \zeta \eta_{CHP}^{electricity} \quad (21)$$

where Y_{yield} = methane production, ml·g-VS^{-1} or m^3·ton-VS^{-1}; m_{VS} = feedstock mass, a metric ton of volatile solids, ton-VS^{-1}; ζ = lower heating value of methane, 35.9 MJ·$(m^3)^{-1}$; η_{boiler}^{heat}, $\zeta\eta_{CHP}^{heat}$, and $\eta_{CHP}^{electricity}$ represent the energy conversion efficiency for the boiler heat and heat and electricity of CHP, 85, 55, and 30%, respectively (Pavlo et al., 2018).

Statistical Analysis

All analyses were performed in triplicate. Data were presented as mean values and standard deviations and processed using Excel 2016. The kinetic models were fitted using Origin 9.1.

Analytical Methods

Soluble chemical oxygen demand (sCOD), TS, VS, alkalinity (ALK), total volatile fatty acids (VFAs), and total ammonia nitrogen (by phenate method) were evaluated according to a standard method (American Public Health Association, 2005). The elemental composition (C, H, N, and O) of each substrate was assessed using an elemental analyzer (Vario EL cube, elementar, Germany); results were reported as a percentage of dry weight. Acetic, propionic, and butyric acids were determined by HPLC (ICSep COREGEL 87H3 Column, the HPLC detector was UV 210) under the following conditions: Flow rate = 0.6 ml min^{-1}; temperature = 60°C, and the mobile phase = 0.008 N H_2SO_4. Total nitrogen was measured according to the method described by Kjeldahl (Metcalf et al., 2002).

TABLE 3 | Anaerobic digestion substrate properties.

	Experimental group	Control group
Weight loss rate (%)	39.4 ± 1.06	0
sCOD (mg/L)	7860.3 ± 244.12	3238.24 ± 123.6
Total sugar (mg/L)	908.33 ± 38.68	201.98 ± 9.19
VFAs (mg/L)	600 ± 48	445 ± 34
Acetic acid (mg/L)	213.39 ± 10	150.89 ± 12
Propionic acid (mg/L)	33.53 ± 3.2	10.31 ± 0.5
Butyric acid (mg/L)	255.38 ± 10	12.95 ± 0.5
Cellulose (%)	10.95 ± 0.16	28.97 ± 0.38
Hemicellulose (%)	11.03 ± 0.08	27.29 ± 0.27
Lignin (%)	4.02 ± 0.02	6.07 ± 0.04

RESULTS AND DISCUSSION

Biological Pretreatment Results

Substrate Biological Pretreatment Results

The substrate properties of AD are shown in **Table 3**. After biological pretreatment, the content of cellulose, hemicellulose, and lignin was reduced by 62.20, 59.58, and 33.77%, respectively. The concentrations of total sugar, sCOD, and VFAs in the pretreatment solution were greatly improved, showing 349.71, 142.73, and 34.83% increase, respectively. This can be attributed to the decomposition of cellulose, hemicellulose, and lignin in the substrate that are difficult to hydrolyze naturally by the cellulolytic microflora in the pretreatment stage. In addition, the concentration of butyric acid in the pretreatment solution was 19.72 times more than that without bio-pretreatment. This indicates that the biological pretreatment of RS and PM may be a metabolic process dominated by butyric acid production. Accumulated butyric acid is rapidly utilized by acetogenic bacteria in the AD stage. Consistent with the work of Caixia and Yebo (2010), metabolites such as organic acids and sugars accumulated in the pretreatment stage are rapidly used by methanogens to shorten the lag period of the AD process.

Methane Production Potential and Biodegradability

A comparison of the cumulative methane production and methane production rate of anaerobic co-digestion of RS and PM mixtures with or without biological pretreatment under the maximum OLR conditions is illustrated in **Figure 1**.

Both the cumulative methane production curves in the experimental and control groups were accorded with the sigmoidal shape; this is similar to the growth curve of methanogens. Therefore, these curves were considered suitable in the application of the modified Gompertz model. Similarly, the process kinetic parameters of AD are mainly affected by hydrolysis and methanogenesis (Taricska et al., 2011). Besides, the cumulative methane production of RS and PM after biological pretreatment (experimental group) reached 342.35 ml·(g-VS)$^{-1}$, which was 45% higher compared to that of the control group [236.03 ml·(g-VS)$^{-1}$]. This may be attributed to highly accumulated nutrients in the system after biological pretreatment. These nutrients are rapidly utilized

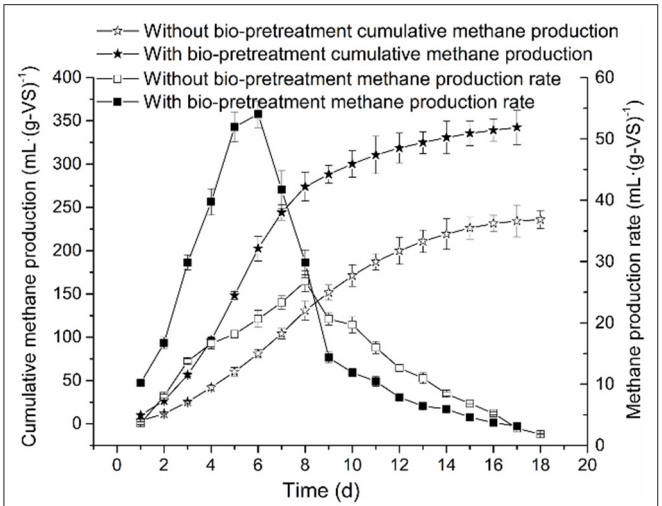

FIGURE 1 | Comparison of cumulative methane production and methane production rate of RS and PM anaerobic co-digestion.

by methanogens so that the methane production in the AD system after biological pretreatment and the bacterial activity are higher than that without biological pretreatment. Also, the lignocellulose structure in the straw and PM in the experimental group system is greatly destroyed; thus, it becomes difficult to prevent microorganisms from attacking the inside. The above findings further demonstrated that the biological pretreatment exerts a productive effect on methane production of RS and PM mixtures.

Moreover, we found that in both the experimental and control groups, after a specific duration, the methane production rate is relatively lower in the early stage of the AD process, which might represent the lag phase. Compared with the experimental group (6 days), this duration of time of the control group (8 days) lasted longer. In the present study, the methane production rate of RS and PM mixtures was at maximum [54.02 ml·(g-VS)$^{-1}$ day^{-1}] on the 6th day after being pretreated with the cellulolytic microflora. In comparison, the maximum methane production rate of the control group was 26.76 ml·(g-VS)$^{-1}$·day^{-1}, on the 8th day. The above findings imply that biological pretreatment destroys the glycosidic bonds in lignocellulose and improves the hydrolysis efficiency of the substrate; thus, microorganisms are more likely to attack the inside of the substrate. In addition, sugars and VFAs are highly concentrated in the pretreatment stage. Therefore, after the pretreatment of RS and PM, the acid-producing microorganisms in the system can quickly adapt to the environment. Methanogens exhibit a higher rate of methane production after they advance past the lag period. We reported that the performance of the experimental group was better than that of the control group. Besides, methane production was believed as the most intuitive indicator that can reflect the efficiency of AD. Notably, the cellulolytic microflora proposed in the present study can effectively improve the AD effect of RS and PM mixture and shorten the lag phase. This might be attributed to the recalcitrant lignocellulosic structures of RS and PM substrates, which can hardly be absorbed and utilized by methanogens, thus resulting in the lower methane production velocity. However, in the experimental group, pretreatment with the cellulolytic microflora could break down the complex lignocellulosic structures, generating sugar, organic acids, and other nutrients that could be easily utilized by methanogens. Therefore, the methanogenesis was accelerated and further enhanced methane production. Previous reports believed that the biological pretreatment process can further benefit the AD and improve the final anaerobic efficiency (Park et al., 2009).

Besides, it was found that after biological pretreatment, the maximum biodegradability predicted by the modified Gompertz models was 68.35%, whereas the actual maximum biodegradability was 66.70%. In AD without bio-pretreatment, the above two values were 47.12 and 45.99%, respectively. This indicates that the AD performance of RS and PM is improved after compound microbial pretreatment, an observation that is consistent with the work of Uma et al. (2013).

Wang S. Q. et al. (2018) used cellulase produced by *Aspergillus niger* to pretreat corn Stover at 50°C for 60 h, and the subsequent AD increased methane production by 36.9% compared with the unpretreated substrate. Fu et al. (2016) used microaerobic bacteria to pretreat effluent from retted corn straw at 55°C and 130 rpm, which improved the methane yield by 21% and the VS removal rate by 10% during AD. This indicates that the pretreatment of lignocellulosic materials using cellulose-degrading microflora has a great application prospect.

Comparison and Analysis of Kinetic Parameters

The kinetic parameters of the AD process help to understand the system evolution of the fermentation process. In the present study, the first-order and modified Gompertz models were proposed to fit the accumulative methane production data observed from the AD experiments with or without bio-pretreatment. The estimated kinetic parameters and model fitting curves are shown in **Table 4** and **Figure 2**. The correlation coefficients (R^2) of the experimental (0.997) and control (0.996) groups revealed that the modified Gompertz models have high correlations and are more suited in simulating the methane production and estimating the lag phase (**Table 2**). Generally, the maximum cumulative methane production potential (M_{max}) and the maximum methane production rate (R_{max}) can directly reflect the efficiency of an AD. In the present study, the M_{max} and R_{max} of RS and PM after biological pretreatment reached 350.79 ml·(g-VS)$^{-1}$ and 45.36 ml·(g-VS)$^{-1}$·day^{-1}, which were 45.1 and 84.3% higher compared to those of the control group, respectively.

Moreover, it was observed that the RS and PM anaerobic co-digestion in the experimental and control groups have an obvious lag phase (λ) of 1.79 and 2.43 days, respectively. Generally, the λ value indicated the time required for methanogens to adapt to the substrates before producing methane (Syaichurrozi et al., 2016). The lower λ value implied that a shorter duration is required to generate methane. As shown in **Table 3**, the λ value in the experimental group with the pretreated RS and PM mixture as the feedstuff was 1.79 days, which was shorter than that of the control group (2.43 days). This concurred

TABLE 4 | Kinetic parameters of anaerobic digestion with or without bio-pretreatment.

	Modified Gompertz model					First-order model		
	R_{emix} ml·(g-VS)$^{-1}$·day^{-1}	M_{max} ml·(g-VS)$^{-1}$	λ (days)	T_{90} (days)	R^2	M_{max} ml·(g-VS)$^{-1}$	k (day^{-1})	R^2
Experimental group	45.36 ± 0.74	350.79 ± 6.2	1.79 ± 0.03	8.92 ± 0.02	0.997	321.78 ± 6.81	0.46 ± 0.03	0.966
Control group	24.60 ± 0.48	241.82 ± 6.1	2.43 ± 0.05	10.7 ± 0.04	0.996	231.13 ± 8.95	0.26 ± 0.02	0.973

All data are shown as means ± standard deviations (n = 3).

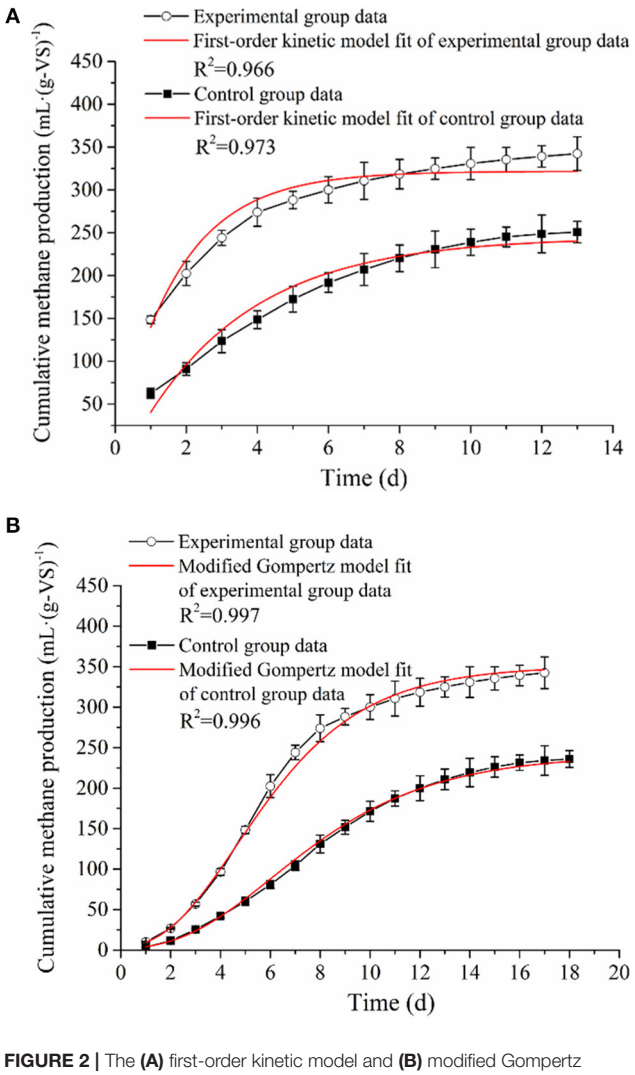

FIGURE 2 | The **(A)** first-order kinetic model and **(B)** modified Gompertz model fitting curves of RS and PM anaerobic co-digestion.

with the findings on the peak gas production time of the experimental group, which occurred earlier than that of the control group in **Figure 1**. A study by Dahunsi et al. also obtained similar results in the pretreatment of lignocellulosic biomass (Dahunsi, 2019). The above results can be attributed to the cellulolytic microflora attacking the rigid structure in cellulose during the pretreatment stage, making it easier for acid and gas-producing microorganisms to use the substrate, thereby improving the utilization efficiency of the substrate. Consequently, the proliferation rate of methanogens is elevated, and the eventual reduction of the lag phase occurs.

Meanwhile, another important kinetic parameter, that is, effective methane production time (T_{90}), was, in most cases, used to predict the duration of AD and methane production. The value of T_{90} was calculated by subtracting λ from the time required to attain 90% of the methane production. Notably, the T_{90} of RS and PM mixtures with or without bio-pretreatment was 8.92 and 10.7 days in the experimental and control groups, respectively (**Table 4**). The above observation revealed that the AD period of the experimental group was shorter compared to that of the control group. Further, through combined analysis of the maximum cumulative methane production potential [350.79 ml·(g-VS)$^{-1}$] and maximum methane production rate [45.36 ml·(g-VS)$^{-1}$·day^{-1}], a shorter lag phase, T_{90}, and higher methane production rate were obtained in the experimental group, indicating that pretreating RS and PM with the cellulolytic microflora could accelerate the AD process and generate more methane at a faster rate.

Furthermore, the hydrolysis constant (k) parameter could be applied to evaluate the process rate-limiting stage and estimate the substrate suitability. Meanwhile, k value describes the degradation rate and the production of methane; in other words, higher k value signifies higher degradation and methane production (Li et al., 2016). In this study, the AD data from the experimental and control groups were efficiently fitted using the first-order model (both their R^2-values were over 0.966). We also observed that the k value of the RS and PM mixture after bio-pretreatment was 0.46 day^{-1}, whereas it was 0.26 day^{-1} in the control group. The above results revealed an increase in the hydrolysis rate of RS and PM by 77% after pretreatment with a cellulolytic microflora. It was believed that the cellulosic components of RS and PM mixtures are difficult to be degraded for their smooth surfaces and compact structures. After biological pretreatment, these dense structures are destroyed, and their contact with hydrolytic bacteria is enhanced. Thus, the structures can easily be broken down by hydrolytic enzymes, which increases the hydrolysis efficiency and k-value (Zhang et al., 2016; Rodriguez et al., 2017).

Analysis of the Process Parameters and Their Correlations With Methane Production and Kinetic Parameters: pH, Alkalinity, and Volatile Fatty Acids

pH is considered as a key indicator that can reflect the proceeding condition of an AD system. Notably, a pH range of 6.8–7.4 has

been reported as most suitable for the growth of methanogens (Li et al., 2016). Additionally, in an AD process, alkalinity (ALK) can neutralize the excessive accumulation of VFAs to stabilize the pH and thus alleviate its inhibitory effect on methanogens (Ripley et al., 1986; Hawkes et al., 1994). Therefore, these parameters are critical process parameters always observed in an anaerobic system.

Herein, the ALK in the AD system of the control and experimental groups slowly decreased from about 3,647–3,168 and 3,754–3,088 mg $CaCO_3 \cdot L^{-1}$, respectively (**Figure 3A**). These ALK values indicated that both the experimental and control AD systems have high buffering capacities. Besides, the pH value of the experimental and control groups showed the same declining tendency in the early stage of the AD process (**Figure 3B**), which may be attributed to the accumulation of VFAs. However, in the late stage, as the methanogens continuously consume VFAs, the pH value gradually increases and is later stabilized. In this work, the pH range of the experimental group in the whole AD process generally was maintained above 7.05. However, the pH in the control group rapidly dropped to about 6.45 in the early anaerobic stage, which was lower than the optimal pH range required by methanogens for growth (6.8–7.4). Because methanogens are sensitive to changes in pH, the pH of the control group in this period potentially impacted the growth of methanogens, which further result in the transition to the lag phase. The above analysis showed that the duration of the lag phase might be related to pH value, in that, a lower pH value would prolong the adaptation time for methanogens to environmental changes, which eventually results in a longer lag phase. Additionally, it was found that the period of rapid decrease of pH in the control group corresponded to that of the increase of methane production rate (see **Figures 1**, **3**). However, the methane production rate was low. This indicated that lower pH potentially affected the maximum methane production rate, thereby reducing the cumulative methane production.

The change in pH is always believed to be associated with the variation of VFAs; therefore, its influence on the lag phase of AD might be caused by the accumulation of VFAs. It is particularly necessary to evaluate the changes in the concentration and composition of VFAs during an AD process. In the hydrolysis phase of the AD process, the lytic monomers or dimers were further transformed into VFAs such as formic, acetic, propionic, and butyric acid, which could be used by methanogens to generate methane. However, the excessive accumulation of these intermediate metabolites would limit methanogenesis due to thermodynamic inhibitions (Xiao et al., 2013). The VFAs of the experimental and control groups were accumulated in the initial stages and were mainly composed of acetic and propionic acids (**Figure 3C**). Notably, acetic acid was regarded as the precursor that can be directly utilized by methanogens, whereas highly concentrated propionic acid exerted a strong toxic effect on methanogens. It was always believed that when the concentration of propionic acid reaches over 1,000 $mg \cdot L^{-1}$, the AD process is inhibited (Hanaki et al., 1994). However, the low propionic acid concentration is believed to possess some benefits for methane fermentation (Yuan et al., 2012). Based on **Figure 3C**, the maximum propionic acid concentration in the control and experimental groups both do not exceed the tolerance concentration. Thus, with the consumption of acetic and propionic acids in the experimental and control groups,

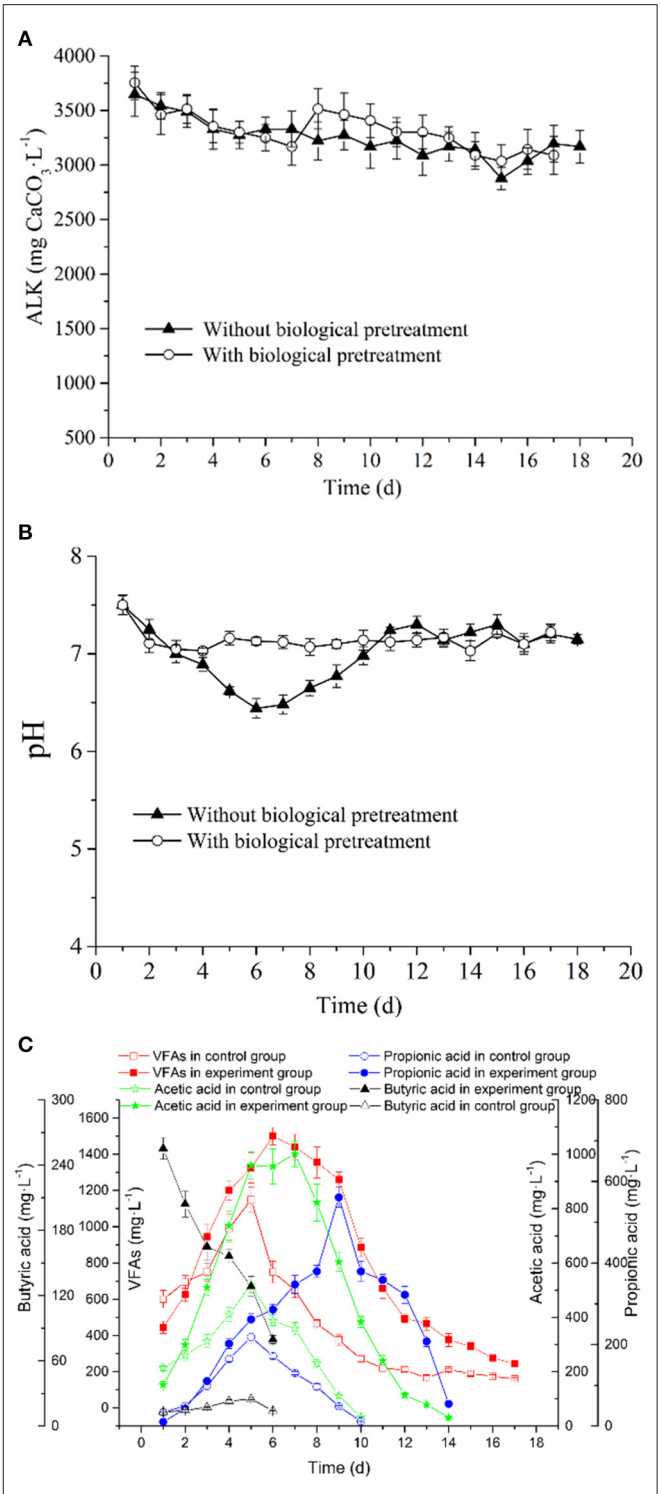

FIGURE 3 | Changes of **(A)** ALK, **(B)** pH and VFAs of RS and PM without or with **(C)** biological pretreatment in the anaerobic co-digestion ($p < 0.05$).

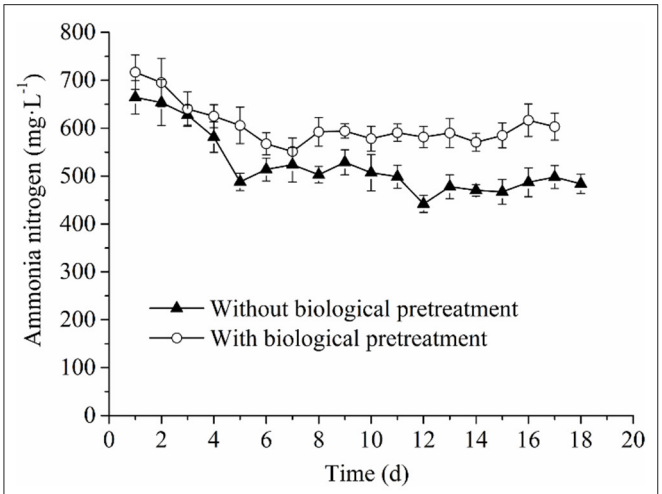

FIGURE 4 | Changes of ammonia nitrogen in the anaerobic co-digestion process.

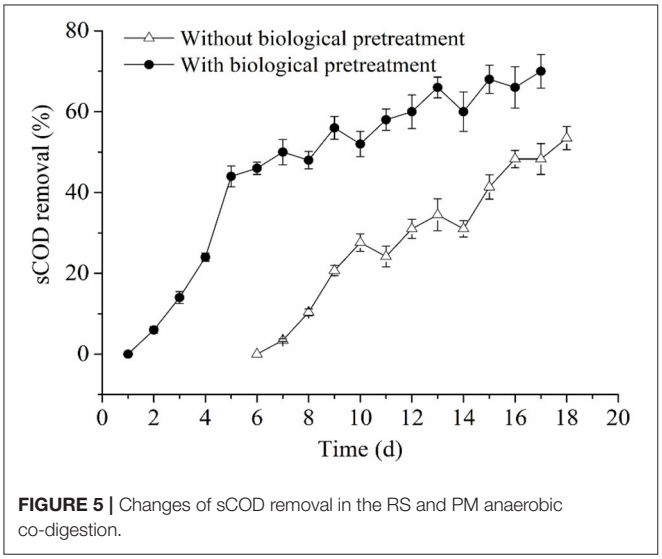

FIGURE 5 | Changes of sCOD removal in the RS and PM anaerobic co-digestion.

the VFA concentration decreased. Besides, the concentration curve of butyric acid was different from other organic acids (**Figure 3C**). Since PM contains a small amount of organic acid, mainly butyric acid, traces of butyric acid can be detected in the initial stage of the control group (Ni et al., 2012). A large amount of butyric acid in the initial phase of the experimental group was produced via the degradation of RS and PM by the cellulolytic microflora during the pretreatment stage. In the AD stage, the butyric acid was rapidly consumed and disappeared on the 6th day; similar results were reported by Fernan et al. (2017).

In the methanogenesis phase, it was believed the accumulation of VFAs would greatly inhibit the growth of methanogens (Xiao et al., 2013). Notably, we found that the accumulation of VFAs in the control group was higher than that in the experimental group (**Figures 1**, **3C**); this inhibited the activity of some methanogens in the AD system. As a result, methanogens were characterized by a decrease in the utilization efficiency of acetic acid, which explains why the cumulative methane production and methane production rate in the control group were lower than those in the experimental group. Furthermore, in the AD process of the experimental and control groups, lag phases could be observed, and propionic acids were accumulated in this period, indicating that the occurrence of the lag phase may be associated with the accumulation of propionic acids. This assumption could also be proved by the following phenomena observed from **Figure 3C**: (1) In the middle stage of the AD process, the degree of accumulation of VFAs in the control group was significantly higher than that in the experimental group, which may be the primary cause of the prolonged period; this result is consistent with a report from the literature (Mao et al., 2017). (2) The time when VFA concentration of the experimental and control groups began to decrease coincided with the time at which methane production was at the peak; however, with the decrease in VFAs, the growth rate of the cumulative methane production rate of the experimental group and the control group was lowered. (3) The peaks of the control group and the experimental group occurred when acetic acid accumulated to the maximum, indicating that R_{max} and T_{90} may be related to the maximum concentration of acetic acid. In subsequent research or application, some methods can be adopted to increase the concentration of acetic acid in the AD system, thus shortening the T_{90}, which is highly vital for the maximum utilization of equipment. Findings by Li H. L. et al. (2016) showed that at an acetic acid concentration of <120,000 mg/L, the rate at which methanogens utilize acetic acid is positively correlated with the acetic acid concentration, and this correlation will be directly reflected in the methane production rate, which is consistent with the above results.

Analysis of Process Parameters and Their Correlations With Methane Production and Kinetic Parameters: Ammonia Nitrogen

The ammonia nitrogen concentration in the experimental and control groups both revealed decreased tendencies with the prolonged AD process, which then stabilized in the late stage (**Figure 4**). Furthermore, it was found that the concentration of ammonia nitrogen in the experimental group was always higher than that of the control group. This could be explained by the fact that in the pretreatment process, more proteins and amino acids were converted into ammonia nitrogen by the cellulolytic microflora during hydrolysis. On the other hand, in the AD process, RS and PM mixtures would still be slowly hydrolyzed, and the existence of more hydrolytic microorganisms from the cellulolytic microflora maintained the production rate of ammonia nitrogen in the experimental group than that of the control group. Subsequently, a higher concentration of ammonia nitrogen in the fermentation solution of the experimental group was reported. According to previous reports, the ammonia nitrogen concentration at 50–200 mg·L^{-1} can promote the growth of microorganisms, whereas ammonia nitrogen concentration at 200–1,000 mg·L^{-1} exerts no antagonistic effect. However, when the concentration reaches 1,500–10,000 mg·L^{-1}, the activity of microorganisms is inhibited (Rajagopal et al., 2013; Sung and Liu, 2013). In this study, the ammonia nitrogen

TABLE 5 | Energy evaluation of anaerobic co-digestion of RS and PM.

Project	$E_{in}^{pretreament}$	$E_{in}^{filling}$	E_{in}^{mixing}	$E_{in}^{recycling}$	$E_{out}^{pretreament}$	E_{boiler}^{heat}	E_{CHP}^{heat}	$E_{out}^{electricity}$	E_{escape}	Net energy
Control group	–	16.57	16.57	10.51	–	657.27	7654.54	4175.15	123.13	12320.18
Experiment group	369.49	16.57	16.57	10.51	246.26	953.33	11103.12	6056.26	492.63	17453.20

Includes heat energy generated but not used at the time of the study.
Unit: kWh.
Calculated by 1 ton of raw material (pig manure and rice straw).

concentration in the experimental and control groups ranged between 200 and 1,000 mg·L^{-1}, which indicated that although the ammonia nitrogen production of the experimental group was higher than that of the control, it could not reduce the benefit of higher methane production. Therefore, the ammonia nitrogen concentration in the AD system could not prolong or shorten the AD lag phase by impacting the activity of methanogens. Meanwhile, it exerted no significant effect on other kinetic parameters (k, T_{90}, $R_{max,}$ and M_{max}). Herein, we suggested that the greater significance of ammonia nitrogen concentration may be the main alkaline substance to maintain ALK, thus ensuring that the anaerobic system would not be acidified (Speece, 1983).

Analysis of Process Parameters and Their Correlations With Methane Production and Kinetic Parameters: sCOD Removal

In an AD system, methanogens can transform some soluble organic substrates into methane. Therefore, the parameter of sCOD (soluble chemical oxygen demand) removal can indicate methanogenic activity. In this work, sCOD removal in the experimental and control groups both showed increased trends (**Figure 5**). However, sCOD removal in the experimental group reached 70%, while that of the control was 53.4% when the AD process was ceased. Besides, it is worth noting that we did not calculate sCOD removal in the control group during the first 6 days of this study due to the slow consumption of sCOD during this period. The reason for this phenomenon might be explained by non-pretreatment of the RS and PM in the control group, such that lignocellulosic components were slowly decomposed into sugars, alcohols, and organic acids, by hydrolyzing microbes. These substances could directly be utilized by methanogens when they are further converted into acetic acid through the activity of acetic acid-producing bacteria. However, due to the tight and complex structure of lignocellulose, this conversion rate is very slow. Therefore, in the early stage, the activity of methanogens was lower than that of hydrolyzing bacteria because of the low levels of available nutrients that could be utilized by methanogens. Thus, the generation of soluble organic matter exceeded the consumption of methanogens, and sCOD was accumulated. After 6 days of incubation, as the methanogens adapted to the environmental conditions and the acetic acid content increased, the activity of methanogens was gradually higher than the hydrolyzing bacteria. Also, a large amount of organic matter was utilized by methanogens to produce methane, which further led to an increase in the sCOD removal ratio.

In the experimental group, a large amount of organic matter, mainly composed of VFAs, were produced from RS and PM with biological pretreatment, which could be rapidly consumed by methanogens in the early stage of the AD process. Therefore, more methane was produced in the early stage, and the AD lag phase and duration in the experimental group were shortened. In addition, we found that the sCOD removal in the experimental group was significantly higher compared to that of the control group; these findings concurred with their accumulative methane production and methane production rate. Further, the above observations revealed that sCOD removal is positively correlated with R_{max} and M_{max}, which was consistent with reports from previous studies (Syaichurrozi and Budiyono, 2013; Li H. L. et al., 2016).

Energy Balance

Bio-pretreatment is an energy-consuming process, whereas AD is an energy production process; therefore, it is important to maintain the energy balance of the bio-pretreatment followed by AD technique. Generally, the additional energy required for bio-pretreatment should be included in the AD process after bio-pretreatment. In this work, to fully evaluate the energy balance and economic feasibility of biological pretreatment, the combined heat and power (CHP) system was adopted with thermal and electrical efficiencies at 50 and 35%, respectively (**Table 5**), which is a highly popular technique in energy conversion across the globe (Lay et al., 1998; Dahunsi et al., 2017). We used the bio-pretreatment method to pretreat RS and PM, which was followed by anaerobic co-digestion. For each ton of material processed, compared to without bio-pretreatment, only 492.73 kWh extra energy was consumed, which could increase the energy output by 5133.02 kWh after AD. Similarly, in previous studies where agricultural waste was subjected to bio-pretreatment methods, positive energy gains were obtained (Yin et al., 2016). Moreover, pretreatments using materialization methods generated similar results (Liang et al., 2016; Kovačić et al., 2019), which showed that in terms of energy gains, pretreatment of materials before AD has great application prospects.

CONCLUSION

In the present study, the methane yield and kinetic parameters of RS and PM anaerobic co-digestion with or without bio-pretreatment showed significant variations. After bio-pretreatment, the cumulative methane production of RS and PM was recorded at 342.35 ml·(g-VS)$^{-1}$, which was a 45% increase, while the biodegradation increased by 45.06%. Based on results generated by the kinetics models, bio-pretreatment improved the

hydrolysis constant, maximum cumulative methane production potential, and the maximum methane production rate, but shortened the lag phase and effective methane production time. Regarding energy balance, biological pretreatment only consumes 738.99 kWh·ton^{-1}, but 5133.02 kWh·ton^{-1} can be obtained in the AD stage, compared to when non-bio-pretreated materials are used. This work demonstrated that bio-pretreatment with a cellulolytic microflora could effectively improve the methane yield of RS and PM anaerobic co-digestion and is an environmentally friendly mechanism. It also could provide technical reference for kinetics and anaerobic co-digestion parameters of RS and PM.

DATA AVAILABILITY STATEMENT

The original contributions presented in the study are included in the article/supplementary material, further inquiries can be directed to the corresponding author/s.

AUTHOR CONTRIBUTIONS

BZ, FS, XA, and QZ: conceptualization, writing—review, and editing. BZ, FS, and WA: methodology and formal analysis. BZ and FS: writing—original draft. QZ: funding acquisition and supervision. All authors contributed to the article and approved the submitted version.

FUNDING

This work was financially supported by the Key Research and Development Project of Jiangxi Province (Grant No. 20192BBF60055), the Outstanding Youth Talent Funding Program of Jiangxi Province (Grant No. 20171BCB23044), the National Natural Science Foundation of China (Grant No. 31260024), and the Science and Technology Project Founded by the Education Department of Jiangxi Province (GJJ180174).

REFERENCES

Ali, S. S., Abomohra, A. E. F., and Sun, J. Z. (2017). Effective bio-pretreatment of sawdust waste with a novel microbial consortium for enhanced biomethanation. *Bioresour Technol.* 238, 425–432. doi: 10.1016/j.biortech.2017.03.187

American Public Health Association (2005). *Standard Methods for the Examination of Water and Wastewater, 21st Edn.* Washington: DC, American Public Health Association.

Andrew, C. V. Z., Hambaliou, B., Anna, C., Robert, J. G., Martin, N., Claudia, W. R., et al. (2018). Potential methane emission reductions for two manure treatment technologies. *Environ. Technol.* 39, 851–858. doi: 10.1080/09593330.2017.1313317

Caixia, W., and Yebo, L. (2010). Microbial pretreatment of corn stover with *Ceriporiopsis subvermispora* for enzymatic hydrolysis and ethanol production. *Bioresour Technol.* 101, 6398–6403. doi: 10.1016/j.biortech.2010.03.070

Chelme-Ayala, P., El-Din, M. G., Smith,. R., Kenneth, R. C., and Jerry, L. (2011). Advanced treatment of liquid swine manure using physico-chemical treatment. *J. Hazard. Mater.* 186, 1632–1638. doi: 10.1016/j.jhazmat.2010.12.047

Dahunsi, S. O. (2019). Mechanical pretreatment of lignocelluloses for enhanced biogas production: methane yield prediction from biomass structural components. *Bioresour. Technol.* 280, 18–26. doi: 10.1016/j.biortech.2019.02.006

Dahunsi, S. O., Oranusi, S., and Efeovbokhan, V. E. (2017). Pretreatment optimization, process control, mass and energy balances and economics of anaerobic co-digestion of *Arachis hypogaea* (Peanut) hull and poultry manure. *Bioresour. Technol.* 241, 454–464. doi: 10.1016/j.biortech.2017.05.152

Deepanraj, B., Sivasubramanian, V., and Jayaraj, S. (2015). Experimental and kinetic study on anaerobic digestion of food waste: the effect of total solids and pH. *J. Renew. Sustain. Energy* 7, 3104–3116. doi: 10.1063/1.4935559

Fernan, D., M. J., Maria, P., M. P., Ackmez, M., Thiago, de, A. N., et al. (2017). Influence of ultrasound irradiation pre-treatment in biohythane generation from the thermophilic anaerobic co-digestion of sugar production residues. *J. Environ. Chem. Eng.* 5, 3749–3758. doi: 10.1016/j.jece.2017.07.030

Fu, S. F., Shi, X. S., Dai, M., and Guo, R. B. (2016). Effect of different mixed microflora on the performance of thermophilic microaerobic pretreatment. *Energy Fuels* 30, 6413–6418. doi: 10.1021/acs.energyfuels.6b00440

Gopi, K. K., Sujala, B., Sang, H. K., and Lide, C. (2014). Anaerobic digestion of Chinese cabbage waste silage with swine manure for biogas production: batch and continuous study. *Environ. Technol.* 35, 2708–2717. doi: 10.1080/09593330.2014.919033

Hanaki, K., Hirunmasuwan, S., and Matsuo, T. (1994). Protection of methanogenic bacteria from low pH and toxic materials by immobilization using polyvinyl alcohol. *Water Res.* 28, 877–885. doi: 10.1016/0043-1354(94)90094-9

Haruta, S., Cui, Z., Huang, Z., Li, M., Ishii, M., and Igarashi, Y. (2002). Construction of a stable microbial community with high cellulose-degradation ability. *Appl. Microbiol. Biotechnol.* 59, 529–534. doi: 10.1007/s00253-002-1026-4

Hawkes, F. R., Guwy, A. J., Hawks, D. L., and Rozzi, A. G. (1994). On-line monitoring of anaerobic digestion: application of a device for continuous measurement of bicarbonate alkalinity. *Water Sci. Technol.* 30, 1–10. doi: 10.2166/wst.1994.0571

Hu, Y. S., Hao, X. D., Wang, J. M., and Cao, Y. L. (2016). Enhancing anaerobic digestion of lignocellulosic materials in excess sludge by bioaugmentation and pre-treatment. *Waste Manage.* 49, 55–63. doi: 10.1016/j.wasman.2015.12.006

James, D. B., Eoin, A., and Jerry, D. M. (2014). Assessing the variability in biomethane production from the organic fraction of municipal solid waste in batch and continuous operation. *Appl. Energy* 128, 307–314. doi: 10.1016/j.apenergy.2014.04.097

Kainthola, J., Kalamdhad, A. S., Goud, V. V., and Goel, R. (2019). Fungal pretreatment and associated kinetics of rice straw hydrolysis to accelerate methane yield from anaerobic digestion. *Bioresour. Technol.* 286:121368. doi: 10.1016/j.biortech.2019.121368

Karimi, K., Shafiei, M., and Kumar, R. (2013). Progress in physical and chemical pretreatment of lignocelluloses biomass. *Biofuel Technol.* 3, 53–96. doi: 10.1007/978-3-642-34519-7_3

Kong, X. P., Du, J., Ye, X. M., Xi, Y. L., Jin, H. M., Zhang, M., et al. (2018). Enhanced methane production from wheat straw with the assistance of lignocellulolytic microbial consortium TC-5. *Bioresour Technol.* 263, 33–39. doi: 10.1016/j.biortech.2018.04.079

Kovačić, Ã., Kralik, D., Rupčić, S., Rupčić, S., Jovičić, D., Spajić, R., et al. (2019). Electroporation of harvest residues for enhanced biogas production in anaerobic co-digestion with dairy cow manure. *Bioresour. Technol.* 274, 215–224. doi: 10.1016/j.biortech.2018.11.086

Lay, J. J., Li, Y. Y., and Noike, T. (1998). Interaction between homoacetogens and methanogens in lake sediments. *J. Ferment. Bioeng.* 86, 467–471. doi: 10.1016/s0922-338x(98)80153-0

Li, H. L., Cao, F. F., and Wang, Y. (2016). The effect of different acetic acid accumulation on the methanogenic population and methane production in dry mesophilic anaerobic digestion. *Energy Sour. Part A* 38, 1678–1684. doi: 10.1080/15567036.2013.773386

Li, L., He, Q., Zhao, X. F., Wu, D., Wang, X. M., and Peng, X. Y. (2018). Anaerobic digestion of food waste: correlation of kinetic parameters with

operational conditions and process performance. *Biochem. Eng. J.* 130, 1–9. doi: 10.1016/j.bej.2017.11.003

Li, Y. Y., Jin, Y. Y., Li, J. H., Li, H. L., and Yu, Z. X. (2016). Effects of thermal pretreatment on the biomethane yield and hydrolysis rate of kitchen waste. *Appl. Energy* 172, 47–58. doi: 10.1016/j.apenergy.2016.03.080

Liang, Y. G., Cheng, B., Si, Y. B., Cao, D. J., Li, D. L., and Chen, J. F. (2016). Effect of solid-state NaOH pretreatment on methane production from thermophilic semi-dry anaerobic digestion of rose stalk. *Water Sci. Technol.* 73, 2913–2920. doi: 10.2166/wst.2016.145

Liu, L. L., Zhang, T., Wan, H. W., Chen, Y. L., Wang, X. J., Yang, G. H., et al. (2015). Anaerobic co-digestion of animal manure and wheat straw for optimized biogas production by the addition of magnetite and zeolite. *Energy Convers. Manage.* 97, 132–139. doi: 10.1016/j.enconman.2015.03.049

Liu, S., Li, X., Wu, S. B., He, J., Pang, C. L., Deng, Y., et al. (2014). Fungal pretreatment by Phanerochaete chrysosporium for enhancement of biogas production from corn stover silage. *Appl. Biochem. Biotechnol.* 174, 1907–1918. doi: 10.1007/s12010-014-1185-7

Lo, H. M., Kurniawan, T. A., Sillanpää M. E. T., Paia, T. Y., Chiangc, C. F., Chaod, K. P., et al. (2010). Modeling biogas production from organic fraction of MSW co-digested with MSWI ashes in anaerobic bioreactors. *Bioresour. Technol.* 101, 6329–6335. doi: 10.1016/j.biortech.2010.03.048

Logan, M., and Visvanathan, C. (2019). Management strategies for anaerobic digestate of organic fraction of municipal solid waste: current status and future prospects. *Waste Manage. Res.* 37, 27–39. doi: 10.1177/0734242X18816793

Luz, F. C., Cordiner, S., Manni, A., Mulone, V., Rocco, V., Braglia, R., et al. (2018). Ampelodesmos mauritanicus pyrolysis biochar in anaerobic digestion process: evaluation of the biogas yield. *Energy* 161, 663–669. doi: 10.1016/j.energy.2018.07.196

Lyu, L., Ruolin, W., Zhenlai, J., Li, W. W., Liu, G. Q., and Chen, C. (2019). Anaerobic digestion of tobacco stalk: biomethane production performance and kinetic analysis. *Environ. Sci. Pollut. Res.* 26, 14250–14258. doi: 10.1007/s11356-019-04677-2

Mao, C. L., Zhang, T., Wang, X. J., Feng, Y. Z., Ren, G. X., and Yang, G. H. (2017). Process performance and methane production optimizing of anaerobic co-digestion of swine manure and corn straw. *Sci. Rep.* 7:9379. doi: 10.1038/s41598-017-09977-6

Mata-Alvarez, J., Kurniawan, T. A., Llabrés-Lueng, P., and Cecchi, F. (1993). Kinetic and performance study of a batch two-phase anaerobic digestion of fruit and vegetable wastes. *Biomass Bioenergy* 5, 481–488. doi: 10.1016/0961-9534(93)90043-4

Metcalf, I., Eddy, G., Tchobanoglou, G., Burton, F. L., and Stensel, H. D. (2002). *Wastewater Engineering: Treatment and Reuse, 4th Edn.* New York, NY: McGraw-Hill Higher Education.

Mustafa, A. M., Poulsen, T. G., and Sheng, K. (2016). Fungal pretreatment of rice straw with *Pleurotus ostreatus* and *Trichoderma reesei* to enhance methane production under solid-state anaerobic digestion. *Appl. Energy* 180, 661–671. doi: 10.1016/j.apenergy.2016.07.135

National Bureau of Statistics (2019). *Announcement of the National Bureau of Statistics on Grain Production Data in 2019.* National Bureau of Statistics. Available online at: http://www.stats.gov.cn/tjsj/zxfb/201912/t20191206_1715827.html (accessed December 6, 2019).

Nguyen, D. D., Jeon, B. H., Jeung, J. H., Rene, E. R., RajeshBanu, J., Ravindran, B., et al. (2019). Thermophilic anaerobic digestion of model organic wastes: evaluation of biomethane production and multiple kinetic models analysis. *Bioresour. Technol.* 280, 269–276. doi: 10.1016/j.biortech.2019.02.033

Ni, J. Q., Robarge, W. P., Xiao, C., and Heber, A. J. (2012). Volatile organic compounds at swine facilities: a critical review. *Chemosphere* 89, 769–788. doi: 10.1016/j.chemosphere.2012.04.061

Park, W. J., Ahn, J. H., Hwang, S. W., and Lee, C. K. (2009). Effect of output power, target temperature, and solid concentration on the solubilization of waste activated sludge using microwave irradiation. *Bioresour. Technol.* 101, S13–S16. doi: 10.1016/j.biortech.2009.02.062

Pavlo, B., Duc, P., Anatoliy, M. K., Steven, C., Edward, J. B., and Michael, J. B. (2018). Synergistic co-digestion of wastewater grown algae-bacteria polyculture biomass and cellulose to optimize carbon-to-nitrogen ratio and application of kinetic models to predict anaerobic digestion energy balance. *Bioresour. Technol.* 269, 210–220. doi: 10.1016/j.biortech.2018.08.085

Qian, X. Y., Shen, G. X., Wang, Z. Q., Guo, C. X., Liu, Y. Q., Lei, Z. F., et al. (2014). Co-composting of livestock manure with rice straw: characterization and establishment of maturity evaluation system. *Waste Manage.* 34, 530–535. doi: 10.1016/j.wasman.2013.10.007

Rajagopal, R., Masse, D. I., and Singh, G. (2013). A critical review on inhibition of anaerobic digestion process by excess ammonia. *Bioresour. Technol.* 143, 632–641. doi: 10.1016/j.biortech.2013.06.030

Ripley, L. E., Boyle, W. C., and Converse, J. C. (1986). Improved alkalimetric monitoring for anaerobic digestion of high-strength wastes. *J. Water Poll. Control Federat.* 58, 406–411. doi: 10.2307/25042933

Rodriguez, C., Alaswad, A., Benyounis, K. Y., and Olabi, A. G. (2017). Pretreatment techniques used in biogas production from grass. *Renew. Sustain. Energy Rev.* 68, 1193–1204. doi: 10.1016/j.rser.2016.02.022

Sagarika, P., Hari, B. S., and Brajesh, K. D. (2020). Anaerobic co-digestion of food waste with pretreated yard waste: a comparative study of methane production, kinetic modeling and energy balance. *J. Cleaner Prod.* 243, 118480. doi: 10.1016/j.jclepro.2019.118480

Shen, F., Li, H. G., Wu, X. Y., Wang, Y. X., and Zhang, Q. H. (2018). Effect of organic loading rate on anaerobic co-digestion of rice straw and pig manure with or without biological pretreatment. *Bioresour. Technol.* 250, 155–162. doi: 10.1016/j.biortech.2017.11.037

Shen, J. C., and Zhu, J. (2016). Kinetics of batch anaerobic co-digestion of poultry litter and wheat straw including a novel strategy of estimation of endogenous decay and yield coefficients using numerical integration. *Bioprocess Biosyst. Eng.* 39, 1553–1565. doi: 10.1007/s00449-016-1630-9

Speece, R. E. (1983). Anaerobic biotechnology for industrial wastewater treatment. *Environ. Sci. Technol.* 17, 416–427. doi: 10.1021/es00115a725

Sung, S., and Liu, T. (2013). Ammonia inhibition on thermophilic digestion anaerobic. *Chemosphere* 53, 43–52. doi: 10.1016/S0045-6535(03)00434-X

Syaichurrozi, I., Budiyono, and Sumardiono, S. (2013). Predicting kinetic model of biogas production and biodegradability organic materials: biogas production from vinasse at variation of COD/N ratio. *Bioresour. Technol.* 149, 390–397. doi: 10.1016/j.biortech.2013.09.088

Syaichurrozi, I., Rusdi, R., and Hidayat, T. (2016). Kinetics studies impact of initial pH and addition of yeast *Saccharomyces cerevisiae* on biogas production from tofu wastewater in Indonesia. *Int. J. Eng. Trans. B* 29, 1037–1046. doi: 10.5829/idosi.ije.2016.29.08b.02

Taricska, J. R., Long, D. A., Chen, J. P., Hung, Y. T., and Zou, S. W. (2011). "Anaerobic digestion," in *Handbook of Environmental Engineer,* eds L. K. Wang, N. K. Shammas, and Y. T. Hung (Totowa, NJ: Humana Press Inc.), 135–176.

Uma, R. R., Adish, K. S., Kaliappan, S., IckTae, Y., and Banu, J. R. (2013). Impacts of microwave pretreatments on the semi-continuous anaerobic digestion of dairy waste activated sludge. *Waste Manage.* 33, 1119–1127. doi: 10.1016/j.wasman.2013.01.016

Villa Gomez, D. K., Becerra Castañeda, P., Montoya Rosales, J. J., and González Rodríguez, L. M. (2019). Anaerobic digestion of bean straw applying a fungal pre-treatment and using cow manure as co-substrate. *Environ. Technol.* 41, 2863–2874. doi: 10.1080/09593330.2019.1587004

Villamil, J. A., Mohedano, A. F., Rodriguez, J. J., and De la Rubia, M. A. (2019). Anaerobic co-digestion of the aqueous phase from hydrothermally treated waste activated sludge with primary sewage sludge. A kinetic study. *J. Environ. Manage.* 231, 726–733. doi: 10.1016/j.jenvman.2018.10.031

Wang, S. Q., Li, F., Wu, D., Zhang, P. Y., Wang, H. J., Tao, X., et al. (2018). Enzyme pretreatment enhancing biogas yield from corn stover: feasibility, optimization, and mechanism analysis. *J. Agric. Food Chem.* 66, 10026–10032. doi: 10.1021/acs.jafc.8b03086

Wang, Y. Y., Li, G. X., Chi, M. H., Sun, Y. B., Zhang, J. X., Jiang, S. X., et al. (2018). Effects of co-digestion of cucumber residues to corn stover and pig manure ratio on methane production in solid state anaerobic digestion. *Bioresour. Technol.* 250, 328–336. doi: 10.1016/j.biortech.2017.11.055

Xiao, K. K., Gu, C. H., Zhou, Y., Maspolim, Y., Wang, J. Y., and Ng, W. J. (2013). Acetic acid inhibition on methanogens in a two-phase anaerobic process. *Biochem. Eng. J.* 75, 1–7. doi: 10.1016/j.bej.2013.03.011

Yangin, G. C., and Ozturk, I. (2013). Effect of maize silage addition on biomethane recovery from mesophilic co-digestion of chicken and cattle

manure to suppress ammonia inhibition. *Energy Convers. Manage*. 71, 92–100. doi: 10.1016/j.enconman.2013.03.020

Yin, D. X., Liu, W., Zhai, N. N., Yang, G. H., Wang, X. J., Feng, Y. Z., et al. (2014). Anaerobic digestion of pig and dairy manure under photo-dark fermentation condition. *Bioresour. Technol.* 166, 373–380. doi: 10.1016/j.biortech.2014.05.037

Yin, Y., Liu, Y. J., Meng, S. J., Kiran, E. U., and Liu, Y. (2016). Enzymatic pretreatment of activated sludge, food waste and their mixture for enhanced bioenergy recovery and waste volume reduction via anaerobic digestion. *Appl. Energy* 179, 1131–1137. doi: 10.1016/j.apenergy.2016.07.083

Yuan, X. F., Cao, Y. Z., Li, J. J., Wen, B. T., Zhu, W. B., Wang, X. F., et al. (2012). Effect of pretreatment by a microbial consortium on methane production of waste paper and cardboard. *Bioresour. Technol.* 118, 281–288. doi: 10.1016/j.biortech.2012.05.058

Zahan, Z., Othman, M. Z., and Muster, T. H. (2018). Anaerobic digestion/co-digestion kinetic potentials of different agro-industrial wastes: a comparative batch study for C/N optimization. *Waste Manage*. 71, 663–674. doi: 10.1016/j.wasman.2017.08.014

Zhai, N., Zhang, T., Yin, D., Yang, G. H., Wang, X. J., Ren, G. X., et al. (2015). Effect of initial pH on anaerobic co-digestion of kitchen waste and cow manure. *Waste Manage.* 38, 126–131. doi: 10.1016/j.wasman.2014.12.027

Zhang, Q. H., He, J., Tian, M., Mao, Z. G., Tang, L., Zhang, J. H., et al. (2011a). Enhancement of methane production from cassava residues by biological pretreatment using a constructed microbial consortium. *Bioresour. Technol.* 102, 8899–8906. doi: 10.1016/j.biortech.2011.06.061

Zhang, Q. H., Li, H. G., Zhu, X. D., Lai, F. J., Zhai, Z. J., and Wang, Y. X. (2016). Exploration of the key functional proteins from an efficient cellulolytic microbial consortium using dilution-to-extinction approach. *J. Environ. Sci.* 43, 199–207. doi: 10.1016/j.jes.2015.09.003

Zhang, Q. H., Tang, L., Zhang, J. H., Mao, Z. G., and Jiang, L. (2011b). Optimization of thermal-dilute sulfuric acid pretreatment for enhancement of methane production from cassava residues. *Bioresour. Technol.* 102, 3958–3965. doi: 10.1016/j.biortech.2010.12.031

Zhang, Y., Piccard, S., and Zhou, W. (2015). Improved ADM1 model for anaerobic digestion process considering physico-chemical reactions. *Bioresour. Technol.* 196, 279–289. doi: 10.1016/j.biortech.2015.07.065

Zhao, X. L., Zheng, Z. H., Cai, Y. F., Zhao, Y., Luo, K., Cui, Z., et al. (2018). Pretreatment by crude enzymatic liquid from *Trichoderma harzianum* and *Aspergillus* sp improving methane production performance during anaerobic digestion of straw. *Trans. Chin. Soc. Agric. Eng.* 34, 219–226. doi: 10.11975/j.issn.1002-6819.2018.03.029

Zhu, J. Y., Han, M. L., Zhang, G. K., and Yang, L. C. (2015). Co-digestion of spent mushroom substrate and corn stover for methane production via solid-state anaerobic digestion. *J. Renew. Sustain. Energy* 7, 3135–3145. doi: 10.1063/1.4919404

Conflict of Interest: The authors declare that the research was conducted in the absence of any commercial or financial relationships that could be construed as a potential conflict of interest.

frontiers in Bioengineering and Biotechnology

ORIGINAL RESEARCH
published: 03 March 2021
doi: 10.3389/fbioe.2021.647853

Identifying and Engineering Bottlenecks of Autotrophic Isobutanol Formation in Recombinant *C. ljungdahlii* by Systemic Analysis

*Maria Hermann[1], Attila Teleki[1], Sandra Weitz[2], Alexander Niess[1], Andreas Freund[1], Frank Robert Bengelsdorf[2], Peter Dürre[2] and Ralf Takors[1]**

[1] Institute of Biochemical Engineering, Faculty of Energy-, Process-, and Bio-Engineering, University of Stuttgart, Stuttgart, Germany, [2] Institute of Microbiology and Biotechnology, Faculty of Natural Sciences, University of Ulm, Ulm, Germany

OPEN ACCESS

Edited by:
Petra Patakova,
University of Chemistry and Technology in Prague, Czechia

Reviewed by:
Fu-Li Li,
Qingdao Institute of Bioenergy and Bioprocess Technology (CAS), China
John A. Morgan,
Purdue University, United States

***Correspondence:**
Ralf Takors
takors@ibvt.uni-stuttgart.de;
ralf.takors@ibvt.uni-stuttgart.de

Specialty section:
This article was submitted to Synthetic Biology, a section of the journal Frontiers in Bioengineering and Biotechnology

Received: 30 December 2020
Accepted: 09 February 2021
Published: 03 March 2021

Citation:
Hermann M, Teleki A, Weitz S, Niess A, Freund A, Bengelsdorf FR, Dürre P and Takors R (2021) Identifying and Engineering Bottlenecks of Autotrophic Isobutanol Formation in Recombinant *C. ljungdahlii* by Systemic Analysis. Front. Bioeng. Biotechnol. 9:647853. doi: 10.3389/fbioe.2021.647853

Clostridium ljungdahlii (*C. ljungdahlii*, CLJU) is natively endowed producing acetic acid, 2,3-butandiol, and ethanol consuming gas mixtures of CO_2, CO, and H_2 (syngas). Here, we present the syngas-based isobutanol formation using *C. ljungdahlii* harboring the recombinant amplification of the "Ehrlich" pathway that converts intracellular KIV to isobutanol. Autotrophic isobutanol production was studied analyzing two different strains in 3-L gassed and stirred bioreactors. Physiological characterization was thoroughly applied together with metabolic profiling and flux balance analysis. Thereof, KIV and pyruvate supply were identified as key "bottlenecking" precursors limiting preliminary isobutanol formation in CLJU[KAIA] to 0.02 g L^{-1}. Additional blocking of valine synthesis in CLJU[KAIA]:*ilvE* increased isobutanol production by factor 6.5 finally reaching 0.13 g L^{-1}. Future metabolic engineering should focus on debottlenecking NADPH availability, whereas NADH supply is already equilibrated in the current generation of strains.

Keywords: *Clostridium ljungdahlii*, intracellular metabolite pools, synthesis gas fermentation, recombinant product formation, isobutanol

INTRODUCTION

Isobutanol is an important commodity in the chemical, food, and pharmaceutical industries with rising global market size (Karabektas and Hosoz, 2009; Grand View Research, 2016). Furthermore, it is a promising fuel substitute showing lower vapor pressure, volatility, and hygroscopicity and higher energy density than bioethanol (Atsumi et al., 2010). Currently, the production of isobutanol is mainly based on petroleum resources. In addition, there are already several biotechnological approaches mainly based on sugars (Chen and Liao, 2016). Synthesis gas (syngas) represents a further promising substrate for biotechnological production of isobutanol as it can replace fossil-based resources and simultaneously prevent a competition with the availability of food. Syngas is a mixture mainly composed of carbon monoxide (CO), carbon dioxide (CO_2), and hydrogen (H_2) derived from agricultural, industrial, and municipal wastes and thus representing an inexpensive

feedstock (Bengelsdorf and Dürre, 2017; Takors et al., 2018). Several anaerobic bacteria are able to metabolize syngas components via hydrogenesis, methanogenesis, or acetogenesis to a wide range of products (Latif et al., 2014; Diender et al., 2015; Takors et al., 2018). Thereof, *C. ljungdahlii* is a promising biocatalyst as it can convert autotrophically syngas, solely CO, and mixtures of CO_2 and H_2 to its natural products acetate, ethanol, 2,3-butanediol, and lactate (Tanner et al., 1993; Köpke et al., 2010, 2011). Its ability to fix CO and CO_2 relies on the Wood-Ljungdahl-Pathway (WLP) that is described in detail in several excellent review articles (Drake et al., 2008; Ragsdale and Pierce, 2008; Schuchmann and Müller, 2014). **Figure 1** shows a scheme of the basic metabolic pathways of syngas-fermenting *C. ljungdahlii*. In short, the WLP is a two-branched reductive pathway characterized by a stepwise reduction of CO_2 to a methyl group (methyl branch) which subsequently is combined with CO (carbonyl branch) to acetyl-CoA, the key-precursor for biomass and products. The WLP is energy-limited as only one ATP may be generated by the conversion of acetyl-CoA to acetate. This, in turn, is needed to reduce CO_2 in the methyl branch, leaving no net ATP formation *via* substrate-level phosphorylation. Hence, a proton gradient coupled to an H^+-translocating ATPase is decisive for the energy provision in *C. ljungdahlii*. In this context, the membrane-bound ferredoxin:NAD oxidoreductase (Rnf complex) plays a crucial role as it couples the electron transfer from reduced ferredoxin (Fd_{red}) to NAD^+ to a simultaneous translocation of protons through the cell membrane (Müller et al., 2008; Tremblay et al., 2012; Hess et al., 2016). The required reducing equivalents are provided by the oxidation of CO *via* carbon monoxide dehydrogenase (CODH) or H_2 using a bifurcating hydrogenase (Hyd) reaction (Köpke et al., 2010; Schuchmann and Müller, 2012; Buckel and Thauer, 2013; Wang et al., 2013). An electron bifurcating transhydrogenase (Nfn) reaction is also involved in the energy conservation of *C. ljungdahlii*. It catalyzes the endergonic reduction of $NADP^+$ with NADH coupled to the exergonic reduction of $NADP^+$ with Fd_{red} (Mock et al., 2015; Aklujkar et al., 2017; Liang et al., 2019). Consequently, Fd_{red} availability tightly links energy management, substrate composition, and product formation in *C. ljungdahlii*. In this context, we identified syngas as a suitable substrate to produce reduced alcohols, presenting the highest 2,3-butanediol formation using a batch process with *C. ljungdahlii* described so far (Hermann et al., 2020). Furthermore, *C. ljungdahlii* is genetically accessible enabling the optimized formation of natural and recombinant products *via* metabolic engineering (Huang et al., 2019; Molitor et al., 2016; Woolston et al., 2018). Weitz et al. (2021) engineered several *C. ljungdahlii* strains and successfully demonstrated isobutanol formation analyzing heterotrophic and autotrophic growth conditions by lab scale batch fermentation experiments. This study builds on the findings of Weitz et al. (2021) by investigating autotrophic syngas-based isobutanol formation applying the two recombinant strains CLJU[KAIA] and CLJU[KAIA]:*ilvE*. Based on 3-L batch cultivations in gassed stirred bioreactors, strains were physiologically characterized, thoroughly investigated *via* intracellular metabolomics, and quantified *via* Flux Balance Analysis (FBA). Thereof, promising metabolic engineering targets were derived finally yielding CLJU[KAIA]:*ilvE* which achieved 130 mg of isobutanol/L.

MATERIALS AND METHODS

A complete description of all methods below can be found in the appendix.

Bacterial Strains, Growth Medium and Pre-culture Preparation

Clostridium ljungdahlii DSM 13528 (Tanner et al., 1993) was obtained from the German Collection of Microorganisms and Cell Cultures (DSMZ). The recombinant *C. ljungdahlii* strains CLJU[KAIA] and CLJU[KAIA]:*ilvE* were kindly provided by the group of Peter Dürre (Institute of Microbiology and Biotechnology, University of Ulm). Details of strain construction are described elsewhere Weitz et al. (2021). Medium and preculture seed train was described earlier (Hermann et al., 2020). The last pre-culture step was based on syngas, characterized by the same gas composition as the bioreactor substrate.

Batch Cultivation Studies in a Stirred-Tank Reactor With Different Substrates

Anaerobic syngas-based batch cultivations were performed in a fully controlled 3-L stirred-tank bioreactor (Bioengineering, Wald, Switzerland) with an operational volume of 1.5 L. The detailed reactor equipment was previously described in Hermann et al. (2020). Temperature and pH were kept constant at 37°C and 5.9, respectively. The agitation speed of the impeller was 500 rpm during the whole cultivation process. The substrate gas was fed continuously into the reactor using one mass flow controller (Bronkhorst High-Tech B. V., Ruurlo, Netherlands) and a predefined gas mixture with a constant gassing rate of 13.2 L h^{-1}. The gas composition was 55% CO, 30% H_2, 5% CO_2, and 10% Ar. To set anaerobic conditions, the medium-containing bioreactor was sparged with nitrogen with a gassing rate of 60 L h^{-1} applied for 2 h. Off-gas measurements guaranteed that oxygen concentrations were always below 0.01% (vv^{-1}). Afterward, the medium was equilibrated with the substrate gas for 5 h. Two hours prior to inoculation of the bioreactor, sterile reducing agent was added (Tanner et al., 1993). To observe growth, extracellular product formation, and intracellular metabolite pools, samples were taken frequently during the cultivations.

All fermentations showed very similar growth and substrate uptake kinetics. Only product formation differed with respect to isobutanol production.

Analytical Methods

Biomass Concentration Analysis

Cell density was determined offline *via* a UV/Visible spectrophotometer at 600 nm. A detailed description is found in Hermann et al. (2020).

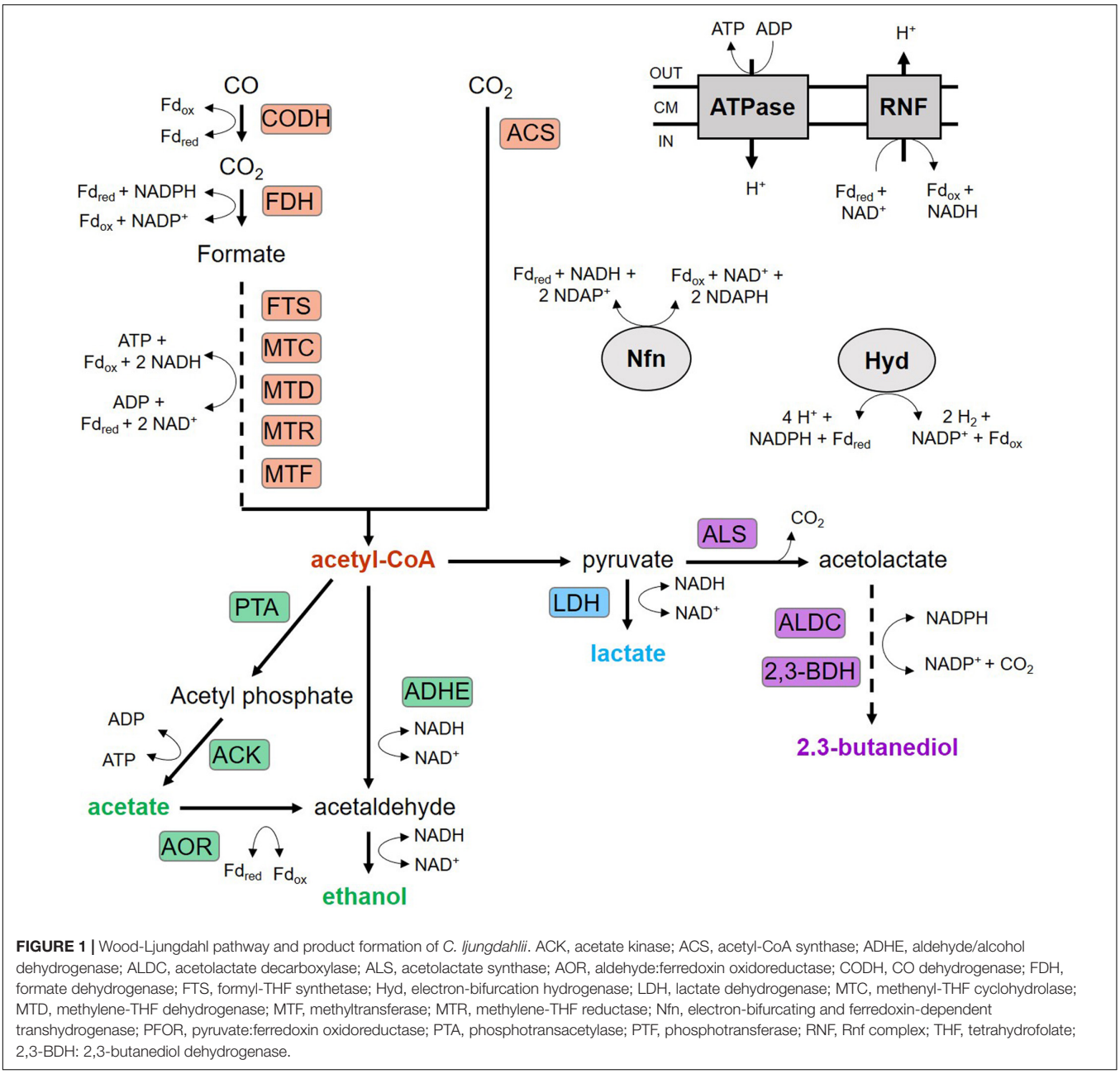

FIGURE 1 | Wood-Ljungdahl pathway and product formation of *C. ljungdahlii*. ACK, acetate kinase; ACS, acetyl-CoA synthase; ADHE, aldehyde/alcohol dehydrogenase; ALDC, acetolactate decarboxylase; ALS, acetolactate synthase; AOR, aldehyde:ferredoxin oxidoreductase; CODH, CO dehydrogenase; FDH, formate dehydrogenase; FTS, formyl-THF synthetase; Hyd, electron-bifurcation hydrogenase; LDH, lactate dehydrogenase; MTC, methenyl-THF cyclohydrolase; MTD, methylene-THF dehydrogenase; MTF, methyltransferase; MTR, methylene-THF reductase; Nfn, electron-bifurcating and ferredoxin-dependent transhydrogenase; PFOR, pyruvate:ferredoxin oxidoreductase; PTA, phosphotransacetylase; PTF, phosphotransferase; RNF, Rnf complex; THF, tetrahydrofolate; 2,3-BDH: 2,3-butanediol dehydrogenase.

Analysis of Extracellular Products

The extracellular formation of ethanol, acetate, 2,3-butanediol, lactate, and isobutanol was observed using an isocratic high-performance liquid chromatography (HPLC) equipped with a RI detector and a Rezex ROA-Organic Acid H^+ column. Measuring parameters and sample preparation are described in Hermann et al. (2020).

LC-MS Based Analysis of Intracellular Metabolites' Concentrations

Intracellular metabolites' concentrations in [μmol $g_{CDW}{}^{-1}$] were quantified using an HPLC system coupled to a triple quadrupole tandem mass spectrometer (QQQ-MS/MS) equipped with an electrospray ion source. Therefore, 5 mL cell suspension each were taken periodically as triplicates in the course of the exponential growth phases of the batch cultures. Extraction and quantification of non-derivatized polar metabolites was described earlier (Teleki et al., 2015; Hermann et al., 2020). Due to their high reactivity, the analysis of α-keto acids (aKG, pyruvate, and OAA) required a preceding derivatization treatment based on the condensation of aldehyde and keto groups by phenylhydrazine (Zimmermann et al., 2014). In addition, a quantification method based on bicratic reverse phase chromatography (RPLC) with acidic mobile phase conditions was applied. For this purpose, an adapted derivatization strategy as well as the respective LC-MS/MS protocol was developed and

described by Junghans et al. (2019). Therefore, for determination of the intracellular pools of pyruvate, KIV, aKG, and OAA 2.5 μL of a freshly prepared 50 mM phenylhydrazine stock solution were added to 24 μL of the metabolite extracts. Additionally, the samples were spiked with 4 μL of a defined standard mix or water and mixed with 1 μL of a 2.2 mM glyoxylate (Gxy) solution. After an incubation at room temperature for 1 h the samples were quenched with 0.5 μL of a 10%(vv^{-1}) formic acid stock solution and 18 μL of acetonitrile. Gxy was considered to monitor instrumental fluctuations and the standard mix was needed for the absolute quantification of the respective α-keto acids. Based on previous measurements, the composition of the standard mix was set to 12 μM pyruvate, 1.6 μM OAA, 2 μM KIV, and 6 μM aKG. By means of different water to standard mix ratios during sample preparation internal calibration curves with four levels for each metabolite were achieved. Thus, internal calibration curves resulted from a standard quadruple addition of defined amounts of the respective metabolite standards directly to the sample.

Online Analysis of the Exhaust Gas

Exhaust gas measurement was performed online by mass spectrometry to determine gas uptake and production as described in Hermann et al. (2020).

Determination of Cell Specific Rates

For each growth phase biomass-specific substrate uptake and product formation rates were calculated by considering the exponential growth rate μ, the biomass substrate yield YX/S, or the biomass product yield YX/P, respectively. A detailed description is found in Hermann et al. (2020).

Determination of the Gibbs Free Energy Changes ΔG_R

Gibbs free reaction energy changes ΔG_R were calculated to compare the individual processes at the energetic level as described by Villadsen et al. (2011). Corresponding calculations for the individual processes are attached in the appendix.

Flux Balance Analysis

Model simulations were performed based on the *Insilico* Discovery™ platform using the previously reconstructed and described model rSMM (Hermann et al., 2020), which was supplemented by a formate-H_2 lyase like reaction (Wang et al., 2013) and recombinant isobutanol formation. This model is characterized by a constant growth-associated maintenance (GAM) value of 46.7 mmol ATP $g_{CDW}{}^{-1}$ (Nagarajan et al., 2013) and the invariable non-growth-associated maintenance value (NGAM) of 5 mmol $(g_{CDW}{}^{*}h)^{-1}$. For NGAM estimation the mean maintenance cost identified for the closely related acetogen *Clostridium autoethanogenum* growing on different gaseous substrates was considered (Valgepea et al., 2018; Heffernan et al., 2020). Further assumption and characteristics of the model are described in Hermann et al. (2020). As the degree of freedom exceeds the maximal number of quantifiable fluxes, FBA was used to investigate the intracellular flux distribution (Schilling et al., 2000; Orth et al., 2010). Maximization of biomass production was set as objective function, while all experimentally determined product formation and substrate uptake rates were used to constrain the solution space (O'Brien et al., 2015). Further details of the applied FBA method are found in Hermann et al. (2020).

RESULTS

Syngas-Based Batch Cultivation of CLJU[WT]

Growth, Product Formation and Substrate Uptake

Before investigating a recombinant isobutanol formation based on syngas, a reference process (REF) was used to analyze growth, product formation, and substrate uptake of the *C. ljungdahlii* wildtype strain (CLJU[WT]) (**Figure 2**). Therefore, a syngas-based batch cultivation in a steadily gassed 3-L bioreactor was performed in duplicates. The detailed composition of the substrate gas is described in the Experimental procedures section. The growth phases, final product concentrations, and substrate-to-product yields of the process are summarized in **Tables 1**, **2**. We identified two growth phases with μ_{exp} = 0.05 ± 0.005 h^{-1} [average ± standard deviation] in the first (approximately 20 – 80 h) and μ_{exp} = 0.01 ± 0.001 h^{-1} in the following period (approximately 90 – 120 h). After approximately 140 h, the final CDW = 0.85 ± 0.06 g L^{-1} was reached representing 2.3 ± 0.6% of totally captured carbon. Furthermore, the two growth periods were characterized by different substrate uptake patterns. During the first phase, CO uptake accompanied by proportional CO_2 formation occurred. Maximum volumetric and biomass specific rates were r_{CO} = 16.3 ± 4.1 mmol $(L^{*}h)^{-1}$ i.e., q_{CO} = 38.8 ± 4.1 mmol $(g_{CDW}{}^{*}h)^{-1}$ and r_{CO2} = 11.3 ± 1.4 mmol $(L^{*}h)^{-1}$ i.e., q_{CO2} = 27.4 ± 3.4 mmol $(g_{CDW}{}^{*}h)^{-1}$, respectively. Subsequently, both rates decreased to r_{CO} = 12.8 ± 2.7 mmol $(L^{*}h)^{-1}$ i.e., q_{CO} = 16.1 ± 3.4 mmol $(g_{CDW}{}^{*}h)^{-1}$ and r_{CO2} = 8.7 mmol ± 1.0 $(L^{*}h)^{-1}$ i.e., q_{CO2} = 11.00 mmol ± 1.3 $(g_{CDW}{}^{*}h)^{-1}$. Only very low H_2 uptake even revealing large deviations between the two biological replicates was observed. On average, r_{H2} = 0.2 ± 0.03 mmol $(L^{*}h)^{-1}$ and $r_{H2} = -0.01 \pm 0.4$ mmol $(L^{*}h)^{-1}$ were measured for the first and second period, respectively. Acetate patterns showed similar trends in biological duplicates with acetate formation during early first phase, reaching a maximum until the beginning of the second period when consumption started. The residual of 0.38 ± 0.08 g L^{-1} represented only 0.9 ± 0.02% of totally captured carbon. On the contrary, the formation of the reduced products ethanol, 2.3-butanediol, and lactate started after the initiation of acetate formation showing a steady rise with final concentrations of 5.9 ± 0.9 g L^{-1} for ethanol, 3.5 ± 0.6 g L^{-1} for 2.3-butanediol, and 0.01 ± 0.03 g L^{-1} for lactate. Accordingly, *C ljungdahlii* converted approximately 30% of consumed carbon into reduced products. The total free Gibbs reaction energy ΔG_R of the process was – 33.55 ± 1.92 kJ C-$mole^{-1}$.

Intracellular Metabolites Pattern

To further characterize the physiological state of the cells 32 intracellular metabolite pools were analyzed (**Figure 3**) at

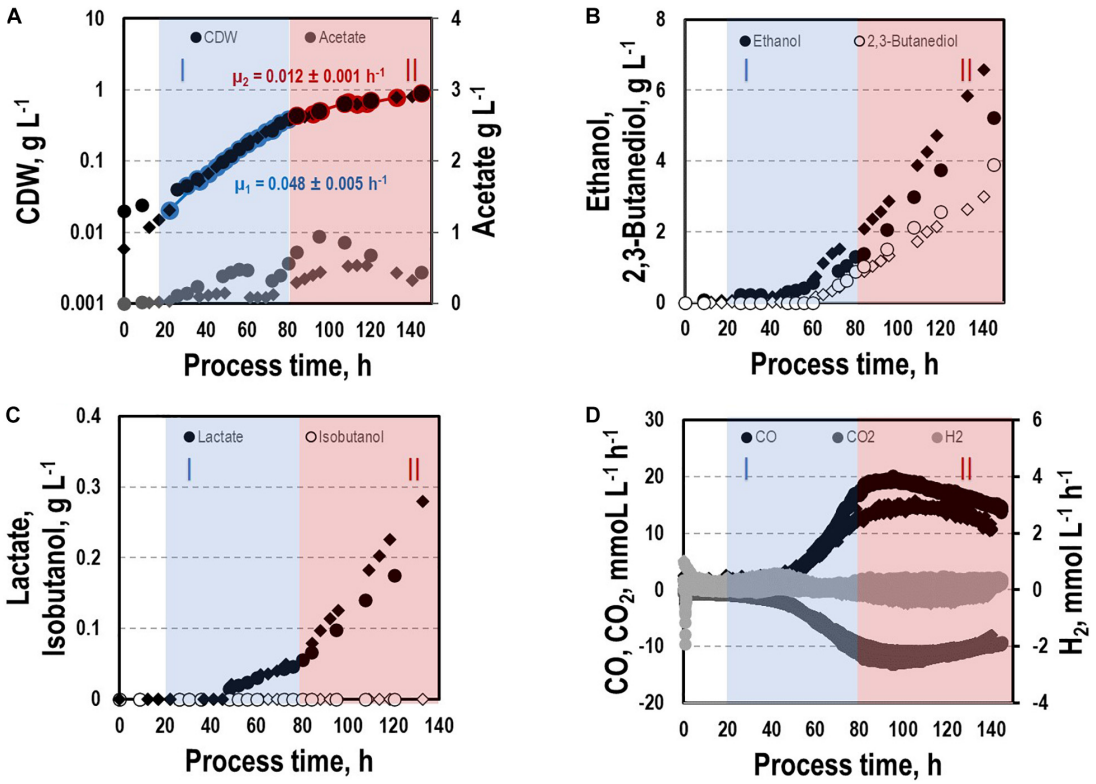

FIGURE 2 | Syngas batch cultivation of CLJU[WT] in a stirred bioreactor with continuous gas supply. Depicted are concentrations of cell dry weight and acetate **(A)**, ethanol and 2,3-butanediol **(B)**, lactate and isobutanol **(C)**, and gas uptake **(D)** of two independent experiments (circles and diamonds). Two growth phases I (blue) and II (red) were identified. Statistical details are given in the **Supplementary Material** (**Supplementary Table 1**).

TABLE 1 | Maximal growth rates and final by-product concentrations of the syngas-based batch cultivations of the different *C. ljungdahlii* strains in a steadily gassed stirred bioreactor.

Strain	μ_{max}, h^{-1}	c_{CDW}, g L^{-1}	$c_{Acetate}$, g L^{-1}	$c_{Ethanol}$, g L^{-1}	$c_{2,3-BD}$, g L^{-1}	$c_{Lactate}$, g L^{-1}	$c_{Isobutanol}$, g L^{-1}
CLJU[WT]	0.048 ± 0.005	0.85 ± 0.06	0.38 ± 0.08	5.90 ± 0.95	3.45 ± 0.64	0.26 ± 0.05	
CLJU[KAIA]	0.071	0.73	0.22	5.25	2.38	0.25	0.02
CLJU[KAIA]:*ilvE*	0.055	0.89	0.83	5.90	3.42	0.09	0.13

Rates reflect exponential growth. Values of the wildtype cultivation indicate mean of duplicates.

TABLE 2 | Final biomass and product yields of the syngas-based batch cultivations of the different *C. ljungdahlii* strains in steadily gassed stirred-tank bioreactor (T = 37°C; pH = 5.9; V_R = 3 L; 500 rpm).

Strain	Y_{CDW}	$Y_{Acetate}$	$Y_{Ethanol}$	$Y_{2,3-BD}$	$Y_{Lactate}$	$Y_{Isobutanol}$	Y_{CO2}
	C-mole $_{(Product)}$ mole^{-1} $_{(CO)}$						
CLJU[WT]	0.023 ± 0.006	0.009 ± 2.3*10^{-5}	0.19 ± 0.07	0.12 ± 0.002	0.007 ± 0.003		0.71 ± 0.005
CLJU[KAIA]	0.026	0.006	0.20	0.09	0.009	0.001	0.70
CLJU[KAIA]:*ilvE*	0.027	0.024	0.17	0.09	0.002	0.003	0.65

Values of the wildtype cultivation indicate mean of duplicates.

representative sampling times. Pool sizes differed individually ranging from about 0.001 μmol g_{CDW}^{-1} for KIV, oxaloacetate (OAA), and 2-ketoglutarate (αKG) to 8 μmol g_{CDW}^{-1} for alanine. Whereas most pool sizes remained constant throughout the process, pyruvate and serine depleted during the second growth phase. In contrast, remarkably large pool sizes were found for valine, glutamate, aspartate, alanine, and lysine.

Intracellular patterns of ATP, ADP, AMP, and the respective adenylate energy charge (AEC) were studied to evaluate whether or not non-wanted energy shortage might exist growing on syngas (**Figure 4**). ATP pools dropped until they leveled out

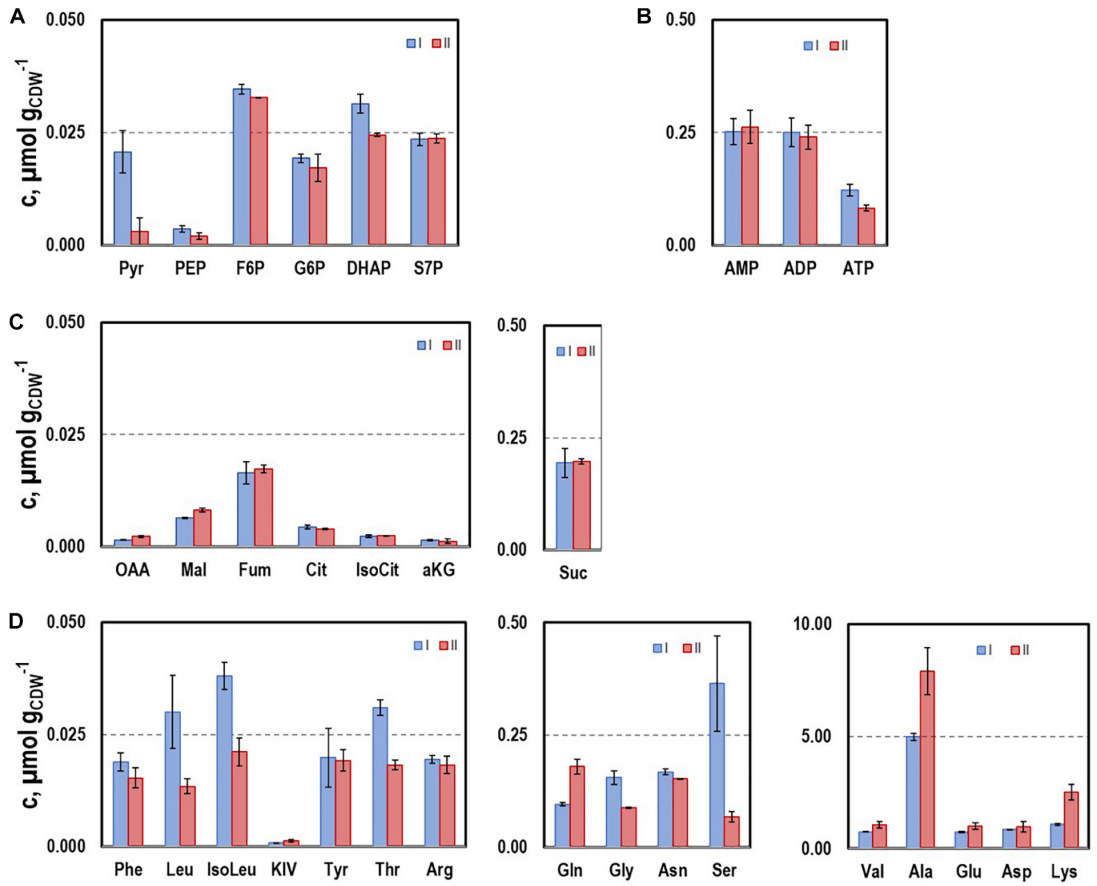

FIGURE 3 | Selected intracellular pools representing Emden-Meyerhof-Parnas and the pentose-phoshate pathway **(A)**, energy metabolism **(B)**, citrate cycle **(C)**, and amino acids **(D)**. Samples were taken during growth phases I and II cultivating CLJU[WT] on syngas in a stirred tank. Error bars are derived from technical replicates.

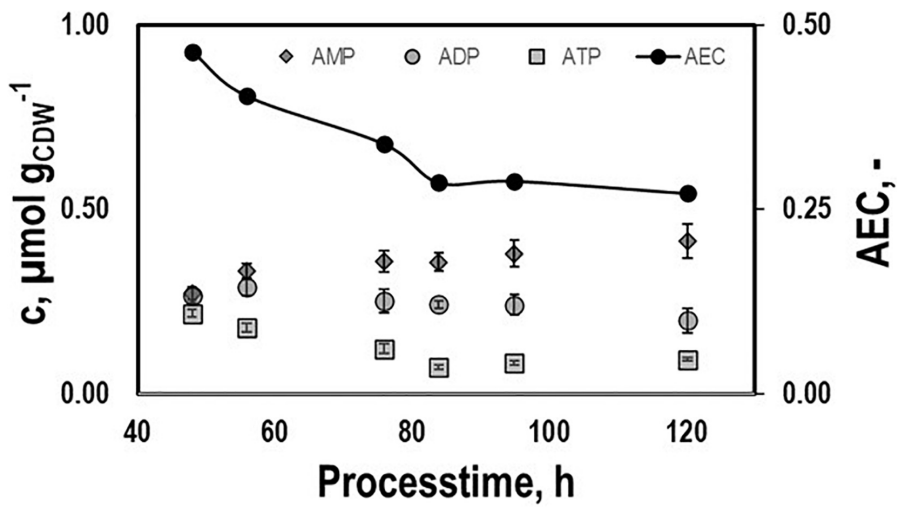

FIGURE 4 | Intracellular pools of AMP, ADP, and ATP and the respective AEC values. Samples were taken during growth phases I and II cultivating CLJU[WT] on syngas in a stirred tank. Error bars are derived from technical replicates.

at 0.08 $\mu molg_{CDW}{}^{-1}$ during the second period. A similar trend was found for AEC starting at 0.46 and ending at 0.28. On contrary, AMP and ADP rather remained at about 0.25 $\mu molg_{CDW}{}^{-1}$.

Batch Cultivations of the Recombinant Strains CLJU[KAIA] and CLJU[KAIA]:ilvE Using Syngas

CLJU[KAIA]

Recombinant isobutanol production from syngas was studied using the strain CLJU[KAIA] which possesses plasmid-encoded amplification of pyruvate-to-KIV conversion followed by the conversion of KIV *via* recombinant Ehrlich pathway (**Figure 5**). Process parameters of the batch equaled those of the REF leading to kinetics and process values indicated in **Figure 6** and in **Tables 1**, **2**. Again, biphasic growth occurred revealing μ_{exp} = 0.07 h^{-1} between 20 – 60 h and μ_{exp} = 0.02 h^{-1} between 60 – 120 h. The final CDW was 0.73 g L^{-1} which equals 2.6% of the entire carbon capture in biomass. Compared to REF, CLJU[KAIA] grew 50% faster during phase I disclosing similar CO-to-CDW yield. Also, substrate uptake kinetics resembled REF showing CO_2 formation accompanying CO uptake during phase I. Maximum volumetric and specific rates were r_{CO} = 17.6 mmol $(L^*h)^{-1}$ i.e., q_{CO} = 34.6 mmol $(g_{CDW}{}^*h)^{-1}$ and r_{CO2} = 13.8 mmol $(L^*h)^{-1}$ i.e., q_{CO2} = 27.0 mmol $(g_{CDW}{}^*h)^{-1}$. During growth period II, biomass specific rates for CO uptake q_{CO} = 25.2 mmol $(g_{CDW}{}^*h)^{-1}$ and CO_2 formation

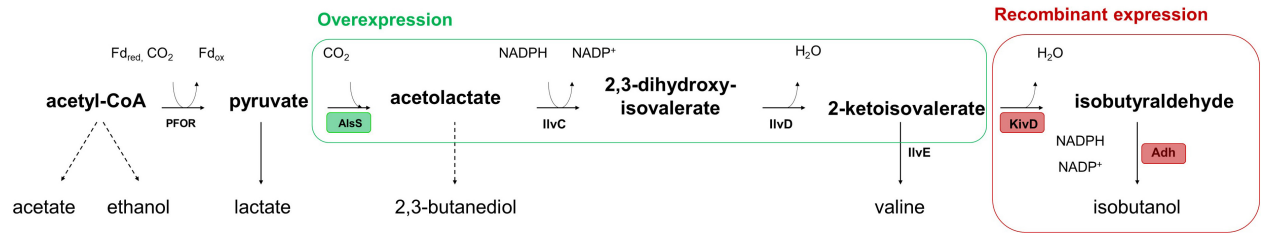

FIGURE 5 | Recombinant isobutanol pathway in CLJU[KAIA] characterized by plasmid-encoded amplification of pyruvate-to-KIV conversion followed by the conversion of KIV via recombinant Ehrlich pathway. PFOR: pyruvate:ferredoxin-oxidoreductase; AlsS: acetolactate synthase; IlvC: ketol-acid reductoisomerase, IlvD: dihydroxy-acid dehydratase; Ilve: amino acid aminotransferase; KivD: ketoisovalerate decarboxalyse; Adh: alcohol dehydrogenase.

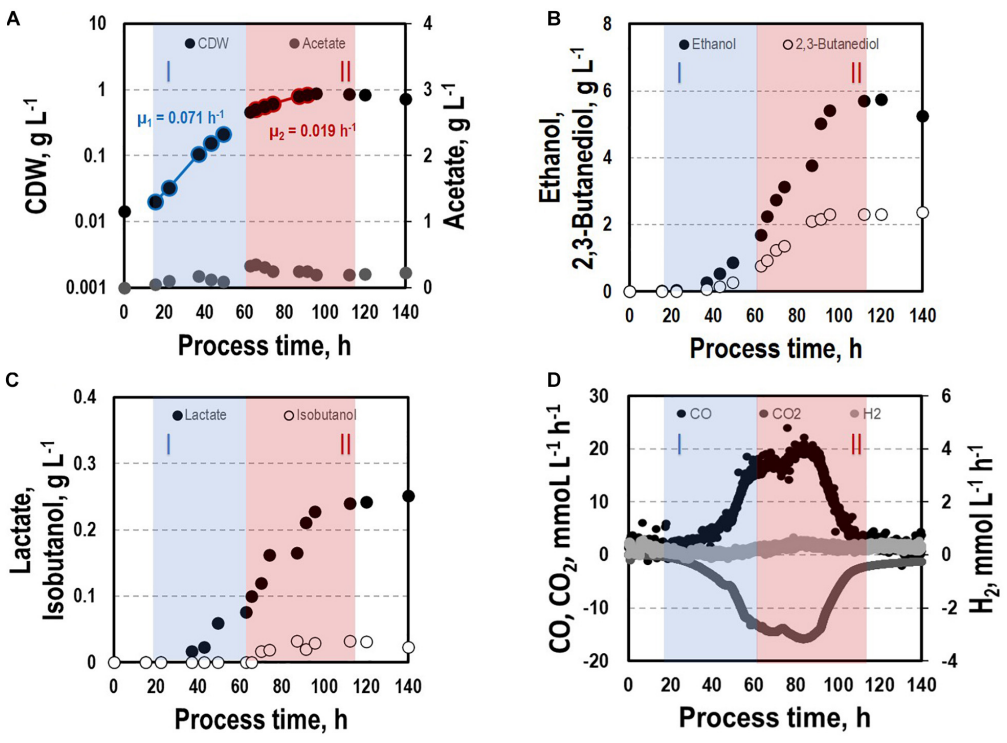

FIGURE 6 | Syngas-based batch cultivation of CLJU[KAIA] in a stirred tank bioreactor with a continuous gas supply. Shown are the concentrations of cell dry weight and acetate **(A)**, ethanol and 2,3-butanediol **(B)**, lactate and isobutanol **(C)**, and the gas uptake **(D)** (T = 37°C; pH = 5.9; VR = 3 L; 500 rpm). Two growth phases I (marked blue) and II (marked red) were identified. Statistical details are given in the **Supplementary Material** (**Supplementary Table 1**)

q_{CO2} = 18.9 mmol $(g_{CDW}{}^*h)^{-1}$ decreased. Low H_2 uptake was observed in each phase with $r_{H2,I}$ = 0.2 mmol $(L^*h)^{-1}$ followed by $r_{H2,II}$ = 0.4 mmol $(L^*h)^{-1}$. The product spectrum was similar to the REF with the final concentrations of 0.22 g L^{-1} of acetate, 5.25 g L^{-1} of ethanol, 2.38 g L^{-1} of 2.3-butanediol, 0.25 g L^{-1} of lactate, and 0.02 g L^{-1} of isobutanol. The total free Gibbs reaction energy ΔG_R of the process was – 36.15 kJ C-mole^{-1} (**Table 3**).

In order to identify possible metabolic engineering targets for optimizing isobutanol production, we compared the patterns of the intracellular metabolites pyruvate, KIV, and valine with those of the REF (**Figure 7**). KIV courses were almost identical, notably revealing the lowest pool sizes of all. Pyruvate levels in CLJU[KAIA] were higher than in REF which might be explained by the elevated growth rate. In addition, substantially higher levels of valine were measured in CLJU[KAIA] compared to REF throughout the entire batch culture.

CLJU[KAIA]:*ilvE*

By interrupting *ilvE* encoding valine amino transferase a block of valine synthesis was achieved. The resulting strain CLJU[KAIA]:*ilvE* was cultivated under reference conditions revealing kinetics as indicated in **Figure 8** and in **Tables 1**, **2**. Growth, substrate uptake, and product formation (except for isobutanol) resemble the wildtype. Again, we identified biphasic growth with $\mu_{exp,I}$ = 0.055 h^{-1} (20 – 80 h) and $\mu_{exp,II}$ = 0.011 h^{-1} (90 – 140 h) reaching CDW = 0.89 g L^{-1} which represents 2.7% of CO captured in biomass. Despite a suspected valine auxotrophy of CLJU[KAIA]:*ilvE* there was no reduction of growth compared to the wildtype. This indicates that the valine concentration provided by the 0.5 g L^{-1} yeast extract in the medium is sufficient. During phase I, maximum volumetric and specific rates were r_{CO} = 16.2 mmol $(L^*h)^{-1}$ i.e., q_{CO} = 33.8 mmol $(g_{CDW}{}^*h)^{-1}$ and r_{CO2} = 11.9 mmol $(L^*h)^{-1}$ i.e., q_{CO2} = 24.9 mmol $(g_{CDW}{}^*h)^{-1}$. The mean volumetric H_2 uptake rate was 0.2 mmol $(L^*h)^{-1}$. In phase II, biomass specific CO uptake and CO_2 formation rates decreased to q_{CO} = 23.5 mmol $(g_{CDW}{}^*h)^{-1}$ and q_{CO2} = 16.1 mmol $(g_{CDW}{}^*h)^{-1}$. Volumetric H_2 uptake rate slightly increased to 0.3 mmol $(L^*h)^{-1}$. At the end of the process, 0.83 g L^{-1} acetate, 5.90 g L^{-1} ethanol, 3.42 g L^{-1} 2.3-butanediol, 0.09 g L^{-1} lactate, and 0.13 g L^{-1} isobutanol were determined. The total free Gibbs reaction energy ΔG_R of the process was – 37.89 kJ C-mole^{-1} (**Table 3**). Both, isobutanol and 2,3 butanediol formation depend on NADPH which is why internal supply was worth investigating.

TABLE 3 | Carbon balances and Gibb's free reaction energies of the syngas-based batch cultivations of the different *C. ljungdahlii* strains in steadily gassed stirred-tank bioreactor (T = 37°C; pH = 5.9; V_R = 3 L; 500 rpm). Values of the wildtype cultivation indicate mean of duplicates.

Strain	C – Balance, %	Δ G_R, kJ C-mole^{-1}
CLJU[WT]	106.1 ± 7.6	−33.6 ± 1.9
CLJU[KAIA]	102.3	−36.2
CLJU[KAIA]:*ilvE*	96.6	−37.9

Simulation of Intracellular Flux Distribution

For determination of NADH and NADPH availabilities in the strains, FBA were performed. Intracellular flux patterns of the "pseudo-steady states" in phases I and II were studied using the stoichiometric metabolic model "modified rSMM" (Hermann et al., 2020), that was extended by recombinant isobutanol formation (see appendix). We applied FBA as the number of the unknown intracellular fluxes exceeded the total number of measured extracellular fluxes. Since growth was exponential in both phases, we chose the maximization of biomass production as objective function in each case. Measured uptake and consumption rates further constrained the solution space. As already shown in Hermann et al. (2020) the approach allowed very well to predict real growth rates further elucidating intracellular flux patterns. Alternate application of determined metabolic flux analysis was not possible as additional measurements e.g., using 13C labeling were not accessible. Since we could not resort to this method, we restricted the solution space by using all experimentally determined uptake and secretion rates as constraints to assure that FBA results reflect real physiological states (O'Brien et al., 2015). As a prerequisite, we qualified the achieved experimental carbon closures of 106.10 ± 7.59, 100.02, and 96.55% as "sufficient" analyzing cultivations of the wild-type (REF), CLJU[KAIA], and CLJU[KAIA]:*ilvE*, respectively (**Table 3**). The overview of all flux patterns is given in **Figure 9**. Furthermore, NADH and NADPH formation related to the consumption of electron donors CO and H_2 are listed in **Table 4**. Yields were derived from the WLP and from the Nfn reaction. In *C. ljungdahlii*, regeneration of NADH and NADPH are strongly intertwined and controlled by the provision of Fd_{red} (Hermann et al., 2020). Utilizing syngas, NADH supply is ensured *via* WLP and *via* the Rnf complex. The transhydrogenase Nfn consumes NADH providing NADPH. In turn, the reduction of CO_2 to formate by the formate dehydrogenase activity represents a NADPH sink. Also, *C. ljungdahlii* directly reduces CO_2 to formate utilizing H_2 through the formate-hydrogen lyase reaction which is carried out by a complex composed of the electron-bifurcating $NADP^+$- and ferredoxin-dependent [FeFe]-hydrogenase and formate dehydrogenase (Wang et al., 2013). Our simulation results show simultaneous activity of both reactions in each cultivation. However, the share of the formate-hydrogen lyase-like reaction strongly decreases due to limited H_2 uptake during phase II. This finding is remarkable as the explicit use of this formate-hydrogen lyase-like reaction for CO_2 reduction was found in continuously cultivated *C. autoethanogenum* (Valgepea et al., 2017). Apparently, *C. ljungdahlii* adapts CO_2 reduction to current needs via flexible enzyme activities of said reductive route. Interestingly enough, NADPH yields were up to 30% higher in isobutanol producers than in the wildtype. Higher activities of transhydrogenase (Nfn) and of the formate-hydrogen reaction rate enable this phenotype. Nevertheless, strongly

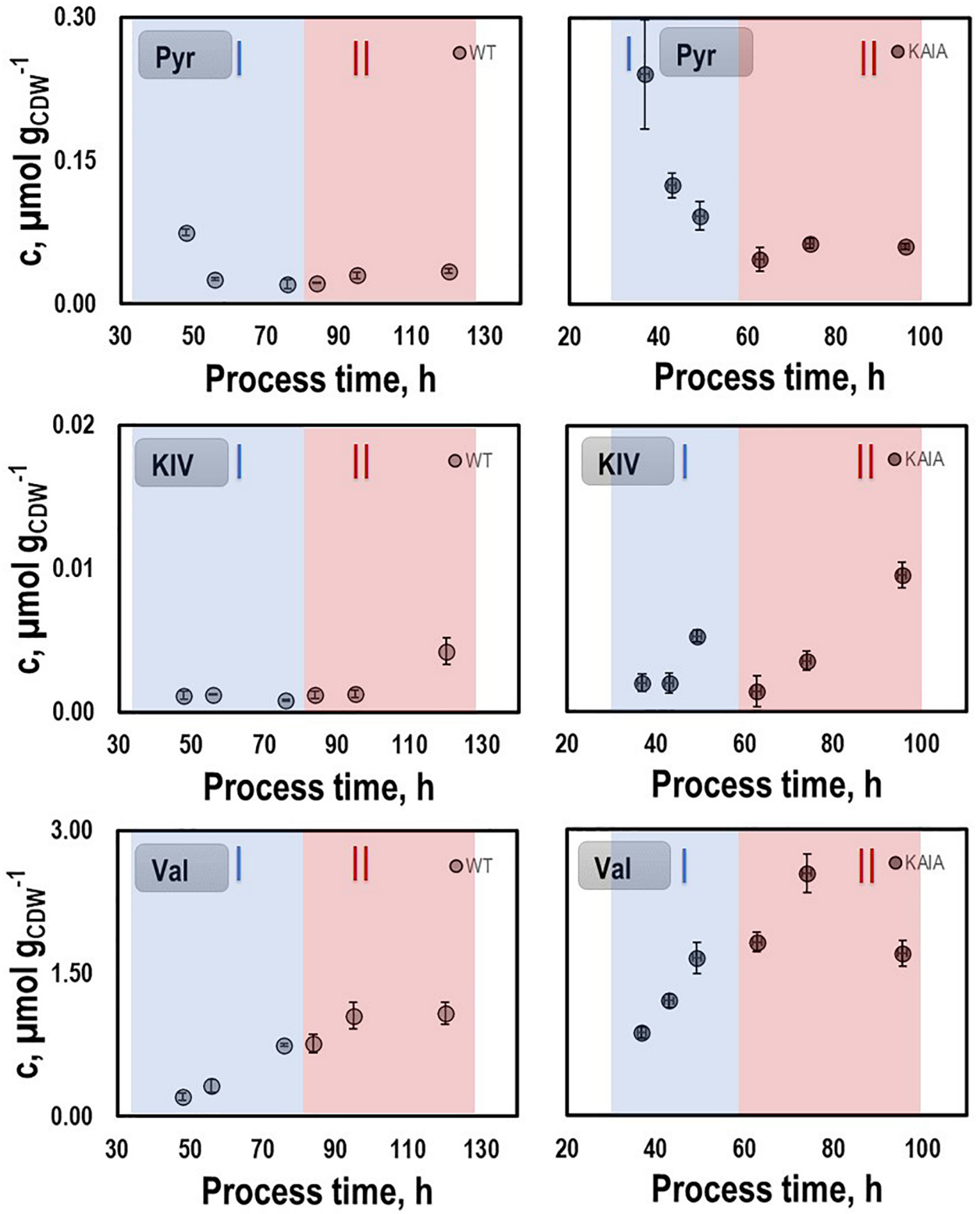

FIGURE 7 | Pyruvate (PYR), ketoisovalerate (KIV), and valine (VAL) pools in autotrophic batch cultivations of CLJU[WT, REF] and CLJU[KAIA] using syngas. Error bars are derived from technical replicates.

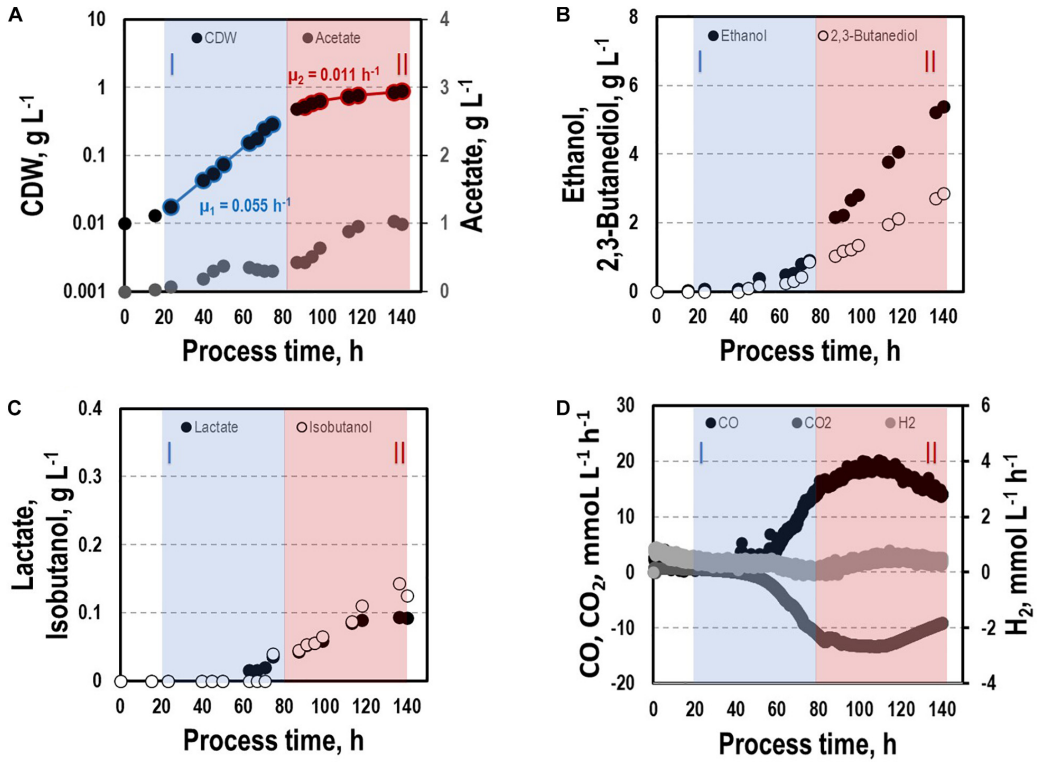

FIGURE 8 | Syngas-based batch cultivation of CLJU[KAIA]:ilvE in a stirred tank bioreactor with a continuous gas supply. Shown are the concentrations of the cell dry weight and acetate **(A)**, ethanol and 2,3-butanediol **(B)**, lactate and isobutanol **(C)**, and the gas uptake **(D)** (T = 37°C; pH = 5.9; VR = 3 L; 500 rpm). Two growth phases I (marked blue) and II (marked red) were identified. Statistical details are given in the **Supplementary Material** (**Supplementary Table 1**).

decreasing NADPH yields of 65 – 70% were determined in the second growth phase for each cultivation. On the contrary, NADH availabilities almost remained constant during phases I and II, only showing a slight 20% decrease for CLJU[KAIA]:*ilvE*.

DISCUSSION

Syngas-Based Reference Process

Metabolizing syngas during a batch cultivation *C. ljungdahlii* shows a biphasic growth behavior, that is characterized by growth reduction with simultaneously increased formation of reduced products. This coincidence was also observed in a two-stage process cultivating *C. ljungdahlii* on syngas (Richter et al., 2016). Previous studies have shown that shifts from acetogenesis to solventogenesis in syngas-fermenting *C. ljungdahlli* are accompanied by growth reduction. Metabolic rearrangements may be induced by pH shifts, nutrient limitation or addition of reducing agents into the growth medium (Gaddy and Clausen, 1992; Cotter et al., 2009; Mohammadi et al., 2016; Richter et al., 2016). In this context, Valgepea et al. (2017) demonstrated that solvent formation in *C. autoethanogenum* may be promoted by simply increasing biomass concentrations. This can be explained by the metabolic link between energy conservation and redox management in acetogens. Shifting to solventogenic alcohol production improves ATP availability *via* the Rnf-ATPase-system (Richter et al., 2016; Valgepea et al., 2017; Hermann et al., 2020). Further evidence was given by Oswald et al. (2016). They measured CO uptake rates of 33 – 100 mmol $(g_{CDW}{}^{*}h)^{-1}$ and CO_2 production rates of 13 – 40 mmol $(g_{CDW}{}^{*}h)^{-1}$ during a batch-cultivation of *C. ljungdahlii* with continuous gas supply. These values fit fairly well to our study. In contrast to our process, however, they identified a simultaneous and equivalent uptake of CO and H_2. The simultaneous utilization of these gases is also shown in further studies describing continuous cultivations performed in chemostat mode installing 0.04 h^{-1} dilution rate (Richter et al., 2013; Martin et al., 2016; Valgepea et al., 2017, 2018). Our observations did not reveal proportionality between CO and H_2 uptake which might be explained by the different syngas composition used (32.5% H_2, 32.5% CO, 16% CO_2, 19% N_2). H_2 uptake and the product spectrum depend on the H_2/CO ratio (Jack et al., 2019) which was 1 in Oswald et al. (2016) and 0.54 in this study. CO is known to be a strong inhibitor of the hydrogenase activity (Jones and Woods, 1986; Goldet et al., 2009; Devarapalli et al., 2016), but CO utilization yields the formation of more reduced products (Jack et al., 2019; Hermann et al., 2020). Moreover, acetate formation is favored by increased H_2 consumption (Jack et al., 2019). Hence, the ratio of H_2/CO affects the product portfolio strongly.

Intracellular metabolites pattern during the process reveals a clear depletion of pyruvate accompanied by a strong

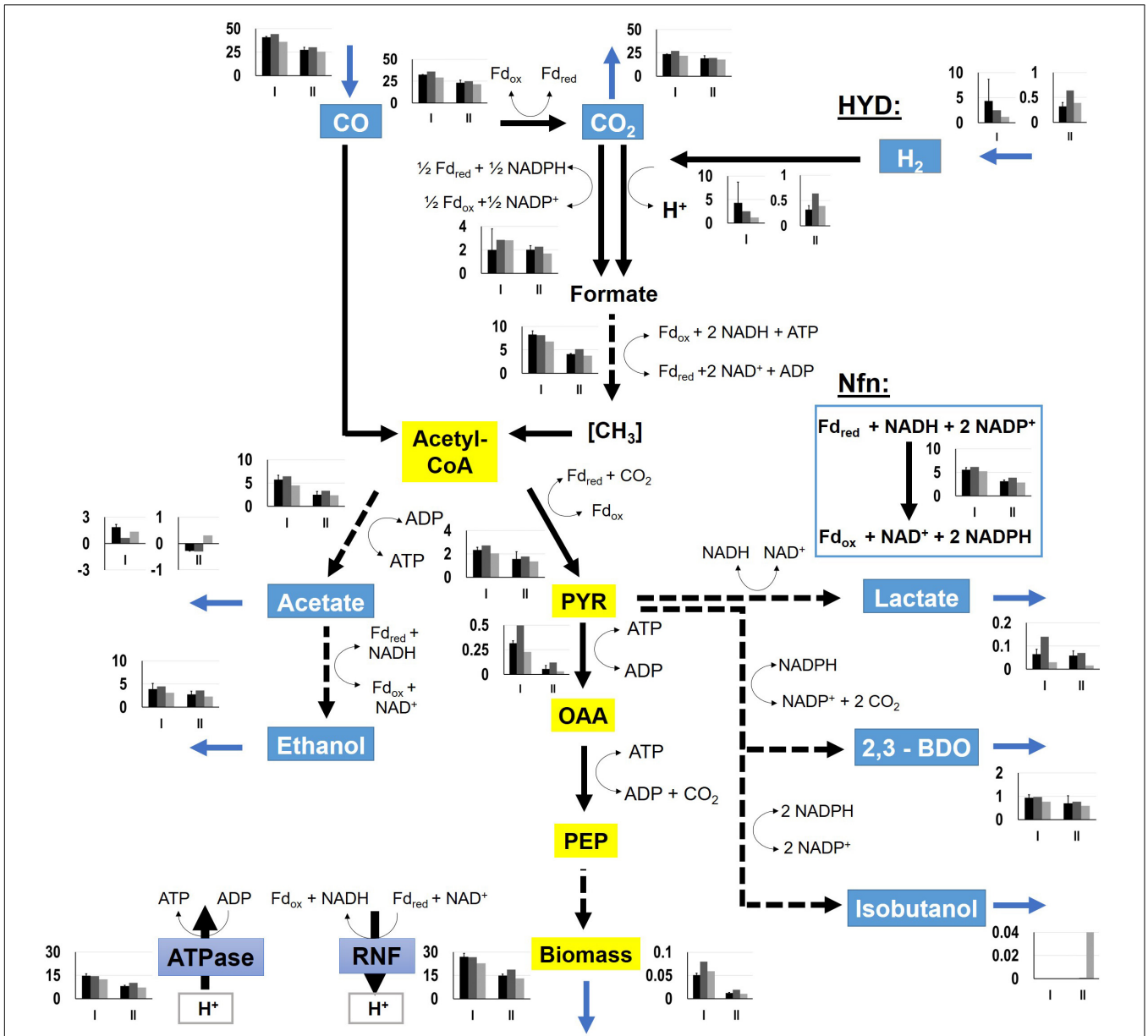

FIGURE 9 | Metabolic flux distributions of CLJU[WT, REF] (black) CLJU[KAIA] (dark gray), and CLJU[KAIA]:ilvE (light gray) based on the conversion of syngas in steadily gassed batch cultivations in stirred-tank bioreactors. Illustrated are the simulated fluxes in mmol $(g_{CDW}{}^{*}h)^{-1}$ for the first (I) and second (II) growth phase. Values of the wildtype cultivation indicate mean of duplicates.

TABLE 4 | NADH and NADPH yields derived from flux balance analysis for the first (I) and second (II) growth phase considering the WLP and the Nfn reaction.

Strain	Phase I		Phase II	
	NADH, mole $mole_{CO + H2}{}^{-1}$	NADPH, mole $mole_{CO + H2}{}^{-1}$	NADH, mole $mole_{CO + H2}{}^{-1}$	NADPH, mole $mole_{CO + H2}{}^{-1}$
CLJU[WT]	0.119 ± 0.026	0.020 ± 0.001	0.131 ± 0.028	0.006 ± 0.001
CLJU[KAIA]	0.095	0.029	0.147	0.01
CLJU[KAIA]:*ilvE*	0.109	0.027	0.086	0.009

Values of the wildtype cultivation indicate mean of duplicates.

accumulation of alanine in the second growth phase. Pyruvate serves as key precursor for 2,3-butanediol and lactate, which are mainly formed in the second phase of the process. In this regard, pyruvate depletion may limit the formation of 2.3-butanediol and isobutanol. Notably, the decreasing L-serine pool might hint to *C. ljungdahlii's* capacity converting L-serine to pyruvate via L-serine dehydratase to refill the pyruvate pool (Köpke et al., 2010).

Alanine may be synthesized by decarboxylation of aspartate and by transamination of valine, glutamate, and pyruvate (Parker and Pratt, 2010). Accordingly, it may serve as carbon and nitrogen storage that could be easily converted to pyruvate. The product formation of *C. ljungdahlii* is driven by its energy and redox management (Hermann et al., 2020). To counteract a surplus of reducing equivalents caused by continuous uptake of CO, *C. ljungdahlii* needs to produce more ethanol and 2.3-butanediol during the phase of retarded growth (Richter et al., 2016; Hermann et al., 2020). In addition, Richter et al. (2016) postulated that the metabolic shift from acidogenesis to solventogenesis of *C. ljungdahlii* is not regulated at the proteome level but rather by thermodynamics. Therefore, we hypothesize that the intracellular accumulation of alanine, valine, and glutamate enables *C. ljungdahlii* to react flexibly on increasing demands for pyruvate, the "doorman" metabolite for getting rid of "surplus" electrons. This hypothesis is supported by the intracellular AEC and AXP patterns. Despite a reduction of AEC and the ATP concentration in the first growth phase, both values remained constant in the following period.

The initial decrease of the ATP pools may be associated with anabolic ATP needs considering that acetogens are living at the edge of thermodynamic feasibility. Retarded growth, consumption of acetate, and enhanced formation of reducing products enable *C. ljungdahlii* to keep its ATP pool constant during the second period. This may be advantageous for the recombinant production of isobutanol. Schatschneider et al. (2018) measured 0.1 $\mu molg_{CDW}^{-1}$ ATP, 0.09 $\mu molg_{CDW}^{-1}$ ADP, and 0.95 $\mu molg_{CDW}^{-1}$ AMP in CO-consuming, steadily growing *C. autoethanogenum*, a close relative of *C. ljungdahlii*. Those values lead to the AEC of 0.13 which fit to the observations of this study. Interestingly, AXP levels and AEC are much lower than the so-called "physiological" levels that range from 0.80 to 0.95 (Chapman et al., 1971). However, the latter rather mirror heterotrophic growth under aerobic conditions with ATP/C ratios of 6.3 – 2.3 (assuming catabolism of glucose with P/O ratios of 2.0 – 1.1). Instead, anaerobic ATP/C gain under autotrophic growth is an order of magnitude lower (Hermann et al., 2020).

Recombinant Isobutanol Formation

Syngas-based recombinant isobutanol formation by CLJU[KAIA] was successfully achieved, although at a low level, still. Given that the total free Gibbs reaction energy ΔG_R was even lower than in REF (**Table 3**), no energy limitation was anticipated. Remarkably higher levels of valine compared to the wildtype cultivation together with the very low pyruvate levels suggested to block valine synthesis for increasing isobutanol formation. By this, a 6.5-fold increase of isobutanol titer compared to CLJU[KAIA] was achieved which supports the findings of Weitz et al. (2021). Energetically, the process should have been well equilibrated (**Table 3**) although intermediary shortcomings of reducing equivalents may not be ruled out completely. However, FBA revealed a limitation of NADPH at the end of the process, while NADH availabilities almost remained constant. Consequently, further improvements of isobutanol formation using CLJU[KAIA]:*ilvE* should be achievable by replacing the cofactor dependency on NADPH by NADH. Using a NADH-dependent variant of the ketol-acid reductoisomerase Weitz (2020) demonstrated increased isobutanol formation (18%). Ethanol and 2,3-butanediol are the main products during syngas-based batch fermentation of *C. ljungdahli* applying a H_2/CO ratio of approximately 0.5 (**Table 1**). Further strain optimization may aim to detour said reductive power into isobutanol formation. In case of ethanol this goal is very challenging as ethanol may be considered as a vital by-product of the acetaldehyde:ferredoxin oxidoreductase (AOR) which links its formation with ATP synthesis (Mock et al., 2015; Liew et al., 2017; Hermann et al., 2020; Liu et al., 2020; Zhu et al., 2020). However, elimination of 2,3-butanediol production may increase isobutanol formation as both products originate from the precursor pyruvate requiring NADPH as electron donor. Unfortunately, a first attempt to eliminate 2,3-butanediol formation in *C. ljungdahlii* was not successful. Thus, further approaches need to be performed (Weitz et al., 2021). Additionally, improved supply of H_2 may also increase the isobutanol formation. To check the hypothesis processes with higher H_2/CO ratios and/or higher reactor pressures during the solventogenic phase could be performed.

CONCLUSION

Clostridium ljungdahlii is well equipped to convert syngas mixtures with H_2:CO ratios of 0.5 into reduced products. 30% of totally consumed carbon were used to produce mostly ethanol and 2.3-butanediol. Predominately, reducing equivalents originate from CO. However, the additional H_2 uptake, even if low, enables *C. ljungdahlii* to adapt simultaneous CO_2 reduction flexibly to NADPH needs. Intracellular pyruvate availability turned out to be a carbon bottleneck of alcohol formation. The implementation of the Ehrlich-pathway partly alleviated the carbon shortage. However, only the additional block of valine formation enabled to harvest the available carbon which resulted in a 6.5-fold increase of isobutanol formation. Analyzing the redox condition in CLJU[KAIA]:*ilvE* gives rise to the conclusion that a novel metabolic engineering target should be addressed next: The increased supply of NADPH. Targeting this goal should be in the focus of future autotrophic isobutanol formation with engineering *C. ljungdahlii*.

DATA AVAILABILITY STATEMENT

The raw data supporting the conclusions of this article will be made available by the authors, without undue reservation.

AUTHOR CONTRIBUTIONS

MH designed the study, conducted the bioreactor experiments, reconstructed the stoichiometric model, performed flux balance analyses, analyzed the datasets, drafted the manuscript, and supported the laboratory conversion. AT and MH designed and performed the metabolomics analysis. AF designed and set up the laboratory for the performance of synthesis gas bioreactor studies. AN advised the network reconstruction and flux balance analysis. SW constructed the recombinant strains CLJU[KAIA] and CLJU[KAIA]:*ilvE*. FB and PD supervised the strain reconstruction and advised the study. RT conceived the study and corrected the manuscript. MH, AT, SW, FB, PD, and RT read and approved the final manuscript. All authors contributed to the article and approved the submitted version.

FUNDING

This work was funded by the Federal Ministry of Education and Research (BMBF, Grant Number: 031A468).

ACKNOWLEDGMENTS

We thank Salaheddine Laghrami for excellent support with bioreactor fermentations and Mira Lenfers-Lücker for assistance with the HPLC analyses. We also thank Flora Siebler for her support and advice during this study. Furthermore, we thank all members of the project "Gase als neue Kohlenstoffquelle für biotechnologische Fermentationen (Gas-Fermentation)" for a great cooperation.

SUPPLEMENTARY MATERIAL

The Supplementary Material for this article can be found online at: https://www.frontiersin.org/articles/10.3389/fbioe.2021.647853/full#supplementary-material

REFERENCES

Aklujkar, M., Leang, C., Shrestha, P. M., Shrestha, M., and Lovley, D. R. (2017). Transcriptomic profiles of *Clostridium ljungdahlii* during lithotrophic growth with syngas or H_2 and CO_2 compared to organotrophic growth with fructose. *Sci. Rep.* 7:13135. doi: 10.1038/s41598-017-12712-w

Atsumi, S., Wu, T.-Y., Eckl, E.-M., Hawkins, S. D., Buelter, T., and Liao, J. C. (2010). Engineering the isobutanol biosynthetic pathway in *Escherichia coli* by comparison of three aldehyde reductase/alcohol dehydrogenase genes. *Appl. Microb. Biotechnol.* 85, 651–657. doi: 10.1007/s00253-009-2085-6

Bengelsdorf, F. R., and Dürre, P. (2017). Gas fermentation for commodity chemicals and fuels. *Microb. Biotechnol.* 10, 1167–1170. doi: 10.1111/1751-7915.12763

Buckel, W., and Thauer, R. K. (2013). Energy conservation via electron bifurcating ferredoxin reduction and proton/Na^+ translocating ferredoxin oxidation. *Biochim. Biophys. Acta Bioenerg.* 1827, 94–113. doi: 10.1016/j.bbabio.2012.07.002

Chapman, A. G., Fall, L., and Atkinson, D. E. (1971). Adenylate energy charge in *Escherichia coli* during growth and starvation. *J. Bacteriol.* 108, 1072–1086.

Chen, C.-T., and Liao, J. C. (2016). Frontiers in microbial 1-butanol and isobutanol production. *FEMS Microb. Lett.* 363:fnw020. doi: 10.1093/femsle/fnw020

Cotter, J. L., Chinn, M. S., and Grunden, A. M. (2009). Ethanol and acetate production by *Clostridium ljungdahlii* and *Clostridium autoethanogenum* using resting cells. *Bioproc. Biosyst. Eng.* 32, 369–380. doi: 10.1007/s00449-008-0256-y

Devarapalli, M., Atiyeh, H. K., Phillips, J. R., Lewis, R. S., and Huhnke, R. L. (2016). Ethanol production during semi-continuous syngas fermentation in a trickle bed reactor using *Clostridium ragsdalei*. *Bioresource Technol.* 209, 56–65. doi: 10.1016/j.biortech.2016.02.086

Diender, M., Stams, A. J. M., and Sousa, D. Z. (2015). Pathways and bioenergetics of anaerobic carbon monoxide fermentation. *Front. Microb.* 6:1275. doi: 10.3389/fmicb.2015.01275

Drake, H. L., Göner, A. S., and Daniel, S. L. (2008). Old acetogens, new light. *Ann. N. Y. Acad. Sci.* 1125, 100–128. doi: 10.1196/annals.1419.016

Gaddy, J. L., and Clausen, E. C. (1992). *Clostridiumm ljungdahlii*, an anaerobic ethanol and acetate producing microorganism. *Google Patent* 5:429.

Goldet, G., Brandmayr, C., Stripp, S. T., Happe, T., Cavazza, C., Fontecilla-Camps, J. C., et al. (2009). Electrochemical kinetic investigations of the reactions of FeFe-hydrogenases with carbon monoxide and oxygen: comparing the importance of gas tunnels and active-site electronic/redox effects. *J. Am. Chem. Soc.* 131, 14979–14989. doi: 10.1021/ja905388j

Grand View Research (2016). *Isobutanol market size to reach $1.18 billion by 2022*. Available online at: https://www.grandviewresearch.com/press-release/global-isobutanol-market (accessed 12 October 2020).

Heffernan, J. K., Valgepea, K., Souza Pinto, Lemgruber, R., de, Casini, I., et al. (2020). Enhancing CO_2 -valorization using *Clostridium autoethanogenum* for sustainable fuel and chemicals production. *Front. Bioeng. Biotechnol.* 8:204. doi: 10.3389/fbioe.2020.00204

Hermann, M., Teleki, A., Weitz, S., Niess, A., Freund, A., Bengelsdorf, F. R., et al. (2020). Electron availability in CO_2, CO and H_2 mixtures constrains flux distribution, energy management and product formation in *Clostridium ljungdahlii*. *Microb. Biotechnol.* 6, 1831–1846. doi: 10.1111/1751-7915.13625

Hess, V., Gallegos, R., Jones, J. A., Barquera, B., Malamy, M. H., and Müller, V. (2016). Occurrence of ferredoxin:NAD(+) oxidoreductase activity and its ion specificity in several Gram-positive and Gram-negative bacteria. *PeerJ.* 4:e1515. doi: 10.7717/peerj.1515

Huang, H., Chai, C., Yang, S., Jiang, W., and Gu, Y. (2019). Phage serine integrase-mediated genome engineering for efficient expression of chemical biosynthetic pathway in gas-fermenting *Clostridium ljungdahlii*. *Metabolic Eng.* 52, 293–302. doi: 10.1016/j.ymben.2019.01.005

Jack, J., Lo, J., Maness, P.-C., and Ren, Z. J. (2019). Directing *Clostridium ljungdahlii* fermentation products via hydrogen to carbon monoxide ratio in syngas. *Biomass Bioener.* 124, 95–101. doi: 10.1016/j.biombioe.2019.03.011

Jones, D. T., and Woods, D. R. (1986). Acetone-butanol fermentation revisited. *Microb. Rev.* 50, 484–524.

Junghans, L., Teleki, A., Wijaya, A. W., Becker, M., Schweikert, M., and Takors, R. (2019). From nutritional wealth to autophagy: In vivo metabolic dynamics in the cytosol, mitochondrion and shuttles of IgG producing CHO cells. *Metab. Eng.* 54, 145–159. doi: 10.1016/j.ymben.2019.02.005

Karabektas, M., and Hosoz, M. (2009). Performance and emission characteristics of a diesel engine using isobutanol–diesel fuel blends. *Renewable Ener.* 34, 1554–1559. doi: 10.1016/J.RENENE.2008.11.003

Köpke, M., Held, C., Hujer, S., Liesegang, H., Wiezer, A., Wollherr, A., et al. (2010). *Clostridium ljungdahlii* represents a microbial production platform based on syngas. *Proc. Natl. Acad. Sci. USA* 107, 13087–13092. doi: 10.1073/pnas.1004716107

Köpke, M., Mihalcea, C., Liew, F., Tizard, J. H., Ali, M. S., Conolly, J. J., et al. (2011). 2,3-Butanediol production by acetogenic bacteria, an alternative route

to chemical synthesis, using industrial waste gas. *Appl. Env. Microb.* 77, 5467–5475. doi: 10.1128/AEM.00355-11

Latif, H., Zeidan, A. A., Nielsen, A. T., and Zengler, K. (2014). Trash to treasure: production of biofuels and commodity chemicals via syngas fermenting microorganisms. *Curr. Opin. Biotech.* 27, 79–87. doi: 10.1016/j.copbio.2013.12.001

Liang, J., Huang, H., and Wang, S. (2019). Distribution, evolution, catalytic mechanism, and physiological functions of the flavin-based electron-bifurcating NADH-dependent reduced ferredoxin: $NADP^+$ oxidoreductase. *Front. Microb.* 10:373. doi: 10.3389/fmicb.2019.00373

Liew, F., Henstra, A. M., Köpke, M., Winzer, K., Simpson, S. D., and Minton, N. P. (2017). Metabolic engineering of *Clostridium autoethanogenum* for selective alcohol production. *Metab. Eng.* 40, 104–114. doi: 10.1016/j.ymben.2017.01.007

Liu, Z.-Y., Jia, D.-C., Zhang, K.-D., Zhu, H.-F., Zhang, Q., Jiang, W.-H., et al. (2020). Ethanol Metabolism Dynamics in *Clostridium ljungdahlii* Grown on Carbon Monoxide. *Appl. Environ. Microbiol.* 86:20. doi: 10.1128/AEM.00730-20

Martin, M. E., Richter, H., Saha, S., and Angenent, L. T. (2016). Traits of selected Clostridium strains for syngas fermentation to ethanol. *Biotechnol. Bioeng.* 113, 531–539. doi: 10.1002/bit.25827

Mock, J., Zheng, Y., Mueller, A. P., Ly, S., Tran, L., Segovia, S., et al. (2015). Energy conservation associated with ethanol formation from H_2 and CO_2 in *Clostridium autoethanogenum* involving electron bifurcation. *J. Bacteriol.* 197, 2965–2980. doi: 10.1128/JB.00399-15

Molitor, B., Kirchner, K., Henrich, A. W., Schmitz, S., and Rosenbaum, M. A. (2016). Expanding the molecular toolkit for the homoacetogen *Clostridium ljungdahlii*. *Sci. Rep.* 6:31518. doi: 10.1038/srep31518

Mohammadi, M., Mohamed, A. R., Najafpour, G., Younesi, H., and Uzir, M. H. (2016). *Clostridium ljungdahlii* for production of biofuel from synthesis gas. *Ener. Sources* 38, 427–434. doi: 10.1080/15567036.2012.729254

Müller, V., Imkamp, F., Biegel, E., Schmidt, S., and Dilling, S. (2008). Discovery of a ferredoxin:NAD+-oxidoreductase (Rnf) in *Acetobacterium woodii*: a novel potential coupling site in acetogens. *Ann. N. Y. Acad. Sci.* 1125, 137–146. doi: 10.1196/annals.1419.011

Nagarajan, H., Sahin, M., Nogales, J., Latif, H., Lovley, D. R., Ebrahim, A., et al. (2013). Characterizing acetogenic metabolism using a genome-scale metabolic reconstruction of *Clostridium ljungdahlii*. *Microb. Cell Fact.* 12:118.

O'Brien, E. J., Monk, J. M., and Palsson, B. O. (2015). Using genome-scale models to predict biological capabilities. *Cell* 161, 971–987. doi: 10.1016/j.cell.2015.05.019

Orth, J. D., Thiele, I., and Palsson, B. (2010). What is flux balance analysis? *Nat. Biotechnol.* 28, 245–248. doi: 10.1038/nbt.1614

Oswald, F., Dörsam, S., Veith, N., Zwick, M., Neumann, A., Ochsenreither, K., et al. (2016). Sequential mixed cultures: From syngas to malic acid. *Front. Microb.* 7:891. doi: 10.3389/fmicb.2016.00891

Parker, E. J., and Pratt, A. J. (2010). "Amino Acid Biosynthesis," in *Amino Acids, Peptides and Proteins in Organic Chemistry*, ed. A. B. Hughes (Germany: Wiley-VCH Verlag GmbH & Co. KGaA), 1–82.

Ragsdale, S. W., and Pierce, E. (2008). Acetogenesis and the Wood-Ljungdahl pathway of CO_2 fixation. *Biochim. Biophys. Acta* 1784, 1873–1898. doi: 10.1016/j.bbapap.2008.08.012

Richter, H., Martin, M., and Angenent, L. (2013). A Two-Stage Continuous Fermentation System for Conversion of Syngas into Ethanol. *Energies* 6, 3987–4000. doi: 10.3390/en6083987

Richter, H., Molitor, B., Wei, H., Chen, W., Aristilde, L., and Angenent, L. T. (2016). Ethanol production in syngas-fermenting *Clostridium ljungdahlii* is controlled by thermodynamics rather than by enzyme expression. *Energy Environ. Sci.* 9, 2392–2399. doi: 10.1039/C6EE01108J

Schatschneider, S., Abdelrazig, S., Safo, L., Henstra, A. M., Millat, T., Kim, D.-H., et al. (2018). Quantitative isotope-dilution high-resolution-mass-spectrometry analysis of multiple intracellular metabolites in *Clostridium autoethanogenum* with uniformly ^{13}C-labeled standards derived from *Spirulina*. *Anal. Chem.* 90, 4470–4477. doi: 10.1021/acs.analchem.7b04758

Schilling, C. H., Edwards, J. S., Letscher, D., and Palsson, B. (2000). Combining pathway analysis with flux balance analysis for the comprehensive study of metabolic systems. *Biotechnol. Bioeng.* 71, 286–306. doi: 10.1002/1097-0290200071:4<286:AID-BIT1018<3.0.CO;2-R

Schuchmann, K., and Müller, V. (2012). A bacterial electron-bifurcating hydrogenase. *J. Biol. Chem.* 28, 31165–31171. doi: 10.1074/jbc.m112.395038

Schuchmann, K., and Müller, V. (2014). Autotrophy at the thermodynamic limit of life: a model for energy conservation in acetogenic bacteria. *Nat. Rev. Microbiol.* 12, 809–821. doi: 10.1038/nrmicro3365

Takors, R., Kopf, M., Mampel, J., Bluemke, W., Blombach, B., Eikmanns, B., et al. (2018). Using gas mixtures of CO, CO_2 and H_2 as microbial substrates: the do's and don'ts of successful technology transfer from laboratory to production scale. *Microb. Biotechnol.* 11, 606–625. doi: 10.1111/1751-7915.13270

Tanner, R. S., Miller, L. M., and Yang, D. (1993). *Clostridium ljungdahlii* sp. nov., an acetogenic species in clostridial rRNA homology group I. *Int. J. Syst. Bacteriol.* 43, 232–236. doi: 10.1099/00207713-43-2-232

Teleki, A., Sánchez-Kopper, A., and Takors, R. (2015). Alkaline conditions in hydrophilic interaction liquid chromatography for intracellular metabolite quantification using tandem mass spectrometry. *Anal. Biochem.* 475, 4–13. doi: 10.1016/j.ab.2015.01.002

Tremblay, P.-L., Zhang, T., Dar, S. A., Leang, C., and Lovley, D. R. (2012). The Rnf complex of *Clostridium ljungdahlii* is a proton-translocating ferredoxin:NAD+ oxidoreductase essential for autotrophic growth. *mBio* 4, e406–e412. doi: 10.1128/mBio.00406-12

Valgepea, K., Souza Pinto, Lemgruber, R., de, Meaghan, K., Palfreyman, R. W., et al. (2017). Maintenance of ATP homeostasis triggers metabolic shifts in gas-fermenting acetogens. *Cell Systems* 4, 505.e–515.e. doi: 10.1016/j.cels.2017.04.008

Valgepea, K., Souza Pinto, Lemgruber, R., de, Abdalla, T., Binos, S., et al. (2018). H_2 drives metabolic rearrangements in gas-fermenting *Clostridium autoethanogenum*. *Biotechnol. Biofuels* 11:55. doi: 10.1186/s13068-018-1052-9

Villadsen, J., Nielsen, J., and Lidén, G. (2011). *Bioreaction engineering principles*, 3rd Edn. New York (NY): Springer Science & Business Media.

Wang, S., Huang, H., Kahnt, J., Mueller, A. P., Köpke, M., and Thauer, R. K. (2013). NADP-specific electron-bifurcating FeFe-hydrogenase in a functional complex with formate dehydrogenase in *Clostridium autoethanogenum* grown on CO. *J. Bacteriol.* 195, 4373–4386. doi: 10.1128/JB.00678-13

Weitz, S. (2020). *Konstruktion und Analyse isobutanolbildender autotropher acetogener Bakterien*. University of Ulm, doi: 10.18725/OPARU-32282 Ph.D. thesis.

Weitz, S., Hermann, M., Linder, S., Bengelsdorf, F. R., Takors, R., and Dürre, P. (2021). Isobutanol production by autotrophic acetogenic bacteria. *Front. Bioeng. Biotechnol.* submitted.

Woolston, B. M., Emerson, D. F., Currie, D. H., and Stephanopoulos, G. (2018). Rediverting carbon flux in *Clostridium ljungdahlii* using CRISPR interference (CRISPRi). *Metab. Eng.* 48, 243–253. doi: 10.1016/j.ymben.2018.06.006

Zhu, H. F., Liu, Z. Y., Zhou, X., Yi, J. H., Lun, Z. M., Wang, S. N., et al. (2020). Energy Conservation and Carbon Flux Distribution During Fermentation of CO or H_2/CO_2 by *Clostridium ljungdahlii*. *Front. Microb.* 11:416. doi: 10.3389/fmicb.2020.00416

Zimmermann, M., Sauer, U., and Zamboni, N. (2014). Quantification and mass isotopomer profiling of α-keto acids in central carbon metabolism. *Analy. Chem.* 86, 3232–3237. doi: 10.1021/ac500472c

Conflict of Interest: The authors declare that the research was conducted in the absence of any commercial or financial relationships that could be construed as a potential conflict of interest.

frontiers in Bioengineering and Biotechnology

ORIGINAL RESEARCH
published: 12 April 2021
doi: 10.3389/fbioe.2021.657253

Isobutanol Production by Autotrophic Acetogenic Bacteria

*Sandra Weitz[1], Maria Hermann[2], Sonja Linder[1], Frank R. Bengelsdorf[1], Ralf Takors[2] and Peter Dürre[1]**

[1] *Institut für Mikrobiologie und Biotechnologie, Universität Ulm, Ulm, Germany,* [2] *Institut für Bioverfahrenstechnik, Universität Stuttgart, Stuttgart, Germany*

Two different isobutanol synthesis pathways were cloned into and expressed in the two model acetogenic bacteria *Acetobacterium woodii* and *Clostridium ljungdahlii*. *A. woodii* is specialized on using $CO_2 + H_2$ gas mixtures for growth and depends on sodium ions for ATP generation by a respective ATPase and Rnf system. On the other hand, *C. ljungdahlii* grows well on syngas ($CO + H_2 + CO_2$ mixture) and depends on protons for energy conservation. The first pathway consisted of ketoisovalerate ferredoxin oxidoreductase (Kor) from *Clostridium thermocellum* and bifunctional aldehyde/alcohol dehydrogenase (AdhE2) from *C. acetobutylicum*. Three different *kor* gene clusters are annotated in *C. thermocellum* and were all tested. Only in recombinant *A. woodii* strains, traces of isobutanol could be detected. Additional feeding of ketoisovalerate increased isobutanol production to 2.9 mM under heterotrophic conditions using *kor*3 and to 1.8 mM under autotrophic conditions using *kor*2. In *C. ljungdahlii*, isobutanol could only be detected upon additional ketoisovalerate feeding under autotrophic conditions. *kor*3 proved to be the best suited gene cluster. The second pathway consisted of ketoisovalerate decarboxylase from *Lactococcus lactis* and alcohol dehydrogenase from *Corynebacterium glutamicum*. For increasing the carbon flux to ketoisovalerate, genes encoding ketol-acid reductoisomerase, dihydroxy-acid dehydratase, and acetolactate synthase from *C. ljungdahlii* were subcloned downstream of *adhA*. Under heterotrophic conditions, *A. woodii* produced 0.2 mM isobutanol and 0.4 mM upon additional ketoisovalerate feeding. Under autotrophic conditions, no isobutanol formation could be detected. Only upon additional ketoisovalerate feeding, recombinant *A. woodii* produced 1.5 mM isobutanol. With *C. ljungdahlii*, no isobutanol was formed under heterotrophic conditions and only 0.1 mM under autotrophic conditions. Additional feeding of ketoisovalerate increased these values to 1.5 mM and 0.6 mM, respectively. A further increase to 2.4 mM and 1 mM, respectively, could be achieved upon inactivation of the *ilvE* gene in the recombinant *C. ljungdahlii* strain. Engineering the coenzyme specificity of IlvC of *C. ljungdahlii* from NADPH to NADH did not result in improved isobutanol production.

Keywords: *Acetobacterium woodii*, acetogens, *Clostridium ljungdahlii*, gas fermentation, isobutanol production, syngas

OPEN ACCESS

Edited by:
Petra Patakova, University of Chemistry and Technology in Prague, Czechia

Reviewed by:
Klaas J. Jan Hellingwerf, University of Amsterdam, Netherlands
Anke Neumann, Karlsruhe Institute of Technology (KIT), Germany

***Correspondence:**
Peter Dürre
peter.duerre@uni-ulm.de

Specialty section:
This article was submitted to Synthetic Biology, a section of the journal Frontiers in Bioengineering and Biotechnology

Received: *22 January 2021*
Accepted: *22 March 2021*
Published: *12 April 2021*

Citation:
Weitz S, Hermann M, Linder S, Bengelsdorf FR, Takors R and Dürre P (2021) Isobutanol Production by Autotrophic Acetogenic Bacteria. Front. Bioeng. Biotechnol. 9:657253. doi: 10.3389/fbioe.2021.657253

INTRODUCTION

Isobutanol is an important platform chemical, representing an app. one billion US $ market in 2019. The compound is mainly used in solvents and coatings, as a chemical intermediate, or as a biofuel (gasoline additive). Synthesis is chemically achieved by hydroformylation of propylene, followed by hydrogenation of the formed aldehyde, but bio-based processes have been developed by companies Gevo Inc. (Douglas County, CO) and Butamax Advanced Biofuels LLC (Wilmington, DE; joint venture of BP and DuPont). The share of bio-based isobutanol is expected to rise in the near future significantly compared to the synthetic compound. A number of microorganisms have been engineered for isobutanol production, including aerobic and anaerobic bacteria as well as *Saccharomyces cerevisiae* (Chen and Liao, 2016). Gevo is using a recombinant yeast for its corn-based process, but details have not yet been disclosed. A landmark publication reported genetically engineered isobutanol formation by modification of amino acid synthesis pathways (Atsumi et al., 2008). 2-Ketoisovalerate, an intermediate in valine and isoleucine biosynthesis, was first decarboxylated by e.g., KivD from *Lactococcus lactis* and then the formed aldehyde was reduced to isobutanol by an alcohol dehydrogenase (e.g., Adh2 from *Saccharomyces cerevisiae*) (**Figure 1**). A natural pathway for production is based on the enzyme ketoisovalerate ferredoxin oxidoreductase (Kor), which was first found and characterized in hyperthermophilic archaea, where it is involved in branched-chain amino acid degradation and biosynthesis (Heider et al., 1996). This isobutanol synthesis pathway (**Figure 1**) was shown to be active in e.g., *Clostridium thermocellum* (Lin et al., 2015).

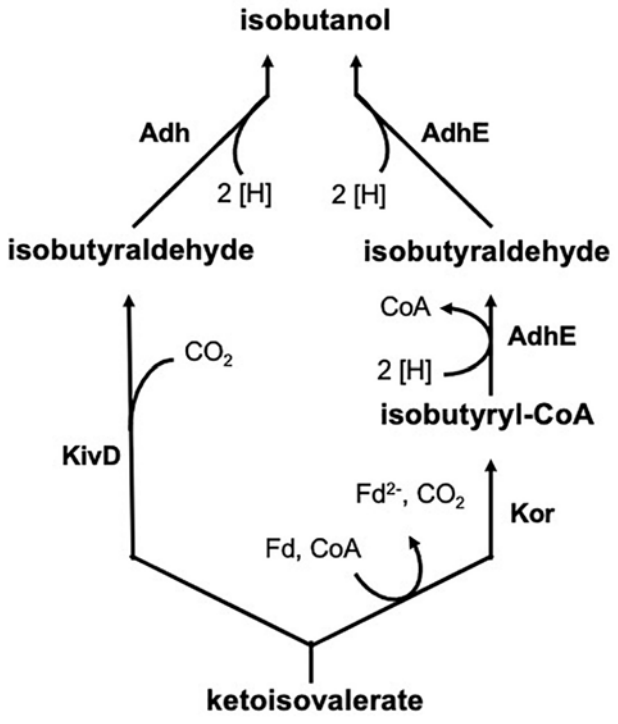

FIGURE 1 | Formation of isobutanol by the enzymes KivD (ketoisovalerate decarboxylase) and Adh (alcohol dehydrogenase) or Kor (ketoisovalerate ferredoxin oxidoreductase) and AdhE (bifunctional aldehyde/alcohol dehydrogenase) from ketoisovalerate, the precursor of valine.

Using biological production with recombinant strains, high isobutanol titers in typical fermentation setups were obtained with e.g., *E. coli* (22 g/l; Atsumi et al., 2008), *Corynebacterium glutamicum* (13 g/l; Blombach et al., 2011), *Clostridium thermocellum* (5.4 g/l; Lin et al., 2015), *Geobacillus thermoglucosidasius* (3.3 g/l; Lin et al., 2014), *S. cerevisiae* (2.1 g/l; Wess et al., 2019), and *Ralstonia eutropha* (0.03 g/l; Black et al., 2018). All these processes used sugar or cellulose as a carbon source. Cheaper substrates would be CO_2 (in combination with a reductant) or CO, which are also waste and greenhouse gases. A photosynthetic isobutanol production of up to 0.9 g/l from CO_2 and solar energy has been reported for *Synechocystis* PCC 6803 (Miao et al., 2018). The electrochemical conversion of CO_2 and water to formate was coupled with formate-dependent growth of recombinant cells of the aerobic "Knallgas" bacterium *R. eutropha*, yielding up to 0.85 g isobutanol/l (Li et al., 2012). However, some challenges still remain for CO_2-based biological isobutanol formation compared to the non-biological production (Brigham, 2019).

Here, we report an approach to isobutanol synthesis using two anaerobic bacteria, which became model organisms of the so-called acetogens: *Acetobacterium woodii*, growing on CO_2/H_2, and *Clostridium ljungdahlii*, growing on syngas (a mixture of mostly CO and H_2).

MATERIALS AND METHODS

Bacterial Strains and Plasmids

Acetobacterium woodii (DSM 1030) and *Clostridium ljungdahlii* (DSM13583) were obtained from the DSMZ (Deutsche Sammlung von Mikroorganismen und Zellkulturen GmbH, Brunswick, Germany). *Escherichia coli* XL1-Blue MRF' [*Δ(mcrA)183Δ(mcrCB-hsdSMR-mrr)173 endA1 supE44 thi-1*] stemmed from Stratagene (La Jolla, CA). All plasmids used in this study are listed in **Table 1**.

Media and Growth Conditions

Escherichia coli was cultivated aerobically in LB (Luria-Bertani) medium (per l: tryptone 10 g, yeast extract 5 g, NaCl 10 g) (Green and Sambrook, 2012) at 37°C on a rotary shaker (175 rpm). For generation of competent cells, *E. coli* was grown in modified SOB (Super Optimal Broth; per l: tryptone 20 g, yeast extract 5 g, NaCl 0.5 g, KCl 1.92 g, $MgCl_2 \times 6\ H_2O$ 2.03 g) (Green and Sambrook, 2012).

Basal medium for *A. woodii* was modified from Balch et al. (1977) and contained per l: KH_2PO_4 0.33 g, K_2HPO_4 0.45 g, $MgSO_4 \times 7\ H_2O$ 0.33 g, NH_4Cl 1 g, yeast extract 2 g, L-cysteine-HCl $\times\ H_2O$ 0.5 g, resazurin 1 mg. To this solution, 20 ml of trace element solution (per l: nitrilotriacetic acid 1.5 g, $MgSO_4 \times 7\ H_2O$ 3 g, $MnSO_4 \times H_2O$ 0.5 g, NaCl 1 g, $FeSO_4 \times 7\ H_2O$ 0.1 g, $CoSO_4 \times 7\ H_2O$ 0.18 g, $CaCl_2 \times 2\ H_2O$ 0.1 g, $ZnSO_4 \times 7\ H_2O$ 0.18 g, $CuSO_4 \times 5\ H_2O$ 0.01 g, $KAl(SO_4)_2 \times 12\ H_2O$

TABLE 1 | Plasmids used in this study.

Plasmid	Relevant features	References
pJUL34	*kivD* from *L. lactis*, P_{tuf} from *L. lactis*, *adhA* from *Corynebacterium glutamicum*; *aph3*; *sacB*, replicon repBL1 for *Corynebacterium*	Gift from Bastian Blombach (Technical University of Munich, Germany) and Bernhard Eikmanns (University of Ulm, Germany)
pMTL007-E2_ilvE	ColE1 ori$^-$, pCB102 ori$^+$, *catP*, *lacZ*, *ltrA*, *oriT*, Pfdx, *ermB*, *traJ*, ClosTron^{TM}plasmid to inactivate *ilvE* in the genome of *C. ljungdahlii*	This study, ATUM, Newark, CA, United States
pMTL83151	*catP*, ColE1 ori$^-$, *lacZ*, pCB102 ori$^+$, *traJ*	Heap et al., 2009
pMTL83151_ptaack_aacht_cac	pMTL83151, $P_{pta-ack}$ and *adhE2* from *C. acetobutylicum*; *abfD* from *C. scatologenes*, *crt*, *hbd*, and *thlA* from *C. acetobutylicum*	This study
pKAIA	pMTL83151, $P_{pta-ack}$ from *C. ljungdahlii, kivD* from *L. lactis*, *adhA* from *Corynebacterium glutamicum*, *ilvC*, *ilvD*, and *alsS* from *C. ljungdahlii*	This study
$pKAI_{NADH}A$	pMTL83151 $P_{pta-ack}$ from *C. ljungdahlii*, *kivD* from *L. lactis, adhA* from *C. glutamicum*, *ilvD* and *alsS* from *C. ljungdahlii*, $ilvC^{P2D1-A1}$ from *E. coli*, codon optimized for clostridia	This study, Thermo Fisher Scientific GENEART GmbH, Regensburg, Germany, Brinkmann-Chen et al., 2013
pKOR2	pMTL83151, $P_{pta-ack}$ from *C. ljungdahlii*, *adhE2* from *C. acetobutylicum*, *kor2* from *C. thermocellum*	This study
pKOR3	pMTL83151, $P_{pta-ack}$ from *C. ljungdahlii*, *adhE2* from *C. acetobutylicum*, *kor3* from *C. thermocellum*	This study

0.02 g, H_3BO_3 0.01 g, $Na_2MoO_4 \times 2\ H_2O$ 0.01 g, $NiCl_2 \times 6\ H_2O$ 0.03 g, $Na_2SeO_3 \times 5\ H_2O$ 0.3 mg, $Na_2WO_4 \times 2\ H_2O$ 0.4 mg) and 20 ml vitamin solution (per l: biotin 2 mg, folic acid 2 mg, pyridoxine-HCl 10 mg, thiamine-HCl 5 mg, riboflavin 5 mg, nicotinic acid 5 mg, D-Ca-pantothenate 5 mg, vitamin B_{12} 0.1 mg, p-aminobenzoic acid 5 mg, lipoic acid 5 mg (DSMZ_Medium141-1.pdf,[1]) were added. Media were prepared under strictly anaerobic conditions. Heterotrophic growth was performed with 40 mM fructose as a carbon source under an atmosphere consisting of N_2 (80%) and CO_2 (20%), autotrophic growth with a $CO_2 + H_2$ gas mixture (33% + 67%), both at 30°C.

Clostridium ljungdahlii was cultivated in a modified medium described by Tanner et al. (1993). It contained per l: 2-(*N*-morpholino) ethanesulfonic acid 20 g, yeast extract 0.5 g, L-cysteine-HCl $\times$ H_2O 1 g, resazurin 1 mg. To this solution, 25 ml of mineral salts solution (per l: $CaCl_2 \times 2\ H_2O$ 4 g, KCl 10 g, KH_2PO_4 10 g, $MgSO_4 \times 7\ H_2O$ 20 g, NaCl 80 g, NH_4Cl 100 g), 10 ml of modified trace element solution (American Type Culture Collection (ATCC);[2]; 1754 PETC medium) (per l: nitrilotriacetic acid 2 g, $MnSO_4 \times H_2O$ 0.5 g, $Fe(SO_4)_2(NH_4)_2 \times 6\ H_2O$ 0.8 g, $CoCl_2 \times 6\ H_2O$ 0.2 g, $ZnSO_4 \times 7\ H_2O$ 1 mg, $CuCl_2 \times 2\ H_2O$ 20 mg, $NiCl_2 \times 6\ H_2O$ 20 mg, $Na_2MoO_4 \times 2\ H_2O$ 20 mg, $Na_2SeO_3 \times 5\ H_2O$ 20 mg, $Na_2WO_4 \times 2\ H_2O$ 20 mg), and 10 ml vitamin solution (per l: biotin 2 mg, folic acid 2 mg, pyridoxine-HCl 10 mg, thiamine-HCl 5 mg, riboflavin 5 mg, nicotinic acid 5 mg, D-Ca-pantothenate 5 mg, vitamin B_{12} 5 mg, p-aminobenzoic acid 5 mg, and lipoic acid 5 mg) were added. Media were prepared under strictly anaerobic conditions. Heterotrophic growth was performed with 40 mM fructose as a carbon source under an atmosphere consisting of N_2 (80%) and CO_2 (20%), autotrophic growth with a syngas mixture (50% CO, 45% H_2, and 5 CO_2), both at 37°C.

For cultivation of *A. woodii* and *C. ljungdahlii* on solid media, a modified version of yeast tryptone fructose medium (Leang et al., 2013) was used (per l: yeast extract 10 g, tryptone 16 g, fructose 5 g, NaCl 4 g, L-cysteine-HCl $\times$ H_2O 1 g, resazurin 1 mg, agar 15 g). Agar plates were poured using anaerobic water in an anaerobic cabinet containing a N_2:H_2 (95:5%) gas atmosphere. Cell suspensions were dripped on plates and spread using glass beads. *A. woodii* cells were incubated at 30°C and *C. ljungdahlii* cells at 37°C in an incubator located in the anaerobic cabinet.

For selection of antibiotic-resistant strains, the following concentrations were used per ml: ampicillin 100 mg, clarithromycin 2.5 mg, chloramphenicol 30 mg, kanamycin 50 mg, thiamphenicol 7.5 mg.

Analytical Methods

Cell growth was monitored offline by measuring the optical density at 600 nm (Ultrospec 3100, Amersham Bioscience Europe GmbH, Freiburg, Germany) in 1-ml cuvettes (width 1 cm).

Ethanol, isobutanol, and isoamyl alcohol were determined using gas chromatograph (GC) "Clarus 680" (PerkinElmer, PerkinElmer, Waltham, MA, United States). GC was equipped with an Elite-FFAP column (i Ø 0.32 mm $\times$ 30 m). H_2 was the carrier gas (2.25 ml min^{-1}, 100°C), injector temperature was 225°C, split 1:20, and flame ionization detector temperature was 300°C. Detector gases were synthetic air (450 ml min^{-1}) and H_2 (45 ml min^{-1}). A temperature profile was predefined: 90°C for 2 min, 40°C min^{-1} increasing steps to 250°C (constant for 1 min). Supernatant (0.48 ml) was acidified with 0.02 mL of 2 M HCl. 1 ml was injected into the GC. Calibration was performed using defined standards of the individual components.

Acetate, 2,3-butanediol, fructose, and ketoisovalerate were determined using high performance liquid chromatography (Agilent 1260 Infinity Series HPLC, Agilent Technologies, Santa Clara, CA) equipped with a refractive index detector (for 2,3-butanediol, fructose, ketoisovalerate) operating at 35°C and a diode array detector (for acetate) at room temperature. The "CS-Chromatographie organic acid column" (CS-Chromatographie

[1]https://www.dsmz.de/collection/catalog/details/culture/DSM-4553

[2]https://www.lgcstandards-atcc.org/products/all/55383.aspx#culturemethod

Service GmbH, Langerwehe, Germany) was kept at 40°C. 5 mM H_2SO_4 was used as mobile phase with a flow rate of 0.7 ml min^{-1}. 20 µl of supernatant were injected into the HPLC system for determination of compounds.

DNA Isolation

Bacterial genomic DNA was isolated using the "MasterPure™ Gram-Positive DNA Purification Kit" (Epicentre, Madison, WI, United States). 2-mL Samples of late exponential cultures were centrifuged (18,000 g, 30 min, 4°C) and further processed according to the manufacturer's instructions. Isolation of plasmid DNA from *E. coli* strains was performed with the "Zyppy™ Plasmid Miniprep Kit" (ZYMO Research Europe GmbH, Freiburg, Germany). 4-ml Samples of overnight cultures were centrifuged (18,000 g, 1 min) and further processed according to the manufacturer's instructions. In case of *A. woodii* and *C. ljungdahlii*, 2 ml were sampled and centrifuged (18,000 g, 30 min, 4°C). The cell pellet was suspended in 600 µl Tris−HCl (20 mM, pH 7). For effective lysis, 60 µl lysozyme (20 mg ml^{-1}) were added, and the solution was incubated for 1 h at 37°C before proceeding according to the manufacturer's instructions.

DNA from *C. thermocellum* DSM 1313 was purchased from the DSMZ (Deutsche Sammlung von Mikroorganismen und Zellkulturen GmbH, Brunswick, Germany).

Sequencing of DNA was performed by GATC Biotech AG (Constance, Germany).

Plasmid Construction

Standard molecular cloning techniques were performed according to established protocols (Green and Sambrook, 2012). In *C. thermocellum*, three gene clusters encoding a putative ketoisovalerate ferredoxin oxidoreductase (Kor) are annotated [*kor1* (Clo1313_0020-0023), *kor2* (Clo1313_0382-0385), *kor3* (Clo1313_1353-1356)]. *kor1* was PCR-amplified using primers clo0020T_fwd and clo0020T_rev, *kor2* was PCR-amplified using primers clo0382T_fwd and clo0382T_rev, and *kor3* was PCR-amplified using primers clo1353T_fwd and clo1353T_rev. Then, each fragment was subcloned into the pMTL83151 backbone (Heap et al., 2009), together (upstream) with the also PCR-amplified $P_{pta\text{-}ack}$ promoter from *C. ljungdahlii* (primers: Ptaack_fwd and Ptaack_rev) and the gene encoding bifunctional butyraldehyde/butanol dehydrogenase AdhE2 from *C. acetobutylicum* [primers: adhE2_pka_fwd and adhE2_pka_rev; plasmid pMTL83151_ptaack_aacht_cac (**Supplementary Figure 1**)]. All primers used are listed in **Table 2**. Subcloning was performed by in-fusion cloning using the NEBuilder Assembly Tool (New England Biolabs Inc., Ipswich, MA, United States;[3]). The resulting plasmids pKOR1, pKOR2, and pKOR3 are shown in **Supplementary Figure 2**. pMTL83151 was kindly provided by Nigel Minton (University of Nottingham, United Kingdom).

The plasmids constructed for elucidation of the ketoisovalerate decarboxylase pathway were also based on the pMTL83151 backbone. The *kivD* gene from *L. lactis* was PCR-amplified using primers kivd_fwd_XhoI and kivd_rev_Eco81I (making use of the inserted restriction sites for subcloning), *adhA* from *C. glutamicum* was PCR-amplified using primers adhA_fwd_XhoI and adhA_rev_NheI (making use of the inserted restriction sites for subcloning). DNA source for amplification was plasmid pJUL34 (**Supplementary Figure 3**), which was kindly provided by Bastian Blombach (Technical University of Munich, Germany) and Bernhard Eikmanns (University of Ulm, Germany) (**Table 1**). Both fragments were subcloned together in several steps into pMTL83151. Upstream of *kivD*, the PCR-amplified $P_{pta-ack}$ promoter fragment from *C. ljungdahlii* (primers: Ptaack_fwd and Ptaack_rev) was inserted. The genes *ilvC* (encoding ketol-acid reductoisomerase) (primers ilvC_fwd and ilvC_rev), *ilvD* (encoding dihydroxy-acid dehydratase) (primers ilvD_fwd and ilvD_rev), and

TABLE 2 | Primer used for cloning procedures.

Name	Sequence	Amplification
clo0020T_fwd	GATATCTATATAAAATCATTTTAACCTCG AGAGGAGGATTACCACATGGGCAA	KOR1 Clo1313_0020-0023
clo0020T_rev	CAAATGCAGGCTTCTTATTTTTATGGCTA GCCAATAATATTTTCTCATTTTAAAAAAT	
clo0382T_fwd	GATATCTATATAAAATCATTTTAACCTCG AGAGGGAGCGATGGAGATGACAGA	KOR2 Clo1313_0382-0385
clo0382T_rev	CAAATGCAGGCTTCTTATTTTTATGGCTA GCCTCCTTTTTTCAAAAAAAGTCCATGTT CC	
clo1353T_fwd	GATATCTATATAAAATCATTTTAACCTCG AGGGGGGATTTACATGGCTAAGGT	KOR3 Clo1313_1353-1356
clo1353T_rev	CAAATGCAGGCTTCTTATTTTTATGGCTA GCCGTATAAGAATTAAAAATAAGAATTA AAAATCAAAACAATCAAAAAAAG	
Ptaack_fwd	ACAGCGGCCGCGTCGACGTTACCACTCAT	$P_{pta-ack}$
Ptaack_rev	ACAACCGGTCCTCAGGTCCTCCCTTTA	
adhE2_pka_fwd	TTAAATTTAAAGGGAGGACCTGAGGATG AAAGTTACAAATCAAAAAGAAC	*adhE2*
adhE2_pka_rev	CTTGGGGTGCAGCAGTGGTCATCCTCGAG TTAAAATGATTTTATATAGATATCCTTAA GTTC	
kivd_fwd_XhoI	CTCGAGGTCCTCCTATTTATAAATTATG	*kivD*
kivd_rev_Eco81I	ACACCTGAGGATGTATACAGTAGGAG	
adhA_fwd_XhoI	CTCGAGATGACCACTGCTGCACCC	*adhA*
adhA_rev_NheI	ACAGCTAGCGCGAGTCGAACAGATGTG	
ilvC_fwd	TGTGGCGATTCGTTTCTAACGACGTCAAA ATAGTATAAATAAATTATTCAGGAGG	*ilvC*
ilvC_rev	TGTAAAAAAATACTAGTTTACTCATTATC AGGATTTTCATTG	
ilvD_fwd	TAATGAGTAAACTAGTATTTTTTTACAAA AAATTTCCAG	*ilvD*
ilvD_rev	GATCTTTATACCATGGTTATTTAAGAACT GCACCTGTATTTG	
alsS_fwd	TTCTTAAATAACCATGGTATAAAGATCAG AGGAAGTTTTATATG	*alsS*
alsS_rev	CAAAGTAGCTTCAGAGCAGTTCTAGATTA CATATTTTCATAAACTTCTTTTAAATG	

Underlined nucleotides are vector overlapping fragments used for In-Fusion® cloning.

[3]https://international.neb.com/products/e5520-nebuilder-hifi-dna-assembly-cloning-kit#ProductInformation

alsS (encoding acetolactate synthase) (primers alsS_fwd and alsS_rev), all from *C. ljungdahlii*, were PCR-amplified (**Table 2**). Subcloning downstream of *adhA* was performed by in-fusion cloning using the NEBuilder Assembly Tool (New England Biolabs inc., Ipswich, MA, United States; see text footnote 3). The resulting plasmid was designated pKAIA (**Supplementary Figure 4**).

For changing the coenzyme specificity of IlvC (ketol-acid reductoisomerase) of *C. ljungdahlii* from NADPH to NADH, the $ilvC^{NADH}$ gene of *E. coli* was commercially synthesized according to Brinkmann-Chen et al. (2013), with appropriate overlaps for in-fusion cloning. Codon optimization for clostridia was suggested by the commercial supplier Thermo Fisher Scientific GENEART GmbH (Regensburg, Germany). The sequence of the codon-optimized, synthesized gene is provided in **Supplementary Figure 5**.

The *ilvC* gene was cut out of pKAIA and the codon-optimized, synthesized gene was subcloned into the linearized vector using in-fusion cloning, resulting in plasmid $pKAI_{NADH}A$ (**Supplementary Figure 6**).

The ClosTron plasmid pMTL007-E2_ilvE (**Table 1**) was synthesized by the company DNA 2.0 (now ATUM, Newark, CA, United States) (see below).

Transformation

In case of *E. coli*, competent cells (Inoue et al., 1990) were obtained by inoculating 250 ml SOB medium with a 5-ml overnight culture grown in the same medium. Incubation was performed in a 2-l Erlenmeyer flask at 18°C under aerobic conditions and shaking (60 rpm), until an optical density (600 nm) of 0.6–0.8 was reached. Then, cells were put on ice for 30 min and afterward centrifuged (4,500 g, 4°C, 10 min). The pellet was suspended in 40 ml buffer (per 125 ml: piperazine-N,N'–bis(2-ethanesulfonic acid) 0.756 g, $CaCl_2$ 0.42 g, pH 6.7; mixed with 125 ml containing 4.66 g KCl and 1.72 g $MnCl_2 \times 4\ H_2O$), incubated on ice for 10 min, and again centrifuged (4,500 g, 4°C, 10 min). The pellet was suspended in 10 ml of the same buffer. 1.5 ml sterile dimethyl sulfoxide were added, and the solution was split into 200 µl aliquots and stored at −80°C. For transformation, such aliquots were thawed on ice, mixed with 10 µl of a DNA solution (in-fusion reaction mix or plasmid), incubated on ice for 10 min, and then at 42°C for 1 min. After an incubation period of 10 min again on ice, 800 µl LB medium were added, and the solution was incubated aerobically for 1 h at 37°C with shaking (160 rpm). Then, cells were centrifuged (4,000 g, room temperature, 3 min), and 800 µl of the supernatant discarded. The pellet was resuspended in the remaining liquid, which was used for plating on solid media with respective selection.

Electroporation of *A. woodii* and *C. ljungdahlii* was performed using a modified protocol of Leang et al. (2013). All plastic materials were stored in an anaerobic cabinet at least 1 day before transformation to eliminate any remaining traces of oxygen. For preparation of competent cells, 100 ml medium were supplemented with 40 mM fructose and 40 mM DL-threonine, inoculated with an early exponential culture, and grown at the appropriate temperature to an optical density (600 nm) of 0.3–0.7. Cultures were centrifuged anaerobically (6,000 g, 4°C, 10 min), and the pellet was washed twice with 50 ml cool, anaerobic SMP buffer (per l: sucrose 92.4 g, $MgCl_2 \times 6\ H_2O$ 0.2 g, NaH_2PO_4 0.84 g; pH 6) and suspended in 0.6 ml SMP buffer. 120 µl cool anti-freezing buffer (mix of 20 ml SMP buffer and 30 ml dimethylformamide) were added, and aliquots stored at −80°C.

Electroporation was carried out in an anaerobic cabinet. 25 µl of electrocompetent cells were mixed with 3–5 µg of plasmid DNA, cooled, and transferred to a pre-cooled 1-mm gap electroporation cuvette (Biozym Scientific GmbH, Hessisch Oldendorf, Germany). Electric pulse was performed with 625 V, resistance of 600 Ω, and a capacitance of 25 µF using a "Gene-Pulser Xcell™" pulse generator (Bio-Rad Laboratories GmbH, Munich, Germany). Afterward, cells were recovered using 5 ml of the respective medium without antibiotic in a Hungate tube and incubated until the optical density (600 nm) doubled. Then, the appropriate antibiotic was added and growth monitored. If growth was detectable, cells were inoculated into fresh medium with antibiotic and, after reaching the early exponential growth phase, plated onto solid media. Single colonies of obtained transformants were picked, and successful transformation was confirmed by isolating genomic or plasmid DNA and PCR amplification of respective sequences for verification.

Gene Inactivation by ClosTron

The ClosTron method was performed according to Heap et al. (2007, 2010). The aim was to create an insertion mutant in *ilvE* of *C. ljungdahlii*, which blocked the last step of valine biosynthesis. Target region for integration was determined using the respective algorithm (Perutka et al., 2004;[4]), and the respective ClosTron plasmid (pMTL007-E2_ilvE) (**Table 1**) was synthesized by the company DNA 2.0 (now ATUM, Newark, CA). After transformation into *C. ljungdahlii*, recombinant strains were verified by PCR amplification and sequencing of the respective gene region.

RESULTS

Isobutanol Production *via* Ketoisovalerate Ferredoxin Oxidoreductase (Kor)

In the genome of *C. thermocellum* three gene clusters are annotated that encode a putative ketoisovalerate ferredoxin oxidoreductase (Kor), i.e., *kor1* (Clo1313_0020-0023), *kor2* (Clo1313_0382-0385), and *kor3* (Clo1313_1353-1356). *kor3* differs significantly from the other two clusters with respect to length (smaller) and gene arrangement (**Supplementary Figure 7**). However, all clusters consist of four genes, encoding the α, β, γ, and δ subunits of Kor. The α subunit carries the core domain of pyruvate-ferredoxin oxidoreductase, β a C-terminal thiamine pyrophosphate-binding domain, γ a catalytic domain of pyruvate/ketoisovalerate oxidoreductase, and δ a binding

[4]www.clostron.com

domain for 4Fe-4S ferredoxin. All clusters were PCR-amplified and subcloned each into the pMTL83151 backbone, together (upstream) with the $P_{pta\text{-}ack}$ promoter from *C. ljungdahlii* and the gene encoding bifunctional butyraldehyde/butanol dehydrogenase AdhE2 from *C. acetobutylicum*. The resulting plasmids (pKOR1, pKOR2, and pKOR3) were transformed into *A. woodii* and *C. ljungdahlii*. Recombinant strains were then tested under heterotrophic conditions with fructose as a carbon source as well as with and without addition of ketoisovalerate (15 mM). Both, *A. woodii* and *C. ljungdahlii* did not grow with ketoisovalerate as sole carbon and energy source and also did not show an increase in optical density when fructose and ketoisovalerate were supplied together, compared to fructose alone. Wild type strains and empty plasmid-carrying strains [*A. woodii* (pM83) and *C. ljungdahlii* (pM83)] were used as controls. Without ketoisovalerate addition, recombinant *A. woodii* strains only formed traces of isobutanol (0.1 mM). However, all pKOR-carrying strains produced increased amounts of ethanol. With addition of ketoisovalerate, *A. woodii*[pKOR1] produced 0.2 mM isobutanol, *A. woodii*[pKOR2] 0.3 mM, and *A. woodii*[pKOR3] 2.9 mM (**Figure 2**). Some isoamyl alcohol (up to 0.3 mM) was formed in addition. The respective data for *C. ljungdahlii* are shown in **Supplementary Figure 8**. With and without ketoisovalerate addition, no isobutanol was formed. pKOR-carrying strains produced increased amounts of ethanol with addition of ketoisovalerate.

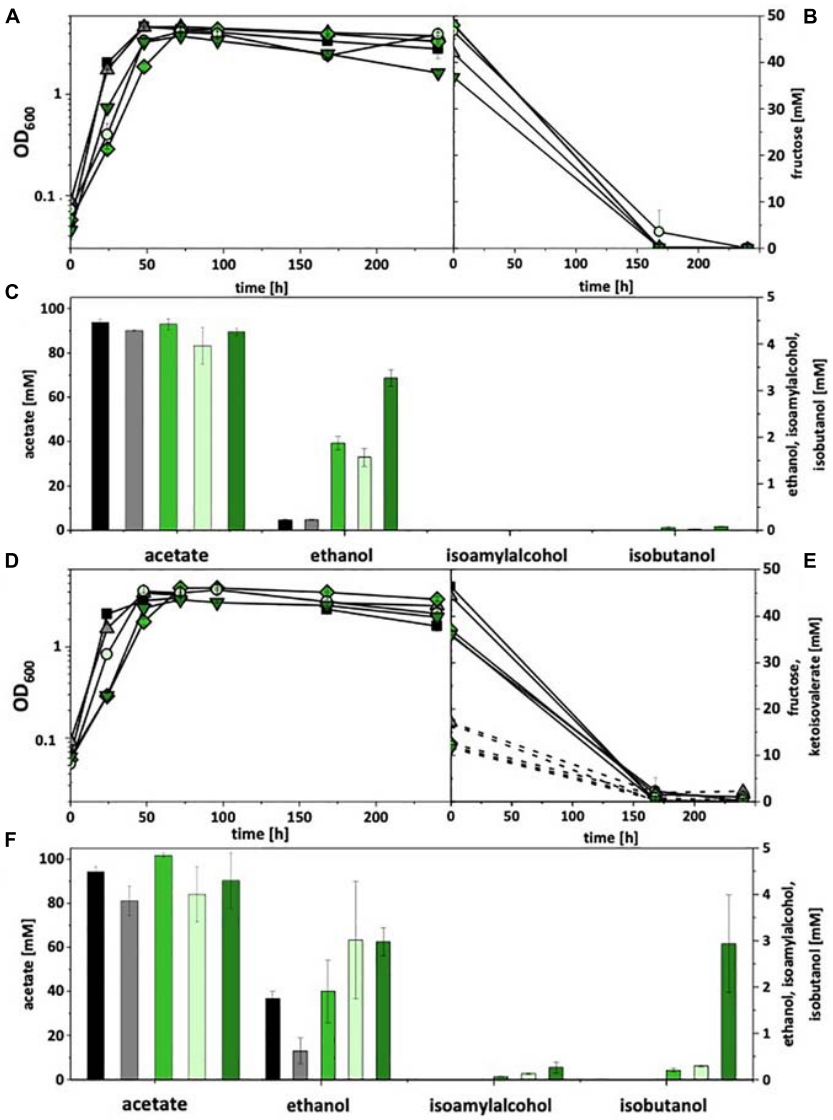

FIGURE 2 | Heterotrophic isobutanol production with recombinant *A. woodii* strains by the Kor pathway. Growth behavior **(A,D)**; fructose consumption **(B,E)**; ketoisovalerate consumption **(E)**; product pattern **(C,F)**. *A. woodii* [WT], black, squares; *A. woodii* [pM83], gray, triangles; *A. woodii* [pKOR1], green, diamonds; *A. woodii* [pKOR2], light green, circles; *A. woodii* [pKOR3], dark green, triangle pointing downward. Panels **(A–C)** without ketoisovalerate supplementation; Panels **(D–F)** with ketoisovalerate supplementation. Each strain was analyzed in biological triplicates ($n = 3$).

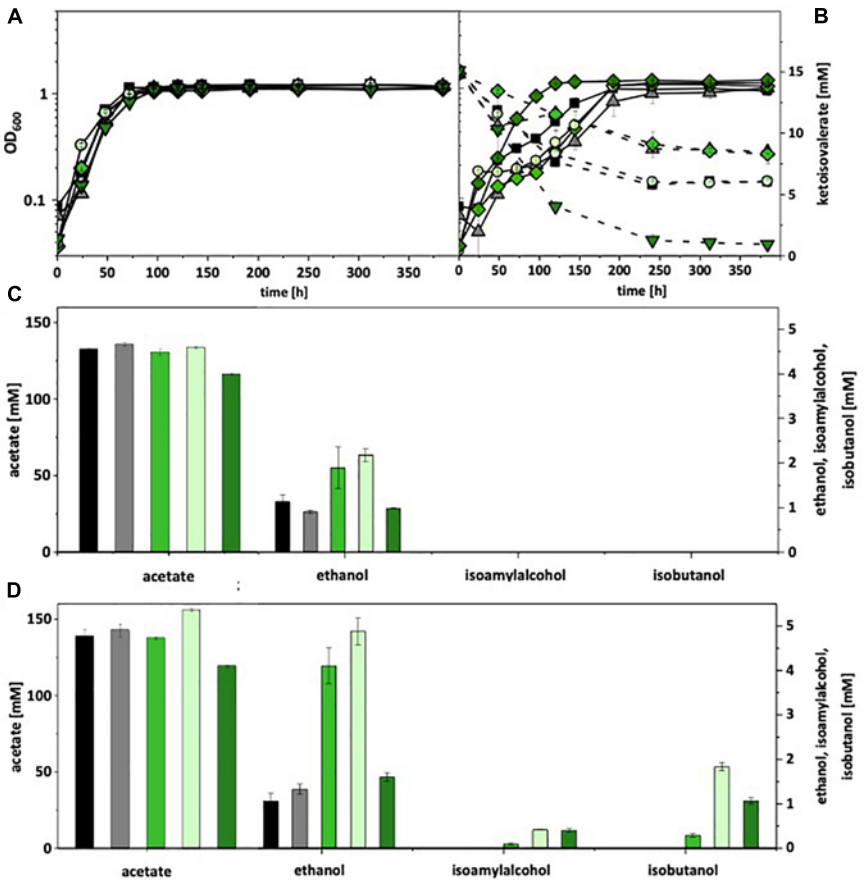

FIGURE 3 | Autotrophic isobutanol production with recombinant *A. woodii* strains by the Kor pathway. Growth behavior **(A,B)**; ketoisovalerate consumption **(B)**; product pattern **(C,D)**. *A. woodii* [WT], black, squares; *A. woodii* [pM83], gray, triangles; *A. woodii* [pKOR1], green, diamonds; *A. woodii* [pKOR2], light green, circles; *A. woodii* [pKOR3], dark green, triangle pointing downward. Panels **(A,C)** without ketoisovalerate supplementation; Panels **(B,D)** with ketoisovalerate supplementation. Each strain was analyzed in biological triplicates (n = 3).

For autotrophic growth, *A. woodii* was cultivated under a CO_2 + H_2 atmosphere, *C. ljungdahlii* under syngas. Without ketoisovalerate addition, recombinant *A. woodii* strains formed no isobutanol. With addition, *A. woodii*[pKOR1] produced 0.3 mM, *A. woodii*[pKOR2] 1.8 mM, and *A. woodii*[pKOR3] 1.1 mM (**Figure 3**). *A. woodii*[pKOR1] and *A. woodii*[pKOR2] produced also increased amounts of ethanol. Some isoamyl alcohol (up to 0.4 mM) was formed in addition. The respective data for *C. ljungdahlii* are shown in **Supplementary Figure 9**. Without ketoisovalerate addition, no isobutanol was formed and even with addition only trace amounts [*C. ljungdahlii*(pKOR2) 0.1 mM; *C. ljungdahlii*(pKOR3) 0.2 mM]. However, *C. ljungdahlii*[pKOR3] showed a significant increase in ethanol formation without ketoisovalerate addition as well as *C. ljungdahlii*[pKOR2] with addition.

Isobutanol Production *via* Ketoisovalerate Decarboxylase (KivD)

Next, the isobutanol synthesis pathway *via* ketoisovalerate decarboxylase and alcohol dehydrogenase in acetogens was elucidated. The *kivD* gene from *L. lactis* and *adhA* from *C. glutamicum* were PCR-amplified and subcloned together into the pMTL83151 backbone, controlled by the also PCR-amplified $P_{pta\text{-}ack}$ promoter from *C. ljungdahlii*. In order to increase the carbon flux from pyruvate to ketoisovalerate, genes *ilvC* (encoding ketol-acid reductoisomerase), *ilvD* (encoding dihydroxy-acid dehydratase), and *alsS* (encoding acetolactate synthase), all from *C. ljungdahlii*, were PCR-amplified and subcloned downstream of *adhA*. The resulting plasmid pKAIA was transformed into *A. woodii* and *C. ljungdahlii*. In case of *C. ljungdahlii*, it was also possible to construct an insertion mutant in *ilvE* (encoding an aminotransferase), which blocked the last step of valine biosynthesis. This strain, *C. ljungdahlii:ilvE* was also transformed with pKAIA. Recombinant strains were then tested under heterotrophic conditions with fructose as a carbon source as well as with and without addition of ketoisovalerate (15 mM). Wild type strains and empty plasmid-carrying strains were used as controls. Without ketoisovalerate addition, only *A. woodii*[pKAIA] formed some isobutanol (0.2 mM). With addition, the same strain produced 0.4 mM (**Supplementary Figure 10**). Some

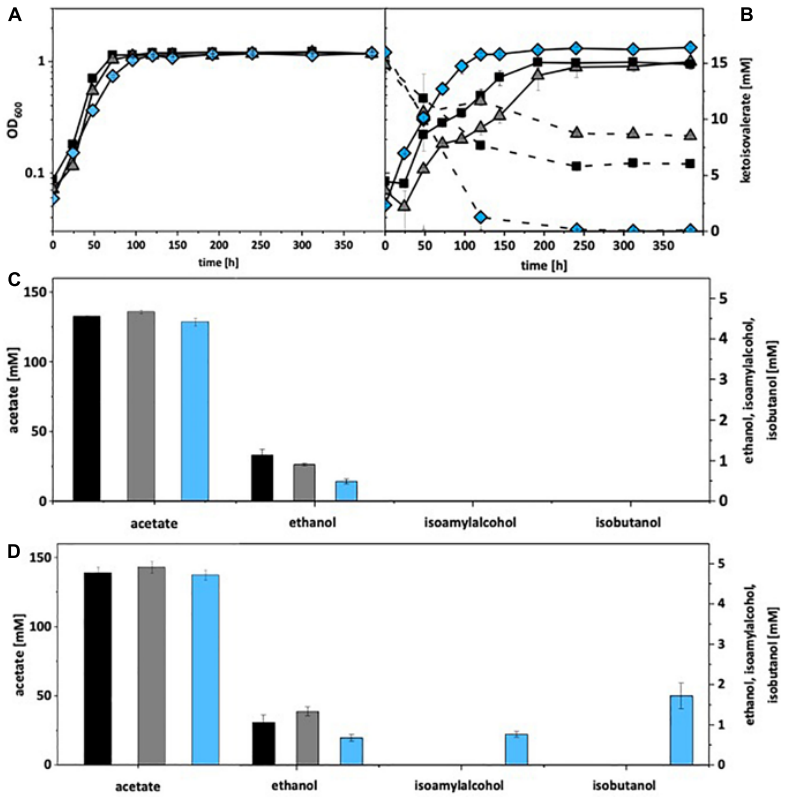

FIGURE 4 | Autotrophic isobutanol production with recombinant *A. woodii* strains by the KivD pathway. Growth behavior **(A,B)**; ketoisovalerate consumption **(B)**; product pattern **(C,D)**. *A. woodii* [WT], black, squares; *A. woodii* [pM83], gray, triangles; *A. woodii* [pKAIA], blue, diamonds. Panels **(A,C)** without ketoisovalerate supplementation; Panels **(B,D)** with ketoisovalerate supplementation. Each strain was analyzed in biological triplicates (n = 3).

isoamyl alcohol (up to 0.2 mM) was formed in addition. The respective data for *C. ljungdahlii* are shown in **Supplementary Figure 11**. Without ketoisovalerate addition, no isobutanol was formed. With addition, *C. ljungdahlii*[pKAIA] and *C. ljungdahlii:ilvE*[pKAIA] produced up to 2.4 mM isobutanol during the exponential growth phase.

Under autotrophic growth conditions, recombinant *A. woodii* strains formed no isobutanol. With addition of 15 mM isovalerate, *A. woodii*[pKAIA] produced 1.7 mM isobutanol and 0.8 mM isoamyl alcohol (**Figure 4**). The respective data for *C. ljungdahlii* are shown in **Figure 5**. Only *C. ljungdahlii*[pKAIA] and *C. ljungdahlii:ilvE*[pKAIA] formed isobutanol (and isoamyl alcohol) without ketoisovalerate addition. The latter strain formed three times more acohols (up to 0.4 mM isobutanol). Addition of ketoisovalerate increased production of both alcohols in the pKAIA-carrying strains (up to 1 mM in *C. ljungdahlii:ilvE*[pKAIA]).

Coenzyme Dependency of Isobutanol Production *via* Ketoisovalerate Decarboxylase (KivD)

The *ilvC* gene product of *C. ljungdahlii*, the ketol-acid reductoisomerase, uses NADPH for reduction of acetolactate to 2,3-dihydroxyisovalerate. However, NADPH might be a limiting factor in a catabolic pathway with high amounts of products. Therefore, this gene in pKAIA was replaced by a similar gene encoding a NADH-dependent IlvC enzyme from *E. coli* (Brinkmann-Chen et al., 2013). The nucleotide sequence of Ec_IlvC$^{P2D1\text{-}A1}$ was codon-optimized for clostridia, PCR-amplified, and subcloned into pKAIA by replacing the *C. ljungdahlii ilvC* gene. The resulting plasmid was designated pKAI$_{NADH}$A (**Supplementary Figure 6**). This plasmid was transformed into *C. ljungdahlii:ilvE*, and the recombinant tested in heterotrophic and autotrophic fermentations. With fructose as a carbon source, *C. ljungdahlii:ilvE*[pKAI$_{NADH}$A] produced isobutanol only upon addition of ketoisovalerate. The production was slightly higher than with the corresponding pKAIA-carrying strain (1.6 vs. 1.4 mM). Under autotrophic conditions without isovalerate supplementation, *C. ljungdahlii:ilvE*[pKAI$_{NADH}$A] formed only trace amounts of isobutanol (0.1 mM). Even with isovalerate addition, lower amounts were produced than by *C. ljungdahlii:ilvE*[pKAIA] (0.8 mM compared to 1 mM).

DISCUSSION

The data presented clearly demonstrate that subcloning of both, the KivD as well as the Kor pathway lead to heterologous expression of isobutanol formation in acetogenic bacteria. Both

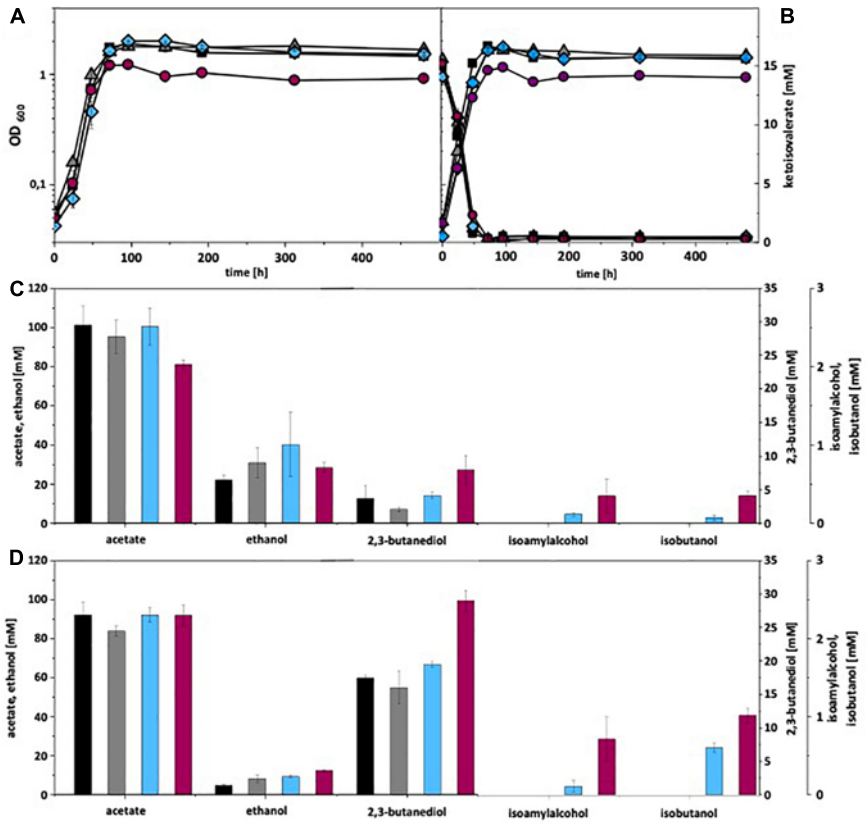

FIGURE 5 | Autotrophic isobutanol production with recombinant *C. ljungdahlii* strains by the KivD pathway. Growth behavior **(A,B)**; ketoisovalerate consumption **(B)**; product pattern **(C,D)**. *C. ljungdahlii* [WT], black, squares; *C. ljungdahlii* [pM83], gray, triangles; *C. ljungdahlii* [pKAIA], blue, diamonds; *C. ljungdahlii:ilvE* [pKAIA], purple, circles; Panels **(A,C)** without ketoisovalerate supplementation; Panels **(B,D)** with ketoisovalerate supplementation. Each strain was analyzed in biological triplicates (n = 3).

key enzymes, ketoisovalerate decarboxylase and ketoisovalerate ferredoxin oxidoreductase, belong to the group of pyruvate decarboxylases/pyruvate oxidoreductases and are dependent on thiamine pyrophosphate (Heider et al., 1996; de la Plaza et al., 2004). The active forms are homo- or heterotetramers, respectively. KivD from *L. lactis* decarboxylates preferentially ketoisovalerate, but also showed specific activity toward other keto compounds, from ketoisocaproate (23% relative activity) to pyruvate (0.6% relative activity) (de la Plaza et al., 2004). The temperature optimum is 45°C, but more than 74% relative activity is found between 30 and 50°C (de la Plaza et al., 2004). The pH optimum is more pronounced, with a peak at pH 6.5 and app. 90% relative activity between pH 6 and 7 (de la Plaza et al., 2004). Kor has been purified from *Pyrococcus* and *Thermococcus* strains, which are proteolytic and hyperthermophilic archaea. Highest activity was observed with ketoisovalerate, lowest activity with phenylpyruvate, pyruvate, and glyoxylate (Heider et al., 1996). Based on the back reaction of acetyl-CoA + CO_2 + reduced ferredoxin to pyruvate, Xiong et al. (2016) characterized the *kor* gene clusters of *C. thermocellum* as reversed pyruvate ferredoxin oxidoreductases. *T. litoralis* Kor exhibits a sharp pH optimum at 7, with less than 50% relative activity of pH 6 and 25% at pH 8 (Heider et al., 1996). The temperature optimum of enzymes from the different archaea varies between 90 and 98°C (Heider et al., 1996).

Our results demonstrate that the *kor3* and *kor2* gene clusters are the best suited candidates for further improvement of isobutanol production in acetogens by the Kor pathway, especially in *A. woodii*. Interestingly, the relatively low similarity between the respective gene products (**Supplementary Figure 7**) does not show a massive effect on product formation. Although the titers are still low (0.1 mM without and up to 2.9 mM with ketoisovalerate addition), it must be kept in mind that in other reported production organisms such as *E. coli* and *C. glutamicum* only numerous additional gene inactivations finally led to promising strains (Atsumi et al., 2008; Blombach et al., 2011). The formation of isoamyl alcohol (3-methyl-1-butanol) is most probably due to the relatively broad substrate spectrum of ketoisovalerate ferredoxin oxidoreductase (and also ketoisovalerate decarboxylase) (Heider et al., 1996; Atsumi et al., 2008). Ketoisocaproate would be the precursor and is metabolized by both enzymes. This substance is formed naturally during leucine biosynthesis. Interestingly, the introduction of the *kor1* and *kor2* gene clusters led in both, *A. woodii* and *C. ljungdahlii* to an app. doubling of the ethanol formation, but only under autotrophic conditions upon addition of

ketoisovalerate. *kor2* in *A. woodii* under heterotrophic conditions resulted in the same phenomenon, whereas in *C. ljungdahlii* rather a decrease in ethanol formation in *kor*-carrying strains under heterotrophic conditions could be observed. The reason for this phenomenon is not obvious, as especially in *A. woodii* the stoichiometry of added ketoisovalerate and formed ethanol does not match. On the other hand, the increase of 2,3-butanediol production in all *C. ljungdahlii* strains upon addition of ketoisovalerate can be easily explained. Obviously, ketoisovalerate was converted to acetolactate, which was then decarboxylated and reduced to yield 2,3-butanediol.

The KivD pathway also allowed formation of trace amounts of isobutanol in *A. woodii* (heterotrophic conditions) and *C. ljungdahlii* (autotrophic conditions). Addition of ketoisovalerate clearly stimulated isobutanol production in both organisms under all tested growth conditions. The inactivation of *ilvE* in *C. ljungdahlii* (blocking the last step of valine biosynthesis) led to a significant increase in isobutanol production. This stresses again the necessity of further tailored metabolic mutations for optimizing the isobutanol fermentation. Unfortunately, an attempt during this project to inactivate the *aldC* gene of *C. ljungdahlii* (encoding the acetolactate decarboxylase, which catalyzes the first step of 2,3-butanediol synthesis) failed. Such a mutant would have prevented the carbon flow toward 2,3-butanediol. It was also disappointing that changing the coenzyme specificity of IlvC, the ketol-acid reductoisomerase, of *C. ljungdahlii* from NADPH to NADH did not result in an increase in isobutanol formation. However, as already stressed before, most probably only a combination of a series of metabolic alterations will result in a suitable production strain, as was the case with other heterotrophic bacteria.

What targets for such mutations can be imagined? Of course, reduction of other products will be the primary goal. Acetate formation is of vital importance for acetogens regarding ATP formation, but it can be further converted to ethanol using aldehyde ferredoxin oxidoreductase and alcohol dehydrogenase. The required reducing equivalents (reduced ferredoxin and NADH) can be easily generated from hydrogen under autotrophic conditions. Thus, 2,3-butanediol is the prime candidate for a product to be eliminated. If the ClosTron technology does not work (as mentioned, our attempt to inactivate the *ilvC* gene failed), CRISPR/Cas9-based genome editing will be an alternative that has recently been developed for *C. ljungdahlii* (Huang et al., 2016; Jin et al., 2020). The optimal temperatures for both key enzymes, ketoisovalerate decarboxylase (45°C) and ketoisovalerate ferredoxin oxidoreductase (growth temperature of *C. thermocellum* is 60°C), significantly exceed the range of mesophilic fermentations. The same applies to the pH optimum of both enzymes. Acetogenic bacteria generate a low pH, which results in reduced enzyme activity. Also, the broad enzyme substrate range is a disadvantage, as is obvious from the formation of isoamyl alcohol by *A. woodii*. Thus, mutational adaptation of the key enzymes with respect to pH and temperature tolerance as well as increase of substrate specificity will be another prime target in future. The change of coenzyme specificity from NADPH to NADH has already been achieved for IlvC from *C. ljungdahlii* and can thus easily be combined with the aforementioned alterations. The benefit of a NADH-depending alcohol dehydrogenase replacement in the natural, decarboxylase-based isobutanol formation pathway of Shimwellia blattae has recently been shown by Acedos et al. (2021). Finally, growing the strains in gassed and stirred bioreactors will certainly improve the fermentation outcome. In fact, a *C. ljungdahlii:ilvE* strain carrying pKAIA showed under such conditions an increased isobutanol production by factor 6.5 (Hermann et al., 2021).

Further metabolic engineering will focus on the *kor3* gene cluster in case of *A. woodii* and the KivD pathway in *C. ljungdahlii:ilvE*[pKAIA], which so far allowed highest product formation. Strains suitably improved as described above might then become a viable option for commercial isobutanol synthesis from waste and greenhouse gases such as CO and CO_2.

DATA AVAILABILITY STATEMENT

The original contributions presented in the study are included in the article/**Supplementary Material**, further inquiries can be directed to the corresponding author/s.

AUTHOR CONTRIBUTIONS

SW, FB, MH, RT, and PD conceived and designed the experiments. SW and SL performed the experiments. SW, MH, SL, FB, RT, and PD analyzed the data. MH, SL, FB, RT, and PD wrote the manuscript. All authors contributed to the article and approved the submitted version.

FUNDING

This work was supported by the Bundesministerium für Bildung und Forschung (BMBF) in its program "Gase als neue Kohlenstoffquelle für biotechnologische Fermentationen," project gas fermentation (031A468A).

ACKNOWLEDGMENTS

We thank Nigel Minton (University of Nottingham, United Kingdom) for providing plasmid pMTL83151 and Bastian Blombach (Technical University of Munich, Germany) as well as Bernhard Eikmanns (University of Ulm, Germany) for providing plasmid pJUL34.

SUPPLEMENTARY MATERIAL

The Supplementary Material for this article can be found online at: https://www.frontiersin.org/articles/10.3389/fbioe.2021.657253/full#supplementary-material

Supplementary Figure 1 | Schematic representation of plasmid pMTL83151_ptaack_aacht_cac. *adhE2*, bifunctional aldehyde/alcohol dehydrogenase gene (*C. acetobutylicum*); *abfD*, 4-hydroxybutyryl-CoA dehydratase gene (*Clostridium scatologenes*); *crt,* crotonase gene (*C. acetobutylicum*); *hbd,* 3-hydroxybutyryl-CoA dehydrogenase gene (*C. acetobutylicum*); *thlA,* acetyl-CoA acetyltransferase gene (*C. acetobutylicum*); *catP*, chloramphenicol resistance gene; ColE1, origin of replication for Gram-negative bacteria; *repH*, origin of replication for Gram-positive bacteria; *lacZ alpha*, truncated β-galactosidase gene (*E. coli*); *traJ*, gene for DNA transfer by conjugation.

Supplementary Figure 2 | Schematic representation of plasmids pKOR1, pKOR2, and pKOR3. *kor1*, *kor2, kor3,* potential ketoisovalerate ferredoxin oxidoreductases gene clusters (*C. thermocellum*); *adhE2*, bifunctional aldehyde/alcohol dehydrogenase gene (*C. acetobutylicum*); $P_{pta-ack}$, promoter upstream of *pta-ack* genes (*C. ljungdahlii*); *catP*, chloramphenicol resistance gene; ColE1, origin of replication for Gram-negative bacteria; *repH*, origin of replication for Gram-positive bacteria; *traJ*, gene for DNA transfer by conjugation.

Supplementary Figure 3 | Schematic representation of plasmid pJUL34. P_{tuf}, promoter upstream of EF-Tu gene (*L. lactis*); *kivD*, ketoisovalerate decarboxylase gene (*L. lactis*); *adhA*, alcohol dehydrogenase gene (*Corynebacterium glutamicum*); *lacZ alpha*, truncated β-galactosidase gene (*E. coli*); *aph3,* kanamycin resistance gene; *sacB,* levansucrase gene; repBL1, origin of replication for *Corynebacterium*.

Supplementary Figure 4 | Schematic representation of plasmid pKAIA. *kivD*, ketoisovalerate decarboxylase gene (*L. lactis*); *adhA*, alcohol dehydrogenase gene (*C. glutamicum*); *ilvC*, ketol-acid reductoisomerase gene (*C. ljungdahlii*); *ilvD*, dihydroxy-acid dehydratase gene (*C. ljungdahlii*); *alsS*, acetolactate synthase gene (*C. ljungdahlii*); $P_{pta-ack}$, promoter upstream of *pta-ack* genes (*C. ljungdahlii*); *catP*, chloramphenicol resistance gene; ColE1, origin of replication for Gram-negative bacteria; *repH*, origin of replication for Gram-positive bacteria; *traJ*, gene for DNA transfer by conjugation.

Supplementary Figure 5 | Sequence of the commercially synthesized and codon-optimized $ilvC^{NADH}$ gene.

Supplementary Figure 6 | Schematic representation of plasmid $pKAI_{NADH}A$. *kivD*, ketoisovalerate decarboxylase gene (*L. lactis*); *adhA*, alcohol dehydrogenase gene (*Corynebacterium glutamicum*); *ilvC*, ketol-acid reductoisomerase gene (*C. ljungdahlii*); $ilvC^{NADH}$, NADH-dependent ketol-acid reductoisomerase gene (Ec_IlvCP2D1-A1 from *E. coli*, codon-optimized for clostridia); *ilvD*, dihydroxy-acid dehydratase gene (*C. ljungdahlii*); *alsS*, acetolactate synthase gene (*C. ljungdahlii*); $P_{pta-ack}$, promoter upstream of *pta-ack* genes (*C. ljungdahlii*); *catP*, chloramphenicol resistance gene; ColE1, origin of replication for Gram-negative bacteria; *repH*, origin of replication for Gram-positive bacteria; *traJ*, gene for DNA transfer by conjugation.

Supplementary Figure 7 | tBLASTx comparison of gene clusters Clo1313_0020-0023 [*kor1*], Clo1313_0382-0385 [*kor2*], and Clo1313_1353-1356 [*kor3*] from *C. thermocellum*.

Supplementary Figure 8 | Heterotrophic isobutanol production with recombinant *C. ljungdahlii* strains by the Kor pathway. Growth behavior **(A,D)**; fructose consumption **(B,E)**; ketoisovalerate consumption **(E)**; product pattern **(C,F)**. *C. ljungdahlii* [WT], black, squares; *C. ljungdahlii* [pM83], gray, triangles; *C. ljungdahlii* [pKOR1], green, diamonds; *C. ljungdahlii* [pKOR2], light green, circles; *C. ljungdahlii* [pKOR3], dark green, triangle pointing downward. Panels **(A–C)** without ketoisovalerate supplementation; Panels **(D–F)** with ketoisovalerate supplementation. Each strain was analyzed in biological triplicates (n = 3).

Supplementary Figure 9 | Autotrophic isobutanol production with recombinant *C. ljungdahlii* strains by the Kor pathway. Growth behavior **(A,B)**; ketoisovalerate consumption **(B)**; product pattern **(C,D)**. *C. ljungdahlii* [WT], black, squares; *C. ljungdahlii* [pM83], gray, triangles; *C. ljungdahlii* [pKOR1], green, diamonds; *C. ljungdahlii* [pKOR2], light green, circles; *C. ljungdahlii* [pKOR3], dark green, triangle pointing downward. Panels **(A,C)** without ketoisovalerate supplementation; Panels **(B,D)** with ketoisovalerate supplementation. Each strain was analyzed in biological triplicates (n = 3).

Supplementary Figure 10 | Heterotrophic isobutanol production with recombinant *A. woodii* strains by the KivD pathway. Growth behavior **(A,D)**; fructose consumption **(B,E)**; ketoisovalerate consumption **(E)**; product pattern **(C,F)**. *A. woodii* [WT], black, squares; *A. woodii* [pM83], gray, triangles; *A. woodii* [pKAIA], blue, diamonds. Panels **(A–C)** without ketoisovalerate supplementation; Panels **(D–F)**, with ketoisovalerate supplementation. Each strain was analyzed in biological triplicates (n = 3).

Supplementary Figure 11 | Heterotrophic isobutanol production with recombinant *C. ljungdahlii* strains by the KivD pathway. Growth behavior **(A,D)**; fructose consumption **(B,E)**; ketoisovalerate consumption **(E)**; product range **(C,F)**. *C. ljungdahlii* [WT], black, squares; *C. ljungdahlii* [pKAIA], blue, diamonds; *C. ljungdahlii:ilvE* [pKAIA], purple, circles. Panels **(A–C)** without ketoisovalerate supplementation; Panels **(D–F)** with ketoisovalerate supplementation. Each strain was analyzed in biological triplicates (n = 3).

REFERENCES

Acedos, M. G., de la Torre, I., Santos, V. E., García-Ochoa, F., García, J. L., and Galán, B. (2021). Modulating redox metabolism to improve isobutanol production in *Shimwellia blattae*. *Biotechnol. Biofuels* 14, 1–11. doi: 10.1186/s13068-020-01862-1

Atsumi, S., Hanai, T., and Liao, J. C. (2008). Non-fermentative pathways for synthesis of branched-chain higher alcohols as biofuels. *Nature* 451, 86–89. doi: 10.1038/nature06450

Balch, W. E., Schoberth, S., Tanner, R. S., and Wolfe, R. S. (1977). *Acetobacterium*, a new genus of hydrogen-oxidizing, carbon dioxide-reducing, anaerobic bacteria. *Int. J. Syst. Bacteriol.* 27, 355–361.

Black, W. B., Zhang, L., Kamoku, C., Liao, J. C., and Li, H. (2018). Rearrangement of coenzyme A-acylated carbon chain enables synthesis of isobutanol via a novel pathway in *Ralstonia eutropha*. *ACS Synth. Biol.* 7, 794–800. doi: 10.1021/acssynbio.7b00409

Blombach, B., Riester, T., Wieschalka, S., Ziert, C., Youn, J.-W., Wendisch, V. F., et al. (2011). *Corynebacterium glutamicum* tailored for efficient isobutanol production. *Appl. Environ. Microbiol.* 77, 3300–3310. doi: 10.1128/AEM.02972-10

Brigham, C. (2019). Perspectives for the biotechnological production of biofuels from CO_2 and H_2 using *Ralstonia eutropha* and other 'Knallgas' bacteria. *Appl. Microbiol. Biotechnol.* 103, 2113–2120. doi: 10.1007/s00253-019-09636-y

Brinkmann-Chen, S., Flock, T., Cahn, J. K. B., Snow, C. D., Brustad, E. M., McIntosh, J. A., et al. (2013). General approach to reversing ketol-acid reductoisomerase cofactor dependence from NADPH to NADH. *Proc. Natl. Acad. Sci. U.S.A.* 110, 10946–10951. doi: 10.1073/pnas.1306073110

Chen, C.-T., and Liao, J. C. (2016). Frontiers in microbial 1-butanol and isobutanol production. *FEMS Microbiol. Lett.* 363:fnw020. doi: 10.1093/femsle/fnw020

de la Plaza, M., de Palencia, P. F., Peláez, C., and Requena, T. (2004). Biochemical and molecular characterization of α-ketoisovalerate decarboxylase, an enzyme involved in the formation of aldehydes from amino acids by *Lactococcus lactis*. *FEMS Microbiol. Lett.* 238, 367–374. doi: 10.1016/j.femsle.2004.07.057

Green, M., and Sambrook, J. (2012). *Molecular Cloning: a Laboratory Manual*. Cold Spring Harbor, NY: Cold Spring Harbor Laboratory Press.

Heap, J. T., Kuehne, S. A., Ehsaan, M., Cartman, S. T., Cooksley, C. M., Scott, J. C., et al. (2010). The ClosTron: mutagenesis in *Clostridium* refined and streamlined. *J. Microbiol. Methods* 80, 49–55. doi: 10.1016/j.mimet.2009.10.018

Heap, J. T., Pennington, O. J., Cartman, S. T., Carter, G. P., and Minton, N. P. (2007). The ClosTron: a universal gene knock-out system for the genus *Clostridium*. *J. Microbiol. Methods* 70, 452–464. doi: 10.1016/j.mimet.2007.05.021

Heap, J. T., Pennington, O. J., Cartman, S. T., and Minton, N. P. (2009). A modular system for *Clostridium* shuttle plasmids. *J. Microbiol. Methods* 78, 79–85. doi: 10.1016/j.mimet.2009.05.004

Heider, J., Mai, X., and Adams, M. W. W. (1996). Characterization of 2-ketoisovalerate ferredoxin oxidoreductase, a new and reversible coenzyme

A-dependent enzyme involved in peptide fermentation by hyperthermophilic archaea. *J. Bacteriol.* 178, 780–787.

Hermann, M., Teleki, A., Weitz, S., Niess, A., Freund, A., Bengelsdorf, F. R., et al. (2021). Debottlenecking autotrophic isobutanol formation in recombinant *C. ljungdahlii* by systemic analysis. *Front. Bioeng. Biotechnol.* 9:647853. doi: 10.3389/fbioe.2021.647853

Huang, H., Chai, C., Li, N., Rowe, P., Minton, N. P., Yang, S., et al. (2016). CRISPR/Cas9-based efficient genome editing in *Clostridium ljungdahlii*, an autotrophic gas-fermenting bacterium. *ACS Synth. Biol.* 5, 1355–1361. doi: 10.1021/acssynbio.6b00044

Inoue, H., Nojima, H., and Okayama, H. (1990). High efficiency transformation of *Escherichia coli* with plasmids. *Gene* 96, 23–28. doi: 10.1016/0378-1119(90)90336-p

Jin, S., Bae, J., Song, Y., Pearcy, N., Shin, J., Kang, S., et al. (2020). Synthetic biology on acetogenic bacteria for highly efficient conversion of C1 gases to biochemicals. *Int. J. Mol. Sci.* 21:7639. doi: 10.3390/ijms21207639

Leang, C., Ueki, T., Nevin, K. P., and Lovley, D. R. (2013). A genetic system for *Clostridium ljungdahlii*: a chassis for autotrophic production of biocommodities and a model homoacetogen. *Appl. Environ. Microbiol.* 79, 1102–1109. doi: 10.1128/AEM.02891-12

Li, H., Opgenorth, P. H., Wernick, D. G., Rogers, S., Wu, T.-Y., Higashide, W., et al. (2012). Integrated electromicrobial conversion of CO_2 to higher alcohols. *Science* 335:1596. doi: 10.1126/science.1217643

Lin, P. P., Mi, L., Morioka, A. H., Yoshino, K. M., Konishi, S., Xu, S. C., et al. (2015). Consolidated bioprocessing of cellulose to isobutanol using *Clostridium thermocellum*. *Metab. Eng.* 31, 44–52. doi: 10.1016/j.ymben.2015.07.001

Lin, P. P., Rabe, K. S., Takasumi, J. L., Kadisch, M., Arnold, F. H., and Liao, J. C. (2014). Isobutanol production at elevated temperatures in thermophilic *Geobacillus thermoglucosidasius*. *Metab. Eng.* 24, 1–8. doi: 10.1016/j.ymben.2014.03.006

Miao, R., Xie, H., and Lindblad, P. (2018). Enhancement of photosynthetic isobutanol production in engineered cells of *Synechocystis* PCC 6803. *Biotechnol. Biofuels* 11:267. doi: 10.1186/s13068-018-1268-8

Perutka, J., Wang, W., Goerlitz, D., and Lambowitz, A. M. (2004). Use of computer-designed group II introns to disrupt *Escherichia coli* DExH/D-box protein and DNA helicase genes. *J. Mol. Biol.* 336, 421–439. doi: 10.1016/j.jmb.2003.12.009

Tanner, R. S., Miller, L. M., and Yang, D. (1993). *Clostridium ljungdahlii* sp. nov., an acetogenic species in clostridial rRNA homology group I. *Int. J. Syst. Bacteriol.* 43, 232–236. doi: 10.1099/00207713-43-2-232

Wess, J., Brinek, M., and Boles, E. (2019). Improving isobutanol production with the yeast *Saccharomyces cerevisiae* by successively blocking competing metabolic pathways as well as ethanol and glycerol formation. *Biotechnol. Biofuels* 12:173. doi: 10.1186/s13086-019-1486-8

Xiong, W., Lin, P. P., Magnusson, L., Warner, L., Liao, J. C., Maness, P.-C., et al. (2016). CO_2-fixing one-carbon metabolism in a cellulose-degrading bacterium *Clostridium thermocellum*. *Proc. Natl. Acad. Sci. U.S.A.* 113, 13180–13185. doi: 10.1073/pnas.1605482113

Conflict of Interest: The authors declare that the research was conducted in the absence of any commercial or financial relationships that could be construed as a potential conflict of interest.

frontiers in Bioengineering and Biotechnology

ORIGINAL RESEARCH
published: 12 April 2021
doi: 10.3389/fbioe.2021.626628

Effect of Solid-State Fermentation on Nutritional Quality of Leaf Flour of the Drumstick Tree (*Moringa oleifera* Lam.)

Honghui Shi[1,2,3,4], *Endian Yang*[1,2,3,4], *Yun Li*[5], *Xiaoyang Chen*[1,2,3,4]* *and Junjie Zhang*[1,2,3,4]*

[1] State Key Laboratory for Conservation and Utilization of Subtropical Agro-Bioresources, South China Agricultural University, Guangzhou, China, [2] Guangdong Key Laboratory for Innovative Development and Utilization of Forest Plant Germplasm, Guangzhou, China, [3] Guangdong Province Research Center of Woody Forage Engineering Technology, Guangzhou, China, [4] College of Forestry and Landscape Architecture, South China Agricultural University, Guangzhou, China, [5] College of Biological Sciences and Technology, Beijing Forestry University, Beijing, China

OPEN ACCESS

Edited by:
Chuang Xue,
Dalian University of Technology, China

Reviewed by:
Apilak Salakkam,
Khon Kaen University, Thailand
Lan Wang,
Institute of Process Engineering (CAS), China

***Correspondence:**
Xiaoyang Chen
xychen@scau.edu.cn
Junjie Zhang
zhangjunjie3168@163.com

Specialty section:
This article was submitted to Bioprocess Engineering, a section of the journal Frontiers in Bioengineering and Biotechnology

Received: 06 November 2020
Accepted: 19 March 2021
Published: 12 April 2021

Citation:
Shi H, Yang E, Li Y, Chen X and Zhang J (2021) Effect of Solid-State Fermentation on Nutritional Quality of Leaf Flour of the Drumstick Tree (Moringa oleifera Lam.). Front. Bioeng. Biotechnol. 9:626628. doi: 10.3389/fbioe.2021.626628

The drumstick tree is a fast-growing multipurpose tree with a large biomass and high nutritional value. However, it has rarely been exploited as a protein source. This study investigated solid-state fermentation induced by *Aspergillus niger*, *Candida utilis* and *Bacillus subtilis* to obtain high-quality protein feed from drumstick leaf flour. The results showed that fermentation induced significant changes in the nutritional composition of drumstick leaf flour. The concentrations of crude protein, small peptides and amino acids increased significantly after fermentation. The protein profile was also affected by the fermentation process. Macromolecular proteins in drumstick leaf flour were degraded, whereas other high molecular weight proteins were increased. However, the concentrations of crude fat, fiber, total sugar and reducing sugar were decreased, as were the anti-nutritional factors tannins, phytic acid and glucosinolates. After 24 h fermentation, the concentrations of total phenolics and flavonoids were increased. The antioxidant capacity was also significantly enhanced.

Keywords: ***Moringa oleifera*** **Lam., solid-state fermentation, nutritional quality, antioxidant activity, protein**

INTRODUCTION

The demand for animal protein for human nutrition is still rising in the developing world and the cost of feed for livestock is also increasing (Tufarelli et al., 2018). Therefore, a new source of feed protein is urgently needed to solve these problems. Among the available forage crops, special focus has been given to the effects of *Moringa oleifera* Lam. on livestock growth and production (Cui et al., 2018; Yusuf et al., 2018; Zeng et al., 2018). *Moringa oleifera* Lam., commonly known as the drumstick tree, belongs to the family of Moringaceae and is widely distributed in tropical and subtropical regions (Popoola and Obembe, 2013; Leone et al., 2015). It is extremely nutritious, containing high levels of protein, vitamins, minerals and phytochemicals (Leone et al., 2015). These nutritional traits together with its high production of leaf mass and adaptability to climate conditions and dry soils make drumstick a potential high quality feed source for livestock

(He et al., 2020). Dietary inclusion of drumstick has been shown to enhance nutritional status, growth performance, milk production and meat quality in several livestock species (Cui et al., 2018; Kholif et al., 2018; Zeng et al., 2018). Such characteristics show that drumstick is a rich source of nutrients and biological activities for livestock, which could help to relieve the shortage of feed resources and decrease the need for antibiotics. However, anti-nutritional factors (ANF) in drumstick, such as tannins, phytic acid and glucosinolates, could affect the palatability, digestion and absorption, limiting its nutrition availability (Stevens et al., 2016). Moreover, most of the proteins are insoluble despite drumstick tree leaves having relatively high protein content (Teixeira et al., 2014). So far, the nutritional value of drumstick leaves has mainly been improved by heating, grinding, cooking and other physical and chemical means (Vongsak et al., 2013; Adedapo et al., 2015; Phatsimo et al., 2015). Although some of the ANF can be removed, the nutrient content may also be destroyed by these processes. Therefore, a more suitable process for improving drumstick feed quality is needed.

Solid-state fermentation (SSF) involves the growth of microorganisms on substrates with limited water content (Dulf et al., 2017). Numerous studies have demonstrated that the functionalities of various agricultural by-products can be enhanced by SSF. Indeed, many beneficial compounds have been produced through SSF, such as organic acids, enzymes, aromatic and flavor compounds, as well as bioactive compounds (Bennett and Yang, 2012; Dulf et al., 2016; Jin et al., 2016). In recent years, SSF has been widely used in the feedstock industry and has shown good prospects for promoting nutrient utilization and decreasing ANF levels (Chi and Cho, 2016; Wang et al., 2018a). Although, several studies have been conducted on the SSF of drumstick leaf flour (DLF), they mainly focused on the selection of strains, optimization of fermentation technology and evaluation of the nutritional value before and after fermentation (Zhang et al., 2017; Wang et al., 2018b). Only a few studies have examined the dynamic changes of nutrients and antioxidant components during fermentation, and even fewer have reported on the antioxidant activity of DLF after fermentation.

The type of microorganism used for inoculation affects the nutritional quality of the fermented feed. Due to the developed enzyme system, *Aspergillus Niger* and *Bacillus subtilis* are commonly used in ANF degradation and hydrolysis of macronutrient factors (Wang et al., 2020). *Candida utilis* is easy to be grown with other strains and often used for the production of single-cell protein for its high content of protein, vitamins B, amino acids and other nutrients (Xie et al., 2016). This study evaluated SSF processes induced by *A. niger*, *C. utilis* and *B. subtilis* for the mixed fermentation of drumstick leaves. Effects on the nutrient composition, physical and chemical properties and functional activity of drumstick leaves were studied. The main aims were to obtain a high nutrition, multi-functional feed, broaden the utilization ways of drumstick feed and provide some theoretical basis for the further processing of drumstick resources.

MATERIALS AND METHODS

Microorganisms

A. niger strain GIM 3.576 and *C. utilis* strain GIM 1.427 were obtained from the Guangdong Microbial Strain Preservation Center. *B. subtilis* CICC 31188 was obtained from the China Center of Industrial Culture Collection (CICC). GIM 3.576 was cultured on potato dextrose agar (PDA) slants for 3 days at 28°C, GIM 1.427 was cultured on yeast extract peptone dextrose (YPD) slants for 3 days at 28°C and CICC 31188 was cultured on Luria-Bertani (LB) slants for 2 days at 30°C. After being activated for 3 generations, GIM 3.576 was cultured in PDA solid medium until mycelia had spread over the entire petri dish. The spores were then rinsed with sterile saline solution, and the concentration of the spore suspension was calculated and diluted to 1×10^7 spores/mL on a blood cell counting board. GIM 1.427 was incubated in YPD liquid medium at 28°C and 150 r/min for 3 days then diluted to a concentration of 1×10^8 spores/mL. CICC 31188 was cultured in LB liquid medium at 30°C and 250 r/min and diluted to a concentration of about 1×10^8 spores/mL.

Solid-State Fermentation

Drumstick leaf samples were harvested from trees of the PKM-1 cultivar. After harvesting, the samples were sun-dried until a constant weight was reached, then ground to a powder and passed through a 40-mesh sieve. Portions of 50 g were packed and sealed in polypropylene bags for sterilization in an autoclave at 121°C for 20 min. After cooling, sterilized water was added to adjust the initial water content to 50%. Then 6% (v/w) of the GIM 3.576 spore suspension was inoculated onto each DLF. After fermentation for 24 h, 6% (v/w) of the GIM 1.427 suspension and 12% (v/w) of the CICC 31188 suspension were inoculated simultaneously and fermented in a biochemical incubator at 32°C for a total of 7 days (Shi et al., 2020). Some of the fermentation samples were stored at −20°C for detection of the active substances, whereas the rest were dried at 50°C, crushed and screened for chemical analysis.

Scanning Electron Microscopy

Samples were prepared by a standard procedure of alcohol dehydration for scanning electron microscopy (SEM, Carl Zeiss, EVO MA15, Germany) analysis. After dehydration, the samples were placed on an aluminum column and sprayed with 12 nm of gold using ion sputtering coater (Leica, EM ACE 600, Germany). SEM images were recorded at 25 kV and with high vacuum modes.

Protein and Amino Acid Analysis

The crude protein (CP) concentration was analyzed using methods of the Association of Official Analytical Chemists (AOAC, 2005). The protein profile was analyzed by sodium dodecyl sulfate-polyacrylamide gel electrophoresis (SDS-PAGE) according to the method described by Zuo et al. (2017) with slight modifications. Proteins from unfermented and fermented samples were extracted using the plant total protein extraction kit (KeyGen Biotech, China), denatured with 2 × Tris-glycine

SDS loading buffer and separated using a 12% gel for SDS-PAGE at 110 V. The gel was stained with Coomassie Brilliant Blue R250 and de-stained with 8% acetic acid until the protein bands were visible. The amino acid (AA) profile was analyzed using an automatic AA analyzer (L-8900, Hitachi, Tokyo, Japan). Trichloroacetic acid-soluble protein (TCA-SP) was analyzed as reported by Ovissipour et al. (2009). Small peptide concentration was calculated by subtracting the concentration of free amino acids from that of TCA-SP.

Chemical Analysis

Dry matter (DM), ether extract (EE), crude fiber (CF), crude ash (CA), calcium (Ca) and phosphorus (P) were analyzed using methods of the Association of Official Analytical Chemists (AOAC, 2005). Neutral detergent fiber (NDF), acid detergent fiber (ADF) and lignin were determined by methods described by Van Soest et al. (1991). Potassium (K), sodium (Na), magnesium (Mg), copper (Cu), zinc (Zn) and iron (Fe) were determined by atomic absorption spectrophotometry as described by the AOAC (2005). Total sugars and reducing sugars were determined by 3,5-dinitrosalicylic acid colorimetry (Miller, 1959). Phytic acid was determined according to the method described by Gao et al. (2007). Glucosinolates were determined by palladium chloride colorimetry as described by Hu et al. (2010).

Determination of Total Phenolic, Tannin and Flavonoid Content

A methanol extract from each sample powder was prepared according to the method described by Zuo and Chen (2002). The lyophilized samples were extracted twice with 80% (v/v) methanol for 3 h at room temperature and filtered through a 0.45 μm injection filter. The total phenolic concentration

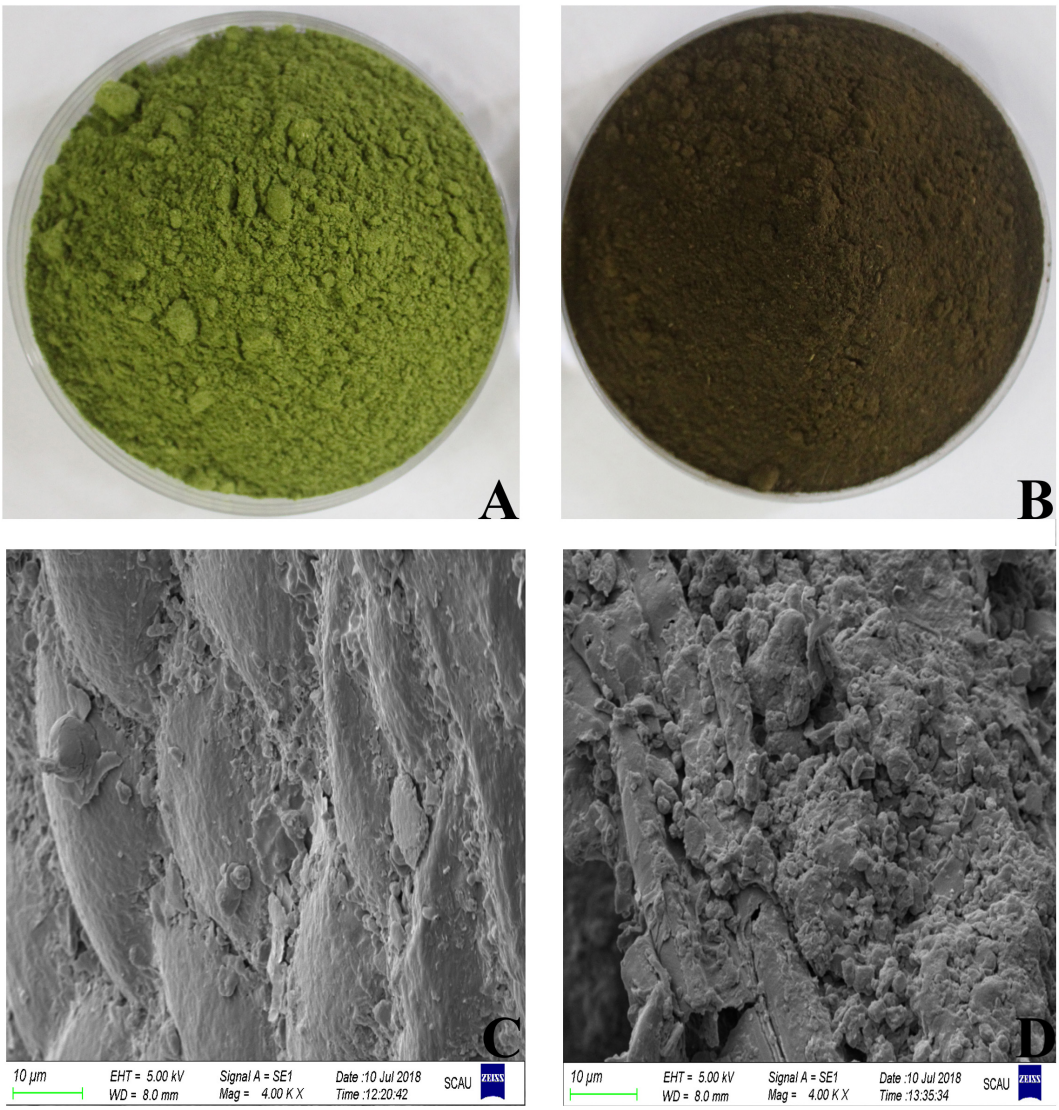

FIGURE 1 | Phenotype and scanning electron microscope images (×4,000) of UDLF **(A,C)** and FDLF **(B,D)**.

of the methanol-extracted samples was determined using the Folin-Ciocalteu procedure and expressed as grams of gallic acid equivalents (GAE) in 100 g of the extract (Generalić Mekinić et al., 2014). The concentration of tannins was calculated as the difference between the concentrations of total phenols and simple phenols after removing tannin from the extract using insoluble polyvinylpyrrolidone. The total flavonoid concentration was analyzed using the aluminum chloride colorimetric method and expressed as grams of rutin equivalents (RUE) in 100 g of the extract (Lin and Tang, 2007).

Determination of Antioxidant Capacity

The $ABTS^+$ (2,2′-azino-bis (3-ethylbenzothiazoline6-sulfonic acid) radical cation) radical-scavenging capacity of methanol extracts of samples were evaluated according to the method of Sasipriya and Siddhuraju (2012) with slight modifications. The stock solution was prepared by reacting 5 mL of 7 mM ABTS with 88 μL of 40 mM potassium persulfate and allowing the mixture to stand in the dark at room temperature for 12–16 h before use. The stock solution was diluted with methanol to give an absorbance of about 0.700 ± 0.020 at 734 nm. To determine the antioxidant capacity, 0.5 mL of methanolic extract samples (final concentration 1 mg/mL) and 4.0 mL of stock solution were mixed and incubated for 6 min. The absorbance was monitored at 734 nm.

The DPPH (2,2-diphenil-1-picrylhydrazyl) radical-scavenging capacity of methanol extracts of samples was evaluated according to the method of Arora and Chandra (2010) with slight modifications. A 100 μM solution of DPPH was prepared in absolute methanol, and 2.0 mL of the DPPH solution was added to 0.5 mL of a methanolic extract of a sample (final concentration 1 mg/mL). After thorough mixing, the solution was kept in the dark at room temperature for 30 min. The absorbance of the samples was measured using an UV-visible spectrophotometer at 517 nm against a methanol blank. Each sample was tested three times and the values were averaged.

The free radical scavenging activity (RSA) was calculated as a percentage using the following equation:

$$\text{RSA}\ (\%) = \left[1 - \left(\text{Ai} - \text{Aj}\right)/\text{Ae}\right] \times 100\%$$

where Ae is the absorbance of the control, Ai is the absorbance of the sample extract and Aj is the absorbance of the control of sample.

The total antioxidant capacity was determined using the ferric reducing ability of plasma antioxidant power (FRAP) assay. The procedure was conducted according to the manufacturer's instruction for the T-AOC kit (Jiancheng Bioengineering Institute, Nanjing, China).

Statistical Analysis

All processing treatments were performed in triplicate. The statistical analysis was carried out using SPSS 23.0 software (SPSS Inc., Chicago, IL, United States), Duncan's multiple range test was used to detect differences among means. A p-value <0.05 was considered significant. Pearson's correlation analysis was also performed.

TABLE 1 | Nutrient composition of FDLF and UDLF.

Item	UDLF	FDLF
CP,%	28.42 ± 1.17^b	40.98 ± 0.59^a
Small peptides,%	5.72 ± 0.20^b	12.03 ± 0.12^a
EE,%	5.43 ± 0.18^a	3.75 ± 0.15^b
CF,%	7.25 ± 0.02^a	2.17 ± 0.04^b
Ash,%	10.49 ± 0.03^b	16.75 ± 0.02^a
Total sugars,%	18.49 ± 0.62^a	5.34 ± 0.88^b
Reducing sugars,%	12.38 ± 0.81^a	1.69 ± 0.16^b
NDF,%	24.41 ± 2.11^b	38.61 ± 2.97^a
ADF,%	13.40 ± 2.06	12.97 ± 2.75
Lignin,%	1.30 ± 0.16^b	2.13 ± 0.38^a
Hemicellulose,%	11.01 ± 0.29^b	22.40 ± 1.68^a
Cellulose,%	12.62 ± 1.49^a	7.50 ± 0.84^b
Ca,%	2.34 ± 0.01^b	3.64 ± 0.06^a
P,%	0.25 ± 0.00^b	0.42 ± 0.01^a
K,%	1.04 ± 0.02^b	1.28 ± 0.01^a
Na,%	0.03 ± 0.01^b	0.12 ± 0.01^a
Mg,%	0.96 ± 0.02^b	1.31 ± 0.02^a
Fe, mg/100 g	41.70 ± 0.57^b	73.05 ± 1.06^a
Cu, mg/100 g	1.25 ± 0.01^b	1.81 ± 0.01^a
Zn, mg/100 g	2.45 ± 0.09^b	3.53 ± 0.06^a
Tannins, mg/g	14.60 ± 0.58^a	8.59 ± 0.45^b
Phytic acid, mg/g	18.31 ± 0.71^a	7.30 ± 0.74^b
Glucosinolates, mg/g	19.11 ± 0.13^a	14.72 ± 0.24^b

Means followed by the different letters in the same line are significantly different from each other at $P \leq 0.05$ level, according to Duncan's multiple range test.

RESULTS AND DISCUSSION

Microscopic Observation

During the fermentation process, the color of DLF changed from green to dark brown(**Figure 1**)accompanied by a sweet smell. The degradation of organic matter produces water, CO_2, and heat during aerobic fermentation. High temperature will accelerate the degradation of chlorophyll and cause caramelization and Maillard reaction, producing Browning. This phenomenon was also observed in the fermentation of lupin flour (Olukomaiya et al., 2020). The microstructure was clearly different between fermented DLF (FDLF) and unfermented DLF (UDLF) (**Figure 1**). An irregularly shaped and rough surface was mainly observed in FDLF, whereas the microstructure of DLF was more regular and the surface smooth. This change of microstructure may increase the surface area of the substrate and facilitate the full reaction between enzyme and substrate.

Effect of Solid-State Fermentation on Proteins and Amino Acids

The protein content is the most important parameter that determines the overall quality of animal feed products. It is well known that the protein content can vary depending on the microorganism used and their carbon and nutrient accessibility, as well as the cultivation conditions, such as carbon and nutrient

sources, water content and pH. The analysis showed that the average concentration of CP in the raw flour was 28.42% (**Table 1**), close to the figure reported by Teixeira et al. (2014) but lower than the values reported by Moyo and Masika (2011), most likely due to differences in the growth stage and planting conditions (Mendieta-Araica et al., 2013). SSF significantly increased the CP concentrations from 28.42 to 40.98% (**Table 1**). The enrichment of CP could be the result of increased fungal biomass, suggesting that the treated substrate could act as a good protein source for livestock. However, it could also be due to the concentration effect caused by the aggravation of dry matter loss.

To analyze the influence of fermentation on the DLF protein profile, SDS-PAGE was performed. SSF affected the characteristics of proteins in DLF. The molecular weight of the main protein fractions in the unfermented DLF was 55 kDa (**Figure 2**). The maximal degradation of large proteins in the FDLF was almost complete after 24 h of fermentation. This was likely because highly active proteases secreted by the microorganisms during fermentation were able to decompose the large proteins (Chi and Cho, 2016). This reduction of protein sizes is important to increase the digestibility of protein. However, from the third day of fermentation, the color of the protein bands gradually deepened and bands appeared at around 33–45 kDa and 60–140 kDa, similar to the results reported by Zuo et al. (2017). This could be due to the production of single-celled proteins in the late fermentation period. This phenomenon indicated that fermentation not only degraded the macromolecular proteins in DLF but also increased the abundance of other proteins with high molecular weight.

Drumstick leaves contain all essential amino acids, but the content varies greatly depending on growth environments, cultivation mode, tree age, leaf maturity and other conditions (Olaofe et al., 2013; Ndubuaku et al., 2014). Evaluation of the amino acid profile confirmed significant differences between the fermented substrate and raw flour (**Table 2**). The levels of most amino acids increased, whereas glutamic acid and lysine decreased. The alterations in amino acid profiles may vary depending on the microorganism used (Medeiros et al., 2018). The inoculated microorganisms may use glutamic acid and lysine for metabolic activity, resulting in a reduction in their concentrations in the fermented substrate compared to those in raw flour. After fermentation, the total amino acid content of DLF was 24.88%, which was significantly higher than that of the unfermented substrate. This may be due to enzymatic hydrolysis of large proteins into small amino acids or the microbial synthesis of some amino acids. The concentration of essential amino acids and non-essential amino acids in the fermented substrate also increased, by 1.81 and 1.76%, respectively. Animals not only have dietary requirements for essential amino acids but also need nutritionally non-essential amino acids to achieve maximum growth and production performance. Therefore, increasing non-essential amino acids in animal feeds is beneficial. It has been

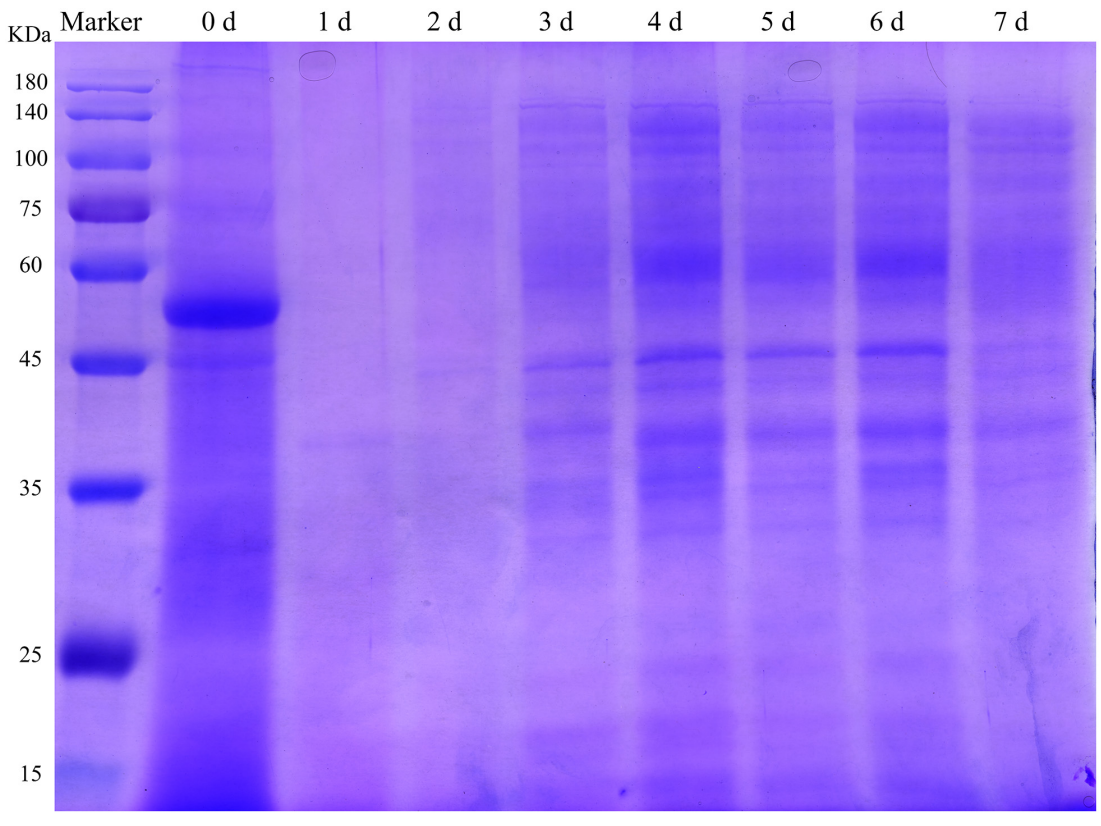

FIGURE 2 | SDS-PAGE analysis of protein profiles in DLF during fermentation.

reported that peptides are more rapidly utilized than proteins and amino acids (Kodera et al., 2006). The small peptide concentration in our study increased from 5.72 to 12.03% after fermentation. The increased peptide content may positively affect the bioactivity of DLF because they may contribute to antioxidative and metal-chelating activities (Chi and Cho, 2016).

Effect of Solid-State Fermentation on the Chemical Composition

The results regarding the chemical composition of the fermented substrate and raw flour are shown in **Table 1**. SSF increased the content of crude ash, neutral washing fiber and lignin. In addition, the CF concentration of the fermented substrate was decreased markedly, by 70.07%, compared to the control. There were also clear reductions in total sugars and reducing sugars from 18.49 and 12.38% to 5.34 and 1.69%, respectively (**Table 1**). Meanwhile, the ether extract (fat) concentration decreased by 30.94% compared with that before fermentation. This suggests that the microbial fermentation process consumed carbohydrates and fats, especially small molecules of sugars. At the same time, SSF resulted in an increase in the mineral content, probably due to the metabolic activity of the microorganisms or dry matter loss.

Effect of Solid-State Fermentation on Total Flavonoid, Phenolic Content and Antioxidant Capacity

Antioxidants are free radical scavengers that can protect the body from free radicals that can cause a variety of diseases, including ischemia, asthma, anemia, dementia and arthritis. Phenols and flavonoids are considered to be some of the safest natural antioxidants, and fermentation technology is an effective way to increase the concentration of these compounds. In this study, the concentration of total phenols and flavones reached the maximum value on the first day of fermentation. Afterward, the content of total phenols and flavonoids decreased as the fermentation continued (**Figure 3**). The proposed reason for the increased content was that various extracellular enzymes such as cellulase, pectinase, xylanase and so on, secreted by microorganisms destroy the intact cell wall structure of plants, releasing flavonoids from within cells and phenols bound to the cell walls during fermentation (Dey et al., 2016). *A. niger* used in the present study is a microorganism which has been found in many SSF studies to liberate the phenolic compounds, such as plum fruit by-products (Dulf et al., 2016), apricot pomace (Dulf et al., 2017). However, prolonged fermentation may lead to the diffusion and oxidation of phenolic substances.

It is crucial to evaluate the antioxidant potential of extracts using more than one method due to the different mechanisms of antioxidant activity. In the present study, the antioxidant activity of fermented substrates was measured using $ABTS^{+}$, DPPH free radical scavenging methods and FRAP. The antioxidant activity showed a trend of first increasing and then decreasing with increasing fermentation time (**Figure 3**), similar to results obtained with okra seeds during fermentation by Adetuyi and Ibrahim (2014). The antioxidant activity of DLF after fermentation was slightly lower than that before fermentation. Hossain et al. (2017) suggested that this might be because of a too long fermentation time and reduced content of phenols and other substances. Many studies have shown that the antioxidant capacity of plants is directly related to the content of phenolic compounds and flavones. In this study, Pearson's correlation analysis showed that flavonoids were only slightly positively correlated with DPPH radical scavenging rate and total antioxidant capacity, whereas total phenols were highly positively correlated with the three antioxidant indexes tested (**Table 3**), indicating that the total phenols and flavonoid concentrations of FDLF were closely related to antioxidant activity. However, total phenols and flavonoids are not the only factors affecting antioxidant activity. Small peptides and amino acids, such as leucine, methionine, tyrosine, histidine, and tryptophan, can also make the fermented sample more reductive (Sarmadi and Ismail, 2010; Sanjukat et al., 2015). In addition, determination of phenolic substances with the Folin-Ciocalteu reagent may be influenced by a variety of non-phenolic compounds, such as reducing sugars, aromatic amino acids and citric acids, which often do not have free radical scavenging capacity. In general, the synergistic effect between phenols and other components in the solid fermentation of DLF may be the main reason for this phenomenon.

TABLE 2 | Amino acid composition of FDLF and UDLF.

Amino acid composition,%	UDLF	FDLF
Arg	1.42 ± 0.02^{b}	1.60 ± 0.01^{a}
His	0.50 ± 0.02^{b}	0.58 ± 0.01^{a}
Ile	0.97 ± 0.06^{b}	1.15 ± 0.03^{a}
Leu	2.06 ± 0.05^{b}	2.38 ± 0.04^{a}
Lys	1.40 ± 0.10	1.35 ± 0.02
Phe	1.31 ± 0.06^{b}	1.53 ± 0.01^{a}
Thr	1.12 ± 0.05^{b}	1.38 ± 0.02^{a}
Val	1.23 ± 0.08^{b}	1.47 ± 0.01^{a}
Trp	0.65 ± 0.07^{b}	1.03 ± 0.11^{a}
Ala	1.49 ± 0.06^{b}	1.80 ± 0.02^{a}
Asp	2.13 ± 0.11^{b}	2.48 ± 0.10^{a}
Cys	0.11 ± 0.04^{b}	0.15 ± 0.02^{a}
Glu	2.80 ± 0.08	2.69 ± 0.20
Gly	1.21 ± 0.01^{b}	1.55 ± 0.05^{a}
Pro	1.01 ± 0.04^{b}	1.44 ± 0.01^{a}
Ser	1.07 ± 0.04^{b}	1.27 ± 0.04^{a}
Tyr	0.84 ± 0.01^{b}	1.03 ± 0.01^{a}
Essential AA,%	10.66 ± 0.51^{b}	12.47 ± 0.26^{a}
Non-essential AA,%	10.65 ± 0.24^{b}	12.41 ± 0.20^{a}
Total AA	21.31 ± 0.75^{b}	24.88 ± 0.46^{a}

Means followed by the different letters in the same line are significantly different from each other at $P \leq 0.05$ level, according to Duncan's multiple range test.

Effect of Solid-State Fermentation on Anti-nutritional Factors

Tannins, phytic acid and glucosinolates are the main anti-nutrients in DLF (Amaglo et al., 2010; Ogbe and Affiku, 2011;

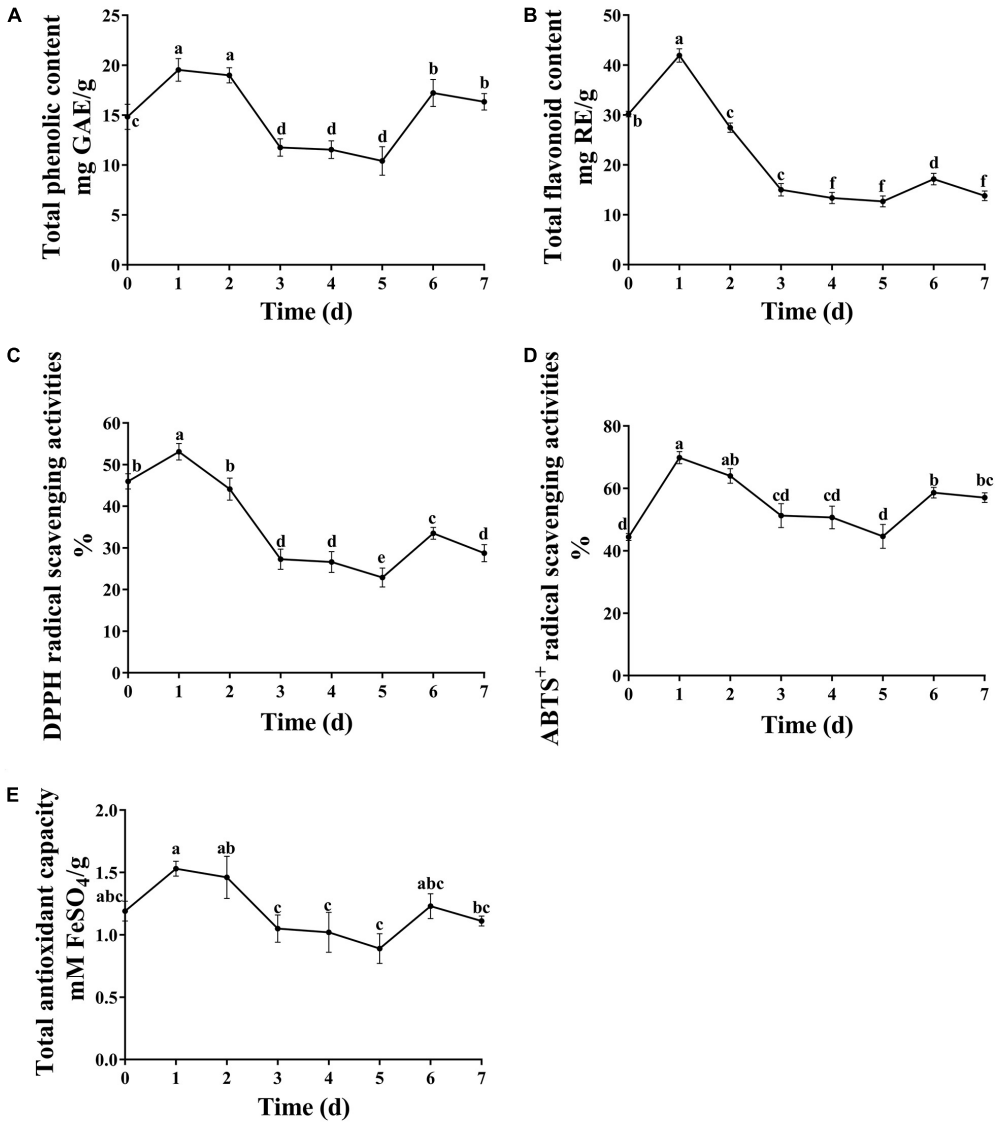

FIGURE 3 | Dynamic changes in total phenolic, flavonoid content and antioxidant capacity. **(A)** Total phenolic content, **(B)** total flavonoid content, **(C)** DPPH radical scavenging activities, **(D)** ABTS$^+$ radical scavenging activities, and **(E)** total antioxidant capacity. Different letters indicate significantly difference at $p \leq 0.05$ level.

Chodur et al., 2018). Tannins can precipitate proteins, amino acids, alkaloids and other organic molecules in aqueous solution, which hinder the absorption of some nutrients due to complexation. Further, the bitter taste of tannins may affect the palatability of feed. High concentrations of tannins have an adverse effect on animal productivity and digestibility. Phytic acid is an organic acid that cannot be digested by animals with a single stomach. Therefore, phytic acid is eventually expelled in an animal's feces, which may be degraded by aquatic microorganisms after entering water, releasing phosphorus and resulting in serious eutrophication of water (Singh and Satyanarayana, 2011). Although glucosinolates are non-toxic, they may decompose into glucose, isothiocyanate, nitrile, thiocarcinate and other toxic compounds through endogenous myrosinase. Their main anti-nutritional effects include reducing the palatability of feed, inducing iodine deficiency and damaging liver and kidney function. They are also more harmful to non-ruminants than ruminants (Tripathi and Mishra, 2007). Nevertheless, phytase, tannase and other enzymes can degrade

TABLE 3 | Correlation analysis of the concentrations of total phenols and flavones and antioxidant activity in FDLF.

Item	DPPH free radical scavenging rate	ABTS$^+$ free radical scavenging rate	Total antioxidant ability
total phenols	0.790*	0.856**	0.932**
flavones	0.975**	0.571	0.855**

**Means significant correlation at P ≤ 0.05 level and ** means highly significantly correlation at P ≤ 0.01 level.*

these substances. *Aspergillus* is considered to be the main source of these enzymes and is known to be capable of degrading tannins, phytic acid and glucosinolates (Shi et al., 2016). In this study, the phytic acid and tannin concentrations of DFL were 18.31 and 14.60 mg/g, respectively, which are close to the values of 22.3 and 16.3 mg/g reported by Stevens et al. (2016). After fermentation, the levels of tannins, phytic acid and glucosinolates were drastically decreased (**Table 1**). This might have been caused by the secretion of tannase, phytase and other biological enzymes, which are able to break down tannins, phytic acid and glucosinolates.

CONCLUSION

In this study, SSF by *A. niger*, *C. utilis* and *B. subtilis* was shown to be beneficial for improving the nutritional value of DLF. It not only increased the content of nutrients, such as CPs and small peptides, but also decreased the content of anti-nutrient factors, such as phytic acid and tannins. Our results suggest that the SSF method offers an effective approach for improving the quality of unconventional proteins sources such as DLF.

DATA AVAILABILITY STATEMENT

The raw data supporting the conclusions of this article will be made available by the authors, without undue reservation.

AUTHOR CONTRIBUTIONS

XC and JZ conceived and designed the research, wrote the manuscript, and obtained fundings. HS conducted the experiments. HS, EY, and YL collected and analyzed the data. All authors contributed to the article and approved the submitted version.

FUNDING

This work was funded by the Forestry Technology Innovation Program, Department of Forestry of Guangdong Province (2018KJCX001), the Characteristic Innovation Program (Natural Science), the Department of Education of Guangdong Province (2018KTSCX018), and the Youth Innovation Program (Natural Science), Department of Education of Guangdong Province (2019KQNCX010).

REFERENCES

Adedapo, A. A., Falayi, O. O., and Oyagbemi, A. A. (2015). Evaluation of the analgesic, antiinflammatory, antioxidant, phytochemical and toxicological properties of the methanolic leaf extract of commercially processed *Moringa oleifera* in some laboratory animals. *J. Basic Clin. Physiol. Pharmacol.* 26, 491–499.

Adetuyi, F. O., and Ibrahim, T. A. (2014). Effect of fermentation time on the phenolic, flavonoid and vitamin C contents and antioxidant activities of okra (*Abelmoschus esculentus*) seeds. *Nigerian Food J.* 32, 128–137. doi: 10.1016/s0189-7241(15)30128-4

Amaglo, N. K., Bennett, R. N., Lo Curto, R. B., Rosa, E. S., and Turco, V. L. (2010). Profiling selected phytochemicals and nutrients in different tissues of the multipurpose tree *Moringa oleifera* L., grown in Ghana. *Food Chem.* 122, 1047–1054. doi: 10.1016/j.foodchem.2010.03.073

AOAC (2005). *Official Methods of Analysis of the AOAC International*. Gaithersburg, MD: Association of Official Analytical Chemists International.

Arora, D. S., and Chandra, P. (2010). Assay of antioxidant potential of two *Aspergillus* isolates by different methods under various physio-chemical conditions. *Braz. J. Microbiol.* 41, 765–777. doi: 10.1590/s1517-83822010000300029

Bennett, P., and Yang, S. T. (2012). Beneficial effect of protracted sterilization of lentils on phytase production by *Aspergillus ficuum* in solid state fermentation. *Biotechnol. Prog.* 28, 1263–1270. doi: 10.1002/btpr.1603

Chi, C. H., and Cho, S. J. (2016). Improvement of bioactivity of soybean meal by solid-state fermentation with *Bacillus amyloliquefaciens* versus *Lactobacillus spp*. and *Saccharomyces cerevisiae*. *J. LWT - Food Sci. Technol.* 68, 619–625. doi: 10.1016/j.lwt.2015.12.002

Chodur, G. M., Olson, M. E., Wade, K. L., Stephenson, K. K., Nouman, W., Garima, et al. (2018). Wild and domesticated *Moringa oleifera* differ in taste, glucosinolate composition, and antioxidant potential, but not myrosinase activity or protein content. *Sci. Rep.* 8, 7910–7995.

Cui, Y. M., Wang, J., Lu, W., Zhang, H. J., and Wu, S. G. (2018). Effect of dietary supplementation with *Moringa oleifera* leaf on performance, meat quality, and oxidative stability of meat in broilers. *J. Poult. Sci.* 97, 2836–2844. doi: 10.3382/ps/pey122

Dey, T. B., Chakraborty, S., Jain, K. K., and Sharma, A. (2016). Antioxidant phenolics and their microbial production by submerged and solid state fermentation process: a review. *Trends Food Sci. Technol.* 53, 60–74. doi: 10.1016/j.tifs.2016.04.007

Dulf, F. V., Vodnar, D. C., Dulf, E. H., and Pintea, A. (2017). Phenolic compounds, flavonoids, lipids and antioxidant potential of apricot (*Prunus armeniaca* L.) pomace fermented by two filamentous fungal strains in solid state system. *Chem. Cent. J.* 11:92.

Dulf, F. V., Vodnar, D. C., and Socaciu, C. (2016). Effects of solid-state fermentation with two filamentous fungi on the total phenolic contents, flavonoids, antioxidant activities and lipid fractions of plum fruit (*Prunus domestica* L.) by-products. *Food Chem.* 209, 27–36. doi: 10.1016/j.foodchem.2016.04.016

Gao, Y., Shang, C., Maroof, M. A. S., Biyashev, R. M., and Buss, G. R. (2007). A modified colorimetric method for phytic acid analysis in soybean. *Crop Sci.* 47, 1797–1803. doi: 10.2135/cropsci2007.03.0122

Generalić Mekinić, I., Skroza, D., Ljubenkov, I., Šimat, V., Smole Možina, S., and Katalinić, V. (2014). In vitro antioxidant and antibacterial activity of Lamiaceae phenolic extracts: a correlation study. *Food Technol. Biotechnol.* 52, 119–127.

He, L., Lv, H., Chen, N., Wang, C., and Zhang, Q. (2020). Improving fermentation, protein preservation and antioxidant activity of *Moringa oleifera* leaves silage with gallic acid and tannin acid. *Bioresour. Technol.* 297:122390. doi: 10.1016/j.biortech.2019.122390

Hossain, A., Khatun, A., Munshi, M. K., Hussain, M. S., and Huque, R. (2017). Study on antibacterial and antioxidant activities of raw and fermented *Moringa oleifera* Lam. leaves. *J. Microbiol. Biotechnol. Res.* 6, 23–29.

Hu, Y., Liang, H., Yuan, Q., and Hong, Y. (2010). Determination of glucosinolates in 19 Chinese medicinal plants with spectrophotometry and high-pressure liquid chromatography. *Nat. Prod. Res.* 24, 1195–1205. doi: 10.1080/14786410902975681

Jin, B., Zepf, F., Bai, Z., Gao, B., and Zhu, N. (2016). A biotech-systematic approach to select fungi for bioconversion of winery biomass wastes to nutrient-rich feed. *Process Saf. Environ. Prot.* 103, 60–68. doi: 10.1016/j.psep.2016.06.034

Kholif, A. E., Gouda, G. A., Olafadehan, O. A., and Abdo, M. M. (2018). Effects of replacement of *Moringa oleifera* for berseem clover in the diets of *Nubian goats* on feed utilisation, and milk yield, composition and fatty acid profile. *Animal* 12, 964–972. doi: 10.1017/s1751731117002336

Kodera, T., Hara, H., Nishimori, Y., and Nio, N. (2006). Amino acid absorption in portal blood after duodenal infusions of a soy protein hydrolysate prepared by a novel soybean protease D3. *J. Food Sci.* 71, S517–S525.

Leone, A., Spada, A., Battezzati, A., Schiraldi, A., Aristil, J., and Bertoli, S. (2015). Cultivation, genetic, ethnopharmacology, phytochemistry and pharmacology of *Moringa oleifera* leaves: an overview. *Int. J. Mol. Sci.* 16, 12791–12835. doi: 10.3390/ijms160612791

Lin, J., and Tang, C. (2007). Determination of total phenolic and flavonoid contents in selected fruits and vegetables, as well as their stimulatory effects on mouse splenocyte proliferation. *Food Chem.* 101, 140–147. doi: 10.1016/j.foodchem.2006.01.014

Medeiros, S., Xie, J., Dyce, P. W., Cai, H. Y., Delange, K., Zhang, H., et al. (2018). Isolation of bacteria from fermented food and grass carp intestine and their efficiencies in improving nutrient value of soybean meal in solid state fermentation. *J. Anim. Sci. Biotechno.* 9:29.

Mendieta-Araica, B., Spörndly, E., Reyes-Sánchez, N., Salmerón-Miranda, F., and Halling, M. (2013). Biomass production and chemical composition of *Moringa oleifera* under different planting densities and levels of nitrogen fertilization. *Agroforestry Systems* 87, 81–92. doi: 10.1007/s10457-012-9525-5

Miller, G. L. (1959). Use of dinitrosalicylic acid reagent for determination of reducing sugar. *Anal. Chem.* 31, 426–428. doi: 10.1021/ac60147a030

Moyo, B., and Masika, P. (2011). Nutritional characterization of Moringa (*Moringa oleifera* Lam.) leaves. *Afr. J. Biotechnol.* 10, 12925–12933. doi: 10.5897/ajb10.1599

Ndubuaku, U. M., Nwankwo, V. U., and Baiyeri, K. P. (2014). Influence of poultry manure application on the leaf amino acid profile, growth and yield of moringa (*Moringa oleifera* Lam.) *plants*. *Albanian J. Agric. Sci.* 13:42.

Ogbe, A. O., and Affiku, J. P. (2011). Proximate study, mineral and anti-nutrient composition of *Moringa oleifera* leaves harvested from lafia, nigeria: potential benefits in poultry nutrition and health. *J. Microbiol. Biotechnol. Food Sci.* 1:296.

Olaofe, O., Adeyeye, E. I., and Ojugbo, S. (2013). Comparative study of proximate, amino acids and fatty acids of *Moringa oleifera* tree. *Elixir Appl. Chem.* 54, 12543–12554.

Olukomaiya, O. O., Adiamo, O. Q., Fernando, W. C., Mereddy, R., Li, X., and Sultanbawa, Y. (2020). Effect of solid-state fermentation on proximate composition, anti-nutritional factor, microbiological and functional properties of lupin flour. *Food Chem.* 315:126238. doi: 10.1016/j.foodchem.2020.126238

Ovissipour, M., Abedian, A., Motamedzadegan, A., Rasco, B., Safari, R., and Shahiri, H. (2009). The effect of enzymatic hydrolysis time and temperature on the properties of protein hydrolysates from *Persian sturgeon* (*Acipenser persicus*) viscera. *Food Chem.* 115, 238–242. doi: 10.1016/j.foodchem.2008.12.013

Phatsimo, G. M., Cukrowska, E., and Chimuka, L. (2015). Development of pressurized hot water extraction (PHWE) for essential compounds from *Moringa oleifera* extracts. *Food Chem.* 172, 423–427. doi: 10.1016/j.foodchem.2014.09.047

Popoola, J. O., and Obembe, O. O. (2013). Local knowledge, use pattern and geographical distribution of *Moringa oleifera* Lam. (*Moringaceae*) in Nigeria. *J. Ethnopharmacol.* 150, 682–691. doi: 10.1016/j.jep.2013.09.043

Sanjukat, S., Rai, A. K., Muhammed, A., Jeyaram, K., and Talukdar, N. C. (2015). Enhancement of antioxidant properties of two soybean varieties of Sikkim Himalayan region by proteolytic Bacillus subtilis fermentation. *J. Funct. Foods.* 14, 650–658. doi: 10.1016/j.jff.2015.02.033

Sarmadi, B. H., and Ismail, A. (2010). Antioxidative peptides from food proteins: a review. *Peptides* 31, 1949–1956. doi: 10.1016/j.peptides.2010.06.020

Sasipriya, G., and Siddhuraju, P. (2012). Effect of different processing methods on antioxidant activity of underutilized legumes, *Entada scandens* seed kernel and *Canavalia gladiata* seeds. *Food Chem. Toxicol.* 50, 2864–2872. doi: 10.1016/j.fct.2012.05.048

Shi, C., He, J., Yu, J., Yu, B., Mao, X., Zheng, P., et al. (2016). Physicochemical properties analysis and secretome of *Aspergillus* niger in fermented rapeseed meal. *PLoS One* 11:e0153230. doi: 10.1371/journal.pone.0153230

Shi, H. H., Su, B., Chen, X. X., and Pian, R. Q. (2020). Solid state fermentation of *Moringa oleifera* leaf meal by mixed strains for the protein enrichment and the improvement of nutritional value. *PeerJ* 8:e10358. doi: 10.7717/peerj.10358

Singh, B., and Satyanarayana, T. (2011). Microbial phytases in phosphorus acquisition and plant growth promotion. *Physiol. Mol. Biol. Plants* 17, 93–103. doi: 10.1007/s12298-011-0062-x

Stevens, C. G., Ugese, F. D., Otitoju, G. T., and Baiyeri, K. P. (2016). Proximate and anti-nutritional composition of leaves and seeds of *Moringa oleifera* in Nigeria: a comparative study. *Agro-Science* 14, 9–17. doi: 10.4314/as.v14i2.2

Teixeira, E. M. B., Carvalho, M. R. B., Neves, V. A., Silva, M. A., and Arantes-Pereira, L. (2014). Chemical characteristics and fractionation of proteins from *Moringa oleifera* Lam. leaves. *Food Chem.* 147, 51–54. doi: 10.1016/j.foodchem.2013.09.135

Tripathi, M. K., and Mishra, A. S. (2007). Glucosinolates in animal nutrition: a review. *Anim. Feed Sci. Technol.* 132, 1–27. doi: 10.1016/j.anifeedsci.2006.03.003

Tufarelli, V., Ragni, M., and Laudadio, V. (2018). Feeding forage in poultry: a promising alternative for the future of production systems. *Agriculture* 8:81. doi: 10.3390/agriculture8060081

Van Soest, P. V., Robertson, J. B., and Lewis, B. A. (1991). Methods for dietary fiber, neutral detergent fiber, and nonstarch polysaccharides in relation to animal nutrition. *J. Dairy Sci.* 74, 3583–3597. doi: 10.3168/jds.s0022-0302(91)78551-2

Vongsak, B., Sithisarn, P., Mangmool, S., Thongpraditchote, S., Wongkrajang, Y., and Gritsanapan, W. (2013). Maximizing total phenolics, total flavaonoids contents and antioxidant activity of *Moringa oleifera* leaf extract by the appropriate extraction method. *Ind. Crops Prod.* 44, 566–571. doi: 10.1016/j.indcrop.2012.09.021

Wang, C., Shi, C., Su, W., Jin, M., Xu, B., Hao, L., et al. (2020). Dynamics of the physicochemical characteristics, microbiota, and metabolic functions of soybean meal and corn mixed substrates during two-stage solid-state fermentation. *mSystems* 5, e501–e519.

Wang, J., Cao, F., Su, E., Zhao, L., and Qin, W. (2018a). Improvement of animal feed additives of ginkgo leaves through solid-state fermentation using *Aspergillus niger*. *Int. J. Biol. Sci.* 14:736. doi: 10.7150/ijbs.24523

Wang, J., Cao, F., Zhu, Z., and Zhang, X. (2018b). Improvement of quality and digestibility of *Moringa oleifera* leaves feed via solid-state fermentation by *Aspergillus niger*. *Int. J. Chem. React. Eng.* 16:20180094.

Xie, P. J., Huang, L. X., Zhang, C. H., and Zhang, Y. L. (2016). Nutrient assessment of olive leaf residues processed by solid-state fermentation as an innovative feedstuff additive. *J. Appl. Microbiol.* 121, 28–40. doi: 10.1111/jam.13131

Yusuf, A. O., Mlambo, V., and Iposu, S. O. (2018). A nutritional and economic evaluation of *Moringa oleifera* leaf meal as a dietary supplement in West African dwarf goats. *S. Afr. J. Anim. Sci.* 48, 81–87. doi: 10.4314/sajas.v48i1.10

Zeng, B., Sun, J. J., Chen, T., Sun, B. L., He, Q., Chen, X. Y., et al. (2018). Effects of *Moringa oleifera* silage on milk yield, nutrient digestibility and serum biochemical indexes of lactating dairy cows. *J. Anim. Physiol. Anim. Nutr.* 102, 75–81. doi: 10.1111/jpn.12660

Zhang, M., Huang, Y., Zhao, H., Wang, T., Xie, C., and Zhang, D. (2017). Solid-state fermentation of *Moringa oleifera* leaf meal using *Bacillus pumilus* CICC 10440. *J. Chem. Technol. Biotechnol.* 92, 2083–2089.

Zuo, S. S., Niu, D. Z., Ning, T. T., Zheng, M. L., and Jiang, D. (2017). Protein enrichment of sweet potato beverage residues mixed with peanut shells by *Aspergillus oryzae* and *Bacillus subtilis* using central composite design. *Waste Biomass Valorization* 9, 835–844. doi: 10.1007/s12649-017-9844-x

Zuo, Y., and Chen, H. (2002). Simultaneous determination of catechins, caffeine and gallic acids in green, Oolong, black and pu-erh teas using HPLC with a photodiode array detector. *Talanta* 57, 307–316. doi: 10.1016/s0039-9140(02)00030-9

Conflict of Interest: The authors declare that the research was conducted in the absence of any commercial or financial relationships that could be construed as a potential conflict of interest.

frontiers in Bioengineering and Biotechnology

ORIGINAL RESEARCH
published: 13 May 2021
doi: 10.3389/fbioe.2021.659895

Development of *Clostridium saccharoperbutylacetonicum* as a Whole Cell Biocatalyst for Production of Chirally Pure (*R*)-1,3-Butanediol

*Alexander Grosse-Honebrink[1], Gareth T. Little[1], Zak Bean[2], Dana Heldt[2], Ruth H. M. Cornock[1], Klaus Winzer[1], Nigel P. Minton[1], Edward Green[2] and Ying Zhang[1]**

[1] Clostridia Research Group, BBSRC/EPSRC Synthetic Biology Research Centre (SBRC), Biodiscovery Institute, School of Life Sciences, University of Nottingham, Nottingham, United Kingdom, [2] CHAIN Biotechnology Ltd., MediCity, Nottingham, United Kingdom

OPEN ACCESS

Edited by:
Petra Patakova,
University of Chemistry and Technology in Prague, Czechia

Reviewed by:
Yi Wang,
Auburn University, United States
Adam William Westbrook,
Genecis Bioindustries Inc., Canada

***Correspondence:**
Ying Zhang
Ying.Zhang@nottingham.ac.uk

Specialty section:
This article was submitted to Synthetic Biology, a section of the journal Frontiers in Bioengineering and Biotechnology

Received: 28 January 2021
Accepted: 12 April 2021
Published: 13 May 2021

Citation:
Grosse-Honebrink A, Little GT, Bean Z, Heldt D, Cornock RHM, Winzer K, Minton NP, Green E and Zhang Y (2021) Development of Clostridium saccharoperbutylacetonicum as a Whole Cell Biocatalyst for Production of Chirally Pure (R)-1,3-Butanediol. Front. Bioeng. Biotechnol. 9:659895. doi: 10.3389/fbioe.2021.659895

Chirally pure (*R*)-1,3-butanediol ((*R*)-1,3-BDO) is a valuable intermediate for the production of fragrances, pheromones, insecticides and antibiotics. Biotechnological production results in superior enantiomeric excess over chemical production and is therefore the preferred production route. In this study (*R*)-1,3-BDO was produced in the industrially important whole cell biocatalyst *Clostridium saccharoperbutylacetonicum* through expression of the enantio-specific *phaB* gene from *Cupriavidus necator*. The heterologous pathway was optimised in three ways: at the transcriptional level choosing strongly expressed promoters and comparing plasmid borne with chromosomal gene expression, at the translational level by optimising the codon usage of the gene to fit the inherent codon adaptation index of *C. saccharoperbutylacetonicum*, and at the enzyme level by introducing point mutations which led to increased enzymatic activity. The resulting whole cell catalyst produced up to 20 mM (1.8 g/l) (*R*)-1,3-BDO in non-optimised batch fermentation which is a promising starting position for economical production of this chiral chemical.

Keywords: *Clostridium saccharoperbutylacetonicum*, biotechnology, *phaB*, Allele Coupled Exchange, (*R*)-1,3-butanediol, *Clostridium*

INTRODUCTION

Chirally active compounds are much sought after by the chemical and pharmaceutical industry. The *R*-form of 1,3-butanediol (1,3-BDO), for example, is used for fragrances, pheromones, insecticides and as starting material for the production of azetidinone derivatives. The latter are intermediates of penem and carbapenem antibiotic synthesis (Nakatsuka et al., 1991; Matsuyama et al., 2001), a major area of development. Old β-lactam antibiotics lose their efficacy against bacteria due to emergent resistances which makes new discoveries crucial (Llarrull et al., 2010; Qin et al., 2014). This makes the cost-effective production of precursor molecules an important field of study.

Chemical production of (*R*)-1,3-BDO from threonine via asymmetric hydrogenation of 4-hydroxy-2-butanone (4H2B) has been studied, but satisfactory enantiomeric purity was not

achieved (Larchevêque et al., 1991; Boaz et al., 2006). Enzymatic production of (*R*)-1,3-BDO has the potential to be cheaper than chemical production from petroleum-based substrates and its stereo-specificity is superior with up to 100% of the product yield having the desired conformation. Different whole cell catalysis approaches have been adopted with mixed results. Reduction through yeast fermentation of 4H2B led to low product yields when the desired stereo-specificity was reached (Matsuyama et al., 2001). However, later research showed promising results when reducing 4H2B using either newly isolated yeast strains, with up to 100% enantiomeric excess and a titre of 38.2 g/l (Zheng et al., 2012; Yang et al., 2014), or genetically engineered *E. coli,* where a 99% enantiomeric excess and 99% substrate yield were obtained (Itoh et al., 2007). Another approach using genetically modified *E. coli* based on the enantio-selective oxidation of (*S*)-1,3-BDO was initially promising (Matsuyama et al., 2001) but proved difficult to scale-up (Yamamoto et al., 2002).

As all of the above studies were reliant on relatively expensive substrates, the use of cheaper alternatives would benefit process economics. Two notable alternative routes to (*R*)-1,3-BDO have been explored. Nemr et al. (2018) assembled an elaborate metabolic pathway in *E. coli* that mediated the condensation of two pyruvate-derived molecules of acetaldehyde to form (*R*)-3-hydroxybutyrate ((*R*)-3-HB) and further to (*R*)-1,3-BDO. (*R*)-1,3-BDO yield equivalent to 13% of the theoretical maximum from glucose was achieved. In another approach, Kataoka et al. (2013) designed a synthetic pathway in *E. coli* encoding the acetyl-CoA acetyltransferase (*phaA*) and the acetoacetyl-CoA reductase (*phaB*) derived from *Cupriavidus necator,* combined with the *Clostridium saccharoperbutylacetonicum*-derived butyraldehyde dehydrogenase (*bld*) to produce 100.4 mM (9.05 g/l) (*R*)-1,3-BDO with 98.5% enantiomeric excess in batch fermentation. Fed-batch operation subsequently increased the product titre to 174.8 mM (15.8 g/l) (Kataoka et al., 2014).

C. saccharoperbutylacetonicum DSM 14923 (Hongo et al., 1968) is a widely used industrial acetone-butanol-ethanol- (ABE-) fermenting organism which is renowned for its particularly high *n*-butanol yields (Shaheen et al., 2000; Herman et al., 2017) and industrially favourable low sporulation capability (Keis et al., 2001). It has been found to grow on a wide range of industrially relevant first- and second-generation feedstocks, such as glucose, cellobiose, xylose, arabinose, mannose, galactose, pentose, starch and molasses (Shaheen et al., 2000; Yoshida et al., 2012; Yao et al., 2017). These characteristics make *C. saccharoperbutylacetonicum* an optimal whole cell biocatalyst for industrial applications. Since *C. saccharoperbutylacetonicum* possesses the necessary alcohol dehydrogenases and an inherently strong acetyl-CoA acetyltransferase (*thl*), introduction of the enantioselective PhaB from *C. necator* should be sufficient to produce (*R*)-1,3-BDO in this organism, obviating the need for multiple engineering steps. Green et al. (2017) expressed a *phaB* gene codon optimised for generic *Clostridium* spp. in *C. saccharoperbutylacetonicum* and observed 0.25 mM of (*R*)-1,3-BDO (plasmid expression) and 6 mM (*R*)-1,3-BDO (chromosomal integration) with no production of (*S*)-1,3-BDO. This study improves on earlier work engineering *C. saccharoperbutylacetonicum* for production of chirally pure (*R*)-1,3-BDO, through optimisation of PhaB-mediated catalysis at transcriptional, translational, enzyme and population levels.

MATERIALS AND METHODS

Bacterial Strains, Growth, and Maintenance Conditions

E. coli HB101 (NEB, United Kingdom) was used as a host strain for plasmid propagation. *E. coli* was grown at 30°C or 37°C in Luria-Bertani (LB) broth or on LB-agar with 500 μg/ml erythromycin or 100 μg/ml spectinomycin. Unless stated otherwise, all chemicals were purchased from Sigma Aldrich, United Kingdom. The parent wild type strain *C. saccharoperbutylacetonicum* N1-4 (HMT) DSM14923 (Hongo et al., 1968) was purchased from the German collection of microorganisms and cell cultures GMBH (DSMZ). All *C. saccharoperbutylacetonicum* strains were grown in an anaerobic cabinet (Don Whitley, Yorkshire, United Kingdom) or tent (Coy Lab Products, United States) with artificial atmosphere (80:10:10 volume% nitrogen: carbon dioxide: hydrogen) at 37°C on solid RCM agar or on solid CBM (O'Brien and Morris, 1971). Standard liquid cultures were grown unshaken in TYA (Tashiro et al., 2004) with, per litre in g: yeast extract, 2; tryptone, 6; ammonium acetate, 3; $MgSO_4.7H_2O$, 0.3; KH_2PO_4, 0.5; $FeSO_4.7H_2O$, 0.01. Growth and solvent production assays of *C. saccharoperbutylacetonicum* were performed in CGM, 2xYTG, CBM, P2 and Biebl medium, with the following compositions per litre in g: CGM was prepared as described by Hartmanis and Gatenbeck with some modification (Hartmanis and Gatenbeck, 1984) yeast extract, 5; KH_2PO_4, 0.75; K_2HPO_4, 0.75; $MgSO_4.7H_2O$, 0.4; $MnSO_4.H_2O$, 0.01; $FeSO_4.7H_2O$, 0.01; NaCl, 1; asparagine, 2; $(NH_4)_2SO_4$, 2; glucose, 50; $CaCO_3$, 20. 2xYTG contained: yeast ectract, 10; tryptone, 16; NaCl, 5. CBM similar to O'Brien and Morris (1971), $MgSO_4.7H_2O$, 0.2; $MnSO_4.H_2O$, 0.00758; $FeSO_4.7H_2O$, 0.01; *p*-aminobenzoic acid, 0.001; biotin, 2×10^{-6}; thiamine HCl, 0.001; casein hydrolysate, 4; K_2HPO_4, 0.5; KH_2PO_4, 0.5 (O'Brien and Morris, 1971). P2 similar to Baer et al. (1987), K_2HPO_4, 0.5; KH_2PO_4, 0.5; ammonium acetate, 2.2; $MgSO_4.7H_2O$, 2; $MnSO_4.H_2O$, 0.1; NaCl, 0.1; $FeSO_4.7H_2O$, 0.1; *p*-aminobenzoic acid, 0.1; thiamine, 0.1; biotine, 0.01 (Baer et al., 1987). Biebl media composition similar to Biebl, 2001: KH_2PO_4, 0.5; K_2HPO_4, 0.5; $(NH_4)_2SO_4$, 5; $MgSO_4.7H_2O$, 0.2; $CaCl_2.2H_2O$, 0.02; $FeSO_4.7H_2O$, 0.00914; biotin, 25×10^{-6}; 2 ml trace element solution made up of, per litre in mg: $MnCl_2.4H_2O$, 100; $ZnCl_2$, 70; H_3BO_3, 60; $NaMoO_4.2H_2O$, 40; $CoCl_2.6H_2O$, 28.7; $CuCl_2.2H_2O$, 20; $NiCl_2.6H_2O$, 20; 1 ml 25% HCl (Biebl, 2001). All media were prepared with 50 g/l glucose and 20 g/l $CaCO_3$ and adjusted to pH 6.2. For antibiotic selection in *C. saccharoperbutylacetonicum,* cultures were supplemented with 50 μg/ml erythromycin or 250 μg/ml spectinomycin.

Growth curves were done by growing *C. saccharoperbutylacetonicum* strains until mid-exponential phase for inoculation of triplicate 35 ml CGM broths to an OD_{600} of 0.05 in 250 ml serum bottles. The bottles were capped

with rubber-butyl stoppers inside a cabinet and transferred outside the cabinet for crimping and static incubation at 37°C. Glucose, acids and solvents including (*R*)-3-HB and (*R*)-1,3-BDO were quantified with HPLC as previously described (Schwarz et al., 2017). Data was analysed with Graphpad PRISM 8.1 (Graphpad Software Inc., United States). The chirality of 3-HB and 1,3-BDO is determined using LC/MS analysis following DATAN (Diacetyl-L-Tartaric Anhydride) derivatisation (Struys et al., 2004).

Clostridium saccharoperbutylacetonicum Electroporation

Electro-competent *Clostridium* cells were prepared based on the method described by Little et al. (2018). Culture in exponential phase was used to inoculate 300 ml TYA to OD_{600} 0.05 and grown to mid-exponential phase (OD_{600} 0.4–0.6). Cells were centrifuged at 7,500 rpm for 10 min and washed twice with ice-cold, reduced EPB buffer (270 mM Sucrose, 5 mM Na_2HPO_4, 5 mM NaH_2PO_4, pH 7.4), resuspended in 9 ml ice-cold EPB buffer containing 10% dimethyl sulphoxide and aliquots frozen at −80°C. For electroporation 580 µl of competent cells and typically 6 µg plasmid were added to a 4 mm electroporation cuvette inside an anaerobic cabinet. The mixture was kept on ice for 5 min before being electroporated with pulse settings of 2 kV, 25 µF and ∞ Ω. Cells were immediately mixed with 10 ml warm TYA to recover for 6 h. Finally, cells were plated out on appropriate medium with appropriate antibiotics for selection.

Plasmid Stability Assay

Plasmid segregational stability was determined as described previously (Heap et al., 2009). Briefly, *C. saccharoperbutylacetonicum* transformants were cultured for 12 h in TYA medium supplemented with the antibiotic erythromycin to select for the plasmid. The culture was washed twice in PBS to remove the antibiotic and then used to inoculate fresh, unsupplemented TYA medium at 1% (vol/vol). This marked the start (i.e., 0 h) of the stability experiment. The unsupplemented culture was then diluted 1% (vol/vol) into fresh medium every 12 h. At 12, 24, 36, 48, 60, 72, 84, and 96 h the culture was plated on both selective and non-selective agar to enumerate erythromycin-resistant colony-forming units and total colony-forming units.

Plasmid Cloning

All restriction enzymes used were fast digest enzymes (ThermoFisher Scientific, United Kingdom), the ligase used throughout this work was the Rapid DNA Ligation Kit (ThermoFisher Scientific, United Kingdom). Plasmids were transformed into chemically competent *E. coli* HB101 according to supplier's instructions (New England Biolabs, United Kingdom). Plasmids are listed in **Supplementary Table 1** and primers and synthetic DNA fragments are listed in **Supplementary Table 2**.

Plasmid pMTL83353::*phaB* and Derivatives

Plasmid pMTL83353::*phaB* (p_*phaB*) was cloned by digesting pMTL83251-p*fdx*_PhaB (Green et al., 2017) (featuring the *phaB* gene from *C. necator* N-1 codon optimised for *Clostridium spp.*) and pMTL83353 (Heap et al., 2009) with *Nde*I and *Nhe*I, ligating the fragment containing *phaB* into the pMTL83353 backbone. The point-mutated p_*phaB* derivatives were produced using the Quikchange site-directed mutagenesis kit according to supplier's instruction (Agilent, United Kingdom) using primers Q47L_F and Q47L_R to produce pMTL83353::*phaB*_Q47L (p_*phaB*_L) and primers T173S_F and T173_R to produce pMTL83353::*phaB*_T173S (p_*phaB*_S). To produce the plasmid pMTL83353::*phaB*_Q47L_T173S (p_*phaB*_LS) carrying the *phaB* double-mutant, plasmid p_*phaB*_L was point-mutated using the Quikchange site directed mutagenesis kit as above with primers T173S_F and T173S_R.

The *C. necator phaB* gene was codon optimised to match the *C. saccharoperbutylacetonicum* codon adaptation index using the codon usage table calculated by Nakamura et al. at https://www.kazusa.or.jp/codon/(accessed 3/9/2019) (Nakamura et al., 2000). The codon optimised *phaB* fragment (*phaB*-opt) and the point mutated derivatives *phaB*-opt_Q47L, *phaB*-opt_T173S and *phaB*-opt_Q47L_T173S were ordered as synthetic DNA fragments (Twist Bioscience, United States) flanked by *Not*I and *Nde*I restriction sites upstream of the gene and *Hin*dIII and *Nhe*I downstream of the gene. The fragments were cloned into pMTL83353 (Heap et al., 2009) by digesting the plasmid and the fragments with *Nde*I and *Nhe*I and ligating each fragment separately into the digested backbone to obtain plasmids pMTL83353::*phaB*-opt_Q47L (p_*phaB*-opt_L), pMTL83353::*phaB*-opt_T173S (p_*phaB*-opt_S) and pMTL83353::*phaB*-opt_Q47L_T173S (p_*phaB*-opt_LS).

ACE Plasmids

The Allele Coupled Exchange (ACE) (Heap et al., 2012) *pyrE* truncation plasmid pMTL-AGH21 (p_AGH21) was cloned by amplifying the following with Phusion High-Fidelity DNA Polymerase (New England Biolabs, United Kingdom): (i) a 300 bp fragment of the DSM14923 *pyrE* gene with primers pE_upstream_F and SOE_pE_trunc_up_R; (ii) the 282 bp multiple cloning site (MCS) from pMTL-ME6C (Heap et al., 2012)with primers SOE_pE_trunc_up_F and SOE_pE_trunc_dwn_R; (iii) the 1,200 bp downstream region of the DSM14923 *pyrE* locus with primers SOE_pE_trunc_dwn_F and pE_downstream_R. All three fragments were spliced together by splicing by overlap extension PCR (SOE-PCR) with primers pE_upstream_F and pE_downstream_R for ligation into pMTL85241 (Heap et al., 2009) at *Sbf*I and *Asc*I sites.

The cargo delivery ACE plasmid pMTL-AGH23 (p_AGH23) was cloned by amplifying the following: (i) a 626 bp fragment of *pyrE* with primers pE_upstream_F and SOE_pE_KI_up_R; (ii) a 323 bp fragment of the MCS from pMTL-ME6C (Heap et al., 2012) with primers SOE_pE_KI_up_F and SOE_pE_KI_dwn_R; (iii) a 1,200 bp fragment downstream of the DSM14923 *pyrE* locus with primers SOE_pE_KI_dwn_F and pE_downstream_R.

The three fragments were used in a SOE-PCR as above with primers pE_upstream_F and pE_downstream_R, for ligation into pMTL85241.

Plasmid pMTL-AGH23::cspo_*fdx-phaB* was cloned by digesting p_*phaB* and p_AGH23 with enzymes *Not*I and *Nhe*I and ligating the resulting *phaB* fragment into the p_AGH23 backbone. The same process led to production of pMTL-AGH23::cspo_*fdx-phaB*-opt using plasmids p_AGH23 and p_*phaB*-opt and pMTL-AGH23::cspo_*fdx-phaB*-opt_Q47L_T173S using p_AGH23 and p_*phaB*-opt_LS. Plasmids pMTL-AGH23::cac_*ptb-phaB*-opt and pMTL-AGH23::cac_*ptb-phaB*-opt_Q47L_T173S were produced by exchanging the promoter P_{cspo_fdx} with promoter P_{cac_ptb} from plasmid pMTL8225::cac_*ptb_gusA* (p_*ptb-gusA*) through digestion of pMTL-AGH23::cspo_*fdx-phaB* or pMTL-AGH23::cac_*ptb-phaB*-opt and p_*ptb-gusA* with *Not*I and *Nde*I cloning the P_{cac_ptb} promoter into the 5,215 bp backbone.

gusA Reporter Plasmids

Reporter plasmids to measure promoter strength were cloned fusing promoters from a promoter library (Willson, 2014) with a *gusA* (β-glucuronidase) gene. The latter was based on plasmid pMTL-JL1 (pMTL8514::fdx-*gusA*) which consisted of the *Streptococcus agalactiae gusA* gene (Wallace et al., 2015) under control of the *C. acetobutylicum* ferredoxin gene promoter in the modular shuttle vector pMTL85141. Plasmids pMTL8225::cac_araE-*gusA* (p_araE-*gusA*), pMTL8225::cac_adhE-*gusA* (p_adhE-*gusA*), pMTL8225::cac_*ptb-gusA* (p_*ptb-gusA*) and pMTL8225::pj23119-*gusA* (p_pj-*gusA*) were constructed by digesting both pMTL8514::fdx-*gusA* and pMTL82251 (Heap et al., 2009) with *Not*I and *Nhe*I and ligating the fdx-*gusA* fragment into the pMTL82251 backbone. Plasmids pMTL8225::cbe_*fdx-gusA* (p_cbe_*fdx-gusA*), pMTL8225::cte_*fdx-gusA* (p_cte_*fdx-gusA*), pMTL8225::sac_*fdx-gusA* (p_sac_*fdx-gusA*), pMTL8225::clk_*fdx-gusA* (p_clk_*fdx-gusA*), pMTL8225::cpf_*fdx-gusA* (p_cpf_*fdx-gusA*), pMTL8225::cbe_*thl-gusA* (p_cbe_*thl-gusA*), pMTL8225::ccv_*thl-gusA* (p_ccv_*thl-gusA*) and pMTL8225::cby_*thl-gusA* (p_cby_thl-*gusA*) were cloned by digesting the corresponding pMTL82254 based plasmids (Willson, 2014; **Supplementary Table 1**) and p_*ptb-gusA* with enzymes *Not*I and *Nde*I and cloning the [promoter] fragment excised from pMTL82254::[promoter] into the backbone of p_*ptb-gusA*. The same process led to production of pMTL8225::cspo_*fdx-gusA* (p_cspo_*fdx-gusA*) by digestion of pMTL83353 (Heap et al., 2009) and p_*ptb-gusA* with *Not*I and *Nde*I and ligating the cspo_*fdx* fragment into the backbone.

Allelic Exchange Mutant Generation

*C. saccharoperbutylacetonicum*Δ*pyrE* truncation and gene insertions downstream of *pyrE* were made as described by Heap et al. (2012). *C. saccharoperbutylacetonicum* DSM14923 was transformed with plasmid p_AGH21 followed by selection on RCM plates containing erythromycin. Faster growing colonies (potential single crossover integrants) were restreaked three times on CBM agar supplemented with 400 μg/ml 5-fluoroorotic acid and 20 μg/ml uracil and tested by colony PCR and subsequent Sanger sequencing (Eurofins Genomics, United Kingdom) for *pyrE* truncation and absence of plasmid. Colony PCR was performed as previously described for *Clostridium pasteurianum* (Pyne et al., 2013) with primers pE_genome_F and pE_genome_R. PCR products were sequenced with primer ACE_insert_seq_F. Plasmid loss was confirmed by colony PCR with primers 85XXX-RF and 8X2XX-RR.

Cargo integrated strains *C. saccharoperbutylacetonicum* Ω Cspo_*fdx-phaB* (Ω*fdx-phaB*), ΩCspo_*fdx-phaB*-opt (Ω*fdx-phaB*-opt), ΩCac_*ptb-phaB*-opt (Ω*ptb-phaB*-opt), ΩCspo_*fdx-phaB*-opt_Q47L_T173S (Ω*fdx-phaB*-opt_LS) and ΩCac_*ptb-phaB*-opt_Q47L_T173S (Ω*ptb-phaB*-opt_LS) were produced by transforming the corresponding pMTL-AGH23 cargo plasmid into *C. saccharoperbutylacetonicum*Δ*pyrE* followed by direct selection for double-crossover integration on CBM plates without uracil. Integration was tested by PCR with primers pE_genome_F and pE_genome_R leading to a 2,836 bp fragment for Ω*fdx-phaB*, a 2,892 bp fragment for both P_{cspo_fdx} promoter based gene insertions and a 2,895 bp fragment for both P_{cac_ptb} promoter-based insertions if integration was successful, compared to 2,213 bp in *C. saccharoperbutylacetonicum*Δ*pyrE*. PCR products were sequenced with primers ACE_insert_seq_F and ACE_insert_seq_R. Plasmid loss was confirmed by PCR with primers 85XXX-RF and 8X2XX-RR.

GusA Reporter Assay

Promoter strength in *C. saccharoperbutylacetonicum* was tested by measuring GusA activity when *gusA* was expressed from different promoters according to protocols by Miller (1972). Cell pellets from 1 ml cultures were defrosted and resuspended in up to 500 μl of Z-buffer (60 mM Na_2HPO_4, 45 mM NaH_2PO_4, 10 mM KCl, 1 mM $MgSO_2.7H_2O$, 50 mM β-mercaptoethanol, pH 8.5) to normalise OD_{600} across all samples. A 75 μl volume of the sample was transferred to a Corning 96 Well Black Polystyrene Microplate with clear bottom (Merck, United Kingdom) and OD_{600} measured in a Clariostar Plus plate reader (BMG Labtech, United Kingdom). Reaction was started by addition of 25 μl of 40 μg/ml 4-methylumbelliferyl-β-D-glucuronide dissolved in Z-buffer to each sample. Fluorescence was measured for 30 min at 450 nm after excitation at 360 nm at a distance of 7 mm and with a gain of 750. The resulting data was analysed in Excel (Microsoft Corporation, United States) by measuring slope of the regression line in the linear phase and the data was further analysed in GraphPad PRISM 8.1 (GraphPad Software Inc., United States).

RESULTS

Based on previous studies in *E. coli* (Kataoka et al., 2013), a pathway to chirally pure (*R*)-1,3-BDO in *C. saccharoperbutylacetonicum* was formulated based on the conversion of acetoacetyl-CoA to (*R*)-3-hydroxybutyryl-CoA using the *C. necator* enzyme acetoacetyl-CoA reductase encoded by *phaB*. In *E. coli* the condensation of two acetyl-CoA to one acetoacetyl-CoA was reliant on the over-expression of the *C. necator phaA* gene (coding for 3-ketothiolase). This was not necessary in *C. saccharoperbutylacetonicum* since the

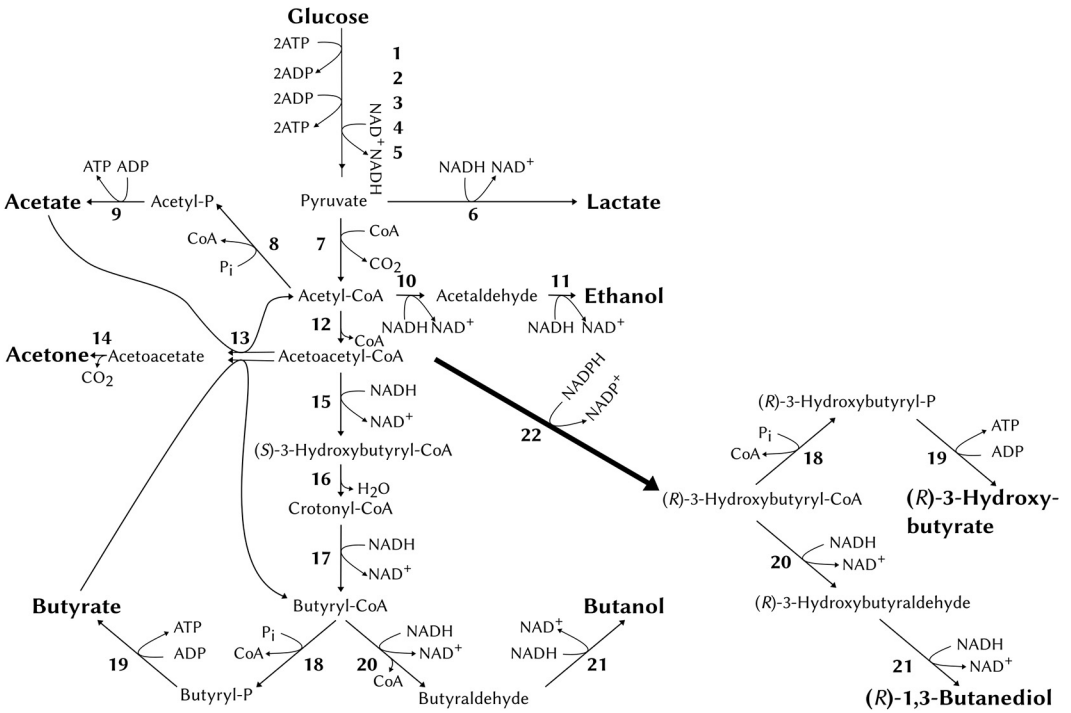

FIGURE 1 | The natural acid- and solvent- producing pathways of *C. saccharoperbutylacetonicum* and the heterologous pathway from acetoacetyl-CoA via PhaB (acetoacetyl-CoA reductase, 22). Numbers correspond to enzymes as follows: 1, hexokinase; 2, phosphoglucose isomerase; 3, phosphofructokinase; 4, glyceraldehyde-3-phosphate dehydrogenase; 5, pyruvate kinase; 6, lactate dehydrogenase; 7, pyruvate-ferredoxin oxidoreductase; 8, phosphate acetyltransferase; 9, acetate kinase; 10, acetaldehyde dehydrogenase; 11, ethanol dehydrogenase; 12, thiolase; 13, acetoacetyl-CoA:acetate:CoA transferase/acetoacetyl-CoA:butyrate:CoA transferase; 14, acetoacetate decarboxylase; 15, β-hydroxybutyryl-CoA dehydrogenase; 16, crotonase; 17, butyryl-CoA dehydrogenase; 18, phosphotransbutyrylase; 19, butyrate kinase; 20, butyraldehyde dehydrogenase; 21, butanol dehydrogenase; 22, acetoacetyl-CoA reductase (*phaB*, from *Cupriavidus necator*).

endogenous thiolase gene (*thlA*) is highly expressed (Wiesenborn et al., 1988). Furthermore, the endogenous enzymes alcohol- and aldehyde-alcohol dehydrogenases (*bdh* and *adh*) should catalyse the reactions from (*R*)-3-hydroxybutyryl-CoA via (*R*)-3-hydroxybutyraldehyde to (*R*)-1,3-BDO analogous to reduction of butyryl-CoA to butanol (**Figure 1**). The side product (*R*)-3-HB was expected to be produced predominantly through conversion of (*R*)-3-hydroxybutyryl-CoA via the endogenous phosphotransbutyrylase (*ptb*) to (*R*)-3-hydroxybutyryl-P and further via butyrate kinase (*buk*) to (*R*)-3-HB in analogy to the natural conversion of butyryl-CoA to butyrate. Additionally, some (*R*)-3-HB maybe produced by unspecific hydrolysis of the CoA thioester bond by endogenous thioesterases analogous to *E. coli* (Guevara-Martínez et al., 2019).

Growth and Solvent Production

Various growth media were tested for solvent production from *C. saccharoperbutylacetonicum* DSM 14923 with the expectation that media supporting high solvent production would also promote (*R*)-1,3-BDO production (**Supplementary Figure 1**). The strain produced the highest yield of solvents per glucose (g solvents/g glucose) when grown in complex media (CGM and TYA) with 0.28 ± 0.02 g/g and 0.28 ± 0.00 g/g, respectively. In minimal Biebl medium the strain still produced 0.24 ± 0.00 g/g solvents. The highest solvent to acid ratio was found when growing on minimal media P2 or Biebl with 4.4 g/g (g solvents/g acids) and 4.3 g/g, respectively, while the ratio was 3.2 g/g for CGM and 3.5 g/g for TYA. However, since PhaB uses the four-carbon intermediate acetoacetyl-CoA to produce (*R*)-3-hydroxybutyryl-CoA, the 4-carbon to 2-carbon product ratio is more important for the production of (*R*)-1,3-BDO. This ratio was 5.1 g/g (g 4-carbon products/g 2-carbon products) for CGM, 3.5 g/g for TYA, 3.9 g/g for P2 and 5.0 g/g for Biebl medium. Thus, as it was expected that the highest yields of (*R*)-1,3-BDO yield in *C. saccharoperbutylacetonicum* strain would be obtained when grown in CGM, this medium was used throughout the rest of this work.

Plasmid Stability Assays

Four Gram-positive replicons (Heap et al., 2009) were tested for segregational stability in *C. saccharoperbutylacetonicum* by following the ratio of antibiotic resistant (plasmid containing) cells to total cell counts in non-selective media over time. The two most stable replicons were pBP1 and pCB102 over 8 generations which corresponded to approximately 96 h (**Figure 2**). Due to its reduced length of 1,625 bp compared to 2,403 bp of pBP1, the second most stable replicon pCB102 was chosen for plasmid-based expression of the heterologous *phaB* gene, as

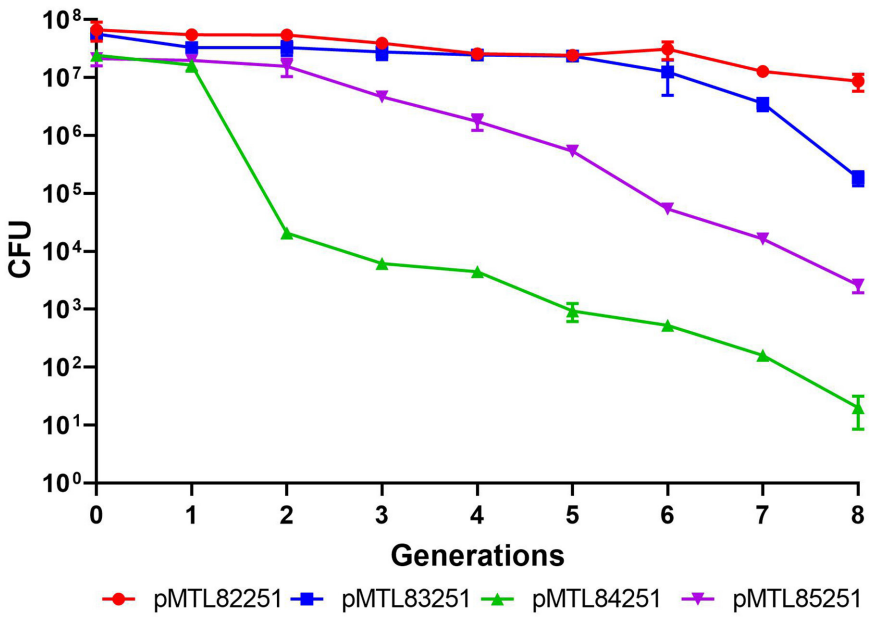

FIGURE 2 | Plasmid stability assay testing four Gram-positive replicons in *C. saccharoperbutylacetonicum*. Plasmid pMTL82251 with pBP1 replicon in red circles, pMTL83251 with pCB102 replicon in blue squares, pMTL84251 with pCD6 replicon in green upward pointing triangles and pMTL85251 with pIM13 replicon in downward pointing triangles.

increasing plasmid size has been shown to negatively correlate with transformation efficiency (Hanahan, 1983).

Plasmid Borne Expression of *phaB* With Increased Catalytic Activity

Production of (*R*)-1,3-BDO was measured in *C. saccharoperbutylacetonicum* cells containing the plasmid p_*phaB* expressing the *C. necator phaB* (coding for acetoacetyl-CoA reductase) gene under the control of the promoter of the *Clostridium sporogenes fdx* gene (P_{cspo_fdx}) (**Figure 3**, also **Supplementary Figure 2**). A control strain carrying the empty vector pMTL83353 was included for comparative purposes. Expression of *phaB* slowed growth of the strain considerably and the highest cell density was reached only after 48 h as compared to 24 h in the control. Strain p_*phaB* produced 6.3 ± 0.1 mM of (*R*)-1,3-BDO after 48 h while the control did not produce the compound, establishing that the pathway was functioning as intended. The by-product (*R*)-3-HB was produced at up to 5.1 ± 0.1 mM and is assumed to be reassimilated in the solventogenic phase via acetoacetate-CoA transferase (*ctfAB*) as it is the case for butyrate and acetate. The chemical chirality of 1,3-BDO and 3-HB were confirmed to be enantio-specific R form in previous study (Green et al., 2017). No S form of either compounds was found in the fermentation broth.

Point mutations Q47L and T173S in PhaB have previously been shown to increase activity and poly-3-HB accumulation in *Corynebacterium glutamicum* (Matsumoto et al., 2013) and in tobacco (Yokoo et al., 2015). Both point mutations were introduced separately into PhaB (plasmids p_*phaB*_L and p_*phaB*_S) and a double mutant (plasmid p_*phaB*_LS) was produced. *C. saccharoperbutylacetonicum* cells carrying plasmids p_*phaB*_L, p_*phaB*_S and p_*phaB*_LS produced 10.2 ± 0.2, 7.8 ± 0.1 and 10.3 ± 0.1 mM (*R*)-1,3-BDO, respectively (**Figure 3**).

Codon Optimisation of Plasmid Expressed Enzyme

The second option chosen to increase product titres after the point mutations, was to translationally optimise the heterologous *C. necator* gene through the alteration of its codon frequency to match that of *C. saccharoperbutylacetonicum*. Codon usage frequencies were determined using the database compiled by Nakamura and coworkers (Nakamura et al., 2000). Synonymous substitutions were made selecting codons with the highest frequency of usage in *C. saccharoperbutylacetonicum*. The resulting gene (*phaB*-opt), single point mutations (*phaB*-opt_L & *phaB*-opt_S) and the double point mutated gene (*phaB*-opt_LS) were ordered as synthetic constructs. Fermentation performance of the strains carrying codon optimised genes was tested against a plasmid control (**Figure 4** and **Supplementary Figure 3**). Plasmids p_*phaB*-opt (6.3 ± 0.7 mM) and p_*phaB*-opt_S (8.8 ± 0.4 mM) produced slightly higher (*R*)-1,3-BDO concentrations while p_*phaB*-opt_L (8 ± 0.2 mM) and p_*phaB*-opt_LS (9.2 ± 0.3 mM) produced slightly less compared to the p_phaB based constructs.

GusA Promoter Strength Assays

Although several native *Clostridium* and synthetic promoters have been used for enzyme expression in *C. saccharoperbutylacetonicum* (Nakayama et al., 2008;

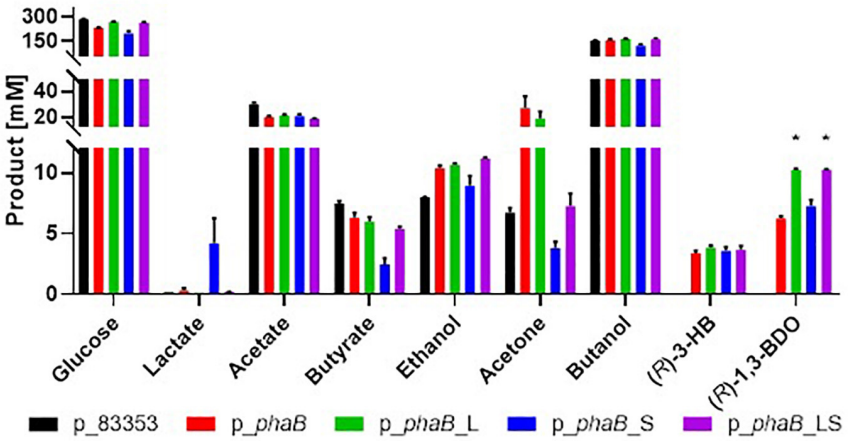

FIGURE 3 | Comparison of product spectrum of *Cupriavidus necator* wild type *phaB* and the derivatives with point mutations and negative control without *phaB* (p_83353) expressed in *C. saccharoperbutylacetonicum* after 48 h. From **left** to **right** for each product p_83353 in black, p_*phaB* in red, p_*phaB*_L in green, p_*phaB*_S in blue, p_*phaB*_LS in purple. For glucose the consumed amount is shown for all other the produced amount. Error-bars represent SEM and * represents statistical significance against p_*phaB* (*t*-test, $p < 0.05$), $n = 3$.

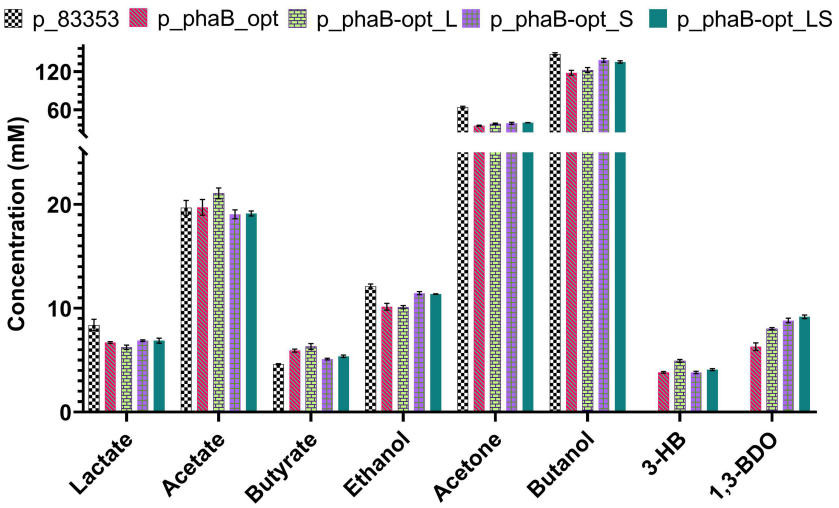

FIGURE 4 | Comparison of product spectrum *C. saccharoperbutylacetonicum* cells carrying the empty plasmid control p_83353 and codon optimised *phaB* and its derivatives with point mutations after 48 h. From left to right for each product p_83353 in chequerboard, p_*phaB*_opt in red diagonal lines, p_*phaB*-opt_L in green bricks, p_*phaB*-opt_S in purple squares and p_phaB-opt_LS in green dots. Error-bars represent SEM.

Zhang et al., 2018) no systematic analysis of promoter strength has been published in this organism so far. A *gusA* (β-glucuronidase) reporter gene was employed to assess the relative strength of various clostridial promoters, including a library derived from the *fdx* and *thl* genes of several different clostridial species (Willson, 2014) as well as a synthetic promoter (iGEM part BBa_J23119). The *gusA* gene derived from *Streptococcus agalactiae* DSM 2134 was chosen because of its compatible GC content and codon usage as well as favourable kinetic properties of the encoded enzyme (Wallace et al., 2015), which were similar to those of *E. coli* GusA previously employed in *C. acetobutylicum* (Girbal et al., 2003). Relative promoter strength at 24 h post-inoculation was measured and the resulting *gusA* activities cluster into weak, mid-strength and strong promoters (**Figure 5**). Although the *C. sporogenes fdx* promoter (P_{cspo_fdx}) is known to be a strong promoter for expression of heterologous genes in *Clostridium* owing to its central position in the ABE-fermentation pathway (Minton et al., 2016), it was ineffective in *C. saccharoperbutylacetonicum*. The strongest promoter identified was that of the *C. acetobutylicum ptb* gene (P_{cac_ptb}) which was nearly 5400-fold stronger than P_{cspo_fdx}. Since the phosphotransbutyrylase (*ptb*) in *Clostridium* is only strongly expressed during exponential (acidogenic) phase in *C. acetobutylicum* (Girbal et al., 2003) and *Clostridium beijerinckii* (Ravagnani et al., 2000), GusA activity with expression from P_{cac_ptb} and P_{cspo_fdx}promoters in *C. saccharoperbutylacetonicum*

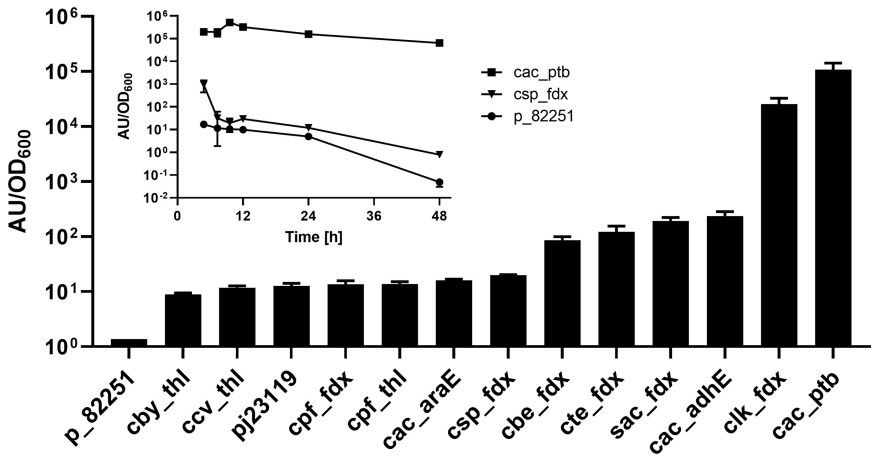

FIGURE 5 | Promoter assay based on GusA production measured by accumulation of fluorescent product. A library of promoters derived from *fdx* and *thl* genes as well as a library of *C. acetobutylicum* promoters were tested for expression strength in *C. saccharoperbutylacetonicum*. Expression profiles over time of the strongest promoter P_{cac_ptb} and the standard promoter P_{cspo_fdx} were further assayed (inset graph). Error-bars represent SEM with $n = 6$ for all samples in the bar chart except p_82251 and P_{cspo_fdx} ($n = 3$) and $n = 3$ for all samples in the inset diagram.

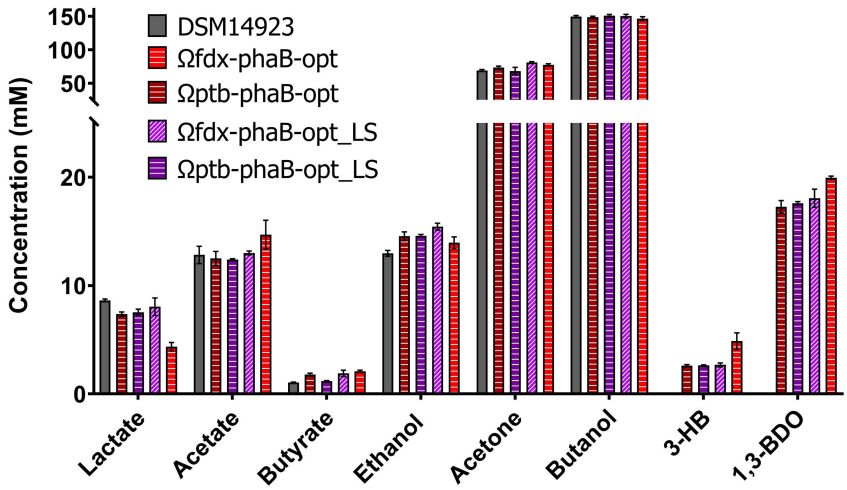

FIGURE 6 | Comparison of product spectrum of the codon optimised *phaB* version and its derivatives encoding PhaB point mutations expressed in *C. saccharoperbutylacetonicum* by either weak promoter P_{cspo_fdx} or strong promoter P_{cac_ptb} from the chromosomal *pyrE* locus after 48 h. From left to right for each product DSM14923 in black, Ω*fdx-phaB*-opt in red horizontal lines, Ω*ptb-phaB*-opt in burgundy horizontal lines, Ω*fdx-phaB*-opt_LS in light purple diagonal lines and Ω*ptb-phaB*-opt_LS in purple horizontal lines. Error-bars represent SEM ($n = 3$).

was measured over 48 h (**Figure 5**). The activity of P_{cac_ptb} was high over the whole time-course, whilst *gusA* expression from the P_{cspo_fdx} promoter was only marginally higher than that of the empty vector control pMTL82251.

phaB Chromosomally Integrated at the *pyrE* Locus

The *C. necator phaB* gene was integrated into the *C. saccharoperbutylacetonicum* chromosome downstream of the *pyrE* gene using the ACE method (Heap et al., 2012). Selection for reversion to uracil prototrophy by restoration of the *pyrE* gene was used as a marker for successful cargo integration. A 3-fold higher (*R*)-1,3-BDO concentration of 19 ± 0.7 mM was produced after 48 h when *phaB* was expressed from the chromosome (Ωcspo_*fdx-phaB*) (**Figure 6**), than when expressed on a plasmid (p_*phaB*). A two-fold increase in product titre was obtained compared to the best performing plasmid-based codon optimised mutant (p_*phaB*-opt_LS).

Production of (*R*)-1,3-BDO by chromosomal expression of codon optimised *phaB* (*phaB-opt*) and the codon optimised double mutant (*phaB*-opt_LS) were measured from the differing strength P_{cac_ptb} and P_{cspo_fdx} promoters. All the codon optimised genes produced increased (*R*)-1,3-BDO concentrations compared to the p_phaB sequence. The weak P_{cspo_fdx} promoter (Ω*fdx-phaB*-opt: 20 ± 0.1 mM;

Ω*fdx-phaB*-opt_LS: 18 ± 1.6 mM) performed marginally better than the strong P_{cac_ptb} promoter (Ω*ptb-phaB*-opt 17.3 ± 1.1 mM; Ω*ptb-phaB*-opt_LS 17.6 ± 0.3 mM) (**Figure 6**).

DISCUSSION

Different growth conditions were tested for maximal solvent production in *C. saccharoperbutylacetonicum* and a stable plasmid selected for expression of heterologous *phaB*. Having shown that expression of *phaB* leads to (*R*)-1,3-BDO production in *C. saccharoperbutylacetonicum*, options to increase the production titre were analysed. Three possibilities on different levels of protein expression were considered. Firstly, at an enzyme level, the catalytic activity of PhaB can be increased through point mutations in sites which were identified previously (Matsumoto et al., 2013). Secondly, translational efficiency can be increased by codon optimisation of the gene to match it to the natural codon adaptation of *C. saccharoperbutylacetonicum* (Quax et al., 2015). And lastly, increasing mRNA levels through boosting of transcription efficiency can be achieved through the use of strong promoters (Deuschle et al., 1986).

Point Mutations in *phaB* Result in a Small Increase of *(R)*-1,3-BDO Production

Matsumoto et al. (2013) engineered and tested a library of approximately 20,000 *phaB* mutants generated by error prone PCR of which two variant genes were isolated that encoded an enzyme that exhibited increased k_{cat} values compared to the wild type enzyme. In one mutant a glutamine at position 47 was changed to leucine (Q47L) and in the other mutant a threonine at position 173 was changed to serine (T173S). Both mutated enzymes showed increased activity and poly-3-hydroxybutyrate accumulation when heterologously expressed in *Corynebacterium glutamicum* (Matsumoto et al., 2013) and in tobacco (Yokoo et al., 2015). It was hypothesised that introduction of these point mutations in *phaB* and expression in *C. saccharoperbutylacetonicum* should analogously lead to higher metabolic flux toward (*R*)-1,3-BDO. Both point mutations were introduced separately and a double mutant carrying both amino acid changes was created. Both single mutants exhibited the desired effect of increased (*R*)-1,3-BDO, however, the double mutant did not show an accumulative titre increase (**Figure 3**).

PhaB Q47L mutant (p_*phaB*_L) produced the highest amount of (*R*)-1,3-BDO, 1.6-fold higher than the PhaB wild type, while the T173S mutant (p_*phaB*_S) only showed a 1.2-fold increase of product titre. The double mutant produced the same amount as p_*phaB*_L which suggested either product inhibition at this level or the fact that the mutations cannot function in conjunction. Product inhibition can be ruled out by a growth assay in increasing *meso*-1,3-BDO concentrations which found *C. saccharoperbutylacetonicum* to grow uninhibited up to 300 mM of *meso*-1,3-BDO (**Supplementary Figure 4**). On the other hand, the fact that the effects of the two mutations would not accumulate could be explained based on data collected by Matsumoto et al. (2013). They found that PhaB T173S increases $k_{cat}/K_{m(Acetoacetate-CoA)}$ and decreases $k_{cat}/K_{m(NADPH)}$ while PhaB Q47L enhances $k_{cat}/K_{m(NADPH)}$ and decreases $k_{cat}/K_{m(Acetoacetate-CoA)}$. Therefore, the positive effects on catalytic enzyme activity of each mutation could cancel the effect of the other.

It was interesting to note that both p_*phaB* and p_*phaB*_S had a detrimental effect on *C. saccharoperbutylacetonicum* growth, evident by a slower growth rate and longer fermentation time (**Supplementary Figure 2**). Both strains also used less glucose than the control. This effect was reversed in p_*phaB*_L and p_*phaB*_LS. Suggesting that the Q47L mutation offsets the deleterious effect of *phaB* expression while increasing product formation. The deleterious effects of *phaB* on *C. saccharoperbutylacetonicum* growth were not observed in any of the codon optimised versions of the gene analysed (**Supplementary Figures 3**, **6**). Since the only difference between the native *phaB* and *phaB*_L are two nucleotides (138-CAG and 130-CTG, respectively) and the same two nucleotides were altered to 138-CAA in *phaB*-opt (**Supplementary Figure 5**) it can be assumed that the deleterious effect stems from translational complications in this region. Correddu et al. (2019) found that co-occurrence of certain amino acid codons in *E. coli* led to a premature stop in the protein chain potentially through a frameshift. Similar effects could be at play here. The codon adaptation frequency pattern found in the vicinity of the mutation, however, does not suggest codon rarity to be a factor (**Supplementary Figure 5**), since the point mutated version uses an uncommon (in *C. saccharoperbutylacetonicum*) CTG codon for lysine (Nakamura et al., 2000). Thus, the ultimate cause of the observed deleterious effect cannot be ascertained.

Codon Optimisation of *phaB* Has Minimal Impact on Product Concentration

Although codon optimisation was expected to lead to higher product yield, this was not found to be the case here (**Figure 4**). This was not entirely unexpected as codon optimisation based on the codon adaption index of an organism is relatively random with no significant correlation between the use of frequent codons and protein expression (Kudla et al., 2009). Future work should include codon harmonisation, where the relative native codon frequency per codon location found in *C. necator* is synchronised in the heterologous host organism. This approach takes into consideration mRNA regions presenting codons with low relative frequency (or codon adaptation index, CAI) which are hypothesised to slow down translation and allowing correct folding of the protein (Quax et al., 2015). Furthermore, it was shown that the 5' mRNA leading sequence has a big influence on protein expression and surprisingly it was found that these sequences are preferably made up of rare codons, allowing appropriate ribosome distribution on the coding mRNA (Kudla et al., 2009; Quax et al., 2015).

Chromosomal Integration Significantly Increases *(R)*-1,3-BDO Formation

Concomitant with testing the influence of codon optimisation on product titres the consequence of locating the heterologous

phaB to the host chromosome as opposed to an autonomous plasmid was evaluated. Stable chromosomal integration is key to biotechnological exploitation of this technology by abolishing the need for antibiotics in fermentation and overcoming the inherent instability of replicative plasmids (Friehs, 2004; Heap et al., 2012). Expression was expected to be lower when the gene was expressed from the chromosome since there are more copies of the plasmid present than of the chromosome. This higher copy number would hypothetically translate into more mRNA and subsequently more protein, which in turn should be reflected in increased product titres. However, 3-fold higher (*R*)-1,3-BDO production was found in the mutant expressing *phaB* from the chromosome (Ωcspo_*fdx-phaB*) compared with it being expressed from a plasmid (p_*phaB*) and double the product titres compared to the best performing plasmid-based codon optimised mutant (p_*phaB*-opt_LS) were found (**Figure 7**). This effect was also previously reported by our team member (Green et al., 2017).

This finding suggests that overexpression of *phaB* has a negative impact on the final product titres. This may be due to pathway overloading, protein aggregation or polymerisation, liquid phase separation or general resource exhaustion of the cell (Bolognesi and Lehner, 2018). If any of these overexpression related issues play a role, then further overexpression would be pointless. To test this hypothesis *phaB* and the double mutant (*phaB*_LS) and codon optimised versions were expressed from the chromosome under the strong P_{cac_ptb} promoter and tested against expression from the weak P_{cspo_fdx} promoter (Ω*fdx-phaB*-opt). Product titres for (*R*)-1,3-BDO were lower when *phaB*-opt was strongly overexpressed with P_{cac_ptb} (Ω*ptb-phaB*-opt) or when the potentially more active double mutant was used (Ω*fdx-phaB*-opt_LS and Ω*ptb-phaB*-opt_LS). However, one-way ANOVA revealed that the reduction was not significant [$F(3,7) = 0.71$, $p = 0.57$].

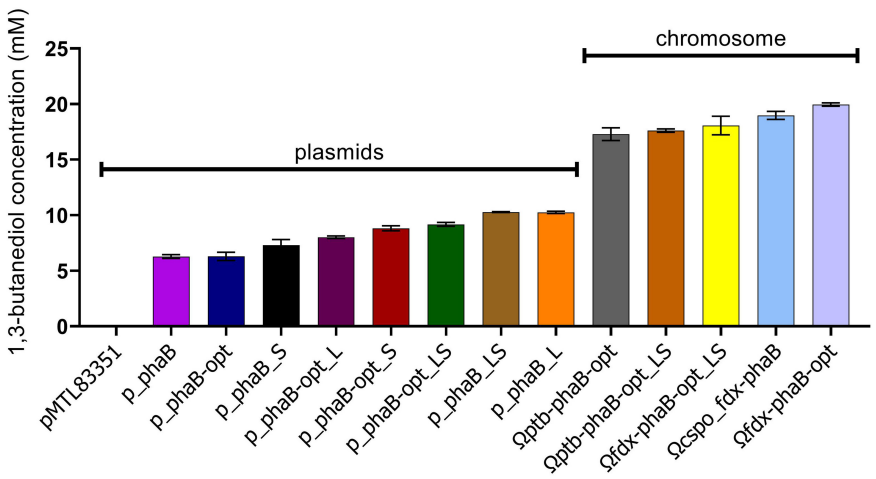

FIGURE 7 | 1,3-butanediol production from all the different constructs tested in this study. Error-bars represent SEM ($n = 3$).

TABLE 1 | Summary of literature to date presenting microbial production of (*R*)-1,3-BDO from different substrates.

Highest titre of (*R*)-1,3-BDO [g/l]	Organism	Substrate	Notes	References
49.5	*E. coli* JM109	4-Hydroxy-2-butanone with 2-propanol as co-substrate	Plasmid borne overexpression of *Leifsonia* alcohol dehydrogenase	Itoh et al., 2007
38.7	*Candida krusei* ZJB-09162	4-Hydroxy-2-butanone with glucose co-substrate	Optimised preparative scale bioconversion process	Zheng et al., 2012
38.3	*Pichia jadinii* HBY61	4-Hydroxy-2-butanone with glucose co-substrate	Optimised preparative scale bioconversion process	Yang et al., 2014
15.6	*E. coli* MG1655 *lacI*q	Glucose	Strain from Kataoka et al. (2013)_ in optimised fed batch fermentation	Kataoka et al., 2014
9.05	*E. coli* MG1655 *lacI*q	Glucose	Plasmid borne overexpression of *phaA* and *phaB* from *Ralstonia eutropha NBRC 102504 and bld*from *C. saccharoperbutylacetonicum* ATCC 27012 in optimised batch fermentation	Kataoka et al., 2013
2.4	*E. coli* BL21	Glucose	Plasmid borne expression of pyruvate decarboxylase (*Zymomonas mobilis*) and the deoxyribose-5-phosphate aldolase (*Bacillus halodurans*) in two stage pH controlled bioreactor fermentation	Nemr et al., 2018
1.1	*E. coli* LMSE51C	Glucose	Aerobic pH controlled fed-batch fermentation of strain from Nemr et al. (2018) with BH1352 harbouring mutations F160Y/M173I	Kim et al., 2020

These findings suggest that the earlier hypothesis was correct and more active or higher expressed *phaB* does not lead to increased product titres. Since not only overexpression but also increasing enzyme activity by introduction of point mutations led to decreased product titre (Ω*fdx-phaB*-opt compared to Ω*fdx-phaB*-opt_LS), protein burden on the cell (Eguchi et al., 2018), protein underwrapping (Birchler and Veitia, 2012) or protein aggregation (Rosano and Ceccarelli, 2014) as a cause can potentially be excluded. Instead, evidence points toward reactant or product inhibition of the reaction. It is not clear through what mechanism this inhibition arises. However, the unfamiliar *R* stereo form of the substrates (*R*)-3-hydroxybutyryl-CoA and (*R*)-3-hydroxybutyraldehyde may not be reduced efficiently by native enzymes butyraldehyde dehydrogenase and butanol dehydrogenase, leading to intracellular build up that may cause feedback inhibition. Moreover, similar effects have been reported before and were attributed to metabolic imbalances caused by highly overexpressed genes and high enzyme activity of heterologously expressed genes (Atsumi et al., 2008; Kataoka et al., 2013).

Final Remarks

It was shown that (*R*)-1,3-BDO can be produced up to 20 mM (1.8 g/l) in a non-optimised batch fermentation with *C. saccharoperbutylacetonicum*. This is the first time (*R*)-1,3-BDO production from glucose has been shown outside of *E. coli* in an anaerobic non-optimised batch fermentation. Titres reached are similar to studies using plasmid borne expression of pyruvate decarboxylase from *Zymomonas mobilis* and deoxyribose-5-phosphate aldolase from *Bacillus halodurans* (Nemr et al., 2018; Kim et al., 2020) but lower than in studies using plasmid borne expression of PhaA and PhaB from *R. eutropha* coupled with expression of Bld from *C. saccharoperbutylacetonicum* (Kataoka et al., 2013, 2014) summarised in **Table 1**. Higher titres can be reached using 4-hydroxy-2-butanone as substrate (Itoh et al., 2007; Zheng et al., 2012; Yang et al., 2014), however glucose is more widely available and more ecenomical than 4-hydroxy-2-butanone. Finally, future work should aim at optimising the fermentation and at upscaling of the production which is easier with an anaerobic organism such as the one used in this work.

Here, three non-exclusive approaches to increase production of (*R*)-1,3-BDO were tested and combined. Firstly, point mutations were applied to increase enzyme activity. Secondly, the gene was codon optimised to fit the *C. saccharoperbutylacetonicum* codon adaptation index. Lastly, the point-mutated and codon-optimised versions of *phaB* were expressed from the chromosome with differing strength promoters. However, it has been shown that increasing transcription and protein activity did not lead to increased product titres. On the contrary these alterations led to decreased product formation by unknown mechanisms. Future work should aim at investigating these imbalances, debottlenecking the downstream pathway (e.g., by overexpression of endogenous genes of the pathway) and optimising the fermentation to increase product titres further.

DATA AVAILABILITY STATEMENT

The original contributions presented in the study are included in the article/**Supplementary Material**, further inquiries can be directed to the corresponding author.

AUTHOR CONTRIBUTIONS

AG-H carried out the laboratory work, data analysis, and drafted the manuscript. ZB and DH provided materials and participated in the laboratory work. EG and NM helped design the study and edited the manuscript. GL and RC coordinated the final part of the study and drafted the manuscript. The manuscript was written through contributions of all authors. YZ conceived the study, oversaw its design and coordination, helped with the data analysis, and revised the manuscript. All authors read and approved the final manuscript.

FUNDING

This work was supported by the Biotechnology and Biological Sciences Research Council (BBSRC; Grant numbers BB/L013940/1, BB/N022718/1, and BB/S011951/1) and the Engineering and Physical Sciences Research Council (EPSRC; Grant number BB/L013940/1). YZ acknowledges the financial support of BBSRC NIBB LBNet: Lignocellulosic Biorefinery Network.

ACKNOWLEDGMENTS

The authors thank Ben Willson and Katalin Kovacs for the provision of their *Clostridium* promoter libraries and Jessica Locker for plasmid pMTL-JL1. Matthew Abbott and James Fothergill for their help with the analytics.

SUPPLEMENTARY MATERIAL

The Supplementary Material for this article can be found online at: https://www.frontiersin.org/articles/10.3389/fbioe.2021.659895/full#supplementary-material

REFERENCES

Atsumi, S., Cann, A. F., Connor, M. R., Shen, C. R., Smith, K. M., Brynildsen, M. P., et al. (2008). Metabolic Engineering of *Escherichia coli* for 1-Butanol Production. *Metab. Eng.* 10, 305–311. doi: 10.1016/j.ymben.2007.08.003

Baer, S. H., Blaschek, H. P., and Smith, T. L. (1987). Effect of Butanol Challenge and Temperature on Lipid Composition and Membrane Fluidity of Butanol-Tolerant *Clostridium acetobutylicum*. *Appl. Environ. Microbiol.* 53, 2854–2861.

Biebl, H. (2001). Fermentation of Glycerol by *Clostridium pasteurianum* - Batch and Continuous Culture Studies. *J. Indust. Microbiol. Biotechnol.* 27, 18–26.

Birchler, J. A., and Veitia, R. A. (2012). Gene Balance Hypothesis: connecting Issues of Dosage Sensitivity across Biological Disciplines. *Proc. Nat. Acad. Sci. U. S. A.* 109, 14746–14753. doi: 10.1073/pnas.1207726109

Boaz, N. W., Ponasik, J. A., and Large, S. E. (2006). Ruthenium Complexes of Phosphine-Aminophosphine Ligands. *Tetrahedr. Lett.* 47, 4033–4035. doi: 10.1016/j.tetlet.2006.04.009

Bolognesi, B., and Lehner, B. (2018). Protein Overexpression: reaching the Limit. *ELife* 7:e39804. doi: 10.7554/eLife.39804

Correddu, D., López, J.d.J.M, Angermayr, S. A., Middleditch, M. J., Payne, L. S., and Leung, I. K. H. (2019). Effect of Consecutive Rare Codons on the Recombinant Production of Human Proteins in *Escherichia coli*. *IUBMB Life* 72, 266–274. doi: 10.1002/iub.2162

Deuschle, U., Kammerer, W., Gentz, R., and Bujard, H. (1986). Promoters of *Escherichia coli*: a Hierarchy of in Vivo Strength Indicates Alternate Structures. *EMBO J.* 5, 2987–2994. doi: 10.1002/j.1460-2075.1986.tb04596.x

Friehs, K. (2004). "Plasmid Copy Number and Plasmid Stability," in *New Trends and Developments in Biochemical Engineering. Advances in Biochemical Engineering*, ed. T. Scheper (United States Springer), doi: 10.1007/b12440

Girbal, L., Mortier-Barrière, I., Raynaud, F., Rouanet, C., Croux, C., and Soucaille, P. (2003). Development of a Sensitive Gene Expression Reporter System and an Inducible Promoter-Repressor System for *Clostridium acetobutylicum*. *Appl. Environ. Microbiol* 69, 4985–4988. doi: 10.1128/aem.69.8.4985-4988.2003

Green, E., Heldt, D., and Bradley, B. (2017). Method and microbes for the production of chiral compounds. *U. S. Patent Appl.* 505:18.

Guevara-Martínez, M., Perez-Zabaleta, M., Gustavsson, M., Quillaguamán, J., Larsson, G., and van Maris, A. J. A. (2019). The role of the acyl-CoA thioesterase "YciA" in the production of (R)-3-hydroxybutyrate by recombinant *Escherichia coli*. *Appl. Microbiol. Biotechnol.* 103, 3693–3704.

Hanahan, D. (1983). Studies on Transformation of *Escherichia coli* with Plasmids. *J. Mole. Biol.* 166, 557–580. doi: 10.1016/S0022-2836(83)80284-8

Hartmanis, M. G., and Gatenbeck, S. (1984). Intermediary Metabolism in *Clostridium acetobutylicum*: levels of Enzymes Involved in the Formation of Acetate and Butyrate. *Appl. Environmental Microbiol.* 47, 1277–1283.

Heap, J. T., Ehsaan, M., Cooksley, C. M., Ng, Y. K., Cartman, S. T., Winzer, K., et al. (2012). Integration of DNA into Bacterial Chromosomes from Plasmids without a Counter-Selection Marker. *Nucl. Acids Res.* 40:e59. doi: 10.1093/nar/gkr1321

Heap, J. T., Pennington, O. J., Cartman, S. T., and Minton, N. P. (2009). A Modular System for *Clostridium* Shuttle Plasmids. *J. Microbiol. Methods* 78, 79–85. doi: 10.1016/j.mimet.2009.05.004

Herman, N. A., Li, J., Bedi, R., Turchi, B., Liu, X., Miller, M. J., et al. (2017). Development of a High-Efficiency Transformation Method and Implementation of Rational Metabolic Engineering for the Industrial Butanol Hyperproducer *Clostridium saccharoperbutylacetonicum* Strain N1-4. *Appl. Environ. Microbiol.* 83, e2942–e2916. doi: 10.1128/AEM.02942-16

Hongo, M., Murata, A., Kono, K., and Kato, F. (1968). Lysogeny and Bacteriocinogeny in Strains of *Clostridium* Species. *Agric. Biol. Chem.* 32, 27–33. doi: 10.1080/00021369.1968.10859021

Itoh, N., Nakamura, M., Inoue, K., and Makino, Y. (2007). Continuous Production of Chiral 1,3-Butanediol Using Immobilized Biocatalysts in a Packed Bed Reactor: promising Biocatalysis Method with an Asymmetric Hydrogen-Transfer Bioreduction. *Appl. Microbiol. Biotechnol.* 75, 1249–1256. doi: 10.1007/s00253-007-0957-1

Kataoka, N., Vangnai, A. S., Tajima, T., Nakashimada, Y., and Kato, J. (2013). Improvement of (R)-1,3-Butanediol Production by Engineered *Escherichia coli*. *J. Biosci. Bioeng.* 115, 475–480. doi: 10.1016/j.jbiosc.2012.11.025

Kataoka, N., Vangnai, A. S., Ueda, H., Tajima, T., Nakashimada, Y., and Kato, J. (2014). Enhancement of (R)-1,3-Butanediol Production by Engineered *Escherichia coli* Using a Bioreactor System with Strict Regulation of Overall Oxygen Transfer Coefficient and PH. *Biosci. Biotechnol., Biochem.* 78, 695–700. doi: 10.1080/09168451.2014.891933

Keis, S., Shaheen, R., and Jones, D. T. (2001). Emended Descriptions of *Clostridium acetobutylicum* and *Clostridium beijerinckii*, and Descriptions of *Clostridium saccharoperbutylacetonicum* Sp Nov and *Clostridium saccharobutylicum* Sp Nov. *Int. J. Syst. Evol. Microbiol.* 51, 2095–2103. doi: 10.1099/00207713-51-6-2095

Kim, T., Stogios, P. J., Khusnutdinova, A. N., Nemr, K., Skarina, T., Flick, R., et al. (2020). Rational engineering of 2-deoxyribose-5-phosphate aldolases for the biosynthesis of (*R*)-1, 3-butanediol. *J. Biol. Chem.* 295, 597–609. doi: 10.1074/jbc.ra119.011363

Kudla, G., Murray, A. W., Tollervey, D., and Plotkin, J. B. (2009). Coding-Sequence Determinants of Gene Expression in *Escherichia coli*. *Science* 324, 255–258. doi: 10.1126/science.1170160

Larchevêque, M., Mambu, L., and Petit, Y. (1991). Preparation of Enantiomerically Pure 1,3-Butanediol from Threonine. *Syn. Commun.* 21, 2295–2300. doi: 10.1080/00397919108021588

Little, G. T., Willson, B. J., Heap, J. T., Winzer, K., and Minton, N. P. (2018). The Butanol Producing Microbe *Clostridium beijerinckii* NCIMB 14988 Manipulated Using Forward and Reverse Genetic Tools. *Biotechnol. J.* 13:1700711. doi: 10.1002/biot.201700711

Llarrull, L. I., Testero, S. A., Fisher, J. F., and Mobashery, S. (2010). The Future of the β-Lactams. *Curr. Opinion Microbiol.* 13, 551–557. doi: 10.1016/j.mib.2010.09.008

Matsumoto, K., Tanaka, Y., Watanabe, T., Motohashi, R., Ikeda, K., Tobitani, K., et al. (2013). Directed Evolution and Structural Analysis of Nadph-Dependent Acetoacetyl Coenzyme A (Acetoacetyl-CoA) Reductase from *Ralstonia eutropha* Reveals Two Mutations Responsible for Enhanced Kinetics. *Appl. Environ. Microbiol.* 79, 6134–6139. doi: 10.1128/AEM.01768-13

Matsuyama, A., Yamamoto, H., Kawada, N., and Kobayashi, Y. (2001). Industrial Production of (R)-1,3-Butanediol by New Biocatalysts. *J. Mol. Catal. B Enzym.* 11, 513–521. doi: 10.1016/S1381-1177(00)00032-1

Miller, J. H. (1972). Experiments in Molecular Genetics. *Q. Rev. Biol.* 42:2.

Minton, N. P., Ehsaan, M., Humphreys, C. M., Little, G. T., Baker, J., Henstra, A. M., et al. (2016). A Roadmap for Gene System Development in Clostridium. *Anaerobe* 41, 104–112. doi: 10.1016/j.anaerobe.2016.05.011

Nakamura, Y., Gojobori, T., and Ikemura, T. (2000). Codon Usage Tabulated from International DNA Sequence Databases: status for the Year 2000. *Nucl. Acids Res* 28, 292–292. doi: 10.1093/nar/28.1.292

Nakatsuka, T., Iwata, H., Tanaka, R., Imajo, S., and Ishiguro, M. (1991). A Facile Conversion of the Phenylthio Group to Acetoxy by Copper Reagents for a Practical Synthesis of 4-Acetoxyazetidin-2-One Derivatives from (R)-Butane-1,3-Diol. *J. Chem. Soc. Chem. Commun.* 9, 662–664. doi: 10.1039/C39910000662

Nakayama, S., Kosaka, T., Hirakawa, H., Matsuura, K., Yoshino, S., and Furukawa, K. (2008). Metabolic Engineering for Solvent Productivity by Downregulation of the Hydrogenase Gene Cluster HupCBA in *Clostridium saccharoperbutylacetonicum* Strain N1-4. *Appl. Microbiol. Biotechnol.* 78, 483–493. doi: 10.1007/s00253-007-1323-z

Nemr, K., Müller, J. E. N., Joo, J. C., Gawand, P., Choudhary, R., Mendonca, B., et al. (2018). Engineering a Short, Aldolase-Based Pathway for (R)-1,3-Butanediol Production in *Escherichia coli*. *Metab. Eng.* 48, 13–24. doi: 10.1016/j.ymben.2018.04.013

O'Brien, R. W., and Morris, J. G. (1971). Oxygen and Growth and Metabolism of *Clostridium acetobutylicum*. *J. Gen. Microbiol.* 68:3.

Pyne, M. E., Moo-Young, M., Chung, D. A., and Chou, C. P. (2013). Development of an Electrotransformation Protocol for Genetic Manipulation of *Clostridium pasteurianum*. *Biotechnol. Biofuels* 6:50. doi: 10.1186/1754-6834-6-50

Qin, W., Panunzio, M., and Biondi, S. (2014). β-Lactam Antibiotics Renaissance. *Antibiotics* 3, 193–215. doi: 10.3390/antibiotics3020193

Quax, T. E. F., Claassens, N. J., Söll, D., and van der Oost, J. (2015). Codon Bias as a Means to Fine-Tune Gene Expression. *Mole. Cell* 59, 149–161. doi: 10.1016/j.molcel.2015.05.035

Ravagnani, A., Jennert, K. C. B., Steiner, E., Grunberg, R., Jefferies, J. R., Wilkinson, S. R., et al. (2000). Spo0A Directly Controls the Switch from Acid to Solvent Production in Solvent-Forming Clostridia. *Mole. Microbiol.* 37, 1172–1185. doi: 10.1046/j.1365-2958.2000.02071.x

Rosano, G. L., and Ceccarelli, E. A. (2014). Recombinant Protein Expression in *Escherichia coli*: advances and Challenges. *Front. Microbiol.* 5:172. doi: 10.3389/fmicb.2014.00172

Schwarz, K. M., Grosse-Honebrink, A., Derecka, K., Rotta, C., Zhang, Y., and Minton, N. P. (2017). Towards Improved Butanol Production through Targeted Genetic Modification of *Clostridium pasteurianum*. *Metabol. Eng* 40, 124–137. doi: 10.1016/j.ymben.2017.01.009

Shaheen, R., Shirley, M., and Jones, D. T. (2000). Comparative Fermentation Studies of Industrial Strains Belonging to Four Species of Solvent-Producing Clostridia. *Journal of Mole. Microbiol. Biotechnol.* 2, 115–124.

Struys, E. A., Jansen, E. E. W., Verhoeven, N. M., and Jakobs, C. (2004). "Measurement of urinary D- and L-2-hydroxyglutarate enantiomers by stable-isotope-dilution liquid chromatography-tandem mass spectrometry after derivatization with diacetyl-L-tartaric anhydride. *Clin. Chem*. 50, 1391–1395.

Tashiro, Y., Takeda, K., Kobayashi, G., Sonomoto, K., Ishizaki, A., and Yoshino, S. (2004). High Butanol Production by *Clostridium saccharoperbutylacetonicum* N1-4 in Fed-Batch Culture with PH-Stat Continuous Butyric Acid and Glucose Feeding Method. *J. Biosci. Bioeng.* 98, 263–268. doi: 10.1016/S1389-1723(04)00279-8

Wallace, B. D., Roberts, A. B., Pollet, R. M., Ingle, J. D., Biernat, K. A., Pellock, S. J., et al. (2015). Structure and Inhibition of Microbiome β-Glucuronidases Essential to the Alleviation of Cancer Drug Toxicity. *Chem. Biol.* 22, 1238–1249. doi: 10.1016/j.chembiol.2015.08.005

Wiesenborn, D. P., Rudolph, F. B., and Papoutsakis, E. T. (1988). Thiolase from *Clostridium acetobutylicum* ATCC 824 and Its Role in the Synthesis of Acids and Solvents. *Appl. Environ. Microbiol.* 54, 2717–2722.

Willson, B. J. (2014). *). Genetic Modification of Clostridium acetobutylicum for Deconstruction of Lignocellulose*. United Kingdom: University of Nottingham. [PhD thesis].

Yamamoto, H., Matsuyama, A., and Kobayashi, Y. (2002). Synthesis of (R)-1,3-Butanediol by Enantioselective Oxidation Using Whole Recombinant *Escherichia coli* Cells Expressing (S)-Specific Secondary Alcohol Dehydrogenase. *Bioscience, Biotechnol. Biochem.* 66, 925–927. doi: 10.1271/bbb.66.925

Yang, T., Man, Z., Rao, Z., Xu, M., Zhang, X., and Xu, Z. (2014). Asymmetric Reduction of 4-Hydroxy-2-Butanone to (R)-1,3-Butanediol with Absolute Stereochemical Selectivity by a Newly Isolated Strain of *Pichia jadinii*. *J. Indust. Microbiol. Biotechnol.* 41, 1743–1752. doi: 10.1007/s10295-014-1521-5

Yao, D., Dong, S., Wang, P., Chen, T., Wang, J., Yue, Z., et al. (2017). Robustness of *Clostridium saccharoperbutylacetonicum* for Acetone-Butanol-Ethanol Production: effects of Lignocellulosic Sugars and Inhibitors. *Fuel* 208, 549–557. doi: 10.1016/J.FUEL.2017.07.004

Yokoo, T., Matsumoto, K., Ooba, T., Morimoto, K., and Taguchi, S. (2015). Enhanced Poly(3-Hydroxybutyrate) Production in Transgenic Tobacco BY-2 Cells Using Engineered Acetoacetyl-CoA Reductase. *Biosci., Biotechnol. Biochem* 79, 986–988. doi: 10.1080/09168451.2014.1002448

Yoshida, T., Tashiro, Y., and Sonomoto, K. (2012). Novel High Butanol Production from Lactic Acid and Pentose by *Clostridium saccharoperbutylacetonicum*. *J. Biosci. Bioeng.* 114, 526–530. doi: 10.1016/J.JBIOSC.2012.06.001

Eguchi, Y., Makanae, K., Hasunuma, T., Ishibashi, Y., Kito, K., and Moriya, H. (2018). Estimating the Protein Burden Limit of Yeast Cells by Measuring the Expression Limits of Glycolytic Proteins. *ELife* 7:e34595. doi: 10.7554/eLife.34595

Zhang, J., Wang, P., Wang, X., Feng, J., Sandhu, H. S., and Wang, Y. (2018). Enhancement of Sucrose Metabolism in *Clostridium saccharoperbutylacetonicum* N1-4 through Metabolic Engineering for Improved Acetone–Butanol–Ethanol (ABE) Fermentation. *Bioresour. Technol.* 270, 430–438. doi: 10.1016/J.BIORTECH.2018.09.059

Zheng, R. C., Ge, Z., Qiu, Z. K., Wang, Y. S., and Zheng, Y. G. (2012). Asymmetric Synthesis of (R)-1,3-Butanediol from 4-Hydroxy-2-Butanone by a Newly Isolated Strain *Candida krusei* ZJB-09162. *Appl. Microbiol Biotechnol* 94, 969–976. doi: 10.1007/s00253-012-3942-2

Conflict of Interest: EG, DH, and ZB work for CHAIN Biotechnology Ltd. which has interest in commercialisation of the present microbial platform. CHAIN Biotechnology Ltd. has filed a patent application encompassing the initial work described in this article, International Application No. PCT/GB2017/050601.

The remaining authors declare that the research was conducted in the absence of any commercial or financial relationships that could be construed as a potential conflict of interest.

frontiers in Bioengineering and Biotechnology

REVIEW
published: 03 June 2021
doi: 10.3389/fbioe.2021.658568

Clostridium acetobutylicum Biofilm: Advances in Understanding the Basis

Huifang Zhang[1†], Pengpeng Yang[1†], Zhenyu Wang[1], Mengting Li[2], Jie Zhang[1], Dong Liu[1,2], Yong Chen[1*] and Hanjie Ying[1,2]*

[1] State Key Laboratory of Materials-Oriented Chemical Engineering, College of Biotechnology and Pharmaceutical Engineering, Nanjing Tech University, Nanjing, China, [2] School of Chemical Engineering and Energy, Zhengzhou University, Zhengzhou, China

Clostridium acetobutylicum is an important industrial platform capable of producing a variety of biofuels and bulk chemicals. Biofilm of *C. acetobutylicum* renders many production advantages and has been long and extensively applied in fermentation. However, molecular and genetic mechanisms underlying the biofilm have been much less studied and remain largely unknown. Here, we review studies to date focusing on *C. acetobutylicum* biofilms, especially on its physiological and molecular aspects, summarizing the production advantages, cell physiological changes, extracellular matrix components and regulatory genes of the biofilm. This represents the first review dedicated to the biofilm of *C. acetobutylicum*. Hopefully, it will deepen our understanding toward *C. acetobutylicum* biofilm and inspire more research to learn and develop more efficient biofilm processes in this industrially important bacterium.

Keywords: *Clostridium acetobutylicum* biofilm, extracellular matrix, physiological changes, non-classically secreted proteins, heteropolysaccharides

OPEN ACCESS

Edited by:
Shang-Tian Yang,
The Ohio State University,
United States

Reviewed by:
Lan Wang,
Institute of Process Engineering (CAS), China
Chi Cheng,
Dalian University of Technology, China

****Correspondence:***
Dong Liu
liudong@njtech.edu.cn
Yong Chen
chenyong1982@njtech.edu.cn

† These authors have contributed equally to this work

Specialty section:
This article was submitted to Bioprocess Engineering, a section of the journal Frontiers in Bioengineering and Biotechnology

Received: *26 January 2021*
Accepted: *10 May 2021*
Published: *03 June 2021*

Citation:
Zhang H, Yang P, Wang Z, Li M, Zhang J, Liu D, Chen Y and Ying H (2021) Clostridium acetobutylicum Biofilm: Advances in Understanding the Basis. Front. Bioeng. Biotechnol. 9:658568. doi: 10.3389/fbioe.2021.658568

INTRODUCTION

Biofilms are the main living structure of microorganisms in nature. They are closely related to our lives. Traces of biofilms can be found in living tissues, medical devices, and industrial settings. It is estimated that more than 90% of bacteria can form this special structure, which makes biofilms a rich and developable biological resource.

In recent years, more and more biofilms are engineered as cell factories for biological manufacturing. A canonical example is the biofilm of the solvent-producing *Clostridium*, which is an important industrial platform and widely employed for biological production of acetone-butanol-ethanol (ABE) and a variety of other important chemicals. As early as 20 years ago, adsorption and immobilization of *C. beijerinckii* on clay bricks as biofilm was reported which greatly improved the ABE fermentation efficiency (Qureshi et al., 2000). In recent years, developments of *Clostridium* biofilms for improved production efficiency are extensively reported. However, compared with the biofilms of other industrial microbes like *Escherichia coli*, *Saccharomyces cerevisiae* and *Bacillus subtilis*, little has been known about the molecular mechanisms underlying the *Clostridium* biofilms. The physiological responses, growth changes, the biofilm composition and its genetic determinants, remain to be further understood. In view of this, we review studies focusing on *C. acetobutylicum* biofilms, especially its physiological and molecular aspects (**Figure 1**). Although there is a review regarding pathogenic clostridia (Pantaleon et al., 2014), this will represent the first review in the field of industrial *C. acetobutylicum*

biofilms. While pathogenic clostridia such as *C. difficile* and *C. perfringens* typically form multi-species biofilm in human gut, they can also form mono-species biofilm on abiotic surfaces like industrial *C. acetobutylicum*. Pathogenic clostridia do share many common characteristics with *C. acetobutylicum*. For example, they all sporulate, possess flagellar motility, and have a master transcription regulator Spo0A, which are important aspects involved in biofilm formation (Dawson et al., 2012; Đapa et al., 2013; Dapa and Unnikrishnan, 2013). However, compared to *C. acetobutylicum*, pathogenic clostridia do not accumulate excessive products and are less studied from a metabolic perspective. Biofilms of pathogenic clostridia were often studied in medical settings in terms of biofilm growth and cell survival over a relative short time period. By contrast, *C. acetobutylicum* biofilm were often studied in bioreactors over hundreds of hours during continuous fermentation. So, research aims and methodology for industrial *Clostridium* biofilm can be quite different from those for pathogenic clostridia. Factors considered important in pathogenic clostridia may not hold for *C. acetobutylicum* and vice versa. Comparison of biofilm between *C. acetobutylicum* and pathogenic clostridia or other industrial clostridia is included in this review when necessary. Hopefully, this review will deepen our understanding of *C. acetobutylicum* biofilm, and inspire more research to learn and develop more efficient *C. acetobutylicum* biofilm processes that can become industrial models of biofilm application.

PHYSIOLOGICAL CHANGES OF CELLS IN THE BIOFILM

Vegetative and Asporogenous Growth

Spore formation is a common physiological characteristic of *C. acetobutylicum*. It is generally believed that *C. acetobutylicum* initiates the expression of spore-producing genes when entering stationary phase. Early studies found that spore formation and solvent production occurred simultaneously. So, sporulation and solventogenesis were widely considered to be coupled (Lütke-Eversloh and Bahl, 2011). However, this seems not true in the biofilm. Liu et al. (2018) found that the spores of *C. acetobutylicum* in biofilm were reduced over time during long-term continuous fermentation. Finally, *C. acetobutylicum* biofilm cells seemed to eliminate sporulation and performed vegetative growth. This suggested that the cells in biofilm could maintain an active metabolic state instead of being in dormancy, leading to extended cell lifespan and prolonged productivity. Temporal transcriptomics analysis confirmed that expression of the genes responsible for spore formation was apparently down-regulated in the biofilm over time. The gene encoding the sporulation regulator σK (sigK, CA_C1689) was down-regulated over time up to eightfold. The genes involved in spore coat synthesis (CA_C0613-0614, CA_C1335, CA_C1337-1338, CA_C2808-2910, and CA_C3317) and the operon CA_C2086-2093 involved in stage III sporulation were decreased over time by 6–24-fold. The most down-regulated genes were those encoding the small, acid-soluble proteins (SASP) that are used to coat DNA in spores (CA_C1487, CA_C1522, and CA_C2365), which were significantly down-regulated by 48–200-fold. It is generally believed that the solvent production in *C. acetobutylicum* is coupled to the formation of spores, but the biofilm shows that *C. acetobutylicum* can greatly increase the solvent production without sporulation. This decoupling is also evidenced by other studies (Jones et al., 2011). Sporulation is also of particular interest in pathogenic clostridia because it is thought to cause persistent infections. Interestingly, elimination of sporulation also appeared in a study of *C. difficile* biofilm (Đapa et al., 2013). In this study, the spore number in *C. difficile* biofilm on day 3 and 5 was extremely low (0.0001%) compared to the control (40–50%). However, other studies showed that the spore number within a 6 days old biofilm varied from 10% to more than 60% depending on the *C. difficile* strains (Dawson et al., 2012; Semenyuk et al., 2014). Different with these pathogenic strains, the biofilm of *C. acetobutylicum* was developed in a long-term fermentation process with continual nutrient supply. This might allow continual cell growth and reduce stress-induced sporulation.

Long-Chain Cells

Besides elimination of sporulation, *C. acetobutylicum* biofilm cells also exhibited significant morphological changes. In traditional planktonic cell culture, cells are dispersed and short rod-shaped. However, cells became longer in the biofilm and were often linked in chain-like structure. Interestingly, the elongated chain-like morphology was also observed for *B. subtilis* biofilm cells. In *B. subtilis*, a transcriptional regulator SinR represses the genes responsible for EPS production and promotes cell motility and separation. During the development of biofilm, SinR activity is decreased and leads to EPS production and loss of cell motility. As a result, motile single cells turn to long chains of non-motile cells (Lemon et al., 2008). *C. acetobutylicum* also has a SinR homolog, but whether the SinR can also cause the long chain of cells in *C. acetobutylicum* biofilm remains to be verified. Similarly, elongated rod morphology was observed for *C. tyrobutyricum* after long-term adaptation in a biofilm reactor (Jiang et al., 2011), and also observed for *C. thermocellum* showing that vegetative cells attached on cellulosic fibers formed progressively longer chains over time (Dumitrache et al., 2013).

Modulated Gene/Protein Expression

Liu et al. (2016) carried out many transcriptomics and proteomics studies of *C. acetobutylicum* biofilm cells and revealed more unique phenotypes of the biofilm cells. They compared transcriptomic differences between free cells and biofilm cells during batch fermentation, studied transcriptomic changes in biofilm cells during long-term repeated batch fermentation (Liu et al., 2018), and performed proteomic analysis of biofilm (Liu et al., 2018; Yang et al., 2020). Genes/proteins that are often differentially regulated in *C. acetobutylicum* biofilm are summarized in **Table 1**. Results showed that 16.2% of genes in *C. acetobutylicum* genome were differentially expressed in the biofilm. The most dramatic changes occurred to amino acid biosynthesis, with sulfur uptake and cysteine biosynthesis genes being the most up-regulated and histidine biosynthesis

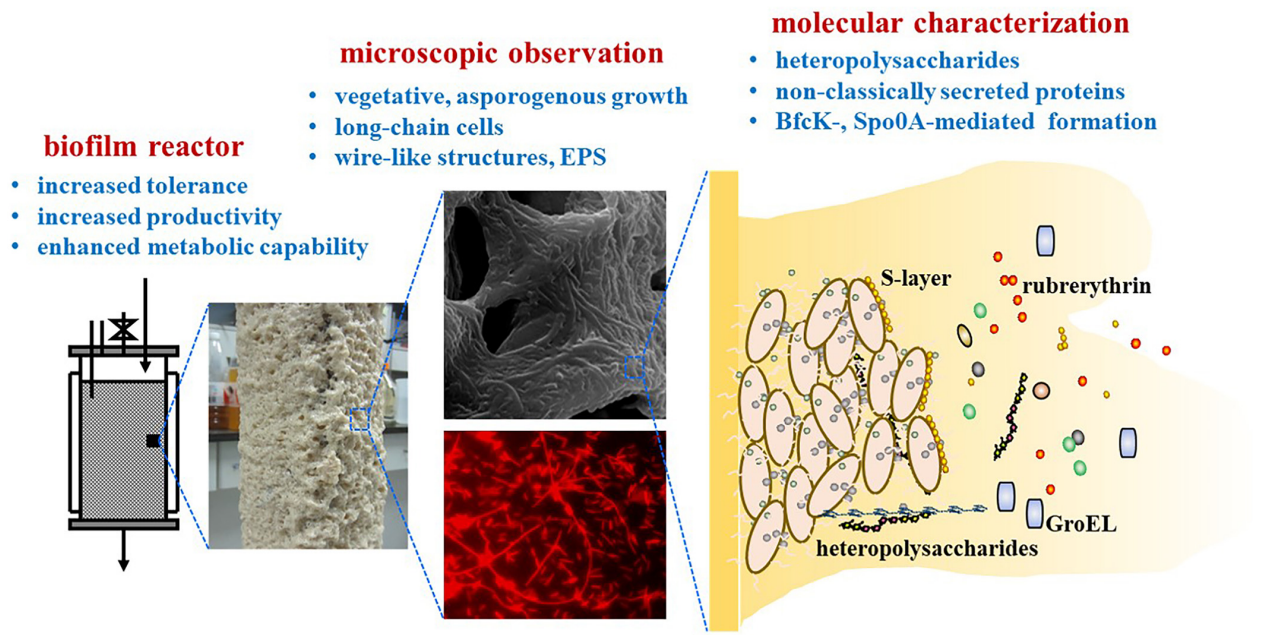

FIGURE 1 | Characterized aspects of *C. acetobutylicum* biofilm.

genes being the most down-regulated. *C. acetobutylicum* biofilm cells also up-regulated iron and sulfur uptake genes, Fe-S cluster biosynthesis genes as well as glycolysis genes, which could probably account for their increased metabolic activity. In addition, granulose formation and extracellular polymers metabolism were also significantly modulated. Cell motility, chemotaxis and flagella biosynthesis were gradually down-regulated in the biofilm during the long-term fermentation process. By contrast, central metabolism such as glycolysis, solvent synthesis and sugar utilization was relatively stable during the long-term biofilm fermentation. Similarly, *C. thermocellum* biofilm cells showed greater expression of genes involved in central metabolism such as glycolysis, H_2 production and ATP regeneration, while relatively lower expression of genes involved in flagellar motility and chemotaxis (Dumitrache et al., 2017). This could explain why cells can maintain long-term metabolic activity in the biofilm. Overall, these studies provide valuable insights into the molecular basis of *C. acetobutylicum* biofilm and should be very useful for understanding and developing biofilm-based processes.

EXTRACELLULAR MATRIX OF THE BIOFILM

EPS and Wire-Like Structures

Biofilm is composed of water, EPS, cells, etc. The EPS is mainly secreted by cells or derived from cell lysis, mainly containing biological macromolecules such as polysaccharides, proteins, nucleic acids, lipids, etc. These components can play important roles in the structure of the biofilm.

Unlike *C. thermocellum* that forms a distinctive monolayer biofilm with no extracellular polymeric matrix (Dumitrache et al., 2013), extracellular polymers are clearly found in *C. acetobutylicum* and many other clostridia. The EPS was so abundant that it often could be visibly observed. Liu et al. (2013) observed a thick and sticky layer of biofilm matrix stacked on the carrier surface. Through SEM observation they found that the cells in the biofilm of *C. acetobutylicum* were present in aggregates and covered by a large number of EPS they produced, forming a multiplayer biofilm. Later Zhuang et al. (2016) observed the extracellular sheet-like EPS with a transmission electron microscope (TEM), and found it was accumulated around the cells during the formation of the biofilm. Recently, Liu et al. (2018) further observed wire-like structures in *C. acetobutylicum* biofilm under fluorescence microscope. The wires were as long as 50 μm and could be cross-connected and imbedded in cell aggregates. Yang et al. (2020) also found wire-like structures that cross-linked cells in *C. acetobutylicum* biofilm. These structures disappeared when *spo0A* was disrupted (Yang et al., 2020). Similarly, Engel et al. (2019) found in a bioelectrochemical system that *C. acetobutylicum* cells in the biofilm formed high number and density of filamentous appendages more than 20 μm in length.

Extracellular Polysaccharides

Extracellular polysaccharide is one of the most common components in biofilms. In many microbes, extracellular polysaccharides play an important role in the formation of biofilms. Mutant strains with defective extracellular polysaccharide synthesis have greatly reduced ability to form biofilms or even produce no biofilms (Danese et al., 2000).

TABLE 1 | Some genes/proteins differentially regulated in *C. acetobutylicum* biofilms*.

Genes/proteins	General change	Description
Glycolysis		
CA_C0570 (glcG)	Up-regulated	PTS sugar transporter subunit
CA_C3657 (gapN)	Up-regulated	$NADP^+$-dependent Glyceraldehyde-3-phosphate dehydrogenase
CA_C0712 (pgm)	Up-regulated	Phosphoglycerate mutase
CA_C0713 (eno)	Up-regulated	Enolase
CA_P0141-0142, CA_C0809-0810	Up-regulated	Hydrogenases and maturation factors
CA_C3552 (ldh)	Up-regulated	L-lactate dehydrogenase
CA_C2967 (alsD)	Down-regulated	α-Acetolactate decarboxylase
Pentose metabolism		
CA_C1339-1341 (araEAD)	Up-regulated	L-arabinose utilization
CA_C2610, CA_C3451	Up-regulated	D-xylose utilization
CA_C1343 (xfp)	Up-regulated	Phosphoketolase
CA_C1347-1348 (tkt, tal)	Up-regulated	Pentose phosphate pathway
Polysaccharides metabolism		
CA_C2383, CA_C0358	Up-regulated	Xylanase/chitin deacetylase
CA_C0804, CA_C1968	Up-regulated	Pectate lyase
CA_C0910	Up-regulated	Cellulosomal scaffolding protein
Iron and sulfur assimilation		
CA_C0788-0791, CA_C1029-1030	Up-regulated	Iron assimilation
CA C0102-0110	Up-regulated	SULFATE assimilation
Sporulation and chemotaxis		
CA_C2086-2093, CA_C2859 (spoIIID)	Up-regulated at early stages then down-regulated over time	Stage III sporulation proteins
CA_C1487, CA_C2365	Down-regulated	Small acid-soluble spore protein
CA_C2908-2910, CA_C1337-1338	Down-regulated	Spore coat protein
CA_C0117	Up-regulated	CheY-like chemotaxis protein
CA_C2745, CA_C2419, CA_C2803	Down-regulated	Methyl-accepting chemotaxis protein
CA_C2205 (fliD)	Down-regulated	Flagellar hook-associated protein
Oxidative stress response		
CA_C1547-1549	Up-regulated at early stages then down-regulated over time	Thioredoxin and thioredoxin reductase
CA_C1570-1571	Up-regulated at early stages then down-regulated over time	Glutathione peroxidase
CA_C3597-3598	Up-regulated at early stages then down-regulated over time	Reverse rubrerythrin
Others		
CA_C0252-0255	Up-regulated	Nitrogen-fixation
CA_C0280-0281	Up-regulated	Molybdate transporter
CA_C3634-3644	Up-regulated	Oligopeptide transporter
CA_C1447, CA_C1504, CA_P0109, CA_P0128	Down-regulated	MDR-type permease

**Results are summarized from the studies of Liu et al. (2016, 2018) and Yang et al. (2020).*

Polysaccharide biosynthesis genes are usually located in operons or gene clusters, encoding proteins responsible for repeat unit synthesis, polysaccharide chain initiation and elongation, chain length control, transmembrane transport and process regulation. In addition to the cell wall peptidoglycan biosynthesis genes, there are at least 4 long gene clusters consisting of 10–15 genes (CA_C3059-CA_C3045, CA_C3073-CA_C3060, CA_C2337-CA_C2325, and CA_C2321-2312) in *C. acetobutylicum* genome that potentially make extracellular polysaccharides. Studies have shown that *C. acetobutylicum* can produce extracellular polysaccharides. An early study showed that an extracellular polysaccharide was produced by *C. acetobutylicum* resting cells during a biocatalysis process, which made the reaction system very viscous. According to the metabolic analysis, it was speculated that the polysaccharide might be acetylate glucose polymers (Häggström and Förberg, 1986). Interestingly, a recent study also found a large quantity of acetylated glucose polymers in *Clostridioides difficile* 630Δerm, which were produced by the operon CDIF630erm_02794—CDIF630erm_02798. Bioinformatics predicted that *C. acetobutylicum* had a similar operon CA_C1561-CA_C1565 (Dannheim et al., 2017). However, whether this operon is involved in the secretion of acetylated glucose polymers in *C. acetobutylicum* remains to be verified.

Wallenius et al. (2016) extracted exopolysaccharides from *C. acetobutylicum* chemostat culture under glucose limited condition and characterized them on monosaccharide level through nuclear magnetic resonance (NMR) spectroscopy. The polysaccharides were mainly composed of 40% (molar ratio, the same hereinafter) rhamnose, 34% glucose, 13% mannose, 10% galactose, and 2% arabinose. Liu et al. (2018) extracted polysaccharides in *C. acetobutylicum* biofilm which were then separated by gel chromatography, degraded, derivatized, and analyzed by liquid chromatography. They identified three different polysaccharides SM1, SM2, and SM3. SM1 represented the largest fraction (53%, w/w) in the polysaccharide extract, followed by SM2 (26%, w/w) and SM3 (21%, w/w). Analysis showed that all the three polysaccharides were heteropolysaccharides with glucose as the primary component. SM2 and SM3 shared similar monosaccharide type and molar ratio, consisting of glucose (47–53%, molar ratio, the same hereinafter), mannose (13–15%), rhamnose (10–16%), galactose (9–10%), glucosamine (7–9%) and ribose (4–5%). Compared with SM2 and SM3, SM1 polysaccharide consisted of more glucose (58%), mannose (21%), and glucosamine (13%), but much less rhamnose (0.8%), galactose (0.8%), and ribose (0.4%). SM1 also consisted of unique galacturonic acid (5.5%). The presence of galacturonic acid explained why the *C. acetobutylicum* biofilm substances was alkali-soluble during the extraction process (Liu et al., 2018). Recently, Dong et al. (2020) also used fluorescent lectins to probe for specific sugars during *C. acetobutylicum* biofilm development, and found that fucose and galactose were present in the biofilm.

Non-classically Secreted Proteins

Extracellular protein has been demonstrated to be another vital component of many bacterial biofilms. In *B. subtilis*, the

TABLE 2 | Comparison of representative fermentation results obtained from *C. acetobutylicum* biofilm or planktonic cells.

Culture	Process mode	Butanol titer (g/L)	Solvent yield(g/g)	Solvent productivity (g/L/h)	References
C. acetobutylicum B3	Free cells	11.8	0.34	0.25	Liu et al., 2014
C. acetobutylicum ATCC 55025	Biofilm-immobilized cells, continuous fermentation	∼5	0.42	4.6	Huang et al., 2004
C. beijerinckii BA101	Biofilm-immobilized cells, continuous fermentation	∼5	0.38	15.8	Qureshi et al., 2000
C. beijerinckii BA101	Biofilm-immobilized cells, batch fermentation	20.9	0.41	0.59	Chen and Blaschek, 1999
C. beijerinckii NCIMB 8052	Biofilm-immobilized cells, continuous fermentation	13.4	0.44	0.40	Lee et al., 2008
C. acetobutylicum B3	Biofilm-immobilized cells, batch fermentation	15.6	0.38	1.88	Liu et al., 2013

TasA, and BslA proteins have been reported to be required for the formation of air–liquid or solid–air interface biofilms. In *Staphylococcus aureus*, the Bap protein at the cell surface facilitates cells attachment to the substrate and cell-to-cell interactions (Obana et al., 2020). Research demonstrated that the protein in the biofilm of *C. acetobutylicum* could reach more than 50% (w/w) of the biofilm matrix. However, no biofilm specific proteins such as TasA and BslA have been found in *C. acetobutylicum* so far. Liu et al. (2018) analyzed the proteomics of the biofilm by LC-MS/MS, two-dimensional SDS-PAGE and MALDI-TOF/TOF mass spectrometry, wherein S-layer protein was found one of the most abundant proteins in the biofilm. S-layer is a crystalline monomolecular assembly of proteins. It is a common outermost cell envelope structure in bacteria (Lai et al., 2003; Plaut et al., 2014; Soavelomandroso et al., 2017). In *C. difficile*, S-layer was demonstrated essential for biofilm formation perhaps because it was essential for anchoring proteins required for biofilm formation (Đapa et al., 2013). In addition to the S-layer protein, a large number of proteins that were expected to be intracellular were also present abundantly in the *C. acetobutylicum* biofilm matrix. GroEL and ruberythrin were two notable examples and they could also be detected in the fermentation supernatant. Proteins released from intracellular pool through unknown secreted pathways have been defined as non-classically secreted proteins. GroEL and rubrerythrin play a canonical role inside cells in correct folding of proteins and adaptation to oxidative stress, respectively. However, there is increasing evidence that non-classically secreted proteins are multifunctional proteins and many of them can moonlight as adhesins (Kainulainen and Korhonen, 2014). In particular, GroEL has often been found involved in cell adherence and biofilm formation in different species (Hennequin et al., 2001; Arai et al., 2015; Arora et al., 2017). Some studies found GroEL was also able to form amyloid-like fibrils under physiological conditions (Chen et al., 2012, 2014), a structure usually important for biofilm formation. Besides GroEL and rubrerythrin, many other non-classically secreted proteins such as the molecular chaperone GroES, elongation factor Tu (Ef-Tu), trigger factor, glyceraldehyde-3-phosphate dehydrogenase (GAPDH), and electron transfer flavoprotein β-subunit were also abundant in the biofilm of *C. acetobutylicum* (Liu et al., 2018). While these non-classically secreted proteins were likely to participate in the formation of biofilm, they were also likely to participate in cellular metabolism because many of them were central metabolic enzymes. Strikingly, these enzymes included almost all the important enzymes for solventogenisis, with the electron transfer flavoprotein (EtfAB), crotonase (Crt), acetoacetyl-CoA: acetate/butyrate CoA-transferase (CtfAB), phosphate butyryltransferase (Ptb), pyruvate:ferredoxin oxidoreductase (Pfor), butyrate kinase (Buk), acetyl coenzyme A acetyltransferase (Thl), acetoacetate decarboxylase (Adc) and alcohol dehydrogenase E (adhE) being the Top 30 abundant extracellular proteins in the biofilm matrix (Liu et al., 2018). However, it is currently unknown how these proteins are secreted outside the cells, and their specific effects on the biofilm of *C. acetobutylicum* need to be studied in detail.

PRODUCTION ADVANTAGES OF BIOFILM

Increased Cell Tolerance

Butanol is toxic to cells. The growth and fermentation of solvent-producing Clostridium such as *C. acetobutylicum* and *C. beijerinckii* are easily inhibited by butanol. In traditional batch fermentation by free cells, the fermentation will cease when butanol titer reaches around 13 g/L, and the total titer of ABE is usually around 20 g/L. At the same time, the fermentation speed is slow, and the fermentation time is usually 60–80 h, with the total solvent productivity only about 0.3 g/L/h. Biofilm increases cellular density inside it, and the highly hydrated extracellular polymeric substances (EPS) of biofilm can act as a protective barrier and timely excrete waste metabolites (Flemming et al., 2016). Therefore, it provides a beneficial microenvironment for cell survival. Thus, the cell viability and environmental adaptability could be improved. Liu et al. (2013) demonstrated that the *C. acetobutylicum* biofilm formed on fibrous matrix significantly increased the butanol resistance of the cells. The survival of the biofilm cells exposed to 15 g/L of butanol for 2 h was 3 orders of magnitude higher than that of the planktonic cells. Later on, they revealed using confocal laser scanning microscope that EPS acted as a barrier to limit the transfer of harmful substances and diluted their concentrations. In addition, cells in different regions of the biofilm displayed different tolerance to harsh environment. Some cells with higher tolerance could continue growth in the biofilm. This heterogeneity of biofilm might be the primary tolerance mechanisms associated with biofilm (Zhuang et al., 2016). The increase in solvent tolerance of *C. acetobutylicum* biofilm cells probably was also associated with their morphological changes. Since the cells in biofilm turned into long-chain cells, compared to the short-rod shape this would decrease their surface-to-volume ratio. As

the cell surface and cell membrane are the major targets for the action of organic compounds, many studies have shown that cells of larger size or smaller specific surface area could be more advantageous under toxic solvents (Neumann et al., 2005; Si et al., 2016; Gupta et al., 2020). It should be noted that while the biofilms increase cell tolerance, it could also become an unfavorable situation under certain circumstance. For example, the heterogeneity of biofilm and EPS protection may void antibiotic selection pressure, and thus make fermentation less efficient with genetically engineered strains that require antibiotics to maintain target genes. A solution to this problem is to integrate target genes into *C. acetobutylicum* genome, which can avoid use of antibiotics and will provide long-term expression of target genes.

Increased Productivity

Performing fermentation using cells in the form of biofilm can greatly improve the productivity (**Table 2**). Qureshi et al. (2000) demonstrated that *C. beijerinckii* biofilm formed on clay bricks could be used for continuous ABE fermentation. At a dilution rate of 2.0 h^{-1}, a total solvent productivity of 15.8 g/L/h was reached, which was approximately 50 times the productivity of free cell batch fermentation. This is the highest productivity ever reported for butanol fermentation. Similarly, Huang et al. (2004) used *C. acetobutylicum* biofilm for continuous fermentation in a fiber bed reactor. The fermentation was continuously performed for more than 600 h, and the best butanol productivity of 4.6 g/L/h was obtained at a dilution rate of 0.9 h^{-1}. Continuous fermentation significantly improves productivity, but there is usually a problem of low product concentration. To address this problem, Liu et al. (2013) developed a repeated batch fermentation process based on *C. acetobutylicum* biofilm. The fermentation period was shortened from the traditional 72 to 12–14 h per batch, which is the shortest batch fermentation time yet reported. Unlike the continuous fermentation, glucose could be completely consumed in the repeated batch fermentation. As a result, a high butanol titer of 15.6 g/L was achieved with a solvent productivity of 1.88 g/L/h. This final butanol titer was 21% higher than that of planktonic cells, which could be explained by the improved butanol tolerance of the biofilm cells. On the other hand, the vegetative and asporogenous growth of biofilm cells could maintain an active metabolic state and help to extend cell lifespan. This should contribute a lot to the increased reaction speed and accelerated fermentation process. Furthermore, biofilms can function as a reservoir of enzymes either extracellular or released from cytoplasm (Flemming and Wingender, 2010). Many of the non-classically secreted proteins in *C. acetobutylicum* biofilm matrix were involved in central metabolism. Thus, the extracellular presence of these metabolic enzymes might also help to increase substrate utilization and conversion speed during the fermentation.

In addition to increasing cell tolerance and productivity, the biofilm also realizes solid-liquid separation and thus is good for product recovery. This makes biofilm fermentation more suitable for process integration. For example, it can be coupled with the product separation process based on resin adsorption or gas stripping. In this way the productivity and equivalent product concentration could be further dramatically improved (Xue et al., 2013; Liu et al., 2014).

Enhanced Metabolic Capability

Studies have also shown that *C. acetobutylicum* biofilm exhibits enhanced metabolic capabilities, such as the utilization of xylose. The utilization of xylose by cells is of great significance to the utilization of lignocellulose as cheap fermentation feedstock. *C. acetobutylicum* is capable of utilizing xylose, but the xylose utilization is relatively inefficient in the presence of glucose, due to the well-known Carbon Catabolite Repression (CCR) effect. Chen et al. (2013) used pretreated cotton towels to support *C. acetobutylicum* biofilm. They showed that the biofilm cells significantly improved the xylose utilization rate. The xylose utilization rate on pure xylose medium was increased by 25.9%, and on glucose-xylose mixture was increased by 70%, compared to those of free cells, respectively. A subsequent transcriptomic study of *C. acetobutylicum* biofilm found that most of the genes involved in xylose and arabinose catabolism were slightly down-regulated at the initial growth stage, but significantly up-regulated throughout the subsequent stages. This was consistent with the experimental results that the xylose utilization capacity of the surface-adsorbed biofilm cells was improved (Liu et al., 2016). In addition, the transcriptomic study also showed that many genes involved in hydrolysis of xylan, chitin, starch and pectate as well as genes involved in cell wall recycling were apparently up-regulated, especially at the late growth stage (Liu et al., 2016). Since the *C. acetobutylicum* biofilm matrix contains heteropolysaccharides composed of various sugars, the enhanced metabolism of sugars may help the cells to derive energy from these extracellular heteropolysaccharides when nutrients are depleted. Potentially, the enhanced metabolism of extracellular sugars could also help to build and restructure the biofilm matrix.

It should be noted that while metabolic capability can be enhanced in biofilm cells, the metabolic fluxes may be shifted and this could lead to undesirable product pattern. For example, transcriptomic analyses showed that expression of hydrogenases was up-regulated in *C. acetobutylicum* and *C. thermocellum* biofilm cells (Liu et al., 2016). Consistently, the biofilm cells appeared to evolve more H_2 and produced 37% more acetone as a result of redox balance (Liu et al., 2013). For strains like *C. tyrobutyricum* that produces H_2 as a target product, this can be a very favorable result (Jo et al., 2008). However, for *C. acetobutylicum* this will cause a decreased butanol selectivity during the ABE fermentation. In this case, metabolic regulation can be considered. Using an exogenous electron carrier to redirect the electron flow toward butanol biosynthesis instead of H_2 evolution could greatly improve the butanol selectivity of the biofilm cells (Liu et al., 2013).

INFLUENCING FACTORS AND REGULATORY GENES

Biofilm Carrier

Carrier is an important factor for cell adsorption, immobilization and biofilm formation. The initial adsorption of cells onto the

carrier can be caused by the interaction between the cells and the carrier surface, which is associated with the properties of the cells and the carrier (hydrophobicity, specific surface area, porosity, etc.) and environmental cues (pH, temperature, ionic strength, etc.). Various materials such as cotton fibers, wood pulp fibers, bamboo fibers, bricks, bone char, ceramic beads, glass slide, bagasse, linen, silk, synthetic sponge and non-woven fabric have been reported as biofilm carriers for *C. acetobutylicum* (Yen et al., 2011; Dolejš et al., 2014; Zhuang et al., 2017). In other industrial clostridia like *C. tyrobutyricum*, common carriers were also reported. Materials with larger surface area and higher roughness were found better for cells to be adsorbed (Chen et al., 2013). Surface modification of carriers is an important way to improve bacterial adsorption and biofilm formation. For example, polyetherimide and steric acid were used for carrier modification to increase the cations on linen surface and the hydrophobicity of linen surface, respectively. Using the modified linen as a biofilm carrier, the adhesion of *C. acetobutylicum* cells was doubled, and the fermentation yield was also improved (Zhuang et al., 2017).

Regulatory Genes

Although *C. acetobutylicum* biofilm has been long and extensively applied in solvent production, its genetic mechanisms have been much less studied. Genetic determinants and regulation processes remain largely unknown. Spo0A has been well studied as a master transcription regulator controlling sporulation and solventogenesis. In *B. subtilis*, Spo0A also regulated *epsA-O* genes that were directly responsible for EPS production and biofilm formation (Banse et al., 2011). However, no such genes have been found in *C. acetobutylicum*. In the pathogenic clostridia *C. perfringens*, *spo0A* mutant was not impaired in biofilm formation, whereas in *C. difficile spo0A* mutant showed a defective biofilm formation (Pantaleon et al., 2014). Yang et al. (2020) disrupted the *spo0A* of *C. acetobutylicum* to investigate its influences on biofilm formation for the first time. They found the aggregation and adhesion abilities of the *spo0A* disruptant and its swarming motility were all dramatically reduced compared to those of the wild strain. Wire-like structures that cross-linked cells were also disappeared upon *spo0A* disruption. As a result, the *spo0A* mutant could hardly form biofilm anymore. These phenotypes could be further explained by the proteomic analysis of the *spo0A* mutant. Similarly, disruption of *spo0A* could also decrease biofilm formation in *C. difficile* though the underlying mechanism remained unclear (Dawson et al., 2012). It should be noted that disruption of *spo0A* also severely impaired cell growth and solvent production in *C. acetobutylicum*. So, the abolished biofilm formation upon *spo0A* disruption could potentially be a result of growth defect. More elaborate experiments are therefore needed to dissect the role of Spo0A in biofilm formation in future.

Signaling processes that usually involve kinases-mediated phosphorylation of regulatory proteins, together with intracellular secondary messengers like c-di-GMP or cAMP, are also important for regulation of biofilm formation (O'Toole and Wong, 2016). In *C. acetobutylicum*, CA_C2730 gene encodes a signal transduction histidine kinase (BfcK). There were five orphan histidine kinases and CA_C2730 was the only one not involved in sporulation (Steiner et al., 2011). A recent research demonstrated that CA_C2730 played an important role in the formation of *C. acetobutylicum* biofilm (Liu et al., unpublished). Disruption of CA_C2730 abolished biofilm formation, and flagella were also disappeared in the disruptant with apparently reduced cell motility. Unlike *spo0A*, disruption of CAC2730 did not cause growth defect or impaired fermentation. So, the impact of this gene on biofilm formation would be more plausible. At the same time, phosphorylation proteomics analysis revealed that the presence of CAC2730 probably repressed the phosphorylation of a serine/threonine protein kinase (encoded by CA_C0404) that might negatively regulate biofilm formation. However, these studies are still at the preliminary research stage. More research is needed in the future to understand the molecular basis underlying *C. acetobutylicum* biofilms.

Studies of other clostridia have shown more possible genes involved in biofilm development. In *C. difficile* or *C. perfringens*, a quorum-sensing regulator LuxS, a cell wall protease Cwp84, a germination protein SleC, a signal peptidase SipW, a type IV pilin PilA2 and an EPS matrix protein BsaA have been demonstrated to greatly impact biofilm formation (Đapa et al., 2013; Obana et al., 2020). Whether homologs of these proteins exist and play similar roles in *C. acetobutylicum* remains to be studied.

CONCLUSION AND PROSPECTS

C. acetobutylicum biofilms have great benefits for industrial applications, but its molecular and genetic basis is still largely unknown. Studies so far have preliminarily characterized the polysaccharide and protein components in the biofilm matrix, studied the cell growth, morphology, metabolism and gene/protein expression pattern in the biofilm, but the studies on biofilm-forming genes and regulatory mechanisms are still insufficient. From our perspective, future research should focus more on the following aspects: (1) understanding the interaction of cells with material surface to better design biofilm-carrying materials; (2) revealing the genetic circuit of biofilm development, and use synthetic biology to re-construct the biosynthetic process for biofilm; (3) exploring the life cycle, physiological changes and clustering effects of the cells in the biofilm under industrial conditions to better develop its potential for industrial applications.

AUTHOR CONTRIBUTIONS

HZ, PY, ZW, ML, JZ, DL, YC, and HY contributed to the research, writing, editing, and formatting of the manuscript. All authors contributed to the article and approved the submitted version.

FUNDING

This work was supported by the National Nature Science Foundation of China (Grant No. 21706123), the key program of

The National Natural Science Foundation of China (Grant No. 21636003), the Natural Science Foundation of Jiangsu Province (Grant Nos. BK20202002 and BK20190035), the National Key Research and Development Program of China (Grant No. 2019YFD1101204), the Program for Changjiang Scholars and Innovative Research Team in University (IRT_14R28), the Priority Academic Program Development of Jiangsu Higher Education Institutions (PAPD), and the Jiangsu Synergetic Innovation Center for Advanced Bio-Manufacture. DL was supported by the Jiangsu Qinglan Talent Program.

ACKNOWLEDGMENTS

We would like to thank the editors and reviewers for their valuable contributions to this special topic.

REFERENCES

Arai, T., Ochiai, K., and Senpuku, H. (2015). *Actinomyces naeslundii* GroEL-dependent initial attachment and biofilm formation in a flow cell system. *J. Microbiol. Methods* 109, 160–166. doi: 10.1016/j.mimet.2014.12.021

Arora, G., Sajid, A., Virmani, R., Singhal, A., Kumar, C. M. S., Dhasmana, N., et al. (2017). Ser/Thr protein kinase PrkC-mediated regulation of GroEL is critical for biofilm formation in *Bacillus anthracis*. *NPJ Biofilms Microbiomes* 3:7. doi: 10.1038/s41522-017-0015-4

Banse, A. V., Hobbs, E. C., and Losick, R. (2011). Phosphorylation of Spo0A by the histidine kinase KinD requires the lipoprotein med in *Bacillus subtilis*. *J. Bacteriol.* 193, 3949–3955. doi: 10.1128/JB.05199-11

Chen, C. K., and Blaschek, H. P. (1999). Acetate enhances solvent production and prevents degeneration in *Clostridium beijerinckii* BA101. *Appl. Microbiol. Biotechnol.* 52, 170–173. doi: 10.1007/s002530051504

Chen, J., Yagi, H., Furutani, Y., Nakamura, T., Inaguma, A., Guo, H., et al. (2014). Self-assembly of the chaperonin GroEL nanocage induced at submicellar detergent. *Sci. Rep.* 4:5614. doi: 10.1038/srep05614

Chen, J., Yagi, H., Sormanni, P., Vendruscolo, M., Makabe, K., Nakamura, T., et al. (2012). Fibrillogenic propensity of the GroEL apical domain: a Janus-faced minichaperone. *FEBS Lett.* 586, 1120–1127. doi: 10.1016/j.febslet.2012.03.019

Chen, Y., Zhou, T., Liu, D., Li, A., Xu, S., Liu, Q., et al. (2013). Production of butanol from glucose and xylose with immobilized cells of *Clostridium acetobutylicum*. *Biotechnol. Bioprocess Eng.* 18, 234–241. doi: 10.1007/s12257-012-0573-5

Danese, P. N., Pratt, L. A., and Kolter, R. (2000). Exopolysaccharide production is required for development of *Escherichia coli* K-12 biofilm architecture. *J. Bacteriol.* 182, 3953–3956. doi: 10.1128/jb.182.12.3593-3596.2000

Dannheim, H., Will, S. E., Schomburg, D., and Neumann-Schaal, M. (2017). *Clostridioides difficile* 630Δerm in silico and in vivo – quantitative growth and extensive polysaccharide secretion. *FEBS Open Bio* 7, 602–615. doi: 10.1002/2211-5463.12208

Đapa, T., Leuzzi, R., Ng, Y. K., Baban, S. T., Adamo, R., Kuehne, S. A., et al. (2013). Multiple factors modulate biofilm formation by the anaerobic pathogen *Clostridium difficile*. *J. Bacteriol.* 195, 545–555. doi: 10.1128/JB.01980-12

Dapa, T., and Unnikrishnan, M. (2013). Biofilm formation by *Clostridium difficile*. *Gut Microbes* 4, 397–402. doi: 10.4161/gmic.25862

Dawson, L. F., Valiente, E., Faulds-Pain, A., Donahue, E. H., and Wren, B. W. (2012). Characterisation of *Clostridium difficile* biofilm formation, a role for Spo0A. *PLoS One* 7:e50527. doi: 10.1371/journal.pone.0050527

Dolejš, I., Rebroš, M., and Rosenberg, M. (2014). Immobilisation of *Clostridium* spp. for production of solvents and organic acids. *Chem. Pap.* 68, 1–14. doi: 10.2478/s11696-013-0414-9

Dong, H., Zhang, W., Wang, Y., Liu, D., and Wang, P. (2020). Biofilm polysaccharide display platform: a natural, renewable, and biocompatible material for improved lipase performance. *J. Agric. Food Chem.* 68, 1373–1381. doi: 10.1021/acs.jafc.9b07209

Dumitrache, A., Klingeman, D. M., Natzke, J., Rodriguez, M. Jr., Giannone, R. J., Hettich, R. L., et al. (2017). Specialized activities and expression differences for *Clostridium thermocellum* biofilm and planktonic cells. *Sci. Rep.* 7:43583. doi: 10.1038/srep43583

Dumitrache, A., Wolfaardt, G., Allen, G., Liss, S. N., and Lynd, L. R. (2013). Form and function of *Clostridium thermocellum* biofilms. *Appl. Environ. Microbiol.* 79, 231–239. doi: 10.1128/AEM.02563-12

Engel, M., Gemünde, A., Holtmann, D., Müller-Renno, C., Ziegler, C., Tippkötter, N., et al. (2019). *Clostridium acetobutylicum*'s connecting world: cell appendage formation in bioelectrochemical systems. *ChemElectroChem* 7, 414–420. doi: 10.1002/celc.201901656

Flemming, H. C., and Wingender, J. (2010). The biofilm matrix. *Nat. Rev. Microbiol.* 8, 623–633. doi: 10.1038/nrmicro2415

Flemming, H. C., Wingender, J., Szewzyk, U., Steinberg, P., Rice, S. A., and Kjelleberg, S. (2016). Biofilms: an emergent form of bacterial life. *Nat. Rev. Microbiol.* 14, 563–575. doi: 10.1038/nrmicro.2016.94

Gupta, J. A., Thapa, S., Verma, M., Som, R., and Mukherjee, K. J. (2020). Genomics and transcriptomics analysis reveals the mechanism of isobutanol tolerance of a laboratory evolved *Lactococcus lactis* strain. *Sci. Rep.* 10:10850. doi: 10.1038/s41598-020-67635-w

Häggström, L., and Förberg, C. (1986). Significance of an extracellular polymer for the energy metabolism in *Clostridium acetobutylicum*: a hypothesis. *Appl. Microbiol. Biotechnol.* 23, 234–239. doi: 10.1007/BF00261921

Hennequin, C., Porcheray, F., Waligora-Dupriet, A. J., Collignon, A., Barc, M. C., Bourlioux, P., et al. (2001). GroEL (Hsp60) of *Clostridium difficile* is involved in cell adherence. *Microbiology* 147, 87–96. doi: 10.1099/00221287-147-1-87

Huang, W., Ramey, D. E., and Yang, S. (2004). Continuous production of butanol by *Clostridium acetobutylicum* immobilized in a fibrous bed bioreactor. *Appl. Biochem. Biotechnol.* 113–116, 0887–0898. doi: 10.1385/ABAB:115:1-3:0887

Jiang, L., Wang, J., Liang, S., Cai, J., Xu, Z., Cen, P., et al. (2011). Enhanced butyric acid tolerance and bioproduction by *Clostridium tyrobutyricum* immobilized in a fibrous bed bioreactor. *Biotechnol. Bioeng.* 108, 31–40. doi: 10.1002/bit.22927

Jo, J. H., Lee, D. S., Park, D., and Park, J. M. (2008). Biological hydrogen production by immobilized cells of *Clostridium tyrobutyricum* JM1 isolated from a food waste treatment process. *Bioresour. Technol.* 99, 6666–6672. doi: 10.1016/j.biortech.2007.11.067

Jones, S. W., Tracy, B. P., Gaida, S. M., and Papoutsakis, E. T. (2011). Inactivation of σ^F in *Clostridium acetobutylicum* ATCC 824 blocks sporulation prior to asymmetric division and abolishes σ^E and σ^G protein expression but does not block solvent formation. *J. Bacteriol.* 193, 2429–2440. doi: 10.1128/JB.00088-11

Kainulainen, V., and Korhonen, T. K. (2014). Dancing to another tune-adhesive moonlighting proteins in bacteria. *Biology* 3, 178–204. doi: 10.3390/biology3010178

Lai, E. M., Phadke, N. D., Kachman, M. T., Giorno, R., Vazquez, S., Vazquez, J. A., et al. (2003). Proteomic analysis of the spore coats of *Bacillus subtilis* and *Bacillus anthracis*. *J. Bacteriol.* 185, 1443–1454. doi: 10.1128/jb.185.4.1443-1454.2003

Lee, S. M., Cho, M. O., Park, C. H., Chung, Y. C., Kim, J. H., Sang, B. I., et al. (2008). Continuous Butanol Production Using Suspended and Immobilized *Clostridium beijerinckii* NCIMB 8052 with Supplementary Butyrate. *Energy Fuels* 22, 3459–3464. doi: 10.1021/ef800076j

Lemon, K. P., Earl, A. M., Vlamakis, H. C., Aguilar, C., and Kolter, R. (2008). Biofilm development with an emphasis on *Bacillus subtilis*. *Curr. Top. Microbiol. Immunol.* 322, 1–16. doi: 10.1007/978-3-540-75418-3_1

Liu, D., Chen, Y., Ding, F. Y., Zhao, T., Wu, J. L., Guo, T., et al. (2014). Biobutanol production in a *Clostridium acetobutylicum* biofilm reactor integrated with simultaneous product recovery by adsorption. *Biotechnol. Biofuels* 7:5. doi: 10.1186/1754-6834-7-5

Liu, D., Chen, Y., Li, A., Ding, F., Zhou, T., He, Y., et al. (2013). Enhanced butanol production by modulation of electron flow in *Clostridium acetobutylicum* B3 immobilized by surface adsorption. *Bioresour. Technol.* 129, 321–328. doi: 10.1016/j.biortech.2012.11.090

Liu, D., Xu, J., Wang, Y., Chen, Y., Shen, X., Niu, H., et al. (2016). Comparative transcriptomic analysis of *Clostridium acetobutylicum* biofilm and planktonic cells. *J. Biotechnol.* 218, 1–12. doi: 10.1016/j.jbiotec.2015.11.017

Liu, D., Yang, Z., Chen, Y., Zhuang, W., Niu, H., Wu, J., et al. (2018). *Clostridium acetobutylicum* grows vegetatively in a biofilm rich in heteropolysaccharides and cytoplasmic proteins. *Biotechnol. Biofuels* 11:315. doi: 10.1186/s13068-018-1316-4

Lütke-Eversloh, T., and Bahl, H. (2011). Metabolic engineering of *Clostridium acetobutylicum*: recent advances to improve butanol production. *Curr. Opin. Biotechnol.* 22, 634–647. doi: 10.1016/j.copbio.2011.01.011

Neumann, G., Veeranagouda, Y., Karegoudar, T. B., Sahin, O., Mausezahl, I., Kabelitz, N., et al. (2005). Cells of *Pseudomonas* putida and *Enterobacter* sp. adapt to toxic organic compounds by increasing their size. *Extremophiles* 9, 163–168. doi: 10.1007/s00792-005-0431-x

Obana, N., Nakamura, K., and Nomura, N. (2020). Temperature-regulated heterogeneous extracellular matrix gene expression defines biofilm morphology in *Clostridium perfringens*. *NPJ Biofilms Microbiomes* 6:29. doi: 10.1038/s41522-020-00139-7

O'Toole, G. A., and Wong, G. C. (2016). Sensational biofilms: surface sensing in bacteria. *Curr. Opin. Microbiol.* 30, 139–146. doi: 10.1016/j.mib.2016.02.004

Pantaleon, V., Bouttier, S., Soavelomandroso, A. P., Janoir, C., and Candela, T. (2014). Biofilms of *Clostridium* species. *Anaerobe* 30, 193–198. doi: 10.1016/j.anaerobe.2014.09.010

Plaut, R. D., Beaber, J. W., Zemansky, J., Kaur, A. P., George, M., Biswas, B., et al. (2014). Genetic evidence for the involvement of the S-layer protein gene *sap* and the sporulation genes *spo0A*, *spo0B*, and *spo0F* in Phage AP50c infection of *Bacillus anthracis*. *J. Bacteriol.* 196, 1143–1154. doi: 10.1128/JB.00739-13

Qureshi, N., Schripsema, J., Lienhardt, J., and Blaschek, H. P. (2000). Continuous solvent production by *Clostridium beijerinckii* BA101 immobilized by adsorption onto brick. *World J. Microbiol. Biotechnol.* 16, 377–382. doi: 10.1023/A:1008984509404

Semenyuk, E. G., Laning, M. L., Foley, J., Johnston, P. F., Knight, K. L., Gerding, D. N., et al. (2014). Spore formation and toxin production in *Clostridium difficile* biofilms. *PLoS One* 9:e87757. doi: 10.1371/journal.pone.0087757

Si, H. M., Zhang, F., Wu, A. N., Han, R. Z., Xu, G. C., and Ni, Y. (2016). DNA microarray of global transcription factor mutant reveals membrane-related proteins involved in *n*-butanol tolerance in *Escherichia coli*. *Biotechnol. Biofuels* 9:114. doi: 10.1186/s13068-016-0527-9

Soavelomandroso, A. P., Gaudin, F., Hoys, S., Nicolas, V., Vedantam, G., Janoir, C., et al. (2017). Biofilm structures in a mono-associated mouse model of *Clostridium difficile* infection. *Front. Microbiol.* 8:2086. doi: 10.3389/fmicb.2017.02086

Steiner, E., Dago, A. E., Young, D. I., Heap, J. T., Minton, N. P., Hoch, J. A., et al. (2011). Multiple orphan histidine kinases interact directly with Spo0A to control the initiation of endospore formation in *Clostridium acetobutylicum*. *Mol. Microbiol.* 80, 641–654. doi: 10.1111/j.1365-2958.2011.07608.x

Wallenius, J., Maaheimo, H., and Eerikainen, T. (2016). Carbon 13-Metabolic Flux Analysis derived constraint-based metabolic modelling of *Clostridium acetobutylicum* in stressed chemostat conditions. *Bioresour. Technol.* 219, 378–386. doi: 10.1016/j.biortech.2016.07.137

Xue, C., Zhao, J., Liu, F., Lu, C., Yang, S., and Bai, F. (2013). Two-stage *in situ* gas stripping for enhanced butanol fermentation and energy-saving product recovery. *Bioresour. Technol.* 135, 396–402. doi: 10.1016/j.biortech.2012.07.062

Yang, Z., Wang, Z., Lei, M., Zhu, J., Yang, Y., Wu, S., et al. (2020). Effects of Spo0A on *Clostridium acetobutylicum* with an emphasis on biofilm formation. *World J. Microbiol. Biotechnol.* 36:80. doi: 10.1007/s11274-020-02859-6

Yen, H. W., Li, R. J., and Ma, T. W. (2011). The development process for a continuous acetone–butanol–ethanol (ABE) fermentation by immobilized *Clostridium acetobutylicum*. *J. Taiwan Inst. Chem. Eng.* 42, 902–907. doi: 10.1016/j.jtice.2011.05.006

Zhuang, W., Liu, X., Yang, J., Wu, J., Zhou, J., Chen, Y., et al. (2017). Immobilization of *Clostridium acetobutylicum* onto natural textiles and its fermentation properties. *Microb. Biotechnol.* 10, 502–512. doi: 10.1111/1751-7915.12557

Zhuang, W., Yang, J., Wu, J., Liu, D., Zhou, J., Chen, Y., et al. (2016). Extracellular polymer substances and the heterogeneity of *Clostridium acetobutylicum* biofilm induced tolerance to acetic acid and butanol. *RSC Adv.* 6, 33695–33704. doi: 10.1039/c5ra24923f

Conflict of Interest: The authors declare that the research was conducted in the absence of any commercial or financial relationships that could be construed as a potential conflict of interest.

frontiers in Bioengineering and Biotechnology

MINI REVIEW
published: 07 June 2021
doi: 10.3389/fbioe.2021.661694

Developing Clostridia as Cell Factories for Short- and Medium-Chain Ester Production

Qingzhuo Wang[1], Naief H. Al Makishah[2], Qi Li[3], Yanan Li[1], Wenzheng Liu[1], Xiaoman Sun[1], Zhiqiang Wen[1]* and Sheng Yang[4,5]*

[1] School of Food Science and Pharmaceutical Engineering, Nanjing Normal University, Nanjing, China, [2] Department of Environmental Sciences, Faculty of Meteorology, Environment and Arid Land Agriculture, King Abdulaziz University, Jeddah, Saudi Arabia, [3] College of Life Sciences, Sichuan Normal University, Chengdu, China, [4] Huzhou Center of Industrial Biotechnology, Shanghai Institutes of Biological Sciences, Chinese Academy of Sciences, Shanghai, China, [5] Key Laboratory of Synthetic Biology, CAS Center for Excellence in Molecular Plant Sciences, Shanghai Institute of Plant Physiology and Ecology, Chinese Academy of Sciences, Shanghai, China

Short- and medium-chain volatile esters with flavors and fruity fragrances, such as ethyl acetate, butyl acetate, and butyl butyrate, are usually value-added in brewing, food, and pharmacy. The esters can be naturally produced by some microorganisms. As ester-forming reactions are increasingly deeply understood, it is possible to produce esters in non-natural but more potential hosts. Clostridia are a group of important industrial microorganisms since they can produce a variety of volatile organic acids and alcohols with high titers, especially butanol and butyric acid through the CoA-dependent carbon chain elongation pathway. This implies sufficient supplies of acyl-CoA, organic acids, and alcohols in cells, which are precursors for ester production. Besides, some Clostridia could utilize lignocellulosic biomass, industrial off-gas, or crude glycerol to produce other branched or straight-chain alcohols and acids. Therefore, Clostridia offer great potential to be engineered to produce short- and medium-chain volatile esters. In the review, the efforts to produce esters from Clostridia via *in vitro* lipase-mediated catalysis and *in vivo* alcohol acyltransferase (AAT)-mediated reaction are comprehensively revisited. Besides, the advantageous characteristics of several Clostridia and clostridial consortia for bio-ester production and the driving force of synthetic biology to clostridial chassis development are also discussed. It is believed that synthetic biotechnology should enable the future development of more effective Clostridia for ester production.

Keywords: *Clostridium*, ester, lipase, alcohol acyltransferase, synthetic biology

OPEN ACCESS

Edited by:
Chuang Xue,
Dalian University of Technology, China

Reviewed by:
Adam William Westbrook,
Genecis Bioindustries Inc., Canada
Angel León-Buitimea,
Universidad Autonoma de Nuevo Leon, Mexico

***Correspondence:**
Zhiqiang Wen
zqwen@njnu.edu.cn
Xiaoman Sun
xiaomansun@njnu.edu.cn

Specialty section:
This article was submitted to Synthetic Biology, a section of the journal Frontiers in Bioengineering and Biotechnology

Received: *31 January 2021*
Accepted: *19 April 2021*
Published: *07 June 2021*

Citation:
Wang Q, Al Makishah NH, Li Q, Li Y, Liu W, Sun X, Wen Z and Yang S (2021) Developing Clostridia as Cell Factories for Short- and Medium-Chain Ester Production. Front. Bioeng. Biotechnol. 9:661694. doi: 10.3389/fbioe.2021.661694

INTRODUCTION

Short- and medium-chain volatile esters (C2–C12) with flavors and fruity fragrances are usually value-added in brewing, food, and pharmacy (Rodriguez et al., 2014; Aleksander et al., 2019). For example, ethyl acetate, ethyl lactate, butyl acetate, and ethyl hexanoate are the main components of the flavor substances in Baijiu (Chinese liquor) (Yi et al., 2019). With the expansion of the application field, the demand of esters continues to rise in recent years.

Traditionally, short- and medium-chain fatty acid esters are mainly produced by concentrated sulfuric acid-mediated esterification of acids and alcohols (Cull et al., 2003). This method has certain risks in terms of safety, health, and environment, because it usually causes serious equipment corrosion, as well as a large amount of wastewater and residues (Jermy and Pandurangan, 2005). The recently developed ionic liquid catalytic method can alleviate these problems to some extent, but it is expensive and not stable (Tankov et al., 2017). Compared to chemical methods, biosynthesis via enzyme catalysis or metabolic engineering is much more environmentally friendly and is expected to be an alternative. Indeed, the esters can be naturally produced by some yeasts and lactic acid bacteria, but the efficiency is far from satisfactory (Mukdsi et al., 2009; Kruis et al., 2018a). Therefore, a lot of efforts have been paid to develop non-natural but more potential strains as microbial cell factories for short- and medium-chain volatile ester production (Rodriguez et al., 2014; Kruis et al., 2017).

Clostridia are especially suitable hosts for ester production due to the diversity of abundant precursors, substrates, and products (Moon et al., 2016; Noh et al., 2019). In the review, we summarized the advances of ester production by Clostridia including *in vitro* lipase catalysis and *in vivo* acyltransferase reaction. Besides, we suggested some promising clostridial chassis for bio-ester production and discussed the driving force of synthetic biology in this field.

ENZYMES AND PATHWAYS IN MICROORGANISMS FOR ESTER PRODUCTION

There are mainly four kinds of ester-forming reactions reported in microorganisms that naturally produce esters. Correspondingly, four kinds of ester synthases including esterase (lipase), hemiacetal dehydrogenase, Baeyer–Villiger monooxygenases, and alcohol acyltransferase (AAT) are involved (Aleksander et al., 2019). Among them, esterase and AAT-mediated reactions are often used for ester overproduction (Aleksander et al., 2019; Noh et al., 2019).

It is a classic strategy to adapt lipase to catalyze the esterification reaction of organic acids and short-chain alcohols (Stergiou et al., 2013; Aleksander et al., 2019). Unfortunately, for the *in vitro* catalytic system, enzymes and substrates need to be produced dedicatedly, which caused complicated process routes and huge equipment costs in most cases (Stergiou et al., 2013; Aleksander et al., 2019).

Theoretically, the integration of enzyme and substrate production and catalytic reaction in one reactor is expected to dramatically reduce costs. Therefore, metabolic engineering by the condensation of alcohols and acyl-CoA using AATs is an emerging strategy, which enables some microorganisms, such as *Escherichia coli*, *Saccharomyces cerevisiae*, and *Kluyveromyces marxianus*, to produce bio-esters (Rodriguez et al., 2014; Kruis et al., 2017; Löbs et al., 2017; Bohnenkamp et al., 2020). The reported AATs are mainly derived from yeast, including *S. cerevisiae*, *K. marxianus*, *Saccharomyces bayanus*, and *Saccharomyces uvarum* (Fujii et al., 1996; Yoshimoto et al., 1998; Saerens et al., 2006). For example, in *S. cerevisiae*, alcohol acetyltransferases are mainly encoded by the genes *ATF1*, *ATF2*, *EEB1*, *EHT1*, and *EAT1* (Fujii et al., 1996; Lilly et al., 2006; Saerens et al., 2006; Kruis et al., 2018a,b). These genes have a certain compensatory effect on each other, but the catalytic activity and substrate preference of these AATs are not completely the same. Besides, AATs from different strain sources usually exhibited different catalytic activities and substrate selectivity, which explains why *E. coli* produces multiple esters after different (and even the same) AATs are introduced (Rodriguez et al., 2014).

In addition to the thoughtful selection and refined expression of AATs, challenges to balance the metabolic pathways for rational precursor distribution need to be addressed. This is because acyl-CoA is an indispensable precursor of esters, as well as fatty acids and alcohols. The metabolism of esters, fatty acids, and fatty alcohols inevitably competes for acyl-CoA (Aleksander et al., 2019; Noh et al., 2019). In *E. coli*, *S. cerevisiae* and *K. marxianus*, acyl-CoA is usually of tight supply, and the metabolic and regulatory networks for acyl-CoA synthesis and consumption are rather complicated. It challenges in distributing precursors reasonably (Rodriguez et al., 2014; Kruis et al., 2017; Löbs et al., 2017).

In contrast, Clostridia can produce a variety of volatile organic acids and alcohols (**Figure 1**), especially butanol and butyrate through the CoA-dependent carbon chain elongation pathway (Tracy et al., 2012; Cho et al., 2015). This implies sufficient supplies of acyl-CoA, organic acids, and alcohols in cells, which are precursors for ester production. Therefore, Clostridia offer great potential to be engineered to produce short- and medium-chain volatile esters. Recently, many important progresses, including lipase catalysis of fermentation broth, AAT heterologous expression, and exploration of different clostridial chassis, have been made in Clostridia-assisted ester production.

LIPASES MEDIATED ESTERIFICATION OF ALCOHOLS AND ACID FROM CLOSTRIDIA

Clostridium is a very important category of prokaryotes, composed of nearly 200 different species (Wiegel et al., 2006). Some non-pathogenic species such as *Clostridium acetobutylicum* and *Clostridium beijerinckii* are known as solventogenic Clostridia because they can utilize starch, molasses, and other sugars to produce bulk chemicals such as ethanol, butanol, and acetone (Lee et al., 2008). Some other species can directly use lignocellulose, glycerol, or syngas (H_2/CO_2, CO) as a sole carbon source to produce short-chain organic acids or alcohols (Ren et al., 2016).

These alcohols and acids are natural substrates for lipase-catalyzed esterification reactions. Therefore, adding lipase to the clostridial fermentation broth is a common strategy for ester production (Noh et al., 2019). In 2013, van den Berg et al. (2013) realized butyl butyrate biosynthesis, by adding commercially available *Candida antarctica* lipase B (CaLB; Novozym 435) into the fermentation broth of *C. acetobutylicum*. Meanwhile,

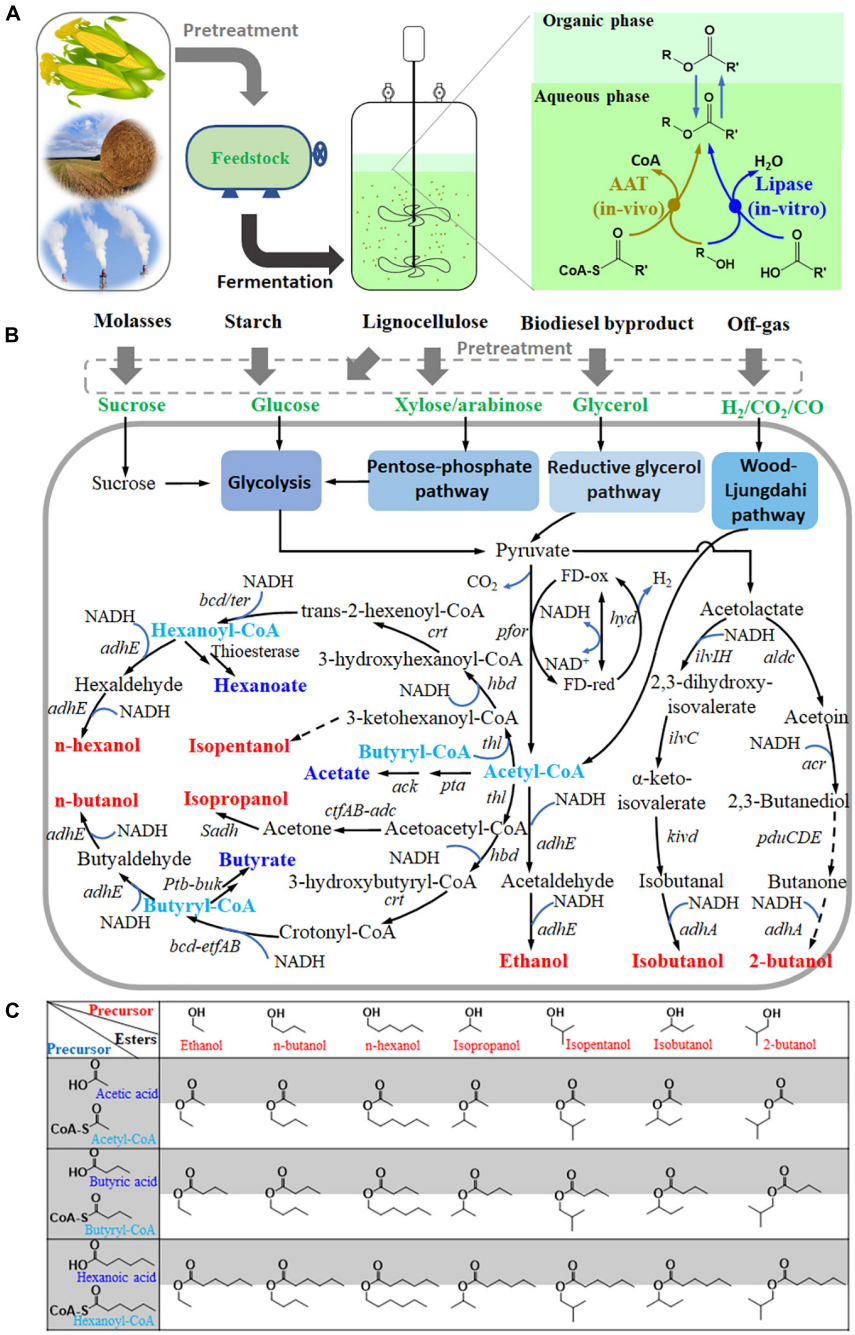

FIGURE 1 | Clostridia are promising cell factories for short- and medium-chain ester production. **(A)**, process and methods for ester production by Clostridia from various feedstocks; **(B)**, metabolic pathway for ester precursors (short-chain acids or acyl CoA, and alcohols) in some Clostridia; **(C)**, matrix of esters putatively produced by Clostridia based on the above precursors. *pfor*, pyruvate: ferredoxin oxidoreductase; *thl*, acetyl-CoA acetyltransferase; *hbd*, beta-hydroxybutyryl-CoA dehydrogenase; *crt*, crotonase; *bcd/ter*, butyryl-CoA dehydrogenase; *adhE* or *adhE1/2*, acetaldehyde/ethanol dehydrogenase; *pta*, phosphotransacetylase; *ack*, acetate kinase; *ctfAB*, acetate/butyrate-acetoacetate COA-transferase; *adc*, acetoacetate decarboxylase; *Sadh*, primary/secondary alcohol dehydrogenase; *ptb*, phosphate butyryl-transferase; *buk*, butyrate kinase; *hyd*, ferredoxin hydrogenase; *bdhA/B*, butanol dehydrogenase; *edh*, alcohol dehydrogenase; *ilvIH*, acetolactate synthase; *ilvC*, keto-acid reductoisomerase; *kivd*, α-ketoisovalerate decarboxylase; *adhA*, alcohol dehydrogenase; *aldc*, acetolactate decarboxylase; acr, acetoin reductase; *pduCDE*, diol dehydratase. Dash lines indicate putative pathways.

hexadecane was adapted to extract butyl butyrate to the organic phase, which helped in product separation and reduced the toxicity of butyl butyrate. Unfortunately, the butyl butyrate titer is only 4.9 g/L in the extractant phase because of low butyrate accumulation during ABE fermentation. Therefore, butyrate was supplemented in a later study in *Clostridium* sp.

strain BOH3 broth (Xin et al., 2016). As for the fermentation broth of *Clostridium tyrobutyricum*, a butyrate hyper-producing strain, butanol supplementation is necessary for butyl butyrate production (Zhang et al., 2017).

In order to reduce substrate costs and fermentation process complexity caused by butyrate or butanol addition, a clostridial consortium composed of *C. tyrobutyricum* and *C. beijerinckii* was established (Cui et al., 2020a). In the consortium, butyrate produced by *C. tyrobutyricum* and butanol and isopropanol produced by *C. beijerinckii* are catalyzed by exogenous lipase to form butyl butyrate and isopropyl butyrate, respectively. In another study (Seo et al., 2017), a *C. beijerinckii spo0A* (a critical regulator to shift metabolism from acidogenesis to solventogenesis) mutant was used for ester production. Since transition from butyrate to butanol is disrupted in the strain, it could produce more butyrate but less butanol compared with the wild type. Accordingly, the addition of butyrate and butanol is avoided, but exogenous lipase is still indispensable.

Although it has been reported that indigenous lipases of *Clostridium* sp. strain BOH3 can be induced by olive oil or Bio-OSR (Xin et al., 2016), indigenous lipases (with low expression level and enzymatic activity) are often not enough, and additional lipases are still required to further increase butyl-butyrate production. What is more, lipase source, lipase loading dosage, and other factors like extractant, agitation speed, and pH also affected the performance of lipase-mediated esterification in fermentation broth (Xin et al., 2016; Zhang et al., 2017).

The bottleneck of lipase-mediated esterification lies in the cost of exogenously added lipase. Fortunately, immobilized lipase and optimal reaction conditions may make the cost acceptable. An alternative option is overexpressing and secreting heterologous lipases by *Clostridium*. However, there has been almost no progress in lipase overexpression in *Clostridium* until now, because it is really challenging to engineer *Clostridium* to secrete proteins well (Wen et al., 2020c). By comparison, the *in vivo* AATs-dependent pathway is more thermodynamically favorable in an aqueous fermentation environment, but more dependent on hosts (Noh et al., 2019).

ALCOHOL ACYLTRANSFERASE-MEDIATED ESTER SYNTHESIS IN CLOSTRIDIA

Ester production in Clostridia by condensation of alcohols and acyl-CoA can be traced back to 2006 (Horton and Bennett, 2006). Horton and Bennett (2006) successfully overexpressed the *ATF2* gene from *S. cerevisiae* in wild *C. acetobutylicum* and a mutant strain M5, respectively, and realized butyl acetate production in strain M5 from glucose for the first time. Noh et al. also observed bio-ester synthesis in *C. acetobutylicum* after introducing alcohol acyltransferases (AATs) from *Fragaria x ananassa* (strawberry) or *Malus* sp. (apple), respectively (Noh et al., 2018). Interestingly, butyl butyrate accounted for about 90% of the total esters, while butyl acetate accounted for a very small proportion. In two recent studies, Fang et al. (2020) and Li et al. (2020) expressed ATF1 in *C. beijerinckii* and *Clostridium diolis*, respectively; the generated strains produced 5.42 and 1.37 g/L of butyl acetate as the main ester products from glucose. The type difference in the main ester products in the above studies may be attributed to substrate selectivity of AATs from different sources (Noh et al., 2018; Aleksander et al., 2019).

In addition to mesophilic Clostridia, the thermophilic Clostridia are also promising hosts for bio-ester production, because higher temperature could facilitate the downstream ester separation (Mazzoli and Olson, 2020). Seo et al. (2019) demonstrated that a thermostable chloramphenicol acetyltransferase from *Staphylococcus aureus* (CATSa) can work as a potential AAT in *Clostridium thermocellum*. CATSa heterologous expression in *C. thermocellum* has enabled the production of ethyl acetate and isobutyl acetate directly from cellulose. A potential drawback is ester degradation caused by the endogenous carbohydrate esterases (CEs), which hindered ester accumulation *in vivo*. Therefore, in a subsequent study, Seo et al. identified and disrupted two putative CEs (encoded by *Clo1313_0613* and *Clo1313_0693*) in *C. thermocellum*, which alleviated ester degradation and further improved isobutyl acetate production by almost 10-fold (Seo et al., 2020).

Generally, Clostridia have been proven to be potential cell factories for ester production. However, these studies mainly focus on the construction and optimization of the ester production process in Clostridia. The characteristics and advantages of Clostridia have not been fully utilized.

SEVERAL POTENTIAL CLOSTRIDIAL HOSTS FOR ESTER SYNTHESIS

Clostridial hosts for ester synthesis have been expanded from typical solventogenic Clostridia to some unconventional strains. These Clostridia with advantageous characteristics in substrate utilization and ester precursor accumulation are worth exploring and developing as novel ester production chassis.

Clostridium tyrobutyricum is one of the most efficient butyrate-producing Clostridia, which can produce about 50 g/L butyrate in batch fermentation under optimized culture conditions (Fu et al., 2017; Bao et al., 2020). Different from the solventogenic Clostridia such as *C. acetobutylicum* and *C. beijerinckii*, there is a special acetate and butyrate reassimilation mechanism in the strain. With its unique CoA transferase CAT1, acetate and butyrate can be efficiently reconverted into acetyl-CoA and butyryl-CoA, respectively, without coupling with acetone synthesis (Bao et al., 2020). The introduction of an aldehyde/alcohol dehydrogenase (encoded by *adhE2*) from *C. acetobutylicum* enabled more than 10 g/L butanol produced from glucose (Yu et al., 2011). Recently, Zhang et al. (2018) developed a gene-editing tool applicable in *C. tyrobutyricum* based on its endogenous Type IB CRISPR/Cas system. They found that when the *cat1* gene was replaced in-frame by *adhE2*, the butanol titer of the mutant reached an unprecedented 26.2 g/L. Moreover, the final concentration of by-products acetate and butyrate reached 15.2 and 2.4 g/L, respectively. High concentrations of butanol, acetate, and butyrate implied the sufficient supply of ester precursors, which

TABLE 1 | Potential Clostridia for the production of short- and medium-chain esters.

Strains or consortia	Genetic tools	Substrates	Acid or acyl-CoA precursors		Alcohol precursors	References
C. thermocellum [a]	Available[b]	Lignocellulose, sugars	Acetate	Acetyl-CoA, butyryl-CoA[c], isobutyryl-CoA	Ethanol, **butanol**[d], **isobutanol**	Lin et al., 2015; Seo et al., 2019; Tian et al., 2019; Mazzoli and Olson, 2020; Seo et al., 2020
C. cellulovorans	Available	Lignocellulose, sugars	Acetate, butyrate	Acetyl-CoA, butyryl-CoA	Ethanol, **butanol**	Sleat et al., 1984; Yang et al., 2015; Wen et al., 2020b
C. cellulolyticum	Available	Lignocellulose, sugars	Acetate	Acetyl-CoA, butyryl-CoA	Ethanol, **butanol**, **isobutanol**	Higashide et al., 2011; Gaida et al., 2016
C. phytofermentans	Unavailable	Lignocellulose, sugars	Acetate	Acetyl-CoA	Ethanol	Tolonen et al., 2015
C. clariflavum	Unavailable	Lignocellulose, sugars	Acetate	Acetyl-CoA	Ethanol	Artzi et al., 2015
C. termitidis CT111	Unavailable	Lignocellulose, sugars	Acetate	Acetyl-CoA	Ethanol	Munir et al., 2016
C. acetobutylicum	Available	Starch, sugars, glycerol	Acetate, butyrate	Acetyl-CoA, butyryl-CoA	Ethanol, butanol, **2,3-butanediol, 1,3-propanediol**	van den Berg et al., 2013; Cho et al., 2015; Noh et al., 2019
C. beijerinckii	Available	Starch, sugars, glycerol	Acetate, butyrate	Acetyl-CoA, butyryl-CoA	Ethanol, butanol	Seo et al., 2017; Fang et al., 2020
C. tyrobutyricum	Available	Starch, sugars, glycerol	Acetate, butyrate	Acetyl-CoA, butyryl-CoA	Ethanol, **butanol**	Yu et al., 2011; Fu et al., 2017; Zhang et al., 2018
C. saccharoperbutylacetonicum	Available	Starch, sugars, glycerol	Acetate, butyrate	Acetyl-CoA, butyryl-CoA	Ethanol, butanol	Noguchi et al., 2013
C. kluyveri	Available	Starch, sugars, glycerol	Acetate, butyrate, hexanoate, octanoate	Acetyl-CoA, butyryl-CoA, hexanoyl-CoA, octanoyl-CoA	Ethanol, butanol, hexanol	Seedorf et al., 2008; Steinbusch et al., 2011
C. propionicum	Available	Starch, sugars, glycerol	Acetate, propionate lactate, succinate	Acetyl-CoA	Propanol	Johns, 1952; Barbirato et al., 1997
C. pasteurianum	Available	Starch, sugars, glycerol	Acetate, butyrate	Acetyl-CoA, butyryl-CoA	1.3-Propanediol, ethanol, butanol, **1, 2-propanediol**	Malaviya et al., 2012; Groeger et al., 2016; Pyne et al., 2016; Schwarz et al., 2017
C. diolis	Available	Starch, sugars, glycerol	Acetate, butyrate	Acetyl-CoA, butyryl-CoA	Ethanol, butanol, 1,3-propanediol	Chen et al., 2018; Li et al., 2020
C. butyricum	Available	Starch, sugars, glycerol	Acetate, butyrate, 2-hydroxy-4-methylpentanoate	Acetyl-CoA, butyryl-CoA	Ethanol, 1,3-propanediol	Butel et al., 1995; Chatzifragkou et al., 2011; Miguel Serrano-Bermudez et al., 2017
Clostridium strain AK1	Unavailable	L-rhamnose	Acetate, lactate, butyrate	Acetyl-CoA, butyryl-CoA	Ethanol, 1,2-propanediol	Ingvadottir et al., 2018
C. thermosaccharolyticum HG-8	Unavailable	Sugars	Acetate, lactate	Acetyl-CoA	Ethanol, 1,2-propanediol	Altaras et al., 2001
C. thermosaccharolyticum ATCC 31960	Unavailable	Sugars	Acetate, lactate	Acetyl-CoA	Ethanol, 1,2-propanediol	Cameron and Cooney, 1986
C. sphenoides	Unavailable	Sugars	Acetate, lactate	Acetyl-CoA	Ethanol, 1,2-propanediol	Tran-Din and Gottschalk, 1985
C. ljungdahlii	Available	H_2/CO_2, CO	Acetate, butyrate, lactate	Acetyl-CoA	Ethanol, 2,3-butanediol, **butanol**	Köpke et al., 2010; Zhang L. et al., 2020
C. carboxidivorans	Unavailable	H_2/CO_2, CO	Acetate, butyrate, lactate	Acetyl-CoA, butyryl-CoA	Ethanol, butanol, hexanol	Shen et al., 2017
C. autoethanogenum	Available	H_2/CO_2, CO	Acetate, lactate	Acetyl-CoA	Ethanol, 2,3-butanediol, **butanol**	Koepke and Liew, 2012

(Continued)

TABLE 1 | Continued

Strains or consortia	Genetic tools	Substrates	Acid or acyl-CoA precursors		Alcohol precursors	References
C. scatologenes	Unavailable	H_2/CO_2, CO	Acetate, butyrate	Acetyl-CoA, butyryl-CoA	Ethanol	Song et al., 2014
C. drakei	Unavailable	H_2/CO_2, CO	Acetate, butyrate	Acetyl-CoA, butyryl-CoA	Ethanol	Gossner et al., 2008
C. thermoaceticum	Available	H_2/CO_2, CO	Acetate	Acetyl-CoA	Ethanol	Pierce et al., 2008
***C. beijerinckii* BGS1 and *C. tyrobutyricum* ATCC 27045**	Available	Starch, sugars	Acetate, butyrate	Acetyl-CoA, butyryl-CoA	Ethanol, butanol	Cui et al., 2020a
C. thermocellum and *C. saccharoperbutylacetonicum strain* N1-4	Available	Crystalline cellulose	Acetate, butyrate	Acetyl-CoA, butyryl-CoA	Ethanol, butanol	Shunichi et al., 2011
C. celevecrescens N3-2 and *C. acetobutylicum* ATCC 824	Unavailable	Filter paper	Acetate, butyrate	Acetyl-CoA, butyryl-CoA	Ethanol, butanol	Wang et al., 2015
C. cellulovorans and *C. beijerinckii*	Available	Alkali extracted corn cobs	Acetate, butyrate	Acetyl-CoA, butyryl-CoA	Ethanol, butanol	Wen et al., 2017; Wen et al., 2020a
C. thermocellum and *C. beijerinckii*	Available	Alkali extracted corn cobs	Acetate, butyrate	Acetyl-CoA, butyryl-CoA	Ethanol, butanol	Wen et al., 2014
C. ljungdahlii and C. kluyveri	Available	H_2/CO_2, CO	Acetate, butyrate, hexanoate	Acetyl-CoA, butyryl-CoA, hexanoyl-CoA	Ethanol	Richter et al., 2016

[a] *Bold fonts indicate strains or consortia that have been engineered to enable ester production.*
[b] *Double underlines indicate advantages of the strain.*
[c] *Single underline indicates limitations of the strain.*
[d] *Bold fonts indicate precursors synthesized via genetic modification.*

may contribute to achieve a very high titer of butyl acetate or butyl butyrate.

Similar to *C. tyrobutyricum*, the main product of *Clostridium cellulovorans* is also butyrate, while the difference is that it can directly grow on lignocellulosic biomass (Sleat et al., 1984). Interestingly, this strain harbors a complete CoA-dependent butanol synthesis pathway without coupled acetone production according to the prediction of KEGG, but it can hardly produce butanol. Modular metabolic engineering has enabled the strain to produce 4.96 g/L butanol from alkali-extracted corn cob (AECC) in 120 h, with 4.81 g/L butyrate and 4.14 g/L acetate residual in broth (Wen et al., 2020b), suggesting sufficient precursors for the synthesis of butyl acetate or butyl butyrate. Recently, Fang et al. claimed that they had realized butyl acetate production in *C. cellulovorans* by overexpressing *ATF1* and *adhE1*, but the detailed experimental data was not shown (Fang et al., 2020). Like *C. cellulovorans*, *Clostridium cellulolyticum* and *C. thermocellum* are also important cellulolytic Clostridia, and *C. thermocellum* has been proven to produce isobutyl acetate and isobutyl isobutyrate directly from cellulose (Seo et al., 2019; Zhang J. et al., 2020). One putative obstacle is that there are no complete pathways from acetyl-CoA to butyrate and butanol existing in *C. cellulolyticum* and *C. thermocellum*. Encouragingly, they have been successfully engineered to produce butanol (Gaida et al., 2016; Tian et al., 2019). In general, cellulolytic Clostridia offered a chance to produce esters from lignocellulose by consolidated bioprocessing.

Another reason why *C. cellulovorans* has potential as an excellent candidate host is its CO_2 fixation ability (Shinohara et al., 2013), although its fixation efficiency is much lower than gas-fermenting Clostridia. Gas-fermenting Clostridia is a major type of chemoautotrophic carbon-fixing bacteria, in which *Clostridium ljungdahlii*, *Clostridium autoethanogenum*, *Clostridium carboxidivorans* have been adapted for ethanol and butanol production from industrial waste gas (Latif et al., 2014; Bengelsdorf and Durre, 2017). Gas-fermenting Clostridia uptake and fix CO_2, CO, and H_2 by a Wood–Ljungdahl (WL) pathway (Fast et al., 2015). The energy metabolism and product synthesis in these strains may be completely different under different growth conditions, which result in product diversity (Bengelsdorf and Durre, 2017). Apart from acetate and ethanol, butyrate can be detected in the fermentation broth of *C. carboxidivorans* (Fernandez-Naveira et al., 2017a), *Clostridium drakei* (Gossner et al., 2008), *Clostridium magnum* (Groher and Weuster-Botz, 2016), and *Clostridium scatologenes* (Song et al., 2014). Moreover, butanol, hexanoate, and hexanol can also be produced by *C. carboxidivorans* (Fernandez-Naveira et al., 2017a) and *C. drakei* (Fernandez-Naveira et al., 2017b). The special substrate spectrum and product (or precursor) diversity make gas-fermenting Clostridia very suitable for different ester synthesis.

ARTIFICIAL CLOSTRIDIAL CONSORTIA OFFER SPECIAL ADVANTAGES FOR BIO-ESTER SYNTHESIS

Ester synthesis is a complex process involving multiple steps, such as the utilization of substrates, precursor production, lipase or AAT expression, and catalysis (Aleksander et al., 2019). A mixed-culture strategy has proven successful in complex

biological processes (Cui et al., 2020b; Wen et al., 2020c). The members in consortia can take on different tasks and exert their unique advantages, thereby reducing the burden, expanding the spectrum of substrates, increasing product diversity, and improving the efficiency of ester synthesis. In an aforementioned study, the titer of butyl butyrate produced from coculture of *C. beijerinckii* (the butanol producer) and *C. tyrobutyricum* (the butyrate producer) is about 10-fold obtained from the *C. beijerinckii* monoculture, implying great potential (Cui et al., 2020a). The consortia that have been adapted for cellulosic butanol production [for example, cellulolytic *C. cellulovorans* and solventogenic *C. beijerinckii* (Wen et al., 2017)] and syngas fermentation [for example, gas-fermenting *C. ljungdahlii* and hexanoate-producing *Clostridium kluyveri* (Richter et al., 2016)] could be engineered for bio-ester production by simply introducing AATs or adding lipase.

Other Clostridia that have the potential to serve as production hosts for bio-esters but have not been discussed are summarized in **Table 1**. According to the table, these distinctive Clostridia and clostridial consortia endow new possibilities for bio-ester synthesis in the aspects of efficiency improvements, broad substrate spectrum, and product diversity. However, the above studies rarely involve the complicated modification of the clostridial host, including metabolic pathway reconstruction, stress resistance modification, and refined expression regulation of AATs, which implies great potential of clostridial synthetic biotechnology to improve bio-ester production.

SYNTHETIC BIOLOGY WILL ACCELERATE DEVELOPMENT OF CLOSTRIDIAL ESTER CELL FACTORIES

Although great progress has been made in bio-ester production, the clostridial potential and advantages have not been fully exploited. Synthetic biology provided many resources and methods for clostridial chassis development, which can be applied to ester production (Joseph et al., 2018; Wen et al., 2020c).

Many genetic manipulation tools such as TargeTron, allelic exchange, CRISPR/Cas system-mediated gene, and base editing tools have been developed in Clostridia (Pyne et al., 2014; McAllister and Sorg, 2019; Wen et al., 2020d). Various genetic operations such as insertion, deletion, substitution, point mutation, and regulation of target gene expression levels can be efficiently implemented in Clostridia, which laid a good foundation for metabolic engineering (Joseph et al., 2018).

Metabolic pathway reconstruction not only increased the titer, yield, and ratio of butanol but also eliminated the by-product acetone in some Clostridia (Cho et al., 2015; Jiang et al., 2015). In addition, it also provides a chance to synthesize some new products (**Figure 1**), such as long straight-chain alcohols and acids (pentanol, hexanoate, hexanol, octanoate, and octanol) or branched-chain alcohols and acids (1,2-propanediol, isopropanol, isobutanol, 2-butanol, and isopentanol) (Pyne et al., 2016; Ren et al., 2016; Bengelsdorf and Durre, 2017). These products can serve as precursors for novel esters, which may increase the diversity of ester products.

In addition, through metabolic engineering, some Clostridia has been improved in the aspects of hexose/pentose co-fermentation (Gu et al., 2014; Mitchell, 2016), syngas utilization (Bengelsdorf and Durre, 2017; Valgepea et al., 2018), and efficient conversion of glycerol to butanol (Schwarz et al., 2017). These Clostridia can utilize inexpensive and renewable resources such as lignocellulosic biomass, industrial off-gas, or crude glycerol to produce bio-ester, which could further reduce bio-ester cost. However, there are still some putative drawbacks for some clostridial hosts (Moon et al., 2016), such as low recombineering efficiency, complex metabolic regulatory networks, by-products (like acetone) accumulation, and inefficient protein secretion system, which are highly dependent on synthetic biotechnology to solve.

It can be expected that with the further development of synthetic biology, bio-ester production by Clostridia will be closely combined with the novel AAT mining, rational metabolic network simulation and prediction, multi-omics analysis, and artificial consortia design. The ideas and technologies of synthetic biology will accelerate to develop Clostridia as more effective cell factories for ester production.

AUTHOR CONTRIBUTIONS

QW, XS, and ZW conceived the project and wrote the manuscript. All authors participated in the discussion, revised the manuscript, and approved the final manuscript.

FUNDING

This study was supported by the National Key Research and Development Program of China (No. 2019YFA0904900), the Tianjin Synthetic Biotechnology Innovation Capacity Improvement Project (TSBICIP-PTJS-003-04), and the grants from the National Natural Science Foundation of China (21706133, 21825804, 31670094, and 31971343).

REFERENCES

Aleksander, J. K. A. B., Anna, C. B. A. B., Constantinos Patinios, B. A., Youri, M. V. N. A., Mark Levisson, C., Astrid, E. M. D., et al. (2019). Microbial production of short and medium chain esters: enzymes, pathways, and applications. *Biotechnol. Adv.* 37:107407.

Altaras, N. E., Etzel, M. R., and Cameron, D. C. (2001). Conversion of sugars to 1,2-propanediol by *Thermoanaerobacterium* thermosaccharolyticum HG-8. *Biotechnol. Progress* 17, 52–56. doi: 10.1021/bp000130b

Artzi, L., Morag, E., Barak, Y., Lamed, R., and Bayer, E. A. (2015). *Clostridium clariflavum*: key cellulosome players are revealed by proteomic analysis. *Mbio* 6:e00411-15. doi: 10.1128/mBio.00411-15

Bao, T., Feng, J., Jiang, W., Fu, H., Wang, J., and Yang, S.-T. (2020). Recent advances in n-butanol and butyrate production using engineered *Clostridium tyrobutyricum*. *World J. Microbiol. Biotechnol.* 36:138. doi: 10.1007/s11274-020-02914-2

Barbirato, F., Chedaille, D., and Bories, A. (1997). Propionic acid fermentation from glycerol: comparison with conventional substrates. *Appl. Microbiol. Biotechnol.* 47, 441–446. doi: 10.1007/s002530050953

Bengelsdorf, F. R., and Durre, P. (2017). Gas fermentation for commodity chemicals and fuels. *Microb. Biotechnol.* 10, 1167–1170. doi: 10.1111/1751-7915.12763

Bohnenkamp, A. C., Kruis, A. J., Mars, A. E., Wijffels, R. H., van der Oost, J., Kengen, S. W. M., et al. (2020). Multilevel optimisation of anaerobic ethyl acetate production in engineered *Escherichia coli*. *Biotechnol. Biofuels* 13:65. doi: 10.1186/s13068-020-01703-1

Butel, M.-J., Rimbault, A., Khelifa, N., Campion, G., Szylit, O., and Rocchiccioli, F. (1995). Formation of 2-hydroxy-4-methylpentanoic acid from l-leucine by *Clostridium butyricum*. *FEMS Microbiol. Lett.* 132, 171–176. doi: 10.1016/0378-1097(95)00306-P

Cameron, D. C., and Cooney, C. L. (1986). A novel fermentation: the production of R(–)–1,2–propanediol and acetol by *Clostridium thermosaccharolyticum*. *Nat. Biotechnol.* 4, 651–654. doi: 10.1038/nbt0786-651

Chatzifragkou, A., Papanikolaou, S., Dietz, D., Doulgeraki, A. I., Nychas, G. J. E., and Zeng, A. P. (2011). Production of 1,3-propanediol by *Clostridium butyricum* growing on biodiesel-derived crude glycerol through a non-sterilized fermentation process. *Appl. Microbiol. Biotechnol.* 91, 101–112.

Chen, C., Sun, C., and Wu, Y.-R. (2018). The draft genome sequence of a novel high-efficient butanol-producing bacterium clostridium diolis strain WST. *Curr. Microbiol.* 75, 1011-1015. doi: 10.1007/s00284-018-1481-5

Cho, C., Jang, Y.-S., Moon, H. G., Lee, J., and Lee, S. Y. (2015). Metabolic engineering of clostridia for the production of chemicals. *Biofuels Bioprod. Biorefin.* 9, 211–225. doi: 10.1002/bbb.1531

Cui, Y., He, J., Yang, K.-L., and Zhou, K. (2020a). Production of isopropyl and butyl esters by *Clostridium* mono-culture and co-culture. *J. Ind. Microbiol. Biotechnol.* 47, 543–550. doi: 10.1007/s10295-020-02279-3

Cui, Y., Yang, K. L., and Zhou, K. (2020b). Using co-culture to functionalize *Clostridium* fermentation. *Trends Biotechnol.* doi: 10.1016/j.tibtech.2020.11.016 [Epub ahead of print].

Cull, S. G., Holbrey, J. D., Vargas-Mora, V., Seddon, K. R., and Lye, G. J. (2003). Room-temperature ionic liquids as replacements for organic solvents in multiphase bioprocess operations. *Biotechnol. Bioeng.* 69, 227–233.

Fang, D., Wen, Z., Lu, M., Li, A., Ma, Y., Tao, Y., et al. (2020). Metabolic and process engineering of *Clostridium beijerinckii* for butyl acetate production in one step. *J. Agric. Food Chem.* 68, 9475–9487. doi: 10.1021/acs.jafc.0c00050

Fast, A. G., Schmidt, E. D., Jones, S. W., and Tracy, B. P. (2015). Acetogenic mixotrophy: novel options for yield improvement in biofuels and biochemicals production. *Curr. Opin. Biotechnol.* 33, 60–72. doi: 10.1016/j.copbio.2014.11.014

Fernandez-Naveira, A., Abubackar, H. N., Veiga, M. C., and Kennes, C. (2017a). Production of chemicals from C1 gases (CO, CO2) by *Clostridium* carboxidivorans. *World J. Microbiol. Biotechnol.* 33:43. doi: 10.1007/s11274-016-2188-z

Fernandez-Naveira, A., Veiga, M. C., and Kennes, C. (2017b). Effect of pH control on the anaerobic H-B-E fermentation of syngas in bioreactors. *J. Chem. Technol. Biotechnol.* 92, 1178–1185.

Fu, H., Yu, L., Lin, M., Wang, J., Xiu, Z., and Yang, S.-T. (2017). Metabolic engineering of *Clostridium tyrobutyricum* for enhanced butyric acid production from glucose and xylose. *Metab. Eng.* 40, 50–58. doi: 10.1016/j.ymben.2016.12.014

Fujii, T., Yoshimoto, H., and Tamai, Y. (1996). Acetate ester production by *Saccharomyces cerevisiae* lacking the ATF1 gene encoding the alcohol acetyltransferase. *J. Ferment. Bioeng.* 81, 538–542. doi: 10.1016/0922-338X(96)81476-0

Gaida, S. M., Liedtke, A., Jentges, A. H., Engels, B., and Jennewein, S. (2016). Metabolic engineering of *Clostridium cellulolyticum* for the production of n-butanol from crystalline cellulose. *Microb Cell Fact.* 15:6. doi: 10.1186/s12934-015-0406-2

Gossner, A. S., Picardal, F., Tanner, R. S., and Drake, H. L. (2008). Carbon metabolism of the moderately acid-tolerant acetogen *Clostridium drakei* isolated from peat. *FEMS Microbiol. Lett.* 287, 236–242. doi: 10.1111/j.1574-6968.2008.01313.x

Groeger, C., Sabra, W., and Zeng, A.-P. (2016). Simultaneous production of 1,3-propanediol and n-butanol by *Clostridium pasteurianum*: in situ gas stripping and cellular metabolism. *Eng. Life Sci.* 16, 664–674. doi: 10.1002/elsc.201600058

Groher, A., and Weuster-Botz, D. (2016). Comparative reaction engineering analysis of different acetogenic bacteria for gas fermentation. *J. Biotechnol.* 228, 82–94. doi: 10.1016/j.jbiotec.2016.04.032

Gu, Y., Jiang, Y., Yang, S., and Jiang, W. (2014). Utilization of economical substrate-derived carbohydrates by solventogenic clostridia: pathway dissection, regulation and engineering. *Curr. Opin. Biotechnol.* 29, 124–131. doi: 10.1016/j.copbio.2014.04.004

Higashide, W., Li, Y., Yang, Y., and Liao, J. C. (2011). Metabolic engineering of *Clostridium cellulolyticum* for production of isobutanol from cellulose. *Appl. Environ. Microbiol.* 77, 2727–2733. doi: 10.1128/AEM.02454-10

Horton, C. E., and Bennett, G. N. (2006). Ester production in E-coli and C-acetobutylicum. *Enzyme Microb. Technol.* 38, 937–943. doi: 10.1016/j.enzmictec.2005.08.025

Ingvadottir, E. M., Scully, S. M., and Orlygsson, J. (2018). Production of (S)-1,2-Propanediol from L-rhamnose using the moderately thermophilic *Clostridium* strain AK1. *Anaerobe* 54, 26–30. doi: 10.1016/j.anaerobe.2018.07.003

Jermy, B. R., and Pandurangan, A. (2005). A highly efficient catalyst for the esterification of acetic acid using n-butyl alcohol. *J. Mol. Catal. A Chem.* 237, 146–154. doi: 10.1016/j.molcata.2005.04.034

Jiang, Y., Liu, J., Jiang, W., Yang, Y., and Yang, S. (2015). Current status and prospects of industrial bio-production of n-butanol in China. *Biotechnol. Adv.* 33, 1493–1501. doi: 10.1016/j.biotechadv.2014.10.007

Johns, A. T. (1952). The mechanism of propionic acid formation by *Clostridium propionicum*. *J. Gen. Microbiol.* 6, 123–127. doi: 10.1099/00221287-6-1-2-123

Joseph, R. C., Kim, N. M., and Sandoval, N. R. (2018). Recent developments of the synthetic biology toolkit for *Clostridium*. *Front. Microbiol.* 9:154. doi: 10.3389/fmicb.2018.00154

Koepke, M., and Liew, F. M. (2012). *Production of Butanol from Carbon Monoxide by a Recombinant Microorganism.* EP Patent Application WO 2012/053905 A1.

Köpke, M., Held, C., Hujer, S., Liesegang, H., Wiezer, A., Wollherr, A., et al. (2010). *Clostridium ljungdahlii* represents a microbial production platform based on syngas. *Proc. Natl. Acad. Sci. U.S.A.* 107:13087. doi: 10.1073/pnas.1004716107

Kruis, A. J., Gallone, B., Jonker, T., Mars, A. E., van Rijswijck, I. M. H., Wolkers–Rooijackers, J. C. M., et al. (2018a). Contribution of Eat1 and other alcohol acyltransferases to ester production in *Saccharomyces cerevisiae*. *Front. Microbiol.* 9:3202. doi: 10.3389/fmicb.2018.03202

Kruis, A. J., Levisson, M., Mars, A. E., van der Ploeg, M., Garcés Daza, F., Ellena, V., et al. (2017). Ethyl acetate production by the elusive alcohol acetyltransferase from yeast. *Metab. Eng.* 41, 92–101. doi: 10.1016/j.ymben.2017.03.004

Kruis, A. J., Mars, A. E., Kengen, S. W. M., Borst, J. W., van der Oost, J., and Weusthuis, R. A. (2018b). Alcohol acetyltransferase Eat1 is located in Yeast Mitochondria. *Appl. Environ. Microbiol.* 84:e01640-18. doi: 10.1128/AEM.01640-18

Latif, H., Zeidan, A. A., Nielsen, A. T., and Zengler, K. (2014). Trash to treasure: production of biofuels and commodity chemicals via syngas fermenting microorganisms. *Curr. Opin. Biotechnol.* 27, 79–87. doi: 10.1016/j.copbio.2013.12.001

Lee, S. Y., Park, J. H., Jang, S. H., Nielsen, L. K., Kim, J., and Jung, K. S. (2008). Fermentative butanol production by clostridia. *Biotechnol. Bioeng.* 101, 209–228. doi: 10.1002/bit.22003

Li, A., Wen, Z., Fang, D., Lu, M., Ma, Y., Xie, Q., et al. (2020). Developing *Clostridium diolis* as a biorefinery chassis by genetic manipulation. *Bioresour. Technol.* 305:123066. doi: 10.1016/j.biortech.2020.123066

Lilly, M., Bauer, F. F., Lambrechts, M. G., Swiegers, J. H., Cozzolino, D., and Pretorius, I. S. (2006). The effect of increased yeast alcohol acetyltransferase and esterase activity on the flavour profiles of wine and distillates. *Yeast* 23, 641–659. doi: 10.1002/yea.1382

Lin, P. P., Mi, L., Morioka, A. H., Yoshino, K. M., Konishi, S., Xu, S. C., et al. (2015). Consolidated bioprocessing of cellulose to isobutanol using *Clostridium* thermocellum. *Metab. Eng.* 31, 44–52. doi: 10.1016/j.ymben.2015.07.001

Löbs, A. K., Engel, R., Schwartz, C., Flores, A., and Wheeldon, I. (2017). CRISPR–Cas9-enabled genetic disruptions for understanding ethanol and ethyl acetate biosynthesis in *Kluyveromyces marxianus*. *Biotechnol. Biofuels* 10:164.

Malaviya, A., Jang, Y.-S., and Lee, S. Y. (2012). Continuous butanol production with reduced byproducts formation from glycerol by a hyper producing mutant

of *Clostridium pasteurianum*. *Appl. Microbiol. Biotechnol.* 93, 1485–1494. doi: 10.1007/s00253-011-3629-0

Mazzoli, R., and Olson, D. G. (2020). *Clostridium thermocellum*: a microbial platform for high-value chemical production from lignocellulose. *Adv. Appl. Microbiol.* 113, 111–161. doi: 10.1016/bs.aambs.2020.07.004

McAllister, K. N., and Sorg, J. A. (2019). CRISPR genome editing systems in the genus *Clostridium*: a timely advancement. *J. Bacteriol.* 201:00219-19. doi: 10.1128/jb.00219-19

Miguel Serrano-Bermudez, L., Fernando Gonzalez Barrios, A., Maranas, C. D., and Montoya, D. (2017). *Clostridium butyricum* maximizes growth while minimizing enzyme usage and ATP production: metabolic flux distribution of a strain cultured in glycerol. *BMC Syst. Biol.* 11:58. doi: 10.1186/s12918-017-0434-0

Mitchell, W. J. (2016). Sugar uptake by the solventogenic clostridia. *World J. Microbiol. Biotechnol.* 32:32. doi: 10.1007/s11274-015-1981-4

Moon, H. G., Jang, Y.-S., Cho, C., Lee, J., Binkley, R., and Lee, S. Y. (2016). One hundred years of clostridial butanol fermentation. *FEMS Microbiol. Lett.* 363:fnw001. doi: 10.1093/femsle/fnw001

Mukdsi, M. C. A., Medina, R. B., Alvarez, M. D. F., and Gonzalez, S. N. (2009). Ester synthesis by lactic acid bacteria isolated from goat's and ewe's milk and cheeses. *Food Chem.* 117, 241–247.

Munir, R. I., Spicer, V., Krokhin, O. V., Shamshurin, D., Zhang, X. L., Taillefer, M., et al. (2016). Transcriptomic and proteomic analyses of core metabolism in *Clostridium termitidis* CT1112 during growth on alpha-cellulose, xylan, cellobiose and xylose. *BMC Microbiol.* 16:91. doi: 10.1186/s12866-016-0711-x

Noguchi, T., Tashiro, Y., Yoshida, T., Zheng, J., Sakai, K., and Sonomoto, K. (2013). Efficient butanol production without carbon catabolite repression from mixed sugars with *Clostridium* saccharoperbutylacetonicum N1-4. *J. Biosci. Bioeng.* 116, 716–721. doi: 10.1016/j.jbiosc.2013.05.030

Noh, H. J., Lee, S. Y., and Jang, Y.-S. (2019). Microbial production of butyl butyrate, a flavor and fragrance compound. *Appl. Microbiol. Biotechnol.* 103, 2079-2086. doi: 10.1007/s00253-018-09603-z

Noh, H. J., Woo, J. E., Lee, S. Y., and Jang, Y.-S. (2018). Metabolic engineering of *Clostridium acetobutylicum* for the production of butyl butyrate. *Appl. Microbiol. Biotechnol.* 102, 8319–8327. doi: 10.1007/s00253-018-9267-z

Pierce, E., Xie, G., Barabote, R. D., Saunders, E., Han, C. S., Detter, J. C., et al. (2008). The complete genome sequence of *Moorella thermoacetica* (f. *Clostridium thermoaceticum*). *Environ. Microbiol.* 10, 2550–2573.

Pyne, M. E., Bruder, M., Moo-Young, M., Chung, D. A., and Chou, C. P. (2014). Technical guide for genetic advancement of underdeveloped and intractable *Clostridium*. *Biotechnol. Adv.* 32, 623–641. doi: 10.1016/j.biotechadv.2014.04.003

Pyne, M. E., Sokolenko, S., Liu, X., Srirangan, K., Bruder, M. R., Aucoin, M. G., et al. (2016). Disruption of the reductive 1,3-propanediol pathway triggers production of 1,2-propanediol for sustained glycerol fermentation by *Clostridium pasteurianum*. *Appl. Environ. Microbiol.* 82, 5375–5388. doi: 10.1128/aem.01354-16

Ren, C., Wen, Z., Xu, Y., Jiang, W., and Gu, Y. (2016). Clostridia: a flexible microbial platform for the production of alcohols. *Curr. Opin. Chem. Biol.* 35, 65–72. doi: 10.1016/j.cbpa.2016.08.024

Richter, H., Molitor, B., Diender, M., Sousa, D. Z., and Angenent, L. T. (2016). A narrow ph range supports butanol, hexanol, and octanol production from syngas in a continuous co-culture of *Clostridium ljungdahlii* and clostridium kluyveri with in-line product extraction. *Front. Microbiol.* 7:1773. doi: 10.3389/fmicb.2016.01773

Rodriguez, G. M., Tashiro, Y., and Atsumi, S. (2014). Expanding ester biosynthesis in *Escherichia coli*. *Nat. Chem. Biol.* 10:259. doi: 10.1038/nchembio.1476

Saerens, S. M., Verstrepen, K. J., Van Laere, S. D., Voet, A. R., Van Dijck, P., Delvaux, F. R., et al. (2006). The *Saccharomyces cerevisiae* EHT1 and EEB1 genes encode novel enzymes with medium-chain fatty acid ethyl ester synthesis and hydrolysis capacity. *J. Biol. Chem.* 281, 4446–4456. doi: 10.1074/jbc.M512028200

Schwarz, K. M., Grosse-Honebrink, A., Derecka, K., Rotta, C., Zhang, Y., and Minton, N. P. (2017). Towards improved butanol production through targeted genetic modification of *Clostridium pasteurianum*. *Metab. Eng.* 40, 124–137. doi: 10.1016/j.ymben.2017.01.009

Seedorf, H., Fricke, W. F., Veith, B., Bruggemann, H., Liesegang, H., Strittimatter, A., et al. (2008). The genome of *Clostridium kluyveri*, a strict anaerobe with unique metabolic features. *Proc. Natl. Acad. Sci. U.S.A.* 105, 2128–2133.

Seo, H., Lee, J.-W., Garcia, S., and Trinh, C. T. (2019). Single mutation at a highly conserved region of chloramphenicol acetyltransferase enables isobutyl acetate production directly from cellulose by *Clostridium thermocellum* at elevated temperatures. *Biotechnol. Biofuels* 12:245. doi: 10.1186/s13068-019-1583-8

Seo, H., Nicely, P. N., and Trinh, C. T. (2020). Endogenous carbohydrate esterases of *Clostridium thermocellum* are identified and disrupted for enhanced isobutyl acetate production from cellulose. *Biotechnol. Bioeng.* 117, 2223–2236. doi: 10.1002/bit.27360

Seo, S.-O., Wang, Y., Lu, T., Jin, Y.-S., and Blaschek, H. P. (2017). Characterization of a *Clostridium beijerinckii* spo0A mutant and its application for butyl butyrate production. *Biotechnol. Bioeng.* 114, 106–112. doi: 10.1002/bit.26057

Shen, S., Gu, Y., Chai, C., Jiang, W., Zhuang, Y., and Wang, Y. (2017). Enhanced alcohol titre and ratio in carbon monoxide-rich off-gas fermentation of *Clostridium carboxidivorans* through combination of trace metals optimization with variable-temperature cultivation. *Bioresour. Technol.* 239, 236–243. doi: 10.1016/j.biortech.2017.04.099

Shinohara, M., Sakuragi, H., Morisaka, H., Miyake, H., Tamaru, Y., Fukusaki, E., et al. (2013). Fixation of CO2 in *Clostridium cellulovorans* analyzed by 13C-isotopomer-based target metabolomics. *AMB Express* 3:61.

Shunichi, N., Keiji, K., Toshimori, K., and Atsumi, N. (2011). Butanol production from crystalline cellulose by cocultured *Clostridium* thermocellum and *Clostridium* saccharoperbutylacetonicum N1-4. *Appl. Environ. Microbiol.* 77, 6470–6475.

Sleat, R., Mah, R. A., and Robinson, R. (1984). Isolation and characterization of an anaerobic, cellulolytic bacterium, *Clostridium cellulovorans* sp. nov. *Appl. Environ. Microbiol.* 48, 88–93.

Song, Y., Jeong, Y., Shin, H. S., and Cho, B. K. (2014). Draft genome sequence of *Clostridium* scatologenes ATCC 25775, a chemolithoautotrophic acetogenic bacterium producing 3-methylindole and 4-methylphenol. *Genome Announc.* 2:e00459-14. doi: 10.1128/genomeA.00459-14

Steinbusch, K. J. J., Hamelers, H. V. M., Plugge, C. M., and Buisman, C. J. N. (2011). Biological formation of caproate and caprylate from acetate: fuel and chemical production from low grade biomass. *Energy Environ. Sci.* 4, 216–224.

Stergiou, P. Y., Foukis, A., Filippou, M., Koukouritaki, M., Parapouli, M., Theodorou, L. G., et al. (2013). Advances in lipase-catalyzed esterification reactions. *Biotechnol. Adv.* 31, 1846–1859. doi: 10.1016/j.biotechadv.2013.08.006

Tankov, I., Mitkova, M., Nikolova, R., Veli, A., and Stratiev, D. (2017). n-Butyl acetate synthesis in the presence of pyridinium-based acidic ionic liquids: influence of the anion nature. *Catal. Lett.* 147, 2279–2289. doi: 10.1007/s10562-017-2135-0

Tian, L., Conway, P. M., Cervenka, N. D., Cui, J., Maloney, M., Olson, D. G., et al. (2019). Metabolic engineering of *Clostridium* thermocellum for n-butanol production from cellulose. *Biotechnol. Biofuels* 12:186. doi: 10.1186/s13068-019-1524-6

Tolonen, A. C., Zuroff, T. R., Ramya, M., Boutard, M., Cerisy, T., and Curtis, W. R. (2015). Physiology, genomics, and pathway engineering of an ethanol-tolerant strain of *Clostridium* phytofermentans. *Appl. Environ. Microbiol.* 81, 5440–5448. doi: 10.1128/aem.00619-15

Tracy, B. P., Jones, S. W., Fast, A. G., Indurthi, D. C., and Papoutsakis, E. T. (2012). Clostridia: the importance of their exceptional substrate and metabolite diversity for biofuel and biorefinery applications. *Curr. Opin. Biotechnol.* 23, 364–381. doi: 10.1016/j.copbio.2011.10.008

Tran-Din, K., and Gottschalk, G. (1985). Formation of d(-)-1,2-propanediol and d(-)-lactate from glucose by *Clostridium* sphenoides under phosphate limitation. *Arch. Microbiol.* 142, 87–92. doi: 10.1007/BF00409243

Valgepea, K., Lemgruber, R. D. S. P., Abdalla, T., Binos, S., Takemori, N., Takemori, A., et al. (2018). H-2 drives metabolic rearrangements in gas-fermenting *Clostridium* autoethanogenum. *Biotechnol. Biofuels* 11:55. doi: 10.1186/s13068-018-1052-9

van den Berg, C., Heeres, A. S., van der Wielen, L. A. M., and Straathof, A. J. J. (2013). Simultaneous clostridial fermentation, lipase-catalyzed esterification, and ester extraction to enrich diesel with butyl butyrate. *Biotechnol. Bioeng.* 110, 137–142. doi: 10.1002/bit.24618

Wang, Z., Cao, G., Zheng, J., Fu, D., Song, J., Zhang, J., et al. (2015). Developing a mesophilic co-culture for direct conversion of cellulose to butanol in consolidated bioprocess. *Biotechnol. Biofuels* 8, 1–9.

Wen, Z., Ledesma-Amaro, R., Lu, M., Jiang, Y., Gao, S., Jin, M., et al. (2020a). Combined evolutionary engineering and genetic manipulation improve low pH tolerance and butanol production in a synthetic microbialClostridiumcommunity. *Biotechnol. Bioeng.* 117, 2008–2022. doi: 10.1002/bit.27333

Wen, Z., Ledesma-Amaro, R., Lu, M., Jin, M., and Yang, S. (2020b). Metabolic engineering of *Clostridium* cellulovorans to improve butanol production by consolidated bioprocessing. *ACS Synth. Biol.* 9:304. doi: 10.1021/acssynbio.9b00331

Wen, Z., Li, Q., Liu, J., Jin, M., and Yang, S. (2020c). Consolidated bioprocessing for butanol production of cellulolytic Clostridia: development and optimization. *Microb. Biotechnol.* 13, 410–422. doi: 10.1111/1751-7915.13478

Wen, Z., Lu, M., Ledesma-Amaro, R., Li, Q., Jin, M., and Yang, S. (2020d). TargeTron technology applicable in solventogenic Clostridia: revisiting 12 Years' advances. *Biotechnol. J.* 15:e1900284. doi: 10.1002/biot.201900284

Wen, Z., Minton, N. P., Zhang, Y., Li, Q., Liu, J., Jiang, Y., et al. (2017). Enhanced solvent production by metabolic engineering of a twin-clostridial consortium. *Metab. Eng.* 39, 38–48. doi: 10.1016/j.ymben.2016.10.013

Wen, Z., Wu, M., Lin, Y., Yang, L., Lin, J., and Cen, P. (2014). A novel strategy for sequential co-culture of *Clostridium thermocellum* and *Clostridium beijerinckii* to produce solvents from alkali extracted corn cobs. *Process Biochem.* 49, 1941–1949. doi: 10.1016/j.procbio.2014.07.009

Wiegel, J., Tanner, R., and Rainey, F. A. (2006). "An introduction to the family clostridiaceae," in *The Prokaryotes*. (eds) M. Dworkin, S. Falkow, E. Rosenberg, K. H. Schleifer, and E. Stackebrandt (New York, NY: Springer)

Xin, F., Basu, A., Yang, K.-L., and He, J. (2016). Strategies for production of butanol and butyl-butyrate through lipase-catalyzed esterification. *Bioresour. Technol.* 202, 214–219. doi: 10.1016/j.biortech.2015.11.068

Yang, X., Xu, M., and Yang, S. T. (2015). Metabolic and process engineering of *Clostridium cellulovorans* for biofuel production from cellulose. *Metab. Eng.* 32, 39–48. doi: 10.1016/j.ymben.2015.09.001

Yi, Z., Jin, Y., Xiao, Y., Chen, L., Tan, L., Du, A., et al. (2019). Unraveling the contribution of high temperature stage to Jiang-Flavor Daqu, a liquor starter for production of Chinese Jiang-flavor Baijiu, with special reference to metatranscriptomics. *Front. Microbiol.* 10:472. doi: 10.3389/fmicb.2019.00472

Yoshimoto, H., Fujiwara, D., Momma, T., Ito, C., Sone, H., Kaneko, Y., et al. (1998). Characterization of the ATF1 and Lg-ATF1 genes encoding alcohol acetyltransferases in the bottom fermenting yeast Saccharomyces pastorianus. *J. Ferment. Bioeng.* 86, 15–20. doi: 10.1016/S0922-338X(98)80027-5

Yu, M., Zhang, Y., Tang, I. C., and Yang, S.-T. (2011). Metabolic engineering of *Clostridium* tyrobutyricum for n-butanol production. *Metab. Eng.* 13, 373–382. doi: 10.1016/j.ymben.2011.04.002

Zhang, J., Hong, W., Guo, L., Wang, Y., and Wang, Y. (2020). Enhancing plasmid transformation efficiency and enabling CRISPR-Cas9/Cpf1-based genome editing in *Clostridium tyrobutyricum*. *Biotechnol. Bioeng.* 117, 2911–2917. doi: 10.1002/BIT.27435

Zhang, J., Zong, W., Hong, W., Zhang, Z.-T., and Wang, Y. (2018). Exploiting endogenous CRISPR-Cas system for multiplex genome editing in *Clostridium tyrobutyricum* and engineer the strain for high-level butanol production. *Metab. Eng.* 47, 49–59. doi: 10.1016/j.ymben.2018.03.007

Zhang, L., Zhao, R., Jia, D., Jiang, W., and Gu, Y. (2020). Engineering *Clostridium ljungdahlii* as the gas-fermenting cell factory for the production of biofuels and biochemicals. *Curr. Opin. Chem. Biol.* 59, 54–61. doi: 10.1016/j.cbpa.2020.04.010

Zhang, Z.-T., Taylor, S., and Wang, Y. (2017). In situ esterification and extractive fermentation for butyl butyrate production with *Clostridium tyrobutyricum*. *Biotechnol. Bioeng.* 114, 1428–1437. doi: 10.1002/bit.26289

Conflict of Interest: The authors declare that the research was conducted in the absence of any commercial or financial relationships that could be construed as a potential conflict of interest.

frontiers in Bioengineering and Biotechnology

ORIGINAL RESEARCH
published: 08 June 2021
doi: 10.3389/fbioe.2021.669462

Ribozyme-Mediated Downregulation Uncovers DNA Integrity Scanning Protein A (DisA) as a Solventogenesis Determinant in *Clostridium beijerinckii*

Victor Chinomso Ujor[1], Lien B. Lai[2], Christopher Chukwudi Okonkwo[3], Venkat Gopalan[2] and Thaddeus Chukwuemeka Ezeji[3]**

[1] Fermentation Science Program, Department of Food Science, University of Wisconsin-Madison, Madison WI, United States, [2] Department of Chemistry and Biochemistry, Center for RNA Biology, The Ohio State University, Columbus, OH, United States, [3] Department of Animal Sciences, Ohio State Agricultural Research and Development Center, The Ohio State University, Wooster, OH, United States

OPEN ACCESS

Edited by:
Petra Patakova,
University of Chemistry and Technology in Prague, Czechia

Reviewed by:
Qiuqiang Gao,
Columbia University, United States
Jingyu Wang,
Westlake Institute for Advanced Study, China
Yi Wang,
Auburn University, United States

***Correspondence:**
Thaddeus Chukwuemeka Ezeji
ezeji.1@osu.edu
Venkat Gopalan
gopalan.5@osu.edu

Specialty section:
This article was submitted to Synthetic Biology, a section of the journal Frontiers in Bioengineering and Biotechnology

Received: 18 February 2021
Accepted: 04 May 2021
Published: 08 June 2021

Citation:
Ujor VC, Lai LB, Okonkwo CC, Gopalan V and Ezeji TC (2021) Ribozyme-Mediated Downregulation Uncovers DNA Integrity Scanning Protein A (DisA) as a Solventogenesis Determinant in Clostridium beijerinckii. Front. Bioeng. Biotechnol. 9:669462. doi: 10.3389/fbioe.2021.669462

Carbon catabolite repression (CCR) limits microbial utilization of lignocellulose-derived pentoses. To relieve CCR in *Clostridium beijerinckii* NCIMB 8052, we sought to downregulate catabolite control protein A (CcpA) using the M1GS ribozyme technology. A CcpA-specific ribozyme was constructed by tethering the catalytic subunit of *Escherichia coli* RNase P (M1 RNA) to a guide sequence (GS) targeting CcpA mRNA ($M1GS^{CcpA}$). As negative controls, the ribozyme $M1GS^{CcpA-Sc}$ (constructed with a scrambled GS^{CcpA}) or the empty plasmid pMTL500E were used. With a ∼3-fold knockdown of CcpA mRNA in *C. beijerinckii* expressing $M1GS^{CcpA}$ (*C. beijerinckii*_$M1GS^{CcpA}$) relative to both controls, a modest enhancement in mixed-sugar utilization and solvent production was achieved. Unexpectedly, *C. beijerinckii*_$M1GS^{CcpA-Sc}$ produced 50% more solvent than *C. beijerinckii*_pMTL500E grown on glucose + arabinose. Sequence complementarity (albeit suboptimal) suggested that $M1GS^{CcpA-Sc}$ could target the mRNA encoding DNA integrity scanning protein A (DisA), an expectation that was confirmed by a 53-fold knockdown in DisA mRNA levels. Therefore, $M1GS^{CcpA-Sc}$ was renamed $M1GS^{DisA}$. Compared to *C. beijerinckii*_$M1GS^{CcpA}$ and _pMTL500E, *C. beijerinckii*_$M1GS^{DisA}$ exhibited a 7-fold decrease in the intracellular c-di-AMP level after 24 h of growth and a near-complete loss of viability upon exposure to DNA-damaging antibiotics. Alterations in c-di-AMP-mediated signaling and cell cycling likely culminate in a sporulation delay and the solvent production gains observed in *C. beijerinckii*_$M1GS^{DisA}$. Successful knockdown of the CcpA and DisA mRNAs demonstrate the feasibility of using M1GS technology as a metabolic engineering tool for increasing butanol production in *C. beijerinckii*.

Keywords: butanol, carbon catabolite repression, M1GS, solventogenesis, metabolic engineering, *Clostridium beijerinckii*, RNase P

INTRODUCTION

The ability of solventogenic *Clostridium* species to utilize a wide range of sugar substrates to produce acetone, butanol, and ethanol (ABE) makes them suitable candidates for generating transport fuels and chemical feedstocks from renewable biomaterials (Jones and Woods, 1986; Grupe and Gottschalk, 1992; Ezeji et al., 2010). Among solvents produced by these Gram-positive, obligately anaerobic, spore-forming bacteria, butanol has drawn the most attention. Owing to its physico-chemical properties, butanol is an ideal transport fuel and has numerous applications in food, plastic, and rubber industries (Ezeji et al., 2003, 2010). However, bio-butanol production is currently economically unviable due to the high cost of substrates, low productivity, and low yield (Ezeji et al., 2007).

Lignocellulose, the most plentiful renewable resource for production of fermentable sugars, has been explored as an inexpensive substrate (Ho et al., 1998; Ezeji et al., 2007; Ren et al., 2010). Hydrolysis of lignocellulose releases mainly glucose and xylose with small amounts of other sugars including arabinose and mannose (Ho et al., 1998; Zverlov et al., 2006; Ezeji et al., 2007). Depending on the source, lignocellulosic biomass hydrolysates (LBH) can contain up to 58% glucose and 36% pentose (xylose + arabinose). While clostridia can utilize all these sugars, pentose utilization is drastically limited in the presence of glucose, an attribute that hampers solvent yield and productivity from LBH (Ounine et al., 1985; Mitchell, 1998; Ren et al., 2010). Thus, overriding this hierarchy in sugar utilization, a phenomenon named carbon catabolite repression (CCR), has been an important research objective in this field.

CCR is globally mediated by catabolite control protein A (CcpA), which in the presence of glucose represses the expression of numerous genes involved in the utilization of non-glucose substrates (Ludwig et al., 2002; Singh et al., 2008; Ren et al., 2010). Indeed, CcpA knockout in *Clostridium acetobutylicum* ATCC 824 led to concomitant utilization of glucose and xylose (Ren et al., 2010). However, compared to the wild type, this knockout strain was (i) less stable, (ii) produced less ABE and more acids (likely due to poor acid re-assimilation), and (iii) exhibited impaired sporulation (Ren et al., 2010, 2012). Such a broad range of effects was perhaps to be expected since CcpA, besides regulating carbon metabolism, exerts a pleiotropic effect on the expression of diverse genes unrelated to carbon utilization in *C. acetobutylicum* (Ren et al., 2012), *Bacillus subtilis* (Ludwig et al., 2002), *Enterococcus faecalis* (Leboeuf et al., 2000), and *Lactobacillus plantarum* (Mazzeo et al., 2012). In *C. acetobutylicum*, global transcriptomic analysis of the CcpA-null mutant relative to the wild type revealed that CcpA upregulates key solventogenic and sporulation genes, while negatively influencing the expression of acidogenic genes (Ren et al., 2012). Given the multiple roles of CcpA, we reasoned that a knockdown strain with some residual function would relieve CCR without engendering all the negative effects observed with the CcpA knockout. We therefore explored a ribozyme (RNase P)-mediated approach to knock down CcpA mRNA in *C. beijerinckii* NCIMB 8052.

In all domains of life, the primary function of RNase P is to remove the 5′ leader from precursor tRNAs (pre-tRNAs; Scott and Engelke, 2006; Altman, 2007; Lai et al., 2010). The ribonucleoprotein (RNP) form of bacterial RNase P comprises a catalytic RNA subunit (termed M1 RNA in *Escherichia coli*) and one protein cofactor. Any cellular RNA could be targeted for cleavage by RNase P (Forster and Altman, 1990; Guerrier-Takada and Altman, 2000) if the binding of the target RNA to a guide sequence (GS) forms a sequence- and structure-specific complex resembling the acceptor–T-stem helical stack in the pre-tRNA, a key recognition determinant of RNase P. The design also includes an (A/G)CCA sequence at the 3′ end of the GS to mimic the 3′ end of pre-tRNAs. An important variation that enhanced the efficiency of this method is the covalent tethering of M1 RNA to the GS (Li and Altman, 1996; Liu, 2010). When the GS in such an engineered M1GS binds an accessible, single-stranded region in its target RNA to form a stem substrate, the bipartite substrate is cleaved *in cis* by the covalently attached M1 RNA (**Figure 1A**). Scrambling the GS while retaining the nucleotide composition provides a control to assess specificity of targeting. Given the proven utility of this method for targeted degradation of RNAs in bacteria, mammalian cells, and mice (Li and Altman, 1996; Bai et al., 2010, 2011; Liu, 2010), we sought its application for knocking down CcpA in *C. beijerinckii*.

While expression of a customized CcpA-specific M1 RNA-based ribozyme ($M1GS^{CcpA}$) in *C. beijerinckii* displayed a 3-fold knockdown in the CcpA mRNA level and a small but discernible increase in ABE production, we unexpectedly found that the specificity control M1GS with a scrambled GS^{CcpA} resulted in a 1.5-fold increase in ABE titer compared to a strain transformed with the empty vector. Upon further investigation, we found that the scrambled GS^{CcpA} targeted the mRNA encoding DNA integrity scanning protein A (DisA) and caused a 53-fold decrease in the DisA mRNA steady-state level. DisA monitors genomic integrity at the onset of sporulation and recruits the DNA repair machinery upon detection of DNA damage (Oppenheimer-Shaanan et al., 2011). While DisA scans the genomic DNA, it produces cyclic diadenosine monophosphate (c-di-AMP), a second messenger critical for cellular homeostasis (Stülke and Krüger, 2020). In fact, c-di-AMP activates Spo0A, a master transcriptional regulator of sporulation. Thus, $M1GS^{DisA}$-mediated knockdown of DisA might enhance solventogenesis by delaying sporulation. In addition to uncovering this unanticipated nexus between DisA, c-di-AMP, and ABE production, our work demonstrates the utility of the M1GS technology as a tool for metabolic engineering of *C. beijerinckii* and likely other solventogenic *Clostridium* species.

MATERIALS AND METHODS

M1GS Design and Cloning

Translational initiation requires binding of the ribosome to a single-stranded region near the start codon. Therefore, we used the mfold web server (Zuker, 2003), which predicts RNA secondary structures based on energy minimization, to

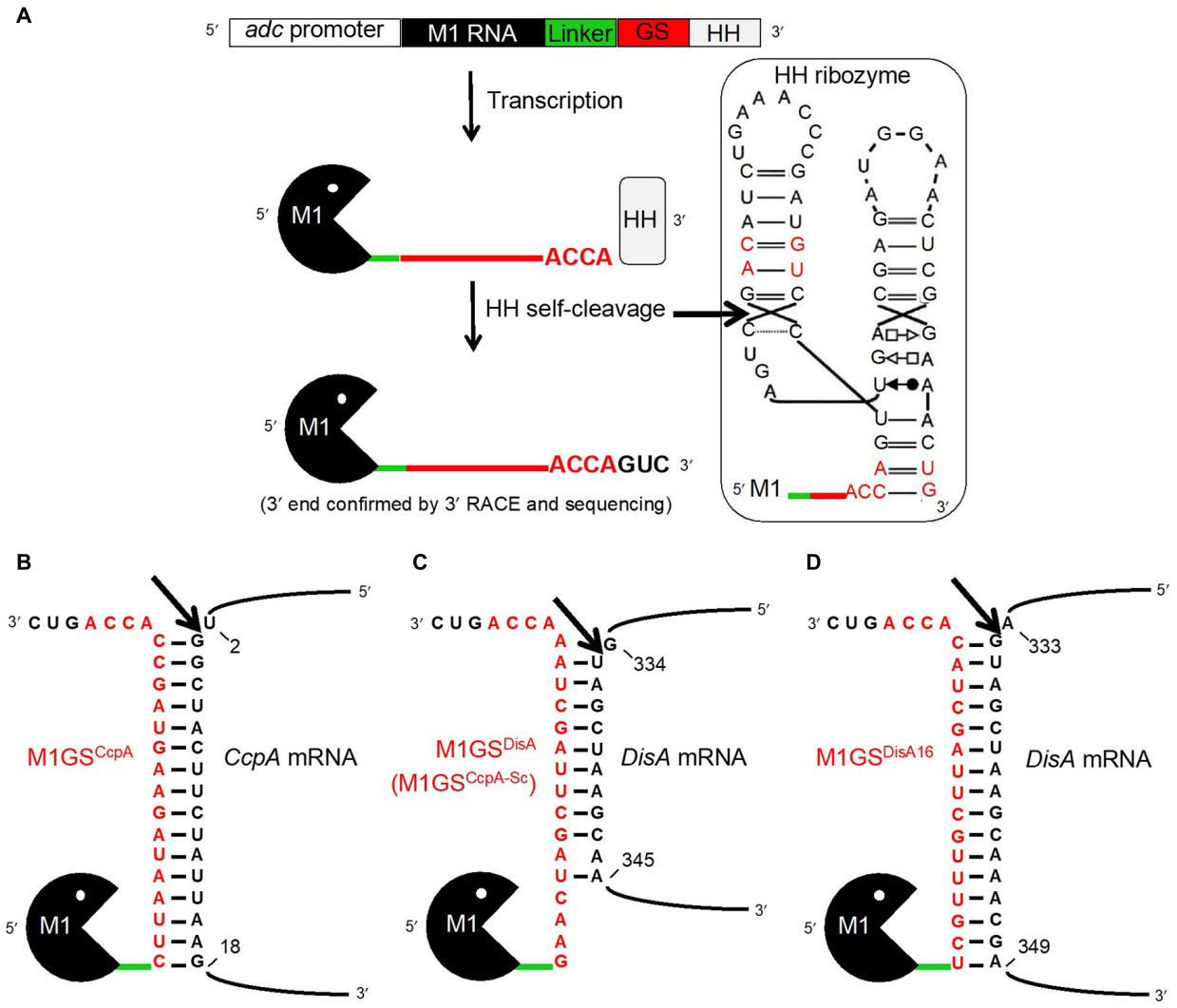

FIGURE 1 | The M1GS approach. **(A)** The M1GS construct was transcriptionally controlled by the *C. acetobutylicum adc* promoter. A 51-nucleotide linker between M1 RNA and the GS was engineered to allow flexibility between them. After transcription, the hammerhead (HH) ribozyme self-cleaved with high efficiency at the precise location indicated by the arrow in the inset, leaving the M1GS transcripts with only three additional 3′ nucleotides. The inset shows the M1GS transcript with the full secondary structure of the HH ribozyme; the red-colored nucleotides are those that were modified to facilitate cloning and to minimize the number of additional bases at the 3′ ends of M1GS. Annealing of M1GS^{CcpA} **(B)**, M1GS^{DisA} **(C)**, and M1GS^{DisA16} **(D)** to their respective target mRNAs. The numbers indicate the nucleotide positions targeted by the ribozymes in the mRNAs (with AUG numbering 1-3). The arrows indicate where the tethered M1 RNA is expected to cleave the mRNAs.

determine single-strandedness in nucleotides −25 to +55 of the CcpA open reading frame (ORF). Such an analysis led us to design GS^{CcpA} for targeting nucleotides 3-18 of the CcpA ORF (**Figure 1B**). The scrambled version GS$^{CcpA-Sc}$, which was originally intended as a negative control for GS^{CcpA}, was subsequently discovered to fortuitously target nucleotides 335-343 of the DisA ORF (**Figure 1C**). These sequences including the 3′ACCA were inserted between the linker and the hammerhead (HH) ribozyme sequences in pBT7–M1-HH, a template vector that harbored sequences for M1 RNA, a 51-nucleotide linker, and a HH ribozyme in tandem (**Figure 1A**) and downstream of the T7 RNA polymerase promoter. Using inverse PCR and back-to-back primers (**Table 1**) flanking the linker-HH border [GS/HH-F and a reverse primer that includes the GS sequence: GS(CcpA)-R or GS(CcpA-Sc)-R], the entire pBT7–M1GS-HH plasmid was amplified, circularized by ligation, and used to transform *E. coli* DH5α cells. Subsequently, primers 5′M1(*Apa*I)-F and 3′HH(*Xho*I)-R were used to introduce an *Apa*I and a *Xho*I site by PCR just upstream of M1 RNA and downstream of HH, respectively, using pBT7–M1GS-HH as the template. After digestion with *Apa*I and *Xho*I, the PCR products were cloned into pWUR459 (under the control of an inducible *adc* promoter; Siemerink et al., 2011) that had been digested with the same restriction enzymes.

Since only nine contiguous nucleotides in DisA ORF were complementary to M1GS^{DisA} (**Figure 1C**), we constructed

TABLE 1 | Sequences of oligonucleotides used in this study.

Primer Name	Target gene/template	Sequence (5′ → 3′)
GS/HH-F	M1GS	ACCAGTCGACA TCTGAAACCC
GS(CcpA)-R	M1GS^{CcpA}	GGCTACTTCTATT AAGAAACCTATG ACCATGATTA
GS(CcpA-Sc)-R	M1GS^{DisA}	TTAGCTAAGCTAGT TCAAACCTATGA CCATGATTA
5′M1(*Apa*I)-F	M1GS	CATGGGCCC GAAGCTGACCAGAC
3′HH(*Xho*I)-R	M1GS	CGTGCTCGAGG TGAAACTGACC
M1-F	*E. coli* M1 RNA	GACCAGTGC AACAGAGAGC
M1-R	*E. coli* M1 RNA	GTCGTGGACA GTCATTCATC
Cbei_R0124-F	*C. beijerinckii* 16S rRNA	GAAGAATACCAG TGGCGAAGGC
Cbei_R0124-R	*C. beijerinckii* 16S rRNA	ATTCATCGTT TACGGCGTGGAC
Cbei_0047-F	*C. beijerinckii* CcpA	GTTGCAAAAG AAGCAGGAG
Cbei_0047-R	*C. beijerinckii* CcpA	CAGCACCTCT TACAATTTCTG
Cbei_0127-F	*C. beijerinckii* DisA	GAAACAGGAAC TAGGCATAGAAC
Cbei_0127-R	*C. beijerinckii* DisA	CTTGATTTGCCT TTCCAAG
M1p3-F (delta-M1GS)	*C. beijerinckii* DisA-16	GCTTCGTCGTC GTCCTCTTCG
M1p12-R (delta-M1GS)	*C. beijerinckii* DisA-16	CCATCGGCGG TTTGCTCTCTG
F-ext	pBT7 vector	CGACGTTGTAAAA CGACGGCCAG
M1GS-3F	M1GS	GAAGCTGACCA GACAGTCGC
M1-4F	M1GS	AGGGTGCCA GGTAACGCC

M1GS^{DisA16} that targets 16 nucleotides (334-349) in DisA ORF (**Figure 1D**). For use as a negative control, we generated ΔM1GS^{DisA16} where an M1 RNA deletion mutant (ΔM1) substituted for the wild type such a control provides an opportunity to assess gene expression changes arising solely from antisense effects (Liu and Altman, 1995; Gopalan et al., 2002). All the cloned inserts were verified by sequencing before using to transform *C. beijerinckii*.

Strains and Culture Conditions

Clostridium beijerinckii NCIMB 8052 was obtained from the American Type Culture Collection (Manassas, VA, United States) as *C. beijerinckii* ATCC 51743 (the same strain is labeled differently as NCIMB 8052 by the NCIMB culture collection, United Kingdom). Laboratory stocks were maintained as spore suspensions in sterile, double-distilled water at 4°C. All cultures were grown at 35 ± 1°C in tryptone-glucose-yeast extract (TGY; 30, 20, and 10 g/L, respectively) broth, and in an anaerobic chamber (Coy Laboratory Products Inc., Grass Lake, MI, United States) with a modified atmosphere of 82% N_2, 15% CO_2, and 3% H_2.

To obtain *C. beijerinckii*_M1GS^{DisA}, _M1GS^{CcpA}, _M1GS^{DisA16}, ΔM1GS^{DisA16}, and _pMTL500E, transformation of *C. beijerinckii* with the corresponding M1GS constructs or the parental plasmid pMTL500E was conducted as described by Kim and Blaschek (1993) with minor modifications. First, a starter culture was grown for 12 h before sub-culturing [10% (v/v) inoculum] into fresh TGY broth and grown until late-exponential phase (OD_{600} ∼1.2). For each transformation, 10 mL of cells were harvested, washed with electroporation solution [10% (w/v) polyethylene glycol 8000 in distilled water], and re-suspended in 1 mL of the same solution. Four hundred μl of this suspension was then mixed with 10 μg of plasmid DNA and subjected to electroporation at 2.5 kV, 25 μF, and infinite resistance in a Gene Pulser (Bio-Rad, Hercules, CA, United States). Subsequently, cells were quickly transferred to 5 mL of TGY broth and grown for 8 h, before being plated on TGY agar [0.45% (w/v) agar] containing erythromycin (25 μg/mL) and incubated overnight at 35 ± 1°C. Single colonies were then suspended in 500 μl of TGY, re-streaked on TGY agar (+25 μg/mL erythromycin), and incubated overnight at 35 ± 1°C. Fresh colonies were then picked and grown in TGY broth for 12 h to make a glycerol stock. In parallel, cells were sub-cultured into P2 medium containing 60 g/L glucose (+25 μg/mL erythromycin) and grown for 7 days to generate spores for subsequent experiments. The P2 medium (100 mL) used for fermentative characterization of the strains contained 60 g/L glucose, arabinose or xylose, or glucose-pentose mixtures totaling 60 g/L sugars [40 g/L glucose and 20 g/L pentose (arabinose or xylose)] and 1 g/L yeast extract supplemented with 1 mL each of buffer, vitamin, and mineral stocks. The buffer stock contained K_2HPO_4 (50 g/L) and ammonium acetate (220 g/L), while the vitamin stock contained *p*-amino-benzoic acid (0.1 g/L), thiamine (0.1 g/L), and biotin (0.001 g/L). The mineral stock comprised $MgSO_4{\cdot}7H_2O$ (20 g/L) $MnSO_4{\cdot}H_2O$ (1 g/L), $FeSO_4{\cdot}7H_2O$ (1 g/L), and NaCl (1 g/L).

For fermentation, all cultures were grown in loosely capped 250-mL Pyrex culture bottles at 35 ± 1°C. For phenotypic characterization of *C. beijerinckii*_M1GS^{DisA}, _M1GS^{CcpA}, _M1GS^{DisA16}, _ΔM1GS^{DisA16}, and _pMTL500E, inoculum generation and fermentation were conducted as described above (also see Ujor et al., 2014). Cultures for the determination of intracellular c-di-AMP levels were grown in the glucose + arabinose medium for 60 h with aliquots withdrawn every 12 h starting at 0 h. In addition to the standard potassium phosphate buffer (K_2HPO_4, 0.5 g/L final concentration), all fermentation media were buffered with 2-(N-morpholino) ethanesulfonic acid (MES; 7 g/L) and supplemented with erythromycin (25 μg/mL).

RNA Isolation and RT-Quantitative PCR (RT-qPCR)

Cell pellets from 6 mL of culture grown in glucose + arabinose medium for 24 h were used for RNA isolation. RNA was isolated individually from triplicate cultures of *C. beijerinckii* strains

(_M1GS^{DisA}, _M1GS^{CcpA}, _M1GS^{DisA16}, _ΔM1GS^{DisA16}, or _pMTL500E). Each cell pellet was suspended in 1 mL of TRI Reagent (Sigma, St. Louis, MO, United States) and lysed by passing through Tissue Lyser LT (Qiagen, Hilden, Germany) at maximal oscillation for 2 min. Subsequent RNA isolation steps were performed as per manufacturer's instructions. Reverse transcription of RNA was carried out with 2 μg of total RNA using random hexamers and M-MLV Reverse Transcriptase (Promega, Madison, WI, United States). Quantitative PCR (20 μl final volume) was then conducted with DyNAmo HS SYBR Green qPCR Master Mix (Thermo Fisher Scientific, Waltham, MA, United States), using gene-specific primers (**Table 1**) for M1 RNA (M1-F & R), ΔM1RNA (M1p3-F & M1p12-R), CcpA (Cbei_0047- F & R), and DisA (Cbei_0127- F & R). Each of the triplicate RNA preparations was analyzed twice in a BioRad iCycler continuous fluorescence detection system (BioRad, Hercules, CA, United States), with the following cycling conditions: 95°C – 15 min; 40 cycles of 95°C – 10 s and 55°C – 60 s. The levels of respective RNAs were normalized to 16S rRNA (Zhang and Ezeji, 2013).

Determination of M1GS and DisA Copy Number per Cell

The reference RNAs were first generated using run-off *in vitro* transcription. For M1GS, the reference M1 RNA was obtained using as template *Fok*I-linearized pJA2′ (Vioque et al., 1988). For the DisA mRNA, a fragment corresponding to nucleotides 301-460 of the DisA ORF was first amplified by PCR using primers Cbei_0127-F and Cbei_0127-R (**Table 1**) and cloned downstream of the T7 promoter in *Stu*I-digested pBT7 (Tsai et al., 2002). Following screening for a clone with an insert in the sense orientation and subsequent confirmation by sequencing, pBT7-DisA was used as the template for PCR with primers F-ext (**Table 1**) and Cbei_0127-R to generate the DNA template for *in vitro* transcription of the DisA RNA fragment. Subsequently, based on the molecular weight and the concentration (determined using a spectrophotometer), the copy number of each transcript was calculated as previously described (Devonshire et al., 2016).

Standard curves were generated by performing RT-qPCR with 10, 20, 30, 50, 80, and 100 copies of M1 RNA and DisA transcripts and with primer sets M1-F + M1-R and Cbei_0127-F + Cbei_0127-R, respectively. The resulting quantification cycles (Cq) were then plotted against the known copy numbers. RNA samples (2 μg) isolated from *C. beijerinckii*_M1GS^{DisA}, _M1GS^{CcpA}, or _pMTL500E were then analyzed by RT-qPCR in the same manner. Based upon the Cq values obtained for each reaction, the corresponding copy numbers for M1GS^{DisA} or M1GS^{CcpA} were interpolated from the respective standard curves and normalized by subtracting the background value obtained using RNA isolated from *C. beijerinckii*_pMTL500E. This background correction was motivated by the expectation that neither M1GS^{DisA} nor M1GS^{CcpA} should be present in *C. beijerinckii* transformed with pMTL500E. The Cq values obtained for M1GS and DisA transcripts were within the range of the standard curve. By plating cells on TGY agar (as described above), we counted the colonies from cells harvested for RNA extraction and calculated the number of cells/culture volume. With this information as well as the RT-qPCR results, we could determine the number of M1GS and DisA copies per cell for the strains in this study.

Rapid Amplification of cDNA 3′ Ends (3′ RACE) Analysis

To assess the efficacy of the HH ribozyme cleavage and generation of the intended M1GS RNA, we sought to map the 3′ termini of the M1GS ribozymes from *C. beijerinckii*_M1GS^{DisA} and _M1GS^{CcpA}. To this end, total RNA was first incubated with polynucleotide kinase (37°C – 2 h) to dephosphorylate the 2′,3′-cyclic phosphate produced by HH cleavage. The RNA was then polyadenylated using the poly(A) Tailing Kit (Invitrogen, Carlsbad, CA, United States). Subsequently, the RNA was reverse transcribed using SuperScript II (Invitrogen) and the anchored oligo dT primer from the GeneRacer Kit (Invitrogen). The resulting cDNAs were then treated with RNase H before amplifying by PCR the 3′ ends of the ribozymes with M1GS-3F and the GeneRacer 3′ Primer using PrimeSTAR GXL (Takara Bio USA, Mountain View, CA, United States). This step was followed by a round of nested PCR using M1-4F and the GeneRacer 3′ Nested Primer. The nested-PCR RACE product, which migrated close to the expected size on an agarose gel, was then sequenced with the M1-4F primer at the OSU Genomics Shared Resources facility. Sequencing results showed that the HH ribozyme cleaved at the expected position and generated the desired 3′ termini (data not shown).

Analytical Methods

Intracellular levels of c-di-AMP were analyzed by HPLC using the Waters 2796 Bioseparations Module (Waters Corporation, Milford, MA, United States), equipped with a photodiode array (PDA) detector (Waters Corporation, Milford, MA, United States) and a 3.5-μm Xbridge C18, 150 mm × 4.6 mm column (Waters Corporation, Milford, MA, United States) according to Oppenheimer-Shaanan et al. (2011). Pure c-di-AMP (BIOLOG Life Science Institute, Bremen, Germany) was used as standard. C-di-AMP was extracted from cell pellets according to Oppenheimer-Shaanan et al. (2011). Pellets were obtained from triplicate 50-mL samples taken every 12 h from cultures grown in glucose + arabinose medium, and each extract was analyzed twice. Extracts were reconstituted in sterile distilled water (400 μl) for HPLC analysis.

Acetone, butanol, ethanol, acetic acid, and butyric acid concentrations were quantitated using a 7890A Agilent gas chromatograph (Agilent Technologies Inc., Santa Clara, CA, United States) as described previously (Ujor et al., 2014). The GC data were analyzed using Agilent Chem Station software (Rev. B.03.02 SR2). Cell growth was determined by measuring optical density (OD_{600}) using a DU® spectrophotometer (Beckman Coulter, Brea, CA, United States). The concentrations of glucose,

arabinose and xylose were determined by HPLC using the Waters 2796 Bioseparations Module (Waters Corporation, Milford, MA, United States) as previously described (Ujor et al., 2014).

Mitomycin C and Nalidixic Acid Sensitivity Assays

At 25 h post inoculation into glucose + arabinose medium, triplicate cultures of *C. beijerinckii*_M1GS^{DisA}, _M1GS^{CcpA} or _pMTL500E were adjusted to the same optical density (OD_{600}), and then diluted 1:500 (in 1 mL) before plating out on semi-solid TGY agar [0.45% (w/v) agar] containing erythromycin (20 ng/mL) and mitomycin C (50, 80, or 120 ng/mL) or nalidixic acid (470, 480, or 495 ng/mL). Plates were incubated for 14 to 24 h at 35°C ± 1°C prior to counting the colony forming units.

Sporulation Test

To determine the progression of sporulation in cultures of *C. beijerinckii*_M1GS^{DisA}, _M1GS^{CcpA}, or _pMTL500E, all three strains were grown in glucose + arabinose medium in triplicate. Samples were taken from each culture every 12 h and diluted 1:100 (in 1 mL). A portion of the sample (500 μl) was heat-shocked at 75°C for 8 min, cooled on ice and plated on TGY agar to determine the number of spores per sample. The remainder of each sample was plated out without heat treatment to determine the number of vegetative cells in the samples relative to the spores (heat-shocked portion). All plates contained erythromycin (25 μg/mL) and were incubated for 24 h as described above, and the colonies were counted.

Statistical Analysis

Statistical analyses were conducted with the General Linear Model (GLM) of Minitab version 17 (Minitab Inc., State College, PA, United States). Statistical analyses compared the differences in the results obtained with *C. beijerinckii*_M1GS^{DisA}, _M1GS^{CcpA}, _M1GS^{DisA16}, or _pMTL500E including butanol and ABE concentrations, yields and productivities, cell growth, c-di-AMP levels, copy numbers and fold changes in M1GS and DisA mRNA levels, and residual sugar concentrations after fermentation with each strain. Data were un-stacked by time and ANOVA was conducted at different time points. Tukey's test at 95% confidence interval was applied to pairwise comparisons to determine the levels of significance. All experiments were performed in triplicate, and the errors reported reflect the standard deviation of the calculated mean.

RESULTS

M1GS Design and Construction

The M1GS approach is depicted in **Figure 1A**. Before designing an M1GS construct against an mRNA, it is necessary to identify a single-stranded region (preferably proximal to the start codon, $A_{+1}UG$) in the target mRNA. Analysis of the CcpA mRNA secondary structure [nucleotides –25 to +55 of the ORF] using the mfold web server (Zuker, 2003) indicated that nucleotides +2 to +18 of its ORF are likely to be accessible for base pairing to a complementary GS. We then constructed the genes encoding two customized ribozymes: one was the test M1GS^{CcpA} and the other a scrambled control M1GS$^{CcpA-Sc}$. The GS$^{CcpA-Sc}$ has the same nucleotide composition as GS^{CcpA} but a different sequence (**Figures 1B,C**); we ascertained by BLAST that the scrambled GS sequence did not have a perfect (16-nucleotide) contiguous match with any other mRNA in the *C. beijerinckii* genome.

To ensure a uniform 3′ terminus for each M1GS transcript generated *in vivo*, we placed a HH ribozyme downstream of M1GS. Self-cleaving HH ribozymes have been used to synthesize RNAs with well-defined termini *in vitro* and *in vivo*. Both M1GS^{CcpA} and M1GS$^{CcpA-Sc}$ constructs (**Figures 1B,C**) were cloned into pWUR459 (Siemerink et al., 2011), displacing the resident *acetoin reductase* gene, and placing the constructs under the control of the acetoacetate decarboxylase (*adc*) promoter, which is active during solventogenesis. As an additional negative control, we used pMTL500E, the vector from which pWUR459 originated. All three plasmids were introduced into *C. beijerinckii* by electroporation to generate the strains *C. beijerinckii*_M1GS^{CcpA}, _M1GS$^{CcpA-Sc}$, and _pMTL500E.

Before examining the effect of CcpA knockdown on solventogenesis, we determined that M1GS ribozymes were expressed in *C. beijerinckii*_M1GS^{CcpA} and _M1GS$^{CcpA-Sc}$ relative to the vector control strain *C. beijerinckii*_pMTL500E (**Table 2**), and that they were synthesized with the correct termini. Although some earlier reports used only a minimal HH catalytic core (Uhlenbeck, 1987), since loop sequences outside the catalytic core were found to enhance the rate of self-cleavage at physiological Mg^{2+} concentrations (Khvorova et al., 2003), we opted for a naturally occurring, loop-containing HH ribozyme found in *Arabidopsis thaliana* (Ara1, k_{obs} ~2 min^{-1} at 25°C in 0.6 mM Mg^{2+}) (Przybilski et al., 2005) with some modifications (**Figure 1A**, inset). Indeed, 3′ RACE followed by sequencing proved that Ara1, albeit of plant origin, functions efficiently in *C. beijerinckii* and cleaves at the expected position to generate a precise 3′ terminus (data not shown). To our knowledge, such use of HHs in the M1GS approach has not been reported.

M1GS^{CcpA} Elicited Knockdown of CcpA mRNA and a Modest Increase in ABE Production

We used RT-qPCR with CcpA-specific primers (**Table 1**) that flank the targeted region to determine the expression of CcpA mRNA in the three *C. beijerinckii* transformants. We found that the CcpA mRNA level in *C. beijerinckii*_M1GS^{CcpA} decreased 2.8-fold ($p < 0.05$) when compared to the other strains (**Table 2**). While examining the ABE production profiles for all strains grown on various sugars, the largest increase observed in *C. beijerinckii*_M1GS^{CcpA} relative to _pMTL500E was ~1.2-fold ($p < 0.05$) when grown on glucose + arabinose (**Figure 2** and **Table 3**). Unexpectedly, we also observed a ~1.5-fold ($p < 0.05$). Increase in ABE production by

TABLE 2 | Determination of fold-change for CcpA and DisA mRNA level and of the cellular copy number for M1GS and DisA transcripts.

C. beijerinckii strain	CcpA mRNA (fold change)	DisA mRNA (fold change)	M1GS transcript (copies/cell)	DisA mRNA (copies/cell)
pMTL500E	1.0 ± 0.0	1.0 ± 0.0	0.0 ± 0.0	791.0 ± 78.0
M1GS^{CcpA}	−2.8 ± 0.4	1.0 ± 0.0	83 ± 9	828.0 ± 74.0
M1GS^{DisA}	1.0 ± 0.0	−44.0 ± 4.4	87 ± 8	15.3 ± 2.8
MIGS^{DisA16}	1.0 ± 0.0	−43.5 ± 1.0	ND	ND
ΔMIGS^{DisA16}	1.0 ± 0.0	−1.5 ± 0.0	ND	ND

ND, not determined. Tukey's pairwise comparison was applied to the means of CcpA mRNA fold changes, M1GS transcript copies, and DisA mRNA copies. RNA copy number was calculated using RT-qPCR (see text for details). All fold changes are relative to C. beijerinckii_pMTL500E. Errors denote the standard deviation of the mean (n = 3).

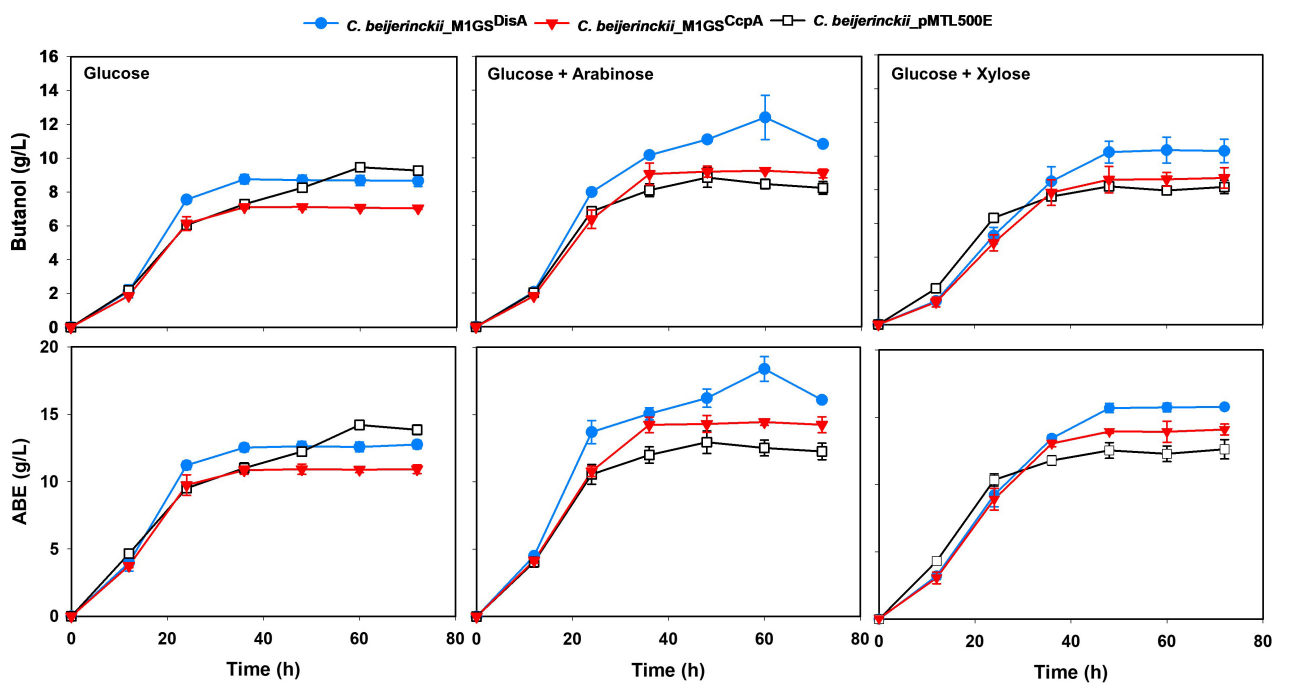

FIGURE 2 | Butanol and ABE titers during a 72-h fermentation in cultures of *C. beijerinckii*_pMTL500E, _M1GS^{CcpA}, and _M1GS^{DisA} on glucose, glucose + arabinose, and glucose + xylose. Error bars represent standard deviation of the mean (n = 3).

*C. beijerinckii*_M1GS$^{CcpA-Sc}$ compared to the vector control, both grown on glucose + arabinose (**Figure 2** and **Table 3**). We leveraged this adventitious finding to direct our study differently.

M1GS$^{CcpA-Sc}$ (M1GS^{DisA}) Leads to a Pronounced Decrease in DisA mRNA Level

To understand the basis for increased ABE production by *C. beijerinckii*_M1GS$^{CcpA-Sc}$, we performed a BLASTn analysis using the GS$^{CcpA-Sc}$ sequence as a query against the *C. beijerinckii* genome. Although we found several genes with a complementarity of nine or more contiguous nucleotides, only six of them seemed likely to affect fermentation. When RT-qPCR analysis of these six mRNAs was conducted (**Supplementary Table 1**), only Cbei_0127 (DisA) mRNA was found to decrease drastically (44-fold; $p < 0.05$) in *C. beijerinckii*_M1GS$^{CcpA-Sc}$ relative to *C. beijerinckii*_M1GS^{CcpA} and _pMTL500E. This finding prompted us to rename M1GS$^{CcpA-Sc}$ as M1GS^{DisA}.

In an independent RT-qPCR experiment, we used an *in vitro* transcribed fragment of the DisA mRNA as a reference for a standard curve and determined that ∼800 copies of DisA mRNA are present per cell in *C. beijerinckii*_M1GS^{CcpA} and _pMTL500E, but only 15 copies in *C. beijerinckii*_M1GS^{DisA}, representing a 53-fold ($p < 0.05$) downregulation mediated by M1GS^{DisA} (**Table 2**). With *in vitro* transcribed M1 RNA as a reference for a standard curve, we found that the normalized copy number of M1GS per cell is 0, 83, and 87, in *C. beijerinckii*_pMTL500E, _M1GS^{CcpA}, and _M1GS^{DisA}, respectively (**Table 2**). The decrease from 828 to 15 copies of DisA mRNA mediated by 87 copies of M1GS^{DisA} in *C. beijerinckii*_M1GS^{DisA} must entail multiple turnover of the ribozyme (at least nine rounds). Although multiple turnover was an implicit expectation for M1GS, *in vivo* evidence has not been documented before.

TABLE 3 | Maximal butanol **(A)** and ABE **(B)** levels in cultures of different *C. beijerinckii* strains grown on different sugars for 60 h.

(A)

Butanol	Glucose medium		Glucose + Arabinose medium		Glucose + Xylose medium		Arabinose medium		Xylose medium	
***C. beijerinckii* strain**	**Conc. (g/L)**	***Fold change**	**Conc. (g/L)**	***Fold change**	**Conc. (g/L)**	***Fold change**	**Conc. (g/L)**	***Fold change**	**Conc. (g/L)**	***Fold change**
pMTL500E	9.5 ± 0.2	1.0 ± 0.0^{a}	8.5 ± 0.4	1.0 ± 0.0^{a}	8.2 ± 0.4	1.0 ± 0.0^{a}	10.2 ± 0.1	1.0 ± 0.0^{a}	9.6 ± 0.3	1.0 ± 0.0^{a}
M1GS^{CcpA}	7.1 ± 0.1	−1.3 ± 0.1^{c}	9.2 ± 0.0	1.1 ± 0.0^{a}	8.7 ± 0.6	1.1 ± 0.1^{a}	11.0 ± 0.1	1.1 ± 0.0^{a}	9.6 ± 0.7	1.0 ± 0.0^{a}
M1GS^{DisA}	8.7 ± 0.3	−1.1 ± 0.1^{a}	12.5 ± 1.6	1.5 ± 0.6^{c}	10.4 ± 0.8	1.3 ± 0.4^{c}	12.2 ± 0.4	1.2 ± 0.1^{c}	10.2 ± 0.8	1.1 ± 0.2^{a}

(B)

ABE	Glucose medium		Glucose + Arabinose medium		Glucose + Xylose medium		Arabinose medium		Xylose medium	
***C. beijerinckii* strain**	**Conc. (g/L)**	***Fold change**	**Conc. (g/L)**	***Fold change**	**Conc. (g/L)**	***Fold change**	**Conc. (g/L)**	***Fold change**	**Conc. (g/L)**	***Fold change**
pMTL500E	14.2 ± 0.4	1.0 ± 0.0^{a}	12.5 ± 0.6	1.0 ± 0.0^{a}	12.6 ± 0.7	1.0 ± 0.0^{a}	14.0 ± 0.2	1.0 ± 0.0^{a}	14.50 ± 0.6	1.0 ± 0.0^{a}
M1GS^{CcpA}	10.9 ± 0.4	−1.3 ± 0.1^{c}	14.5 ± 0.2	1.2 ± 0.1^{c}	14.1 ± 0.4	1.1 ± 0.1^{c}	15.0 ± 0.4	1.1 ± 0.1^{a}	14.5 ± 1.5	1.0 ± 0.8^{a}
M1GS^{DisA}	12.8 ± 0.3	−1.1 ± 0.1^{c}	18.4 ± 0.9	1.5 ± 0.0^{c}	15.8 ± 0.2	1.3 ± 0.0^{c}	17.5 ± 0.5	1.3 ± 0.2^{c}	15.6 ± 0.6	1.1 ± 0.2^{a}

**All fold changes are relative to C. beijerinckii_pMTL500E. Tukey's pairwise comparison was applied to the mean fold changes in butanol and ABE concentrations in cultures of C. beijerinckii_M1GS^{CcpA} and _M1GS^{DisA} relative to those of C. beijerinckii_pMTL500E. Fold changes for C. beijerinckii_pMTL500E, _M1GS^{CcpA}, and _M1GS^{DisA} with different superscripts within a column are significant ($p \leq 0.05$). Errors denote standard deviation of the mean ($n = 3$).*

*C. beijerinckii*_M1GS^{DisA} Displayed a Decreased c-di-AMP Level, Increased Sensitivity to DNA-Damaging Antibiotics, and a Slower Sporulation Rate

Since DisA is a diadenylate cyclase (DAC) that synthesizes c-di-AMP (Bejerano-Sagie et al., 2006; Oppenheimer-Shaanan et al., 2011), its knockdown should result in decreased c-di-AMP production. Indeed, when intracellular levels of c-di-AMP in 24-h cultures of *C. beijerinckii*_M1GS^{DisA}, _M1GS^{CcpA}, and _pMTL500E were quantitated by HPLC, we observed a 7-fold ($p < 0.05$) decrease in *C. beijerinckii*_M1GS^{DisA} compared to the other two strains (**Figure 3A**).

Because DisA scans genomic DNA and initiates the repair of lesions, we also postulated that *C. beijerinckii*_M1GS^{DisA} would be more susceptible to DNA-damaging agents due to DisA knockdown. Therefore, *C. beijerinckii*_M1GS^{DisA} and _M1GS^{CcpA} were challenged with mitomycin C and nalidixic acid, two well-established DNA-damaging antibiotics. Both drugs drastically decreased the viability of *C. beijerinckii*_M1GS^{DisA} compared to _M1GS^{CcpA} (**Figure 3B** and **Supplementary Figure 1**). At 120 ng/mL of mitomycin C, the viability of M1GS^{DisA} decreased by 99.9% ($p < 0.05$). A similar effect was observed with nalidixic acid, which decreased the viability of *C. beijerinckii*_M1GS^{DisA} by 99.8% ($p < 0.05$) at 470 ng/mL and by 100% at 480-495 ng/mL. These results indicate that *C. beijerinckii*_M1GS^{DisA} is hypersensitive to DNA-damaging antibiotics.

DisA monitors genomic integrity particularly at the onset of sporulation. To allow a cell to fix damages to DNA that might disrupt its replication or cause defects in chromosome partitioning, DisA halts sporulation by delaying the activation of Spo0A, a master transcriptional activator critical for sporulation. Thus, DisA knockdown is expected to alter the sporulation dynamics in *C. beijerinckii*_M1GS^{DisA}. Since cultures of solventogenic clostridia exist as mixtures of vegetative cells and spores upon transition to solventogenesis, we assessed the progression of sporulation in cultures of *C. beijerinckii*_M1GS^{DisA}, _M1GS^{CcpA}, and _pMTL500E over a 60-h fermentation (**Figure 3C**). As expected, *C. beijerinckii*_M1GS^{DisA} showed a delay relative to *C. beijerinckii*_pMTL500E (**Figure 3C**). We observed 7.4−, 2.5− and 1.6-fold decrease in percent sporulation at 24, 36, and 48 h, respectively, for *C. beijerinckii*_M1GS^{DisA} compared to *C. beijerinckii*_pMTL500E ($p < 0.05$). Although CcpA is known to partake in sporulation, no substantial delay was found in *C. beijerinckii*_M1GS^{CcpA} cultures compared to the sporulation rate found in *C. beijerinckii*_pMTL500E cultures. It is also possible that the ∼3-fold decrease in CcpA mRNA level is insufficient to cause a change in the sporulation dynamics.

Both *C. beijerinckii*_M1GS^{CcpA} and _M1GS^{DisA} Exhibited Increased Solvent Production in Pentose-Containing Media

The effects of CcpA and DisA knockdown on butanol and ABE production were assessed while growing on media

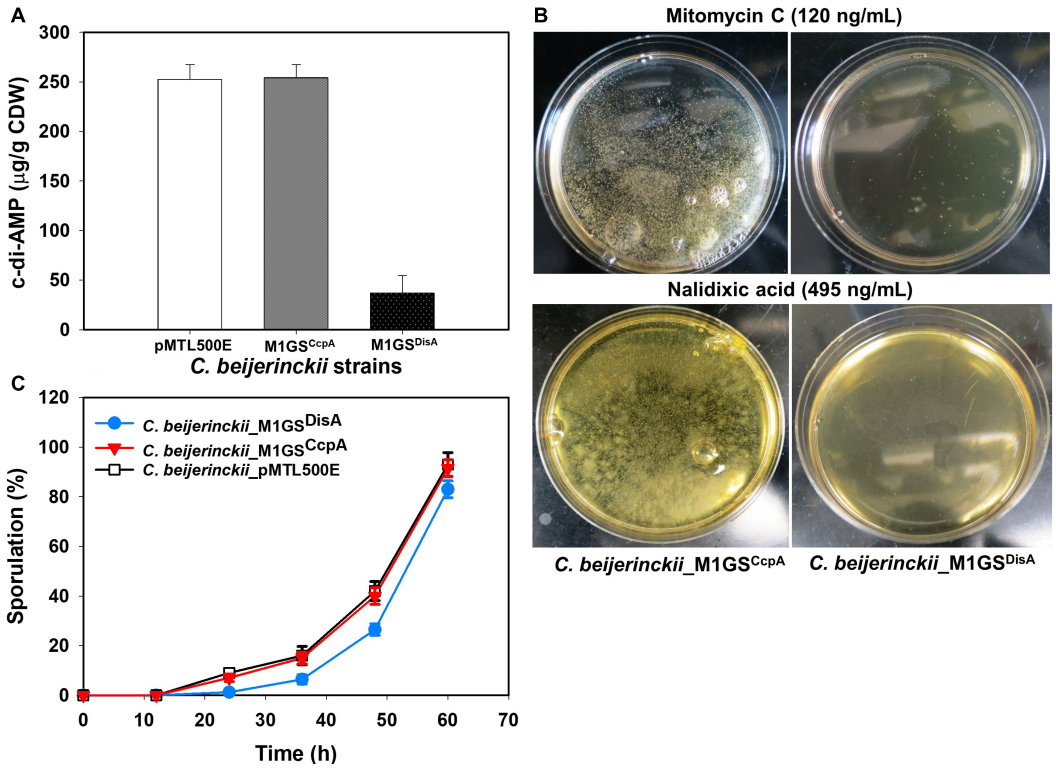

FIGURE 3 | Phenotypic changes elicited by M1GS^{DisA}. **(A)** Intracellular c-di-AMP levels in *C. beijerinckii*_M1GS^{DisA} decreased 7-fold relative to *C. beijerinckii* _M1GS^{CcpA} and _pMTL500E at 24 h of growth. CDW, cell dry weight. **(B)** *C. beijerinckii*_M1GS^{DisA} was more sensitive to mitomycin C and nalidixic acid than *C. beijerinckii*_M1GS^{CcpA}. At the specified concentrations, both antibiotics caused ∼100% loss of cell viability in *C. beijerinckii*_M1GS^{DisA} (see **Supplementary Figure 1** for more details). Generation of carbon dioxide and hydrogen during cellular growth and metabolism caused bubbles on *C. beijerinckii*_M1GS^{CcpA} plates. **(C)** Sporulation profiles of *C. beijerinckii*_M1GS^{DisA} relative to *C. beijerinckii*_M1GS^{CcpA} and _pMTL500E. Error bars represent standard deviation of the mean (n = 3).

with single (glucose, arabinose, or xylose) and mixed sugars (glucose + arabinose or glucose + xylose) as carbon source(s). Interestingly, butanol production by both *C. beijerinckii*_M1GS^{CcpA} and _M1GS^{DisA} was lower than the control (*C. beijerinckii*_pMTL500E) when grown on glucose (**Table 3**), although *C. beijerinckii*_M1GS^{DisA} initially (12-48 h) produced more than the other two strains (**Figure 2**). Except for *C. beijerinckii*_M1GS^{CcpA} being on par with the control in xylose medium (**Figure 4**), *C. beijerinckii*_M1GS^{CcpA} and _M1GS^{DisA} showed higher butanol production than the control strain in all pentose-containing media (**Figures 2**, **4** and **Table 3**). This difference was most pronounced in media containing arabinose, either alone or in combination with glucose (**Figures 2**, **4**). In the arabinose medium, maximal butanol concentration was 1.2-fold ($p < 0.05$) higher in *C. beijerinckii*_M1GS^{DisA} than *C. beijerinckii*_pMTL500E; remarkably, this change increased to 1.5-fold ($p < 0.05$) with the addition of glucose (**Figures 2**, **4** and **Table 3A**). In xylose medium, *C. beijerinckii*_M1GS^{DisA} achieved a maximal butanol titer that is 1.1-fold higher than *C. beijerinckii*_pMTL500E; this change increased to 1.3-fold ($p < 0.05$) with the addition of glucose. Thus, butanol production notably increased by either 50% or 30% in *C. beijerinckii* _M1GS^{DisA} grown in media with either glucose + arabinose or glucose + xylose, respectively, when compared to the control strain; the basis for this solventogenesis difference between the two pentoses remains to be determined by future transcriptomic studies. In contrast, the gains with *C. beijerinckii*_M1GS^{CcpA} were more modest (less than 10% regardless of the combinations tested). In all fermentations, the extent of changes in ABE levels mirrored the corresponding butanol titers (**Figures 2**, **4** and **Table 3**). Calculated yield, productivity, and residual sugars in cultures of *C. beijerinckii*_M1GS^{CcpA}, _M1GS^{DisA} and _pMTL500E after a 60-h fermentation are consistent with the solvent production profiles (**Supplementary Tables 2**, **3**).

To further characterize the phenotypes of *C. beijerinckii*_M1GS^{CcpA}, _M1GS^{DisA}, and _pMTL500E, their optical densities (OD_{600}) during fermentation on the various carbon substrates mentioned above were measured (**Supplementary Figure 2A**). Growth for all three strains was comparable in glucose- and arabinose-containing media. *C. beijerinckii*_M1GS^{CcpA} grew well in glucose + arabinose medium, whereas the maximal OD_{600} values of the other two strains (*C. beijerinckii*_M1GS^{DisA} and _pMTL500E) were both ∼1.2-fold lower ($p < 0.05$) than the glucose-containing medium. In glucose + xylose and xylose-alone media, *C. beijerinckii*_M1GS^{DisA} showed the poorest growth, with maximal OD_{600} values up to 1.4-fold lower ($p < 0.05$) than

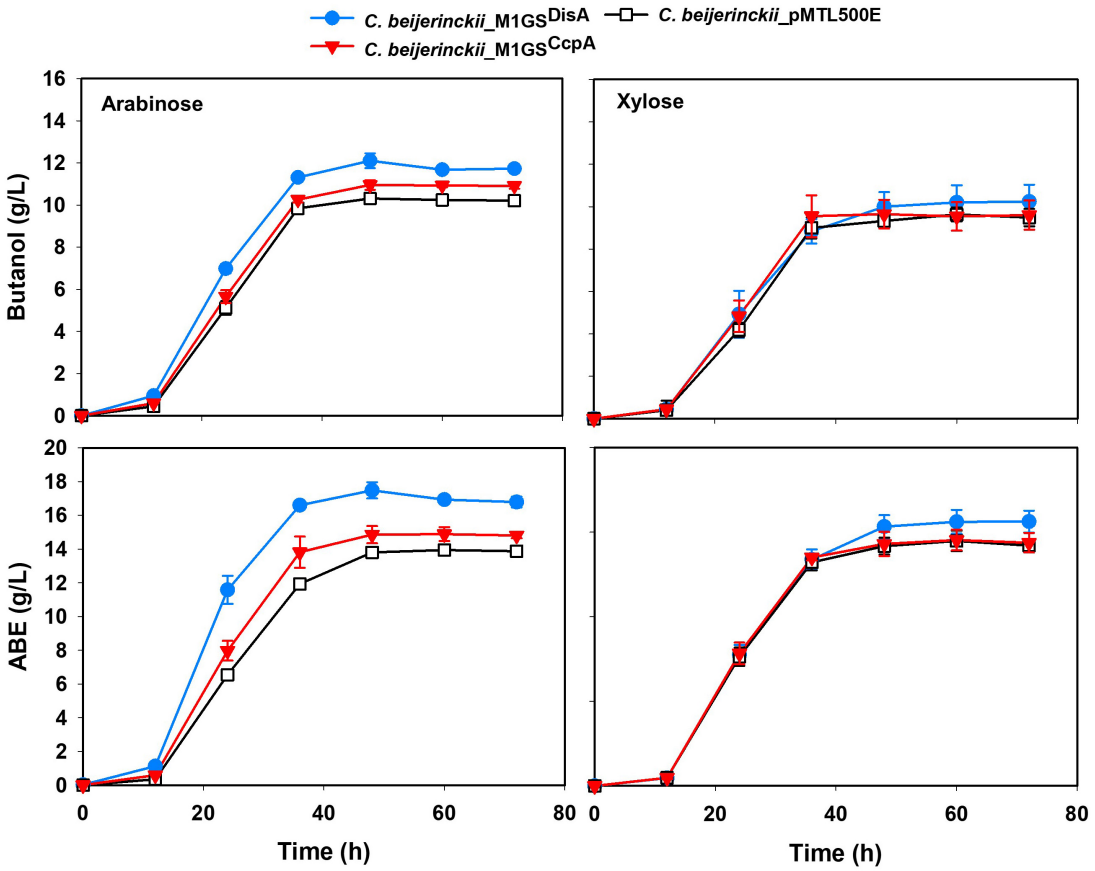

FIGURE 4 | Butanol and ABE titers during a 72-h fermentation in cultures of *C. beijerinckii*_ pMTL500E, _M1GS^{CcpA}, and _M1GS^{DisA} grown on arabinose and xylose. Error bars represent standard deviation of the mean (n = 3).

those of *C. beijerinckii*_M1GS^{CcpA} or _pMTL500E grown on different combinations (**Supplementary Figure 2A**). We could not gain clear insights as to solventogenesis gains based on these growth curves.

Increased Complementarity in GS^{DisA} Did Not Lead to Solventogenic Gain

Given the enhanced solventogenesis elicited by M1GS^{DisA} even though its GS has only 9-bp complementarity with the DisA mRNA, we then examined whether an M1GS with additional base pairing would be even more effective. To this end, we constructed *C. beijerinckii*_M1GS^{DisA16} that has a full 16-nucleotide complementarity to DisA mRNA. As an additional control, we generated *C. beijerinckii*_ΔM1GS^{DisA16} in which the latter half of M1 RNA was deleted to render it inactive; this control helps determine the antisense effect of the GS portion. We found that DisA mRNA decreased ∼44- and 1.5-fold in *C. beijerinckii*_M1GS^{DisA16} and _ΔM1GS^{DisA16}, respectively (**Table 2**). Despite a comparable knockdown in DisA mRNA level relative to *C. beijerinckii*_M1GS^{DisA} (53-fold), *C. beijerinckii*_M1GS^{DisA16} showed a very different growth and solvent profile relative to *C. beijerinckii*_M1GS^{DisA}.

The different strains of *C. beijerinckii* studied herein exhibited varying growth profiles with different sugar substrates. For instance, cultures of *C. beijerinckii*_M1GS^{DisA16} reached maximum optical densities at 60 h when grown on glucose and glucose + arabinose, whereas *C. beijerinckii*_M1GS^{DisA}, _ΔM1GS^{DisA16}, _M1GS^{CcpA}, and _pMTL500E reached maximum optical densities at 24 h on glucose and glucose + arabinose, except for *C. beijerinckii*_ΔM1GS^{DisA} that grew to a maximum optical density at 36 h on glucose and arabinose (**Supplementary Figures 2A,B**). Conversely, when grown on glucose + xylose, _M1GS^{DisA16} attained greater optical density and in considerably less time (36 h), when compared to its growth on glucose or glucose + arabinose (**Supplementary Figures 2A,B**).

To further assess the effects of DisA knockdown on solvent production, we compared the solvent profiles of *C. beijerinckii*_ΔM1GS^{DisA16} and _M1GS^{DisA16} to those of _M1GS^{DisA}, _M1GS^{CcpA}, and _pMTL500E in media containing glucose, glucose + arabinose, and glucose + xylose (**Figures 2**, **4** and **Supplementary Figure 3**). Like its growth profile (**Supplementary Figure 2B**), *C. beijerinckii*_M1GS^{DisA16} exhibited a considerable lag in solvent accumulation (**Supplementary Figure 3**) when grown on glucose or

glucose + arabinose but not on glucose + xylose. Notably, *C. beijerinckii*_ΔM1GS^{DisA16} achieved similar maximum solvent concentrations as *C. beijerinckii*_M1GS^{DisA16} and _M1GS^{DisA} when grown on glucose and glucose + xylose (**Supplementary Figure 3**). However, when all three strains were grown on glucose + arabinose, *C. beijerinckii*_M1GS^{DisA} produced significantly more butanol and ABE than *C. beijerinckii*_ΔM1GS^{DisA16} and _M1GS^{DisA16}.

DISCUSSION

Although we fulfilled our goal of improving ABE production in *C. beijerinckii* grown on mixed sugars, it was accomplished more through fortuitous knockdown of DisA than of CcpA, which was our intended target originally for dampening CCR. While a modest ABE increase was observed with CcpA downregulation, our results provide insights into the M1GS-based knockdown approach in *C. beijerinckii* and the hitherto unknown role of DisA (via c-di-AMP) in solventogenesis (**Figure 5**).

The M1GS-based mRNA degradation approach has been used successfully to cleave mRNAs in bacteria, mammalian cells, and mice (Liu, 2010). Nevertheless, our finding of the 53-fold decrease in the DisA mRNA level in *C. beijerinckii* elicited by M1GS^{DisA} is notable for a few reasons. First, we show the utility of this method in an anaerobic, Gram-positive bacterium and demonstrate its merit as a tool for studying the physiology and metabolic engineering of *Clostridium* species. Second, our copy number determination of the DisA mRNA and M1GS^{DisA} confirms the unproven expectation of multiple turnover by this ribozyme *in vivo* (**Table 2**). Third, the M1GS method typically aims for 13-15 base pairs between the GS and the target mRNA to achieve optimal binding and cleavage, with the caveat that long stems favorable for GS-mRNA complex formation might inhibit turnover by preventing product release. That M1GS^{DisA} can form only 9 base pairs with the DisA mRNA (**Figure 1C**) may account for the efficient turnover that we observed; it is possible that intracellular factors (e.g., chaperones) contribute favorably either to the annealing and thermodynamic stability of the GS-mRNA complex or to product dissociation. While such short GS-mRNA duplexes raise the specter of off-target effects, this concern is partly alleviated by accessibility considerations. In fact, the degree of knockdown observed for DisA mRNA suggests that the target sequence on this mRNA is accessible. This expectation is consistent with our observation that extending the GS-DisA mRNA complementarity from 9- (**Figure 1C**) to 16-base pairs (**Figure 1D**) resulted in a similar extent of DisA mRNA knockdown (∼44-fold), relative to the plasmid control strain (*C. beijerinckii*_pMTL500E). Fourth, these DisA-targeted GSs bind to the 334-349 region of DisA mRNA (numbering with reference to the start codon; **Figures 1C,D**), whereas GSs are typically designed to target nucleotides immediately downstream of the start codon because they are often single-stranded to ensure high translatability. The efficient knockdown with these DisA-targeted GSs suggests that local secondary structure elsewhere in the mRNA, which is hard to predict under cellular conditions, might offer more accessible targets (Cobaleda and Sánchez-García, 2000; Lundblad et al., 2008). New methods that map RNA secondary structure *in vivo* will be valuable in this regard (Spitale et al., 2013; Watters et al., 2016; Zhao et al., 2019). Last, *in vitro* studies suggest that M1GS prefers to cleave between a pyrimidine and a guanosine (**Figure 1B**; Li and Altman, 1996), but this cleavage site requirement is not absolute. Indeed, based on the predicted targeting site in the DisA mRNA (**Figures 1C,D**), it appears that this is not a strict requirement *in vivo*.

It is surprising that while we set out to knock down CcpA in *C. beijerinckii* to abolish or at least dampen CCR, we achieved only a 3-fold decrease in the CcpA mRNA level with M1GS^{CcpA} when M1GS^{DisA} could reduce the DisA mRNA level by 53-fold. Nevertheless, the 3-fold decrease in CcpA mRNA levels was accompanied by a 10-20% increase in ABE production compared to the control when grown on arabinose, glucose + arabinose, or glucose + xylose media (**Figures 2**, **4** and **Table 3**). The fact that the increase was associated with pentose-containing media suggests that M1GS^{CcpA} was able to dampen CCR. That M1GS^{CcpA} was not more effective could be explained by gene duplication in *C. beijerinckii* (Hall et al., 2009; Shi et al., 2010). While our customized M1GS^{CcpA} was designed to target *Cbei_0047*, which is annotated to encode a CcpA/alanine racemase, the *C. beijerinckii* genome has seven other genes annotated to encode putative alanine racemases that have sequence similarity to *Cbei_0047* as well as to the *C. acetobutylicum* CcpA (**Supplementary Table 4**). Given that all these seven proteins harbor DNA-binding helix-turn-helix and sugar-binding domains like those found in *Cbei_0047*, a 3-fold downregulation of the CcpA mRNA encoded by *Cbei_0047* may not be sufficient to eliminate CCR.

Decreased DisA mRNA and c-di-AMP levels, increased sensitivity to DNA-damaging antibiotics, and delayed sporulation in *C. beijerinckii*_M1GS^{DisA} are consistent with the 53-fold knockdown of DisA mRNA. However, the 7-fold decrease in cellular c-di-AMP level in *C. beijerinckii*_M1GS^{DisA} was lower than expected but easily rationalized. While most organisms have only one diadenylate cyclase (DAC; a c-di-AMP–producing enzyme), *Clostridium* and *Bacillus* species possess two to three DACs, all subject to spatio-temporal regulation (Corrigan and Gründling, 2013; Mehne et al., 2013). In fact, the presence of c-di-AMP in a DisA-null mutant of *B. subtilis* during vegetative growth confirmed the involvement of other DACs in c-di-AMP production (Oppenheimer-Shaanan et al., 2011). To determine if there are additional DACs in the *C. beijerinckii* genome, we searched for proteins annotated with a DAC domain (DUF147; Mehne et al., 2013). In addition to *Cbei_0127* (DisA), we found only *Cbei_0200*, a conserved hypothetical protein, to have this domain. *Cbei_0200* was also the only *C. beijerinckii* protein uncovered in a BLASTp search when the sequences of *Cbei_0127* (DisA) and the three *B. subtilis* DACs (CdaA, CdaS, and DisA) were each used as a query. While the protein product of *Cbei_0200* might be a DAC homolog that contributes to intracellular c-di-AMP levels, it is unlikely that *Cbei_0200* encodes a DisA homolog as it shares only 22% similarity with *Cbei_0127*. Importantly, the poor complementarity between *Cbei_0200* and GS^{DisA} would allow *Cbei_0200* to escape downregulation by M1GS^{DisA} and to continue contributing to the cellular c-di-AMP level in *C. beijerinckii*_M1GS^{DisA}. As in

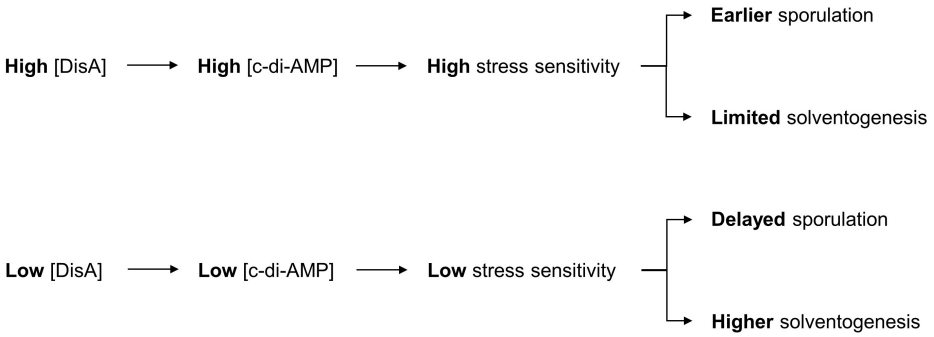

FIGURE 5 | Model for the role of c-di-AMP in ABE production. The depiction includes the normal sequence of events during c-di-AMP production in *C. beijerinckii* and the role of c-di-AMP in the initiation of sporulation, which impacts the duration of ABE biosynthesis. Decrease in c-di-AMP production following DisA knockdown in *C. beijerinckii*_M1GS^{DisA} would delay activation of Spo0A, and hence, the onset of sporulation. This delay would therefore extend the solventogenic phase, thereby allowing increased accumulation of ABE pre-sporulation.

B. subtilis, where DisA is expressed predominantly at high cell density and at the onset of sporulation (Bejerano-Sagie et al., 2006; Mehne et al., 2013), decreases in the c-di-AMP level in *C. beijerinckii*_M1GS^{DisA} relative to the control strains were pronounced at high cell density (7-fold at 24 h of growth) and at the peak of sporulation (5-fold at 60 h; **Figure 3A** and **Supplementary Figure 4**).

In some media, *C. beijerinckii*_M1GS^{DisA} grew slower but produced more ABE than other strains (**Figures 2**, **4** and **Supplementary Figures 2**, **3**). c-di-AMP is essential for growth in rich media but is dispensable in minimal media (Whiteley et al., 2015). Decreased c-di-AMP level is the likely cause for the poorer growth in the first 24 h when nutrients in the media is high. We can also rationalize our observation that a more efficient channeling of carbon to ABE biosynthesis over biomass accumulation exists in this strain, a desirable trait for large-scale fermentation. As c-di-AMP can directly inactivate pyruvate carboxylase (Sureka et al., 2014), decreasing the level of this secondary messenger could support the TCA cycle and thereby solventogenesis in *C. beijerinckii*_M1GS^{DisA}. In addition, high c-di-AMP level leads to increased stress sensitivity, especially to high salt concentrations (and, perhaps, other stressors including ABE products); the low c-di-AMP level in *C. beijerinckii*_M1GS^{DisA} likely mitigated such stress sensitivity. Coupled to the delayed onset of sporulation mediated by DisA knockdown (**Figure 3C**), solvent production in *C. beijerinckii*_M1GS^{DisA} can continue unabated longer than other strains.

While *C. beijerinckii*_M1GS^{DisA} and _M1GS^{DisA16} showed a similar degree of DisA mRNA fold change (∼44-fold decrease; **Table 2**), their growth and solvent profiles (**Figures 2**, **4**) are seemingly disparate but share a pattern. First, their slow growth, though worse in the latter strain, occurred only at the early stages of culturing. Second, while higher solvent production is evident in *C. beijerinckii*_M1GS^{DisA} after 12 h of growth, *C. beijerinckii*_M1GS^{DisA16} displayed an initial lag but the ABE production increased thereafter to at least a level that matched that of other strains. Both observations could be explained by decreased c-di-AMP levels as discussed above: poor growth in rich media and a rapid increase in ABE productivity in later stages. The reason for differences in phenotypes between *C. beijerinckii*_M1GS^{DisA} and *C. beijerinckii*_M1GS^{DisA16} is unclear but may involve stronger off-target effects by GS^{DisA16}. Support for this possibility comes from the observation that of the five mRNAs encoding transporters examined by RT-qPCR as possible off-targets of M1GS^{DisA} (**Supplementary Table 1**), three (including ABC transporter component of monosaccharide transport system and ATP-binding cassette domain of the histidine-glutamine transporters) showed several-fold downregulation. These findings suggest that for organisms with AT-rich genomes such as *C. beijerinckii*, promiscuity with the M1GS approach is inevitable. Even a naturally occurring small RNA in solventogenic clostridia was found to be a pleiotropic regulator due to its ability to target multiple mRNAs simultaneously (Yang et al., 2020). Thus, the specificity issues that we found unpredictable might be attributable to the compositional make-up of the transcriptome and repertoire of cellular factors in *C. beijerinckii*.

Asporogenic strains of solventogenic clostridia have long been considered ideal for continuous fermentation and longer-lasting batch fermentation with improved sugar utilization and ABE production. However, obtaining such a strain has thus far proven elusive. Our observation of enhanced ABE production by knocking down a gene not directly involved in the onset of sporulation (**Figure 5**) merits further investigation and highlights the importance of understanding the intricate coupling between sporulation and solventogenesis. While DisA knockdown exhibited improved ABE production, it also increased sensitivity to DNA damage (**Figure 3B**). Future studies to decrease intracellular c-di-AMP levels either by downregulating other DACs (not involved in genome scanning and DNA repair) or by upregulating the c-di-AMP phosphodiesterases may be a viable and appealing alternative.

Overall, our results confirm that DisA is a significant player in the regulation of solvent production in *C. beijerinckii*. It is plausible that a similar phenomenon exists in other solventogenic *Clostridium* species. While our findings demonstrate the utility

of knockdown over knockout, the confounding issue of off-target effects need to be addressed before deployment of the ribozyme approach in solventogenic *Clostridium* species. Such concerns may be partly offset as long as the defined payoffs are accomplished as illustrated here for solventogenesis. Regardless, the M1GS ribozyme approach could be harnessed to uncover new determinants of phenotypes such as growth, solventogenesis, and sporulation, and inspire targeted genetic manipulations to boost ABE production. Indeed, this work shows that MIGS technology has the potential of being a metabolic engineering tool of solventogenic *Clostridium* species, and perhaps, other microorganisms. The recent demonstration of the utility of the endogenous type IB CRISPR-Cas machinery as a powerful tool for engineering solventogenic *Clostridium* species (Payne et al., 2016; Zhang et al., 2018; Atmadjaja et al., 2019) further highlights the potential for using the RNase P-based approach as a gene-knockdown complement to a knockout method.

DATA AVAILABILITY STATEMENT

The original contributions presented in the study are included in the article/**Supplementary Material**, further inquiries can be directed to the corresponding author/s.

AUTHOR CONTRIBUTIONS

TE and VG conceived and designed the study. VU, LL, and CO performed the experiments. VU analyzed the data. VU and LL wrote the first draft of the manuscript. All authors contributed to the writing of the final draft and approved the submitted version.

FUNDING

Funding for this research was provided in part by the USDA NIFA Hatch grant (Project No. OHO01333), National Science Foundation Cellular & Biochemical Engineering program (Award Number: 1803022), by state funds allocated to the Ohio Agricultural Research and Development Center (OARDC, OHOA1682), and the Behrman Research Fund (to VG).

ACKNOWLEDGMENTS

We thank Dr. Wouter Kuit (Wageningen University and Research Centre, Wageningen, Netherlands) for kindly providing us pWUR459 and pWUR460 expression plasmids.

SUPPLEMENTARY MATERIAL

The Supplementary Material for this article can be found online at: https://www.frontiersin.org/articles/10.3389/fbioe.2021.669462/full#supplementary-material

REFERENCES

Altman, S. (2007). A view of RNase P. *Mol. Biosyst.* 3, 604–607. doi: 10.1039/b707850c

Atmadjaja, A. N., Holby, V., Harding, A. J., Krabben, P., Smith, H. K., and Jenkinson, E. R. (2019). CRISPR-Cas, a highly effective tool for genome editing in *Clostridium saccharoperbutylacetonicum* N1-4(HMT). *FEMS Microbiol. Lett.* 366:fnz059. doi: 10.1093/femsle/fnz059

Bai, Y., Gong, H., Li, H., Vu, G. P., Lu, S., and Liu, F. (2011). Oral delivery of RNase P ribozymes by *Salmonella* inhibits viral infection in mice. *Proc. Natl. Acad. Sci. U.S.A.* 108, 3222–3227. doi: 10.1073/pnas.1014975108

Bai, Y., Rider, P. J., and Liu, F. (2010). Catalytic M1GS RNA as an antiviral agent in animals. *Methods Mol. Biol.* 629, 339–353.

Bejerano-Sagie, M., Oppenheimer-Shaanan, Y., Berlatzky, I., Rouvinski, A., Meyerovich, M., and Ben-Yehuda, S. (2006). A checkpoint protein that scans the chromosome for damage at the start of sporulation in *Bacillus subtilis*. *Cell* 125, 679–690. doi: 10.1016/j.cell.2006.03.039

Cobaleda, C., and Sánchez-García, I. (2000). In vivo inhibition by a site-specific catalytic RNA subunit of RNase P designed against the BCR-ABL oncogenic products: a novel approach for cancer treatment. *Blood* 95, 731–737. doi: 10.1182/blood.v95.3.731.003k28_731_737

Corrigan, R. M., and Gründling, A. (2013). Cyclic di-AMP: another second messenger enters the fray. *Nat. Rev. Microbiol.* 11, 513–524. doi: 10.1038/nrmicro3069

Devonshire, A. S., Sanders, R., Whale, A. S., Nixon, G. J., Cowen, S., Ellison, S. L. R., et al. (2016). An international comparability study on quantification of mRNA gene expression ratios: CCQM-P103.1. *Biomol. Detect. Quantif.* 8, 12–28.

Ezeji, T. C., Groberg, M., Qureshi, N., and Blaschek, H. P. (2003). Continuous production of butanol from starch-based packing peanuts. *Appl. Biochem. Biotechnol.* 108, 375–382. doi: 10.1385/abab:106:1-3:375

Ezeji, T. C., Milne, C., Price, N. D., and Blaschek, H. P. (2010). Achievements and perspectives to overcome the poor solvent resistance in acetone and butanol-producing microorganisms. *Appl. Microbiol. Biotechnol.* 85, 1697–1712. doi: 10.1007/s00253-009-2390-0

Ezeji, T. C., Qureshi, N., and Blaschek, H. P. (2007). Butanol production from agricultural residues: impact of degradation products on *Clostridium beijerinckii* growth and butanol fermentation. *Biotechnol. Bioeng.* 97, 1460–1469. doi: 10.1002/bit.21373

Forster, A. C., and Altman, S. (1990). External guide sequence for an RNA enzyme. *Science* 249, 783–786. doi: 10.1126/science.1697102

Gopalan, V., Vioque, A., and Altman, S. (2002). RNase P: variations and uses. *J. Biol. Chem.* 277, 6759–6762. doi: 10.1074/jbc.r100067200

Grupe, H., and Gottschalk, G. (1992). Physiological events in *Clostridium acetobutylicum* during the shift from acidogenesis to solventogenesis in continuous culture and presentation of a model for shift induction. *Appl. Environ. Microbiol.* 58, 3896–3902. doi: 10.1128/aem.58.12.3896-3902.1992

Guerrier-Takada, C., and Altman, S. (2000). Inactivation of gene expression using ribonuclease P and external guide sequences. *Methods Enzymol.* 313, 442–456. doi: 10.1016/s0076-6879(00)13028-9

Hall, B. G., Pikis, A., and Thompson, J. (2009). Evolution and biochemistry of family 4 glycosidases: implications for assigning enzyme function in sequence annotations. *Mol. Biol. Evol.* 26, 2487–2497. doi: 10.1093/molbev/msp162

Ho, N. W., Chen, Z., and Brainard, A. P. (1998). Genetically engineered Saccharomyces yeast capable of effective cofermentation of glucose and xylose. *Appl. Environ. Microbiol.* 64, 1852–1859. doi: 10.1128/aem.64.5.1852-1859.1998

Jones, D. T., and Woods, D. R. (1986). Acetone-butanol fermentation revisited. *Microbiol. Rev.* 50, 484–524. doi: 10.1128/mr.50.4.484-524.1986

Khvorova, A., Lescoute, A., Westhof, E., and Jayasena, S. D. (2003). Sequence elements outside the hammerhead ribozyme catalytic core enable intracellular activity. *Nat. Struct. Biol.* 10, 708–712. doi: 10.1038/nsb959

Kim, A. Y., and Blaschek, H. P. (1993). Construction and characterization of a phage-plasmid hybrid (phagemid), pCAK1, containing the replicative form of virus-like particle CAKi isolated from *Clostridium acetobutylicum* NCIB 64444. *J. Bacteriol.* 175, 3838–3842. doi: 10.1128/jb.175.12.3838-3843.1993

Lai, L. B., Vioque, A., Kirsebom, L. A., and Gopalan, V. (2010). Unexpected diversity of RNase P, an ancient tRNA processing enzyme: challenges and prospects. *FEBS Lett.* 584, 287–296. doi: 10.1016/j.febslet.2009.11.048

Leboeuf, C., Leblanc, L., Auffray, Y., and Hartke, A. (2000). Characterization of the CcpA gene of Enterococcus faecalis: identification of starvation-inducible proteins regulated by CcpA. *J. Bacteriol.* 182, 5799–5806. doi: 10.1128/jb.182.20.5799-5806.2000

Li, Y., and Altman, S. (1996). Cleavage by RNase P of gene N mRNA reduces bacteriophage lambda burst size. *Nucleic Acids Res.* 24, 835–842. doi: 10.1093/nar/24.5.835

Liu, F. (2010). "Ribonuclease P as a tool," in *Ribonuclease P*, eds F. Liu and S. Altman (New York: Springer), 153–172.

Liu, F., and Altman, S. (1995). Inhibition of viral gene expression by the catalytic RNA subunit of RNase P from *Escherichia coli*. *Genes Dev.* 9, 471–480. doi: 10.1101/gad.9.4.471

Ludwig, H., Meinken, C., Martin, A., and Stulke, J. (2002). Insufficient expression of the ilv-leu operon encoding enzymes and branched-chain amino acid biosynthesis limits growth of *Bacillus subtilis* CcpA mutant. *J. Bacteriol.* 184, 5174–5178. doi: 10.1128/jb.184.18.5174-5178.2002

Lundblad, E. W., Xiao, G., Ko, J. H., and Altman, S. (2008). Rapid selection of accessible and cleavable sites in RNA by *Escherichia coli* RNase P and random external guide sequences. *Proc. Natl. Acad. Sci. U.S.A.* 105, 2354–2357. doi: 10.1073/pnas.0711977105

Mazzeo, M. F., Cacace, G., Peluso, A., Zotta, T., Muscariello, L., Vastano, V., et al. (2012). Effect of inactivation of CcpA and aerobic growth in *Lactobacillus plantarum*: A proteomic perspective. *J. Proteomics* 75, 4050–4061. doi: 10.1016/j.jprot.2012.05.019

Mehne, F. M. P., Gunka, K., Eilers, H., Herzberg, C., Kaever, V., and Stülke, J. (2013). Cyclic di-AMP homeostasis in *Bacillus subtilis*: both lack and high level accumulation of the nucleotide are detrimental for cell growth. *J. Biol. Chem.* 288, 2004–2017. doi: 10.1074/jbc.m112.395491

Mitchell, W. J. (1998). Physiology of carbohydrate to solvent conversion by clostridia. *Adv. Microb. Physiol.* 39, 31–130. doi: 10.1016/s0065-2911(08)60015-6

Oppenheimer-Shaanan, Y., Wexeselblatt, E., Katzhendler, J., Yavin, E., and Ben-Yehuda, S. (2011). c-di-AMP reports DNA integrity during sporulation in *Bacillus subtilis*. *EMBO Rep.* 12, 594–601. doi: 10.1038/embor.2011.77

Ounine, K., Petitdemange, H., Raval, G., and Gay, G. (1985). Regulation and butanol inhibition of D-xylose and D-glucose uptake in *Clostridium acetobutylicum*. *Appl. Environ. Microbiol.* 49, 874–878. doi: 10.1128/aem.49.4.874-878.1985

Payne, M. E., Bruder, M. R., Moo-Young, M., Chung, D. A., and Chou, C. P. (2016). Harnessing heterologous and endogenous CRISPR-Cas machineries for efficient markerless genome editing in *Clostridium*. *Sci. Rep.* 6:25666.

Przybilski, R., Gräf, S., Lescoute, A., Nellen, W., Westhof, E., Steger, G., et al. (2005). Functional hammerhead ribozymes naturally encoded in the genome of *Arabidopsis thaliana*. *Plant Cell* 17, 1877–1885. doi: 10.1105/tpc.105.032730

Ren, C., Gu, Y., Hu, S., Wu, Y., Wang, P., Yang, Y., et al. (2010). Identification and inactivation of pleiotropic regulator CcpA to eliminate glucose repression of xylose utilization in *Clostridium acetobutylicum*. *Metab. Eng.* 12, 446–454. doi: 10.1016/j.ymben.2010.05.002

Ren, C., Gu, Y., Wu, Y., Zhang, W., Yang, C., Yang, S., et al. (2012). Pleiotropic functions of catabolite control protein CcpA in butanol-producing *Clostridium acetobutylicum*. *BMC Genomics* 13:349. doi: 10.1186/1471-2164-13-349

Scott, C. W., and Engelke, D. R. (2006). Ribonuclease P: the evolution of an ancient RNA enzyme. *Crit. Rev. Biochem. Mol. Biol.* 41, 77–102. doi: 10.1080/10409230600602634

Shi, Y., Li, Y. X., and Li, Y. Y. (2010). Large number of phosphotransferase gens in the *Clostridium beijerinckii* NCIMB 8052 genome and study on their evolution. *BMC Bioinformatics* 11(Suppl. 11):S9.

Siemerink, A. J., Kuit, W., López-Contreras, A. M., Eggink, G., van der Oost, J., and Kengen, S. W. M. (2011). D-2,3-butanediol production due to heterologous expression of an acetoin reductase in *Clostridium acetobutylicum*. *Appl. Environ. Microbiol.* 77, 2582–2588. doi: 10.1128/aem.01616-10

Singh, K. D., Schmalisch, M. H., Stülke, J., and Görke, B. (2008). Carbon catabolite repression in *Bacillus subtilis*: quantitative analysis of repression exerted by different carbon sources. *J. Bacteriol.* 190, 7275–7284. doi: 10.1128/jb.00848-08

Spitale, R. C., Crisalli, P., Flynn, R. A., Torre, E. A., Kool, E. T., and Chang, H. Y. (2013). RNA SHAPE analysis in living cells. *Nat. Chem. Biol.* 9, 18–20. doi: 10.1038/nchembio.1131

Stülke, J., and Krüger, L. (2020). Cyclic di-AMP signaling in bacteria. *Annu. Rev. Microbiol.* 74, 159–179. doi: 10.1146/annurev-micro-020518-115943

Sureka, K., Choi, P. H., Precit, M., Delince, M., Pensinger, D. A., Huynh, T. N., et al. (2014). The cyclic dinucleotide c-di-AMP is an allosteric regulator of metabolic enzyme function. *Cell* 158, 1389–1401. doi: 10.1016/j.cell.2014.07.046

Tsai, H. Y., Lai, L. B., and Gopalan, V. (2002). A modified Bluescript vector for facile cloning and transcription of RNA. *Anal. Biochem.* 303, 214–217. doi: 10.1006/abio.2001.5567

Uhlenbeck, O. C. (1987). A small catalytic oligoribonucleotide. *Nature* 328, 596–600. doi: 10.1038/328596a0

Ujor, V., Agu, C. V., Gopalan, V., and Ezeji, T. C. (2014). Glycerol supplementation enhances furfural detoxification by *Clostridium beijerinckii* during butanol fermentation. *Appl. Microbiol. Biotechnol.* 98, 6511–6521. doi: 10.1007/s00253-014-5802-8

Vioque, A., Arnez, J., and Altman, S. (1988). Protein-RNA interactions in the RNase P holoenzyme from *Escherichia coli*. *J. Mol. Biol.* 202, 835–848. doi: 10.1016/0022-2836(88)90562-1

Watters, K. E., Abott, T. R., and Lucks, J. B. (2016). Simultaneous characterization of cellular RNA structure and function with in-cell SHAPE-Seq. *Nucleic Acids Res.* 44:e12. doi: 10.1093/nar/gkv879

Whiteley, A. T., Pollock, A. J., and Portnoy, D. A. (2015). The PAMP c-di-AMP is essential for Listeria monocytogenes growth in rich but not minimal media due to a toxic increase in (p)ppGpp. *Cell Host Microbe* 17, 788–798. doi: 10.1016/j.chom.2015.05.006

Yang, Y., Zhang, H., Lang, N., Zhang, L., Chai, C., He, H., et al. (2020). The small RNA sr8384 is a crucial regulator of cell growth in solventogenic clostridia. *Appl. Envi. Microbiol.* 86:e00665-20.

Zhang, J., Zong, W., Hong, W., Zhang, Z.-T., and Wang, Y. (2018). Exploiting endogenous CRISPR-Cas system for multiplex genome editing in *Clostridium tyrobutyricum* and engineer the strain for high-level butanol production. *Metab. Eng.* 47, 49–59. doi: 10.1016/j.ymben.2018.03.007

Zhang, Y., and Ezeji, T. C. (2013). Transcriptional analysis of *Clostridium beijerinckii* NCIMB 8052 to elucidate the role of furfural stress during acetone butanol fermentation. *Biotechnol. Biofuels* 6, 66–82. doi: 10.1186/1754-6834-6-66

Zhao, J., Qian, X., Yeung, P. Y., Zhang, Q. F., and Kwok, C. K. (2019). Mapping in vivo RNA structures and interactions. *Trends Biochem. Sci.* 44, 555–556. doi: 10.1016/j.tibs.2019.01.012

Zuker, M. (2003). Mfold web server for nucleic acid folding and hybridization prediction. *Nucleic Acids Res.* 31, 3406–3415. doi: 10.1093/nar/gkg595

Zverlov, V. V., Berezina, O., Velikodvorskaya, G. A., and Schwarz, W. H. (2006). Bacterial acetone and butanol production by industrial fermentation in the Soviet Union: use of hydrolyzed agricultural waste for biorefinery. *Appl. Microbiol. Biotechnol.* 71, 587–597. doi: 10.1007/s00253-006-0445-z

Conflict of Interest: The authors declare that the research was conducted in the absence of any commercial or financial relationships that could be construed as a potential conflict of interest.

frontiers in Bioengineering and Biotechnology

ORIGINAL RESEARCH
published: 16 June 2021
doi: 10.3389/fbioe.2021.609345

A Series of Efficient Umbrella Modeling Strategies to Track Irradiation-Mutation Strains Improving Butyric Acid Production From the Pre-development Earlier Stage Point of View

*Li Cao[1†], Yue Gao[2,3†], Xue-Zhen Wang[1], Guang-Yuan Shu[1], Ya-Nan Hu[1], Zong-Ping Xie[1], Wei Cui[1], Xiao-Peng Guo[2,3] and Xiang Zhou[2,3]**

[1] College of Life Sciences and Engineering, Hexi University, Zhangye, China, [2] Institute of Modern Physics, Chinese Academy of Sciences, Lanzhou, China, [3] College of Life Science, University of Chinese Academy of Sciences, Beijing, China

Clostridium tyrobutyricum (*C. tyrobutyricum*) is a fermentation strain used to produce butyric acid. A promising new biofuel, n-butanol, can be produced by catalysis of butyrate, which can be obtained through microbial fermentation. Butyric acid has various uses in food additives and flavor agents, antiseptic substances, drug formulations, and fragrances. Its use as a food flavoring has been approved by the European Union, and it has therefore been listed on the EU Lists of Flavorings. As butyric acid fermentation is a cost-efficient process, butyric acid is an attractive feedstock for various biofuels and food commercialization products. $^{12}C^{6+}$ irradiation has advantages over conventional mutation methods for fermentation production due to its dosage conformity and excellent biological availability. Nevertheless, the effects of these heavy-ion irradiations on the specific productiveness of *C. tyrobutyricum* are still uncertain. We developed non-structured mathematical models to represent the heavy-ion irradiation of *C. tyrobutyricum* in biofermentation reactors. The kinetic models reflect various fermentation features of the mutants, including the mutant strain growth model, butyric acid formation model, and medium consumption model. The models were constructed based on the Markov chain Monte Carlo model and logistic regression. Models were verified using experimental data in response to different initial glucose concentrations (0–180 g/L). The parameters of fixed proposals are applied in the various fermentation stages. Predictions of these models were in accordance well with the results of fermentation assays. The maximum butyric acid production was 56.3 g/L. Our study provides reliable information for increasing butyric acid production and for evaluating the feasibility of using mutant strains of *C. tyrobutyricum* at the pre-development phase.

Keywords: *Clostridium tyrobutyricum*, butyric acid, MCMC model, logistic regression, luedeking—piret model, fermentation

OPEN ACCESS

Edited by:
Hongxin Fu,
South China University of Technology, China

Reviewed by:
Wenjing Cui,
Jiangnan University, China
Qiuqiang Gao,
Columbia University, United States

***Correspondence:**
Xiang Zhou
syannovich@gmail.com;
syannovich@impcas.ac.cn

†These authors have contributed equally to this work

Specialty section:
This article was submitted to Synthetic Biology, a section of the journal Frontiers in Bioengineering and Biotechnology

Received: *23 September 2020*
Accepted: *10 May 2021*
Published: *16 June 2021*

Citation:
Cao L, Gao Y, Wang X-Z, Shu G-Y, Hu Y-N, Xie Z-P, Cui W, Guo X-P and Zhou X (2021) A Series of Efficient Umbrella Modeling Strategies to Track Irradiation-Mutation Strains Improving Butyric Acid Production From the Pre-development Earlier Stage Point of View. Front. Bioeng. Biotechnol. 9:609345. doi: 10.3389/fbioe.2021.609345

INTRODUCTION

Butyrate ($C_4H_8O_2$) possesses a structure of saturated tetra-carboxylic acid; the name, butyric acid is derived from the Latin word for butter (Gutteridge, 1981; Ren et al., 1997; Bettelheim et al., 2012). Butyric acid and its acid salts are used in numerous commercial products, including food additives and flavors, antiseptics, cellulose-based plastic products, drug formulations, and aromatics (Zigová and Sturdik, 2000; Agler et al., 2011; Jiang et al., 2011). Further, butyric acid can be used to prepare various butyrate esters. Methyl butyrate, which is a low-molecular-weight ester of butyric acid; it has a more pleasant aroma or better taste compared to those associated with butyric acid. Therefore, methyl butyrate is used as a food and perfume additive. Animal feed is also supplied in combination with methyl butyrate to reduce colonization of pathogenic bacteria. The use of butyric acid as a food flavoring has been approved by the European Union, and it has therefore been listed on the EU Lists of Flavorings in the EU FLAVIS database (Flavis number: 08.005). Butyric acid is generally present at concentrations of 82 mg/kg in candy, 60–270 mg/kg in chewing gum, 32 mg/kg in baked foods, 18 mg/kg in margarine, and 6.5 mg/kg in cold drinks. It has also been used as a fishing bait additive due to its powerful odor. Many commercially available flavors that are used in carp bait use butyric as their ester base. Butyric acid was previously produced through the oxidation of butyraldehyde [CH_3 $(CH_2)_2$ CHO] (Henstra et al., 2007; Dagaut et al., 2009; Jin et al., 2011). However, customers tend to choose food additives, flavors as well as fragrances containing natural ingredients (Ragauskas et al., 2006; Nigam and Singh, 2011; Zhou et al., 2013a,b).

Butyric acid was previously widely produced through the oxidation of butyraldehyde. However, limited fossil resources and increasing environmental concerns have resulted in a switch to microbial fermentation, a green and renewable technology. A promising new biofuel, n-butanol, can be produced by the catalysis of butyrate, which can be obtained through microbial fermentation (Munasinghe and Khanal, 2010). Previous studies have demonstrated that *Clostridium tyrobutyricum (C. tyrobutyricum)* produces more butyrate than other strains. *C. tyrobutyricum* produces a relatively large amount of butyrate from five- or six-carbon sugars with high efficiency. Recently, research has identified improved *C. tyrobutyricum* strains (compared to traditional mutation and molecular biology methods). Mutagenic technology is reliable and is widely used for strain improvement. Various mutation approaches are commonly employed in mutational engineering to produce bacteria with novel traits; these include chemical and physical mutagenesis. Afterward, bacteria strains produced using such technologies are screened by selective medium to identify mutant strains with remarkable performance and application value. Because of the frequent use of traditional mutagenic approaches, several engineering strains have build up tolerance. Hence, investigators have begun to establish novel methods for enabling microbe mutagenesis; heavy ion beam irradiation, considered as a highly efficient irradiating method, has been employed in a variety of studies aimed at developing novel bacterial strains using mutagenesis, and this strategy has achieved remarkable success with good economic benefits (**Table 1**). At present, fermentation-derived butyric acid plays an important role as a food additive. Microorganism fermentation engineering is the cornerstone of bioengineering and biotechnology. It is the fundamental application of biotechnology and its use is at the core of the biotechnology industry. Butyric acid fermentation processes have been limited by two factors, i.e., the production performance of *C. tyrobutyricum* with respect to butyric acid, and the fermentation conditions. In recent decades, the fermentation industry has developed rapidly, and its scale has grown. In order to obtain maximum efficiency from industrial-scale production, we must ensure optimal conditions for *C. tyrobutyricum* to grow and synthesize metabolites. Therefore, the optimization of fermentation conditions is becoming increasingly important. Previous studies have demonstrated that *C. tyrobutyricum* produces more butyrate than other strains (Lan and Liao, 2012; Jang et al., 2012, 2014). *C. tyrobutyricum* produces high levels butyrate from five- or six-carbon sugars (Tao et al., 2008; Peralta-Yahya et al., 2012; Zhou et al., 2014a) with high efficiency. Recently, *C. tyrobutyricum* strains with improved performance compared to that of *C. tyrobutyricum* strains produced using traditional mutation and molecular biology methods have been developed (Choi et al., 2012; Dwidar et al., 2012; Pappu et al., 2013). Artificial manipulation of traditional mutation strategies used for butyrate production was unable to result in the production of mutants with satisfactory butyric acid mass production abilities. Thus, it cannot be used as a suitable technique for scaling up industrial fermentation (Yu et al., 2011; Mattam and Yazdani, 2013; Zhou et al., 2017).

One breeding tactics were put forward with respect to existing situation, as an important breeding method, heavy ion beam radiation mutagenesis breeding has the advantages of high mutation rate, wide mutation spectrum, stable mutants, and short breeding cycle. Induced heavy ion beam radiation mutagenesis is one of the most effective and economy means for the proper utilization of the existing well-characterized *C. tyrobutyricum* strains resources, especially self-owned traits improvement and enhancement without altering good optimization-genetic background of the strains. The heavy ion beam radiation mutagenesis has enormous potential to accelerate the mutation breeding in *C. tyrobutyricum* strains, it will be become fully aware of as a fact that rapid improvement of *C. tyrobutyricum* quality and its yield of butyric acid. Rheological properties of the bioprocessing and the downstream manufacturing of butyric acid are greatly rely on the production capacity of mutant *C. tyrobutyricum*, therefore cautiously designed $^{12}C^{6+}$ heavy-ion radiation indices are required. An appropriate mathematical model is the basis and prerequisite for process control and optimization. Toward this, in the context of $^{12}C^{6+}$ heavy-ion radiation the first step is the modeling of $^{12}C^{6+}$ heavy-ion radiation parameters and the fermentation process, and the second step is the process control and optimization. In this study, the $^{12}C^{6+}$ heavy-ion radiation has been used for bioprocess and biological fermentation devisal and scale-up cultivation. Associated empirical models aimed at the biological fermentation of mutant strains have been proposed to optimize operation conditions for mutational strain growth, butyric acid generation, and glucose consuming, because promoting butyric

TABLE 1 | Traditional mutagenesis methods and heavy-ion irradiation with the reported mutation methods are widely used in strain improvement.

Mutants	Sources	Mutant methods	References
Aurantiochytrium sp. T-99	*Aurantiochytrium* sp. CGMCC 6208	Heavy-ions mutagenesis	Cheng et al., 2016
Trichoderma viride CIT 626	*T. viride* GSICC 62010	$^{12}C^{6+}$-ion beam irradiation and Electron beam irradiation	Li et al., 2016
Streptomyces fungicidicus M30	*S. fungicidicus* SG-01	Heavy ion mutagenesis	Liu et al., 2018
Chlorella K05	*C. pyrenoidosa* FACHB-9	Heavy-ion irradiation mutagenesis	Song et al., 2018
Mortierella alpina F-23	*M. alpina* SD003 (CGMCC No.7960)	Heavy ion mutagenesis	Zhang et al., 2018
Lactobacillus thermophilus A69	*L. thermophilus*	Heavy ion irradiation	Tian et al., 2019
Streptomyces avermitilis 147-$G_5$8	*S. avermitilis* AV-J-AO	Heavy-Ion beam Irradiation	Wang et al., 2017
Arthrobacter strain C2	*A. strain* C1	$^{12}C^{6+}$ heavy-ion beam	Li et al., 2018
Blakeslea trispora WY-239	*B. trispora* NRRL 2895	Mutation with ARTP	Wang et al., 2020
Chiba maru No. 10	*Colocasia esculenta* L. Schott	Heavy-ion beam irradiation	Matsuyama et al., 2020
Gamma ray-induced mutants (M_7)	Rice (*Oryza sativa* L.)	Gamma Ray	Hwang et al., 2020
Clostridium carboxidivorans P7-EMS$_{III-J}$	*C. carboxidivorans* (P7)	Ethyl methanesulfonate (EMS)	Lakhssassi et al., 2020
Oryza sativa L. *m3*	*Indica* landrace BBS.	Carbon ion irradiation	Peng et al., 2019
Aspergillus fumigatus MS160.53	*A. fumigatus* MS13.1	Heavy ion beam mutagenesis	Dong et al., 2019
Aspergillus niger H_{11201} *Clostridium tyrobutyricum* No. H51–8–4	*A. niger* H_{11} *C. tyrobutyricum* strains ATCC 25755	$^{12}C^{6+}$ ion beam	Jiang et al., 2016
Yarrowia lipolytica Mut-96	*Y. lipolytica* Wt-11	Low-energy ion implantation	Ping et al., 2018
Monascus purpureus KS301U and KS302U	*M. purpureus* KUPM5	UV (Ultraviolet) irradiation and NTG (N-methyl-N'-nitro-N-nitrosoguanidine) treatment	Ketkaeo et al., 2020
C. tyrobutyricum C.T^{UV}	*C. tyrobutyricum* DSM 2637	UV irradiation, nitrous acid, and ethidium bromide treatment	Akhtar et al., 2018

acid production is vital for future utilizations of the process in bio-fermentation field.

MATERIALS AND METHODS

$^{12}C^{6+}$ Heavy-Ion Beam Irradiation

Previous studies have been reported the heavy-ion radiation experimental setups (Zhou et al., 2014b). The extracting time of $^{12}C^{6+}$ heavy ions (about 220 AMeV) was about 3 s, additionally the dosage of priming was 50–90 Gy. The dose rates were 5 Gy/min. Following operation parameters were used: energy input of radiation, 220 AMeV; the distance from $^{12}C^{6+}$ heavy ion nozzle exits to spore suspensions, 4 mm; temperature of the $^{12}C^{6+}$ heavy-ion beams, < 36–38°C. Inoculum was prepared as previous research reported by Roos et al. (1985) and Wiesenborn et al. (1988). Cell strains from an independent colony on a 3 × Reinforced Clostridial semi-defined P2 medium base plate (RCM-DRCM, AppliChem, Germany), were transferred to 250 mL of semi-defined P2 medium and cultured for 18 h.

Strain Growth and Cultivation Medium

Wild-type *Clostridium. tyrobutyricum* (ATCC 25755) was obtained from the Biophysics Research Laboratory, Institute of Modern Physics, Chinese Academy of Sciences, China. The optimized culture medium included the following (g/L): yeast extract, 4.2; peptone, 3.1; K_2HPO_4, 2.7; KH_2PO_4, 3.6; $MgSO_4$, 0.3; $MnSO_4$, 0.25; $FeSO_4$, 0.03; NaCl, 0.03; yeast extract, 1.6 (Difco, Detroit, MI, United States); ammonium acetate, 2.5; *p*-aminobenzoate, 0.0003; thiamin, 0.0003; biotin, 5×10^{-5}; thiamphenicol, 3.5×10^{-5}. Samples were stored in an anaerobic chamber. The inoculum preparation and batch anaerobic fermentations were conducted in the 7-L BioFlo®/CelliGen^{TM} 115 fermentor/bioreactor (New Brunswick Scientific Co., Edison, NJ) including 270 mL inoculum added to 2 L of reinforced clostridial semi-defined P2 medium. The P2 medium contained the following ingredients (g/L): yeast extract powder, 1; KH_2PO_4, 0.5; K_2HPO_4, 0.5; para-aminobenzoic acid, 0.001; thiamin, 0.001; biotin, 1×10^{-5}; $MgSO_47H_2O$, 0.2; $MnSO_47H_2O$, 0.01; $Fe_2SO_47H_2O$, 0.01; NaCl, 0.01; and ammonium acetate, 2.2. The initial glucose concentrations were 0–180 g/L. The temperature, pH value, and agitating speed remained at 36–38°C, 6.0–6.2, and 160 rpm, respectively. A nitrogen without oxygen supply rate of 60–65 mL/min was maintained. The optimal concentrations were 650 g/L of glucose as well as 22.5 g/L of $MgSO_4{\cdot}7H_2O$.

Analysis Methods

The system of high-performance liquid chromatography (HPLC) was applied to detect and analyze carbohydrates (containing glucose) in the liquid medium for fermentation. This HPLC system was comprised of an auto-injector (Agilent 1100, G1313A), a Zorbax carbohydrate analytical column

(250 mm × 4.6 mm, 5 μm; Agilent, United States), a high-pressure pump (Agilent 1100, G1311A), a refractive index detector (Agilent 1100, G1362A) as well as a column oven retained at 30°C (Agilent 1100, G1316A). Ethyl nitrile was selected as mobile phase (the ratio of water/ethyl nitrile = 1:3), and the flow rate was 1.5 mL/min. Butyrate and acetate were detected by a gas chromatograph (GC) (Shimadzu, Columbia, MD, United States, GC-2014) which was furnished with a fused silica column (0.25 mm film thickness and 0.25 mm ID, 30 m, Stabilwax-DA) as well as a flame ionization detector. The injection temperature of GC was 200°C, and per microliter sample was injected through an automatic injector (Shimadzu, AOC-20i). The temperature of column remained at 80°C within 3 min, then increased to 150°C at a rate of 30°C per minute, eventually remained at 150°C lasting 3.7 min. Moreover, the cell density was analyzed via testing the optical density values (OD) of the cell suspensions at 600 nm by a UV-spectrophotometer (Genesys 20, Thermo Scientific, United States) with a transition of 0.412 ± 0.012 g/L of dry cell weight (DCW) for each OD unit. The levels of elemental carbon (C), hydrogen (H), oxygen (O) and nitrogen (N) were detected by Sercon-GSL (CE Instruments, Milan, Italy).

Survival Fraction Determination: Mtt Assay

The survival fraction can be identified as previously noted (Buch et al., 2012). Hundred microliter MTT reagent (0.25 g/L) per well was added into Dulbecco's revised Eagle's medium (DMEM, Gibco Glasgow, United Kingdom), and cultured at 36–38°C for 40 min. MTT experiment was conducted by 128-well plates which contained 5,500–7,500 cells for each well. The survival fraction was calculated using the following equation (Price and McMillan, 1990):

$$Survival\ fraction = 2^{-n}, \quad \mathrm{n} = \frac{T_{delay}}{T_{doubling\ time}} \tag{1}$$

where T_{delay} is the time for achieving the specific absorption values of the control groups vs. the irradiation cells, while $T_{doublingtime}$ is the time needed for doubling the content of cells.

Monod Kinetic Model

The Monod equation is regarded as a kinetic model which exhibits microbe growth as a function of specific growth rate and an essential substrate concentration (Lobry et al., 1992). The Monod model was modified by introducing a substrate inhibition term (Drapcho, 2006):

$$\frac{dX}{dt} = \mu X = \frac{\mu_m S}{\left(S + K_s + {S^2}/{K_I}\right)} \times X \tag{2}$$

$$\frac{dX}{dt} = \mu X = \frac{\mu_m S}{\left(S + K_s + {S^2}/{K_I}\right)} \times \left(1 - \frac{P}{P_\mathrm{d}}\right)^i X \tag{3}$$

where X is the dry cell weight (g/L), μ represents the growth rate (1/h), μ_m represents the maximal growth rate (1/h), S means the growth-restricting substrate concentration (g/L), K_S, and K_I are constants of substrate saturation and substrate inhibition, respectively (g/L), P means the products concentration (g/L), P_d represents the product concentration without cell growth, then i represents the inhibitory extent of product. In this study, P is the total amount of butyric acid (g/L), and P_d is the total amount of acetic acid (g/L).

Luedeking—Piret Model

The Luedeking—Piret model is a microbe growth model possessed a growth-related portion as well as a non-growth-related portion. The Luedeking–Piret model can be revised by introduction of a term of substrate inhibition (Luedeking and Piret, 1959; Kubicek et al., 1985):

$$\frac{dP}{dt} = \alpha\frac{dX}{dt} + \beta X\left(1 - \frac{[HL]}{HL_{inh}}\right) \tag{4}$$

We rewrote the formula as follows:

$$\frac{dP_1}{dt} = \alpha_1\frac{dX}{dt} + \beta_1 X, \ \frac{dP_2}{dt} = \alpha_2\frac{dX}{dt} + \beta_2 X \tag{5}$$

where P_1 is the concentration of butyrate (g/L), P_2 is the concentration of acetate (g/L), α is cell growth related (g/g), and β is non-growth-related (g/g/h).

Statistical Analysis

Several mathematical formulas, such as the Jacobian matrix of the vector function, the sum-of-squares function, loglog counting, logistic regression as well as Probit regression, were used to analyze predicted simulation values.

RESULTS AND DISCUSSION

$^{12}C^{6+}$ Heavy-Ion Energy Input and Dose Dominating Survivors

Several experiments were conducted using varying irradiation dose parameters (50–80 Gy), and the survival rates (10.2–84.7%) were in comparison with a representative group of experimental results to determine the optimal $^{12}C^{6+}$ heavy ions for 220-AMeV energy input and the appropriate dose. Based on the strain characteristics and survival rates, sample points were randomly assigned prior to any data-processing tasks. This selection strategy helped avoid bias from the human operator. The heavy-ion beam irradiation experiments were classified into three groups of seven samples each (**Table 2**), No. Q36–8–1, No. S24–3–2, No. H51–8–3, H51–8–4, No. S24–3–5, No. Q36–8–6, and Q36–8–7. These experiments were composed of 21 independent irradiating tests and their results. The survival probability decreased upon increasing the irradiation dose (**Table 2**). A total of n = 5,900 cell strains were irradiated, eventually causing 900 of cell death. In strains subjected to random $^{12}C^{6+}$ heavy-ion irradiation, n = 5,900 strains received the lowest irradiation dose (50 Gy), and the survival proportion varied from 0 to 1. We modeled cell strain lethality as a function of irradiation dosage

TABLE 2 | Random sampling locations after $^{12}C^{6+}$ heavy-ion irradiation with an energy input of 220 AMeV and a dose of 50∼80 Gy.

SampleNo. Q36-8	Irradiation dose	Log of irradiation dose	Total of cells strains	Total of cells strains lethal	Survival proportion
1	50 Gy	1.6989	5,900	900	0.8475
2	55 Gy	1.7403	6,250	2,470	0.6048
3	60 Gy	1.7782	5,500	2,940	0.4655
4	65 Gy	1.8129	5,600	3,250	0.4196
5	70 Gy	1.8451	6,300	5,170	0.1794
6	75 Gy	1.8575	5,900	5,300	0.1017
7	80 Gy	1.9031	6,200	6,200	0
SampleNo. S24–3	**Irradiation dose**	**Log of irradiation dose**	**Total of cells strains**	**Total of cells strains lethal**	**Survival proportion**
1	50 Gy	1.6989	6,100	740	0.8787
2	55 Gy	1.7403	6,000	2,300	0.6167
3	60 Gy	1.7782	5,900	3,150	0.4661
4	65 Gy	1.8129	5,600	3,270	0.4161
5	70 Gy	1.8451	6,300	5,200	0.1746
6	75 Gy	1.8575	6,200	5,490	0.1145
7	80 Gy	1.9031	6,100	6,100	0
SampleNo. H51–8	**Irradiation dose**	**Log of irradiation dose**	**Total of cells strains**	**Total of cells strains lethal**	**Survival proportion**
1	50 Gy	1.6989	6,200	730	0.8823
2	55 Gy	1.7403	5,500	3,430	0.6236
3	60 Gy	1.7782	6,200	3,200	0.4839
4	65 Gy	1.8129	5,600	3,100	0.4464
5	70 Gy	1.8451	5,500	4,560	0.1709
6	75 Gy	1.8575	6,300	5,600	0.1111
7	80 Gy	1.9031	5,600	5,600	0

by means of a regression model and a −2 log-likelihood function. If y is the number of dead cells (strains), then y can be used as a random variable along with a binomial distribution expressed by the formula as shown below:

$$P\left(y=k\right)=\binom{n}{k}p^{k}\left(1-p\right)^{n-k} \tag{6}$$

where y assumes a value called k, and k = 0, 1,. . .5,900. We thus have a binomial distribution where p (the success probability) depends upon the irradiating dose x:

$$\mathrm{p}\left(x\right)=\frac{e^{\beta_0+\beta_1 x}}{1+e^{\beta_0+\beta_1 x}} \tag{7}$$

where β_0 and β_1 = the regression parameters, and $p\ (x)$ varies from 0 to 1. Then a new logistic regression function can be deformed from the formula (7) to:

$$Logit\left(p\left(x\right)\right)=Log\left[p\left(x\right)/\left(1-p\left(x\right)\right)\right]=\beta_0+\beta_1 x \tag{8}$$

This equation is the link function for the logistic regression. In the random $^{12}C^{6+}$ heavy ion irradiated samples, the minimum irradiating dosage set as x_1 = 50 Gy; n_1 = 5,900 cell strains were irradiated in the dose above, leading to y_1 = 900 cell strain deaths. The likelihood function is written as:

$$L=\binom{\mathrm{n}_1}{y_1}p\left(x_1\right)^{y_1}\left(1-p\left(x_1\right)\right)^{n_1-y_1}\times\cdots\times \binom{n_m}{y_m}p\left(x_m\right)^{y_m}\left(1-p\left(x_m\right)\right)^{n_m-y_m} \tag{9}$$

where L = as and β_0 and β_1, like in function (7). The parameters of logistic regression are following:

$$\mathrm{p}\left(x\right)=\frac{e^{\beta_0+\beta_1 x_\mathrm{i}}}{1+e^{\beta_0+\beta_1 x_i}},\quad for\ \mathrm{i}=1,2,\ldots,\mathrm{m}. \tag{10}$$

During the statistical analysis, the coding work for the Markov chain Monte Carlo model and the delayed rejection and adaptive metropolis portion were used as previously described (Haario et al., 2006; Dobson and Barnett, 2008). We aimed to model lethal situations in which the proposed distributions are selected with excessively large or small variances related to the target distribution. We performed the runs repeatedly with increasing dimensions. In order to obtaining credible random experimental results, two-dimension Markov chain Monte Carlo chain as well as one-dimension parameter chain lengths can be set at 50,000 steps for whole dimensions (**Figure 1A**). For **Figure 1A**, enlarged the "Top right figures: the 1D parameter chains" (**Supplementary Figure 1**). Each dimension was required to repeat 500 times. The simulations began by randomly generating a point from the experimental data. Simple linear regression parameters were

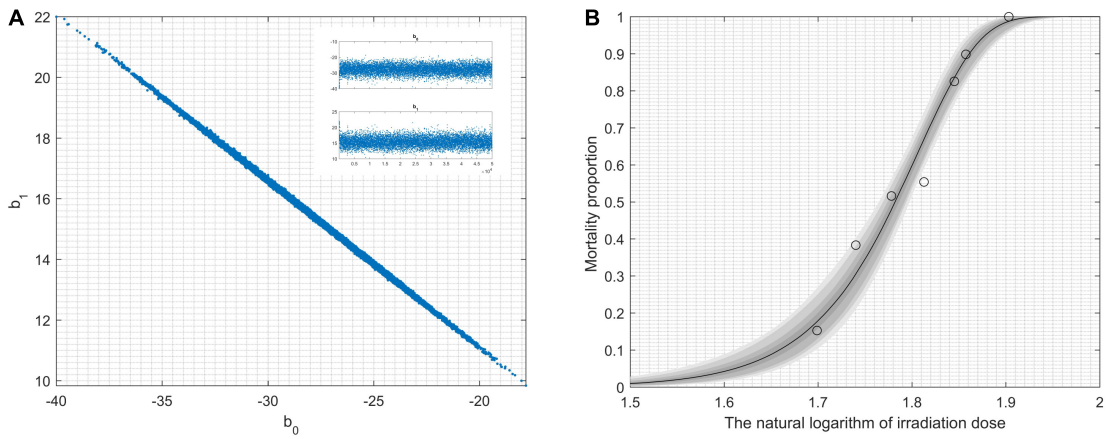

FIGURE 1 | Results obtained by modeling lethality-associated a function of irradiation-dose, and applied delayed-rejection adaptive metropolis Markov chain Monte Carlo chain (MCMC). **(A)** 2D MCMC-chain using 5.0 × 10^4 consecutive steps of delayed-rejection adaptive metropolis MCMC. Top right figures: the 1D parameter chains. **(B)** The model fit randomly selected the chain subsets, and the model-predictive envelope was developed. The gray protection system of the plot corresponds to 50, 90, 95, and 99% posterior regions.

found, including the intercept and slope from Equations (7) and (8). The maximum value of the log-likelihood function ($D = 2\left[l\left(b_{\max}\right) - l\left(b\right)\right]$) for the maximal model was -40.28. The data helped create a logistic regression model that was used to identify a correlation between radiation-related mortality of strain cells (*C. tyrobutyricum*) and $^{12}C^{6+}$ heavy ions with 220 AMeV energy input as well as a dosage of log (50–80 Gy); meanwhile the model also resulted in the production of an approximated logistic regression curve (**Figure 1B**). The gray regions correspond, respectively, to 50, 90, 95, and 99% of posterior regions. The predictions of the model were consistent with the results of the *n*-independent irradiation tests (and radiation results). The probability *(p)* of success was identical for each irradiation test. Random $^{12}C^{6+}$ heavy-ion radiation is a time-consuming technique and is not conducive to use in industrial applications. Thus, a carefully designed $^{12}C^{6+}$ heavy-ion irradiation model is invaluable and can be widely used for *C. tyrobutyricum* irradiation in industrial applications.

Determination of Positive or Negative Mutants

The generation of improved *C. tyrobutyricum* strains using mutagenesis and selection represents a better technique compared to traditional mutation methods. Molecular biology methods are essential to commercial exploitation of microbe fermentation processes. Applied heavy-ion irradiation technology represents a new, green method to produce butyric acid. The performance of *C. tyrobutyricum* mutants must be determined for use in industrial applications. Previously, we had reported that high producing mutant strains exhibited survival rates of 10.2–11.7% after $^{12}C^{6+}$ heavy-ion irradiation, and validated the expression of proteins (∼85 kDa molecular weight) in these mutants. A protein of approximately 90–106 kDa correlated with higher survival rates (10.2–11.7%) than those of the wild-type strain (Zhou et al., 2014a). The results revealed large variations in molecular weight. All mutants were identified as "*Positive*" or "*Negative*" mutants. Random $^{12}C^{6+}$ heavy-ion irradiation cannot result in the mutation of the *ack* and *pta* genes or cause accurate and reproducible damage to individual organisms. A "*Positive*" mutant demonstrated an increased ratio of $Y_{butyricacid}$:$Y_{aceticacid}$. We selected mutants at random from the 75 Gy irradiated samples (No. Q36–8–6, No. S24–3–6, and No. H51–8–6), and mixed them. These blends of samples were named as No. QSH-M-F_{80} and divided into eight groups, additionally each group contained seven samples. From these, we randomly selected two samples (**Table 3**). **Table 3** presents the $Y_{butyricacid}/Y_{aceticacid}$ ratios (δ) for all mutants and for the wild-type *C. tyrobutyricum*. In the wild-type strain, δ was typically 3.05:1, 3.25:1, or 3.32:1, whereas in the mutants, δ exceeded 5.45:1. The butyric acid productivity of the *C. tyrobutyricum* mutants had $P < 0.05$ random error, based on the mean values of five-time measurement. Strains with an increased ratio exceeding 3.05:1 exhibited a δ similar to that of the wild-type strain and were identified as "*Positive*" mutants. The $R_{M/T}$ was estimated at 19.8% and the $R_{P/T}$ at 5.8% according to the detected specific productivities of 16 mutants and the colony-forming number of each group (**Table 3**). The "*Positive*" mutant QSH-M-$F_{75_}$6–1 demonstrated the highest-butyric acid production among the randomly sampled and detected strains. The productivity of this mutant was more than 1.72-fold greater compared to wild-type strains. The models used for the optimization of the "*Positive*" mutant QSH-M-$F_{75_}$6–1 growth and acid production will be detailed below.

"*Positive*" Mutant Growth

Biofermentation was investigated using varying glucose concentrations (5, 10, 15, 20, 25, 50, 75, 100, 125, 150, and 175 g/L). To identify he kinetic parameters of the growth models of the "*Positive*" mutants, the sum-of-squares function between experimental results gained from batch fermentations and predicted results of the Monod model need to be minimized. The

TABLE 3 | Comparison butyric and acetic acid productivity after mutation via $^{12}C^{6+}$ heavy-ion irradiation with an energy input of 220 AMeV and a dose of 75 Gy at 37°C, pH = 5.5 and 6.0 during the first 70 h of fermentation (n = 5).

Group	Colony number	No. Sample	$R_{butyricacids}$ *	$R_{aceticacids}$ *	δ**
		W	34.32 ± 0.13	11.24 ± 0.09	3.05:1
QSH-M-F_{75}–1	9	QSH-M-F_{75}–1–1	43.56 ± 0.19	10.37 ± 0.23	3.43:1
		QSH-M-F_{75}–1–2	47.86 ± 0.12	9.78 ± 0.17	4.98:1
QSH-M-F_{75}–2	15	QSH-M-F_{75}–2–1	44.46 ± 0.15	10.17 ± 0.21	4.37:1
		QSH-M-F_{75}–2–2	39.78 ± 0.23	9.64 ± 0.12	4.13:1
P	*24*				
QSH-M-F_{75}–3	19	QSH-M-F_{75}–3–1	40.78 ± 0.11	12.56 ± 0.17	3.25:1
		QSH-M-F_{75}–3–2	36.35 ± 0.21	12.78 ± 0.06	2.85:1
QSH-M-F_{75}–4	17	QSH-M-F_{75}–4–1	31.67 ± 0.23	13.42 ± 0.09	2.36:1
		QSH-M-F_{75}–4–2	35.36 ± 0.32	11.87 ± 0.21	2.98:1
QSH-M-F_{75}–5	8	QSH-M-F_{75}–5–1	51.18 ± 0.16	10.27 ± 0.11	4.98:1
		QSH-M-F_{75}–5–2	49.65 ± 0.23	9.62 ± 0.12	5.16:1
QSH-M-F_{75}–6	23	QSH-M-F_{75}–6–1	58.93 ± 0.27	10.78 ± 0.13	5.45:1
		QSH-M-F_{75}–6–2	49.36 ± 0.21	9.92 ± 0.19	4.98:1
QSH-M-F_{75}–7	9	QSH-M-F_{75}–7–1	33.75 ± 0.13	12.35 ± 0.27	2.73:1
		QSH-M-F_{75}–7–2	35.63 ± 0.09	11.21 ± 0.17	3.18:1
M	81				
QSH-M-F_{75}–8	328	QSH-M-F_{75}–8–1	53.36 ± 0.18	11.36 ± 0.09	4.70:1
		QSH-M-F_{75}–8–2	35.67 ± 0.24	12.31 ± 0.18	2.90:1
T	*409*				
$R_{M/T}$ = M/T = 19.8%			$R_{P/T}$ = P/T = 5.8%		

** $R_{butyricacid}$ and *$R_{aceticacid}$ represent the percentages of the specific productivity of all mutants. $R_{butyricacid}$ and $R_{aceticacid}$ represent the percentages of the wild-type strain C. tyrobutyricum (W). **δ indicates the $Y_{butyricacid}$:$Y_{aceticacid}$ ratio. P represents the total colony number of positive mutants. M represents the total number of mutants, including positive and negative mutations. T represents the total colony number of P and M.*

Monod model is expressed by the following system of non-linear equations:

$$y_i = \frac{\theta_1 x_i}{\theta_2 + x_i} + e_i \tag{11}$$

where y_i represents the growth rate (1/h) obtained at substrate concentration x, θ_1 is the highest growth rate (1/h), and θ_2 means the saturation constant (in units of the substrate concentration). The non-linear models estimate θ_1 and θ_2 at low initial glucose concentrations (5, 10, 15, 20, and 25 g/L) by simplifying Equations (1–5). The parameters related to the substrate, $\theta_1 = K_S$ (Equation 1) *and* $\theta_2 = K_I$ (Equation 1), were identified from the data obtained during the early exp-date of the "*Positive*" mutants' growth phase, when no excrete organic acid inhibition occurred. θ_1 and θ_2 were estimated by minimizing the sum-of-squares function:

$$Minimize\ S = \sum \left(y_i - \frac{\theta_1 x}{\theta_2 + x} \right)^2 \tag{12}$$

The right-hand panel (**Figure 2D**) shows the model fitted to the experimental data corresponding to the approximately 99% joint confidence region (**Figure 2**). **Figure 2D** was mapped using the sum-of-squares values calculated over a grid of paired experimental values for θ_1 and θ_2. The initial values of the experimental parameters were estimated using the plotted data (**Figure 2A**). We minimized the sum-of-squares function using *fminsearch*. For our study data, $S_R = 0.0003$, $n = 5$, *and* $p = 2$. The chain variable is the *nsimu* × *npar* matrix (**Figure 2C**). Chain plots, plots one and two, and the dimensional marginal kernel density approximations for posterior distributions were created. Plots 1 and 2 consisted of pairwise scatterplots of the columns of the chain (**Figure 2B**). The square root of the *s2chain* was obtained and used to determine the histogram of the chain error (standard deviation) (**Figure 2C**). A point estimate for model parameters can be computed from the average of the chain. We plotted the fitted model using the posterior means of the parameters (**Figure 2D**) and fit the fermentation data to the model predictions for high initial glucose concentrations (50, 75, 100, 125, 150, and 175 g/L). The values of the "*Positive*" mutants for the kinetic parameters μ_m, K_S, and K_I are listed in **Table 4**. As shown in **Figure 2**, the value of θ_2 (K_S) was supposed to be less than 45 g/L, because θ_1 (μ_m) was calculated from the plot of $1/y_i$ ($1/\mu$) vs. $1/x$ ($1/S$). The initial glucose solution gradient was used to establish the predictive envelopes of the model. The variable y_i (μ) was fitted to the experimental data during the early exp-date growth phase of the "*Positive*" mutant, and revealed the original glucose solution gradient was higher than the glucose solution gradient in the culture medium. Because $y_i = \theta_1$ and $S = \sqrt{\theta_2}$from Equations (11) and (12), $S = \sqrt{K_S \cdot K_I}$ from Equation (1). The highest specific growth rate (θ_1) of the "*Positive*" mutant would be obtained when the glucose gradient was approximate 50 g/L in the cultivation medium. A high dissolved CO_2 concentration is a critical factor for achieving a high growth rate at a high cell density. The pathways of glucose metabolism in *Clostridium. tyrobutyricum* indicate that CO_2 is released through the decarboxylic reaction of pyruvic acid to acetyl-CoA, leading to butyric and acetic acid production

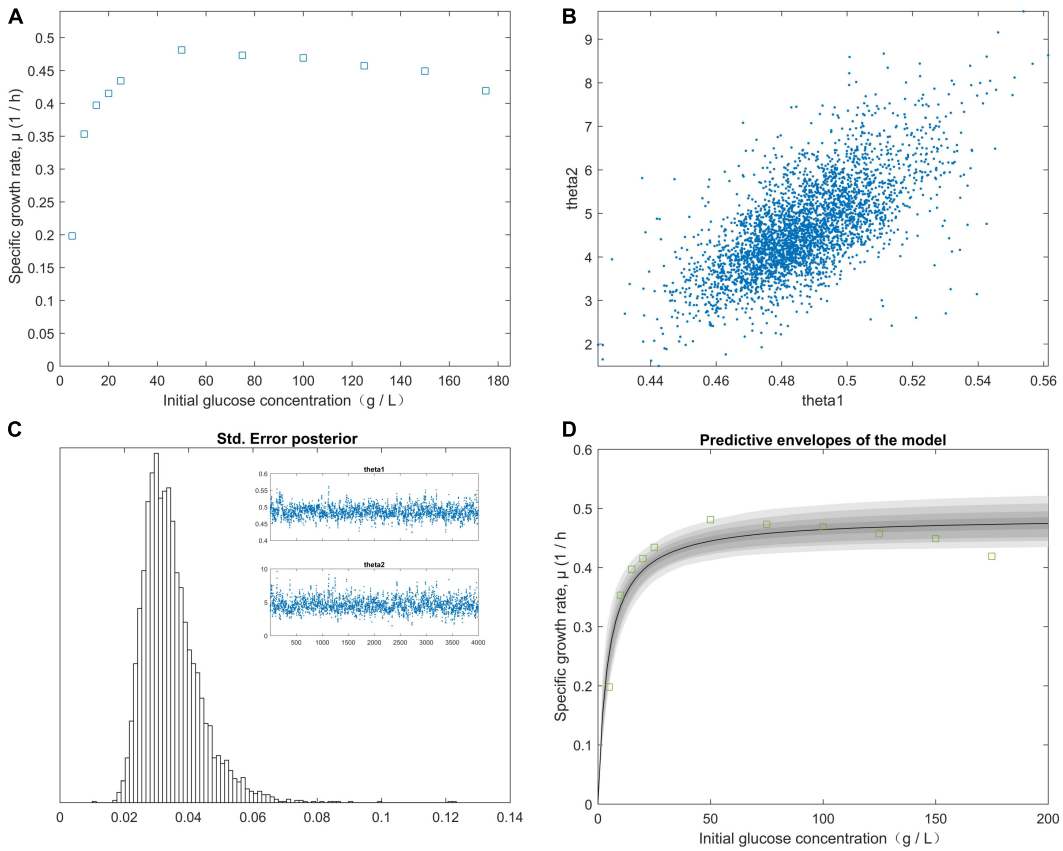

FIGURE 2 | The effect of the initial glucose concentration gradient from predictive posterior distribution on the specific growth rate of the *C. tyrobutyricum* mutant. **(A)** The different specific growth rates of *C. tyrobutyricum* mutant correlated with the initial glucose concentration gradient. **(B)** Chain plots, plots 1 and 2, and dimensional marginal kernel density estimates of the posterior distributions. **(C)** Standard deviation was displayed at the square root of the s2chain. Top right figures: the 1D parameter chains with 4.0×10^3 consecutive steps of delayed-rejection adaptive metropolis MCMC. **(D)** Predictive envelopes of the model: The gray protection system corresponds to 50, 90, 95, and 99% in the posterior regions as illustrated in the plot.

TABLE 4 | Notations, units for Equations (2–5 and 15), parameters, data and constants.

Symbol	Description and units data and constants
I	Suppression degree of metabolite product 5.32
K_d	Specific the strain of cell mortality rate (1/h) 0.0027
K_I	Normal factor of substrate inhibition (g/L) 383
K_S	Normal factor of substrate saturation (g/L) 1.71
m_S	Maintenance coefficient of system (1/h) 0.015
P	Gradient of product of metabolism (g/L) –
P_d	Critical gradient of product of metabolism (g/L) 53.8
S	Gradient of substrate (g/L) –
X	Gradient of biomass (g/L) –
Y_{Aa}	Stoichiometric yield-factor of acetic acid (g/g) 0.997
Y_{Ba}	Stoichiometric yield-factor of butyric acid (g/g) 0.973
Y_X	Stoichiometric yield-factor of biomass (g/g) 0.812
Greek letters	
α_{Aa}	Formation parameters of acetic acid associated with growth (g/g DCW) 0.83
α_{Ba}	Formation parameters of butyric acid associated with growth (g/g DCW) 3.12
β_{Aa}	Formation parameters of acetic acid associated with non-growth (g/g DCW/h) –
β_{Ba}	Formation parameters of butyric acid associated with non-growth (g/g DCW/h) 0.049
M	Specific the strain of cell growth-rate (1/h) -
μ_m	Maximum specific the strain of cell growth-rate (1/h) 0.48

(Zverlov et al., 2006; Ezeji et al., 2007). The carbon mass balance based on the stoichiometric reactions is expressed as:

$$C_6H_{12}O_6 \rightarrow C_3H_7COOH + 2H_2 + 2CO_2 \quad (13)$$

$$C_6H_{12}O_6 + 2H_2O \rightarrow 2CH_3COOH + 4H_2 + 2CO_2 \quad (14)$$

$$-\frac{dS}{dt} = \frac{1}{Y_X}\frac{dX}{dt} + \frac{1}{Y_{Ba}}\frac{dP_{Ba}}{dt} + \frac{1}{Y_{Aa}}\frac{dP_{Aa}}{dt} + m_S X \quad (15)$$

These parameters are listed in **Table 4**. Gassing with N_2 decreased the dissolved CO_2 and H_2, both of which evolved from the "*Positive*" mutant. The dissolution of CO_2 in the culture medium is necessary for the biosynthesis of the components of "*Positive*" mutants. Increasing the growth rate of the mutant also increases the biomass concentration and productivity because the reaction of acetyl coenzyme A, and carbon dioxide is catalyzed via the specific enzyme acetyl-coenzyme A carboxylase. Substrate inhibition must be minimized before the growth of

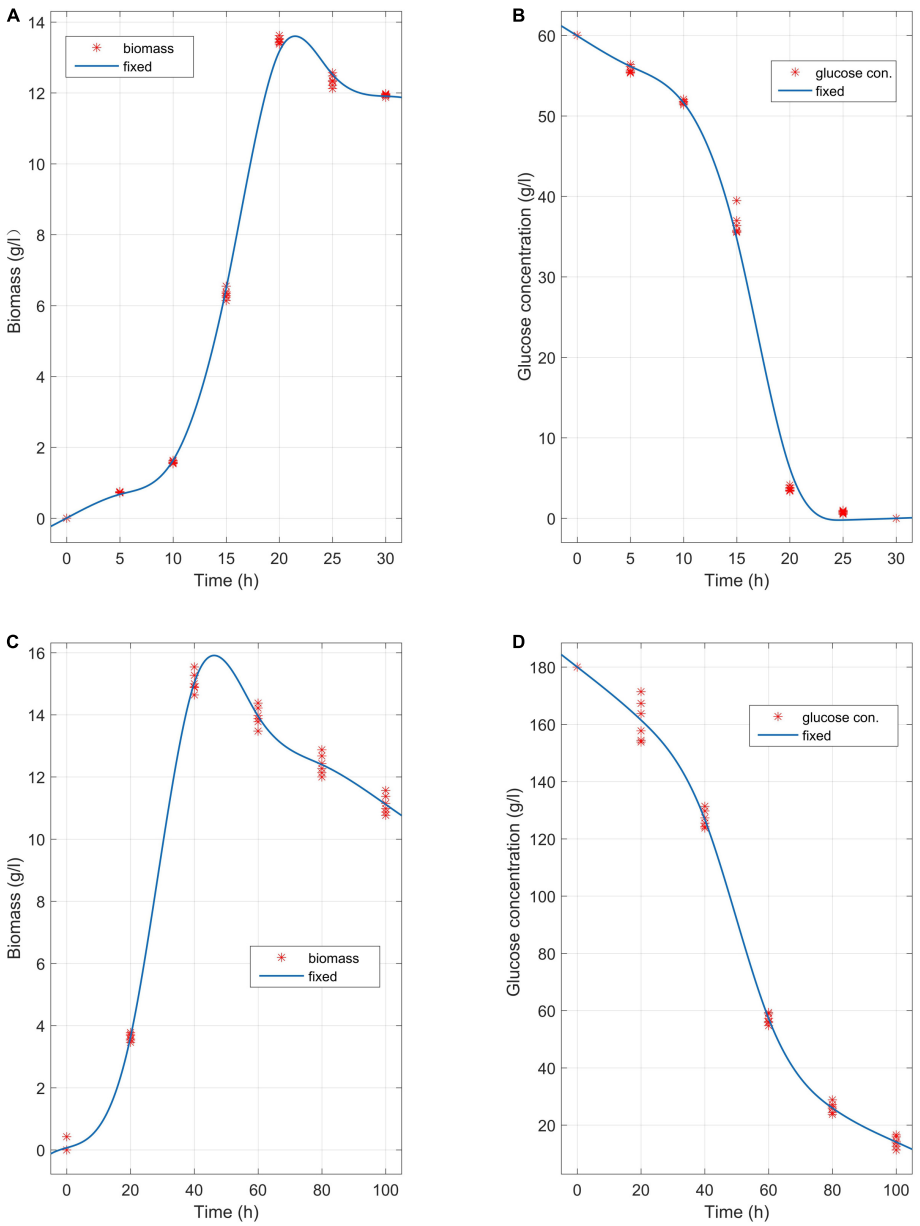

FIGURE 3 | Biomass change and glucose consumption at different time points in the biofermentations of *C. tyrobutyricum* mutants in media with a concentration gradient of 60 g/L and 180 g/L glucose, respectively. **(A)** The mutants' butyric and acetic acid productivity at 37°C, pH = 6.0 over 45 h of biofermentation (n = 6). **(B)** Glucose consumption (60 g/L) at different time points in the biofermentation of the *C. tyrobutyricum* mutant (45 h). **(C)** The mutants' butyric and acetic acid productivity at 37°C, pH = 6.0 over 120 h of biofermentation (n = 6). **(D)** Glucose consumption (180 g/L) at different time points in the biofermentation of the *C. tyrobutyricum* mutant (120 h). Experimental (red asterisks); simulated (blue lines).

the mutant becomes retarded by the accumulated products in the bioreactor or scale-up. Butyric acid and acetic acid were the major and minor fermentation products, respectively. These acidic products inhibit growth and result in cell death (Martinez et al., 1998; Hanahan and Weinberg, 2011). Cell growth was previously demonstrated to be determined by pK_a (the dissociation constants for organic acids) and pH values of the cultivation medium (Cherrington et al., 1991; Narendranath et al., 2001). Butyrate and acetate have similar values of pK_a (4.93 and 4.83, respectively), additionally the pH value of the fermentation during the experiment remained at pH 6.0. The pH of the bioreactor was 6.0. The degrees of inhibition of the organic acids were identical. The degree of the product inhibition parameter (i = 5.32) was approximated from Equations (4) and (5) (**Table 4**). The growth of the "*Positive*" mutant decreased along with the bioreaction proceeded and stopped when the total quantity of acetic and butyric acids (P_d) was 53.8 g/L. A drastic decrease in the biomass occurred at K_d = 0.0027.

Organic Acid-Specific Productivity of the "Positive" Mutant

The media involving glucose concentrations of 60 g/L and 180 g/L were observed at different time points, and the biomass change and glucose consumption were measured during the biofermentation of *C. tyrobutyricum* mutants (**Figure 3**). α_{Ba} = 0.83 (Equations 2–5 and 15) and α_{Ba} =3.12 were estimated by fitting the biofermentation results of the model. The butyric acid-specific productivity of the "*Positive*" mutant was more affected by the μ parameter than the biomass change, as suggested by the higher value of the parameter β_{Ba} compared to β_{Aa}. Previous study has been suggested that butyrate can suppress cell growth. As organic acid concentrations reach a key value in the biofermentation process, cell death occurs (Muller-Feuga et al., 2004). Those "*Positive*" mutant cells dividing actively, mutant cells that exhibit a physiological lag stage, cells which are impaired and require repair prior to resolving lag and then those cells are dead. The lag phase durations for mutant cells in various physiological conditions metabolize different gradients of organic acids; exponentially growing wild-type cells have minimum stationary phases, lag phases, and longer lag stages in mutant strains. However, no gradual inhibiting effect of "*Positive*" mutant growth was noted. Indeed, no growth could be found when the biomass concentration exceeded 16 g/L or the butyric acid concentration exceeded 68 g/L (**Figures 3**, **4**). The maximum biomass concentrations occurred at 20 and 40 h (**Figures 3A,C**). This result was slightly different from the

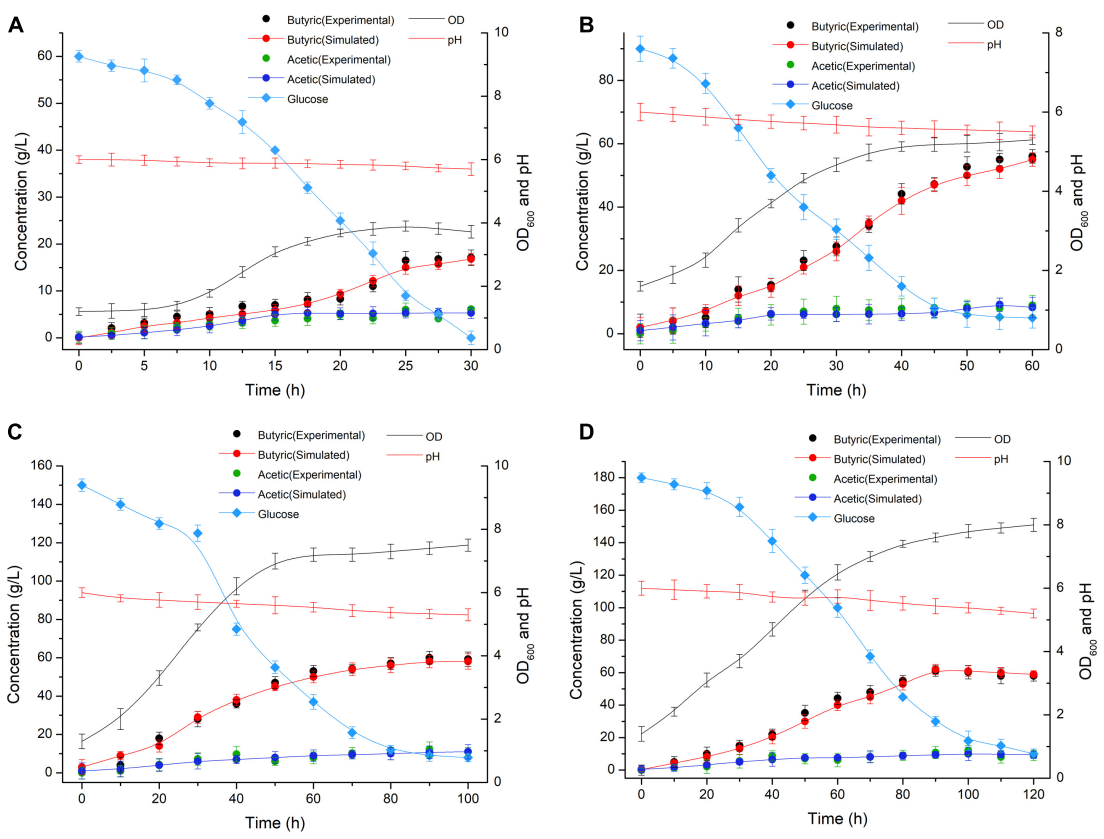

FIGURE 4 | Butyric (Experimental: black symbols; Simulated: red symbols and red lines) and acetic (Experimental: green symbols; Simulated: blue symbols and blue lines) acid production at different time points in the biofermentations of the *C. tyrobutyricum* mutant in media containing glucose concentration gradients of **(A)** 60 g/L, **(B)** 90 g/L, **(C)** 150 g/L, and **(D)** 180 g/L glucose.

results of model prediction. No significant differences were found in terms of glucose consumption between the two experimental conditions (**Figures 3B,D**). Additional energy expenditure can be used for the glucose transport through cellular membranes, which is powered by a phosphoenolpyruvate-controlling phosphotransferase system usually aimed at glucose transport. It is worth noting that more acetate can be generated from glucose, presumably to satisfy demand for higher ATP levels in glucose fermentation which could grow more quickly and greatly (**Figure 4**). A higher level of ATP can be produced when pyruvate generated from substrates is transformed into acetate instead of butyrate. These results indicated that the acetate/butyrate ratio improved depending on the growth rate, thus a low cell growth velocity was beneficial to the production of butyric acids. By calculating the stoichiometric Equations (13) and (14), the butyric acid yield gained from this research was approximate to the theoretical highest acetate/butyrate yield (0.489 g/g). These findings demonstrated that the metabolic burden was reduced for the "*Positive*" mutant. Our experimental results showed that the acetate/butyrate yield ranged from 0.27∼0.31 g/g for original glucose concentrations from 60 to 180 g/L. This observation is consistent with fast cell mutant growth and organic acid formation (Dawes and Ribbons, 1964; Barsanti et al., 2001). The obtained glucose consumption prediction model curves are consistent with the experimental data. The results of the maximum butyric and acetic acid productivities of the "*Positive*" mutant with different glucose concentration gradients (60, 90, 150, and 180 g/L) are shown in **Figure 4**. Butyric acid production ranged from15.5 to 56.3 g/L and acetic acid production from 4.8 to 13.5 g/L for original glucose concentrations from 60 to 180 g/L. Fine-grained differences were noted in the organic acid production between the assay data and the model predicted estimates (**Figure 4**). These differences may be attributed to the m_S = 0.015 1/h (maintenance parameter) in Equation (15). This parameter was approximated through fitting the assay results to the above model. The m_S parameter during the lag phase was also assumed to be proportional to the biomass. Therefore, the established model cannot predict the lag phase accurately, which probably require further adjustment for parameters to better depict this phase.

CONCLUSION

Factors influencing the irradiation-mutation strains that improve butyric acid production have been discussed based on the experimental results presented in this paper, and major modeling approaches concerning the estimation of butyric acid production have been critically estimated. In predictive irradiation-mutation strains, a multi-step modeling approach was employed. Primary models described the evolution of irradiation-mutation strain amounts along with duration, and they can be further divided into two groups: deterministic model and stochastic model. Primary deterministic models described the metabolism of mutation strains via a serie of deterministic model parameters. Among stochastic models, the parameters were identified as distributed variable or random variable. Secondary models were used to depict the relationship between the primary model parameters and affecting factors. In this study, a series of efficient umbrella modeling strategies were used to track and generate reliable data supporting the improvement of butyric acid production were presented. These modeling strategies confirmed the feasibility of using a mutant strain of *C. tyrobutyricum* at the pre-development phase.

DATA AVAILABILITY STATEMENT

The original contributions presented in the study are included in the article/**Supplementary Material**, further inquiries can be directed to the corresponding author/s.

AUTHOR CONTRIBUTIONS

LC and YG conceived, designed, and supervised the study. LC, YG, X-ZW, G-YS, Y-NH, Z-PX, WC, and X-PG performed the experiments, analyzed the data and contributed reagents, materials, and analysis tools. LC wrote the manuscript. LC and YG critically revised the manuscript. XZ final approval of the version to be published. All authors contributed to the discussion and comments on the manuscript and approved the submitted version.

FUNDING

This work was supported by grants from the National Natural Science Foundation of China (Grant No. 31560029), CAS Light of West China Program [Ke-Fa-Ren-Zi (2015) No. 77] and Natural Science Foundation of Gansu Provincial Sci. and Tech. Department (Grant No. 1506RJZA293) and Project of Lanzhou Science and Technology (Grant No. 2019-1–39).

ACKNOWLEDGMENTS

We sincerely thank the National Laboratory of HIRFL and the National Natural Science Foundation of China for giving us opportunity to perform this project.

SUPPLEMENTARY MATERIAL

The Supplementary Material for this article can be found online at: https://www.frontiersin.org/articles/10.3389/fbioe.2021.609345/full#supplementary-material

Supplementary Figure 1 | For **Figure 1A**, enlarged the "Top right figures: the 1D parameter chains."

REFERENCES

Agler, M. T., Wrenn, B. A., Zinder, S. H., and Angenent, L. T. (2011). Waste to bioproduct conversion with undefined mixed cultures:The carboxylate platform. *Trends Biotechnol.* 29, 70–78. doi: 10.1016/j.tibtech.2010.11.006

Akhtar, T., Hashmi, A. S., Tayyab, M., Anjum, A. A., and Saeed, S. (2018). Enhanced production of butyric acid by solid-state fermentation of rice polishings by a mutant strain of Clostridium tyrobutyricum. *Trop. J. Pharm. Res.* 17:1235. doi: 10.4314/tjpr.v17i7.2

Barsanti, L., Vismara, R., Passarelli, V., and Gualtieri, P. (2001). Paramylon (β-1, 3-glucan)content in wild type and WZSL mutant of euglena gracilis. Effects of growth conditions. *J. Appl. Phycol.* 13, 59–65. doi: 10.1023/A:1008105416065

Bettelheim, F., Brown, W., Campbell, M., Farrell, S., and Torres, O. (2012). *Introduction to organic and biochemistry*. Boston: Cengage Learning, doi: 10.1021/ed050pA511.1

Buch, K., Peters, T., Nawroth, T., Sänger, M., Schmidberger, H., and Langguth, P. (2012). Determination of cell survival after irradiation via clonogenic assay versus multiple MTT assay-a comparative study. *Radiat. Oncol.* 7:1. doi: 10.1186/1748-717X-7-1

Cheng, Y. R., Sun, Z. J., Cui, G. Z., Song, X., and Cui, Q. (2016). A new strategy for strain improvement of Aurantiochytrium sp. based on heavy-ions mutagenesis and synergistic effects of cold stress and inhibitors of enoyl-ACP reductase. *Enzyme Microb. Technol.* 93-94, 182–190. doi: 10.1016/j.enzmictec.2016.08.019

Cherrington, C. A., Hinton, M., Mead, G. C., and Chopra, I. (1991). Organic acids: chemistry, antibacterial activity and practical applications. *Adv. Microb. Physiol.* 32, 87–108. doi: 10.1016/S0065-2911(08)60006-5

Choi, O., Um, Y., and Sang, B. I. (2012). Butyrate production enhancement by clostridium tyrobutyricum using electron mediators and a cathodic electron donor. *Biotechnol. Bioeng.* 109, 2494–2502. doi: 10.1002/bit.24520

Dagaut, P., Sarathy, S. M., and Thomson, M. J. (2009). A chemical kinetic study of n butanoloxidation at elevated pressure in a jet stirred reactor. *Proc. Combust. Inst.* 32, 229–237. doi: 10.1016/j.proci.2008.05.005

Dawes, E. A., and Ribbons, D. W. (1964). Some aspects of the endogenous metabolism of bacteria. *Bacteriol. Rev.* 28, 126. doi: 10.1128/MMBR.28.2.126-149.1964

Dobson, A. J., and Barnett, A. (2008). *An introduction to generalized linear models*. Boca Raton: CRC press, doi: 10.1002/9780470556986.ch1

Dong, M. Y., Wang, S. Y., Xiao, G. Q., Xu, F. Q., Hu, W., and Li, Q. Q. (2019). Cellulase production by Aspergillus fumigatus MS13.1 mutant generated by heavy ion mutagenesis and its efficient saccharification of pretreated sweet sorghum straw. *Proc. Biochem.* 84, 22–29. doi: 10.1016/j.procbio.2019.06.006

Drapcho, C. (2006). "Microbial modeling as basis for bioreactor design for nutraceutical production," in *Functional food ingredients and nutraceuticals: proceeding technologies*, ed. J. Shin (Boca Raton: CRC Press, Taylor and Francis Group), 237–268. doi: 10.1201/b19426-21

Dwidar, M., Lee, S., and Mitchell, R. J. (2012). The production of biofuels from carbonated beverages. *Appl. Energ.* 100, 47–51. doi: 10.1016/j.apenergy.2012.02.054

Ezeji, T. C., Qureshi, N., and Blaschek, H. P. (2007). Bioproduction of butanol from biomass:From genes to bioreactors. *Curr. Opin. Biotechnol.* 18, 220–227. doi: 10.1016/j.copbio.2007.04.002

Gutteridge, J. M. C. (1981). Thiobarbituric acid-reactivity following iron-dependen free-radical damage to amino acids and carbohydrates. *FEBS Lett.* 128, 343–346. doi: 10.1016/0014-5793(81)80113-5

Haario, H., Laine, M., Mira, A., and Saksman, E. (2006). DRAM: Efficient adaptive MCMC. *Statist. Comput.* 16, 339–354. doi: 10.1007/s11222-006-9438-0

Hanahan, D., and Weinberg, R. A. (2011). Hallmarks of cancer: The next generation. *Cell* 144, 646–674. doi: 10.1016/j.cell.2011.02.013

Henstra, A. M., Sipma, J., Rinzema, A., and Stams, A. J. (2007). Microbiology of synthesis gas fermentation for biofuel production. *J. Curr. Opin. Biotechnol.* 18, 200–206. doi: 10.1016/j.copbio.2007.03.008

Hwang, S. G., Lee, S. C., Lee, J., Lee, J. W., Kim, J. H., Choi, S. Y., et al. (2020). Resequencing of a Core Rice Mutant Population Induced by Gamma-Ray Irradiation and Its Application in a Genome-Wide Association Study. *J. Plant Biol.* 2020:9266. doi: 10.1007/s12374-020-09266-2

Jang, Y. S., Im, J. A., Choi, S. Y., Lee, J. I., and Lee, S. Y. (2014). Metabolic engineering of Clostridium acetobutylicum for butyric acid production with high butyric acid selectivity. *Metab. Eng.* 23, 165–174. doi: 10.1016/j.ymben.2014.03.004

Jang, Y. S., Malaviya, A., Cho, C., Lee, J., and Lee, S. Y. (2012). Butanol production from renewable biomass by Clostridia. *Bioresource Tech.* 123, 653–663. doi: 10.1016/j.biortech.2012.07.104

Jiang, B. L., Wang, S. Y., Wang, Y. C., Chen, J. H., Li, W. J., Liu, J., et al. (2016). A high-throughput screening method for breeding Aspergillus niger with 12C6+ ion beam-improved cellulase. *Nuclear Sci. Techniq.* 28:8. doi: 10.1007/s41365-016-0157-8

Jiang, L., Wang, J., Liang, S., Cai, J., Xu, Z., Cen, P., et al. (2011). Enhanced butyric acid tolerance and bioproduction by clostridium tyrobutyricum immobilized in a fibrous bed bioreactor. *Biotechnol. Bioeng.* 108, 31–40. doi: 10.1002/bit.22927

Jin, C., Yao, M., Liu, H., Lee, C. F., and Ji, J. (2011). Progress in the production and application of n-butanol as a biofuel. *J. Renewable Sustain Energ. Rev.* 15, 4080–4106. doi: 10.1016/j.rser.2011.06.001

Ketkaeo, S., Sanpamongkolchai, W., Morakul, S., Baba, S., Kobayashi, G., and Goto, M. (2020). Induction of mutation in Monascus purpureus isolated from Thai fermented food to develop low citrinin-producing strain for application in the red koji industry. *J. Gen. Appl. Microbiol.* 66, 163–168. doi: 10.2323/jgam.2019.04.008

Kubicek, C. P., Röhr, M., and Rehm, H. J. (1985). Citric acid fermentation. *Crit. Rev. Biotechnol.* 3, 331–373. doi: 10.3109/07388558509150788

Lakhssassi, N., Baharlouei, A., Meksem, J., Hamilton-Brehm, S. D., Lightfoot, D. A., Meksem, K., et al. (2020). EMS-Induced Mutagenesis of Clostridium carboxidivorans for Increased Atmospheric CO2 Reduction Efficiency and Solvent Production. *Microorganisms* 8:8081239. doi: 10.3390/microorganisms8081239

Lan, E. I., and Liao, J. C. (2012). ATP drives direct photosynthetic production of 1-butanol in cyanobacteria. *Proc. Natl. Acad. Sci. USA.* 109, 6018–6023. doi: 10.1073/pnas.1200074109

Li, X., Wang, J., Tan, Z., Ma, L., Lu, D., Li, W., et al. (2018). Cd resistant characterization of mutant strain irradiated by carbon-ion beam. *J. Hazard Mater.* 353, 1–8. doi: 10.1016/j.jhazmat.2018.03.036

Li, Z., Chen, X., Li, Z., Li, D., Wang, Y., Gao, H., et al. (2016). Strain improvement of Trichoderma viride for increased cellulase production by irradiation of electron and 12C6+-ion beams. *Biotechnol. Lett.* 38, 983–989. doi: 10.1007/s10529-016-2066-7

Liu, L., Hu, W., Li, W. J., Wang, S. Y., Lu, D., Tian, X. J., et al. (2018). Heavy-ion mutagenesis significantly enhances enduracidin production by Streptomyces fungicidicus. *Eng. Life Sci.* 2018:109. doi: 10.1002/elsc.201800109

Lobry, J. R., Flandrois, J. P., Carret, G., and Pave, A. (1992). Monod's bacterial modelrevisited. *Bull Math Biol.* 54, 117–122. doi: 10.1007/bf02458623

Luedeking, R., and Piret, E. L. (1959). A kinetic study of the lactic acid fermentation: Batch process at controlled pH. *J. Biochem. Microbiol. Technol.* 1, 393–412. doi: 10.1002/jbmte.390010406

Matsuyama, T., Watanabe, M., Murota, Y., Nakata, N., Kitamura, H., Shimokawa, T., et al. (2020). Efficient mutation induction using heavy-ion beam irradiation and simple genomic screening with random primers in taro (Colocasia esculenta L. Schott). *Sci. Horticult.* 272:109568. doi: 10.1016/j.scienta.2020.109568

Martinez, J. D., Stratagoules, E. D., LaRue, J. M., Powell, A. A., Gause, P. R., Craven, M. T., et al. (1998). Different bile acids exhibit distinct biological effects: The tumorpromoter deoxycholic acid induces apoptosis and the chemopreventive agentursodeoxycholic acid inhibits cell proliferation. *Nutrit. Cancer* 31, 111–118. doi: 10.1080/01635589809514689

Mattam, A. J., and Yazdani, S. S. (2013). Engineering E. coli strain for conversion of shortchain fatty acids to bioalcohols. *Biotech. Biofuels* 6:128. doi: 10.1186/1754-6834-6-128

Muller-Feuga, A., Le Guédes, R., and Le Déan, L. (2004). Cell weight kinetics simulationin chemostat and batch culture of the rhodophyte porphyridium cruentum. *Biotechnol. Bioeng.* 88, 759–766. doi: 10.1002/bit.20255

Munasinghe, P. C., and Khanal, S. K. (2010). Biomass-derived syngas fermentation into biofuels: opportunities and challenges. *Bioresour. Technol.* 101, 5013–5022. doi: 10.1016/j.biortech.2009.12.098

Ragauskas, A. J., Williams, C. K., Davison, B. H., Britovsek, G., Cairney, J., Eckert, C. A., et al. (2006). The path forward for biofuels and biomaterials. *Science* 311, 484–489. doi: 10.1126/science.1114736

Narendranath, N. V., Thomas, K. C., and Ingledew, W. M. (2001). Effects of acetic acid and lactic acid on the growth of saccharomyces cerevisiae in a minimal medium. *J. Ind. Microbiol. Biotechnol.* 26, 171–177. doi: 10.1038/sj.jim.7000090

Nigam, P. S., and Singh, A. (2011). Production of liquid biofuels from renewable resources. *Prog. Energ. Combust. Sci.* 37, 52–68.

Pappu, V. K., Kanyi, V., Santhanakrishnan, A., Lira, C. T., and Miller, D. J. (2013). Butyric acidesterification kinetics over Amberlyst solid acid catalysts: The effect of alcoholcarbon chain length. *Bioresour. Technol.* 130, 793–797.

Peralta-Yahya, P. P., Zhang, F., Del Cardayre, S. B., and Keasling, J. D. (2012). Microbial engineering for the production of advanced biofuels. *Nature* 488, 320–328. doi: 10.1038/nature11478

Peng, X., Luo, L., Cui, H., Wang, H., Guo, T., Liu, Y., et al. (2019). Characterization and Fine Mapping of a Leaf Wilt Mutant, m3, Induced by Heavy Ion Irradiation of Rice. *Crop Sci.* 59, 2679–2688. doi: 10.2135/cropsci2019.03.0167

Ping, L., Yuan, X., Zhang, M., Chai, Y., and Shan, S. (2018). Improvement of extracellular lipase production by a newly isolated Yarrowia lipolytica mutant and its application in the biosynthesis of L-ascorbyl palmitate. *Int. J. Biol. Macromol.* 106, 302–311. doi: 10.1016/j.ijbiomac.2017.08.016

Price, P., and McMillan, T. J. (1990). Use of the tetrazolium assay in measuring the response of human tumor cells to ionizing radiation. *Cancer Res.* 50, 1392–1396. doi: 10.1016/0304-3835(90)90166-U

Ren, N., Wang, B., and Huang, J. C. (1997). Ethanol-type fermentation from carbohydrate in high rate acidogenic reactor. *Biotechnol. Bioeng.* 544, 28–33. doi: 10.1002/(SICI)1097-0290(19970605)54:5<428::AID-BIT3<3.0.CO;2-G

Roos, J. W., McLaughlin, J. K., and Papoutsakis, E. T. (1985). The effect of pH on nitrogen supply, cell lysis, and solvent production in fermentations of Clostridium acetobutylicum. *Biotechnol Bioeng.* 27, 681–694. doi: 10.1002/bit.260270518

Song, X., Wang, J., Wang, Y., Feng, Y., Cui, Q., and Lu, Y. (2018). Artificial creation of Chlorella pyrenoidosa mutants for economic sustainable food production. *Bioresour. Technol.* 268, 340–345. doi: 10.1016/j.biortech.2018.08.007

Tao, Y., He, Y., and Wu, Y. (2008). Characteristics of a new photosynthetic bacterial strain for hydrogen production and its application in wastewater treatment. *Int. J. Hydrogen. Energ.* 33, 963–973. doi: 10.1016/j.ijhydene.2007.11.021

Tian, X. J., Jiang, A. L., Mao, Y. Q., Wu, B., He, M. X., Hu, W., et al. (2019). Efficient L −lactic acid production from purified sweet sorghum juice coupled with soybean hydrolysate as nitrogen source by Lactobacillus thermophilus A69 strain. *J. Chem. Technol. Biotechnol.* 94, 1752–1759. doi: 10.1002/jctb.5939

Wang, Q., Chen, Y., Fu, J., Yang, Q., and Feng, L. (2020). High-throughput screening of lycopene-overproducing mutants of Blakeslea trispora by combining ARTP mutation with microtiter plate cultivation and transcriptional changes revealed by RNA-seq. *Biochem. Eng. J.* 161:107664. doi: 10.1016/j.bej.2020.107664

Wang, S. Y., Bo, Y. H., Zhou, X., Chen, J. H., Li, W. J., Liang, J. P., et al. (2017). Significance of Heavy-Ion Beam Irradiation-Induced Avermectin B1a Production by Engineered Streptomyces avermitilis. *Biomed. Res. Int.* 2017:5373262. doi: 10.1155/2017/5373262

Wiesenborn, D. P., Rudolph, F. B., and Papoutsakis, E. T. (1988). Thiolase from Clostridium acetobutylicum ATCC 824 and its role in the synthesis of acids and solvents. *Appl. Environ. Microbiol.* 54, 2717–2722. doi: 10.1016/03856380(88)90069-6

Yu, M., Zhang, Y., Tang, I. C., and Yang, S. T. (2011). Metabolic engineering of clostridiumtyrobutyricum for n-butanol production. *Metab. Eng.* 2011, 373–382. doi: 10.1016/j.ymben.2011.04.002

Zhang, H., Lu, D., Li, X., Feng, Y., Cui, Q., and Song, X. (2018). Heavy ion mutagenesis combined with triclosan screening provides a new strategy for improving the arachidonic acid yield in Mortierella alpina. *BMC Biotechnol.* 18:23. doi: 10.1186/s12896-018-0437-y

Zhou, X., Xie, J. R., Tao, L., Xin, Z. J., Zhao, F. W., Lu, X. H. (2013a). The effect of microdosimetric 12C6+ heavy ion irradiation and Mg2+ on canthaxanthin production in a novel strain of Dietzia natronolimnaea. *BMC Microbiol.* 13:213. doi: 10.1086/343136

Zhou, X., Xin, Z. J., Lu, X. H., Yang, X. P., Zhao, M. R., and Wang, L. (2013b). High efficiency degradation crude oil by a novel mutant irradiated from Dietzia strain by 12C6+ heavy ion using response surface methodology. *Bioresour. Technol.* 137, 386–393. doi: 10.1016/j.biortech.2013.03.097

Zhou, X., Lu, X. H., Li, X. H., Xin, Z. J., Xie, J. R., Zhao, M. R., et al. (2014a). Radiation induces acid tolerance of clostridium tyrobutyricum and enhances bioproduction of butyric acid through a metabolic switch. *Biotechnol. Biofuels* 7:22. doi: 10.1186/1754-6834-7-22

Zhou, X., Xu, D., and Jiang, T. T. (2017). Simplifying multidimensional fermentation dataset analysis and visualization: One step closer to capturing high-quality mutant strains. *Sci. Rep.* 7:39875. doi: 10.1038/srep39875

Zhou, X., Wang, S. Y., Lu, X. H., and Liang, J. P. (2014b). Comparison of the effects of high energy carbon heavy ion irradiation and eucommia ulmoides oliv. On biosynthesis butyric acid efficiency in clostridium tyrobutyricum. *Bioresour. Technol.* 161, 221–229. doi: 10.1016/j.biortech.2014.03.039

Zigová, J., and Sturdik, E. (2000). Advances in biotechnological production of butyric acid. *J. Ind. Microbiol. Biotechnol.* 24, 153–160. doi: 10.1038/sj.jim.2900795

Zverlov, V. V., Berezina, O., Velikodvorskaya, G. A., and Schwarz, W. H. (2006). Bacterial acetone and butanol production by industrial fermentation in the soviet union: use of hydrolyzed agricultural waste for biorefinery. *Appl. Microbiol. Biotechnol.* 71:045. doi: 10.1007/s00253-006-0445-z

Conflict of Interest: The authors declare that the research was conducted in the absence of any commercial or financial relationships that could be construed as a potential conflict of interest.

frontiers in Microbiology

ORIGINAL RESEARCH
published: 08 October 2021
doi: 10.3389/fmicb.2021.754306

Metabolic Engineering of *Enterobacter aerogenes* for Improved 2,3-Butanediol Production by Manipulating NADH Levels and Overexpressing the Small RNA RyhB

Yan Wu[1,2†], Wanying Chu[1†], Jiayao Yang[1], Yudong Xu[1], Qi Shen[1], Haoning Yang[3], Fangxu Xu[4], Yefei Liu[4], Ping Lu[1], Ke Jiang[1] and Hongxin Zhao[1]*

[1]Zhejiang Province Key Laboratory of Plant Secondary Metabolism and Regulation, College of Life Sciences and Medicine, Zhejiang Sci-Tech University, Hangzhou, China, [2]Key Laboratory of Urban Agriculture by Ministry of Agriculture of China, School of Agriculture and Biology, Shanghai Jiao Tong University, Shanghai, China, [3]Department of Bioengineering, Liaoning Technical University, Fuxin, China, [4]Experimental Teaching Center, College of Life Science, Shenyang Normal University, Shenyang, China

OPEN ACCESS

Edited by:
Shang-Tian Yang,
The Ohio State University,
United States

Reviewed by:
Xiao-Jun Ji,
Nanjing Tech University, China
Liya Liang,
University of Colorado Boulder,
United States

***Correspondence:**
Hongxin Zhao
bxxbj2003@gmail.com

†These authors have contributed equally to this work

Specialty section:
This article was submitted to Microbiotechnology, a section of the journal Frontiers in Microbiology

Received: 06 August 2021
Accepted: 16 September 2021
Published: 08 October 2021

Citation:
Wu Y, Chu W, Yang J, Xu Y, Shen Q, Yang H, Xu F, Liu Y, Lu P, Jiang K and Zhao H (2021) Metabolic Engineering of Enterobacter aerogenes for Improved 2,3-Butanediol Production by Manipulating NADH Levels and Overexpressing the Small RNA RyhB. Front. Microbiol. 12:754306. doi: 10.3389/fmicb.2021.754306

Biotechnological production of 2,3-butanediol (2,3-BD), a versatile platform bio-chemical and a potential biofuel, is limited due to by-product toxicity. In this study, we aimed to redirect the metabolic flux toward 2,3-BD in *Enterobacter aerogenes* (*E. aerogenes*) by increasing the intracellular NADH pool. Increasing the NADH/NAD^+ ratio by knocking out the NADH dehydrogenase genes (*nuoC*/*nuoD*) enhanced 2,3-BD production by up to 67% compared with wild-type *E. aerogenes*. When lactate dehydrogenase (*ldh*) was knocked out, the yield of 2,3-BD was increased by 71.2% compared to the wild type. Metabolic flux analysis revealed that upregulated expression of the sRNA RyhB led to a noteworthy shift in metabolism. The 2,3-BD titer of the best mutant Ea-2 was almost seven times higher than that of the parent strain in a 5-L fermenter. In this study, an effective metabolic engineering strategy for improved 2,3-BD production was implemented by increasing the NADH/NAD^+ ratio and blocking competing pathways.

Keywords: *Enterobacter aerogenes*, NADH dehydrogenase, lactate dehydrogenase, small RNA RyhB, 2,3-butanediol

INTRODUCTION

The biotechnological production of bulk chemicals is partially driven by the wish to reduce the reliance on fossil fuels because of limited reserves and increasing environmental concerns. The small molecule 2,3-BD is listed by the United States Department of Energy as a platform chemical with great potential for industrial applications (Song et al., 2019). The production of 2,3-BD by bacteria such as *Escherichia* sp. (Park et al., 2020), *Bacillus* sp. (Petrova et al., 2020), *Klebsiella* sp. (Sharma et al., 2018), and *Enterobacter* sp. (Thapa et al., 2019) has been investigated in depth in the last few years on account of its potential applications in the chemical industry for the production of polymers and solvents. As a versatile chemical feedstock and liquid fuel, 2,3-BD is extensively applied in the food, chemical, pharmaceutical, petrochemical,

and aerospace industries (Ge et al., 2016). The development of biorefinery technology was further boosted due to concerns surrounding high energy costs and environmental problems (Ragauskas et al., 2006; Haveren et al., 2008). Most microbiological methods for the production of 2,3-BD rely on the biotransformation of expensive glucose. However, the utilization rate of glucose is still low, resulting in a pressing need for more efficient biological production methods for 2,3-BD.

Enterobacter aerogenes (syn. *Klebsiella aerogenes*) is a facultatively anaerobic Gram-negative bacterium that naturally produces 2,3-BD during fermentation at low O_2 concentrations. Due to its role in maintaining the intracellular redox balance of the pyridine nucleotide pool during glycolysis and biosynthesis, 2,3-BD was regarded as a classical end-product of anaerobic fermentation (Converti et al., 2003). The conversion of acetoin by 2,3-BD dehydrogenase regenerates NADH for continued glycolysis, and this reaction is increased to maintain the NAD^+/NADH balance when there is a lack of oxygen (Blomqvist et al., 1993). Because NADH from glycolysis is regenerated *via* respiration under aerobic conditions, the switch from biomass synthesis to production of mixed acids and 2,3-BD is critical for maintaining the redox balance (Hung et al., 2011).

Many studies have demonstrated that small RNAs play critical roles in the metabolic regulation of both eukaryotes and bacteria (Beauchene et al., 2015; Machner and Storz, 2016). The small noncoding RNA RyhB undergoes base pairing with mRNAs to suppress gene expression (Massé et al., 2003). RyhB is related to a variety of crucial cellular functions such as iron homeostasis, antioxidant defenses, and TCA cycle activity in many bacteria, including *Klebsiella pneumoniae* and *Escherichia coli* (*E. coli*; Massé et al., 2003; Huang et al., 2012; Beauchene et al., 2015). In *E. coli*, formate dehydrogenase is downregulated by RyhB (Massé et al., 2005), suggesting that RyhB might regulate 2,3-BD production in *E. aerogenes* by suppressing formate production. Moreover, RyhB also influences the expression of NADH dehydrogenase I (Massé et al., 2005), which may influence the NAD^+/NADH ratio during the production of 2,3-BD.

Enterobacter aerogenes can produce high titers of 2,3-BD from many different carbon sources, while producing different fermentation gases and soluble byproducts. Lactate is the main byproduct during the anaerobic fermentation process of *E. aerogenes* and blocking the lactate synthesis pathway can increase the yield of 2,3-BD due to their competition for NADH as a cofactor and pyruvate as a precursor. However, there are few reports on metabolic engineering in *E. aerogenes*. Nevertheless, a previous study improved hydrogen production in *E. aerogenes* by deleting a hydrogenase subunit and formate hydrogen lyase subunit, while also overexpressing a heterologous formate dehydrogenase and its positive regulator (Lu et al., 2009, 2016; Zhao et al., 2009). Similarly, Lu et al. (2010) investigated the effects of overexpressing formate hydrogenase and deleting lactate dehydrogenase (LDH) on hydrogen production. In a more recent study, CRISPR-Cas9 was used to knock out the *nuoCD* genes in the NADH dehydrogenase cluster of *E. aerogenes* IAM1183. The resulting double mutant Ea-1 (Δ*nuoC*/Δ*nuoD*) showed improved hydrogen production (Wu et al., 2017).

In this study, the gene *ldh* encoding LDH was deleted using the λ-Red recombination system to reduce byproduct accumulation, generating Ea-2 (Δ*nuoC*/Δ*nuoD*/Δ*ldh*). To regulate the 2,3-BD production of IAM1183 *via* the small RNA RyhB, it was overexpressed in both strains Ea-1 and Ea-2, respectively, resulting in Ea-3 and Ea-4. We constructed a metabolic network model to quantify the metabolic fluxes of IAM1183 and its mutants and thereby analyze the changes in the metabolic pattern of the mutants. The best mutant exhibited a high 2,3-BD titer in both shake-flasks and batch fermentation, indicating its potential for scaled-up 2,3-BD production.

MATERIALS AND METHODS

Strains, Plasmids, and Reagents

Table 1 lists the primers, plasmids, and strains used in this work. The Green Industry Biotechnology Laboratory of Tsinghua University kindly provided the *E. aerogenes* wild-type strain IAM1183. *Escherichia coli* DH5α (TaKaRa Biotechnology, Dalian, China) was used for genetic engineering. Kits for the isolation of genomic DNA, DNA gel extraction, and plasmid DNA purification were from GenScript (GenScript USA Inc. United States). All DNA-modifying enzymes, restriction endonucleases, and DNA polymerase were bought from New England BioLabs (Beverly, MA, United States). Tryptone and yeast extract were purchased from Thermo Fisher Biochemicals (Beijing Ltd.). Unless specified otherwise, all other reagents used in this study were purchased from Sigma-Aldrich (St. Louis, MO, United States).

Media and Culture Conditions

Luria–Bertani (LB) broth including (g/L) 10 tryptone, 5 yeast extract, and 10 NaCl was used to culture *E. coli* for cloning and cryopreservation. The cultivation medium consisted of several reagents including (g/L) 6.8 Na_2HPO_4, 3 KH_2PO_4, 0.75 KCl, 0.28 Na_2SO_4, 5.35 $(NH_4)_2SO_4$, 34.2 $ZnCl_2$, 0.26 $MgSO_4{\cdot}7H_2O$, 0.42 citric acid, 10 Casamino acids, 5 yeast extract, and 0.3 ml trace element solution containing (g/L) 2.7 $FeCl_3{\cdot}6H_2O$, 10 0.85 $CuCl_2{\cdot}2H_2O$, $MnCl_2{\cdot}4H_2O$, and 0.31 H_3BO_3 (Jung et al., 2012) used to produce 2,3-BD. Glucose, sucrose, galactose, and fructose (40 g/L) were used as carbon sources. The 50 ml cultures in 250-ml Erlenmeyer flasks were closed using silicone stoppers and incubated micro-aerobically at 37°C and 250 rpm. Kanamycin (50 mg/ml), chloramphenicol (25 mg/ml), or ampicillin (50 mg/ml) was added to the medium, respectively, when necessary.

Fermentation experiments were performed in a 5-L bioreactor (Biostat A, Sartorius, Germany) with 3 L of fermentation medium, at 250 rpm and 37°C. The same medium was used for fermentation as the flask culture, and the carbon source was glucose. Chloramphenicol (50 mg/ml) was supplied to promote plasmid retention. The fermentation was conducted at 37°C and 250 rpm, with air supplied at 1 vvm. The pH was maintained in the range from 6.5 to 7.0 by adding 5 M NaOH (Jung et al., 2012).

TABLE 1 | Strains, plasmids, and primers used in the experiments.

Strains, plasmids, and primers	Genotype and relevant characteristics	Source or literature
Strains		
IAM1183	Wild type	IAM (Tokyo, Japan)
E.a-1	*E. aerogenes* IAM1183 *ΔnuoC*/*ΔnuoD*	Wu et al., 2017
E.a-2	*E. aerogenes* IAM1183 *ΔnuoC*/*ΔnuoD*/*Δldh*	This study
E.a-3	*E. aerogenes* IAM1183 *ΔnuoC*/*ΔnuoD*, harboring plasmid pKK102-ryhB-cm	Wu et al., 2017
E.a-4	*E. aerogenes* IAM1183 *ΔnuoC*/*ΔnuoD*/*Δldh*, harboring plasmid pKK102-ryhB-cm	This study
E. coli DH5a	*F-, φ 80dlacZ ΔM15*, Δ (*lacZYA -argF*) *U169*, *deoR*, *recA1*, *endA1*, *hsdR17* (*rK-, mK+*), *phoA*, *supE44*, *λ-, thi −1*, *gyrA96*, *relA1*	TaRaKa
Plasmids		
pKD46	*FRT flanked resistance cassette involved vector*, *oriRγ*, *Ampr*	TaRaKa
pKD46-cm	FRT flanked resistance cassette involved vector, oriRγ, *Cmr*	This study
pKD46-ldh	*ldh*-homologous arm FRT flanked resistance cassette involved vector, oriRγ, *Cmr*	This study
pCP20	FLP recombinase producing vector, *Ampr*, *Cmr*	TaRaKa
pMD18-T Vector	TA Cloning vector, *Ampr*	TaRaKa
FRT	Kan+, FRT site	TaRaKa
pKK102-ryhB-cm	RyhB, *Cmr* deriving pKK102-ryhB	This lab
Primers (5'–3')		
Primer-cm-F	TGCACGGTGCACAGTGCCAAGC TTGCATGCCT	This study
Primer-cm-R	CGGCATGACTCCCCGTCAGTATACACT CCGCTAGCGC	This study
Ea-ldh-F	TTGTACGATTATTTTAAATATGCTACCGTGACGGTATAATC *ACTGGAGAAAAGTCTT*AATTAACCCTCACTAAAGGGCG	This study
Ea-ldh-R	*CTGTGGGGATTATCTGAATGTGCTCCCCCCGGGAGAGGAG CACAAAAGGGAAAGGC*ATAATACGACTCACTATAGGGCTC	This study
ldh-Con-A	AATTAACCCTCACTAAAGGGCG	This study
ldh-Con-B	TAATACGACTCACTATAGGGCTC	This study
ldh-Con-C	CCGTGACGGTATAATCACTGGAG	This study
ldh-Con-D	ATCTTCGAAG AACAGGTCGC	This study

Genetic Manipulation

Table 1 lists all primers used in this study. The *ldh* gene, which encodes LDH, was knocked out in the Ea-1 strain (*E. aerogenes* IAM1183 *ΔnuoC*/*ΔnuoD*) using a published λ-Red recombination method (Datsenko and Wanner, 2000), resulting in strain Ea-2 (*E. aerogenes* IAM1183 *ΔnuoC*/*ΔnuoD*/*Δldh*). Genomic DNA was isolated from *E. aerogenes* IAM1183 according to a published method (Miller, 1972) or using a commercial kit. The QIAprep Spin Miniprep kit and GenScript DNA gel extraction kit were used for plasmid isolation and DNA purification, respectively. The 50 μl PCR reactions contained: PCR reaction buffer (5 μl), dNTPs (10 mM each), primers (10 pmol each), 1 U of Pfu DNA polymerase or Taq polymerase, and 10–20 ng of the DNA template were conducted with a Bio-Rad thermocycler (Hercules, CA, United States). The correct products were confirmed by sequencing (Life Technologies, Shanghai Invitrogen, China). The purified plasmid pKK102-ryhB-cm, which was used to overexpress the small RNA RyhB, was introduced into Ea-3 by electroporation, and the resulting strain was named Ea-4 (*E. aerogenes* IAM1183 *ΔnuoC*/*ΔnuoD*/*Δldh* [pKK102-ryhB-cm]). RyhB expression was induced by adding 0.6 g/L l-arabinose (Wu et al., 2017).

NADH/NAD$^+$ Assay

The intracellular NADH/NAD$^+$ ratio was determined using a method described in a previous study (Yang et al., 2015). The steady-state cells were harvested by centrifuging at 12,000 rpm, 4°C for 10 min. A colorimetric NAD/NADH Assay Kit (ab65348; Abcam, United Kingdom) was used to quantify the NADH/NAD$^+$ in cell extracts.

Analytical Methods

Cell density was assessed by measuring the optical density of the cultures at 600 nm (OD_{600}) using a UV-721G spectrophotometer. The dry cell weight (DCW) of *E. aerogenes* was subsequently calculated using the empirical formula: DCW (mg/ml) = $0.132 \times OD_{600}$ (Zhao et al., 2015). Analytes in the gas space, including 2,3-BD and ethanol, were measured using a GC-2010 Plus gas chromatography apparatus (Shimadzu, Japan) equipped with a thermal conductivity detector at 40°C and a Parapak Q column at 200°C, with He as the carrier gas.

Samples comprising 10 ml of the fermentation cultures were centrifuged at 10,000× *g* and 4°C for 15 min, and the supernatant was then harvested for analysis of metabolites and residual sugar. The concentrations of formate, acetate, lactate, succinate, citrate, acetoin, and ethanol in the culture supernatant were determined by HPLC (LC-20A; Shimadzu, Japan), using a PREP-ODS (H) KIT C-18 column (Shimadzu) kept at 33°C, and a refractive index detector (RID-10A, Shimadzu). The mobile phase was composed of 0.2% aqueous phosphoric acid at a flow rate of 0.8 ml/min. Formate, ethanol, lactate, acetate,

citric acid, and 2,3-BD had retention times of 4.42, 5.12, 5.38, 5.67, 6.49, and 11.51 min, respectively.

RESULTS AND DISCUSSION

Effects of Knocking Out the *nuoC*, *nuoD*, and *ldh* Genes on 2,3-BD Production

To examine the relationship between NADH dehydrogenase activity, 2,3-BD synthesis, and carbon flux distribution, CRISPR/Cas9 precise editing technology (Wu et al., 2017) was used to delete the *nuoC* and *nuoD* genes, encoding the two subunits of NADH dehydrogenase, resulting in the *E. aerogenes* IAM1183 derivative Ea-1 (**Table 1**). To increase the production of 2,3-BD, the *ldh* gene was further deleted using λ-Red recombination to limit lactate production in Ea-1, resulting in strain Ea-2 (**Table 1**). To study the effects of the mutations on metabolite production and carbon source consumption, the strains were cultured in medium containing 40 g/L of glucose.

To measure 2,3-BD production, all strains were cultivated under aerobic conditions in 250-ml shake-flasks with 50 ml of glucose medium. The parental strain IAM1183 served as the control. After 20 h of cultivation, the cell density of both Ea-1 and Ea-2 was greater than that of IAM1183 (**Figure 1A**). Compared with the exponential phase of wild-type IAM1183, which lasted 6 h, the constructed strains Ea-1 and Ea-2 showed corresponding phases that were ~4 and ~8 h longer, respectively (**Figure 1A**). The pH of the culture broth of Ea-1 and Ea-2 decreased during 20 h of batch fermentation at a lower rate than that of IAM1183 (**Figure 1B**). These results demonstrated that the deletion of *nuoC*, *nuoD*, and *ldh* reduced the acidification rate of Ea-1 and Ea-2, resulting in a higher plateau phase of the mutants (**Figure 1**). NADH availability and its reduction potential (the intracellular reduced NADH pool) has a stronger effect on the overall yield of 2,3-BD (Yang et al., 2015). Ji et al. (2010) constructed a *Klebsiella oxytoca* strain that does not accumulate 2,3-BD by deleting the aldehyde dehydrogenase gene *aldA*.

In this study, the 2,3-BD titer of Ea-1 reached 70.64 mM within 20 h of cultivation, which was much higher than the 45.72 mM of the wild type (**Table 2**), indicating that the removal of NADH dehydrogenase significantly improved 2,3-BD production in *E. aerogenes* IAM1138. As shown in **Table 2**, the double-knockout strain Ea-2 was obviously a superior 2,3-BD producer, with a 84.6% higher product titer than that of the wild-type IAM1183. Furthermore, the 2,3-BD yield from glucose improved 61% compared with the wild-type strain (**Table 2**). Additionally, the increased growth rate of the Ea-2 mutant also led to an increase in 2,3-butanediol production. It was reported that when LDH is eliminated, the increased NADH availability and redistribution of carbon fluxes lead to an increase in 2,3-BD production (Jung et al., 2012). Metabolically engineered microbes often have lower growth rates than the wild type. The increased microbial growth of the double mutants in this study might be the result of reduced acidification of the medium. Guo et al. (2020) constructed a mutant *K. pneumoniae* strain by deleting three genes, *ldhA*, *adhE* (encoding alcohol dehydrogenase), and *pta* (encoding phosphotransacetylase), resulting in significantly increase the yield of 2,3-BD. Currently, undesirable byproducts (such as lactate, ethanol, and acetate) are also produced during the 2,3-BD fermentation process, which shunts the carbon flow and dramatically decreases the efficiency of 2,3-BD synthesis. Thus, blocking pathways that competitively consume NADH to redistribute carbon flux will be more conducive to the 2,3-BD synthesis.

Effect of Overexpressing the sRNA RyhB on 2,3-BD Production

The plasmid pKK102-ryhB-cm, which overexpresses the small RNA *RyhB*, was introduced into Ea-1 and Ea-2 to generate Ea-3 and Ea-4, respectively. Based on the OD_{600}, the final cell densities of Ea-3 and Ea-4 were lower than that of *E. aerogenes* IAM1183 by 13 and 24%, respectively (**Figure 2A**). Moreover, the two mutants Ea-3 and Ea-4 entered the plateau phase ~4–6 h later than the wild-type strain IAM1183, which reached the plateau at 6 h (**Figure 2A**). During 20 h of shake-flask cultivation, the pH of the Ea-3 and Ea-4 cultures decreased more slowly than that of IAM1183 (**Figure 2B**). However, the final pH of the Ea-3 and Ea-4 cultures was lower than that of strains Ea-1 and Ea-2, respectively, implying that overexpressing the sRNA RyhB had an effect on acid production, which inhibited the growth of the strain (**Figure 2**).

We also found that overexpression of *RyhB* caused significant decrease in 2,3-BD production (18.3%) in Ea-3 compared with Ea-1, and a modest decrease in Ea-4 (14.6%) compared with Ea-2 when grown on glucose (**Table 2**; **Figure 3**). A previous study demonstrated that overexpression of *RyhB* could improve 2,3-BD production under anaerobic conditions, while we found that *RyhB* had no effect on aerobic 2,3-BD production (Wu et al., 2017). In *E. coli*, formate dehydrogenase is downregulated by *RyhB* under aerobic conditions (Massé et al., 2005). Indeed, the formate production of Ea-3 and Ea-4 was significantly lower than that of Ea-1 and Ea-2 (**Table 2**; **Figure 3**). Among the by-products, Ea-3 produced 7.17 mM lactate and 23.71 mM acetate, representing 39.5 and 79.9% increases compared to Ea-1, respectively. Furthermore, Ea-4 produced more acetate and lactate than Ea-2 (**Table 2**; **Figure 3**). The resulting acidification of the Ea-3 and Ea-4 cultures may explain their lower 2,3-BD titer. Interestingly, the production of acetate by Ea-3 was increased 2.67-fold compared with Ea-1, while Ea-4 produced 27% more acetate than Ea-2. Similarly, Kang et al. (2012) reported that overexpression of *RyhB* led to a threefold increase in acetate accumulation in *E. coli*, which indicated that *RyhB* had a comprehensive influence on the central glucose metabolism of *E. aerogenes*.

Effects of Different Carbon Sources on the Mutants

Enterobacter aerogenes can effectively utilize many different carbon sources (Perego et al., 2000). To detect the effects of different carbon sources on the mutants, shake-flask fermentations were conducted using 40 g/L of glucose, fructose, sucrose or

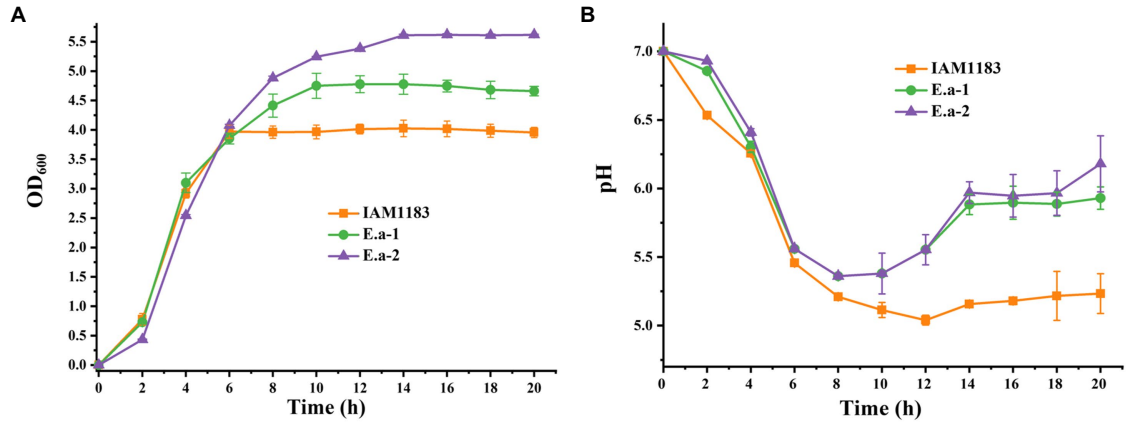

FIGURE 1 | Time-profiles of biomass accumulation (OD_{600}) and culture pH for IAM1183 and its mutants. **(A)** Biomass of IAM1183, Ea-1 and Ea-2. **(B)** Culture pH of IAM1183, Ea-1 and Ea-2 ($n = 3$).

TABLE 2 | Comparison of wild-type *Enterobacter aerogenes* IAM1183 and the mutants Ea-1 to -4 in 20-h shake-flask fermentations using 40 g/L of glucose as the carbon source ($n = 3$).

End products	Strains				
	IAM1183	Ea-1	Ea-2	Ea-3	Ea-4
Consumed carbon source (mM)	76.93 ± 0.43	75.43 ± 0.77	88.07 ± 0.97	71.99 ± 0.85	76.12 ± 0.36
2,3-Butanediol (mM)	45.72 ± 3.82	70.64 ± 0.29	84.38 ± 2.71	57.73 ± 6.23	72.10 ± 3.94
Formate (mM)	6.03 ± 1.17	4.94 ± 0.53	2.52 ± 0.30	3.19 ± 0.63	1.62 ± 0.99
Acetoin (mM)	45.25 ± 1.76	21.58 ± 1.94	38.57 ± 2.03	31.93 ± 0.77	36.05 ± 1.79
Lactate (mM)	3.21 ± 0.21	4.14 ± 0.41	0.34 ± 0.008	7.17 ± 0.88	0.92 ± 0.33
Ethanol (mM)	6.27 ± 0.77	9.29 ± 0.53	13.95 ± 0.36	6.37 ± 0.63	14.55 ± 1.76
Acetate (mM)	9.14 ± 0.62	6.18 ± 1.03	14.32 ± 1.62	23.71 ± 1.19	17.75 ± 1.54
Citric acid (mM)	1.51 ± 0.08	3.29 ± 0.13	1.16 ± 0.003	0.33 ± 0.08	2.10 ± 0.30
2,3-Butanediol yield (mol/mol Glc)	0.59 ± 0.09	0.93 ± 0.03	0.95 ± 0.02	0.80 ± 0.13	0.94 ± 0.01

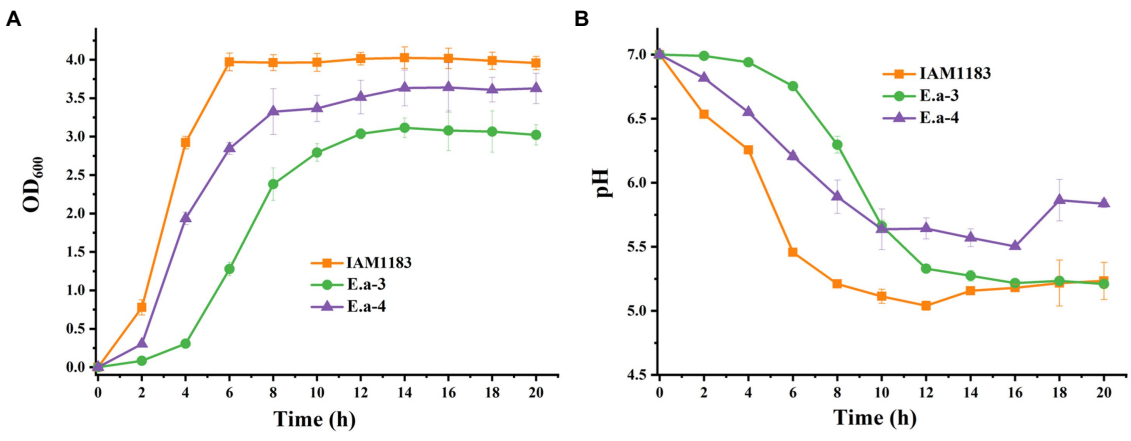

FIGURE 2 | Time-profiles of biomass accumulation (OD_{600}) and culture pH for IAM1183 and its mutants. **(A)** Biomass of IAM1183, Ea-3 and Ea-4. **(B)** Culture pH of IAM1183, Ea-3 and Ea-4 ($n = 3$).

galactose (sections "Effects of Knocking Out the nuoC, nuoD, and ldh Genes on 2,3-BD Production" and "Effect of Overexpressing the sRNA RyhB on 2,3-BD Production") With galactose and fructose, the production of 2,3-BD by Ea-1 was significantly increased, while the carbon source consumption rate was modestly decreased compared with IAM1183 (**Table 3**;

Figure 4A), which was presumably caused by the lower NADH dehydrogenase activity in the two constructed strains, which conserved energy during the exponential growth phase. The concentrations of other fermentation byproducts, such as formate and acetate, all decreased >20% in Ea-1. However, there was a significant increase in lactate production, which, respectively, increased 28.9, 41.8, and 79.6% compared with IAM1183 with all carbon sources except for sucrose (**Table 3**), which was detrimental for the productivity and yield of 2,3-butanediol (**Figure 4A**).

When grown on galactose and fructose, the 2,3-BD production and carbon source utilization rate of Ea-2 also increased (**Table 3**;

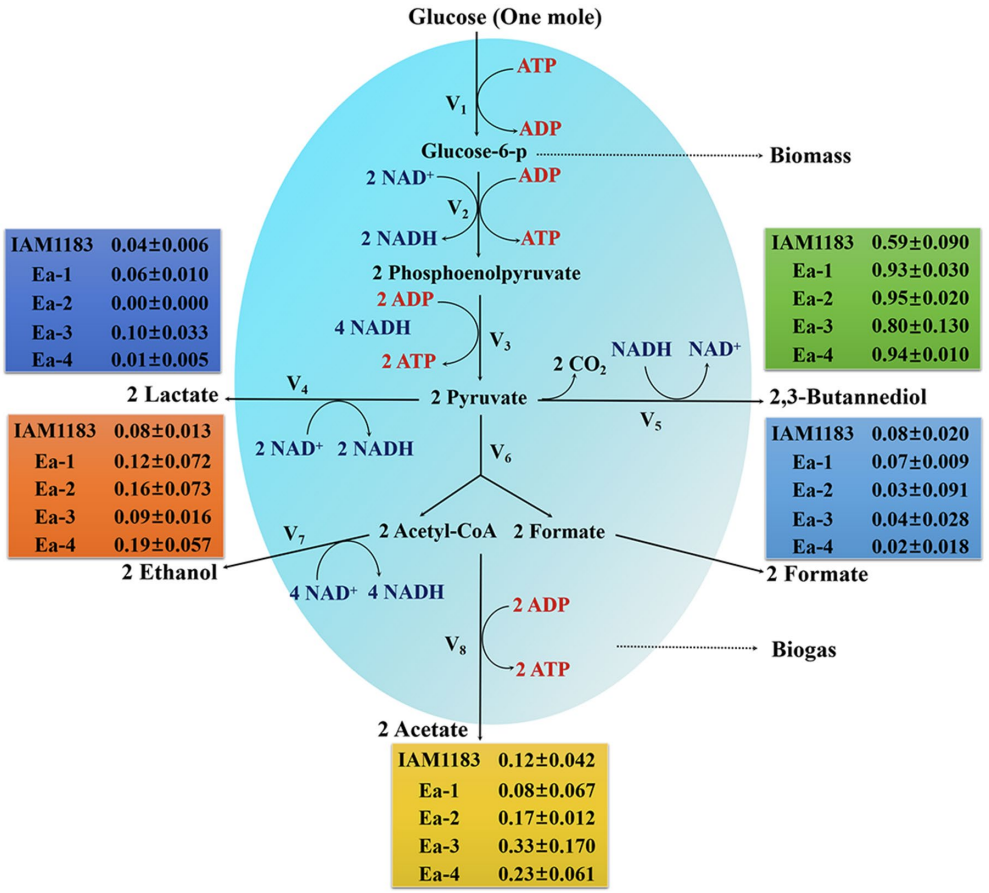

FIGURE 3 | Metabolite profiles of IAM1183 and the mutants Ea-1 to -4 after 20 h of shake-flask cultivation with glucose as carbon source ($n = 3$). The data shown in **Table 2** were used for the calculations.

TABLE 3 | Comparison of wild-type *E. aerogenes* IAM1183 with the mutants Ea-1 and Ea-2 grown for 20 h in shake-flask cultures on different carbon sources ($n = 3$).

End products	Strains								
	IAM1183			Ea-1			Ea-2		
Carbon source (40 g/L)	**Galactose**	**Fructose**	**Sucrose**	**Galactose**	**Fructose**	**Sucrose**	**Galactose**	**Fructose**	**Sucrose**
Consumed carbon source (mM)	77.22 ± 0.18	79.07 ± 0.19	80.82 ± 0.22	76.81 ± 0.68	78.63 ± 0.81	74.33 ± 0.80	92.06 ± 0.72	84.94 ± 0.95	83.89 ± 0.92
2,3-Butanediol (mM)	42.72 ± 1.57	48.94 ± 2.55	73.00 ± 0.58	74.72 ± 11.80	72.44 ± 0.45	41.51 ± 0.71	88.97 ± 5.41	75.59 ± 0.37	32.10 ± 0.19
Formate (mM)	7.10 ± 0.70	2.45 ± 0.37	5.37 ± 1.46	5.54 ± 1.32	1.62 ± 0.39	6.27 ± 0.31	2.99 ± 0.12	2.14 ± 0.16	3.18 ± 0.47
Acetoin (mM)	31.05 ± 1.61	12.83 ± 0.77	35.08 ± 0.69	18.69 ± 0.36	20.83 ± 0.77	21.46 ± 1.99	31.77 ± 1.62	37.35 ± 0.46	25.29 ± 2.19
Lactate (mM)	2.49 ± 0.66	1.13 ± 0.06	1.98 ± 0.22	3.58 ± 0.90	2.03 ± 0.77	0.93 ± 0.03	0.21 ± 0.002	0.52 ± 0.004	0.16 ± 0.013
Ethanol (mM)	5.31 ± 0.45	7.47 ± 1.11	9.61 ± 0.56	5.08 ± 0.17	6.86 ± 0.47	7.42 ± 0.68	12.72 ± 0.04	9.91 ± 0.31	18.91 ± 0.44
Acetate (mM)	4.88 ± 1.36	2.26 ± 0.08	4.71 ± 1.68	4.63 ± 1.15	6.49 ± 0.42	4.68 ± 0.14	6.29 ± 0.58	8.09 ± 0.35	4.89 ± 0.34
Citric acid (mM)	1.56 ± 0.45	1.21 ± 0.12	1.58 ± 0.46	2.99 ± 0.75	4.35 ± 0.32	2.67 ± 0.07	2.12 ± 0.52	1.43 ± 0.28	1.16 ± 0.26
2,3-Butanediol yield (mol/mol Glc)	0.55 ± 0.07	0.62 ± 0.09	0.90 ± 0.03	0.97 ± 0.01	0.92 ± 0.06	0.56 ± 0.07	0.96 ± 0.04	0.89 ± 0.03	0.38 ± 0.06

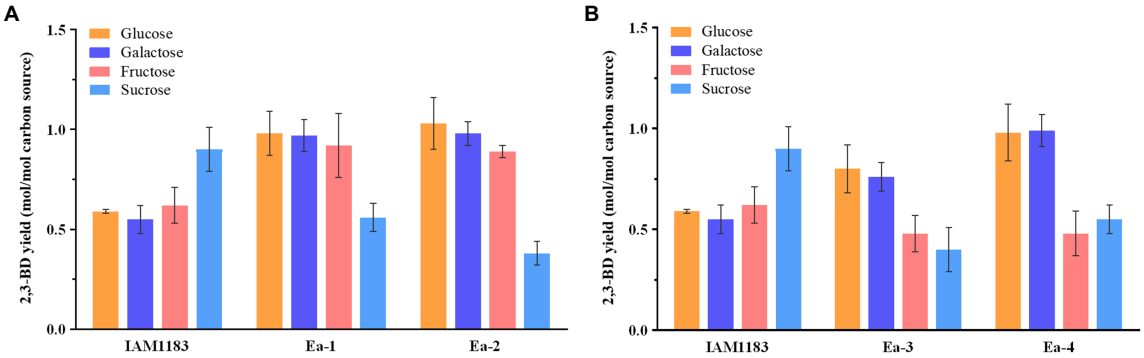

FIGURE 4 | Comparison of 2,3-BD yields from different carbon sources for the wild-type strain and the mutants. **(A)** 2,3-BD yield of IAM1183, Ea-1, and Ea-2. **(B)** 2,3-BD yield of IAM1183, Ea-3, and Ea-4 (n=3). The data shown in **Tables 2** and **3** were used for the calculations.

TABLE 4 | Comparison of Ea-3 and Ea-4 mutants in 20-h shake-flask cultivations using different carbon sources (n = 3).

End products	Strains					
	Ea-3			Ea-4		
Carbon source (40 g/L)	**Galactose**	**Fructose**	**Sucrose**	**Galactose**	**Fructose**	**Sucrose**
Consumed carbon source (mM)	81.13 ± 0.94	79.07 ± 0.22	72.33 ± 0.65	82.13 ± 0.57	80.36 ± 0.76	69.89 ± 0.62
2,3-Butanediol (mM)	61.67 ± 2.85	37.99 ± 7.28	29.18 ± 0.32	82.01 ± 2.60	38.67 ± 4.17	38.55 ± 3.26
Formate (mM)	1.69 ± 0.34	2.98 ± 0.13	2.20 ± 0.10	1.82 ± 0.28	4.07 ± 0.31	3.23 ± 0.31
Acetoin (mM)	27.72 ± 0. 39	29.27 ± 0.73	25.59 ± 0.70	30.35 ± 1.74	28.63 ± 0.02	23.67 ± 1.51
Lactate (mM)	8.62 ± 0.46	6.94 ± 0.13	9.27 ± 0.75	1.43 ± 0.12	1.66 ± 0.77	1.15 ± 0.01
Ethanol (mM)	7.88 ± 0.26	3.30 ± 1.11	3.02 ± 0.40	23.16 ± 4.40	4.94 ± 1.11	8.18 ± 1.95
Acetate (mM)	7.54 ± 0.25	6.83 ± 0.17	10.27 ± 1.07	4.52 ± 1.12	7.37 ± 0.31	10.20 ± 0.47
Citric acid (mM)	1.45 ± 0.04	1.64 ± 0.12	1.25 ± 0.02	1.60 ± 0.14	1.54 ± 0.14	1.49 ± 0.08
2,3-Butanediol yield (mol/mol sugar)	0.76 ± 0.07	0.48 ± 0.09	0.40 ± 0.11	0.99 ± 0.08	0.48 ± 0.16	0.55 ± 0.07

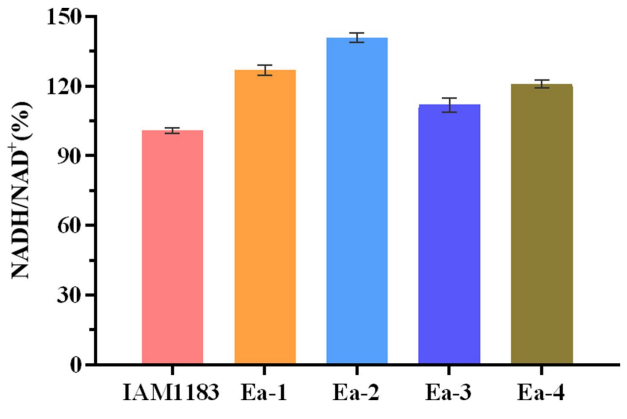

FIGURE 5 | Time profiles of the intracellular NADH/NAD$^+$ ratio of the wild-type strain AM1183 and the mutants Ea-1 to -4 (n = 3). Error bars show the SDs from biological triplicates.

Figure 4A). Similar to glucose, these carbon sources are metabolized *via* the glycolysis pathway. Due to the likely presence of a secondary LDH or a side activity of an unrelated enzyme, Ea-2 still produced a small amount of lactate. The large decrease in lactate accumulation had positive impacts to 2,3-BD productivity, which, respectively, increased by 17.5 and 4.3% compared with Ea-1 on galactose and fructose (**Table 3**; **Figure 4A**). The slower decrease in the culture pH in the double mutant likely led to the increase in productivity (Booth, 1985). The double mutant showed an improvement in the consumption rates of all carbon sources. Notably, obvious ethanol accumulation was observed in the double mutant with sucrose as the carbon source, and this increase was accompanied by a reduced 2,3-BD titer. Glucose directly enters the glycolysis pathway and does not require any additional energy to convert it into a usable form (Öhgren et al., 2006). This explains why glucose was the most efficient carbon source, since sucrose requires an additional enzyme and energy input in order for it to be converted into glucose and processed in glycolysis. These processes may lead to the production of more by-products such as ethanol (Bonestroo et al., 1992).

The effect of overexpressing the sRNA *RyhB* was tested in four cultures with various carbon sources (**Table 4**). The Ea-3 and Ea-4 strains showed a reduction in carbon source consumption, 2,3-BD production (**Figure 4B**), and yield with all carbon sources compared with Ea-1 and Ea-2, respectively. The accumulation of acidic by-products such as lactate and acetate reduced the 2,3-BD productivity (**Table 4**; **Figure 4B**). *RyhB* was reported

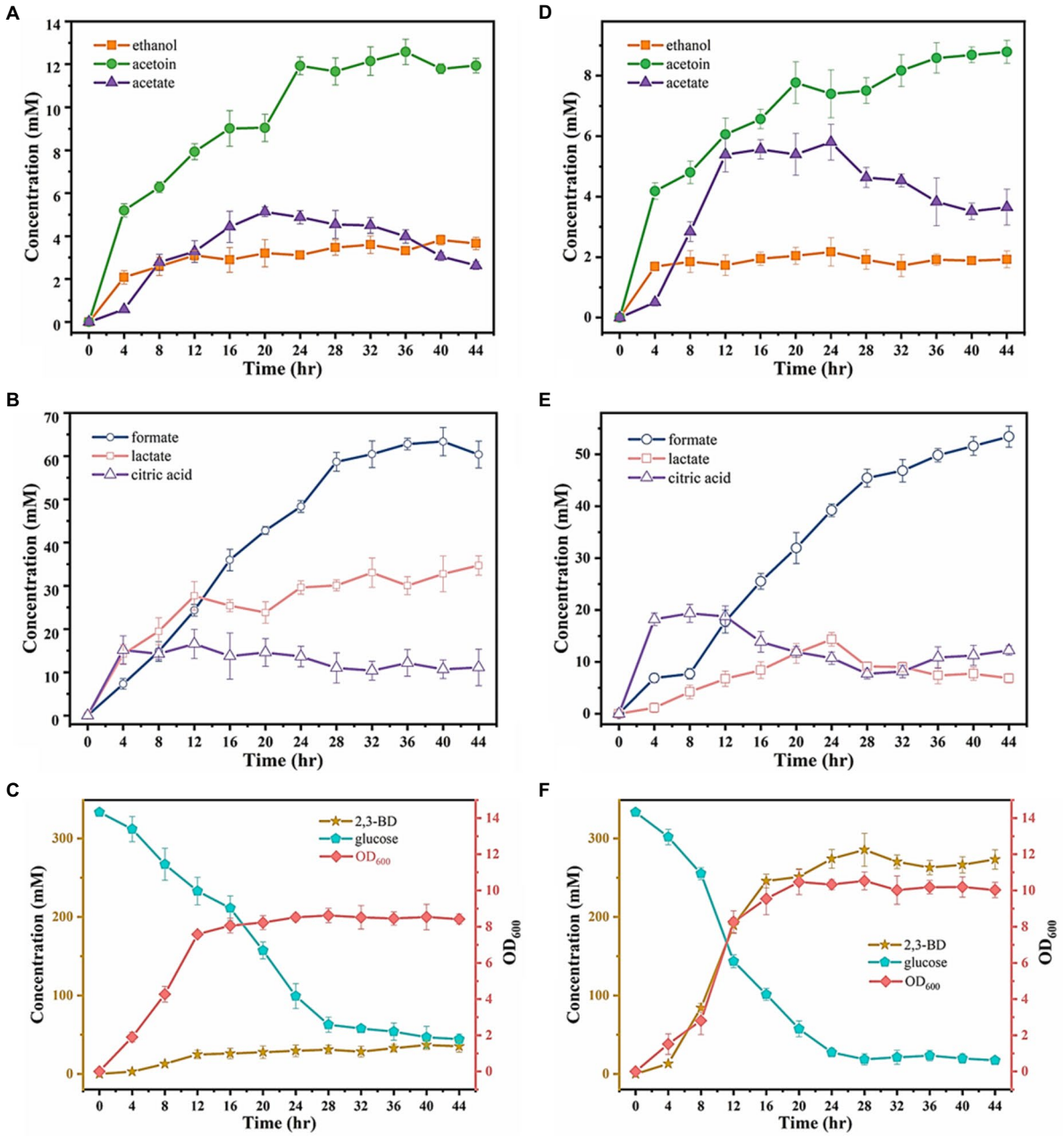

FIGURE 6 | Substrate consumption and produced metabolites after 44 h of fermentation for the wild-type strain IAM1183 and the best mutant Ea-2 in a 5-L fermenter. **(A)** Metabolite concentrations of acetate, acetoin, and ethanol in the culture supernatant IAM1183. **(B)** Metabolite concentrations of formate, lactate, and citric acid in the culture supernatant of IAM1183. **(C)** OD_{600}, glucose consumption, and concentration of 2,3-BD in the culture supernatant of IAM1183. **(D)** Metabolite concentrations of acetate, acetoin, and ethanol in the culture supernatant of Ea-2. **(E)** Metabolite concentrations of formate, lactate, and citric acid in the culture supernatant of Ea-2. **(F)** OD_{600}, glucose consumption, and concentration of 2,3-BD in the culture supernatant of Ea-2. Symbols represent acetoin (green circles), acetate (dark purple triangles), ethanol (orange squares), formate (blue circles), lactate (pink squares), citric acid (light purple triangles), optical density (pink diamonds), consumed glucose (blue pentagons), 2,3-BD (orange stars).

to have an even stronger effects on intermediary metabolism than on the TCA cycle enzymes, downregulating many different Fe-S-containing metabolic enzymes (Massé et al., 2005; Beauchene et al., 2015), which may explain the reduction in 2,3-BD production in Ea-3 and Ea-4. sRNAs are important regulators of gene expression and physiology in bacteria. RyhB is an iron-responsive sRNA well characterized in *E. coli* and conserved in other *Enterobacteriaceae* (Lillian et al., 2021). Zhang et al. (2018) have demonstrated that increased ATP levels were observed in the ryhB-knockout mutant of *E. coli*, which indicated that the decrease in ATP level has an impact on the lower 2,3-BD production of ryhB-overexpress mutant in our study.

Interestingly, we found the 2,3-BD production of all mutants on sucrose was significantly decreased compared with the wild type (**Figure 4**), which was potentially caused by a redox imbalance due to the disruption of NADH dehydrogenase when sucrose was used as substrate (Jung et al., 2014).

The Intracellular NADH/NAD⁺ Ratios of Different Strains

The effects of knocking out *nuoC*, *nuoD*, and *ldhA* on the intracellular NADH/NAD⁺ ratio are shown in **Figure 5**. After 20 h of shake-flask cultivation, the NADH/NAD⁺ ratios of strains Ea-1 and Ea-2, respectively, increased by 25.7 and 39.6% compared with the parental strain. This suggested that the redox balance of strains Ea-1 and Ea-2 was disrupted, which also explained the causes that significantly affect cell growth (**Figure 1**). As an intrinsic component of the respiratory chain, the mitochondrial NADH: ubiquinone oxidoreductase (complex I) mediates the transmembrane translocation of protons e in the first step of intracellular or mitochondrial NADH oxidation (or alternatively, NAD⁺ reduction; Vinogradov, 2008). The knockout of *nuoC* and *nuoD*, encoding complex I, increased the NADH/NAD⁺ ratio of Ea-1 and redistributed metabolic fluxes to increase 2,3-BD production. Similarly, a previous study showed that deletion of LDH increased NADH availability (Jung et al., 2012). In this study, the molar yield of 2,3-BD and NADH/NAD⁺ ratio of Ea-2 was, respectively, 23 and 11% higher than in Ea-1 (**Figure 5**; **Table 2**). This suggests that the deletion of *ldh* also made additional NADH available for other pathways, especially the biosynthesis of 2,3-BD. The strain Ea-3 and Ea-4 showed significant downregulation in NADH/NAD⁺ ratio when compared with the Ea-1 and Ea-2, respectively (**Figure 5**), which suggested that sRNA RyhB can significantly affect cell metabolism in addition to its role as a regulator of gene expression. Interestingly, a decrease in NADH/NAD⁺ ratios can be observed upon ryhB activation in *E. coli* (Lyu et al., 2019). Thus, RyhB is not merely a genetic-level regulator, its function can also have profound impacts on cell metabolism.

Calderón et al. (2013) reported that the NADH/NAD⁺ ratio was higher in a *ryhB*-deletion strain than in the parental wild

TABLE 5 | Analysis of consumed substrate and anaerobic metabolites after 44 h of cultivation of wild-type *E. aerogenes* IAM1183 and Ea-2 in 5-L fermenter.

End products	Strains			
	IAM1183	Ea-2	Change trend	Up or down (%)
Glucose consumption (%)	86.74	94.11	↑	8.49
Residual sugar (mM)	44.21	19.75	↓	55.33
Lactate (mM)	34.70	6.89	↓	80.14
Acetate (mM)	2.63	3.65	↑	38.78
Formate (mM)	60.36	53.63	↓	11.15
Ethanol (mM)	3.66	1.96	↓	46.45
Citric acid (mM)	11.12	12.31	↑	10.7
Acetoin (mM)	11.94	8.79	↓	26.38
2,3-Butanediol (mM)	35.04	252.06	↑	619.35

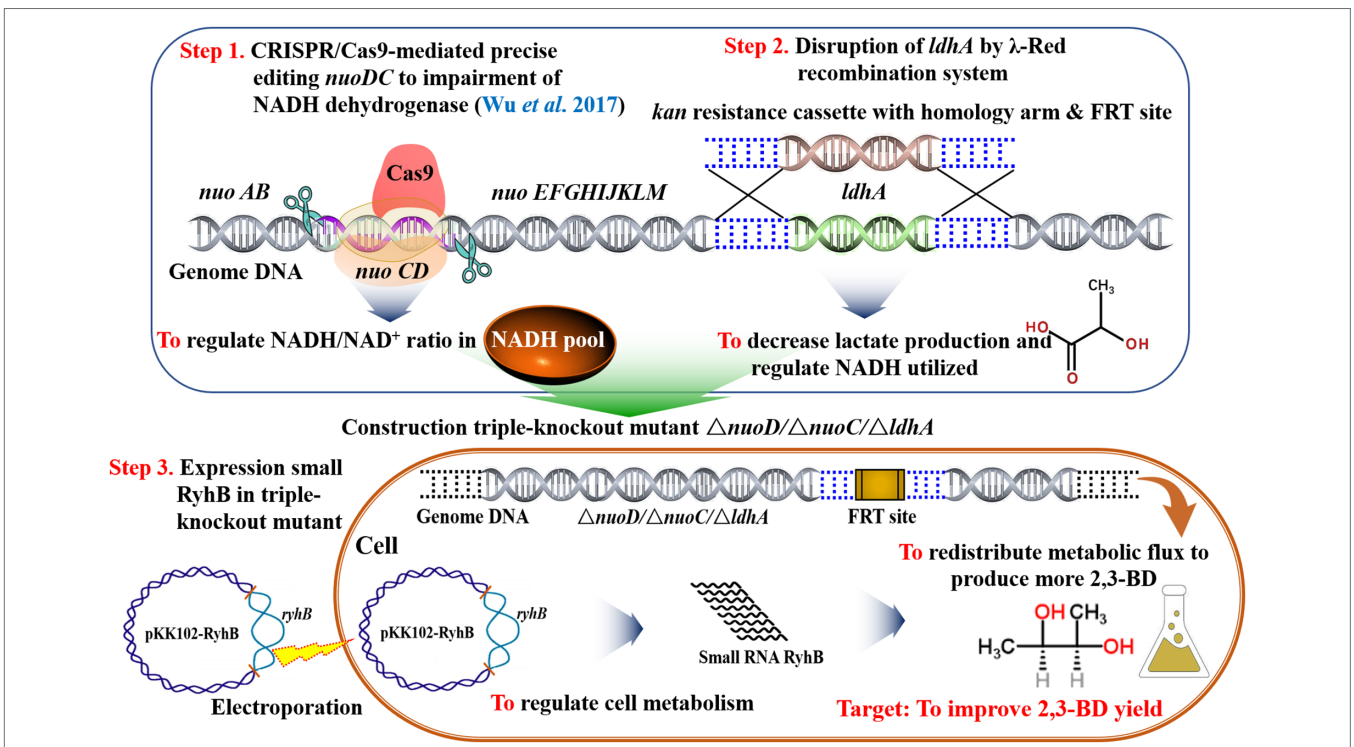

FIGURE 7 | Diagram of primary aerobic metabolic pathways for bacterial 2,3-BD production. Shown are three putative strategies to enhance 2,3-BD yield as outlined in this study.

type-strain *Salmonella typhimurium*. We found that the NADH/NAD$^+$ ratios of Ea-3 and Ea-4 were, respectively, decreased by 11.8 and 14.2% relative to Ea-1 and Ea-2 (**Figure 5**). These results support a role of *RyhB* in regulating the NADH/NAD$^+$ ratio, suggesting that the redox balance of the *E. aerogenes* mutants was disturbed. A similar observation was made in *E. coli* by Lyu et al. (2019), which explains why *RyhB* can significantly affect cell metabolism in addition to its negative effect on 2,3-BD production. Since RyhB acts as a global regulator of glucose metabolism (Kang et al., 2012), it stands to reason that since several of the targets of *RyhB* encode proteins of the TCA cycle, the overexpression of *RyhB* could result in lower levels of NADH in *E. aerogenes*.

2,3-BD Production by Ea-2 in a Fermenter

Ea-2 exhibited the highest 2,3-BD productivity in shake-flask fermentations among all the tested strains, with a yield from glucose reaching 1.01 mol/mol (**Figure 3**). We therefore used Ea-2 for a scale-up experiment in a 5-L fermenter with 3 L of glucose-containing medium. Ea-2 displayed a more pronounced exponential phase (4 h longer than in IAM1183), reaching a 40% higher cell density after cultivation for 44 h (**Figures 6C,F**). More glucose was consumed by Ea-2 during the fermentation, which resulted in an almost 7-fold higher 2,3-BD titer compared with the wild type (**Figures 6C,F**). There was also an increase in acetate production (**Figures 6A,D**), while the lactate accumulation rate was clearly reduced in Ea-2 (**Figures 6B,E**).

The final titers of the major byproducts after 44 h of fermentation in the 5-L bioreactor were measured for both Ea-2 and WT, as summarized in **Table 5**. The WT exhibited higher final concentrations of formate and lactate, while the concentration of ethanol decreased. This was in agreement with the shake-flask fermentations. The mutants generated in this work offer a solid basis for further studies on the fermentative metabolism of *E. aerogenes*, with great application potential for industrial 2,3-BD production.

CONCLUSION

There are three metabolic pathways for the production of 2,3-BD in *E. aerogenes* (**Figure 7**). The present work demonstrates that the deletion of NADH dehydrogenase (*ΔnuoC*/*ΔnuoD* strain Ea-1), alone or in combination with the deletion of LDH (*ΔnuoC*/*ΔnuoD*/*Δldh* strain Ea-2), can significantly improve the 2,3-BD yield of *E. aerogenes* (**Figure 7**). However, overexpression of the sRNA RyhB reduced the NADH/NAD$^+$ ratio and 2,3-BD production (**Figure 7**). Metabolic flux analysis of the parental strain IAM1183 and mutants grown on four different carbon sources indicated that the impairment of dehydrogenase is beneficial for 2,3-BD production due to a reduction in acidic by-products, and also indicated that RyhB could redistribute metabolic fluxes in *E. aerogenes*. The 2,3-BD titer produced by the mutant strain Ea-2 in a 5-L fermenter exhibited an almost 7-fold improvement over the wild type. Hence, Ea-2 may be a basis for further improvement of 2,3-BD production *via* metabolic engineering, offering hope to finally achieve biotechnological 2,3-BD production on an industrial scale.

DATA AVAILABILITY STATEMENT

The original contributions presented in the study are included in the article/supplementary material, further inquiries can be directed to the corresponding author.

AUTHOR CONTRIBUTIONS

HZ conceived and supervised the research, analyzed the results, and reviewed and edited the manuscript. HZ and YW designed the experiments. YW, QS, WC, and JY performed the investigations. YX, QS, HY, and FX validated the data. YW, WC, YL, PL, and KJ analyzed the results. YW wrote the original draft of the manuscript. WC modified the manuscript. All authors contributed to the article and approved the submitted version.

FUNDING

This work was financially supported by the National Science Foundation of China (grant no. 31970038), the Key Program Funds of Science and Technology Development of Liaoning Province of China (grant no. 2019JH2/10200003).

ACKNOWLEDGMENTS

The authors are grateful to the Wuxi Research Institute of Applied Technologies, Tsinghua University for technical support with the BatchPro software used for bioreactor monitoring and management.

REFERENCES

Beauchene, N. A., Myers, K. S., Chung, D. J., Park, D. M., Weisnicht, A. M., Keleş, S., et al. (2015). Impact of anaerobiosis on expression of the iron-responsive fur and RyhB regulons. *MBio* 6, e01947–e02015. doi: 10.1128/mBio.01947-15

Blomqvist, K., Nikkola, M., Lehtovaara, P., Suihko, M. L., Airaksinen, U., Straby, K. B., et al. (1993). Characterization of the genes of the 2,3-butanediol operons from *Klebsiella terrigena* and *Enterobacter aerogenes*. *J. Bacteriol.* 175, 1392–1404. doi: 10.1128/jb.175.5.1392-1404.1993

Bonestroo, M. H., Kusters, B. J. M., Wit, J. C. D., and Rombouts, F. M. (1992). Glucose and sucrose fermenting capacity of homofermentative lactic acid bacteria used as starters in fermented salads. *Int. J. Food Microbiol.* 15, 365–376. doi: 10.1016/0168-1605(92)90070-J

Booth, I. R. (1985). Regulation of cytoplasmic pH in bacteria. *Microbiol. Rev.* 11, 353–369. doi: 10.1007/BF02016817

Calderón, I. L., Morales, E. H., Collao, B., Calderón, P. F., Chahúan, C. A., Acuña, L. G., et al. (2013). Role of *salmonella Typhimurium* small RNAs RyhB-1 and RyhB-2 in the oxidative stress response. *Res. Microbiol.* 165, 30–40. doi: 10.1016/j.resmic.2013.10.008

Converti, A., Perego, P., and Borghi, M. D. (2003). Effect of specific oxygen uptake rate on *Enterobacter aerogenes* energetics: carbon and reduction degree balances in batch cultivations. *Biotechnol. Bioeng.* 82, 370–377. doi: 10.1002/bit.10570

Datsenko, K. A., and Wanner, B. L. (2000). One-step inactivation of chromosomal genes in *Escherichia coli* K-12 using PCR products. *Proc. Natl. Acad. Sci. U.S.A.* 97, 6640–6645. doi: 10.1073/pnas.120163297

Ge, Y. S., Li, K., Li, L. X., Gao, C., Zhang, L. J., Ma, C. Q., et al. (2016). Contracted but effective: production of enantiopure 2,3-butanediol by thermophilic and GRAS *bacillus licheniformis*. *Green Chem.* 18, 4693–4703. doi: 10.1039/C6GC01023G

Guo, Z. W., Ou, X. Y., Xu, P., Gao, H. F., Zhang, L. Y., Zong, M. H., et al. (2020). Energy- and cost-effective non-sterilized fermentation of 2,3-butanediol by an engineered *Klebsiella pneumoniae* OU7 with an anti-microbial contamination system. *Green Chem.* 22, 8584–8593. doi: 10.1039/D0GC03044A

Haveren, J. V., Scott, E. L., and Sanders, J. (2008). Bulk chemicals from biomass. *Biofuels Bioprod. Biorefin.* 2, 41–57. doi: 10.1002/bbb.43

Huang, S. H., Wang, C. K., Peng, H. L., Wu, C. C., Chen, Y. T., Hong, Y. M., et al. (2012). Role of the small RNA RyhB in the fur regulon in mediating the capsular polysaccharide biosynthesis and iron acquisition systems in *Klebsiella pneumonia*. *BMC Microbiol.* 12:148. doi: 10.1186/1471-2180-12-148

Hung, Y. P., Albeck, J., Tantama, M., and Yellen, G. (2011). Imaging cytosolic NADH-NAD^+ redox state with a genetically encoded fluorescent biosensor. *Cell Metab.* 14, 545–554. doi: 10.1016/j.cmet. 2011.08.012

Ji, X. J., Huang, H., Zhu, J. G., Ren, L. J., Nie, Z. K., Du, J., et al. (2010). Engineering *Klebsiella oxytoca* for efficient 2, 3-butanediol production through insertional inactivation of acetaldehyde dehydrogenase gene. *Appl. Microbiol. Biotechnol.* 85, 1751–1758. doi: 10.1007/s00253-009-2222-2

Jung, M. Y., Mazumdar, S., Shin, S. H., Yang, K. S., Lee, J., and Oh, M. K. (2014). Improvement of 2,3-butanediol yield in *Klebsiella pneumoniae* by deletion of the pyruvate formate-lyase gene. *Appl. Environ. Microbiol.* 80, 6195–6203. doi: 10.1128/aem.02069-14

Jung, M. Y., Ng, C. Y., Song, H., Lee, J., and Oh, M. K. (2012). Deletion of lactate dehydrogenase in *Enterobacter aerogenes* to enhance 2,3-butanediol production. *Appl. Microbiol. Biotechnol.* 95, 461–469. doi: 10.1007/s00253-012-3883-9

Kang, Z., Wang, X. R., Li, Y. K., Wang, Q., and Qi, Q. S. (2012). Small RNA RyhB as a potential tool used for metabolic engineering in *Escherichia coli*. *Biotechnol. Lett.* 34, 527–531. doi: 10.1007/s10529-011-0794-2

Lillian, G. A., Barros, M. J., Montt, F., Peñaloza, D., Núñez, P., Valdés, I., et al. (2021). Participation of two sRNA RyhB homologs from the fish pathogen *Yersinia ruckeri* in bacterial physiology. *Microbiol. Res.* 242, 126629–126638. doi: 10.1016/j.micres.2020.126629

Lu, Y., Zhao, H. X., Zhang, C., Lai, Q. H., Wu, X., and Xing, X. H. (2010). Alteration of hydrogen metabolism of *ldh*-deleted *Enterobacter aerogenes* by overexpression of NAD^+-dependent formate dehydrogenase. *Appl. Microbiol. Biotechnol.* 86, 255–262. doi: 10.1007/s00253-009-2274-3

Lu, Y., Zhao, H. X., Zhang, C., Lai, Q. H., and Xing, X. H. (2009). Perturbation of formate pathway for hydrogen production by expressions of formate hydrogen lyase and its transcriptional activator in wild *Enterobacter aerogenes* and its mutants. *Int. J. Hydrog. Energy* 34, 5072–5079. doi: 10.1016/j.ijhydene.2009.04.025

Lu, Y., Zhao, H. X., Zhang, C., and Xing, X. H. (2016). Insights into the global regulation of anaerobic metabolism for improved biohydrogen production. *Bioresour. Technol.* 200, 36–41. doi: 10.1016/j. biortech.2015.10.007

Lyu, Y., Wu, J. H., and Shi, Y. Y. (2019). Metabolic and physiological perturbations of *Escherichia coli* W3100 by bacterial small RNA RyhB. *Biochimie* 162, 144–155. doi: 10.1016/j.biochi.2019.04.016

Machner, M. P., and Storz, G. (2016). Small RNA with a large impact. *Nature* 529, 472–473. doi: 10.1038/nature16872

Massé, E., Escorcia, F. E., and Gottesman, S. (2003). Coupled degradation of a small regulatory RNA and its mRNA targets in *Escherichia coli*. *Genes Dev.* 17, 2374–2383. doi: 10.1101/gad.1127103

Massé, E., Vanderpool, C. K., and Gottesman, S. (2005). Effect of RyhB small RNA on global iron use in *Escherichia coli*. *J. Bacteriol.* 187, 6962–6971. doi: 10.1128/JB.187.20.6962-6971.2005

Miller, J. H. (1972). *Experiments in Molecular Genetics*. *Vol. 172*. New York: Cold Spring Harbor Laboratory Press.

Öhgren, K., Bengtsson, O., Gorwa-Grauslund, M. F., Galbe, M., Hahn-Hägerdal, B., and Zacchi, G. (2006). Simultaneous saccharification and co-fermentation of glucose and xylose in steam-pretreated corn stover at high fiber content with *Saccharomyces cerevisiae* TMB3400. *J. Biotechnol.* 126, 488–498. doi: 10.1016/j.jbiotec.2006.05.001

Park, S. J., Sohn, Y. J., Park, S. J., and Choi, J. I. (2020). Enhanced production of 2,3-butanediol in recombinant *Escherichia coli* using response regulator DR1558 derived from *Deinococcus radiodurans*. *Biotechnol. Bioproc. E.* 25, 45–52. doi: 10.1007/s12257-019-0306-0

Perego, P., Converti, A., Borghi, A. D., and Canepa, P. (2000). 2,3-Butanediol production by *Enterobacter aerogenes*: selection of the optimal conditions and application to food industry residues. *Bioprocess Biosyst. Eng.* 23, 613–620. doi: 10.1007/s004490000210

Petrova, P., Petlichka, S., and Petrov, K. (2020). New *bacillus spp.* with potential for 2,3-butanediol production from biomass. *J. Biosci. Bioeng.* 130, 20–28. doi: 10.1016/j.jbiosc.2020.02.009

Ragauskas, A. J., Williams, C. K., Davison, B. H., Britovsek, G., Cairney, J., Eckert, C. A., et al. (2006). The path forward for biofuels and biomaterials. *Science* 311, 484–489. doi: 10.1126/science.1114736

Sharma, A., Nain, V., Tiwari, R., Singh, S., and Nain, L. (2018). Optimization of fermentation condition for co-production of ethanol and 2,3-butanediol (2,3-BD) from hemicellolosic hydrolysates by *Klebsiella oxytoca* XF7. *Chem. Eng. Commun.* 205, 402–410. doi: 10.1080/00986445.2017.1398743

Song, C. W., Park, J. M., Chung, S., Lee, S. Y., and Song, H. (2019). Microbial production of 2,3-butanediol for industrial applications. *J. Ind. Microbiol. Biotechnol.* 46, 1583–1601. doi: 10.1007/s10295-019-02231-0

Thapa, L. P., Lee, S. J., Park, C., and Kim, S. W. (2019). Metabolic engineering of *Enterobacter aerogenes* to improve the production of 2,3-butanediol. *Biochem. Eng. J.* 143, 169–178. doi: 10.1016/j.bej.2018.12.019

Vinogradov, A. D. (2008). NADH/NAD^+ interaction with NADH: ubiquinone oxidoreductase (complex I). *Biochim. Biophys. Acta Bioenerg.* 1777, 729–734. doi: 10.1016/j.bbabio.2008.04.014

Wu, Y., Hao, Y. Q., Wei, X., Shen, Q., Ding, X. W., Wang, L. Y., et al. (2017). Impairment of NADH dehydrogenase and regulation of anaerobic metabolism by the small RNA RyhB and NadE for improved biohydrogen production in *Enterobacter aerogenes*. *Biotechnol. Biofuels* 10, 248–262. doi: 10.1186/s13068-017-0938-2

Yang, T. W., Rao, Z. W., Hu, G. Y., Zhang, X., Liu, M., Dai, Y., et al. (2015). Metabolic engineering of *Bacillus subtilis* for redistributing the carbon flux to 2,3-butanediol by manipulating NADH levels. *Biotechnol. Biofuels* 8, 129–137. doi: 10.1186/s13068-015-0320-1

Zhang, S., Shuang, L., Nan, W., Yuan, Y., Zhang, W., and Ying, Z. (2018). Small non-coding rna ryhb mediates persistence to multiple antibiotics and stresses in uropathogenic *Escherichia coli* by reducing cellular metabolism. *Front. Microbiol.* 9:136. doi: 10.3389/fmicb.2018.00136

Zhao, H. X., Lu, Y., Wang, L. Y., Zhang, C., Yang, C., and Xing, X. H. (2015). Disruption of lactate dehydrogenase and alcohol dehydrogenase for increased hydrogen production and its effect on metabolic flux in *Enterobacter aerogenes*. *Bioresour. Technol.* 194, 99–107. doi: 10.1016/j. biortech.2015. 06.149

Zhao, H. X., Ma, K., Lu, Y., Zhang, C., and Xing, X. H. (2009). Cloning and knockout of formate hydrogen lyase and H_2-uptake hydrogenase genes in *Enterobacter aerogenes* for enhanced hydrogen production. *Int. J. Hydrog. Energy* 34, 186–194. doi: 10.1016/j.ijhydene.2008.10.025

Conflict of Interest: The authors declare that the research was conducted in the absence of any commercial or financial relationships that could be construed as a potential conflict of interest.

Publisher's Note: All claims expressed in this article are solely those of the authors and do not necessarily represent those of their affiliated organizations, or those of the publisher, the editors and the reviewers. Any product that may be evaluated in this article, or claim that may be made by its manufacturer, is not guaranteed or endorsed by the publisher.

Advantages of publishing in Frontiers

OPEN ACCESS
Articles are free to read for greatest visibility and readership

FAST PUBLICATION
Around 90 days from submission to decision

HIGH QUALITY PEER-REVIEW
Rigorous, collaborative, and constructive peer-review

TRANSPARENT PEER-REVIEW
Editors and reviewers acknowledged by name on published articles

Frontiers
Avenue du Tribunal-Fédéral 34
1005 Lausanne | Switzerland

Visit us: www.frontiersin.org
Contact us:frontiersin.org/about/contact

REPRODUCIBILITY OF RESEARCH
Support open data and methods to enhance research reproducibility

DIGITAL PUBLISHING
Articles designed for optimal readership across devices

FOLLOW US
@frontiersin

IMPACT METRICS
Advanced article metrics track visibility across digital media

EXTENSIVE PROMOTION
Marketing and promotion of impactful research

LOOP RESEARCH NETWORK
Our network increases your article's readership